



JANET MARGARET SUMNER

**THE TRANSPORT AND DEPOSITIONAL
MECHANISM OF HIGH GRADE
MIXED-MAGMA IGNIMBRITE TL,
GRAN CANARIA: THE MORPHOLOGY OF
A LAVA-LIKE FLOW**

GEOMAR
Forschungszentrum
für marine Geowissenschaften
der Christian-Albrechts-Universität
zu Kiel

Kiel 1994

GEOMAR REPORT 27

GEOMAR
Research Center
for Marine Geosciences
Christian Albrechts University
in Kiel



JANET MARGARET SUMNER

Dissertation
zur Erlangung des Doktorgrades
der mathematisch-naturwissenschaftlichen Fakultät
der Christian-Albrechts-Universität zu Kiel
Zum Druck genehmigt am 22.12.1993

Redaktion der Serie: Gerhard Haass
Umschlag: Kerstin Kreis, Harald Gross,
GEOMAR Technologie GmbH

Managing Editor: Gerhard Haass
Cover: Kerstin Kreis, Harald Gross,
GEOMAR Technologie GmbH

GEOMAR REPORT
ISSN 0936 - 5788

GEOMAR REPORT
ISSN 0936 - 5788

GEOMAR
Forschungszentrum
für marine Geowissenschaften
D-24148 Kiel
Wischhofstr. 1-3
Telefon (0431) 7202-0
Telefax (0431) 72 53 91, 7 20 22 93, 72 56 50

GEOMAR
Research Center
for Marine Geosciences
D-24148 Kiel / Germany
Wischhofstr. 1-3
Telephone (49) 431 / 7202-0
Telefax (49) 431 / 72 53 91, 7 20 22 93, 72 56 50

TABLE OF CONTENTS

ABSTRACT	i
CHAPTER 1: INTRODUCTION	1
1.1 The Problems to be studied	1
1.2 Previous studies on ignimbrite TL	1
1.3 Perspectives of this study	2
1.4 The geology of Gran Canaria	3
1.4.1 Regional setting	3
1.4.2 Gran Canaria	3
1.4.3 Mogan Formation	7
1.5 Terminology	7
CHAPTER 2: FIELD STUDIES	10
2.1 Introduction	10
2.2 Internal Stratigraphy of TL	10
2.3 Definition and classification of lithofacies	13
2.3.1 Lithofacies groups	14
2.4 Lithofacies in unit TL1	21
2.4.1 TL comendite Lithofacies Group	23
2.4.2 TL mixed rock Lithofacies Group	27
2.4.3 TL trachyte Lithofacies Group	32
2.5 Lithofacies in unit TL2	33
2.5.1 Proximal Lithofacies of TL2	33
2.5.1.1 TL comendite Lithofacies Group	35
2.5.1.2 TL mixed rock Lithofacies Group	38
2.5.1.3 TL trachyte Lithofacies Group	39
2.5.2 Distal Lithofacies of TL2	41
2.5.2.1 TL comendite Lithofacies Group	44
2.5.2.2 TL mixed rock Lithofacies Group	45
2.5.2.3 TL trachyte Lithofacies Group	52
2.6 Regional variation	57
2.7 Topography controlled variation	59
2.7.1 Distribution of TL1 and TL2	59
2.7.2 Distribution of Lithofacies	62
2.7.3 Asymmetric welding	66
2.8 CONCLUSIONS	68
CHAPTER 3: TEXTURES AND FABRICS	69
3.1 Introduction	69
3.2 Variation in particle composition with height	69
3.3 Fiamme morphology and deformation	70
3.4 Axial ratios of fiamme as indicators of welding intensity	74

3.5	Variation in axial ratios of fiamme in TL	74
3.6	Microfabrics	76
3.6.1	Results of pilot study	77
3.7	Geographical distribution and flow lineations	85
3.8	Conclusions	88
CHAPTER 4: PETROGRAPHY OF TL LITHOFACIES		89
4.1	Introduction	89
4.2	Lithofacies and composition of TL	89
4.3.	Mineralogy	90
4.3.1	Crystal assemblage in TL comendite	90
4.3.2	Crystal assemblage in TL trachyte	93
4.3.3	Mineral chemistry	95
4.4	Other components in TL	111
4.4.1	TL trachybasalt globules	111
4.4.2	Pyroclasts	114
4.4.3	Non-juvenile rock fragments	117
4.4.4	Lenticules	118
4.5	Matrix textures in TL	118
4.5.1	Welding textures	119
4.5.2	Devitrification textures	122
4.6	Vapour phase crystallisation	122
4.7	Secondary alteration	125
4.8	Discussion	125
4.9	Conclusions	128
CHAPTER 5: WHOLE ROCK CHEMISTRY		129
5.1	Introduction	129
5.2	Geochemistry of the Lithofacies	129
5.2.1	Identification of Lithofacies Groups	129
5.2.2	Vertical variation in the composition of TL	134
5.2.3	Major and trace element variation	138
5.2.4	Fractionation trends	139
5.3	Discussion	142
5.3.1	Differentiation of TL magmas by fractionational crystallisation and mixing	142
5.3.2	Implications of peralkaline chemistry	144
5.4	Conclusions	147
CHAPTER 6: MAGMA MIXING AND MINGLING IN TL		148
6.1	Introduction	148
6.2	Mixing and mingling in the magma chamber	149
6.2.1	Mixing	149
6.2.2	Mingling	150
6.3	Mingling in the conduit during withdrawal	154
6.4	Particulate mixing during transport	157

6.5	Mingling of facies during post-depositional deformation	158
6.6	Discussion	159
6.6.1	Model for mixing, mingling and eruption of TL	159
6.6.2	Generation of TL1 and TL2	161
6.7	Conclusions	166
CHAPTER 7: DEPOSITION AND DEFORMATION OF TL		167
7.1	Introduction	167
7.2	Characteristics of high grade peralkaline ignimbrites	167
7.3	Flow dynamics	169
7.4	Discussion of terminology	170
7.5	Review of high grade ignimbrite emplacement mechanisms	174
7.6	Evidence for progressive aggradation of TL	178
7.7	Textural evidence of a particulate to non-particulate flow transition in TL2	184
7.8	Summary and conclusions	187
7.9	Agglutinate stability and viscosity	189
7.10	Post-depositional deformation of TL2	194
7.10.1	Lateral spreading and slumping: The effect of competency contrasts	194
7.10.2	Brecciation: Brittle deformation	195
7.10.3	Hot Loading: Plastic deformation	198
7.11	Deformation in response to topography	200
7.11.1	Extensional deformation	200
7.11.2	Compressional deformation	200
7.12	The morphology of a lava-like ignimbrite	206
7.13	Conclusions	209
CHAPTER 8: CONCLUSIONS		212
REFERENCES		217

APPENDICES A copy of the appendices, available for reference, is held in the GEOMAR Library. (Address on cover page).

ABSTRACT

The Miocene (ca. 13.88 Ma) ignimbrite TL (43km³ estimated minimum volume) is a complex extra-caldera cooling unit deposited around the western and southern parts of the Tejede Caldera, Gran Canaria. This outflow facies consists of two spatially discrete but overlapping flow units, TL1 (106km²) and TL2 (51km²). Flow unit TL1 (ca. 10m thick) is a 'high grade' ignimbrite which is welded to its upper surface and contains rheomorphic zones. TL2 (ca. 14m thick) is an 'extremely high grade' ignimbrite welded to its upper surface, with vertical and lateral gradations to lava-like lithofacies. Both units have an extremely complicated textural stratigraphy, but a relatively simple compositional stratigraphy based on the varying proportions of comenditic trachyte and comendite. Both units consist of a base dominated by TL comendite lithofacies, a central zone of TL mixed rock lithofacies, and an upper zone dominated by TL trachyte lithofacies. TL comendite lithofacies are mostly vitroclastic and only locally lava-like. TL mixed rock lithofacies show both vitroclastic and lava-like lithofacies, and are marbled and flow banded. TL trachyte lithofacies are generally lava-like, but locally even these grade vertically and laterally into vitroclastic lithofacies.

Glass, mineral and fiamme compositions suggest that three original magma compositions are represented in TL: comendite, comenditic trachyte and trachybasalt. The comendite is an anorthoclase, amphibole (magnesian katophorite and ferro-eckermanite) bearing peralkaline rhyolite (ca. 67 wt.% SiO₂ for bulk rock and 69 wt.% for fiamme), with rare hypersthene phenocrysts. Mineralogically the comenditic trachyte (ca. SiO₂ content 65 wt.% for bulk rock and 62 wt.% for fiamme) is composed of anorthoclase and sodic plagioclase (albite, oligoclase and andesine) with subordinate augite and hypersthene, and rare sodic-calcic amphibole. The trachybasalt occurs as minute (< 7mm) globules finely dispersed throughout TL trachyte in TL2. It is glassy, aphyric and is identified by microprobe analysis only.

The major and trace element trends indicate that fractional crystallisation of comenditic trachyte was the main process of differentiation in the TL trachyte - TL comendite series. Comendite is interpreted as being produced from comenditic trachyte by the fractional crystallisation of pyroxene, ilmenite, plagioclase and anorthoclase feldspar, with anorthoclase feldspar being the most important phase. The presence of comenditic trachyte (TL trachyte) cannot be explained by simple fractionation and is probably the result of an early magma mixing event between basalt and comendite. Mingling of the component magmas is indicated by the occurrence of compositionally banded pumice, now represented by fiamme. The suggestion that magmas were physically mingled rather than mixed is supported by the lack of mutual mineral inclusions, and the rare occurrence of disequilibrium textures, such as rounding or corrosion of phenocrysts interpreted as xenocrysts. Globules of trachybasalt occurring within TL trachyte and TL mixed rock in TL2 have amoeboid and crenulate margins. They are glassy and are often mantled in comenditic trachyte. These features are consistent with simultaneous liquidity of the magmas and suggest that mingling occurred predominantly in a magmatic state within the chamber, before fragmentation. The morphology and texture suggests that the trachybasalt globules were produced when more mafic magma was injected into, and quenched within, cooler more silicic magma (comenditic trachyte).

Intense mixing of the two main component magmas, comendite (occupying the upper half of the chamber) and comenditic-trachyte (occupying the lower half of the chamber), was inhibited by a difference in viscosity. Fiamme compositions suggest that mixing was 'stepwise,' through a series of hybrid intermediate compositions, as opposed to directly between comendite and trachyte. Evacuation of the magma chamber was driven by forceful injection of trachybasalt into the lower portion of the chamber. This hotter more basic magma was quenched on contact with the comenditic trachyte. 'Vesiculation induced disintegration' of the trachybasalt caused disruption of the stable comenditic trachyte-comendite zonation. The chamber was evacuated from the top down. Comendite was erupted first (TL comendite lithofacies), as the thickness of this layer was progressively reduced, intermediate compositions and comenditic trachyte were drawn up towards the conduit in the form of an inverted funnel. Simultaneous eruption of comendite, intermediate compositions and comenditic trachyte lead to in-conduit mingling, e.g. banded pumice and TL mixed rock lithofacies. On continued eruption, the amount of comenditic trachyte ejected gradually increased, finally dominating the eruption and leading to the deposition of TL trachyte lithofacies.

The sectorial differences in the distribution of TL1 and TL2, together with the presence of trachybasalt in TL2 and its absence in TL1, argue strongly for *two* sequential eruptions issuing from *two* vents but related to a single compositionally heterogeneous magma chamber.

The compositionally and texturally discrete layers within flow units TL1 and TL2 are separated by diffuse boundaries, grading over tens of centimetres. TL comendite and TL mixed rock layers are mostly vitroclastic (eutaxitic) but show rare lateral gradation into lava-like lithofacies. Trachyte layers are generally holocrystalline and lava-like, but locally grade laterally into vitroclastic lithofacies. There is no evidence that the chemically distinct layers are discrete flow units, and the entire deposit is considered to consist of only two flow units. Vertical welding compaction/agglutination profiles are highly irregular. Local, lateral gradations from vitroclastic to lava-like occur

within individual compositional layers. Lineated fiamme are locally imbricated throughout massive layers and from one layer to the next.

This combination of features indicates that the two flow units deposited incrementally from the base upwards with agglutination and particle deformation occurring *during* as well as after deposition. The variations from slightly welded to lava-like lithofacies therefore reflect viscosity variations in successive particle populations supplied to the depositional regimes of the two flows. The complex lithofacies variations in TL2 suggest this was the deposit of a more unsteady flow than TL1.

Flow unit TL2 is divided into a proximal ponded region and a distal region. The distal portion of TL2 is dominated by holocrystalline, lava-like textures and features, previously considered diagnostic of lavas, e.g. basal autobreccia, extensive upper autobreccia, steep distal margin and marginal autobreccia, and locally holocrystalline trachytic texture. These features are interpreted to have formed during the non-particulate flow of TL2.

TL2 aggraded rapidly and the agglutinate pile continued to deform after deposition. The chemical zoning in TL from first erupted TL comendite to last erupted TL trachyte resulted in an unstable reverse density layering. The aggrading pile of agglutinate layers underwent loading, shear, mechanical mixing, and auto intrusion prior to cooling and lithification. Viscosity relationships between TL comendite and TL trachyte changed significantly from magma chamber conditions through to the last stages of deformation. TL trachyte and TL comendite show evidence of brittle *and* plastic behaviour throughout their deformation history. The changes in deformation behaviour are interpreted to be the result of, preferential cooling and degassing of TL trachyte in the top portion of the flow, insulation of TL comendite, coupled with reheating by heat transfer from TL comendite, and possibly retention of dissolved volatiles in TL comendite due to overlying impermeable TL trachyte.

The resultant ignimbrite TL is complex. It locally exhibits features previously regarded as diagnostic of lavas, yet its lithofacies associations clearly show that its origin is pyroclastic.

*'The time has come,' the Walrus said,
'To talk of many things:
Of shoes-and ships-and sealing-wax-
Of cabbages-and kings-
And why the sea is boiling hot-
And whether pigs have wings.'*

*- Lewis Carroll 1832-1898,
Through the Looking Glass*

ACKNOWLEDGEMENTS

The first three years of this work was funded by a SERC/NATO Overseas Studentship and the final year was financed by a grant from Prof. H-U Schmincke, this funding is gratefully acknowledged. I thank Prof. H-U Schmincke for his support and encouragement and am indebted to Mike Branney and Jocelyn McPhie for their detailed reviews of this manuscript. Special thanks go to Jon Dehn for his time and assistance in the preparation and format of this report.

CHAPTER 1

INTRODUCTION

1.1 THE PROBLEMS TO BE STUDIED

The distinction between lava-like ignimbrites and widespread siliceous lavas has long been controversial. This is because the distinguishing vitroclastic textures of ignimbrites are commonly destroyed during intense welding and rheomorphism, and when devitrification occurs. This produces problematic deposits that show complex facies variations and makes determination of the mode of deposition difficult.

Lithofacies can be especially difficult to interpret in terms of emplacement and depositional processes where apparent lavas and highly welded tuffs pass vertically and laterally into weakly welded and non-welded tuffs. The determination of emplacement and depositional mechanisms in high grade ignimbrites can be further compounded where the ignimbrite shows marked textural changes related to pronounced changes in the chemical stratification. The following two problems are addressed in this thesis:

1. Identifying, and defining the depositional, transport and emplacement mechanisms of high grade ignimbrite TL on Gran Canaria.

2. Determination of the magma mixing and mingling processes which occurred during the withdrawal, eruption, transport and deposition of high grade ignimbrite TL on Gran Canaria.

Ignimbrite TL of the Middle Mogán formation (Section 1.4.3) on Gran Canaria is ideally suited for the study of these two problems. TL is a high grade, peralkaline ignimbrite showing marked vertical and lateral changes in welding intensity, and it is compositionally zoned from comendite to comenditic trachyte.

1.2 PREVIOUS STUDIES ON IGNIMBRITE TL

Ignimbrite TL is a conspicuous marker horizon in the field, commonly forming a line of small but steep, dark grey-brown cliffs. It commonly has a highly irregular, spinose and undulating, lava-like surface morphology with top breccia and ramp structures, resembling the upper surface of blocky Aa lava flows. Locally it has a basal autobreccia.

Schmincke (1969 b) carried out the initial investigatory work on TL. The initials 'TL' stand for Tufolava, which was a term commonly used for lava-like ignimbrites (Abich, 1982; Cook, 1966).

Schmincke (op. cit.) identified the vitroclastic and lava-like components, as well as the comenditic and comenditic trachyte components in TL. These are mixed in all proportions and on all scales ranging from the submicroscopic to domains of several meters. He suggested that the fine scale mixing of comendite and comenditic trachyte took place in the conduit or magma chamber just prior to eruption. Eruption was hypothesised from a zoned magma-column with pronounced changes in eruptive behaviour. The more volatile rich comenditic magma erupted early, largely as pyroclastic flows, and the comenditic trachyte generally later, as lava flows from lava fountains.

Also recognised by Schmincke was a locally separate ignimbrite with black fiamme occurring below the lava-like TL flow unit, in Barranco (Bco.) de Mogán and Taurito areas. This study now confirms this ignimbrite as being the first flow unit of compound cooling unit TL, and divides TL into two distinct units:

TL1- Flow unit 1, a high grade ignimbrite (classification after Walker, 1983), with vitroclastic texture ranging from non-welded and weakly welded, through to eutaxitic and parataxitic.

TL2- Flow unit 2, which is an extremely high grade (classification after Walker, 1983) lava-like ignimbrite.

1.3 PERSPECTIVES OF THIS STUDY

Three major topics will be discussed in detail:

1. The **mixing and mingling** of the component magmas in TL, in the magma chamber and conduit, the particulate mixing of juvenile particles in the transport regime of the flow, and the mechanical mingling of facies during post-depositional non-particulate flow.
2. The **emplacement and depositional mechanisms** of TL1 and TL2, relating to the peralkaline chemistry and the type of flow. Particular consideration is given to the way in which individual particles deposit and the timing of welding.
3. The **post-emplacement cooling and deformation history**, with particular reference to the devitrification and vapour phase crystallisation of TL, and the post-depositional deformation of TL during non-particulate flow.

The discussion of these topics will be based on data collected during detailed field studies and petrographic and geochemical analyses of samples.

Field studies, structural and textural analysis

1. Detailed regional mapping together with vertical profiles through complete stratigraphic sections of TL are used to:
 - (a) Determine the geographical extent of flow units TL1 and TL2.
 - (b) Show proximal to distal facies variations in flow units TL1 and 2.
 - (c) Examine the effect of palaeotopography on distribution of the two flow units and the facies within them.
2. Samples through stratigraphic sections at selected localities around the caldera are used to:
 - (a) Detect regional changes in the chemical and textural stratification.
3. Samples and horizontal photomontages at key outcrops are used to:
 - (a) Define facies and facies associations.
 - (b) Detect small scale vertical and lateral changes in the chemical and textural stratigraphy.
 - (c) Demonstrate local differences in mixing and mingling patterns.
 - (d) Record extensional and compressional deformation structures produced by post-depositional non-particulate flow.

Petrography and geochemistry

1. Samples of bulk rock, globules or inclusions and fiamme are studied, together with chemical analysis of phenocryst phases, with the object of identifying the mixtures of the component magmas, and to determine the timing and mechanisms of mixing and mingling events.
2. Detailed chemical analysis of vapour phase minerals, and petrographic studies of glassy and crystalline groundmass are used to reconstruct the cooling, devitrification and vapour phase crystallisation history of TL.

Viscosity calculations

The determination of viscosity, as a function of thermal diffusivity and changing temperature over time, between the compositionally diverse magmas, is calculated because this places major constraints on the mingling processes and type of deformation (brittle versus ductile) which occurs.

1.4 THE GEOLOGY OF GRAN CANARIA

1.4.1 Regional setting

Gran Canaria is one of the central islands of the Canarian archipelago, a group of 7 major islands built on the continental rise and slope about 100km off the north west coast of Africa (Fig. 1.1).

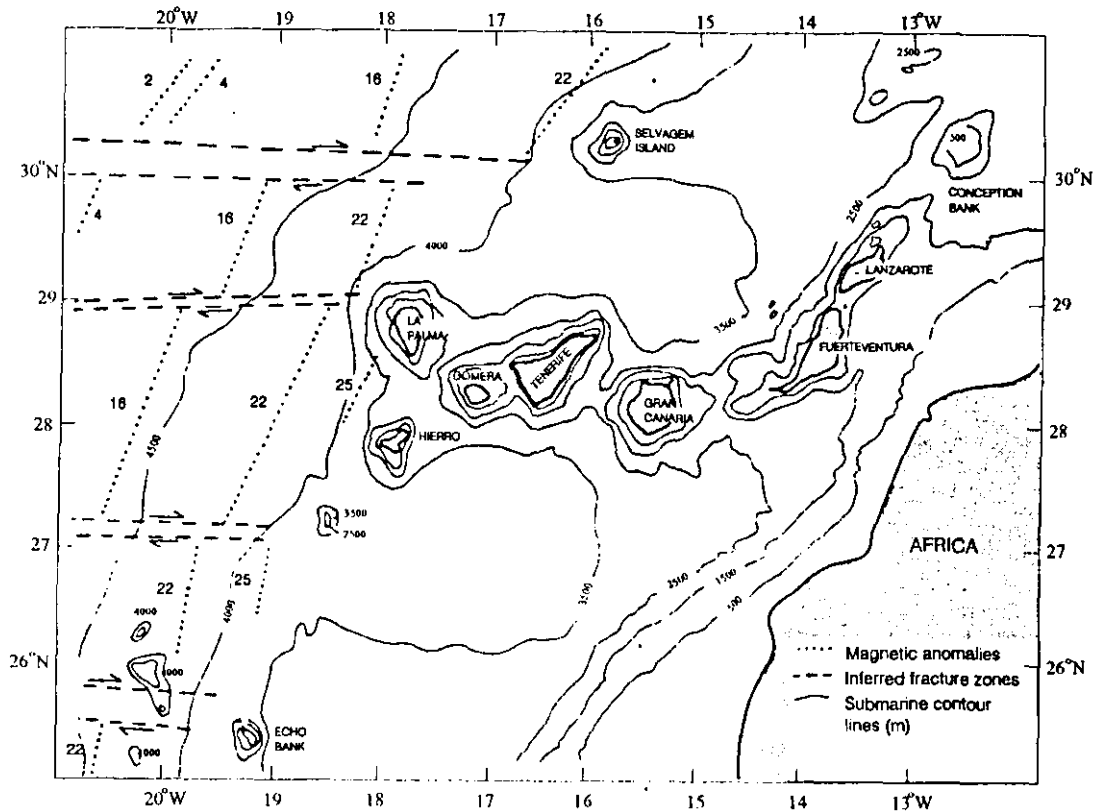


Figure 1.1. The Canary Island archipelago, including bathymetric and magnetic anomalies in the eastern Atlantic ocean (Reproduced from Schmincke, 1987).

1.4.2 Gran Canaria

The island of Gran Canaria is roughly circular in contour, with a diameter of 45km. The coastward sloping topography is dissected by deep near vertical walled canyons (Barrancos) which extend radially outwards from the island's highest point (1,950m). The geology of the island can be roughly divided into three broad sections; the Miocene extracaldera facies in the SW and S (Fig. 1.2), the resurgent Tejeda caldera in the centre and younger volcanic rocks which are concentrated in the NE half of the island.

Gran Canaria

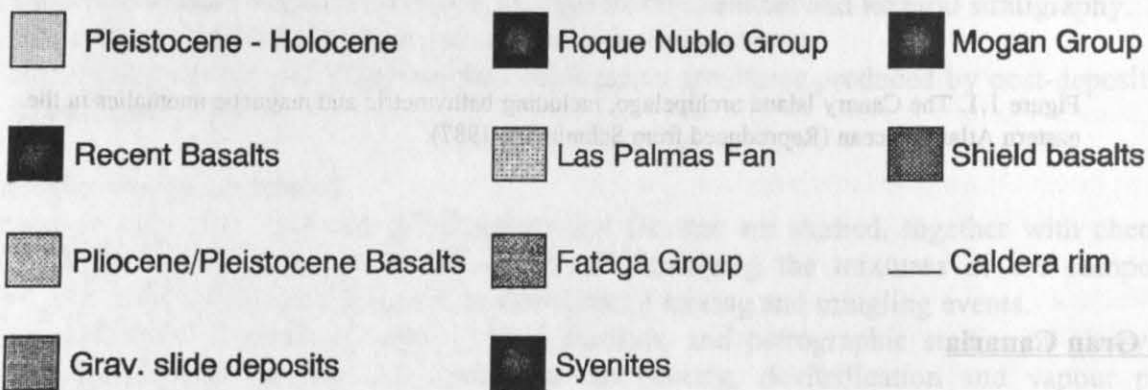
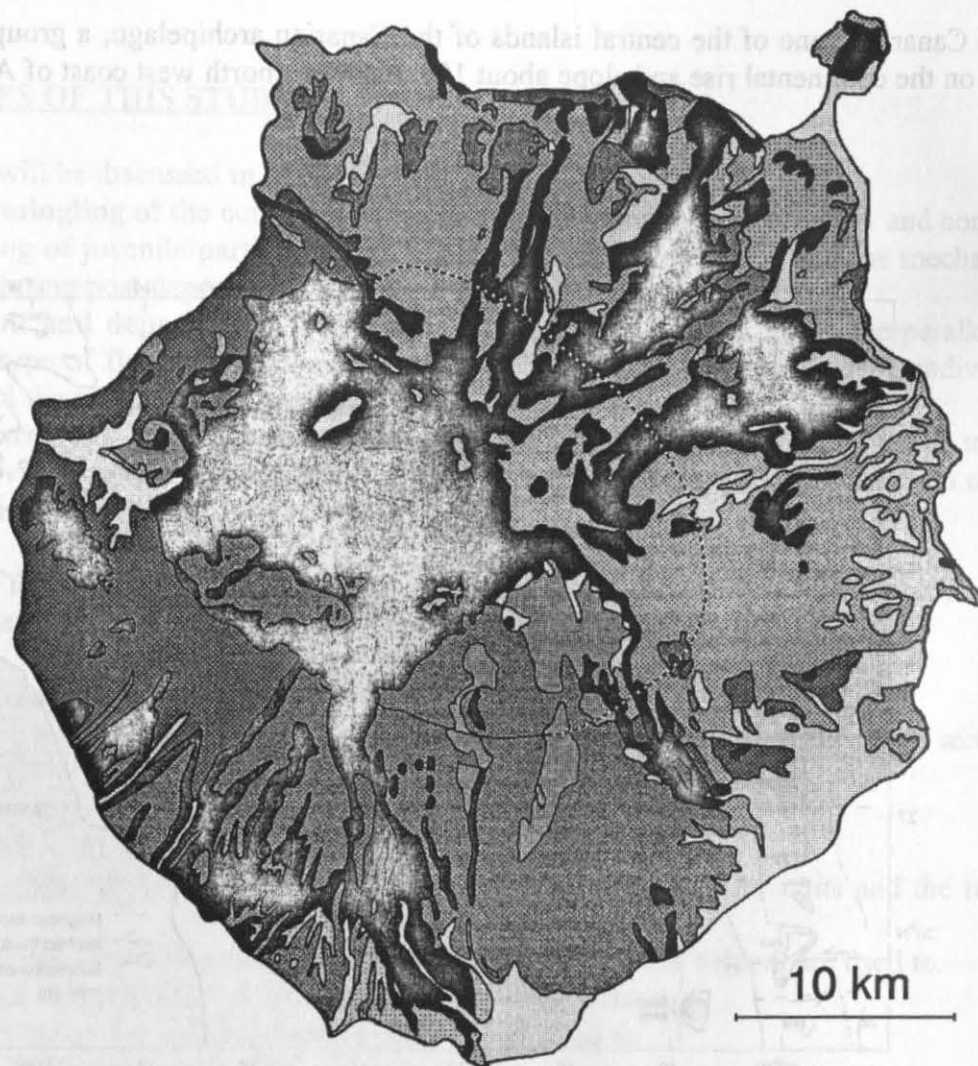


Figure 1.2. Geological map of Gran Canaria, simplified and modified after Fuster et al. (1968) and Schmincke (1976).

The following formalised lithostratigraphic subdivision (Fig. 1.3) is taken from Schmincke, 1993:

Miocene Basalt Group (ca. 14 to 14.5Ma)

The oldest rocks on Gran Canaria are a series of basalt flows forming complex shield volcanoes, which crop out in the western and southwestern parts of the island (Fig. 1.2) and reach a height of a 1000 m above sea level. The oldest shield forming lavas (Fig. 1.3), the **Güigüi Formation**, are a series of picrites and ankaramites which appear at sea level in Bco. de Güigüi and rise southward to several hundred meters above sea level. A major erosional unconformity separates the older Güigüi Formation from the younger **Hogarzales Formation**, which is a series of fine grained, thick, brecciated trachybasalt flows (hawaiites and mugearites).

Miocene Felsic Rock Group

Extracaldera Outflow Facies

The Miocene basalts are overlain by >500m of felsic extrusive rocks which form the *outflow or extracaldera* facies (Fig. 1.2) of a large caldera (ca. 20km in diameter). The caldera is filled with >1000m of sedimentary, extrusive and intrusive felsic rocks. The outflow or extracaldera facies has been divided into two groups (Fig. 1.3): the lower series of trachytic to rhyolitic sub alkalic to strongly peralkalic lavas and ignimbrites forming the **Mogán Group** (ca. 13.5 to 14.1Ma), up to ca. 300m thick; and the **Fataga Group** (ca. 10 to 13Ma), consisting of a series of trachyphonolitic lavas and ignimbrites, locally >500m thick. TL is part of the Mogán Group, which is described in detail in the following section.

Intracaldera Facies (ca. 10 to 8.5Ma)

The intracaldera Miocene felsic rocks are a series of epiclastic and pyroclastic volcanoclastics interbedded with and overlain by trachytic to rhyolitic lithic rich ignimbrites (**Montana Tirma Formation**). These comprise the outer intracaldera filling, and a series of comenditic to pantelleritic ignimbrites, tuffs and local intrusions make up the outer intracaldera belt between Montana Tirma and Bco. de Agiuneguín (**Montana Horno Formation**). The intracaldera intrusive rocks consist of syenite stocks, trachytic cone sheets and younger phonolite dikes and stocks (**Tejeda Formation**, Fig. 1.2); and trachyphonolitic dikes, intrusions and tephra deposits (**Cruz Grande Formation**).

Miocene and Pliocene Sedimentary Group

A series of sedimentary rocks predominantly conglomerates, fanglomerates, mudflows and landslide deposits represent a period of intense erosion in the interval between the end of Miocene phonolitic and the beginning of Roque Nublo volcanism.

Roque Nublo Group (ca. 4.4 to 3.4Ma)

The Roque Nublo group (Fig. 1.2) is made up of lava flows in its basal part, breccia sheets interbedded with lava flows and thick, massive breccia sheets in the middle, and strongly hauyne-phyric intrusives and a few hauyne-rich lava flows in its upper part. Lava compositions range from transitional tholeiites and alkali basalts to trachytes, and from basanites through phonolites, as well as nephelinites.

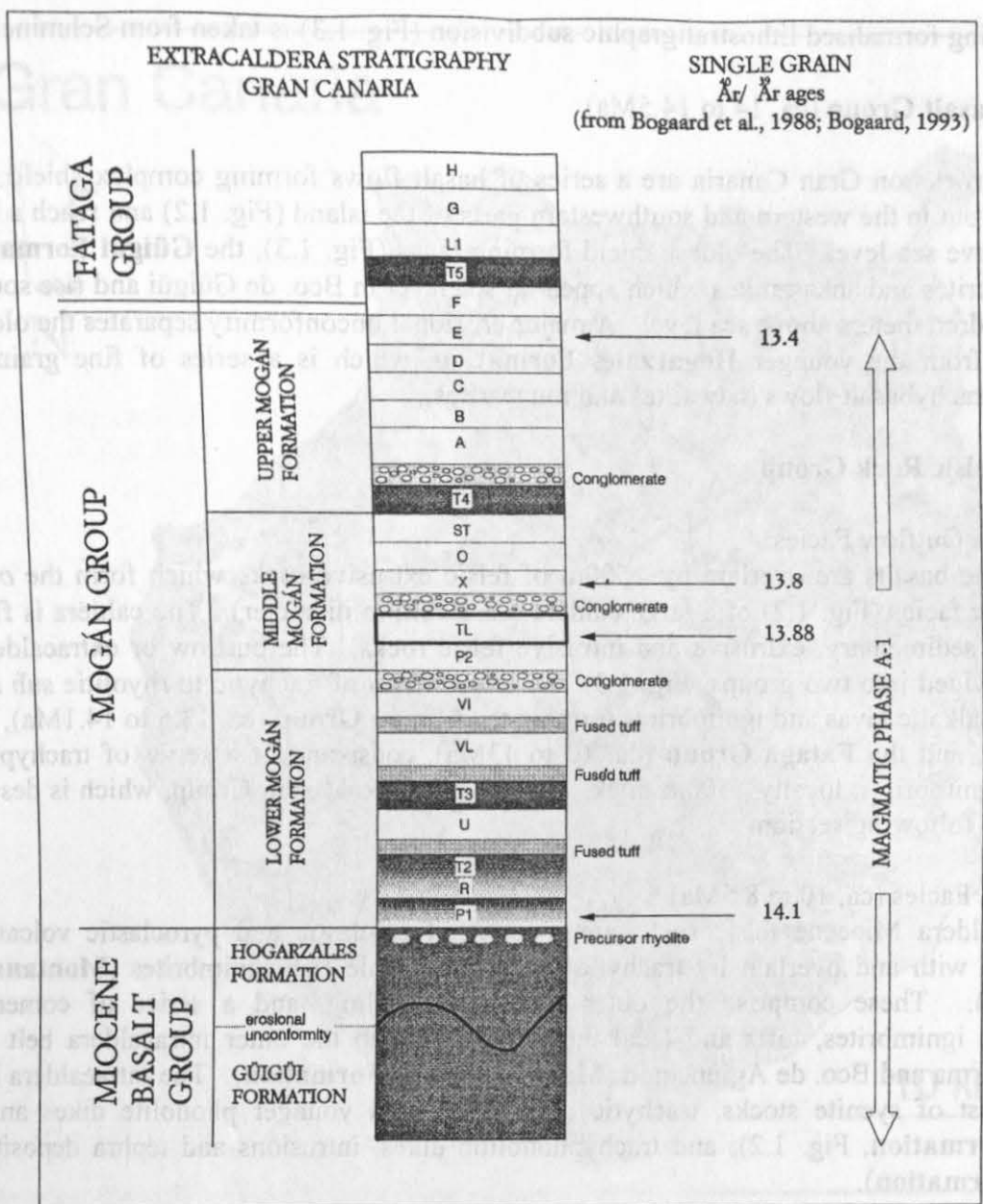


Figure 1.3. Schematic stratigraphic column of the rock series deposited during the first Miocene magmatic phase (A-I). Modified after Schmincke (1987). The position of ignimbrite TL is outlined in black.

Post Roque Nublo Volcanics Group (ca. 3Ma to subrecent)

Following a second, relatively brief, but intense period of erosion a major phase of nephelinite volcanism occurred, with lava flows filling canyons in the north and northeastern sectors of the island. This phase was followed by basanite and nephelinite scoria and lava flows which erupted from many vents in the northern and eastern sectors of the island during the Middle Quaternary (Fig. 1.2). The most recent volcanism is a series of prehistoric basanitic scoria cones and lava flows in the north of the island.

The subaerially exposed volcanic and intrusive rocks on Gran Canaria all formed within the last 15Ma (McDougall and Schmincke, 1976; Bogaard et al., 1988), with the most recent prehistoric eruption on Gran Canaria (see above) occurring some 3057 years ago (Nogales and Schmincke,

1969). During this period magmatism was not continuous, but evolved in cycles. Schmincke (1982, 1987; most recent review in Schmincke, 1993) defined two major cycles (A and B), each comprising three phases (I- III). Phase A-I was the rapid formation (during Ma) of the volcanic shield (submarine and subaerial), making up 90 volume percent of the island and consisting of mildly alkalic to alkalic basaltic lavas capped by a minor volume of trachytic to peralkaline rhyolitic lavas and ignimbrites. Silica-undersaturated trachyphonolites and nepheline phonolites were erupted and intruded during phase A-II, lasting from about 12.5 to 8.5Ma. After an erosional interval, small volumes of nephelinite were locally erupted about 5Ma ago, representing phase A-III. The second cycle began 4.4Ma ago, with the emplacement of a small volume of transitional tholeiitic basalt lavas (phase B-I), followed by the large volume, basanitic-tephritic basalts of the Roque Nublo Volcanics Group (phase B-II). This terminated with the deposition of massive hauyne-phonolite breccia flows at 3.5Ma. After a second erosional interval, nephelinite magmas younger than 2.9Ma were erupted during phase B-III.

1.4.3 Mogán Formation

The Mogán Group (Fig. 1.3) is subdivided into:

- (a) **Lower Mogán Formation**, consisting of three basalt flows Ta, Tb, Tc (at least one of which contains significant traces of precursor rhyolite, Schmincke, 1987), porphyritic ignimbrite P1, high grade ignimbrites R and U, benmoreite lava flow T3, rhyolite lava flow VL and very high grade ignimbrite VI.
- (b) **Middle Mogán Formation**, consisting of porphyritic ignimbrite P2, very high grade ignimbrite TL, and ignimbrites L, X, and O.
- (c) **Upper Mogán Formation**, consisting of lava flow T4 and ignimbrites A, B, C, D and E. Cooling unit F is transitional to the overlying Fataga Formation.

Most of the cooling units of the Mogán Group are weakly to strongly peralkaline (comenditic to pantelleritic), compositionally zoned, low-silica rhyolitic to trachytic ignimbrites, whose chemistry can be largely explained by the fractional crystallisation of anorthoclase feldspar (Schmincke, 1969a). The ignimbrites are commonly highly welded to within a few cm's of the upper surface and are characterised by a number of spectacular internal deformation structures which are typical of peralkaline ignimbrites (Schmincke and Swanson, 1967; Schmincke, 1974). The Mogán ignimbrite sequence in general is characterised by a paucity of initial fallout tephra underlying the ignimbrites. The cooling unit P1 marks the beginning of voluminous eruption of highly evolved magmas after the formation of the basaltic shield, and the eruption of this unit was synchronous with the collapse of a huge caldera basin at least 15km in diameter (Fig. 1.2).

1.5 TERMINOLOGY

The following usage of terms will be applied throughout this work. The terms are listed in alphabetical order for easy reference:

Agglutination: the process by which low viscosity particles weld immediately on contact and the particle outline is, in part, retained.

Aggradation: material layer construction by sedimentation.

Coalescence: the process by which fluidal droplets form a homogeneous liquid in which the remnant particle outlines are obliterated (Ekren et al., 1984).

Compound cooling unit: several flow units (multiple flow unit) containing a cooling hiatus (Smith, 1960b; Fisher and Schmincke, 1984).

Cooling unit: an assemblage of flow units produced during one eruption (Smith, 1960b). The term 'ignimbrite' is used synonymously with cooling unit.

Eutaxitic: a discontinuous planar fabric produced by the flattening of vitroclastic textures (Wright, Smith and Self, 1980).

Fiamme: any sheared juvenile clast. The term is not synonymous with 'flattened pumice lapilli' and does not imply emplacement by pyroclastic flow. Normally prefixed by the compositional classification e.g. comenditic fiamme, also including *mixed rock fiamme* which are subdivided into (a) *compositionally banded fiamme*: composed of compositionally discrete interlayered bands of varying vesicularity and (b) *intermediate fiamme*: which are compositionally homogeneous flattened juvenile clasts of intermediate composition (composition determined by geochemical analysis).

Flow unit: the deposit of a single pyroclastic flow (Smith, 1960).

Globules: roughly spherical glassy inclusions, regular or amoeboid in outline. Can be vesicular or non-vesicular.

Grade: terminology proposed by Walker (1983) to refer to the amount of welding compaction exhibited by ignimbrites. This reflects the cooling history and embraces the concept of a grade continuum, which can be divided into 4 arbitrary categories: (a) Extremely high grade ignimbrites- are intensely welded to their upper surfaces and include lithofacies that are lava-like, (b) High grade ignimbrites- these are predominantly welded throughout and have intensely welded and rheomorphic zones, (c) Moderate grade ignimbrites- have both welded and non-welded facies, (d) Low grade ignimbrites- show little or no evidence of welding and range down to those ignimbrites emplaced at ambient temperatures.

The term is non-genetic and reflects the variability of particle viscosity and yield strength during ignimbrite emplacement; without implying which of the many factors (e.g. eruption temperature, magma chemistry, volatile content, syn-emplacement cooling) may be the cause.

Hot slumping: mass movement of viscous welded tuff in response to gravity, either downslope or by gravity spreading on flat surfaces.

Inclusions/blebs: rock bodies that show signs (e.g. plastic deformation, amoeboid or crenulated margins, chilled margins) of incorporation in a partly liquid state, suggesting they were co-magmatic with their host.

Lava-like: texturally indistinguishable from a lava.

Layer: a discrete facies, traceable over several tens of meters, which is bounded by upper and lower contacts which may be sharp or gradational, planar or undulating.

Lenticules: flattened, elongate vesicles in densely welded tuff (Mackin, 1960) may or may not be infilled with vapour phase minerals.

Lithofacies Group: groups of compositionally similar lithofacies.

Lithofacies: rock units that can be defined by their morphology, stratigraphic position, composition, texture, grain size characteristics and colour. (Following usage of the term by Middleton, 1978).

Load-ball: an isolated pod of material detached from the parent body, also includes large, lobate protrusions transgressing down into underlying facies or layers.

Mechanical mingling: the process by which facies are physically mingled during the post-depositional non-particulate flow of high grade ignimbrite.

Microfacies: compositionally distinct lithologies occurring within a lithofacies or subfacies, determined by geochemical analysis.

Mingling: the incomplete mixing of two or more compositionally distinct magmas, such that the magmas reach the surface without entirely losing their identity and are still compositional and texturally distinguishable (Yoder, 1973).

Mixing: the process by which two or more compositionally distinct magmas are blended together such that the melts of each are blended into a compositionally uniform single magma (Anderson, 1976).

Non-juvenile rock fragments/accidental lithics: rock fragments which were not fluid when entrained in the magma or transport regime of the pyroclastic flow. These include: (a) *accessory lithics*: lithic fragments which are unrelated to the magma and were derived from the conduit and vent wall rocks; and (b) *pick-ups*: lithic fragments which are unrelated to the magma and were derived from the surface.

Non-particulate: material composed of particles that are stuck together such that they cannot move independently of each other.

Parataxitic: Extreme lengthening and distortion of eutaxitic texture, but still discontinuous (Wright, Smith and Self, 1980).

Particulate mixing: the process by which pre-existing juvenile particle populations are physically mixed by semi-turbulent flow in the transport regime of a pyroclastic flow.

Pillows/micropillows: the term used to describe inclusions resembling, in both morphology and texture, the cross sections of pillows produced by the subaqueous eruption of basaltic lava.

Post-depositional deformation: process of deformation producing structures affecting entire flow units to the upper surface.

Post-depositional welding compaction: the post depositional adhesion and compaction of higher viscosity shards under the influence of a deposits *in situ* cooling rate and load pressure.

Rheomorphism: non-particulate flow of welded tuff.

Shear cavities: irregularly shaped open cavities in densely welded tuff, usually surrounding accidental lithic clasts.

Shear zones: narrow (ca. 4cm) vesicular zones crossed by slanting, sub-parallel, open fractures and sigmoidal cracks, in densely welded tuff.

Simple cooling unit: a single flow unit or several flow units (multiple flow unit of Smith, 1960b) which cooled together without any break in the temperature gradient.

Sintering: the process by which the point contacts of hot vesicular fragments or shards adhere. This process may or may not result in the plastic deformation of shards giving a eutaxitic texture.

Subfacies: texturally distinct lithologies occurring within a lithofacies, generally as finer grained discontinuous layers, pods or lenses.

Syn-depositional deformation: process of deformation which produces structures constituting classic criteria for rotational shear.

TL trachyte: rock composed of >60 volume % comenditic trachyte and <40 volume % comendite, with up to 2 volume % trachybasalt.

TL comendite: rock composed of >60 volume % comendite and <40 volume % comenditic trachyte.

TL mixed rock: rock composed of two or more compositionally and texturally distinct components mingled down to a microscopic level. The overall composition is 60-40 volume % comenditic trachyte and 60-40 volume % comendite, with up to 2 volume % trachybasalt.

Trachytic texture: a sub-parallel arrangement of elongate feldspars in the groundmass of a holocrystalline or hypocrySTALLINE rock, usage of the term is not restricted to rocks of trachytic composition.

Trachytoid texture: the sub-parallel alignment of large feldspar phenocrysts that can be observed in hand specimen.

Welding: the term used to describe a range of processes by which hot, viscous particles adhere and deform. The term embraces the processes of coalescence, agglutination and sintering, which are part of a continuum.

CHAPTER 2

FIELD DATA

2.1 INTRODUCTION

This chapter presents data, obtained by logging and mapping at a scale of 1:5 000, describing (1) the regional and local variations of TL, (2) the proximal to distal lithofacies variations (3) the localised lithofacies variations and subfacies associations and (4) the deformation structures in TL.

The most continuous exposures of ignimbrite TL are in the western and southwestern sectors of the Gran Canaria (Fig. 2.1). Thirty vertical sections were studied and sampled, and over 100 logs described. Short horizontal sections were mapped out onto oblique photographs where the lithofacies associations are particularly complex. Rocks adjacent to these sections were mapped at a scale of 1:50 000, to determine the influence of palaeotopography on the distribution and deformation of TL. Where possible, described sections were selected in axial parts of palaeovalleys to avoid gaps in the sequence caused by units pinching out towards palaeovalley margins.

This chapter is divided into two sections. The first section describes the lithofacies and lithofacies associations, and the second analyses the regional and local variations in TL.

General terminology is given in Section 1.5. A discussion of the genetic implications of terminology pertaining to ignimbrite emplacement and depositional mechanisms is given in Section 7.4.

2.2 INTERNAL STRATIGRAPHY OF TL

Ignimbrite TL is a compound cooling unit consisting of two **spatially discrete but overlapping** flow units, TL1 and TL2 (Fig. 2.1). Where TL1 and TL2 overlap they are locally separated by a thin layer of fallout tuff. Further subdivision of TL1 and TL2 into multiple flow units is not readily apparent in the field and, because this involves interpretation, flow units are discussed after the descriptions have been presented objectively (Chapter 7, Section 7.4). TL1 is mainly vitroclastic in texture, TL2 is predominantly holocrystalline and displays features characteristic of lava flows (Section 2.5).

TL1 was deposited over an area of 106km², on the southern flanks of the shield volcano, whereas TL2 was deposited over a more restricted area, 51km², to the southwest. The type localities for TL1 and TL2 are respectively Montaña de las Carboneras and the west side of Bco. de Mogán, where several profiles are well exposed. Where TL2 overlies TL1 in the southwest the two units are separated by a thin impersistent fallout layer. TL1 is generally thinner than TL2. Its average thickness is 10.4m, but it is locally ponded up to 28m. TL2 averages 14m thick, but locally is 17m thick due to thrust-stacking and 26m thick due to ponding.

Both TL1 and TL2 have a broadly similar lithostratigraphy. The basal portion of both units is composed of TL comendite, the central portions are TL mixed rock and the upper part of each unit is TL trachyte (Fig. 2.2). This chemical stratification is best preserved in TL1 which exhibits a gradational change from TL comendite at the base, through TL mixed rock, to TL trachyte at the top (Fig. 2.3).

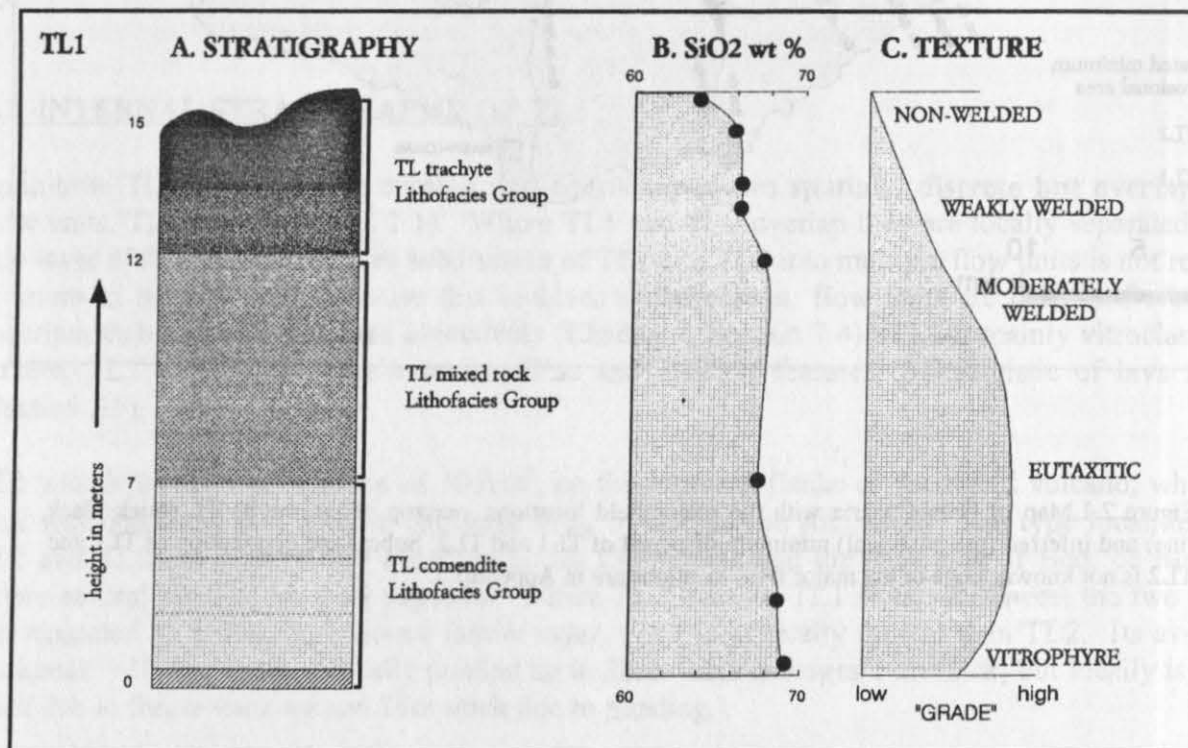
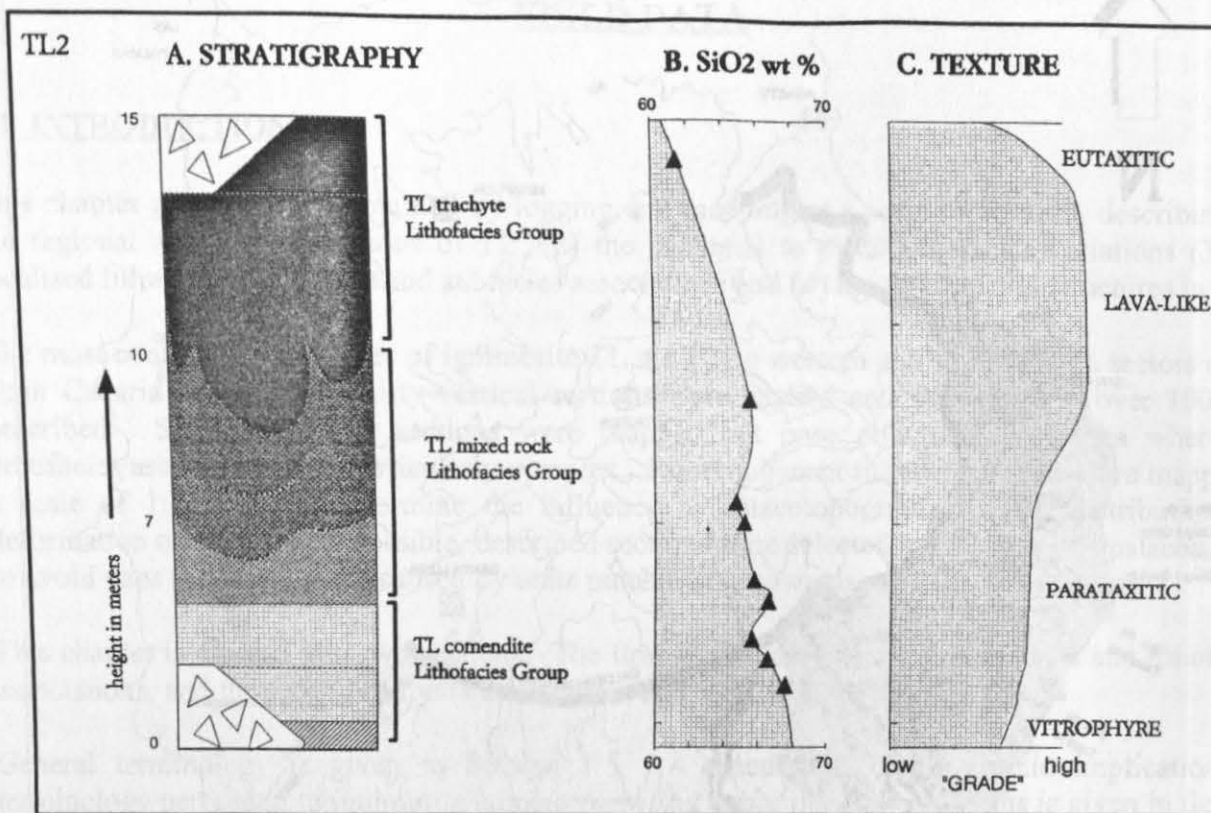


Figure 2.2. Simplified stratigraphy of TL1 (bottom) and TL2 (top) showing: (A) The Lithofacies Groups: TL comendite, TL mixed rock and TL trachyte, (B) variation in chemical composition and (C) textural variations.

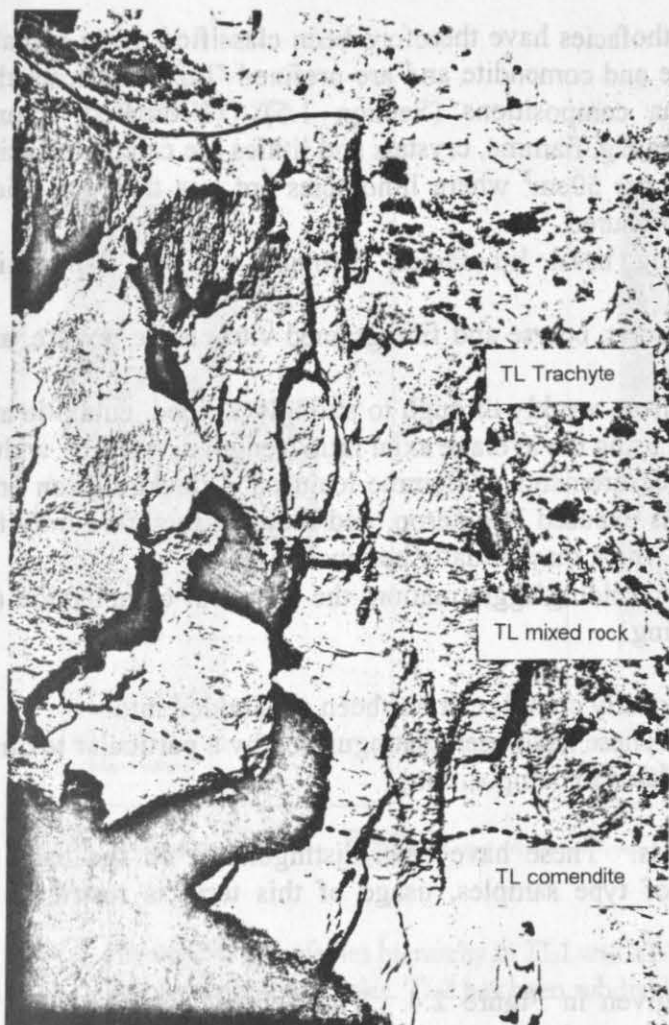


Figure 2.3. Lithostratigraphy of TL1 at the type locality, Montaña de las Carboneras (Exp. 60). The light coloured tuff at the base is composed of TL comendite lithofacies. The central portion is composed of TL mixed rock lithofacies and the upper dark coloured portion is composed of TL trachyte lithofacies. Boundaries between the lithofacies are gradational over several tens of centimetres. The largest fiamme size is in the central portion of the deposit and fiamme are imbricated throughout the unit. The top is less highly welded than the central and basal portions of the flow unit.

SECTION II

LITHOFACIES IN TL

2.3 DEFINITION AND CLASSIFICATION OF LITHOFACIES

TL1 and TL2 exhibit complex morphologies and relations and so each is described in terms of lithofacies and lithofacies associations. A simple flow unit model, where the stratigraphic relations of the deposits of successive pyroclastic flows are compared and contrasted is not applicable, because laterally persistent internal flow unit boundaries cannot be defined in the field.

The term 'lithofacies' is used to describe the characteristics of a local part of the tuff, its stratigraphic position, composition, colour, texture, fabrics and its relationships to adjacent lithofacies.

The following characteristics have been used to define lithofacies:

Composition: from TL comendite, through TL mixed rock to TL trachyte. Due to deposition from a particulate system, end-member magma compositions are NOT represented in TL lithofacies. Petrography (Chapter 4) and geochemistry (Chapter 5) shows that although TL lithofacies plot in the comendite and comenditic trachyte fields on standard classification diagrams (e.g. Figs. 5.1 and 5.2), bulk rock compositions result from varying mixtures of **comendite** and **comenditic trachyte**,

with rare fragments of **trachybasalt**. TL lithofacies have therefore been classified using visually estimated percentages of comenditic trachyte and comendite and are prefixed 'TL' to indicate that the compositions do not represent magma compositions (Section 1.5). Estimated volume percentages for a particular particle population e.g. fiamme, crystals and lithics are calculated using the number and size of particles per m², or per 50cm² where lithofacies are less than 1m thick. Quantitative volume percentages cannot be measured.

Stratigraphic position: from 'B' indicating basal lithofacies, through numbers 1-6 which correspond to the compositional layering.

Texture: including agglutinate beds and breccias, coarse and fine grained vitroclastic texture, and holocrystalline lava-like texture. The

Fabric: including the intensity of welding, from weakly through to strongly welded, eutaxitic and parataxitic. Intensity of welding is estimated using the average axial ratio (length divided by width) of the fiamme population. Note that field measurements of fiamme length and thickness can only be made on the proportion of the clast that is exposed at outcrop, and they are therefore only the **apparent** maximum dimensions of the clast, which may actually be much larger.

Colour: which varies according to degree of welding/agglutination, the chemical composition (of matrix and clasts), and the degree of weathering.

Where a lithofacies is texturally or compositionally complex, it has been subdivided into:

Subfacies: which occur within a lithofacies. These have been distinguished by a particular textural characteristic or diagnostic colour (usually related to composition).

Microfacies: which occur within a subfacies. These have been distinguished on the basis of composition determined by XRF analysis of type samples, usage of this term is restricted to lava-like, marble mingled rocks.

The lithofacies and subfacies in TL1 are given in Figure 2.4. The nomenclature and list of abbreviations for lithofacies and subfacies names is given on Table 2.1, adjoining Figure 2.4. Microfacies are detailed in the text.

Exceptions to the standard nomenclature are as follows:

1. Basal lithofacies: are prefixed Basal for simplicity and are not allocated a temporal stratigraphic character. Basal Vitrophyres; are not allocated a compositional character since glass compositions could not be identified in the field, likewise, Basal Autobreccia; as this is composed of clasts of diverse composition.
2. The 'Big globule lithofacies' is named separately (B.G.I.Z) since it forms an intrusive zone and has a transgressive relationship to the surrounding lithofacies.
3. Rheomorphically displaced lithofacies e.g. C0b - comendite upper autobreccia (TL2) are not allocated a temporal stratigraphic character as their original stratigraphic position cannot be accurately determined.

2.3.1 Lithofacies Groups

At the simplest level, flow units TL1 and TL2 have been subdivided by their chemical composition, into three lithofacies groups.

TL Comendite Lithofacies Group

Lithofacies belonging to this group are prefixed 'C' for TL comendite, and comprise the basal portion of TL1 and TL2 (shown in pale grey on Fig. 2.4). This lithofacies group contains the following lithofacies:

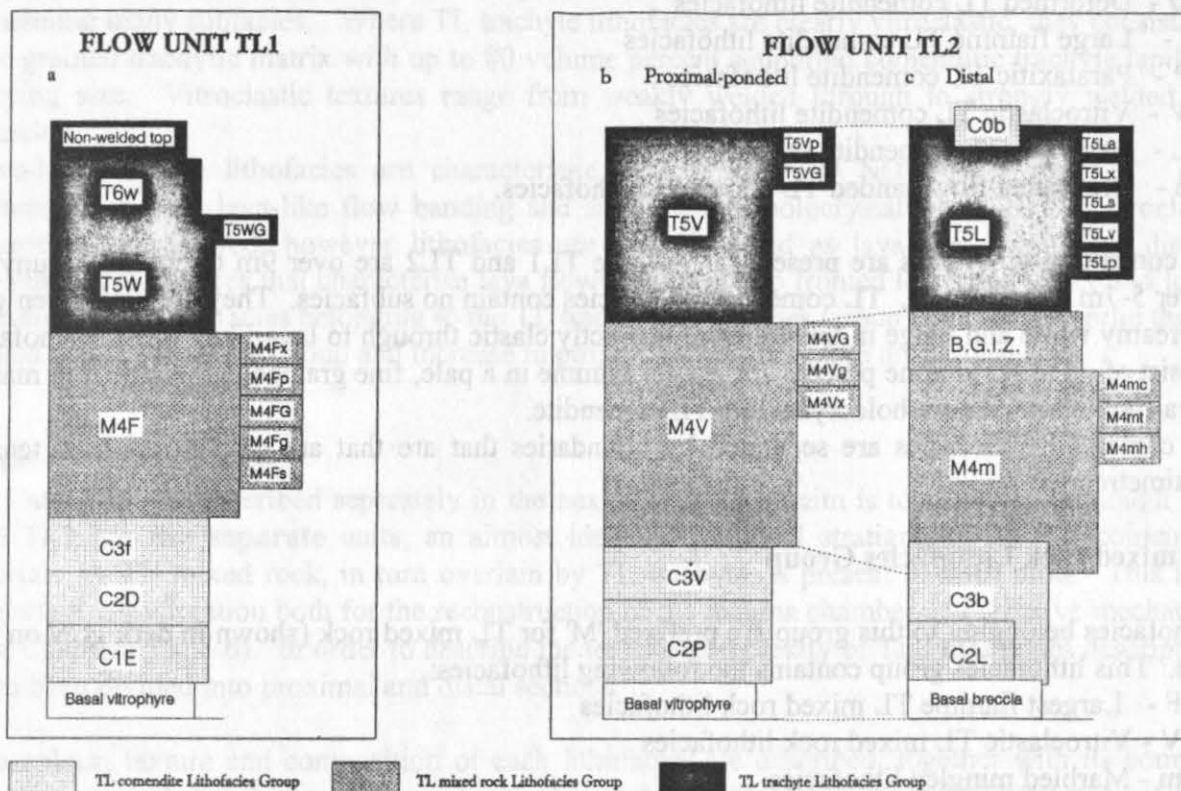


Figure 2.4. Lithofacies hierarchy in TL1 and TL2, including Lithofacies Groups, lithofacies and subsfacies. TL2 has been subdivided into proximal and distal regions.

Nomenclature				
Lithofacies Group	Lithofacies		Subfacies	
Compositional character	Temporal character	Major textural character	Minor textural character	
TL1	C, M, T	1, 2, 3, 4, 5, 6	E, D, F, f, W, w	G, g, s, p, x
TL2	C, M, T	2, 3, 4, 5, 0	V, L, b, m, P	h, c, t, a, v, G, g, s, p, x
Abbreviations				
C = TL comendite M = TL mixed rock T = TL trachyte	0 = original stratigraphic position not known	E = Eutaxitic D = Deformed F = Fiamme (largest) f = fiamme (large) W = Welded, moderately w = weakly welded V = Vitroclastic L = Lava-like b = breccia m = marble mingled P = Parataxitic B.G.I.Z. = Big Blobule lithofacies	G = Grain size, coarse g = grain size, Fine x = transitional s = small fiamme p = purple h = half and half mixture, peppered c = comendite dominated t = trachyte dominated a = agglutinate (clastic) v = vesicular	

Table 2.1. Nomenclature for the classification of lithofacies and subsfacies in TL1 and TL2.

- C1E - Eutaxitic TL comendite lithofacies
- C2D - Deformed TL comendite lithofacies
- C3f - Large fiamme TL comendite lithofacies
- C2P - Parataxitic TL comendite lithofacies
- C3V - Vitroclastic TL comendite lithofacies
- C2L - Lava-like TL comendite lithofacies
- C3b - Brecciated flow banded TL comendite lithofacies.

TL comendite lithofacies are present only where TL1 and TL2 are over 9m thick and occupy the lower 5-7m of both units. TL comendite lithofacies contain no subfacies. They are pale green-grey to creamy white and range in texture from distinctly clastic through to lava-like. Clastic lithofacies consist of up to 80 volume percent comendite fiamme in a pale, fine grained comendite rich matrix. Lava-like lithofacies are holocrystalline TL comendite.

TL comendite lithofacies are separated by boundaries that are that are gradational over tens of centimetres.

TL mixed rock Lithofacies Group

Lithofacies belonging to this group are prefixed 'M' for TL mixed rock (shown in dark grey on Fig. 2.4). This lithofacies group contains the following lithofacies:

- M4F - Largest fiamme TL mixed rock lithofacies
- M4V - Vitroclastic TL mixed rock lithofacies
- M4m - Marbled mingled lithofacies
- B.G.I.Z - Big globule lithofacies (intrusive zone)

Where TL1 is thicker than 10m TL mixed rock lithofacies comprise up to 10m of the central portion of the unit. In TL2 and where TL1 is less than ca. 10m thick they commonly directly overlie the basal vitrophyre or a basal autobreccia and comprise 7-12m of the lower portion of the deposit.

Lithofacies belonging to the TL mixed rock Lithofacies Group are highly complex, each containing several subfacies defined by the degree of welding and the estimated volume percent of comendite to comenditic trachyte in both matrix and fiamme. The lithofacies range from weakly welded through highly rheomorphic, to lava-like and holocrystalline and have variable proportions of comendite and comenditic trachyte.

TL trachyte Lithofacies Group

Lithofacies belonging to this lithofacies group are prefixed 'T' for TL trachyte (shown in black on Fig. 2.4). This lithofacies group contains the following lithofacies:

- T5W - Moderately welded TL trachyte lithofacies
- T6w - Weakly welded TL trachyte lithofacies
- T5V - Vitroclastic TL trachyte lithofacies
- T5L - Lava-like TL trachyte lithofacies

Lithofacies belonging to the TL trachyte Lithofacies Group occur in both TL1 and TL2 at all localities, even where TL1 is less than 1m thick. Where TL1 is greater than 10m thick they comprise up to the top 6m of the unit. In TL2 at proximal localities this thickness increases to up to 8m. At distal localities of TL2, for example, the distal margin, TL trachyte lithofacies can comprise the entire thickness of the deposit (i.e. from 7 to 17m thick). The vertical and lateral contacts between lithofacies are generally gradational over tens of centimetres. TL trachyte lithofacies

range in texture from vitroclastic to holocrystalline and lava-like and are extremely complex, each containing many subfacies. Where TL trachyte lithofacies are clearly vitroclastic, they consist of a fine grained trachytic matrix with up to 80 volume percent supported comenditic trachyte lapilli of varying size. Vitroclastic textures range from weakly welded through to strongly welded and eutaxitic.

Lava-like trachyte lithofacies are characteristic of TL2 and DO NOT occur in TL1. They commonly display lava-like flow banding and are generally holocrystalline. Locally vitroclastic textures are preserved, however lithofacies are still classified as lava-like where they display medium scale features that characterise lava flows such as steep fronted lobes and upper and lower autobreccias. Lithofacies belonging to the TL trachyte Lithofacies Group commonly overlie the TL mixed rock Lithofacies Group and increase in proportion towards more distal locations.

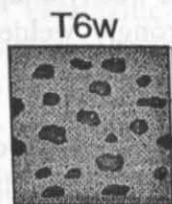
Note:

TL1 and TL2 are described separately in the next section. The aim is to show that although TL1 and TL2 are two **separate** units, an almost identical chemical stratigraphy i.e. TL comendite, overlain by TL mixed rock, in turn overlain by TL trachyte, is present in **both** units. This is an important consideration both for the reconstruction of the magma chamber and eruptive mechanism (see Chapters 5 and 6). In order to describe the textural complexity of TL2 lithofacies descriptions have been divided into proximal and distal sections.

The colour, texture and composition of each lithofacies are described, together with its common associations and distribution. The petrography of the lithofacies is given in Chapter 4. A type locality, a type sample and the maximum thickness for each lithofacies are given in Table 1.1 in Appendix 1. Type localities are shown on Figure 2.1. and logs of type localities are in Appendix 1. Box diagrams of each lithofacies, its associated subfacies, and key diagnostic features are shown in Figure 2.5.

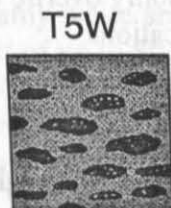
LITHOFACIES

SUBFACIES



T6W
Weakly welded TL trachyte lithofacies

Subrounded trachytic lapilli
Orange trachytic matrix



T5W
Moderately welded TL trachyte lithofacies

Flattened vesicular trachytic fiamme
Red-brown trachytic matrix



T5WG
Coarse grained TL trachyte subfacies

Large, blocky scoriaceous
comenditic trachyte fiamme,
fractured and broken



M4F
L argest fiamme TL mixed rock lithofacies

Flattened vesicular comenditic
trachyte fiamme
Red-brown trachytic matrix



M4FG
Coarse grained porous subfacies

Subrounded, weakly flattened comenditic
trachyte lapilli
Porous, buff mixed rock matrix



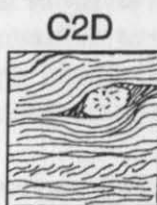
C3f
Large fiamme TL comendite lithofacies

Highly attenuated comendite fiamme, rare
comenditic trachyte fiamme
Pale green-grey comenditic matrix



M4Fg
Fine grained porous subfacies

Rare small comenditic trachyte fiamme,
amphibole megacrysts, feldspar phenocrysts
Porous mixed rock matrix, faintly stratified



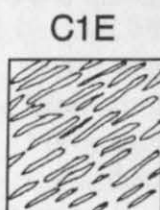
C2D
Deformed TL comendite lithofacies

Folded paratextitic texture, shear cavities and
shear zones



M4Fp
Fine grained purple matrix subfacies

Comenditic trachyte fiamme, and comendite
blebs in dark purple matrix



C1E
Eutaxitic TL comendite lithofacies

Lineated, imbricated, rodded comendite
fiamme



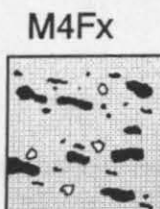
M4Fs
Small fiamme mixed rock subfacies

Small comenditic trachyte, intermediate and
comendite fiamme
Fine grained mixed rock matrix



Basal vitrophyre

Large glassy fiamme, slightly divitrified pale
brown matrix
Lithic rich



M4Fx
Transitional to lava-like subfacies

Small subrounded comenditic trachyte lapilli,
rare comendite blebs
Dense, blue-grey crystalline matrix

Figure 2.5. For figure caption please see next page.

TL2 - Proximal Region

LITHOFACIES

SUBFACIES




Fig 2.5 Summary of the lithofacies and subfacies in TL1 and TL2 (including TL2 proximal or ponded, and distal lithofacies groupings). Box diagrams depict the major textural and compositional characteristics, which are briefly described to the right of each diagram. Lithofacies and subfacies are shown stratigraphically from the base of each unit upwards.

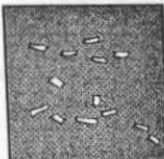
LITHOFACIES

SUBFACIES


C0b
Comenditic top breccia
 White heterolithologic clast supported breccia
 Fine grained friable matrix




T5L
Lava-like TL trachyte lithofacies
 Dense holocrystalline TL trachyte
 Feldspar phenocrysts occasionally aligned forming trachytoid texture




B.G.I.Z.
Big Globule lithofacies
 Intrusive zone - fine grained comendite matrix with pillows and micropillows of comenditic trachyte




M4m
Marble mingled lithofacies
 Lava-like mixed rock composed of an estimated 50:50 volume % comendite and comenditic trachyte. Incompletely mingled




C3B
Flow banded TL comendite lithofacies
 Holocrystalline to faintly vitroclastic TL comendite, forming breccia and shear planes




C2L
Lava-like TL comendite lithofacies
 Dense crystalline TL comendite
 Rare trachytoid texture




Basal Breccia
 Irregularly distributed heterolithologic clast supported breccia
 Numerous subangular clasts of overlying TL comendite lithofacies




T5La
Lava-like agglutinate subfacies
 Agglutinated comenditic trachyte spatter lumps
 Holocrystalline trachytic matrix




T5Lx
Transitional to agglutinate subfacies
 Rare outlines of agglutinated comenditic trachyte clasts locally flow foliated



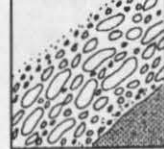
T5Ls
Highly welded subfacies
 Dense predominantly holocrystalline trachyte with rare small subparallel aligned comenditic trachyte fiamme




T5Lp
Purple lava-like subfacies
 Holocrystalline trachyte
 Porous with numerous vesicles




T5Lv
Lava-like vesicular subfacies
 Usually TL comendite with up to 60 volume % vesicles



M4mc
Marble mingled TL comendite subfacies
 Lava-like, dominated by incompletely mingled TL comendite microfacies



M4mt
Marble mingled TL trachyte subfacies
 Lava-like, dominated by incompletely mingled TL trachyte microfacies



M4mh
Peppered mixed subfacies
 Coarse 'salt and pepper' mixture of comendite and comenditic trachyte with feldspar phenocrysts and trachybasalt globules




Figure 2.5. continued.

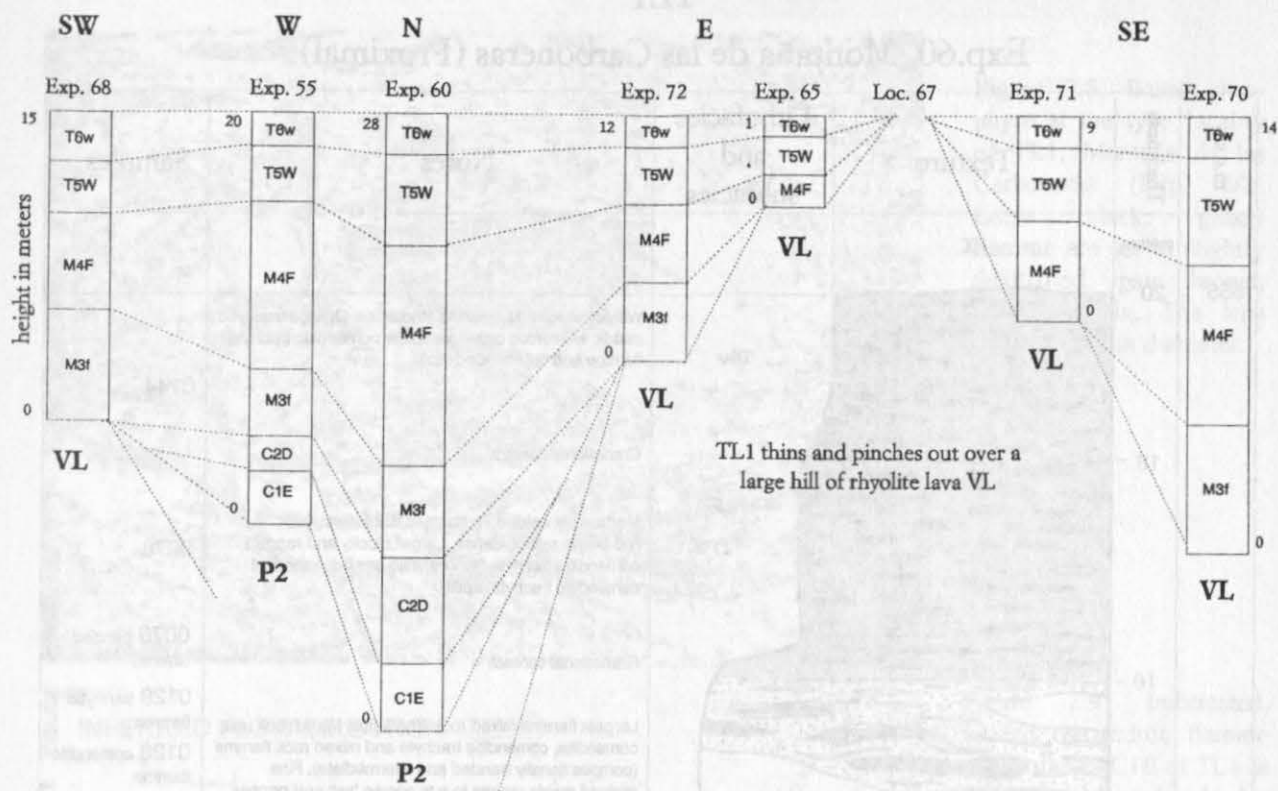


Figure 2.6. Stratigraphic profiles showing the lithofacies and their associations at the type locality for TL1, Montaña de las Carboneras. Contacts between adjacent lithofacies are gradational but are shown as solid lines for clarity and to avoid confusion with underlying units of the Lower Mogán Formation. Refer to Fig. 2.5 for details of the lithofacies and subfacies.

2.4 LITHOFACIES IN UNIT TL1

The lithofacies and subfacies in TL1 are summarised in Figure 2.5 (a). Lithofacies are described stratigraphically from the base of TL1 upwards. TL1 is vitroclastic throughout and vertical variations between lithofacies are gradational rather than sharp. Lithofacies associations at the type locality for TL1, Montaña de las Carboneras, are shown in Figure 2.6. Figure 2.7 is a sample log from this locality.

Basal Vitrophyre

Basal vitrophyre of TL1 is commonly <15cm in thick, but is up to 30cm thick where TL1 is thickest. For example, at the type locality, TL1 is 20m thick and the basal vitrophyre is 30cm thick. The basal vitrophyre is particulate and large black fiamme (<36cm in length) are clearly visible where the surrounding matrix has devitrified slightly (Fig. 2.8). In thin section (Chapter 4), flattened glassy shards can be identified in the matrix, defining a strongly welded texture (Ross and Smith, 1961). Both shards and fiamme are comenditic in composition. Fiamme up to 36cm in length occur in the vitrophyre, indicating that from the beginning of the eruption, the eruption rate was sufficiently high to produce large clasts.

The basal vitrophyre of TL1 contains many lithics (<3cm in diameter, 18 per 30cm², ca. 12 volume percent), ranging from angular pick-ups (Section 1.5) of underlying layers, P2, VI, and VL to subangular accessory lithics of trachyte, syenite and basalt.

Exp.60, Montaña de las Carboneras (Proximal)

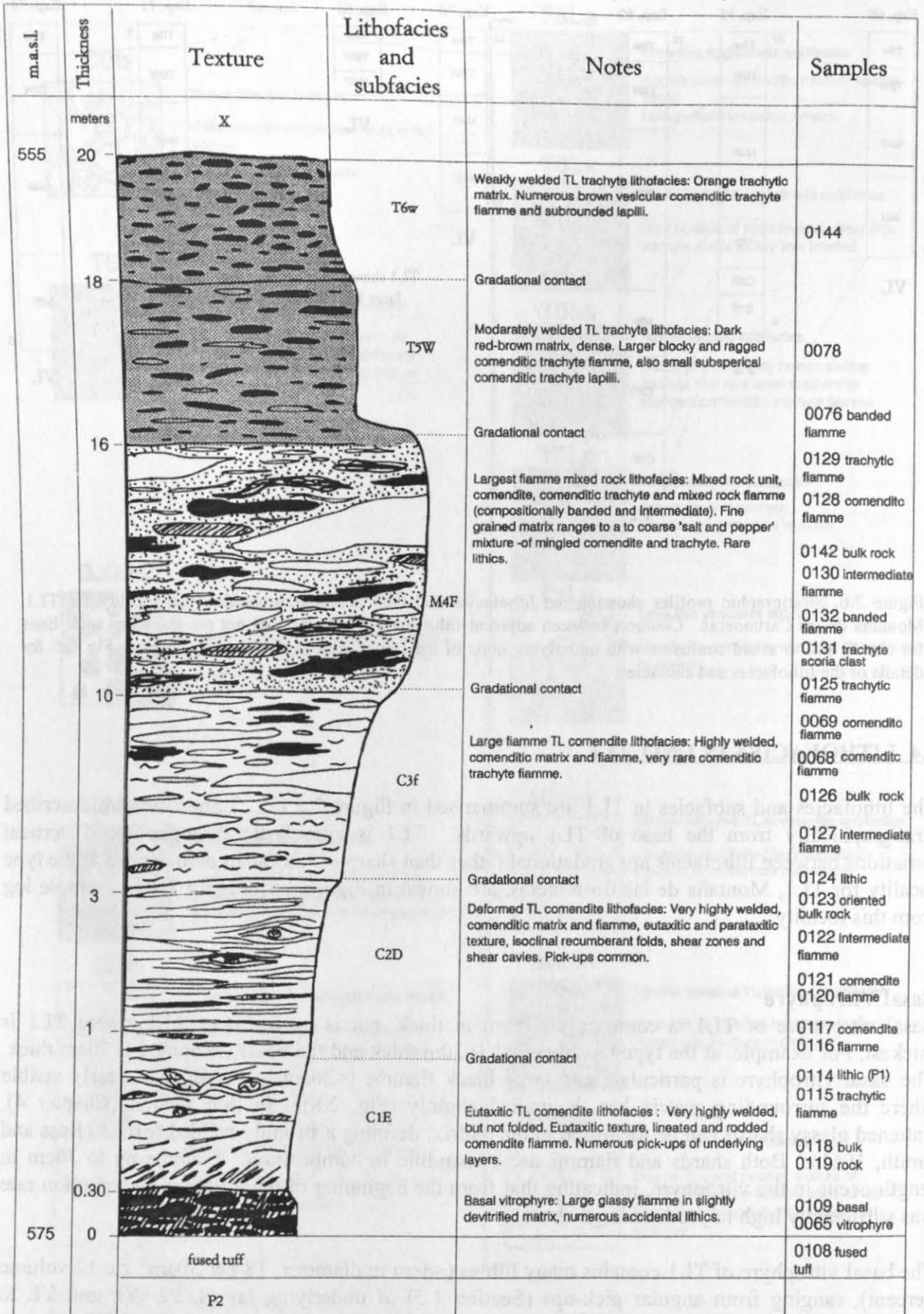


Figure 2.7. Log showing the lithofacies associations at the type locality of TL1, Montaña de las Carboneras (Exp. 60). XRF analyses of samples are in Appendix II.



Figure 2.8. Basal vitrophyre at the type locality of TL1, Montaña de las Carboneras (Exp. 60). Large black, glassy fiamme are set in slightly devitrified, pale brown, porous matrix. The lens cap is 5.5cm in diameter.

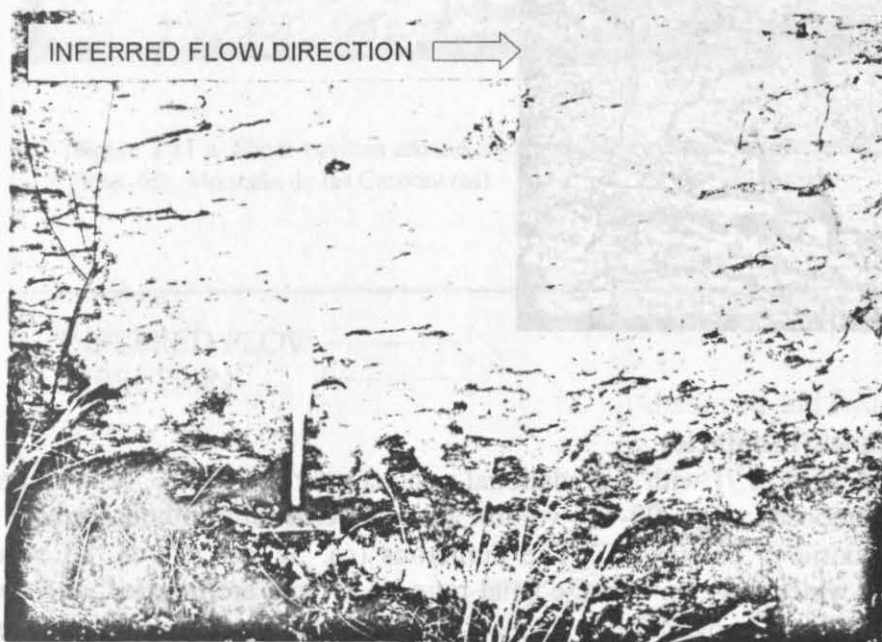


Figure 2.9. Imbricated, rodded comenditic fiamme in lithofacies C1E of TL1 at Exp. 60, Montaña de las Carboneras. Note the horizontal base of TL1 behind the hammer head. The hammer is 30cm long.

2.4.1 TL comendite Lithofacies Group

C1E - Eutaxitic TL comendite lithofacies

This lithofacies overlies the vitrophyre. It is cream to pale grey, poorly sorted and is composed of ca. 90-100 volume percent comendite in both clasts and matrix, the remainder being comenditic trachyte fiamme and ash, or a hybrid mixture of comendite and comenditic trachyte, forming intermediate fiamme and ash. The lithofacies is clearly vitroclastic, and the highly welded eutaxitic texture is defined by large numbers of highly flattened comenditic fiamme (<48 per m², ca 20 volume percent, average axial ratio 11:1cm; maximum size 18cm long by 2cm thick). Comenditic trachyte fiamme are rare (0 to 4 per m², <1 volume percent). Fiamme are often imbricated or rodded and define a lination (Fig. 2.9). Numerous lithics (18 per m², ca. 4 volume percent, maximum size: 8cm in diameter), have been incorporated from underlying units P2, VI and VL. They are well rounded and show rotation due to rheomorphic flow. Adjacent matrix is chilled indicating that they were cold, and were not significantly heated up during transport in TL (Fig. 2.10).



Figure 2.10. Large pick-up of rhyolite lava VL, in lithofacies C1E of TL1. The lithic is 'wrapped' by matrix and fiamme and rotated over in the flow direction (right to left in photograph), the sense of shear is sinistral. The pencil is 16cm long (Exp. 55, Montaña de las Carboneras).

C2D - Deformed TL comendite lithofacies

This lithofacies overlies C1E (Fig. 2.7) with a gradational contact over ca. 15cm. It is cream to pale grey, vitroclastic and composed of ca. 90-100 volume percent comendite in both fiamme and matrix. The texture is eutaxitic to parataxitic. The numerous (ca. 52 per m², ca. 83 volume percent) comenditic fiamme, which have an average axial ratio of 13:1cm are lineated, and define discontinuous flow banding which is often flow folded. No comenditic trachyte fiamme were found in this lithofacies. Lithics are less common than in C1E, 6 lithics per m² (ca. 1.5 volume percent), maximum lithic size is 5cm in diameter. The maximum fiamme size is 108cm in length and 7cm thick.

C2D is characterised by rheomorphic deformation structures (Fig. 2.11a and b). It contains large numbers of open 'shear cavities' (Section 1.5) which resulted from anisotropic deformation around lithic clasts during non-particulate flow. The welded matrix has pulled apart around larger lithics producing open cavities. Locally three clearly defined 'shear zones' (Section 1.5) occur towards the base of this lithofacies. These 4cm thick zones are vesicular and are crossed by open sigmoidal fractures (Fig. 2.12).

C3f - Large fiamme TL comendite lithofacies

This pale grey-green lithofacies commonly occurs overlying C2D (Fig. 2.6, Exp. 55). Where TL1 is less than 12m thick it directly overlies the basal vitrophyre (Fig. 2.6, Exp. 68). It is vitroclastic and is characterised by large, prolate, white comenditic fiamme (52 per m², ca. 40 volume percent). Black, comenditic trachyte fiamme are less common (<4 per m², ca. 3 volume percent). Rarely,

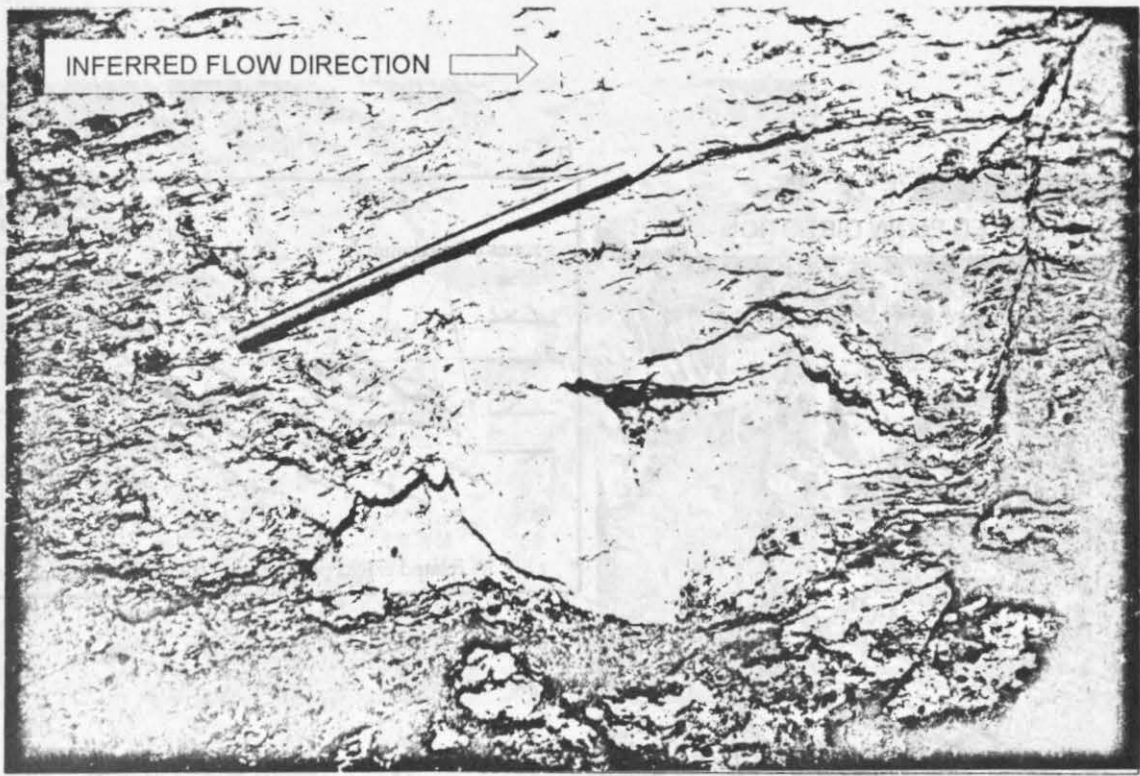


Figure 2.11 a. Shear cavities around a rotated lithic clast in lithofacies C2D. The pencil is 16cm long (Exp. 60, Montaña de las Carboneras).

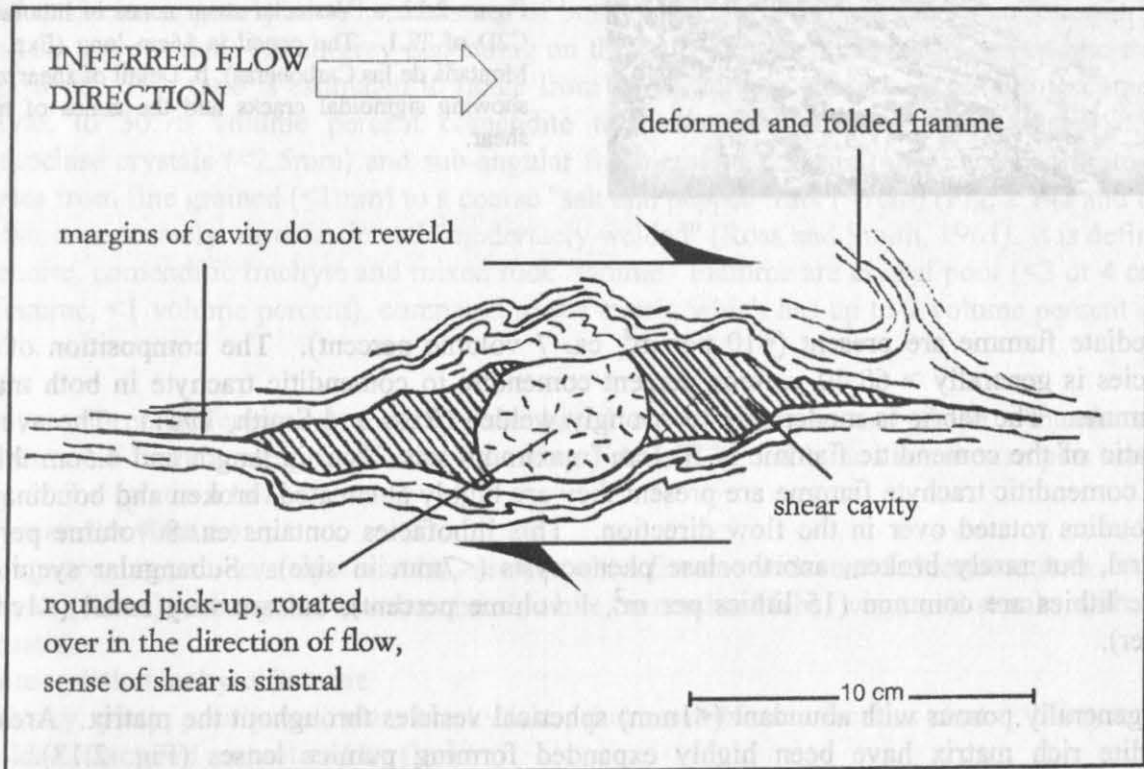


Figure 2.11 b. Sketch showing a vertical section through a rotated lithic clast (pick-up of underlying ignimbrite P2). The lithic clast is flanked by shear cavities, which are interpreted to have formed during late stage rheomorphism.

a



b

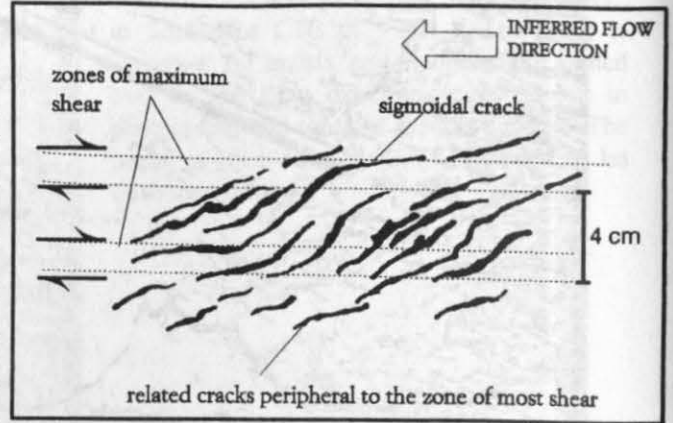


Figure 2.12. a. Vesicular shear zones in lithofacies C2D of TL1. The pencil is 16cm long (Exp. 55, Montaña de las Carboneras). b. Detail of shear zone showing sigmoidal cracks and the zones of most shear.

intermediate fiamme are present (<10 per m^2 , ca. 7 volume percent). The composition of this lithofacies is generally $> 60:40$ volume percent comendite to comenditic trachyte in both matrix and fiamme. The fabric is moderately to strongly welded (Ross and Smith, 1961). The average axial ratio of the comenditic fiamme is 10:1cm (maximum size 37cm in length and 4.5cm thick). Where comenditic trachyte fiamme are present they are highly attenuated, broken and boudinaged, with boudins rotated over in the flow direction. This lithofacies contains ca. 8 volume percent subhedral, but rarely broken, anorthoclase phenocrysts (<7 mm in size). Subangular syenite or trachyte lithics are common (15 lithics per m^2 , 1 volume percent), but are very small (<1 cm in diameter).

C3f is generally porous with abundant (<1 mm) spherical vesicles throughout the matrix. Areas of comendite rich matrix have been highly expanded forming pumice lenses (Fig. 2.13). The spherical shape of the vesicles suggests that they were formed during late-stage exsolution of volatiles, after welding compaction and rheomorphism had ceased. The areas of pumiceous matrix may be due to the post-welding-vesiculation of comendite as a result of heating during mingling with comenditic trachyte (discussed in Chapter 7, Section 7.9).



Figure 2.13. Vesicular lense of comendite in lithofacies C3f. This was probably not an original pumice clast, rather an area of comenditic matrix which underwent intense post depositional vesiculation due to reheating on initial contact with comenditic trachyte. Note the brown, highly flattened comenditic trachyte fiamme in the lower half of the picture (Exp. 60, Montaña de las Carboneras).

2.4.2 TL mixed rock Lithofacies Group

M4f - Largest fiamme TL mixed rock lithofacies

This lithofacies generally overlies C2D or C3f (Fig. 2.6), but locally where TL1 is thin it lies directly over the basal vitrophyre, for example Exp. 76, Bco. de Mogán (Appendix I, vertical profile 76).

M4F lithofacies is poorly sorted, consisting of both matrix and fiamme. The matrix colour varies from pale grey to dark bluish-grey depending on the ratio of comendite ash to comenditic trachyte ash present. This ratio is estimated to range from 60:40 volume percent comendite to comenditic trachyte, to 30:70 volume percent comendite to comenditic trachyte. The matrix contains anorthoclase crystals (<2.5mm) and sub-angular fragments of comendite and comenditic trachyte. It varies from fine grained (<1mm) to a coarse "salt and pepper" mix (<1cm) (Fig. 2.14a and b).

The fabric is coarsely vitroclastic and "moderately welded" (Ross and Smith, 1961). It is defined by comendite, comenditic trachyte and mixed rock fiamme. Fiamme are crystal poor (<3 or 4 crystals per fiamme, <1 volume percent), compared to the matrix which has up to 7 volume percent crystal content.

There are three different types of fiamme based on composition and shape. Abundance and dimensions of fiamme are given in the following Tables 2.2a and b, and some examples are given in Figure 3.2 (plates a to f) :

A. Comendite fiamme

- (1) Large, prolate, moderately vesicular, smooth white fiamme with rounded terminations.
- (2) Small (<3cm), subangular to subrounded, white comendite blebs, wisps and streaks with frayed terminations.

B. Comenditic trachyte fiamme

- (1) Blocky, platy, poorly vesicular, black clasts, that resemble scoriaceous clasts. Many of these are folded, fractured and rotated by flow.
- (2) Small, dark brown, highly flattened fiamme containing flattened vesicles, some of which form a discontinuous flow banding around larger clasts.

C. Mixed Rock fiamme

- (1) *Intermediate fiamme*: uniform creamy-brown, highly vesicular fiamme. These are prolate and smooth with rounded terminations.

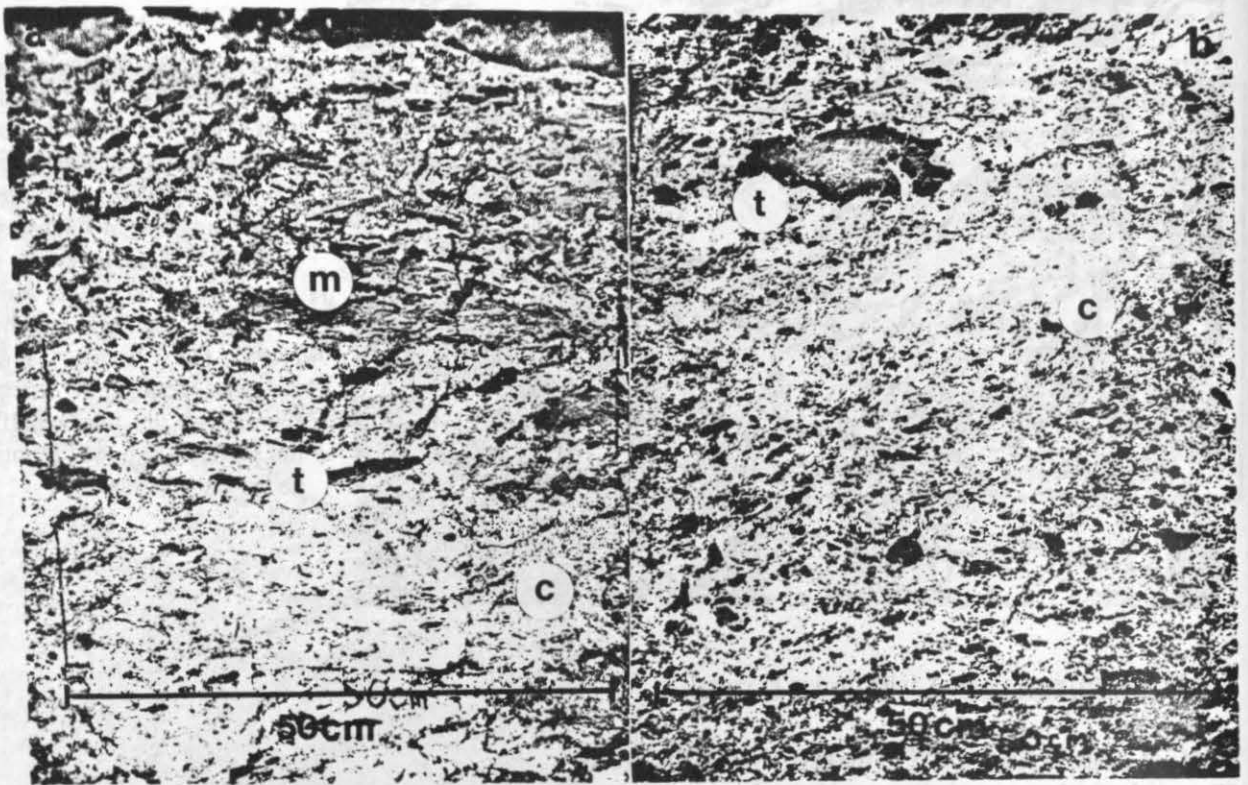


Figure 2.14. Textural variations in lithofacies M4F of TL1. (A) Large comendite (c), comenditic trachyte (t) and mixed fiamme (m) set in fine grained matrix. (B) Coarse grained 'salt and pepper' matrix, with rare large fiamme (Exp. 60, Montaña de las Carboneras).

(2) *Compositionally banded fiamme*: subangular to subrounded, slightly prolate fiamme. These are composed of interlayered bands of comenditic trachyte and comendite of varying vesicularity.

M4F is often finer grained towards the base especially where it is thin and directly overlies the vitrophyre. Where stratigraphic sections are complete it fines upwards and this corresponds to a change in the size, number and type of fiamme (Chapter 3, Section 3.4). With height the abundance of comenditic fiamme decreases, the abundance of trachyte fiamme increases and the average grain size decreases (see Tables 2.2a and b).

Table 2.2a

Top 2 m of layer 4	Number per m ²	Estimated Volume Percent	Axial ratio	Maximum apparent dimensions
Comendite fiamme	22	13	5:1	17:2.5
Comenditic trachyte fiamme	21	10	4:1	11:1.7
Intermediate fiamme	6	<1	2.5:1	5:1.3
Compositionally banded fiamme	7	1	3:1	11:1.2

Table 2.2b

Basal 2 m of unit 4	Number per m ²	Estimated Volume Percent	Axial ratio	Maximum apparent dimensions
Comendite fiamme	57	34	4.6 : 1	70:13
Comenditic trachyte fiamme	6	4	8 : 1	32:2.5
Mixed fiamme	15	8	4 : 1	16:3.5

M4F lithofacies is complex and shows local, vertical and lateral gradations from coarser to finer grained subfacies (see next section).

SUBFACIES OF M4F :

M4FG - Coarse grained porous subfacies

This subfacies occurs as discontinuous pods and lenses (<2m in width and 4m in length) within lithofacies M4F, and in association with subfacies M4Fg and M4Fx (see below). Contacts with the surrounding facies vary from sharp to wispy with streaky boundaries, locally contacts are gradational.

Lithofacies M4FG is weakly welded and porous. It is poorly sorted with a fine grained matrix and clasts. The matrix is pale creamy-brown and compositionally estimated as 60:40 volume percent comendite to comenditic trachyte. Clasts are small, black, weakly flattened comenditic trachyte fiamme (ca. 22 volume percent, average axial ratio 3:1cm). These are predominantly platy and blocky, <5 volume percent are ragged with frayed terminations. Comenditic fiamme and lithics are rare (ca. 1 per m², <0.5 volume percent). This subfacies is occasionally brecciated and weathers back in a rubbly manner.

M4Fg - Fine grained porous subfacies

Subfacies M4Fg occurs in association with M4FG as discontinuous lenses (up to 1m wide and <8m in length) within the upper 1-2m of lithofacies M4F. It has a gradational planar upper contact, and a gradational, undulating lower contact with M4F (Fig. 2.15). Locally it forms discrete lenses and pockets of internal autobreccia, composed of subangular clasts (Section 7.9.2).

This subfacies is fine grained (<2mm), porous and "weakly welded" (Ross and Smith, 1961), weathering to a granular surface. It is distinguished by the absence of large fiamme. Rarely it contains small, wispy comenditic trachyte fiamme (ca. <12 per m², <1 volume percent, maximum size 2:0.5cm).

M4Fg is characterised by numerous hornblende megacrysts (up to 3mm in diameter) and euhedral, feldspar phenocrysts (ca. 5 volume percent, maximum size 3mm) which give the rock a speckled appearance.

It is faintly stratified with diffuse layers of pale, yellow-brown comendite rich matrix alternating with orange -brown trachytic rich matrix (Fig. 2.15).

M4Fp - Fine grained purple subfacies

M4Fp occurs as laterally discontinuous layers. It is transitional with subfacies M4Fg and with subfacies M4Fx (next section).

SUBFACIES
M4Fg

LITHOFACIES
M4F

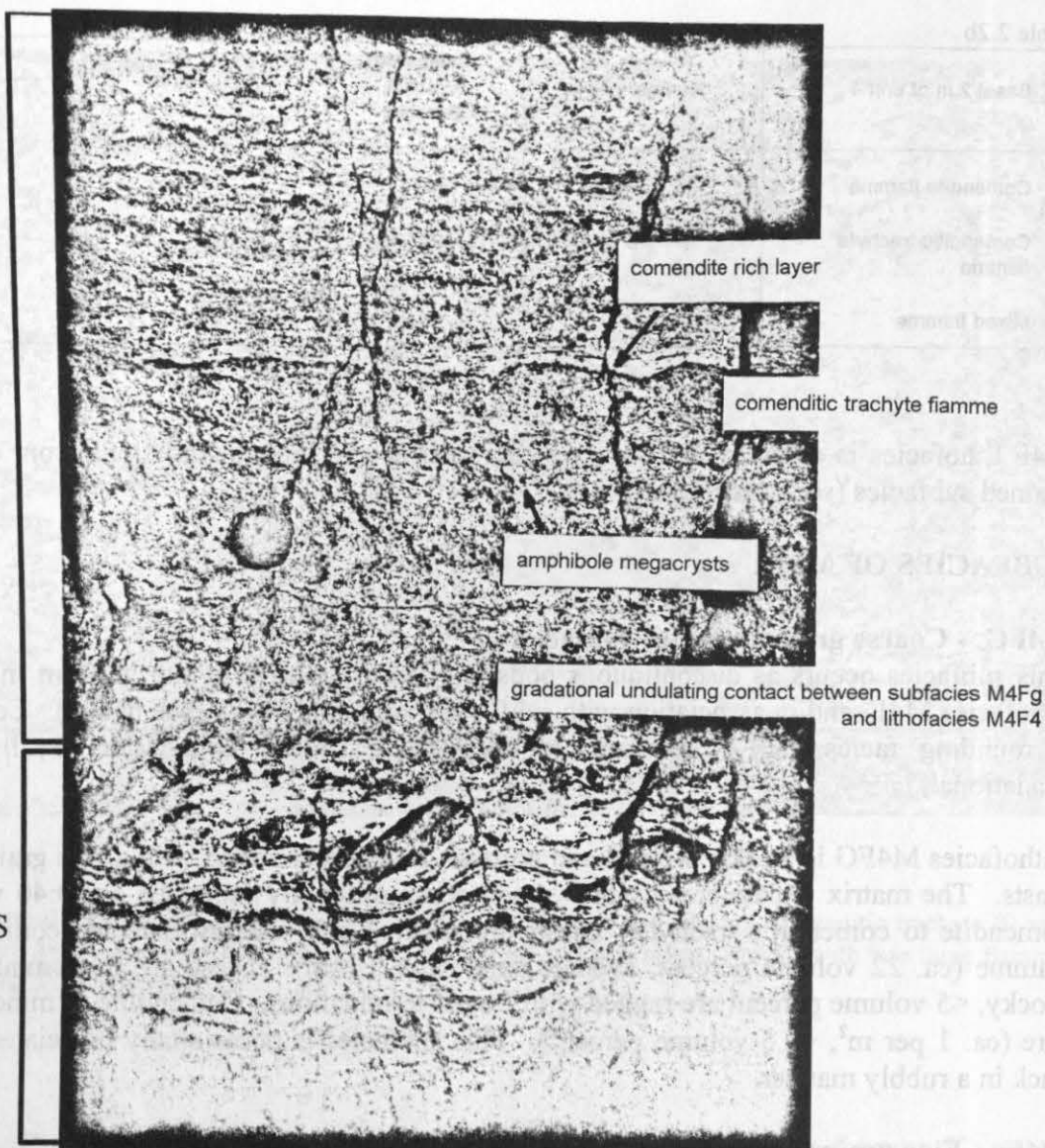


Figure 2.15. Fine grained subfacies M4Fg. Note the gradational, undulating contact with lithofacies M4F, and the localised layering within M4Fg. These layers are not laterally persistent (when traced away from the photograph they die out within 5m), and thus cannot represent flow unit boundaries. The lens cap is 5.5cm in diameter (Exp. 76, Bco. de Mogán).

It is characteristically densely welded and dark purple-brown (Fig. 2.16). It is poorly sorted consisting of fine grained matrix and clasts. The fine grained matrix is estimated to contain 60:40 volume percent comenditic trachyte to comendite, which gives it a distinctive purplish colour when weathered. Clasts are comenditic trachyte, and range from subvitric, angular, fragments, <3mm in diameter, to weakly flattened, highly vesicular fiamme (average axial ratio 4:1, average size 4.7:2.2cm).

This subfacies also contains broken, subhedral anorthoclase phenocrysts (<2mm). Rare, small lithic clasts are subangular (<0.5 volume percent, <1cm in diameter).

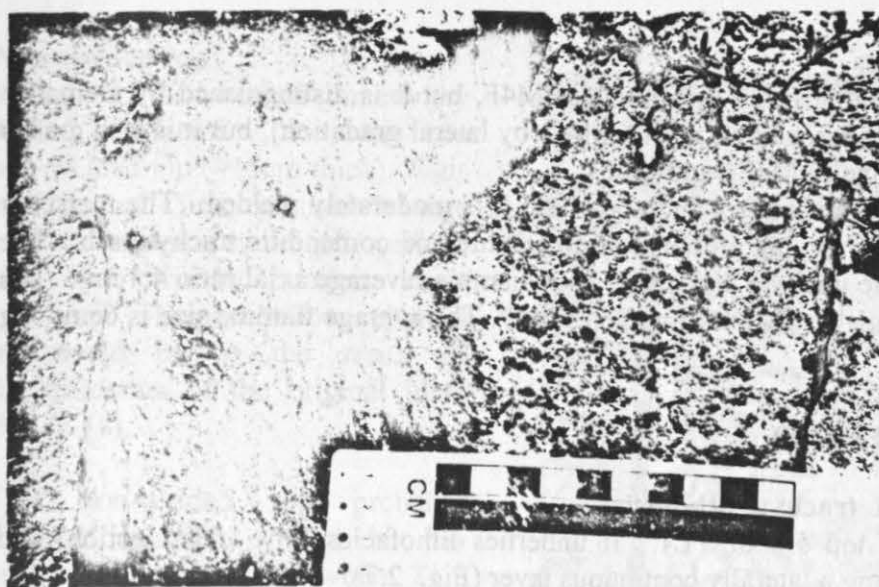


Figure 2.16. Comparison of hand specimens from subfacies M4Fp (right) and M4Fx (left), showing the characteristic purplish-brown colour of M4Fp, compared to the blue-grey of lithofacies M4Fx.

M4Fx - Transitional to lava-like subfacies

M4Fx occurs as a laterally discontinuous layer within M4F lithofacies. It commonly underlies M4Fp subfacies and the contact between the two is gradational over tens of cm's (Fig. 2.27).

This subfacies is particulate and poorly sorted, consisting of both fine grained matrix and clasts. The dark blue-grey matrix is densely welded, finely crystalline and composed of an estimated equal proportion of comenditic trachyte to comendite ash, which distinguishes it from the comenditic trachyte rich purple matrix of subfacies M4Fp. Rare patches of pale grey matrix are comendite rich. These areas are highly vesicular with diffuse outlines (<10cm in length).

The size and shape of fiamme distinguish this subfacies (Figs 2.16 and 2.17). Fiamme are predominantly small, black, subvitic comenditic trachyte (ca. 30 volume percent). In spite of the very dense crystalline matrix, fiamme are rounded to subrounded and appear only weakly flattened (average axial ratio 1.5:1cm).

Comenditic clasts are rare small, angular fragments (ca. 1 per m², <0.5 volume percent, <0.7cm in diameter). One large comendite 'bleb' was found (Fig. 2.17), its rounded, amoeboid outline and slightly crenulate margins suggest that this inclusion was probably incorporated while still partly molten.

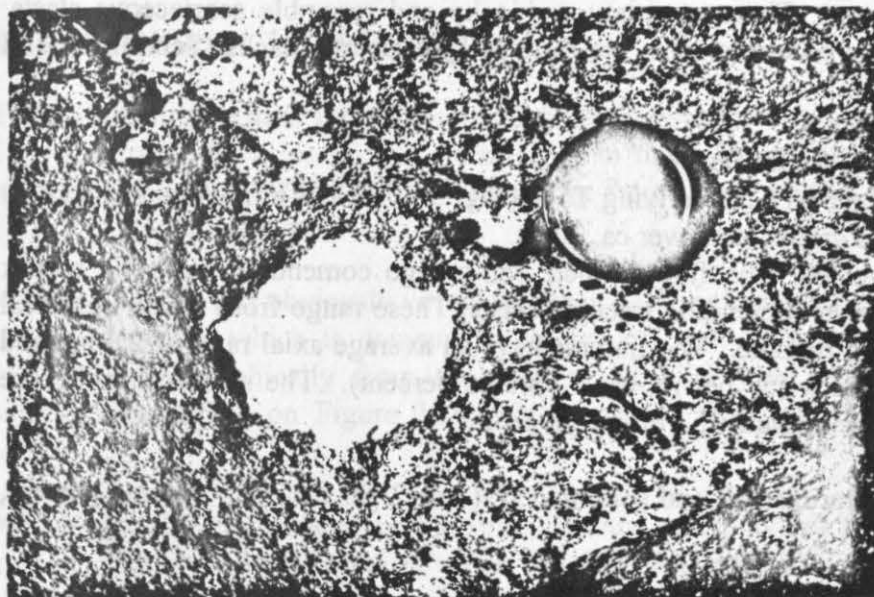


Figure 2.17. Isolated comendite inclusion (6cm in diameter) in subfacies M4Fx. Note the rounded amoeboid outline, suggesting it may have been partially molten when incorporated (Exp. 88, Bco. de Mogán).

M4Fs - Small fiamme subfacies

This subfacies is identical in composition to lithofacies M4F, but it is distinguished by a smaller fiamme size. Its common facies association is with M4F' (by lateral gradation), but it is also grades vertically and laterally into subfacies M4Fp and M4Fx.

M4Fs is poorly sorted, consisting of matrix and clasts and it is moderately welded. The matrix is light coloured, and patchy, with varying amounts of comendite and comenditic trachyte ash. The clasts are comendite, comenditic trachyte and mixed rock fiamme (average axial ratio 4:1cm). The fiamme are characteristically smaller than in lithofacies M4F. The average fiamme size is 6cm long by 1.3 cm thick.

2.4.3 TL trachyte Lithofacies Group

T5W - Moderately welded TL trachyte lithofacies

This lithofacies occurs in the top 5m of TL1. It underlies lithofacies T6w (next section) and overlies M4F lithofacies, forming a laterally continuous layer (Fig. 2.7).

T5W is poorly sorted consisting of fine grained matrix with clasts. The texture is 'weakly' to 'moderately welded' (Ross and Smith, 1961). The matrix is characteristically dark red-brown and is compositionally estimated as 80:20 volume percent comenditic trachyte to comendite ash.

The numerous clasts are comenditic trachyte fiamme. These range from small weakly flattened lapilli (248 per 50cm², ca. 10 volume percent, <1cm in diameter) with round vesicles, to moderately flattened, poorly vesicular fiamme (>57 per 50cm², ca. 13 volume percent) which have an average axial ratio of 4:1cm. The largest fiamme (maximum size, 17cm long and 8cm thick) are blocky and broken (Section 3.2, Fig. 3.3).

Comenditic clasts are rare (<11 per 50 cm², <0.5 volume percent) and are small and subangular (> 1cm). Rare lithics are small, subrounded clasts of basalt or syenite (<1 per m², <0.1 volume percent, maximum lithic size 3cm).

SUBFACIES OF T5W :

T5WG - Coarse grained TL trachyte subfacies

Subfacies T5WG occurs as lenses within the T5W lithofacies. It is characterised by a large grain size. The fine grained trachytic matrix contains comenditic trachyte fiamme up to 15cm long and 7cm thick (ca. 20 volume percent). These are platy or blocky and resemble scoriaceous clasts. They show evidence of late stage deformation in the form of "pull-apart" cracks (Schmincke and Swanson, 1967).

T6w - Weakly welded TL trachyte lithofacies

Lithofacies T6w occurs at the top of TL1, overlying T5W (Fig. 2.7). It has a maximum thickness of 2m. The contact with T5W is gradational over ca. 20cm.

It is particulate and weakly welded. The fine grained, red-orange comenditic trachytic matrix contains numerous, dark red-brown comenditic trachyte clasts. These range from small, spherical pumice lapilli to weakly flattened fiamme. The fiamme have an average axial ratio of 2:1cm, and are up to 7cm long and 5.5cm thick (65 per m, ca. 5 volume percent). The spherical lapilli are <2cm in diameter (>378 per m², minimum 15 volume percent).

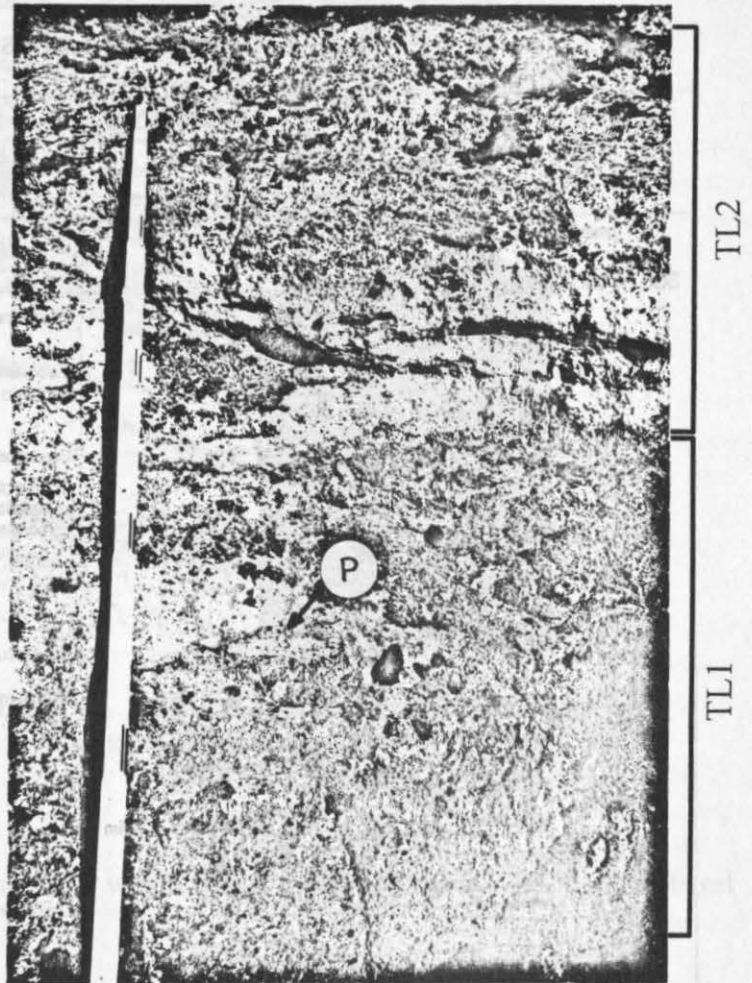
Comenditic clasts are extremely rare, small and subrounded (1 or 2 per m², <0.5 volume percent, <0.8cm in diameter).

Non-welded top

Where TL1 is overlain directly by TL2, lithofacies T6w has a non-welded top (>15cm thick). This consists of fine grained orange matrix containing small, pale yellow, soft and friable pumice clasts (<0.7cm). The pale yellow colour is interpreted to be the result of devitrification of the original glass (Fig. 2.18).

This non-welded top probably covered the whole of TL1, but has been completely eroded where TL1 is not overlapped by TL2.

Figure 2.18. Non-welded top of TL1, containing pale yellow, devitrified pumice lapilli (p). TL1 is overlain by TL2 (Exp.89, Bco. de Mogán).



2.5 LITHOFACIES IN UNIT TL2

On a regional scale flow unit TL2 can be divided into: a proximal or ponded lithofacies group (Fig. 2.4b) and a distal lithofacies group (Fig. 2.4c). The lithofacies within these two regions are distinguished on a textural basis, but the stratigraphic position and chemical composition correlate directly, as shown in Figure 2.4.

2.5.1 PROXIMAL LITHOFACIES OF TL2

The following proximal lithofacies and lithofacies associations are summarised on Figure 2.5 (b). The proximal lithofacies of TL2 occur close to the caldera margin (e.g. Exp. 108-112, Bco. de Mogán, and Exp. 73, Montaña Lobas), and in areas where TL2 is ponded, up to 26m thick, (e.g. Exp. 108, Bco. de Tasarte).

Although TL2 is less obviously vitroclastic than TL1, a chemical stratification and textural layering can be identified which is comparable to that of TL1. To enable comparison, lithofacies are described stratigraphically from the base of TL2 upwards. An example of the stratigraphic succession is shown on Figure 2.19, which is a log from proximal locality, Exp. 73, Montaña Lobas.

Only the lithofacies characterising the proximal and thick, layered parts of TL2 are discussed in this section. The lava-like lithofacies, which widely characterise TL2, occur at all localities in varying proportions, but as they dominate distal regions of TL2, they are discussed under Section 2.5.2.

Exp. 73, Montaña Lobas (Proximal)

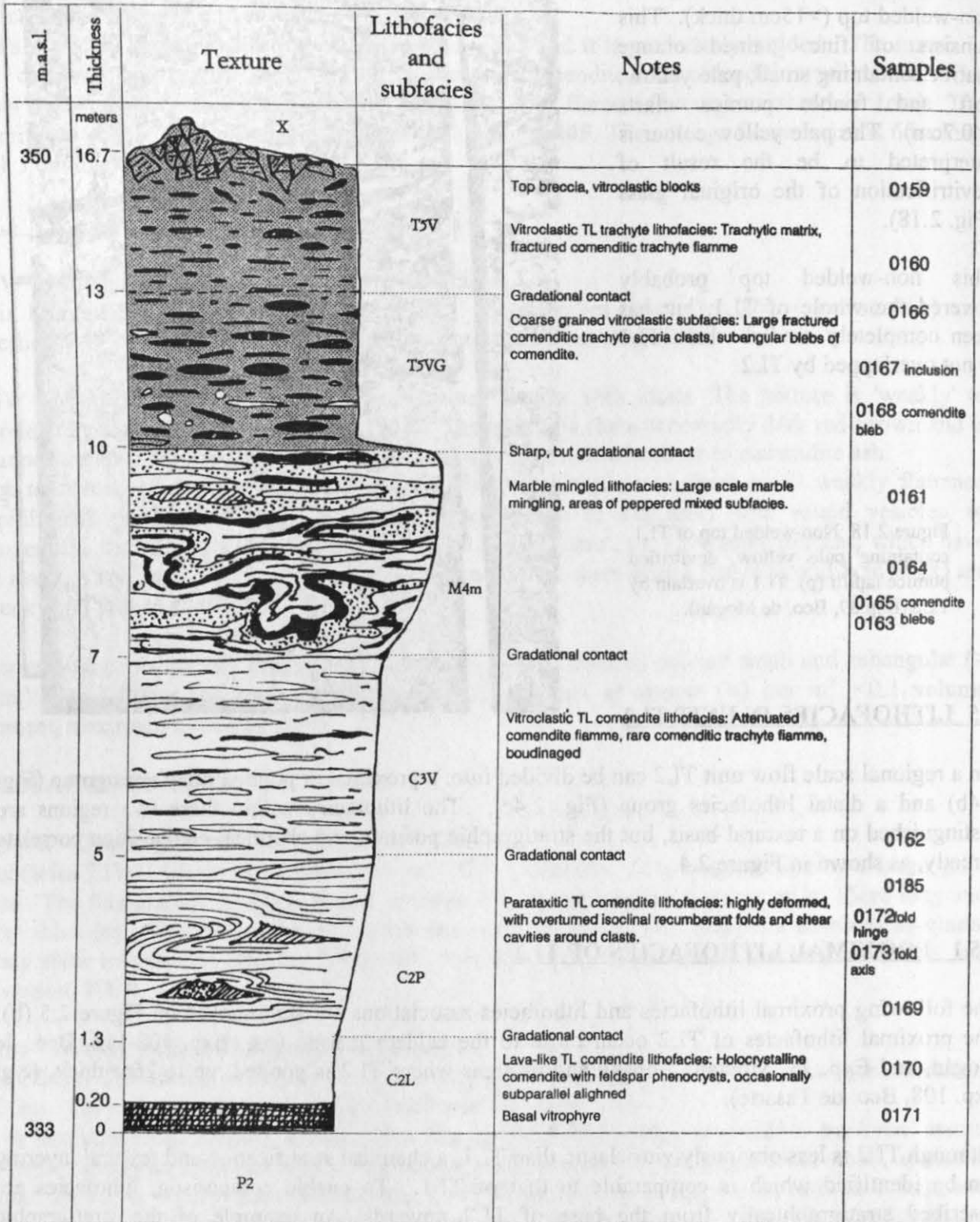


Figure 2.19. Proximal lithofacies and their associations at Exp. 73, Montaña Lobas.

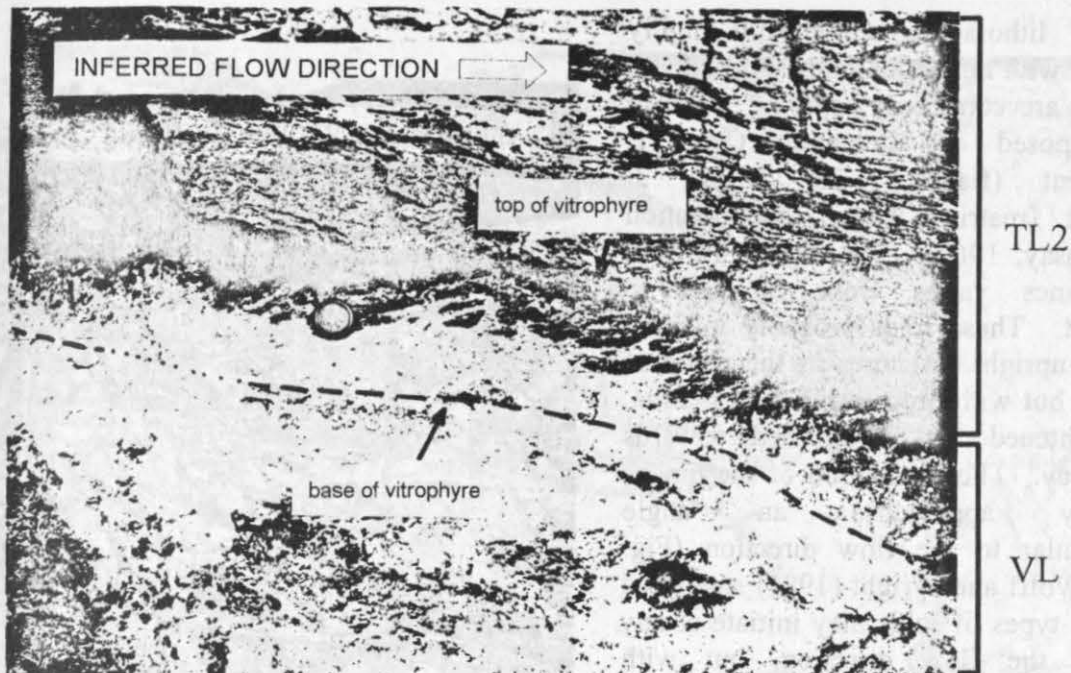


Figure 2.20. Basal vitrophyre of TL2. Fiamme are imbricated right to the base of the vitrophyre (extreme right of picture). The palaeohorizontal is marked with a dashed line. The lens cap is 5.5cm in diameter (Exp. 108, Bco. de Tasarte).

Basal vitrophyre

The basal vitrophyre of TL2 is up to 40cm thick, which is (minimum) 10cm thicker than the basal vitrophyre of TL1.

The basal vitrophyre contains black, glassy fiamme which are flattened and imbricated right to the base of the unit (Fig. 2.20). The fiamme size is generally smaller than in the basal vitrophyre of TL1 (maximum fiamme size, 13cm in length). The vitrophyre ranges in texture from eutaxitic to parataxitic and the fiamme and shards are more highly attenuated than in TL1 (Fig. 4.27). The composition of both matrix and fiamme is comendite (XRF analysis; Appendix II) and most fiamme are aphyric. The basal vitrophyre of TL2 is lithic poor (ca. 2 volume percent), compared to that of TL1. Lithics are small, subrounded fragments of trachyte or syenite with irregular crenulate margins, the maximum lithic size is 2cm.

2.5.1.1 TL comendite Lithofacies Group

C2P - Parataxitic TL comendite lithofacies

Lithofacies C2P occurs overlying the vitrophyre. It is poorly sorted, and the fine grained pale green-brown matrix contains large white, vesicular, comenditic fiamme. This lithofacies is characteristically densely welded and foliated (Fig. 2.21). Discontinuous flow banding is defined by the highly attenuated fiamme which have an approximate axial ratio of 50:1. This ratio can only be estimated as the high degree of deformation and attenuation of fiamme makes particle outline difficult to trace accurately.

Locally C2P is faintly vitroclastic and porous. These porous areas show faint banding of interlayered pale, vesicular bands (probably comenditic fiamme) and darker, densely crystalline matrix. Lithics are rare subangular pick-ups of VI and VL (<1 per m², ca. 0.5 volume percent).

The C2P lithofacies is typically highly deformed, with numerous folds (Fig. 2.22a). The folds are commonly "similar" in form and composed of alternating Class 1, incompetent (fiamme) and Class 3, competent (matrix) layers (classification after Ramsay, 1967). The dip of the fold axial planes varies from inclined to recumbent. These folds probably initiated as gentle upright structures in the plane of the layer, but with progressive deformation, were tightened and overturned towards recumbency. The orientation of the hinges commonly approaches an angle perpendicular to the flow direction (Fig. 2.22b). Wolff and Wright (1981) suggested that these types of folds may initiate at any angle to the flow direction, but with progressive deformation they rotate towards a 90 degree angle.

C3V - Vitroclastic TL comendite lithofacies

Lithofacies C3V overlies C2P and the contact between the two is gradational (Fig. 2.19).

C3V is vitroclastic and poorly sorted consisting of fine grained matrix with clasts. The finely crystalline blue-grey matrix consists of a mixture of comendite and comenditic trachyte ash. The pale colour suggests it is dominated by comendite ash. Large juvenile clasts are predominantly (ca. 32 volume percent) white, comenditic fiamme.

This lithofacies is distinguished from underlying C2P by the characteristic presence of black, comenditic trachyte fiamme (ca. 10 volume percent). The comenditic trachyte fiamme are very highly attenuated and form discontinuous flow banding. They average 24cm in length and 0.7cm in width and have an average axial ratio of 34:1. Axial ratios are difficult to measure accurately in the field as the fiamme are fractured and boudinaged. Boudins are often rotated over in the flow direction (Fig. 2.23).

Highly expanded, vesicular, granular lenses of comendite also occur in this layer (e.g. Fig. 3.3f). These were probably never originally pumice, rather comendite rich portions of the matrix which have undergone intense post-welding-vesiculation on contact with hotter comenditic trachyte magma (see discussion in Chapter 3, Section 3.3).

Lithofacies C3V also contains numerous, large, subangular feldspar phenocrysts (ca. 5 volume, maximum size 6mm). Lithics are rare (<3 per m², <0.1 volume percent). Small (<2cm in diameter) subangular to angular fragments of comendite occur near the top part of the lithofacies.



Figure 2.21. Discontinuous flow banding in proximal lithofacies C2P of TL2 is produced by extreme attenuation of comendite fiamme. The hammer is 30cm long (Exp.94 III, Bco. de Mogán).

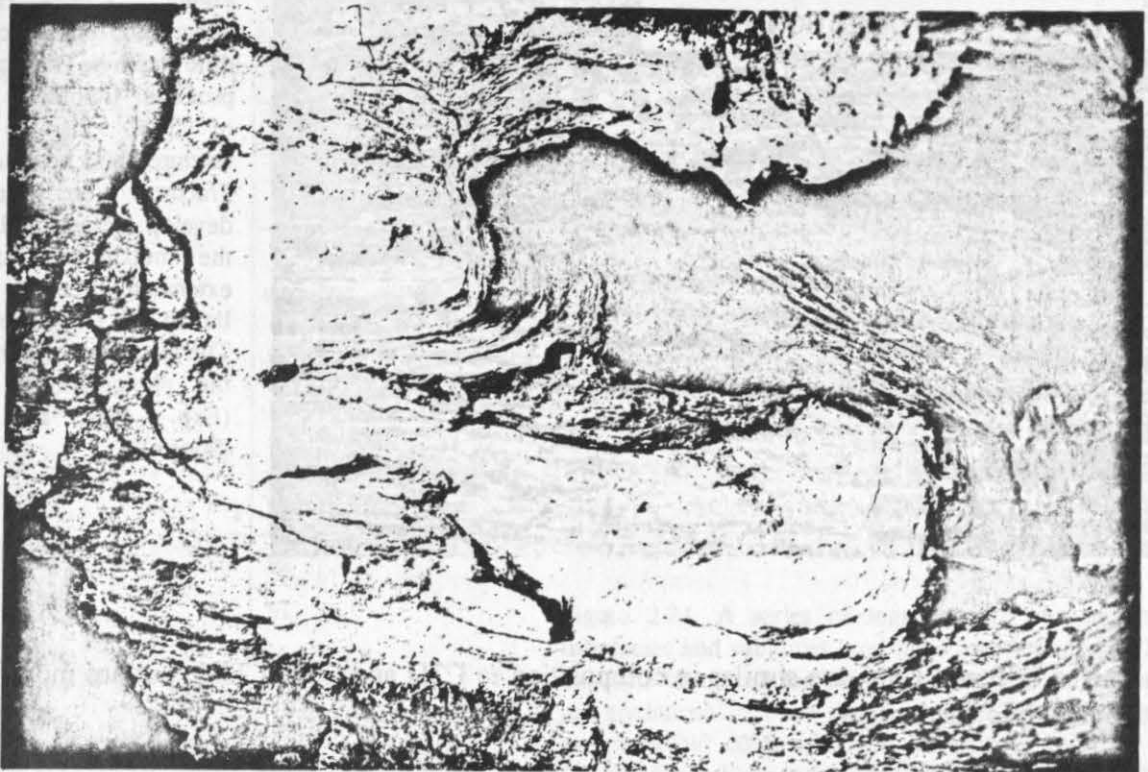


Figure 2.22 a. Folds in proximal lithofacies C2P of TL2. The dip of the axial surfaces of such folds are commonly recumbent and most hinge directions are perpendicular to the flow direction. The pen is 15cm long (Exp. 73, Montaña Lobas).

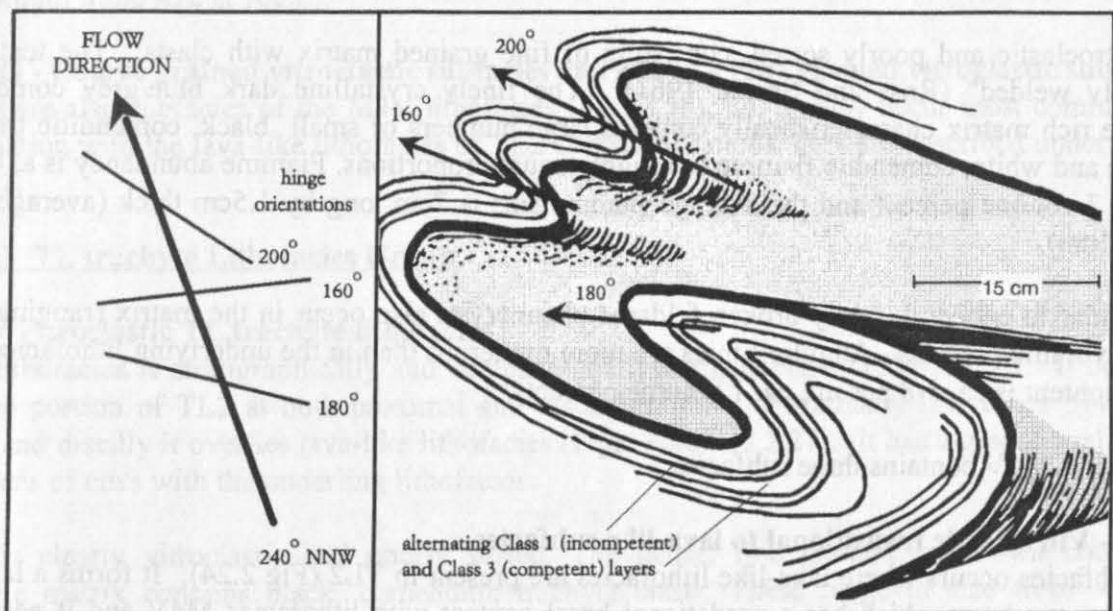


Figure 2.22 b. Sketch of recumbent fold in lithofacies C2P (as above). The fold is composed of alternating Class 1, incompetent (fiamme) and Class 3, competent (matrix) layers, (terminology after Ramsay, 1967). The hinge directions of folds commonly have angles approaching perpendicular to the flow direction (see inset).

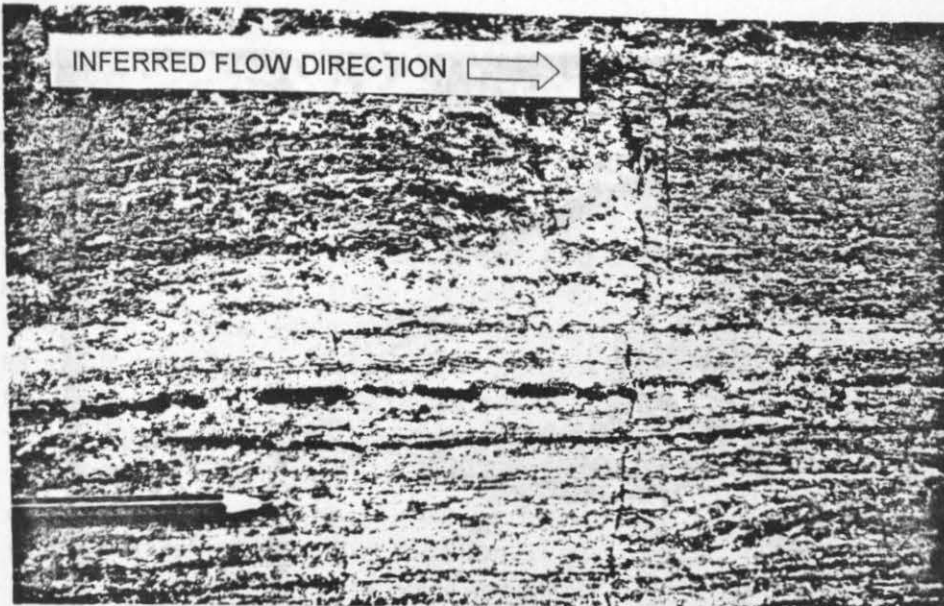


Figure 2.23. Highly attenuated, black comenditic trachyte fiamme in proximal lithofacies C3V of TL2. Fiamme are fractured and boudinaged. Fractures in fiamme develop perpendicular to the maximum inferred extension direction, parallel to the flow direction. The length of the pencil in the photograph is 7cm (Exp. 108, Bco. de Tasarte).

Lithofacies C2P and C3V, are similar in composition to C2D and C3f in TL1, but are more highly welded and deformed.

2.5.1.2 TL mixed rock Lithofacies Group

M4V - Vitroclastic TL mixed rock lithofacies

Lithofacies M4V is compositionally and stratigraphically comparable to lithofacies M4F in TL1 (Fig. 2.4a and b). It occurs in the lower and central portions of TL2 and has a gradational contact (over 15-20cm) with underlying lithofacies C3V (Fig. 2.24).

It is vitroclastic and poorly sorted, consisting of fine grained matrix with clasts. The texture is "strongly welded" (Ross and Smith, 1961). The finely crystalline dark blue/grey comenditic trachyte rich matrix characteristically contains large numbers of small black, comenditic trachyte fiamme and white, comendite fiamme in roughly equal proportions. Fiamme abundance is a. 47 per m², ca. 7 volume percent and the average fiamme size is 7cm long by 1.5cm thick (average axial ratio 5:1cm).

Subangular to euhedral, rarely broken feldspar phenocrysts also occur in the matrix (ranging from ca. 3-5 volume percent). Angular lithics are more numerous than in the underlying lithofacies C3V (lithic content is ca. 5-8 per m², ca. 1 volume percent).

Lithofacies M4V contains three subfacies :

M4Vx - Vitroclastic transitional to lava-like subfacies

This subfacies occurs where lava-like lithofacies are present in TL2 (Fig 2.24). It forms a laterally discontinuous layer which has a gradational basal contact with lithofacies M4V and it passes by vertical gradation into overlying lava-like lithofacies.

Subfacies M4Vx is dense, compact, and finely crystalline. Faint outlines of black comenditic trachyte fiamme, which appear highly flattened can be observed in the crystalline matrix. These fiamme range up to approximately 5cm in length, however this subfacies is so densely welded that the outlines of fiamme are difficult to trace accurately.

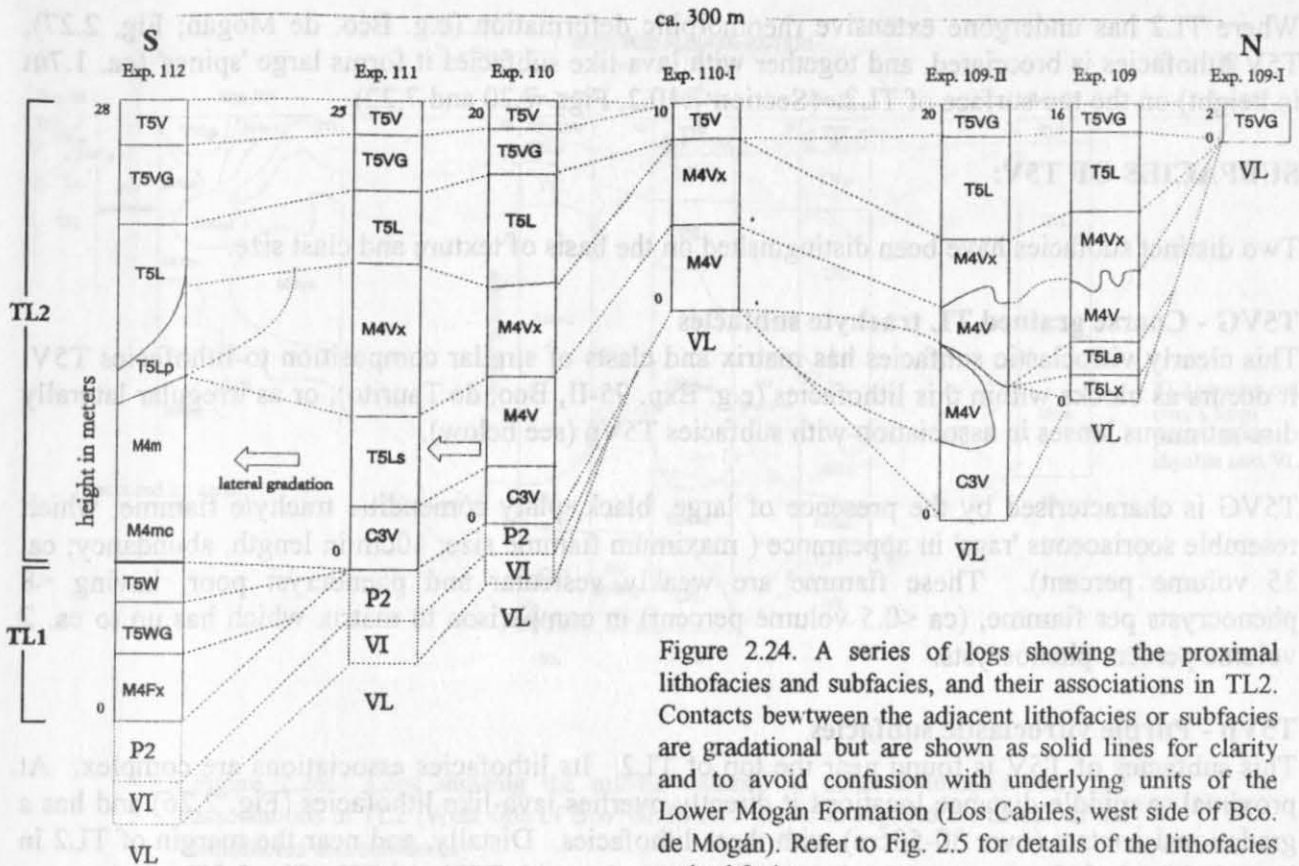


Figure 2.24. A series of logs showing the proximal lithofacies and subsfacies, and their associations in TL2. Contacts between the adjacent lithofacies or subsfacies are gradational but are shown as solid lines for clarity and to avoid confusion with underlying units of the Lower Mogán Formation (Los Cabiles, west side of Bco. de Mogán). Refer to Fig. 2.5 for details of the lithofacies and subsfacies.

M4Vx is lithic rich (<12 per m², ca. 8 volume percent). The lithic population consists of rounded syenite accessory lithics, highly angular pick-ups of P1, and subangular pickups of VL and VI (maximum lithic size is 10cm).

M4VG - Coarse grained vitroclastic subsfacies and M4Vg - Fine grained vitroclastic subsfacies: These are also subsfacies of the M4V lithofacies (Fig. 2.5b), but as they occur most commonly in association with the lava-like lithofacies of TL2 at distal locations, they are described under section 2.5.2.2.

2.5.1.3 TL trachyte Lithofacies Group

T5V - Vitroclastic TL trachyte lithofacies

This lithofacies is stratigraphically and compositionally comparable to T5W in TL1. It occurs in the top portion of TL2 at both proximal and distal locations. Proximally it overlies M4V (Fig. 2.24) and distally it overlies lava-like lithofacies (Figs. 2.26 and 2.27). It has a gradational contact over tens of cm's with the underlying lithofacies.

T5V is clearly vitroclastic and poorly sorted. The dense, fine grained red-brown comenditic trachyte matrix contains black, comenditic trachyte clasts. These range in size from <1cm in diameter to 5cm in length. The shape of the clasts varies from subspherical, vesicular lapilli, to flattened, wispy, poorly vesicular fiamme.

The matrix contains numerous, euhedral, rarely broken, feldspar phenocrysts (ca. 5 volume percent). In places, large (ca. 6mm) phenocrysts are sub-parallel aligned, forming a weak trachytoid texture. Comendite clasts are rare, small, angular fragments (<7 per m², <0.5 volume percent, <2.8cm in diameter).

Where TL2 has undergone extensive rheomorphic deformation (e.g. Bco. de Mogán; Fig. 2.27), T5V lithofacies is brecciated, and together with lava-like subfacies it forms large 'spines' (ca. 1.7m in height) on the top surface of TL2. (Section 7.10.2, Figs. 7.20 and 7.22)

SUBFACIES OF T5V:

Two distinct subfacies have been distinguished on the basis of texture and clast size.

T5VG - Coarse grained TL trachyte subfacies

This clearly vitroclastic subfacies has matrix and clasts of similar composition to lithofacies T5V. It occurs as blocks within this lithofacies (e.g. Exp. 95-II, Bco. de Taurito), or as irregular laterally discontinuous lenses in association with subfacies T5Vp (see below).

T5VG is characterised by the presence of large, black, platy comenditic trachyte fiamme, which resemble scoriaceous 'rags' in appearance (maximum fiamme size; 10cm in length, abundance; ca. 35 volume percent). These fiamme are weakly vesicular and phenocryst poor, having <8 phenocrysts per fiamme, (ca <0.5 volume percent) in comparison to matrix which has up to ca. 2 volume percent phenocrysts.

T5Vp - Purple vitroclastic subfacies

This subfacies of T5V is found near the top of TL2. Its lithofacies associations are complex. At proximal to middle-distance locations it directly overlies lava-like lithofacies (Fig. 2.26) and has a gradational contact (over 30-50cm) with these lithofacies. Distally, and near the margin of TL2 in Bco. de Mogán it forms upper autobreccia in association with T5V and C0b (Fig. 2.27).

Subfacies T5Vp is compact and densely welded. It is characteristically purple-brown (Fig. 2.25). It displays discontinuous flow banding produced by alternating dark purple and reddish-purple streaks. The reddish-purple streaks are more vesicular and are probably highly attenuated comenditic trachyte fiamme. These alternate with dense dark purple bands which are probably areas of dense, finely crystalline matrix.

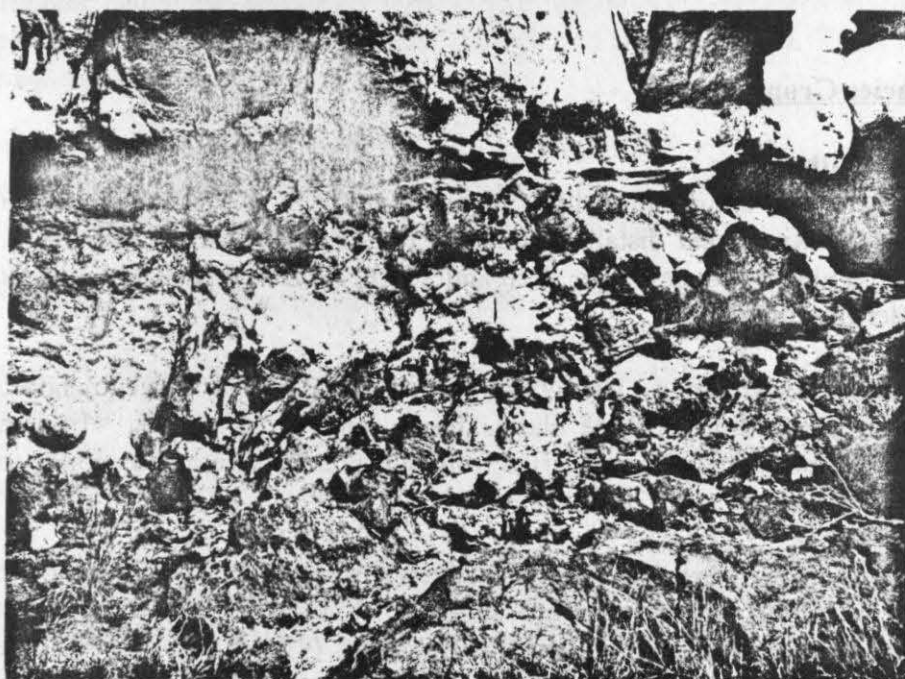


Figure 2.25. The characteristically purple subfacies T5Vp forms upper autobreccia at the top of TL2. TL2 is overlain by ignimbrite X at this locality. The hammer is 30cm long (Exp. 100, Bco. de Taurito).

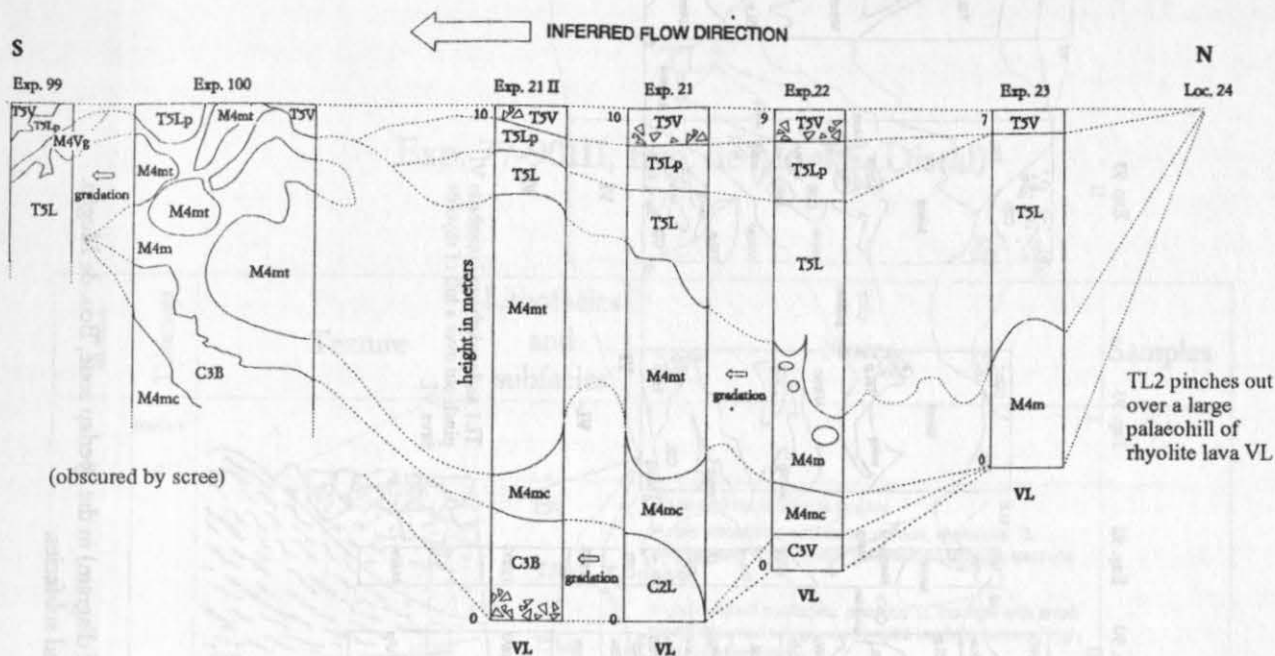


Figure 2.26. Logs showing the middle distance to distal lithofacies and their associations in TL2 (West side of Bco. de Tauro). Refer to Fig. 2.5 for details of the lithofacies and subfacies.

2.5.2 DISTAL LITHOFACIES OF TL2

The lithofacies and subfacies described in this section occur at distal locations of TL2, up to 15km away from the caldera margin (e.g. Exp. 99-102, Bco. de Tauro, Fig. 2.26). Distally most of TL2 is lava-like and remnant vitroclastic textures are identifiable only near the top of the deposit.

Much of the original layering has been disturbed during post-depositional non-particulate flow (Chapter 7) and lithofacies associations are very complex. The broad chemical stratification from TL comendite, through TL mixed rock to TL trachyte however, is still identifiable and this allows direct correlation with the proximal or ponded lithofacies of TL2 (Fig. 2.4).

The distal lithofacies and subfacies of TL2 are summarised on Figure 2.5 (c). Lithofacies at the type locality for TL2, Bco. de Mogán, are shown in Figure 2.27. Figure 2.28 is a sample log from this locality.

Basal Autobreccia

Distally TL2 is characterised by the presence of basal autobreccia, rather than a basal vitrophyre. The irregularly distributed, clast supported, heterolithologic basal autobreccia is generally composed of subangular blocks of adjacent lithofacies. As the base of the deposit is usually composed of TL comendite lithofacies, basal autobreccia is most commonly composed of blocks (<40cm) of C2L and C3b (see below). Near the distal margin of TL2 however (Fig. 2.27), basal autobreccia consists of a diverse range of blocks of varying lithofacies, including blocks from lithofacies normally found near the top of the deposit. This suggests that basal autobreccia is not formed by a simple process of in situ brecciation of lithofacies. (Chapter 7, Section 7.10.2)

TL2

Exp. 77-90III, Bco. de Mogán (Distal)


m.a.s.l.	Thickness	Texture	Lithofacies and subfacies	Notes	Samples
95	15		T5V	Spine and back breccia pocket	
			T5Lp	Purple vitroclastic subfacies: porous, vesicular TL trachyte with small weakly flattened comenditic trachyte lapi.lli.	
			T5Ls	Highly welded subfacies: eutaxitic TL trachyte with small highly flattened wispy comenditic trachyte fiamme, high angle of imbrication.	
			M4Vg	Sharp contact	
			M4Vg	Fine grained vitroclastic subfacies: Moderately welded TL trachyte lenses, rare small trachytic fiamme, often fining upwards.	
			T5Ls	Sharp contact	
			T5Ls	Highly welded subfacies: Lava-like trachyte, faintly vitroclastic, wispy highly attenuated comenditic trachyte fiamme.	M0193
	6		M4Vg	Sharp contact	0439
			M4Vg	Marble mingled TL trachyte subfacies: Dominated by TL trachyte microfacies.	M0192
			M4mt	Sharp contact	M0191
			M4Vg	Coarse grained vitroclastic subfacies: Lense of weakly welded tuff, trachytic matrix, small, platy and blocky vesicularcomenditic trachyte fiamme, sharp contact with surrounding lava-like facies.	M0189
			M4Vg	Sharp contact	
			M4Vg	Sharp contact	
	3.5		M4Vg	Sharp contact	M0188
			M4m	Marble mingled TL mixed rock lithofacies: Equal estimated proportions of TL trachyte and TL comendite microfacies	
	2		M4mc	Gradational contact	
			M4mc	Marble mingled TL comendite subfacies: Dominated by TL comendite microfacies	
			C2L	Gradational contact	
			C2L	Lava-like TL comendite lithofacies: Holocrystalline TL comendite	
80	0		C3B	Gradational contact	0306
			C3B	Comenditic basal autobreccia	

Figure 2.28. Distal lithofacies and their associations in TL2 (Exp. 77-90III, Bco. de Mogán).

2.5.2.1 TL comendite Lithofacies Group

C2L - Lava-like TL comendite lithofacies

C2L forms a laterally discontinuous layer in the basal 2m of TL2. It occurs as small pods and lenses in association with C3b (see below). It is generally overlain by TL mixed rock lithofacies (Fig. 2.28).

C2L correlates to proximal lithofacies C2P in both composition and stratigraphic position (Fig. 2.4), but is distinguished from this lithofacies by the absence of any original vitroclastic texture.

C2L is dense and holocrystalline comendite. It contains numerous, euhedral to subhedral feldspar phenocrysts (phenocryst abundance ca. 5-7 volume percent, maximum phenocryst size 5mm). The largest feldspar phenocrysts are commonly flow aligned forming trachytoid texture. Rare, smaller mafic phenocrysts are probably amphibole (Chapter 4). No lithics were recorded in this lithofacies.

C2L has variable contacts with the surrounding lithofacies. These range from sharp and planar to gradational. The variation in the type of contact is interpreted to be the result of viscosity differences between lithofacies C2L and the adjacent lithofacies (Chapter 7, Section 7.9).

C3B - Flow banded brecciated TL comendite lithofacies

C3B forms shear zones and low angle thrusts in the lower 5-7m of TL2 (e.g. Fig. 2.27, Exposures 90-II to 93-I). It has a transgressive relationship with surrounding lithofacies C2L and M4m (next section) and more rarely (higher up in the deposit) with lava-like trachytic lithofacies T5L. The contacts between C3B and the surrounding lithofacies vary from sharp and crenulate to gradational (Fig. 2.29).

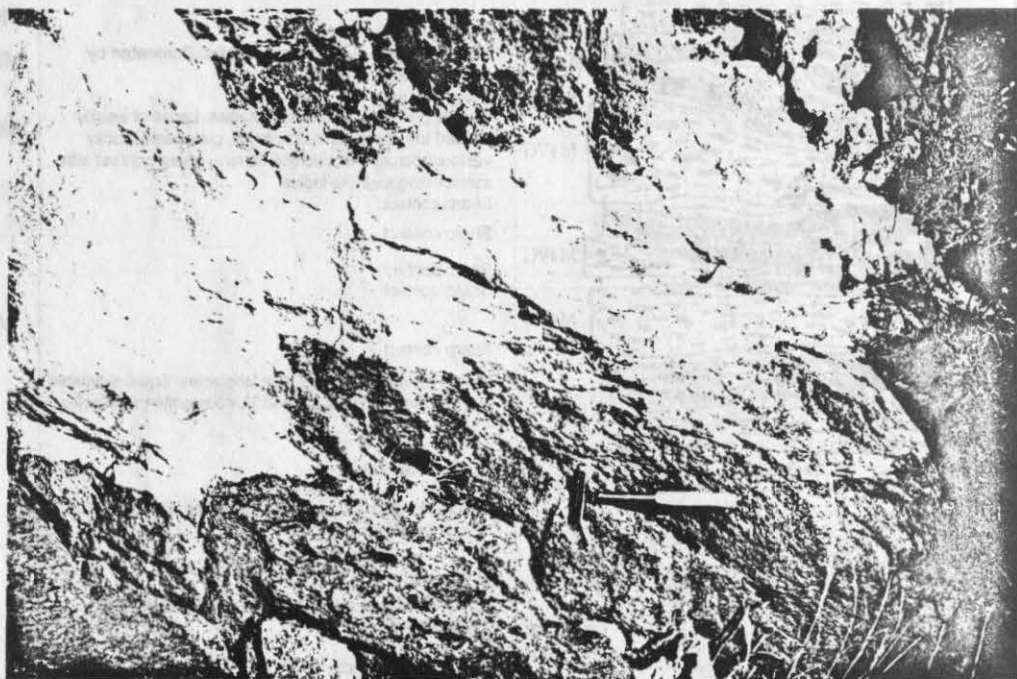


Figure 2.29. Distal lithofacies C3B forming a low angle shear or ramping plane at the base of TL2. Note the sharp but undulating contact between C3B (white) and underlying M4Vg (brown). The hammer is 30cm long (Exp. 93-I, Bco. de Mogán).

C3B lithofacies is characteristically flow banded (Fig. 2.29). Its texture varies from dense and holocrystalline to porous and faintly vitroclastic. Its pale cream colour indicates that the composition is predominantly comendite. C3B contains 3-5 volume percent euhedral and occasionally broken, anorthoclase phenocrysts (ca. <2.5mm).

The low angle thrusts or ramping planes are less than 70cm thick and contain lenses of "in situ" autobreccia (Bonnichsen and Kauffman, 1987) which is interpreted to form during the late stage, brittle failure of layers, during continued deformation. The autobreccia is clast supported and the clasts are subangular to subrounded (<30cm in diameter). The autobreccia is poorly sorted, with a fine grained matrix probably produced by autobrecciation and attrition between clasts (autobreccia formation is discussed in Chapter 7, Section 7.10.2).

2.5.2.2 TL mixed rock Lithofacies Group

M4m - Marble mingled lithofacies

M4m lithofacies occupies the same stratigraphic position in TL2 as lithofacies M4F in TL1 (Fig. 2.4 a and c). It correlates directly with TL2 proximal lithofacies M4V (Fig. 2.4 b and c).



LITHOFACIES
M4m

SUBFACIES
M4mh

Figure 2.30. Marbled mingling between darker TL trachyte and lighter TL comendite microfacies in the distal M4m lithofacies of TL2. This type of complex fluidal mingling pattern characterises the M4m lithofacies. In comparison subfacies M4mh (bottom half of photograph) appears speckled due to the presence of small globules of comenditic trachyte and trachybasalt (Exp. 77-6, Bco. de Mogán).

This lithofacies occurs as a thick layer from middle distance to distal localities, It overlies TL comendite lithofacies (e.g. Fig. 2.26, Exp. 22) and underlies TL trachyte lava-like lithofacies. It has gradational upper and lower contacts.

M4m is characteristically marbled and is composed of incompletely mingled holocrystalline TL comendite and TL trachyte (Fig. 2.30). It is finely crystalline, dense and compact, showing no evidence of vitroclastic texture. M4m lithofacies is predominantly blue-grey, marbled with streaks of dark blue-grey and pale blue.

Sample number	Lithofacies	Subfacies	Microfacies	SiO ₂ wt%	Fe ₂ O ₃ wt%	MgO wt%	MnO wt%	Zr ppm	Nb ppm
0283	M4m	M4mt	90:10 t	64	5.45	1.19	0.21	996	137
0376			80:20 t	64.4	6	0.8	0.16	1037	141
0001			70:30 t	64.7	5.59	1.02	0.19	836	120
0002			60:40 t	65	5.80	1.20	0.19	1021	144
C		M4mc	50:50	65.5	4.93	0.77	0.17	1002	131
B			60:40 c	66.5	4.90	0.75	0.18	963	137
A			80:20 c	66.9	4.65	0.79	0.18	891	139

Table 2.3. Identification of microfacies in lithofacies M4m of TL₂, using selected chemical components from bulk rock analyses (Chapter 5, Appendix II).

The marbling streaks have been subdivided into **microfacies** using the weight percent of SiO₂ for bulk rock samples (Table 2.3). The colour of the streaks corresponds directly to the composition, thus compositions can be visually estimated. M4m is roughly composed of roughly 50% comenditic microfacies and 50% trachytic microfacies i.e.;

50:50 microfacies = 50:50 volume percent comendite : comenditic trachyte - blue grey

60:40c microfacies = 60:40 volume percent comendite : comenditic trachyte - pale blue

60:40t microfacies = 60:40 volume percent comenditic trachyte : comendite - dark blue grey

70:30t microfacies = 70:30 volume percent comenditic trachyte : comendite - dark grey

M4m is compositionally and texturally complex, it contains three subfacies, two of which have been distinguished on the basis of field estimated percentages of TL comendite to TL trachyte. The third is characterised by its distinctive particulate appearance.

SUBFACIES OF M4m:

M4mc - Marble mingled TL comendite subfacies

Subfacies M4mc is composed of marbled mingled comenditic microfacies. The predominance of comenditic microfacies gives this subfacies and overall very light blue grey colour. It contains the following comenditic microfacies listed in decreasing order of abundance :

60:40c = 60:40 volume percent comendite : comenditic trachyte -pale blue-grey

80:20c = 80:20 volume percent comendite : comenditic trachyte -white

50:50 = 50:50 volume percent comendite : comenditic trachyte -blue grey

Rare streaks of the following trachytic microfacies highlight the marbling pattern :

60:40t = 60:40 volume percent comenditic trachyte : comendite -dark blue grey

70:30t = 70:30 volume percent comenditic trachyte : comendite -dark grey

M4mt - Marble mingled TL trachyte subfacies

This subfacies has a higher overall volume percent of TL trachyte. It is composed predominantly of TL trachyte microfacies (Table 2.3) and is dark grey in colour. The following trachytic microfacies are distinguished in decreasing order of abundance:

70:30t = 70:30 volume percent comenditic trachyte : comendite -dark grey

60:40t = 60:40 volume percent comenditic trachyte : comendite -dark blue grey

80:20t = 80:20 volume percent comenditic trachyte : comendite -very dark grey

90:10t = 90:10 volume percent comenditic trachyte : comendite -blue-black

Marbling within this lithofacies is highlighted by rare streaks of:

60:40c = 60:40 volume percent comendite : comenditic trachyte -pale blue grey

Subfacies M4mt underlies lava-like trachyte lithofacies (Section 2.5.2.3). On a large scale it forms massive lenses with a pinch and swell structure and large rounded pods or load-balls underlain by lithofacies M4m (Section 7.10.1, Fig. 7.21) or subfacies M4mc (Fig. 2.34).

M4mh - Peppered mixed subfacies

Subfacies M4mh occurs within lithofacies M4m as localised lenses or irregular patches with gradational margins. It is characterised by a speckled, mixed 'salt and pepper' appearance.

It appears particulate, with a fine grained clastic texture, however the it is dense and finely crystalline throughout. M4mh varies in colour from light grey to blue grey depending on the relative amount of comendite and comenditic trachyte present, this is estimated to range from 60:40 volume percent comendite to comenditic trachyte, to 50:50 volume percent comendite to comenditic trachyte (Table 2.3).

The particulate speckled appearance is produced by white feldspar phenocrysts (<0.3mm) and comenditic blebs (<0.5cm in diameter), together with dark blebs of comenditic trachyte and minute globules of black vitric trachybasalt (<0.6cm in diameter, <2 volume percent). The trachybasalt globules and comenditic trachyte blebs cannot be distinguished in the field. Trachybasalt was identified later by microprobe analysis (Section 4.4.1).

SUBFACIES M4VG AND M4Vg:

The following are subfacies of lithofacies M4V (Section 2.5.1.2) but are described here as they typically occur at distal locations (e.g. Fig. 2.28).

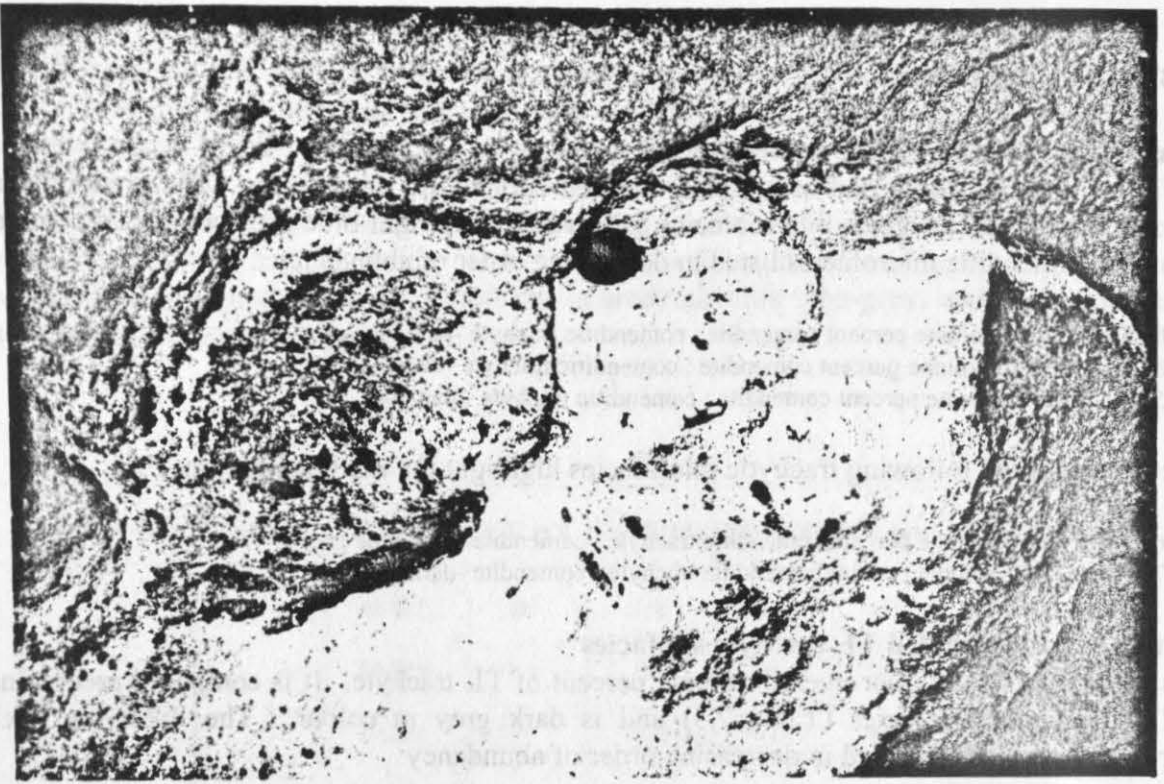


Figure 2.31 a. Lava-like TL trachyte lithofacies T5L in association with vitroclastic subfacies M4VG and M4Vg in TL2. The lens cap is 5.5cm in diameter (Exp. 93 II, Bco. de Mogán).

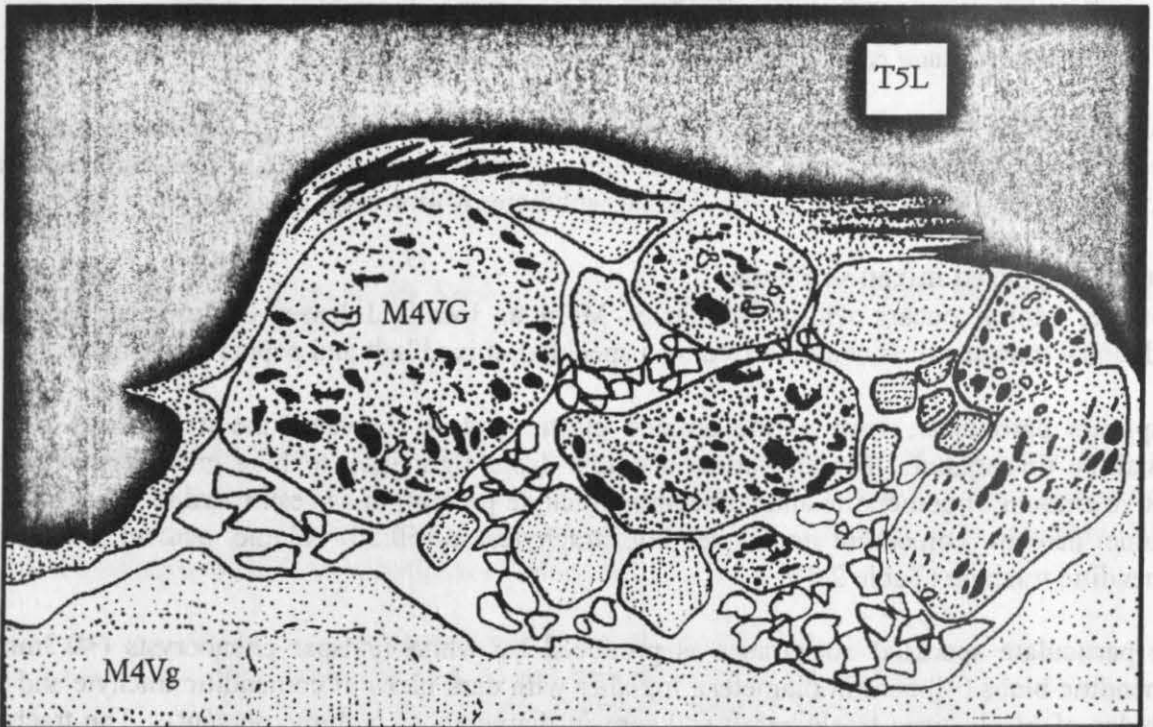


Figure 2.31 b. Sketch of the associations between T5L and M4VG and M4Vg (as above). Weakly welded subfacies M4VG and M4Vg form pockets of internal autobreccia (Chapter 7) within lava-like lithofacies T5L.

These subfacies occur in a similar stratigraphic position to subfacies M4FG and M4Fg in TL1 (Fig. 2.4 a). Subfacies M4VG and M4Vg are restricted to the lower 10m of TL2, and like subfacies M4FG and M4Fg of TL1, they are usually intimately related. The boundaries between M4VG and M4Vg are gradational over tens of centimetres.

M4VG - Coarse grained vitroclastic subfacies

Subfacies M4VG occurs as isolated lenses within lithofacies M4m (Figs. 2.28 and 2.32) and more rarely in TL trachyte lava-like lithofacies. It also occurs as bands and lenses, and rounded autobreccia blocks in more continuous layers and large pods of subfacies M4VG (Fig. 2.31a and b).

Subfacies M4VG is clearly vitroclastic. It is particulate and poorly sorted, consisting of fine grained matrix with clasts. The dense, finely crystalline pale cream-brown matrix is comendite rich. Clasts are predominantly small, black, subangular to subrounded comenditic trachyte lapilli. These are poorly vesicular and weakly flattened (<4.3cm in diameter).

Where M4VG occurs as discrete lenses within the M4m lithofacies (Figs. 2.32 and 2.33), the fiamme near the margins of the lense are more highly attenuated. This suggests that; either the matrix and clasts were still able to deform plastically when incorporated in the lithofacies M4m; or that the margins of the lenses were heated by juxtaposition with hotter lithofacies M4m (probably during non-particulate flow). When hot they deformed plastically, causing attenuation of clasts and producing crenulate and wispy lense margins.

Locally M4VG also occurs as laterally discontinuous layers (ca. 150cm in length and 60cm in width) forming 'mounds' at the base of the deposit (Fig. 2.27). The distribution and complex lithofacies associations of this subfacies are further discussed in Chapter 7 (Section 7.10.1).

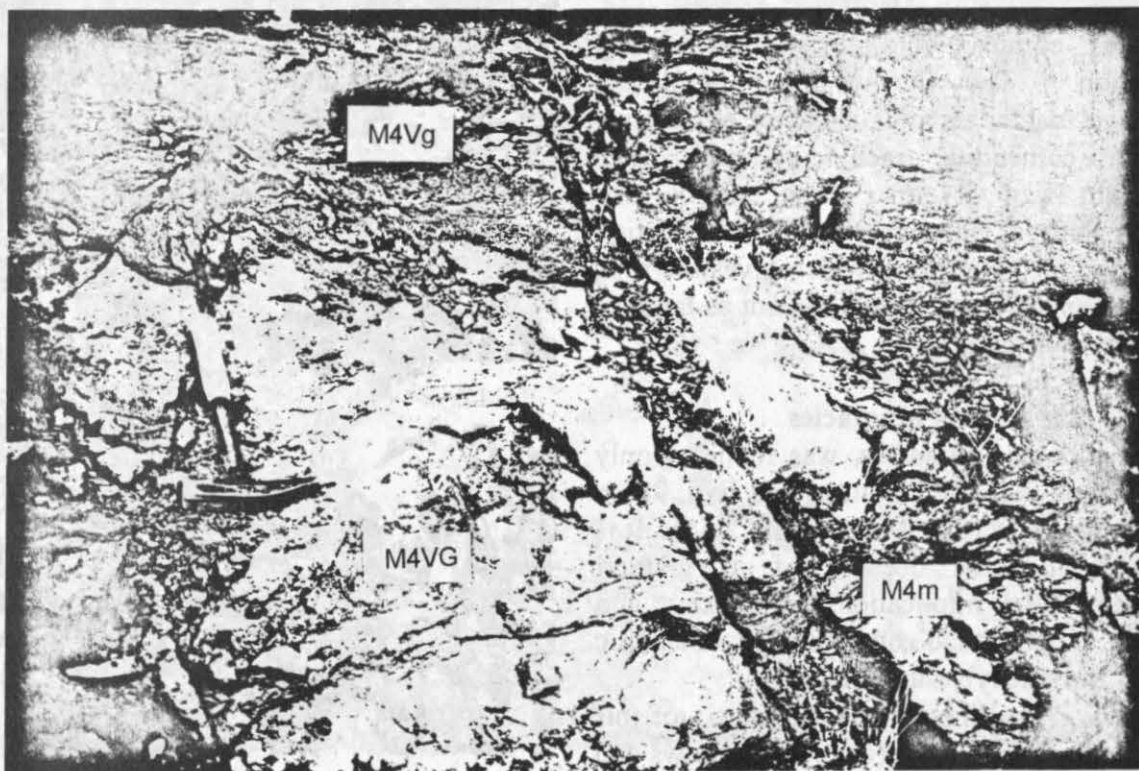


Figure 2.32. Textural variations and changes in intensity of welding in TL2, demonstrated by interlayering of lava-like lithofacies M4m with vitroclastic subfacies M4VG and M4Vg. The hammer is 30cm long (Exp. 77-6, Bco. de Mogán).

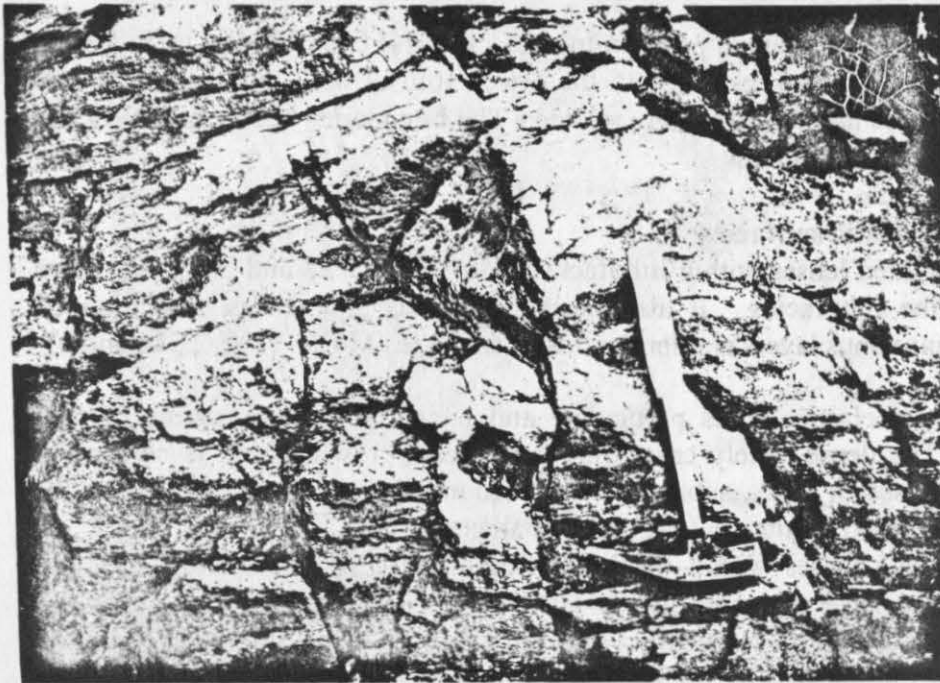


Figure 2.33. Lense of subfacies M4VG within lithofacies M4m in TL2. Note the attenuated fiamme around the margins of the lense, suggesting that subfacies M4VG was still hot enough to deform plastically, as lithofacies M4m sheared around it. The hammer is 30cm long (Exp. 77-6, Bco de Mogán).

M4Vg - Fine grained vitroclastic subfacies

This subfacies occurs in the lower 5-10m of TL2 in close association with M4VG (Fig 2.32). Lenses of M4Vg are partly enclosed within lithofacies M4m and occasionally within TL comendite lithofacies at the base of the deposit.

M4Vg is compact and dense, but clearly vitroclastic. The fine grained, purple to red-brown matrix contains clasts of red-brown, vesicular, comenditic trachyte, <1cm in size (maximum size 2.7cm). The matrix also contains feldspar phenocrysts (<2mm) and tiny comenditic blebs (<1mm), which gives the rock a mottled appearance. Clasts are not as large or as numerous as in M4VG.

B.G.I.Z - Big globule lithofacies

The big globule lithofacies, was found at only two outcrops, Bco. de Lechugal and Exp. 96 on the east side of Bco. de Mogán (Fig. 2.34). It is described in detail because of its textural significance and implications for mixing and mingling between comendite, comenditic trachyte and trachybasalt (Chapter 6).

The finely crystalline comenditic matrix of this lithofacies contains large (ca. 7cm), pillows and micropillows (Section 1.5) of comenditic trachyte (Fig. 2.35a). These have fine grained, cryptocrystalline margins, which may represent chilled or quenched margins, and more vesicular, coarse grained cores.

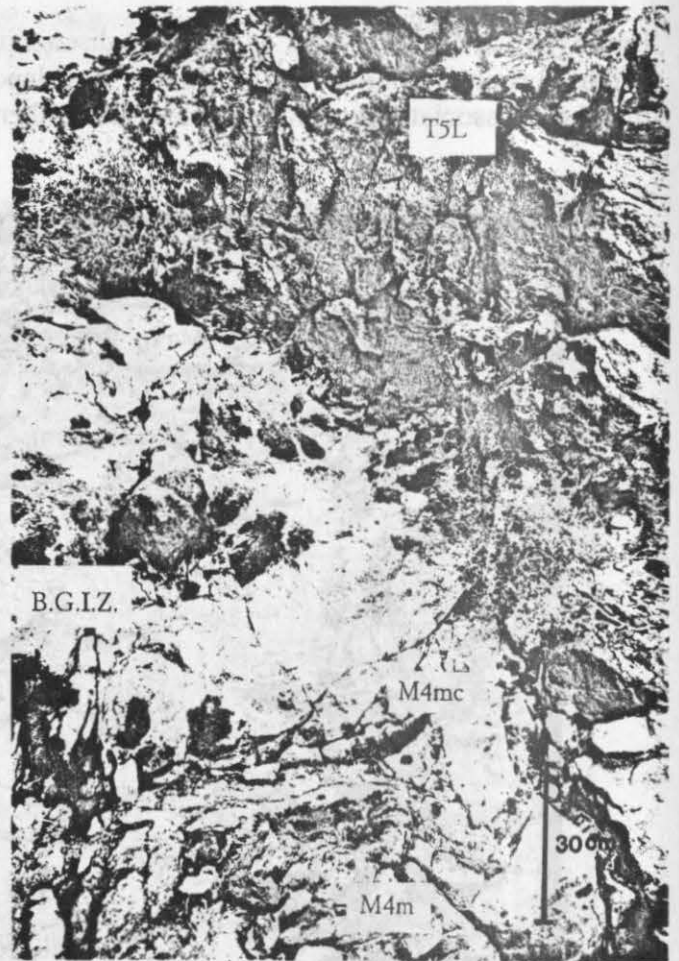


Figure 2.34. Detail of the complex subfacies and their microfacies associations in lithofacies M4m and B.G.I.Z. of TL2 (Exp. 96, Bco. de Mogán).

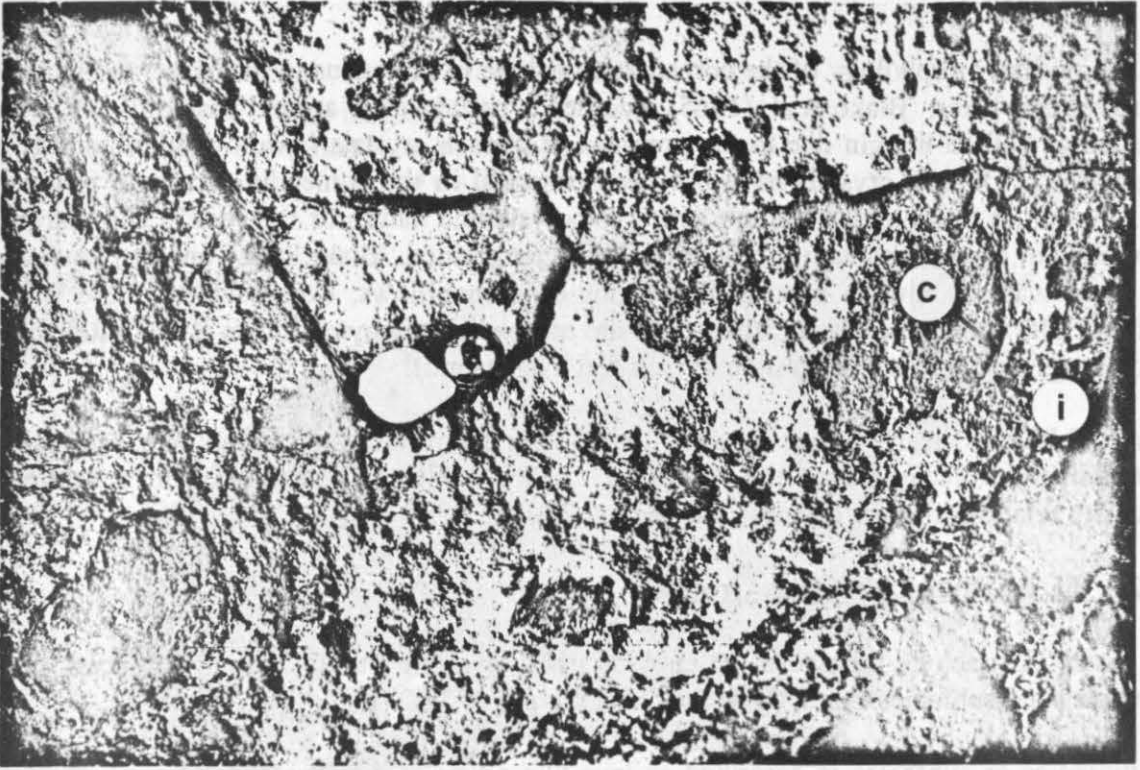


Figure 2.35 a. Big globule lithofacies forming an intrusive zone (B.G.I.Z.) in TL2. Comenditic trachyte 'pillows' have a chilled, cryptocrystalline margin (c), comenditic matrix adjacent to the pillows is indurated (i) and enriched in iron and magnesium. The open hand lens is 3cm in diameter (Exp 58-59, Bco. de Lechugal).

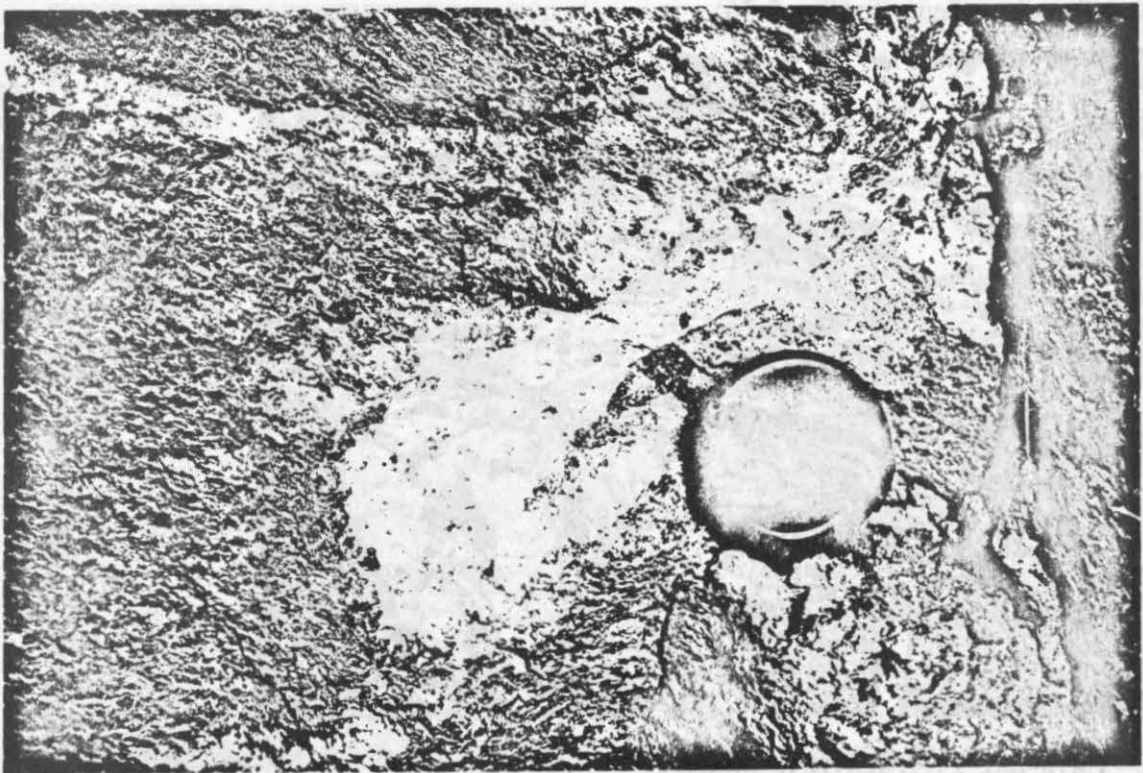


Figure 2.35 b. Dike-like intrusion of the comenditic matrix of the B.G.I.Z. into surrounding M4mt subfacies. TL2. The lens cap is 5.5cm in diameter (Exp. 58-59, Bco. de Lechugal).

The pillow-like morphology of the comenditic trachyte is analogous to that observed in net-veined intrusive complexes. Blake et al. (1965) recorded a 'pseudo-chill' around basic pillows, which was regarded as chilled margin due to the presence of quench crystals (swallow tailed and 'H' shaped plagioclase). Quench crystals have not been observed in the comenditic trachyte pillows in the B.G.I.Z. due to the microcrystalline and cryptocrystalline nature of the rock. The margin to the pillows is not glassy, although it is significantly finer grained. Blake et al. (op. cit.) however noted that glass was not always present at margins of such pillows, except where there was drastic chilling. The comendite matrix adjacent to the comenditic trachyte pillows is indurated and darker in colour (probably due to migration of iron and magnesium).

This B.G.I.Z. is clearly intrusive and forms a series of dike and spine like protrusions into surrounding lithofacies M4m and T5L (Fig. 2.35b), which have fractured in a brittle manner (viscosity relationships are discussed in Section 7.9).

2.5.2.3 TL trachyte Lithofacies Group

The distal TL trachyte lithofacies group consists of lava-like lithofacies and subfacies. Lava-like lithofacies and subfacies characterise the distal margin of TL2 (Fig. 2.37a and b).

A lithofacies or subfacies is described as lava-like where it displays one or more characteristics normally considered characteristic of a lava. This includes for example; flow banding, upper and lower autobreccia, holocrystallinity, trachytic texture etc. Lava-like lithofacies are distinguished even though they may pass vertically and laterally into lithofacies with unequivocal vitroclastic texture because the presence of fiamme, producing apparent vitroclastic texture, is not necessarily diagnostic of pyroclastic flow origin. Fiamme also occur in lavas, for example the rhyolite lavas of Mount Tejedi on Tenerife (Fig. 2.36).



Figure 2.36. Apparent fiamme, produced by irregular devitrification, in an obsidian lava flow (Tenerife, Canary Islands), demonstrating that fiamme are not exclusive to ignimbrites, and are not diagnostic of pyroclastic origin.

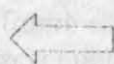
T5L - Lava-like TL trachyte lithofacies

T5L generally forms the upper 5-10m of TL2 (depending on deposit thickness). It is not restricted to the distal margin and occurs at proximal locations and where TL2 is ponded (e.g. Exp. 111, Bco. de Mogán and Exp. 108, Bco. de Tasarte respectively). Locally it has been rheomorphically displaced to near the base of the flow (Chapter 7, Section 7.10.3).

a.

TOP BRECCIA:

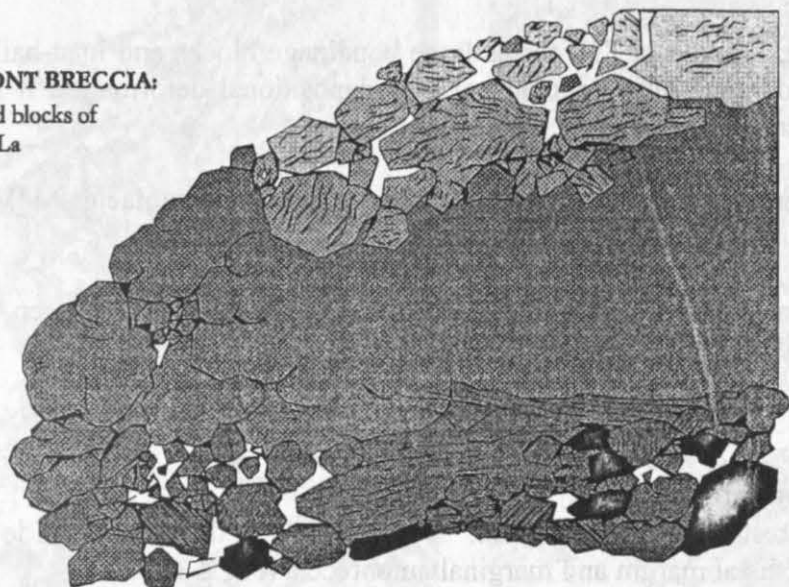
Rotated blocks of lithofacies T5V and subfacies T5Ls and T5La.



INFERRED FLOW DIRECTION

FLOW FRONT BRECCIA:

Large slipped blocks of subfacies T5La



- T5V
- T5Ls
- T5La
- T5L
- T5Lx
- Vitrophyre
- Devitrified matrix

2 m

BASAL BRECCIA:

Angular blocks of basal vitrophyre, lithofacies T5L and subfacies T5La and T5Lx (laminated)

b.

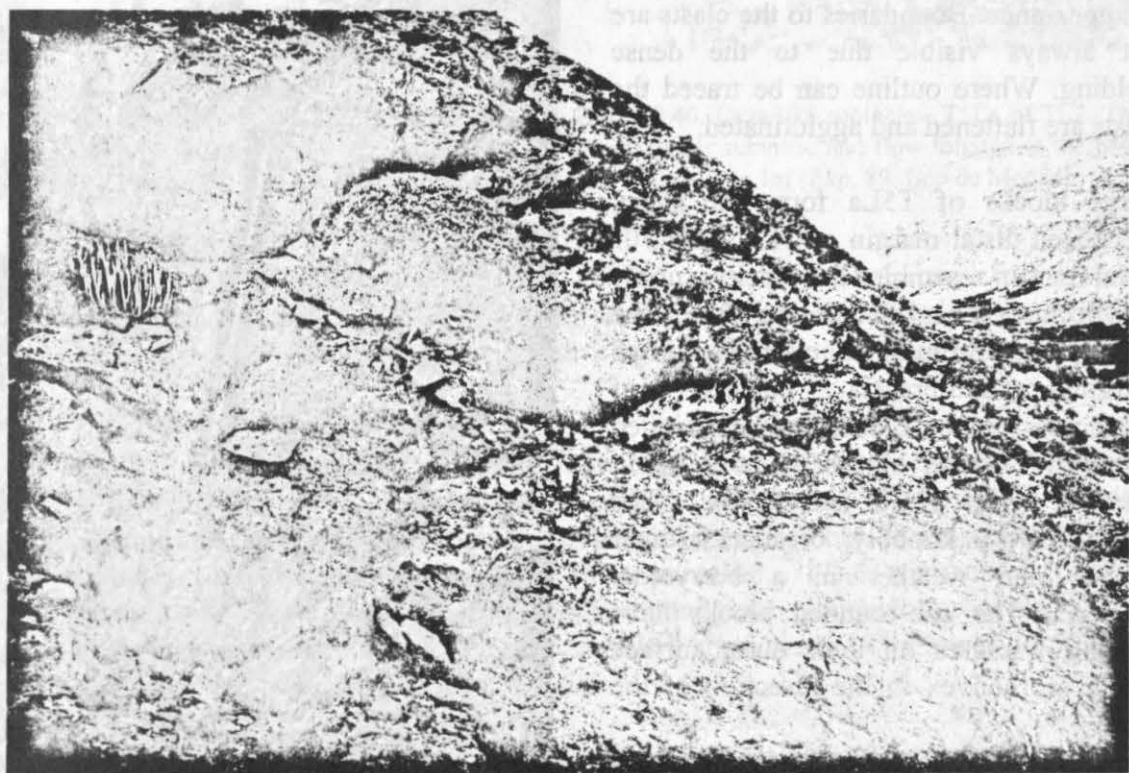


Figure 2.37. Sketch (a) and photograph (b) showing the distribution of autobreccia and lithofacies and subfacies associations at the distal margin of TL2. TL2 is underlain by TL1 at this locality. The rucksack is 50cm high (Exp. 88, Bco. de Mogán).

This dark grey-black lithofacies is dense, compact, holocrystalline TL trachyte with no evidence of vitroclastic texture. Numerous, euhedral feldspar phenocrysts (up to ca. 8 volume percent, maximum phenocryst size 4mm) are often sub parallel aligned, forming a weak trachytoid texture (Section 1.5). No comendite was observed in this lithofacies.

Where TL2 is deformed, lithofacies T5L forms large boudinage blocks and load-balls (Fig. 2.27). Where TL2 has not undergone large amounts of post-depositional deformation it forms a more laterally continuous layer (Fig. 2.26).

T5L has sharp planar contacts with surrounding lithofacies M4m and subfacies M4VG and M4Vg (Fig. 2.32a and b).

Lithofacies T5V contains five texturally distinct subfacies. The contacts between subfacies and lithofacies M5L are all gradational over several tens of cm's.

SUBFACIES OF T5L:

T5La - Lava-like agglutinate subfacies

Subfacies T5La is very restricted in distribution. It occurs only at the most distal locality of TL2, where it forms the steep distal margin and marginal autobreccia (Fig 2.37).

This dark purple-black subfacies is composed of subvitric vesicular comenditic trachyte clasts (maximum clast size; 15cm) which resemble spatter lumps in appearance. Boundaries to the clasts are not always visible due to the dense welding. Where outline can be traced the clasts are flattened and agglutinated.

Large blocks of T5La form the steep, brecciated distal margin of TL2. This 70° distal margin resembles the blocky, rubbly flow front of a basaltic Aa lava flow. The coarse, monolithologic, clast supported marginal autobreccia consists of subangular, slabby blocks and subrounded to 'pillow' shaped blocks up to 2.7m in diameter (Figs. 2.38 and 2.39). The blocks have a knobby, breadcrust outer surface and weather in a botryoidal fashion. The sub-rounded blocks have curving fractures on their outer surface which are convex in the direction of the flow.

Between the larger blocks are narrow (<20cm) zones of fine grained autobreccia and lineated fracture zones occur between slipped or slumped blocks (Fig. 2.39).

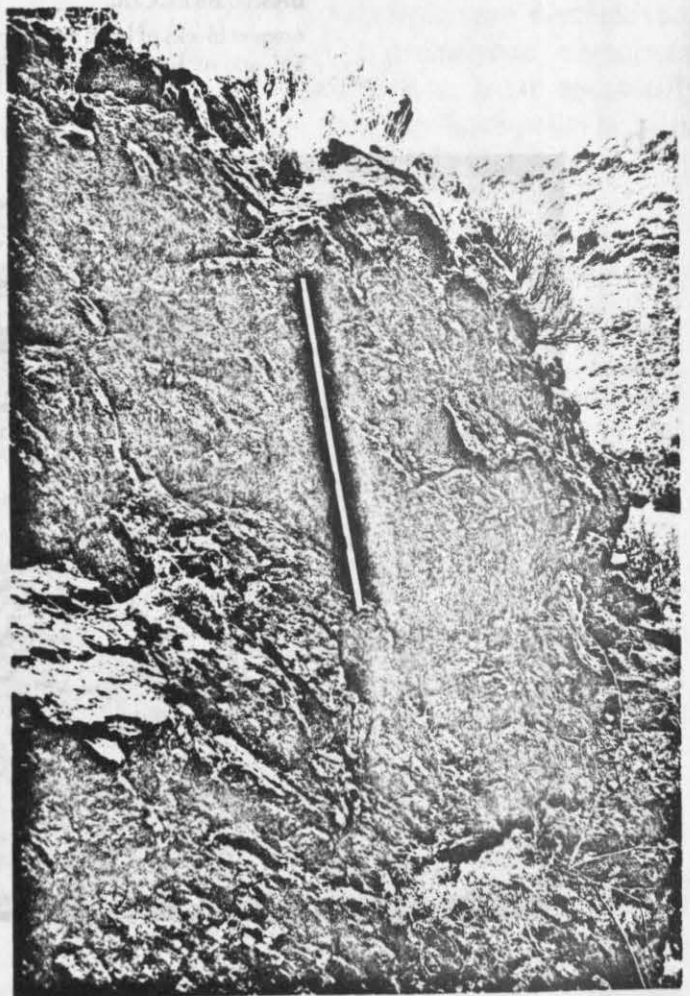


Figure 2.38. Large slipped block (behind 1 meter rule) of lava-like subfacies T5La at the steep distal margin of TL2 (Exp. 88, Bco. de Mogán).

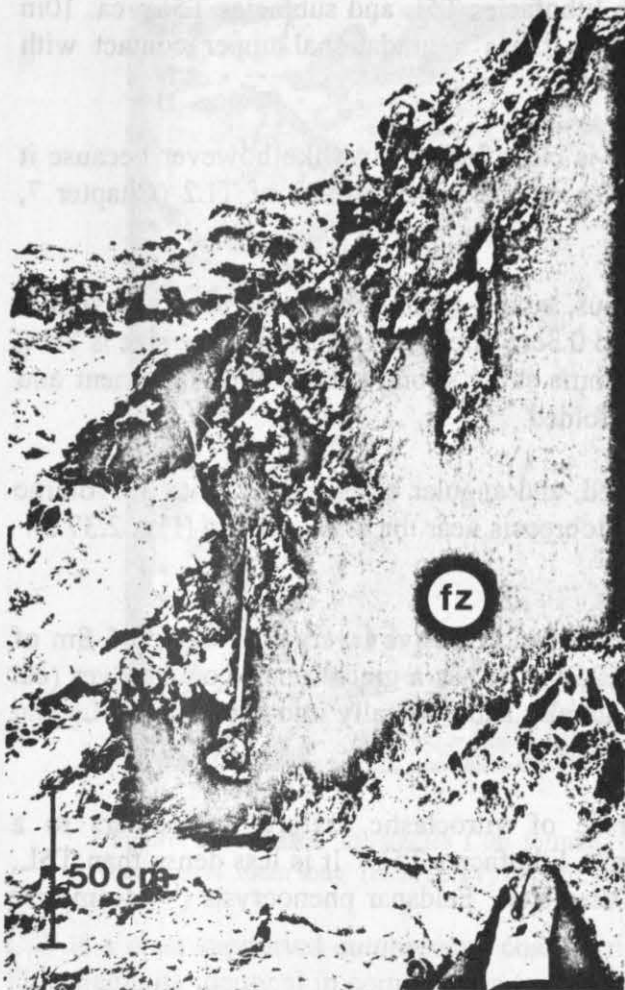


Figure 2.39. Jointed blocks of lava-like subfacies T5La separated by thin fracture zones (fz) at the distal margin of TL2 (Exp. 88, Bco. de Mogán).



Figure 2.40. Lava-like subfacies T5Lx of TL2. This lithofacies is subvitric and flow foliated at the base. The scale rule is 1m (Exp. 89, Bco de Mogán).

T5Lx - Transitional to agglutinate subfacies

Subfacies T5Lx first occurs approximately 7-8m away from the distal margin. It is up to 4m thick and occurs at the base of TL2. It is transitional with lithofacies T5La, and underlying T5Ls (see below).

Subfacies T5Lx is dark grey and finely crystalline. It contains numerous rarely broken, subangular to subhedral feldspar phenocrysts (<3mm in size, <5 volume percent). T5Lx generally appears dense and holocrystalline at outcrop, locally however, there are patches of faint vitroclastic texture. Rare, poorly defined, subangular to subrounded, microcrystalline, black comenditic trachyte fragments can sometimes be identified. These are predominantly non-vesicular and average <5cm in diameter. They give weathered surfaces a faintly 'mottled' appearance. The lower 30-50cm of this subfacies is subvitric and flow foliated (Fig. 2.40).

Comendite occurs rarely as subangular blebs (<1.7cm in diameter, 1 or 2 per m², <0.5 volume percent).

T5Ls - Highly welded subfacies

Subfacies T5Ls is found at the top of TL2, near the distal margin (Fig. 2.27). It is commonly 3-5m thick, but ranges up to 8m thick where thrust stacking occurs (Chapter 7, Fig. 7.19). It is

transitional with T5La at the distal margin, and with lithofacies T5L and subfacies T5Lp ca. 10m inland. One kilometer away from the distal margin it has a gradational upper contact with lithofacies T5V (Fig. 2.26).

This subfacies is vitroclastic and densely welded. It is classified as lava-like however because it contains upper autobreccia and forms spines or ogives on the upper surface of TL2 (Chapter 7, Section 7.11.2).

T5Ls is eutaxitic, the texture is defined by numerous, small, highly flattened, poorly vesicular comenditic trachyte fiamme, averaging <4cm long and 0.3cm thick (maximum fiamme size is 7cm, the average axial ratio of fiamme is 13:1). The fiamme show strong sub-parallel alignment and define a highly variable lineation which is often flow folded.

Subfacies T5Ls is usually fractured and autobrecciated, and angular blocks form up to 30 volume percent of the thick (7-10m) heterolithologic upper autobreccia near the distal margin (Fig. 2.37 a).

T5Lp - Purple lava-like subfacies

Subfacies T5Lp occurs as large boudinage blocks, lenses and massive layers near the top 5-8m of TL2 at both proximal and distal localities (e.g. Fig. 2.26). It has a gradational contact over (ca. 40cm) with underlying lithofacies T5L and grades laterally and vertically into subfacies T5Ls and lithofacies T5V.

T5Lp is holocrystalline TL trachyte, with no trace of vitroclastic texture it weathers to a characteristic purple colour which distinguishes it from lithofacies T5L. It is less dense than T5L, containing numerous tiny round vesicles, <1mm in diameter. Feldspar phenocrysts (<4.4mm) are less common than in T5L (ca. 5-7 volume percent).

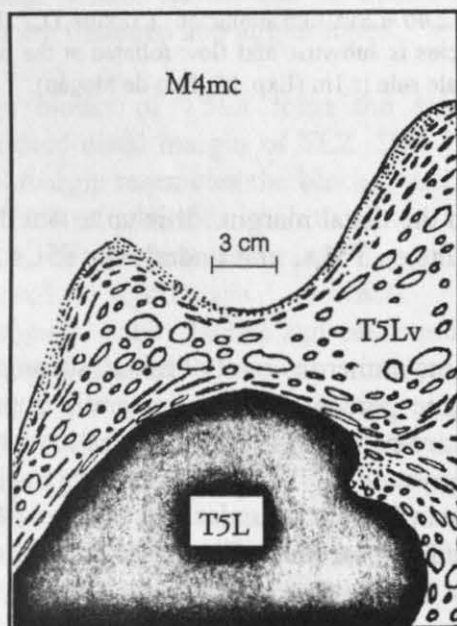


Figure 2.41. Lava-like vesicular subfacies T5Lv in TL2. This lithofacies occurs between subfacies M4mc and lithofacies T5L (Exp. 93 IV, Bco. de Mogán).

T5Lv - Lava-like vesicular subfacies

Subfacies T5Lv is distinguished by its texture. It is found where lava-like TL comendite and TL trachyte are adjacent to each other. It occurs where there is a significant difference in composition between lithofacies and commonly develops along the boundary between lithofacies in the more comenditic end member.

T5Lv is characteristically highly vesicular (Fig. 2.41). Vesicularity can be as much as 60 volume percent, with either rounded vesicles <5cm in diameter (ca. 0.7cm in diameter) or flattened 'long-tube' vesicles (<3cm long and 0.6cm in diameter). The shape of vesicles indicates that vesiculation occurred both during and after plastic deformation of the layers.

C0b - Comenditic upper autobreccia

Lithofacies C0b is restricted to the top of flow unit TL2. It occurs in 'valleys' between 'highs' created by ramps and spines in the more trachytic lithofacies e.g. Fig. 2.42.

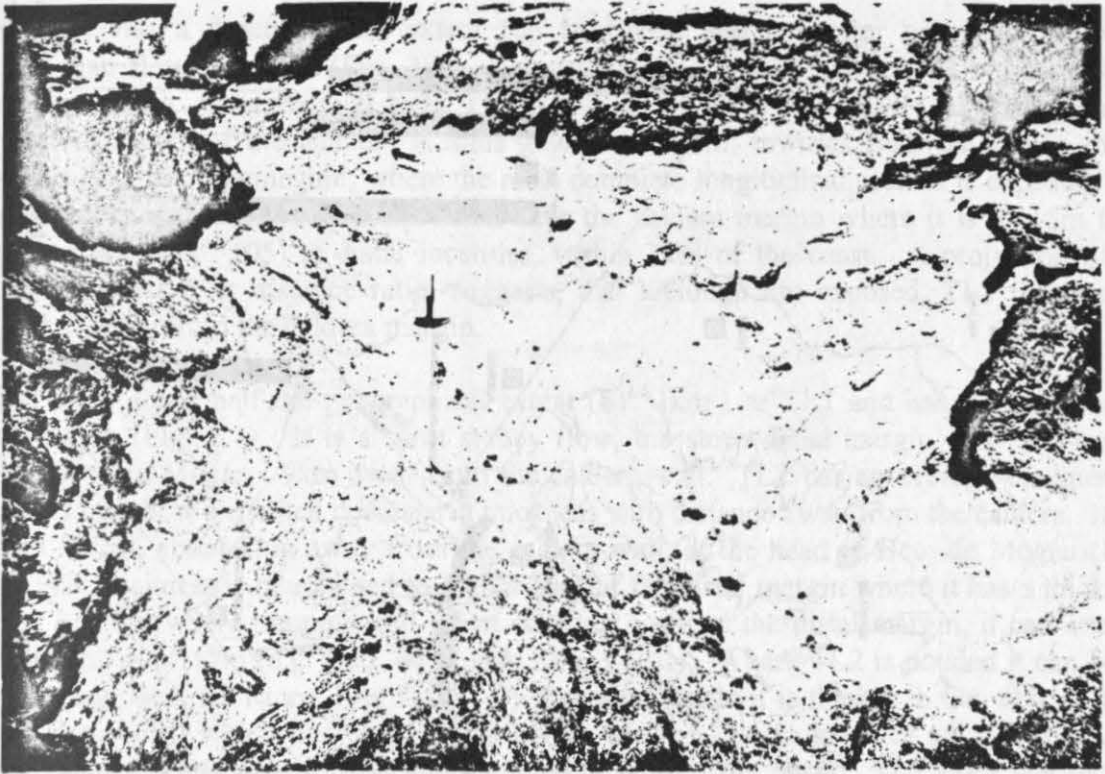


Figure 2.42. Distal lithofacies C0b forming comenditic upper autobreccia at the top of TL2. The hammer is 30cm long (Exp. 93 IV, Bco. de Mogán).

C0b is a clast supported autobreccia, characterised by white clasts and matrix. It is composed of TL comendite identical in composition to that found near the base of the deposit. The upper ca. 1m of breccia is often stained orange due to the presence of an overlying thin red soil. The lower ca. 3m of the breccia is white and purplish grey. This heterolithic autobreccia is predominantly composed of rounded to subangular clasts (<1m in diameter) of TL comendite. These are friable, and crumble to a white powder. Rarer more consolidated clasts composed of mingled TL comendite and TL trachyte are flow banded in white and purple. These flow banded clasts demonstrate that the breccia blocks have been rotated. The heterogeneity of the autobreccia and the banding and rotation of clasts suggests that this was not simple 'in situ' brecciation of a comenditic layer (Section 7.10.3).

SECTION II

LATERAL VARIATION IN TL

2.6 REGIONAL VARIATION

Flow units TL1 and TL2 and the individual lithofacies within them vary in thickness regionally around the caldera and with distance away from the caldera wall. The thickness variations are also markedly influenced by the underlying paleotopography (next section).

Figure 2.43 shows the varying thickness of TL1 and TL2, and of the lithofacies groups within them. The thickness variations are most clearly demonstrated using the simple lithostratigraphic subdivision, applicable to both units i.e. a the lower zone, composed of TL comendite lithofacies; a central zone of TL mixed rock lithofacies and an upper zone of TL trachyte lithofacies.

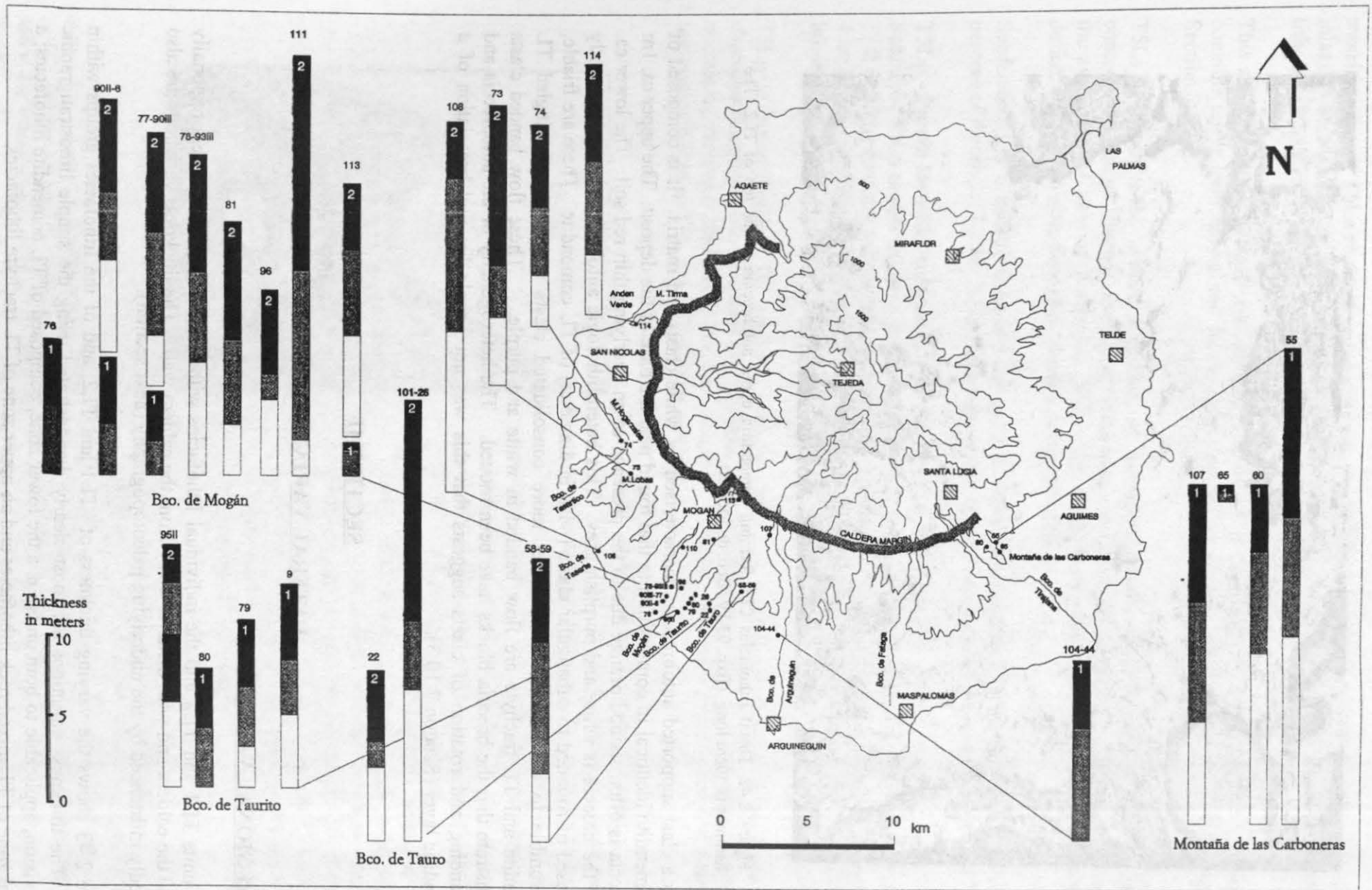


Figure 2.43. Simplified stratigraphic columns showing the regional variation in the relative proportions of lithofacies groups: TL trachyte (black), TL mixed rock (grey) and TL comendite (white) in flow units TL1 and TL2. Numbers within the columns indicate the flow unit, exposure numbers are at the top of each column, locations are given at the base of each column. Detailed logs for the localities are in Appendix I.

Flow unit TL1 has a greater radial extent (up to 16km) and a greater geographical extent (106.17km²) than flow unit TL2 (Fig. 2.1). Generally, except where ponded, TL1 thins distally away from the caldera. On a regional scale, TL1 is thickest (28m) at Montaña de las Carboneras, in the southeastern sector of the island. It thins gradually to 5m, towards Bco. de Mogán in the southwest. In Bco. de Arguineguin, where the most complete longitudinal section is exposed, TL1 decreases in thickness from proximal localities near the caldera margin where it is 20.15m thick (Exp. 107), to 6m (Exp. 105) at distal localities, within 3km of the coast. A projection of the decrease in thickness over distance ratio, suggests, that although not exposed, TL1 pinches out about 20-25km away from the caldera margin.

Flow unit TL2 is about half the geographical extent (51.51km²) of TL1 and has a much smaller radial distribution (Fig. 2.1). It is a short stubby flow, the steep distal margin of which can be observed in Bco. de Mogán, 9km away from the caldera wall. TL2 has an average thickness of 14m, and does not show a marked decrease in thickness with distance away from the caldera. It has a thickness of 12m, about 2km away from the caldera wall, at the head of Bco. de Mogán (Exp. 109-112). This thickness is maintained to within 30m of the distal margin where it has a thickness of 12-15m. Locally where ramping and thrust stacking occur at the distal margin, it can attain a maximum thickness of 17m (e.g. Bco. de Mogán Exp. 93-III). Where TL2 is ponded it can be up to 26m thick (e.g. Bco. de Tauro, Fig. 2.43). On a regional scale it is thicker to the west, in Bco. de Tasarte (Exp. 108), which lies on the edge of the Montaña de Hogarzales palaeobasin. The thickness of 25m at these localities is due to ponding within this basin. TL2 does not show a regional thinning radially around the caldera.

Both TL1 and TL2 are thicker in valleys and basins and thin over topographic highs. They are clearly topography-controlled, supporting their origin as flow deposits, rather than fall-out deposits.

Three factors affected the distribution of the lithofacies in TL1 and TL2:

- 1) Vent migration; which influences the duration of the eruption at any one place and thus the thickness of the deposit which aggrades during sustained flow.
- 2) Eruption rate; which affects the volume of eruptive material available for deposition.
- 3) Palaeotopography; which causes unequal distribution of erupted material.

It is impossible to tell which of these factors was dominant at any one time, and the thickness variation of lithofacies was probably due to a complex combination of all three. Detailed mapping indicates that the distribution of the lithofacies within TL1 and TL2 is primarily influenced by small-scale channels which dissect the gross relief of the area, and on a local scale by the 'hummocky' relief produced by underlying rhyolite lava VL. These variations are described in detail in the following section. There are some variations however, which appear to occur on a regional scale. Figure 2.43 shows that moving S to NW around the caldera there appears to be a decrease in relative thickness of TL comendite in both TL1 and TL2. This suggests that in both cases this phase of the eruption proceeded for a longer time at localities to the south and southwest respectively.

2.7. TOPOGRAPHY CONTROLLED VARIATION

2.7.1 Distribution of TL1 and TL2

Two aspects of the effect of topography will be considered in this section. Firstly the effect of the underlying palaeotopography on the distribution of flow units in TL and secondly the effect of the surface topography produced by TL on the deposition of subsequent units in the Mogán Formation. These variations are on a local scale and are recorded from individual localities within separate

barrancos. The palaeotopography has been mapped in detail and the variations are directly related to specific topographical irregularities.

The influence of rheology on the response to palaeotopography

Due to their differing rheologies, flow units TL1 and TL2 show a differing response to palaeotopography. At localities 76-93 on the west side of Bco. de Mogán, both flow units occur together and TL1 is overlapped by TL2 (Fig. 2.27). At this locality rhyolite lava VL of the Lower Mogán Formation (Fig. 1.3) forms a large hill (ca. 25m high, the base of this unit is buried below the road). The hill is draped by high grade ignimbrite VI of the Lower Mogán Formation, which thins drastically over the crest. Unit P2 is missing and VI is directly overlain by flow unit TL1, which in turn is overlapped by TL2 (Fig. 2.44). Although TL1 thins considerably at the crest it completely covers VI on both the upflow and the downflow side of the hill, TL2 however is only present on the upflow side of the hill and forms a steep distal margin near the crest. This difference in distribution of TL1 and TL2 is interpreted to be the result of the differing rheology of the two flows.

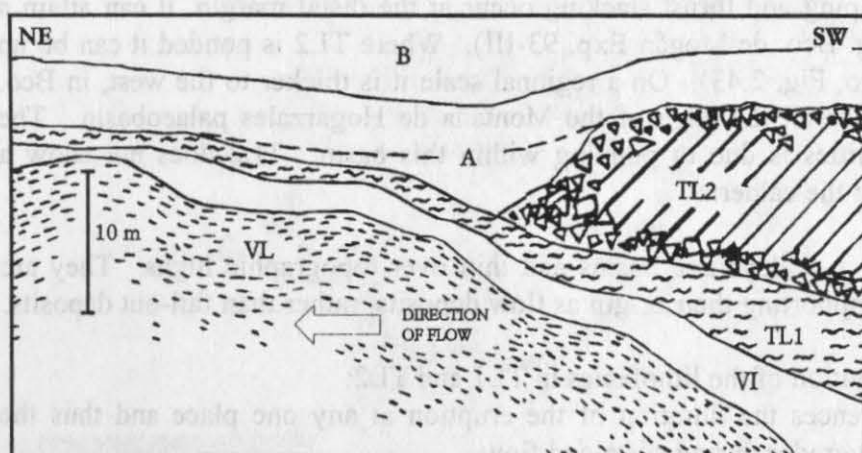


Figure 2.44. Sketch section showing the effect of palaeotopography on the distribution of flow units TL1 and TL2 (Exp. 88, Bco. de Mogán). This variation in distribution is interpreted to be the result of the differing rheology of the two flows (Chapter 7, Section I).

TL1 is a 'high grade' ignimbrite (Section 7.2), with clear vitroclastic texture throughout, while TL2 is an 'extremely high grade' ignimbrite (Section 7.2) showing vertical and lateral gradations to lava-like lithofacies. The preservation of vitroclastic textures throughout TL1 suggests that it was probably the deposit of a relatively cooler flow than TL2. The clasts in the TL1 flow probably welded, during and following deposition, as opposed to those in the TL2 flow which must have mostly agglutinated and coalesced *during* deposition to produce lava-like, lithofacies (depositional mechanisms and timing of welding are discussed in Chapter 7).

The particulate TL1 flow was able to surmount the obstacle produced by VL, and was deposited over the entire hill. The textures in TL2 suggest that it probably flowed in a non-particulate manner for most of its run out and particulate flow may even have ceased by this point (ca. 9km from the vent). Continued non-particulate flow of the pile of agglutinated and coalesced layers would however, have allowed further flow of TL2 beyond its original depositional extent. Without particle supply from the overlying transport regime however, the non-particulate flow then lacked the impetus to flow up and over the palaeohill. As a result the flow crept slowly to a halt forming a steep autobrecciated distal margin (Figs. 2.37 and 2.44).

Effect of TL surface topography on deposition of subsequent units in the Mogán Formation

The irregular surface morphology of TL2 consists of a series of spines (up to 2m in height, Fig. 2.45), resembling those on the upper surface of viscous lava flows. This spiny upper surface has caused a marked variation in the thickness of overlying ignimbrite X.



Figure 2.45. Irregular 'spiny' surface topography of TL2, produced by alternating ramp structures and autobreccia pockets (Section 7.11.2). TL2 is overlain by ignimbrite X at this locality (Exp. 58-59, Bco. de Lechugal).

On the west side of Bco. de Mogán, TL1 is <10m thick and sheet-like. It is overlapped to the west by TL2, which terminates at this locality with a steep (ca. 70 degree) distal margin (Fig. 2.37). This topographical barrier has caused a complex stratigraphy to develop in the overlying units. (Fig. 2.46).

Between exposure 86 and 88, TL1 is overlain by a thin (<80cm) lense of ignimbrite X. Overlying this and TL2 at exposure 88 are two small lenses of trachyandesite lava-flow T4 which is rubbly and poorly consolidated and <6m thick. A thin (<30cm) crystal vitric tuff overlies T4 and overlaps TL2.

Ignimbrite A (<20m thick) has cut a deep side channel over the steep distal margin of TL2 and eroded the crystal vitric tuff, T4 and ignimbrite X until it rests directly on TL1. The following sequence of events (Fig. 2.47) may explain the features observed at this outcrop:

A) Pyroclastic flow X was deposited mantling existing TL2 and TL1 paleotopography. X was very thin, poorly welded and was partly eroded leaving only small remnant lenses.

B) Lava T4 was deposited after ignimbrite X, and flowed over TL2. The rubbly texture suggests it underwent extensive autobrecciation, probably generated by oversteepening of the flow as it passed over the steep distal margin of TL2. This produced a poorly consolidated, thick pile of rubble and loose autobreccia.

C) Fallout lead to the deposition of a thin (<30cm) crystal vitric tuff.

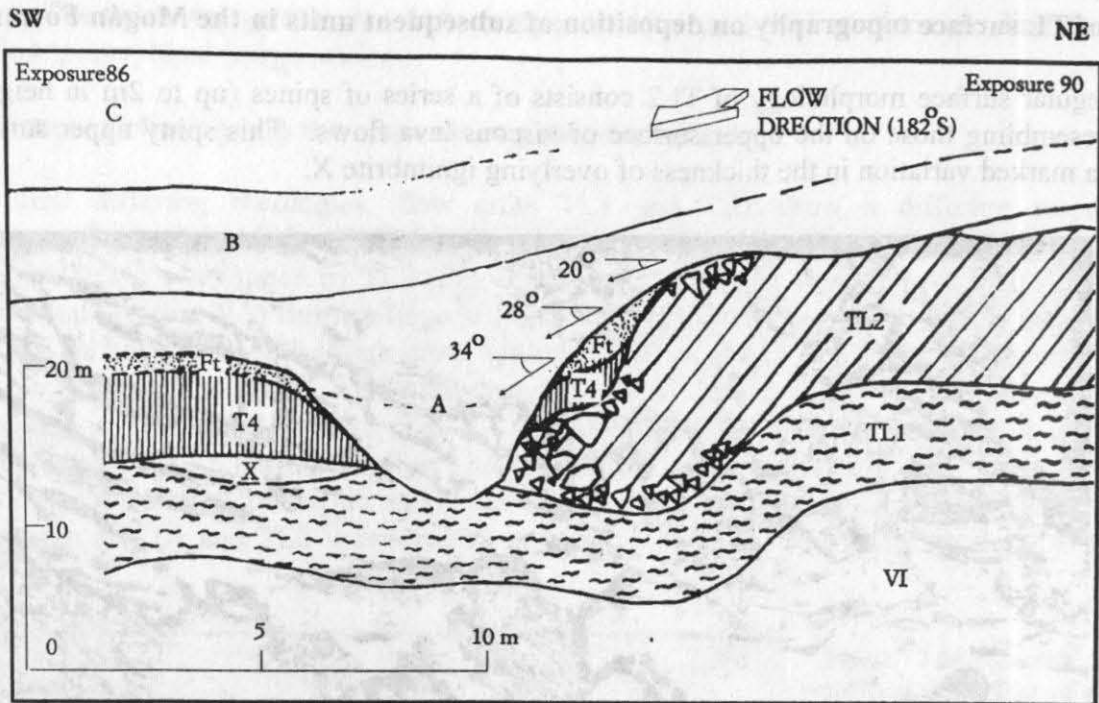


Figure 2.46. Sketch of the steep distal margin of TL2 with overlying units in the Mogán Formation. Degree angles relate to the inclination of fiamme in Upper Mogán Formation ignimbrite A (Localities 86-90, on the west side of Bco. de Mogán).

- D) Ignimbrite A was then deposited by a pyroclastic flow. The steep distal margin of TL2 provided a focal point for erosive channelling and the flow eroded through the poorly consolidated breccia of T4, the thin crystal vitric tuff and weakly welded ignimbrite X.

This has produced a steep channel filled with ignimbrite A, bordered on one side by the distal margin of TL2, with only marginal remnants of T4. On one side this is overlain by thin lenses of the crystal vitric tuff, and on the other side by remnants of X, overlain by T4 and a thin layer of crystal vitric tuff (Fig. 2.46).

2.7.2 Distribution of lithofacies

The regional variation in the distribution TL1 and TL2 and the lithofacies within them is interpreted to be the result of vent migration, magma withdrawal pattern, eruption rate and the duration of each eruptive phase at any given locality (Chapter 6, Section 6.6.2).

Detailed mapping at selected localities however, demonstrates that local variations are due to small-scale irregularities in the palaeorelief, predominantly produced by rhyolite lava VL. These variations are best observed in TL1, as the stratigraphy has not been disrupted by post-depositional deformation.

There is a positive correlation between the thickness of TL1 and the number of lithofacies observed (Section 2.4). Where TL is thickest the maximum number of lithofacies occurs (Fig. 2.7). This suggests that the thickness is not only due to ponding and draining back downslope.

The initial incursion of the TL1 flow deposited the TL comendite Lithofacies Group (Section 2.4.1). Lithofacies of this group filled up the hollows and depressions in the palaeotopography and reduced the surface relief for the later, successively deposited, TL mixed rock Lithofacies Group (Section 2.4.2), and last deposited TL trachyte Lithofacies Group (Section 2.4.3).

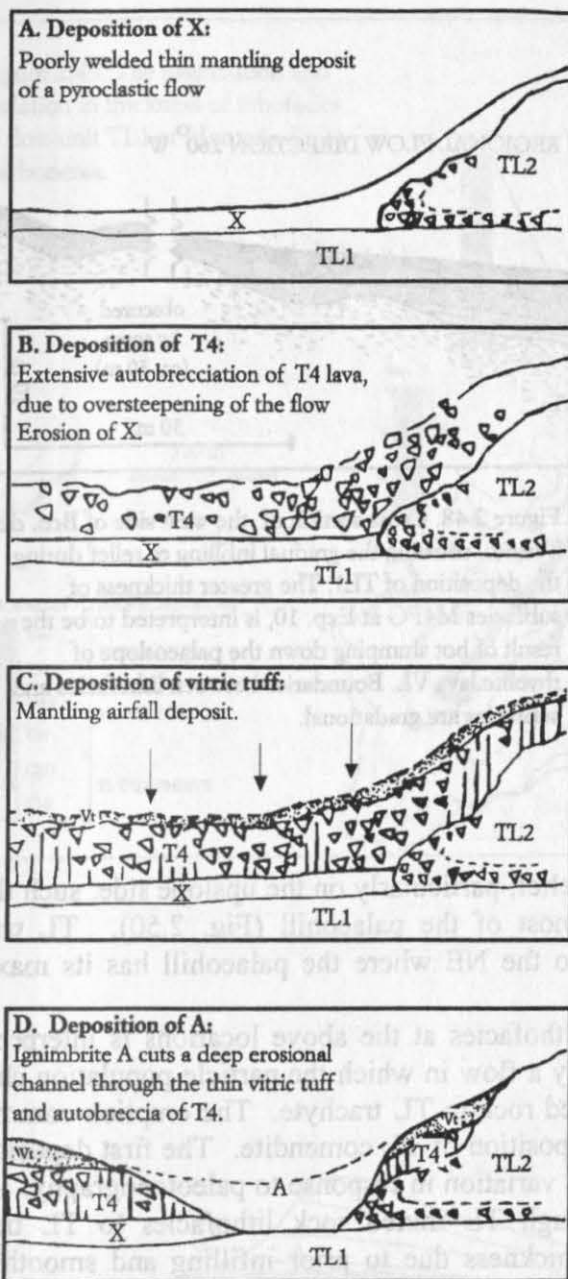
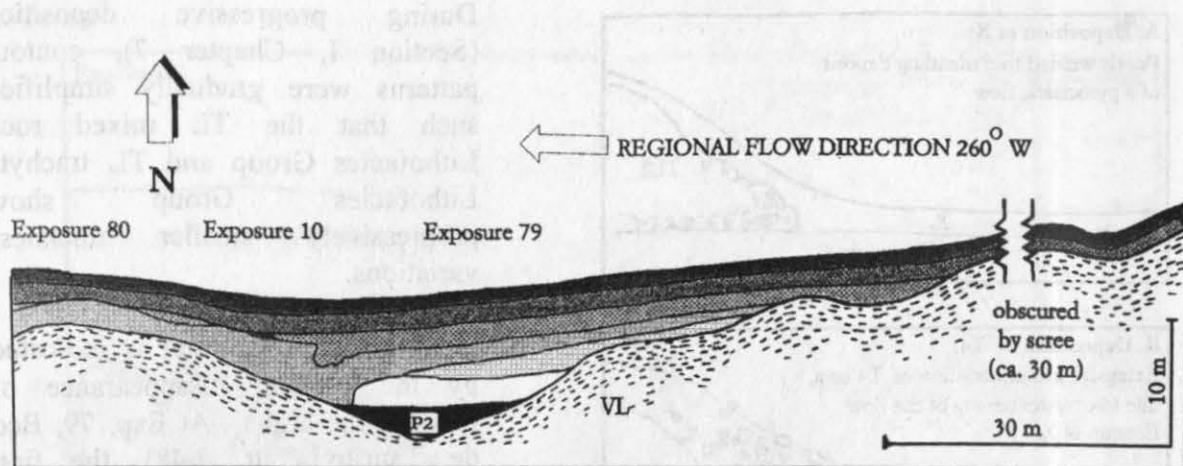


Figure 2.47. Sequential diagrams showing the effect of the steep distal margin of TL2 on the deposition of successive units in the Mogán Formation (see text for details).

During progressive deposition (Section I, Chapter 7), contour patterns were gradually simplified such that the TL mixed rock Lithofacies Group and TL trachyte Lithofacies Group show progressively smaller thickness variations.

Infilling of palaeorelief is indicated by the gradual disappearance of topographic highs. At Exp. 79, Bco de Taurito (Fig. 2.48), the first deposited TL comendite lithofacies thin and pinch out at the channel margins. TL mixed rock lithofacies are present in the channel and over the western overbank area, but thin to a few centimetres and pinch out on the eastern overbank. Build-up of these lithofacies, infilled and smoothed the topography to the extent that later deposited TL trachyte lithofacies were able to completely surmount and cover the ridges in VL (Fig. 2.46), thus blanketing the topography.

Gradual but incomplete burial of topography by TL1 is also illustrated at Montaña de las Carboneras, where a large hill in rhyolite lava VL (draped by VI) is partially covered by TL1 (Figs. 2.49 and 2.50). Measured logs around this palaeotopographic high show the distribution and thickness of lithofacies (Fig. 2.49). Lineations, measured throughout the deposit indicate that the direction of flow was from northwest to southeast (Chapter 3, Fig. 3.11). First deposited TL comendite lithofacies are present on the north and western flanks of the palaeohill (Fig. 2.50). However, they are thickest on the northwestern side where TL1 abuts against the hill. TL mixed rock lithofacies overly TL comendite to the northwest, but transgress and lie directly on the palaeosurface to the southwest and south. Deposition of



Lithofacies and subfacies	Lithofacies Group	
T6w	TL trachyte	FLOW UNIT TL1
T5W		
M4F		
M4FG	TL mixed rock	FLOW UNIT TL1
C3f		
C2D	TL comendite	

Figure 2.48. Cross section of the west side of Bco. de Taurito, showing the gradual infilling of relief during the deposition of TL1. The greater thickness of subfacies M4FG at Exp. 10, is interpreted to be the result of hot slumping down the palaeoslope of rhyolite lava VL. Boundaries between lithofacies and subfacies are gradational.

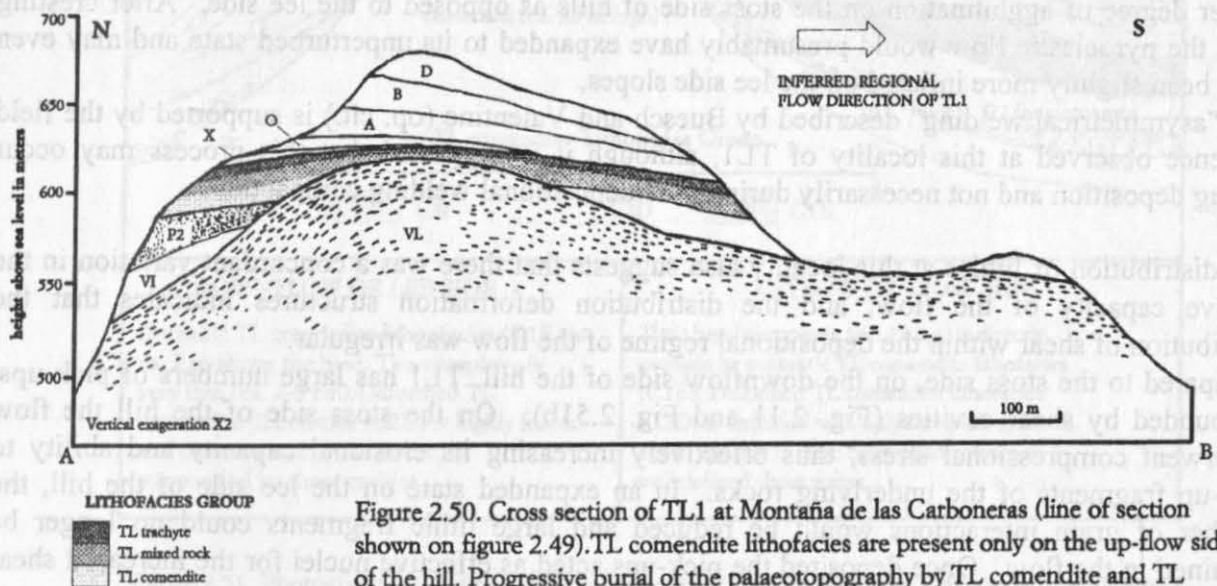
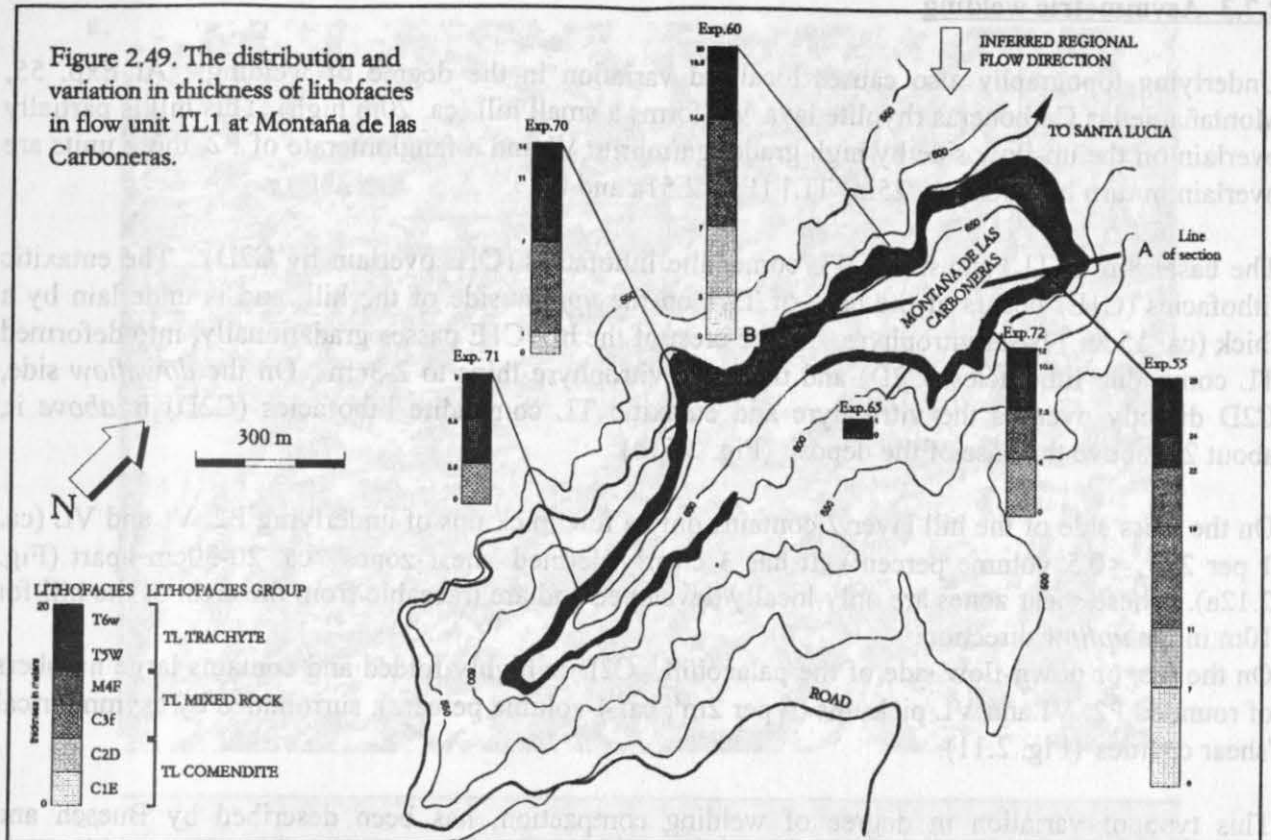
these lithofacies reduced the angle of the palaeorelief, particularly on the upslope side, such that the later deposited TL trachyte lithofacies cover most of the palaeohill (Fig. 2.50). TL trachyte lithofacies are missing only in a small sector to the NE where the palaeohill has its maximum height of 654m.a.s.l. (Fig. 2.49).

The variation in thickness and distribution of lithofacies at the above locations is interpreted to represent the progressive burial of topography, by a flow in which the particle population changed over time, from TL comendite, through TL mixed rock to TL trachyte. The eruption commenced with the evacuation, transport and subsequent deposition of TL comendite. The first deposited TL comendite lithofacies show the greatest thickness variation in response to paleotopography. As the eruption continued, deposition progressed through TL mixed rock lithofacies to TL trachyte lithofacies, which show the least variation in thickness due to prior infilling and smoothing of surface relief.

The thickness variations are a result of the flows' ability to surmount elevations which increases as the topography is buried. However the duration of deposition (at any one locality) during sustained passage of the flow, post depositional welding compaction and late stage hot slumping downslope also influence the thickness of the flow unit and the lithofacies within it.

Hot slumping has occurred at exposure 79, in Bco. de Taurito (Fig. 2.48). TL mixed rock lithofacies (subfacies M4FG) show a marked increase in thickness at the western edge of the channel in Bco. de Taurito and appear to have partially displaced underlying TL comendite lithofacies in the base of the channel.

In general however, the preservation of smooth, gradual transitions from lithofacies to lithofacies argues against large scale rheomorphism, which would almost certainly have disturbed the layering and caused disruption of the gradational boundaries.



2.7.3 Asymmetric welding

Underlying topography also causes localised variation in the degree of welding. At Exp. 55, Montaña de las Carboneras rhyolite lava VL forms a small hill (ca. 20m high). This hill is partially overlain on the up-flow side by high grade ignimbrite VI and a fanglomerate of P2, these units are overlain in turn by thick (ca. 25m) TL1 (Fig. 2.51a and b).

The basal 8m of TL1 consist of TL comendite lithofacies (C1E overlain by C2D). The eutaxitic lithofacies (C1E) occurs at the base of TL1 on the *upflow* side of the hill, and is underlain by a thick (ca. 15cm) basal vitrophyre. At the crest of the hill C1E passes gradationally, into deformed TL comendite lithofacies (C2D) and the basal vitrophyre thins to 2-3cm. On the *downflow* side, C2D directly overlies the vitrophyre and eutaxitic TL comendite lithofacies (C2D) is *above* it, about 2m above the base of the deposit (Fig. 2.51b).

On the stoss side of the hill layer 2 contains only a few pick ups of underlying P2, VI and VL (ca. 1 per 2m², <0.5 volume percent). It has 3 clearly defined 'shear zones' ca. 20-30cm apart (Fig. 2.12a). These shear zones are only locally developed and are traceable from the crest of the hill for 10m in the *upflow* direction.

On the lee, or down-flow side of the palaeohill, C2D is highly folded and contains large numbers of rounded P2, VI and VL pick-ups (6 per 2m², ca. 4 volume percent), surrounded by asymmetrical 'shear cavities' (Fig. 2.11).

This type of variation in degree of welding compaction, has been described by Buesch and Valentine (1989) from the Peach Springs Tuff. They attribute this "asymmetrical welding" to increased compaction of the pyroclastic flow material when it impinges on the stoss side of palaeohills. In a compacted state, the shards have greater sheared compaction areas, resulting in better welding efficiency.

However 'asymmetrical welding' could also be produced *during* deposition by slowing down and compression of the transport regime or particulate flow (Fig. 7.9). This would lead to a greater number of clast collisions and deposited particles would be more highly compacted, resulting in a higher degree of agglutination on the stoss side of hills as opposed to the lee side. After cresting hills, the pyroclastic flow would presumably have expanded to its unperturbed state and may even have been slightly more inflated on the lee side slopes.

The "asymmetrical welding" described by Buesch and Valentine (op. cit.) is supported by the field evidence observed at this locality of TL1, although it is suggested that this process may occur *during* deposition and not necessarily during post-depositional welding compaction.

The distribution of lithics at this locality also suggests that there was a concordant variation in the erosive capacity of the flow, and the distribution deformation structures indicates that the distribution of shear within the depositional regime of the flow was irregular.

Compared to the stoss side, on the downflow side of the hill, TL1 has large numbers of pick-ups, surrounded by shear cavities (Fig. 2.11 and Fig. 2.51b). On the stoss side of the hill the flow underwent compressional stress, thus effectively increasing its erosional capacity and ability to pick-up fragments of the underlying rocks. In an expanded state on the lee side of the hill, the number of grain interactions would be reduced and large lithic fragments could no longer be entrained in the flow. Once deposited the pick-ups acted as effective nuclei for the increased shear produced by the speeding up of the flow in its expanded state.

On the stoss side of the hill, as the flow compacted, the interstitial gas would be trapped within the deposit and compressed into a smaller volume, or transferred from the lower part to the upper part of the flow by a process similar to filter pressing. Buesch and Valentine (op. cit.) suggested that

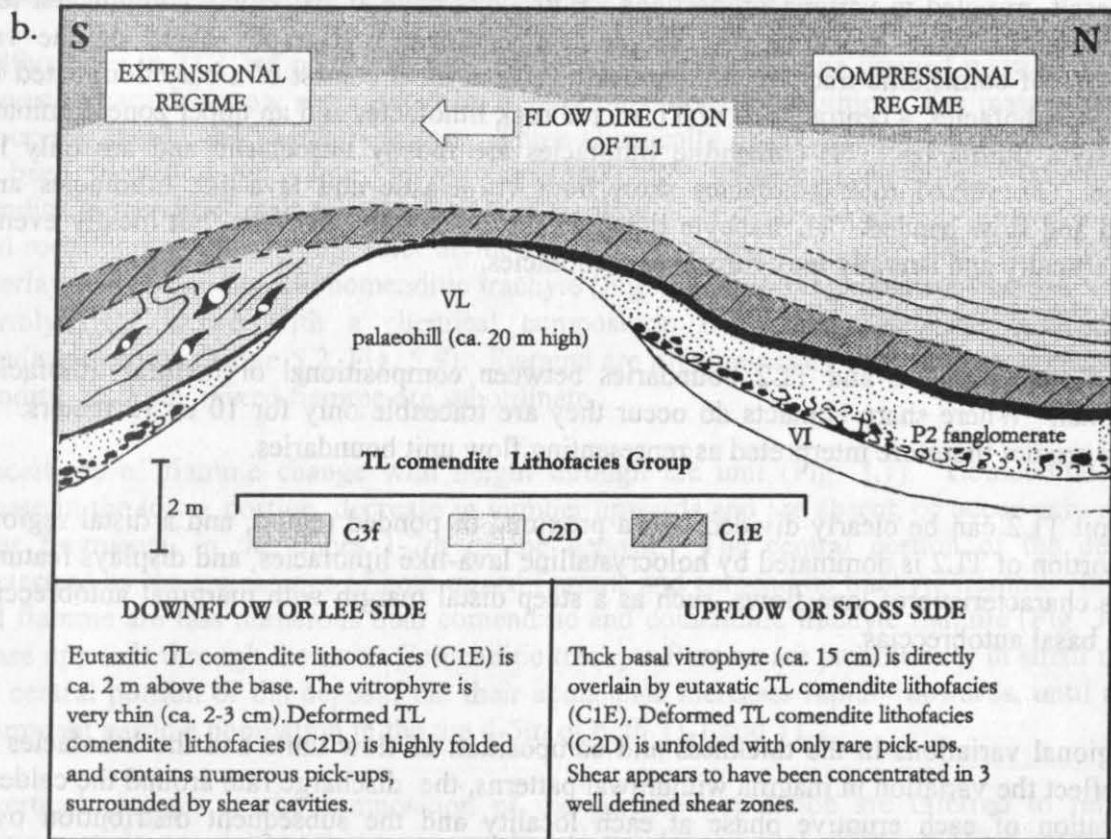
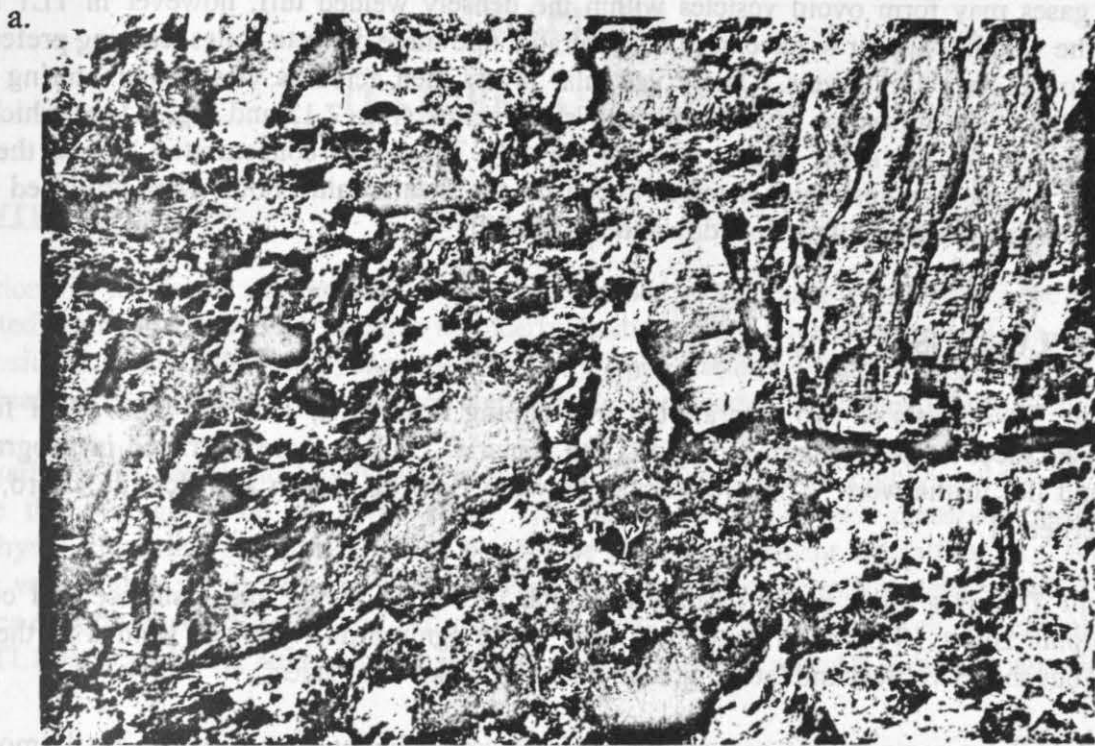


Figure 2.51. Photograph (a) and field sketch (b) showing how the height of the 'zone of maximum intensity of welding' (lithofacies C1E) varies around palaeotopographic highs. Welding is asymmetrical, this is interpreted to be the result of variation in the stress regime during deposition (TL1, Exp. 55, Montafia de las Carboneras).

trapped gases may form ovoid vesicles within the densely welded tuff, however in TL1 at this locality the volatiles appear to have been concentrated into three discrete zones, causing preferential vesiculation in very thin layers. These vesicular layers then acted as weak points during shear. This resulted in the formation of three discrete 'shear zones' (Fig. 2.12 and Fig. 2.51b) which took up the majority of the shear strain. On the lee side, 'shear was concentrated around the large number of ridged pick-ups which acted as nuclei for the shear strain. Folds were produced by hot slumping of the non-particulate flow down the palaeohill.

2.8 CONCLUSIONS

Ignimbrite TL consists of two separate but overlapping flow units; TL1 and TL2. TL1 forms a widespread sheet in the southern sector of Gran Canaria. TL2 is more restricted in geographical extent and lies to the west. The two overlap between Bco. de Mogán and Bco. de Tauro, where TL2 overlies TL1.

Flow unit TL1 is a 'high grade' ignimbrite which is welded to the upper surface and contains rheomorphic zones. TL2 is an 'extremely high grade' ignimbrite, which is welded to the upper surface, but shows vertical and lateral gradations to lava-like lithofacies.

TL1 and TL2 are composed of comenditic trachyte, comendite and more rarely small amounts of trachybasalt, mingled in varying proportions. Both units have an extremely complicated textural stratigraphy, but there is a relatively simple compositional stratigraphy based on the varying proportions of comenditic trachyte and comendite. Both units consist of a base dominated by TL comendite lithofacies, a central zone of TL mixed rock lithofacies and an upper zone dominated by TL trachyte lithofacies. TL comendite lithofacies are mostly vitroclastic and are only locally lava-like. TL mixed rock lithofacies show both vitroclastic and lava-like lithofacies and are marbled and flow banded. TL trachyte lithofacies are generally lava-like, but locally even these grade vertically and laterally into vitroclastic lithofacies.

Within flow units TL1 and TL2 boundaries between compositional or textural lithofacies are gradational. Where sharp contacts do occur they are traceable only for 10 or 12 meters. These contacts are not therefore interpreted as representing flow unit boundaries.

Flow unit TL2 can be clearly divided into a proximal or ponded region, and a distal region. The distal portion of TL2 is dominated by holocrystalline lava-like lithofacies, and displays features and textures characteristic of lava flows, such as a steep distal margin with marginal autobreccia, and top and basal autobreccias.

The regional variations in the thickness and composition of flow units and the lithofacies within them reflect the variation in magma withdrawal patterns, the discharge rate around the caldera rim, the duration of each eruptive phase at each locality and the subsequent distribution over the palaeorelief. The tri-part division of the two flow units at all localities is strong evidence for the eruption of these components from the same magma chamber (Schmincke 1969a).

CHAPTER 3

TEXTURES AND FABRICS

3.1 INTRODUCTION

Variations in the fabric and texture of TL are described in this chapter. Most of the data were collected from flow unit TL1 because its clearly clastic texture allows analysis of the shapes and compositions of individual component particles. TL1 has a relatively simple chemical and textural stratification (Fig. 2.4a) that has not been significantly disturbed by late stage deformation.

TL1 varies from weakly to highly welded (Fig. 4.27). 'Weakly' and 'highly' welded are used to denote the average strain of pyroclasts. Vitroclastic texture is best preserved in the basal vitrophyre, which has not been effected by intense post-emplacement crystallisation. Where the tuff is very highly welded e.g. in TL2, extreme distortion of clasts makes determination of clast outlines of individual particles very difficult. Thus, moderately to highly welded vertical profiles from TL1 were analysed, although examples are drawn from TL2 where it is clearly vitroclastic.

3.2 VARIATION IN PARTICLE COMPOSITION WITH HEIGHT

The lithofacies in TL1 are poorly sorted, consisting of lapilli and fine grained matrix. The lapilli are juvenile particles (now represented by fiamme) and accidental lithics. The matrix consists of phenocrysts, shards and shard fragments. Three chemically discrete juvenile particle populations have been identified by colour, morphology and XRF analysis (Chapter 5). These include comendite, comenditic trachyte and mixed rock fiamme.

Mixed rock fiamme have been further divided into: compositionally banded fiamme, which consist of interlayered comendite and comenditic trachyte (Fig. 6.4d), and intermediate fiamme, which are uniformly light brown with a chemical composition intermediate between comendite and comenditic trachyte (Table 5.2, Fig. 5.9). Fiamme are predominantly composed of comendite and comenditic trachyte, mixed fiamme are subordinate.

Compositions of fiamme change with height through the unit (Fig. 3.1). Comenditic fiamme dominate in the lower portion, decrease in number upwards and are absent, or occur only rarely as angular fragments, in the upper 1-2m of the deposit. The central portion of the deposit is characterised by the appearance of both mixed fiamme and comenditic trachyte fiamme. In general mixed fiamme are less numerous than comenditic and comenditic trachyte fiamme (Fig. 3.1), and decrease upwards through the unit. Comenditic trachyte fiamme are present only in small numbers in the central portion of the deposit, but their abundance increases rapidly upwards, until they are the dominant particle population in the top 4-5m of both TL1 and TL2.

The vertical changes in the composition of the particle population are inferred to reflect the changing particle populations that were supplied to the depositional regime of the flow with time. The systematic vertical variation in the distribution of comendite, comenditic trachyte and mixed fiamme indicate that the depositional regime of the flow was initially supplied with comendite particles, followed by increasing proportions of mixed and comenditic trachyte particles, with a corresponding decrease in the number of comendite particles. Finally only comenditic trachyte particles were supplied to the site of deposition.

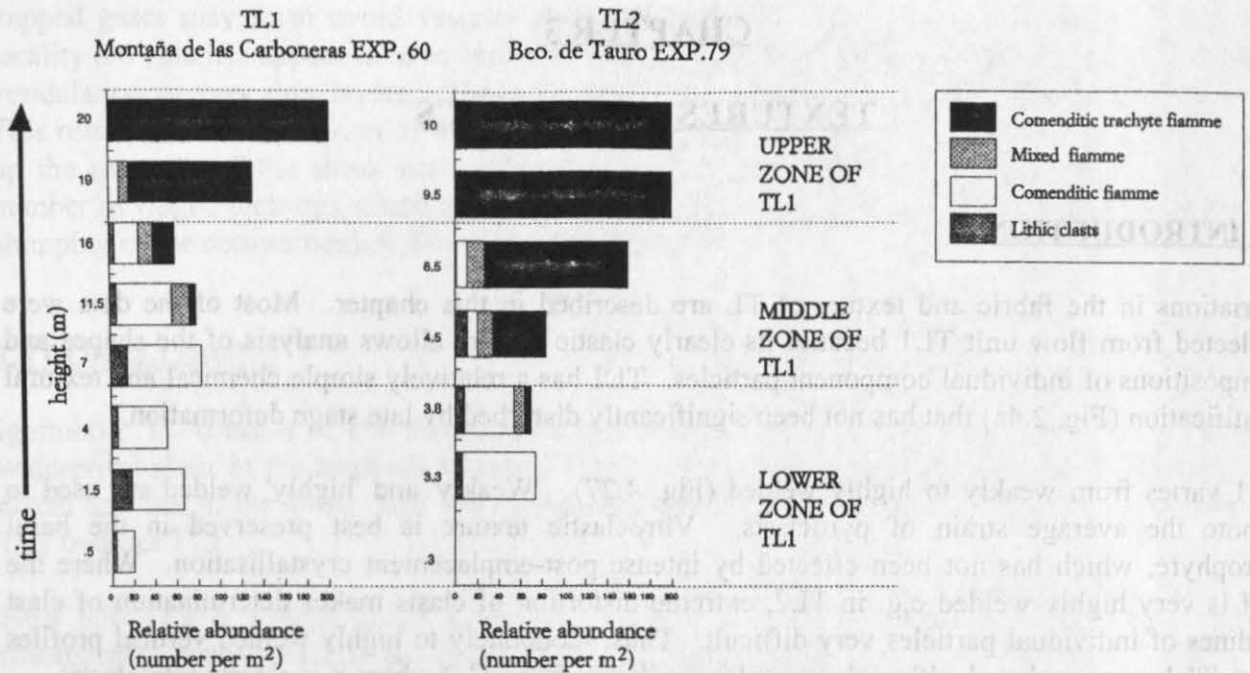


Figure 3.1. Variation in chemical composition of juvenile clasts, with height, in TL1. Accidental lithics are also included. Changes in juvenile particle composition with height are interpreted to represent the changing supply of particles to the depositional regime of the flow over time.

The non-juvenile clasts in TL are accidental lithic fragments, which were rigid when they were entrained in the magma or transport regime of the pyroclastic flow. These include 'pick-ups' derived from erosion of the underlying stratigraphy and accessory lithics incorporated during conduit and vent erosion (Section 4.4.3).

Accidental lithics also decrease in number with increasing height through the unit. This variation is also consistent with a changing particle supply to the depositional regime of the flow, and may relate to the progressive burial of the landscape by aggrading tuff, and a decrease in wall rock erosion at the conduit and vent during the course of the eruption.

Lithics are absent in the upper 4-5m of the deposit. This part of the ignimbrite is interpreted as having been deposited during waning flow conditions (Section 3.5) when the lithic transport limits had migrated considerably upstream and dense lithics could no longer be transported for large distances. Alternatively if flow was waning the vent would be closing up due to accretion and not eroding, and the flow may have ceased to be erosional in proximal areas.

3.3 FIAMME MORPHOLOGY AND DEFORMATION

Having considered the variations in particle composition with height as a function of time, the variations within the compositionally discrete particle populations are now described. Five basic clast shapes are displayed by the juvenile particles in TL1, these also occur in vitroclastic parts of TL2 (Table 3.1).

Although the post-deposition and deformation morphology of fiamme does not necessarily reflect the original morphology of the juvenile clast, it is important to consider the pre-deposition morphology of the clasts as this may provide some information about the magma chemistry, viscosity, volatile content, eruptive temperature and type of volcanic explosivity. The height and

Composition	Post deposition and welding morphology	Suggested original morphology produced by fragmentation	Controlling Factors
comendite	flattened pumice clast	expanded pumice lapilli	
↓	flattened poorly vesicular scoria	poorly vesicular spatter lump	
comenditic trachyte	broken, folded, blocky or platy scoria	elongate, weakly vesicular scoria rag	
↓	highly folded ribbons	scoria ribbons, unfolded but possibly twisted during flight	
↓	spherical lapilli	fluidal droplets	

Table 3.1. Variation in fiamme morphology with changing chemical composition in TL. Suggested pre-deformation morphology and possible controlling factors are given.

particle concentration of the eruption column effects the degree of cooling of the clasts during transport through the air, and the eruption violence influences the sizes of the clasts.

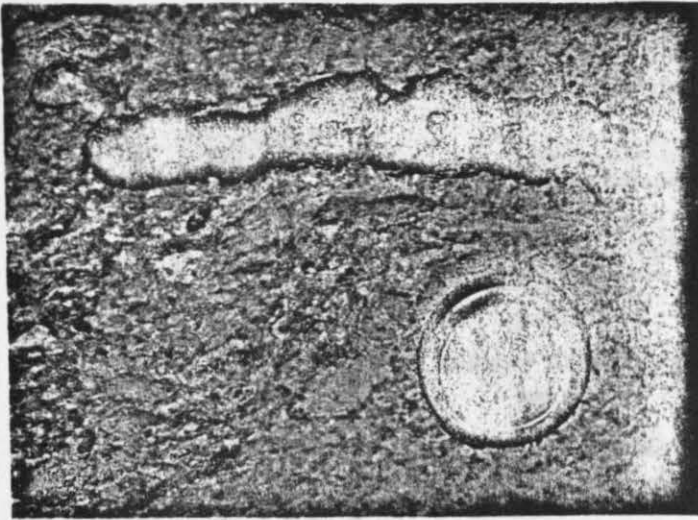
The term 'fiamme' is commonly used synonymously with "flattened pumice lapilli" and has been used to imply welding, and even emplacement by pyroclastic flow (e.g. Millward and Lawrence, 1985). However fiamme have been recorded in many other rocks, including lavas (Fig. 2.36), agglutinates, scoria flows, welded air fall, and can even be produced by diagenetic processes (Branney and Sparks, 1991) and magma-mixing. Gibson and Tazieff (1967) described lumps of spatter, as 'fiamme' and these can be indistinguishable from fiamme derived from flattened pumice lapilli. Clearly, 'fiamme' should not be used to denote a certain type of pyroclast, or a specific mode of emplacement or flattening. For the purpose of this work, the term fiamme (Section 1.5) is used to describe *any* sheared juvenile clast.

Figure 3.2 shows that many of the fiamme in TL were never originally highly expanded pumice lapilli, subsequently flattened during agglutination and syn-depositional shear, or by post depositional welding compaction.

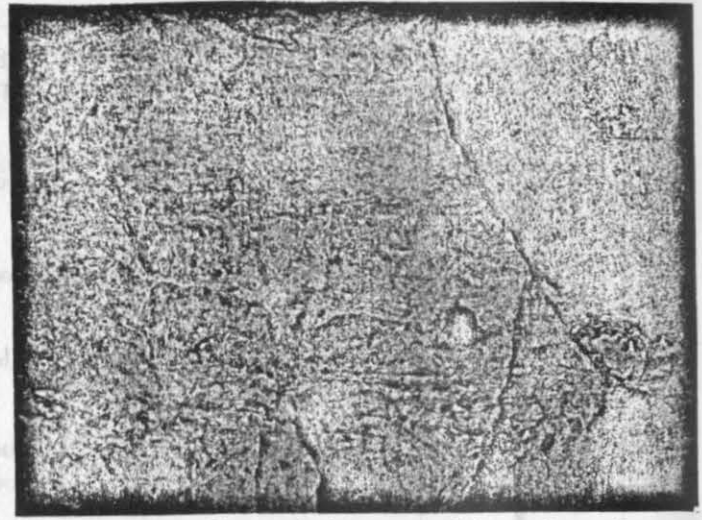
Juvenile clast morphologies range from flattened pumice lapilli through scoria rags and ribbons to near spherical lapilli. The shape of the clasts varies with chemical composition (Table 3.1). Comenditic clasts are usually highly vesicular, flattened pumice lapilli, that show several stages of vesiculation, collapse and re-vesiculation (Fig. 4.20). Comenditic trachyte fiamme have more diverse morphologies and range from flattened, poorly vesicular scoria or spatter (Fig. 3.2a); through folded or fractured, blocky, platy, poorly vesicular scoria (Fig. 3.2d) to highly folded scoria "ribbons" (Fig. 3.2b and c) and spherical lapilli (Fig. 2.17).

Two types of discontinuous, flattened vesicular "lenses" of comendite (Fig. 3.2f), resembling comenditic fiamme have also been identified in TL: (1) Highly expanded, intensely vesiculated

Figure 3.2. Variation in morphology of juvenile clasts in TL. The lens cap is 5.5 cm in diameter.



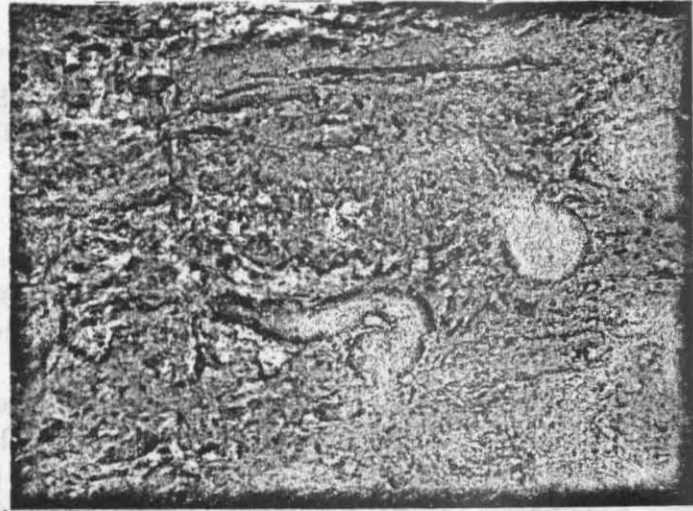
a) Blocky comenditic trachyte fiamme, interpreted as platey poorly vesicular scoria rag. Enclosing pale matrix is comendite rich.



b) Folded, weakly vesicular comenditic trachyte fiamme, interpreted as formerly elongate scoria rag. Inferred flow direction from left to right of photograph. Enclosing pale matrix is comendite rich.



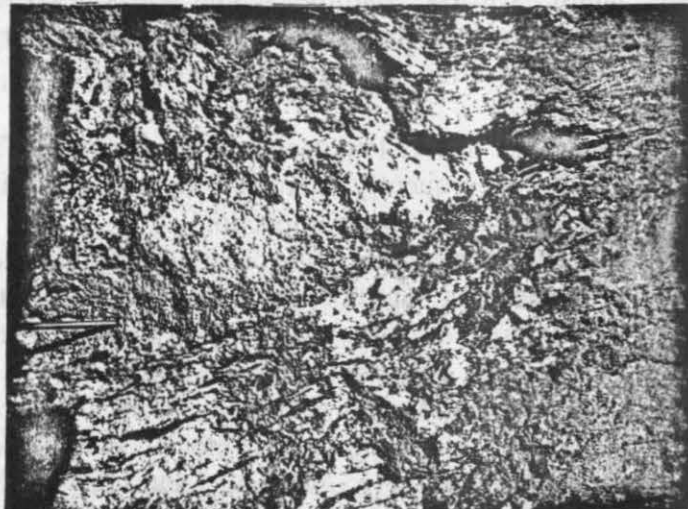
c) Highly folded comenditic trachyte fiamme, interpreted as a former scoria ribbon during particulate transport. The fold axes point in the downflow direction (inferred to be towards the right of the photograph).



d) Blocky comenditic trachyte fiamme interpreted as a former scoria clast, overfolded in the downflow direction (towards the right of the photograph).



e) Two populations of juvenile particles. White, vesicular comenditic fiamme, some of which may be flattened pumice lapilli, and black, poorly vesicular comenditic trachyte fiamme, which are interpreted as former scoria clasts or rags. Note vertical orientation of the large comenditic trachyte scoria rag (to right of photograph) and the blocky, platy comenditic trachyte clasts (centre of photograph).



f) A highly vesicular comenditic pumice lense. Because of its large size this is interpreted as an area of intensely reveesiculated comenditic matrix, not a former pumice clast. The scale is 14cm long.

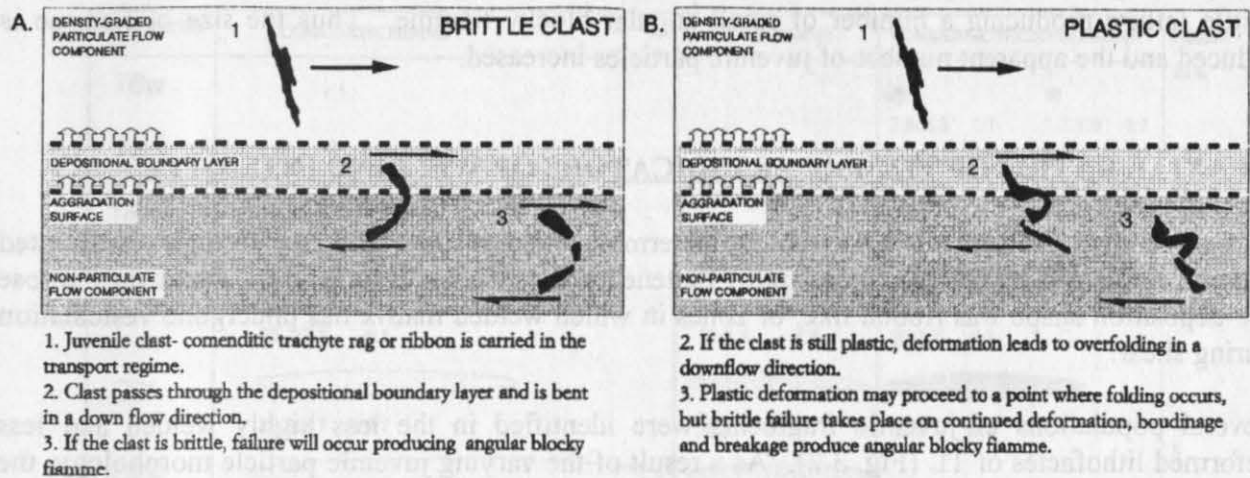


Figure 3.3. Development of differing morphologies in comenditic trachyte fiamme of lithofacies M4F in TL1.

lenses (up to 56cm in length and 35 cm in width) with sharp to gradational boundaries resembling "pumice lenses", and (2) Weakly vesicular comendite lenses (up to 2m in length and 50cm in width). It is unlikely that either of these features are flattened pumice lapilli, as they would have to represent clasts which were <1m in diameter prior to flattening. It seems unrealistic that the high explosivity resulting in the formation of pumice could have produced clasts of this size, and that delicate pumice could have been transported to distal regions without being broken up. These lenses probably represent large clots of juvenile magma evacuated from the chamber during the maximum mass flux of the eruption, and subsequently entrained in the non-particulate flow. Their chemistry (Fig. 5.9, group A) is the most evolved composition for comendite and probably represents the most fractionated magma, residing near the top of the chamber. This magma may have remained trapped at the 'shoulders' of the chamber until the mass flux was sufficiently high to cause entrainment in the eruption stream. The rounded shape of the vesicles suggests that these lenses underwent post-depositional vesiculation which in some cases was intense, producing pumice lenses.

In many cases, deformation of fiamme during deposition and rheomorphism has made it difficult to define the original clast morphology. Figure 3.3 shows the suggested sequence of events leading to the observed morphologies of comenditic trachyte fiamme in TL1. There are two possible explanations for the observed clast morphologies: If deposition occurred 'en masse' followed by welding compaction, deformation of fiamme may have occurred during subsequent rheomorphism (Fig. 7.4, 1). Under these circumstances, deformation of the welded matrix around the clasts should be observed. This however, is not the case, only individual fiamme are deformed and folded and they are enclosed in non-deformed matrix (e.g. Fig 3.2c).

The low strain exhibited by matrix compared to large clasts suggests that deformation was syn-depositional, occurring during aggradation of the unit (Fig. 7.4, 3), and preferentially affecting larger juvenile clasts. If for example, due to spinning during transport, a scoria rag was in a near vertical position when it reached the aggradation surface (Fig. 3.3a), rather than being sheared towards a horizontal position, it would be bent over, convex to the downflow direction, as it passed through the depositional boundary layer. If the clast was brittle (e.g. cool or degassed), failure would occur producing two or more angular blocky or platy fiamme. However, if the clast was sufficiently plastic (e.g. hot and gas rich), it may fold, forming a sigmoidal fiamme with the fold

axis pointing downflow (Fig. 3.3b). With continued folding, plastic behaviour may give way to brittle failure producing a number of small angular blocky fiamme. Thus the size of fiamme is reduced and the apparent number of juvenile particles increased.

3.4 AXIAL RATIOS OF FIAMME AS INDICATORS OF WELDING INTENSITY

In many high grade tuffs it is impossible to determine whether some lenticular or highly attenuated fiamme represent flattened pumice lapilli; flattened non-vesicular lava lumps; scoria rags whose pre-deposition shape was ribbon like; or zones in which welded matrix has undergone vesiculation during shear.

Several populations of juvenile fragments were identified in the less highly welded and less deformed lithofacies of TL (Fig. 3.2). As a result of the varying juvenile particle morphology, the value of axial ratios of fiamme, commonly used to show the variation in the degree of welding compaction through vertical profiles, must be seriously questioned. Fiamme axial ratios *do not* simply record welding intensity. The axial ratio of a highly folded comenditic trachyte ribbon in TL cannot be compared to that of a flattened comenditic pumice clast in TL, because their original shapes were quite different.

However once discrete populations of juvenile clasts are recognised, the axial ratios *within* a single population can be compared to give an indication of the variation in intensity of welding and deformation. Variation in eruption rate, based on the size of clasts, can also be inferred from the size variation within each population.

3.5 VARIATION IN AXIAL RATIOS OF FIAMME IN TL

The variation intensity of agglutination and post-emplacement welding is described for the chemically discrete particle populations in TL1 from two separate localities (Exp. 60, Montaña de las Carboneras and Exp. 79, Bco. de Taurito). Vertical profiles at these localities show how the axial ratios of fiamme change with height through the unit.

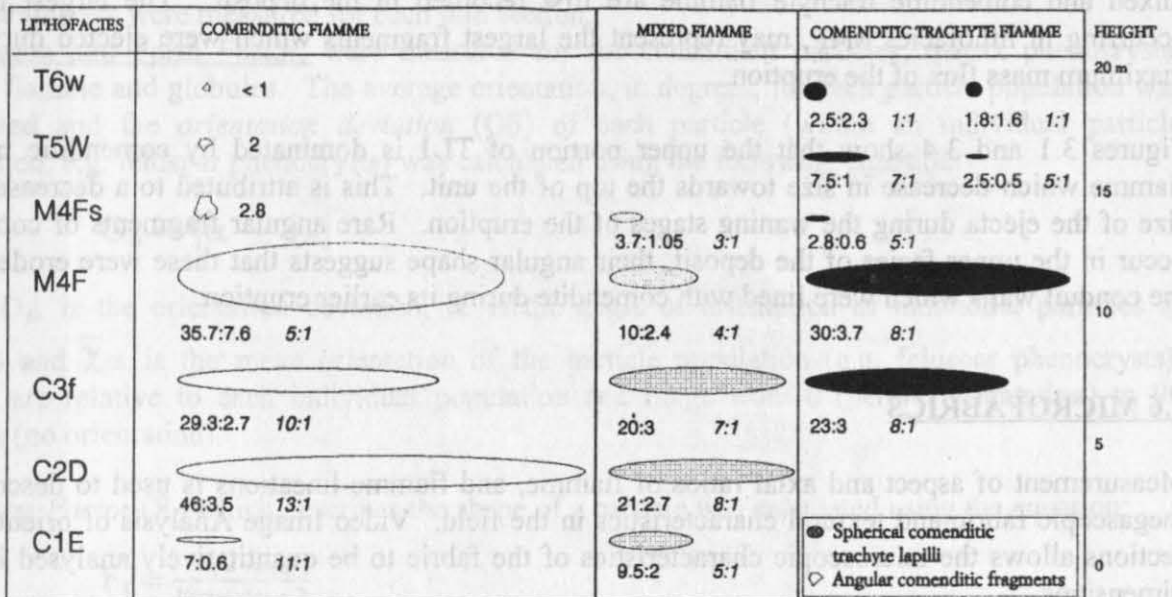
The size of individual clasts and the dominance of a particular particle population also change with height. This is attributed to variation in erupted material and hence the change in the particle population supplied to the depositional regime of a sustained flow through time. In addition, segregation processes within the flow may also contribute to localised accumulations of particles of a particular composition and density.

Figure 3.4 shows the variation in the average apparent size and average axial ratio of fiamme with height through flow unit TL1 at (a) Exp. 60, Montaña de las Carboneras and (b) Exp. 79, Bco. de Taurito. In both cases, fiamme show a variation in size which may be related to eruption rate, with the largest fiamme size being produced during the maximum mass flux. This does not necessarily coincide with the explosivity maxima, as this would produce particles of a smaller size. At both localities (Fig. 3.4) the largest fiamme occur in lithofacies M4F (approximately in the middle of the deposit). This significantly coincides with the first appearance in the deposit of both mixed and comenditic trachyte fiamme. Sparks, Sigurdsson and Wilson (1977) have demonstrated that the injection of hotter, more basic magma (in this case trachyte) into an eruptive stream of more acid magma (comendite) can cause an increase in eruption rate.

An increased eruption rate facilitates erosion and widening of the conduit, which then further increases the eruption rate. Evidence for erosion and widening of the conduit is suggested by the 'peak' in the accidental lithic content on the histograms in Figure 3.1. This peak occurs where

a.

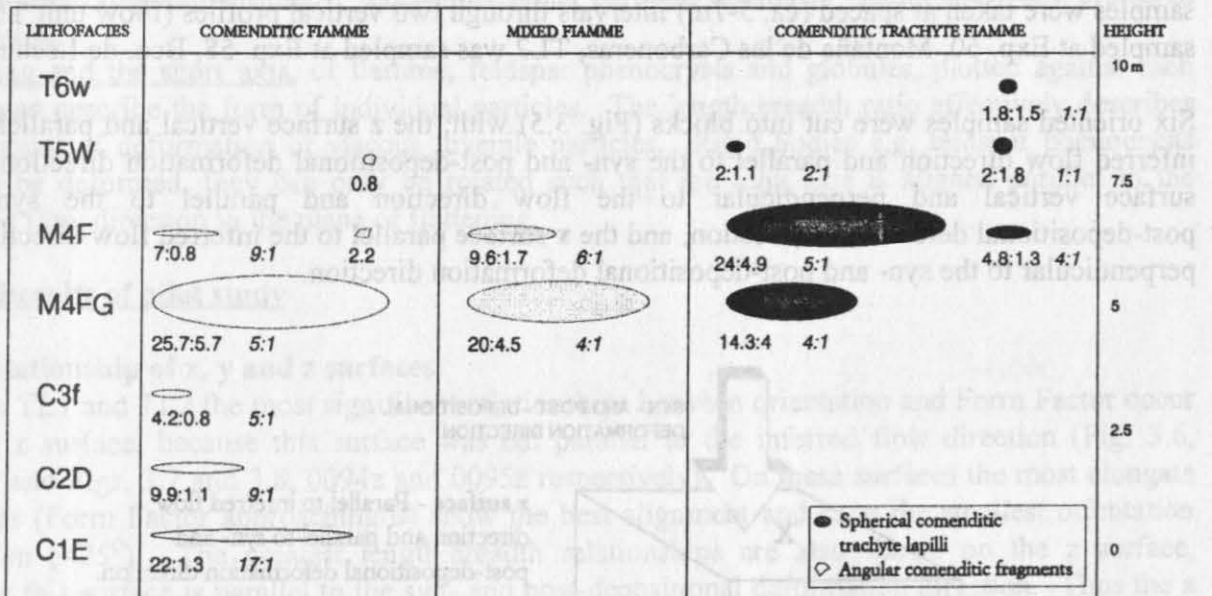
Axial Ratio (width vs. height in cm)



2 = diameter in cm
 46:3.5 = average apparent size in cm
 13:1 = average axial ratio

b.

Axial Ratio (width vs. height in cm)



2 = diameter in cm
 46:3.5 = average apparent size in cm
 13:1 = average axial ratio

c.

Aspect Ratio	Facies	a:b:c
	6	2.5 : 2.9 : 1.75
	5	3.6 : 7.5 : 7
	4	16.8 : 32.3 : 8
	3	10.3 : 19.3 : 1.5
	2	3.2 : 14 : 0.8
	1	3.1 : 6.8 : 0.5

Figure 3.4. Variation in average apparent size and average axial ratio of fiamme, related to chemical composition and height, within flow unit TL1. (a) Exp. 60, Montaña de las Carboneras, (b) Exp. 76, Bco. de Taurito, (c) variation in aspect ratio of composite fiamme population with height at Exp. 60, Montaña de las Carboneras.

mixed and comenditic trachyte fiamme are first recorded in the deposit. The largest fiamme occurring in lithofacies M4F, may represent the largest fragments which were ejected during the maximum mass flux of the eruption.

Figures 3.1 and 3.4 show that the upper portion of TL1 is dominated by comenditic trachyte fiamme which decrease in size towards the top of the unit. This is attributed to a decrease in the size of the ejecta during the waning stages of the eruption. Rare angular fragments of comendite occur in the upper facies of the deposit, their angular shape suggests that these were eroded from the conduit walls which were lined with comendite during its earlier eruption.

3.6 MICROFABRICS

Measurement of aspect and axial ratios of fiamme, and fiamme lineations is used to describe the megascopic fabric and textural characteristics in the field. Video Image Analysis of oriented thin sections allows the microscopic characteristics of the fabric to be quantitatively analysed in three dimensions.

As a pilot study, several oriented samples were taken parallel to the regional inferred flow direction. Flow direction was inferred from the dip and strike of lineations within a barranco. The samples were taken at spaced (ca. 5-7m) intervals through two vertical profiles (Flow unit TL1 was sampled at Exp. 60, Montaña de las Carboneras, TL2 was sampled at Exp. 58, Bco. de Lechugal).

Six oriented samples were cut into blocks (Fig. 3.5) with; the z surface vertical and parallel to the inferred flow direction and parallel to the syn- and post-depositional deformation direction, the y surface vertical and perpendicular to the flow direction and parallel to the syn- and post-depositional deformation direction, and the x surface parallel to the inferred flow direction and perpendicular to the syn- and post-depositional deformation direction.

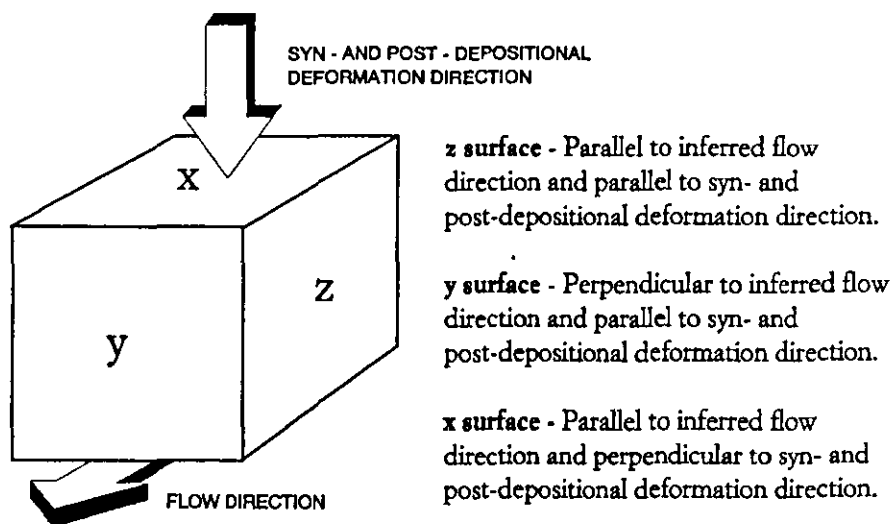


Figure 3.5. Orientation of cut surfaces with respect to inferred flow direction and syn- and post-depositional deformation direction. Thin sections of x, y and z surfaces were used for video image analysis.

Four parameters were measured for each thin section;

Orientation and Form Factor, were measured for the constituent particles; matrix phenocrysts, lithics, fiamme and globules. The average orientation, in degrees, for each particle population was calculated and the *orientation deviation* ($O\delta$) of each particle (within an individual particle population, e.g. feldspar phenocrysts) was calculated using the following equation:

$$O\delta = |\alpha - \bar{\chi}_\alpha|$$

where $O\delta$ is the orientation deviation, α is the angle of orientation of individual particles in degrees and $\bar{\chi}_\alpha$ is the mean orientation of the particle population (e.g. feldspar phenocrysts). Values are relative to each individual population and range from 0 (perfect orientation) to 90 degrees (no orientation).

The *Form Factor* (F_f) which describes the shape of a particle was calculated using the equation:

$$F_f = \frac{4\pi \cdot \text{Area}}{\text{Perimeter} \cdot 2}$$

The area and perimeter of the clasts were measured on the x, y or z surface depending on the cut of the section (Fig. 3.5). Values range from 0, where the form is a stick, to 1 where the form is a perfect circle (equidimensional). Equidimensional particles obviously cannot show any preferred orientation.

The long and the short axis, of fiamme, feldspar phenocrysts and globules, plotted against each other also describe the form of individual particles. The length:breadth ratio effectively describes the amount of deformation of viscous juvenile particles. Rigid bodies e.g. feldspar phenocrysts cannot be deformed, they can only be rotated such that the long axis is aligned parallel to the inferred flow direction in the plane of flattening.

3.6.1 Results of pilot study

The relationship of x, y and z surfaces

In both TL1 and TL2 the most significant relationships between orientation and Form Factor occur on the z surface, because this surface was cut parallel to the inferred flow direction (Fig. 3.6, 0123z; and Figs. 3.7 and 3.8, 0094z and 0095z respectively). On these surfaces the most elongate particles (Form Factor approaching 0) show the best alignment and have the smallest orientation deviation ($<25^\circ$). The greatest length:breadth relationships are also shown on the z surface, because this surface is parallel to the syn- and post-depositional deformation direction. Thus the z surface shows the effects of *both* shear during non-particulate flow and static compaction.

Moderately good orientation versus Form Factor relationships and moderate length:breadth ratios are observed on the y surfaces (Fig. 3.6, 0123y; Figs. 3.7 and 3.8, 0094y and 0095y respectively) since these surfaces were cut parallel to the syn- and post-depositional deformation direction, but perpendicular to the inferred flow direction. Thus y surfaces show primarily the effects of static compaction and not the effect of elongation through shear during non-particulate flow.

The weakest orientation versus Form Factor relationships and the smallest length to breadth ratios are observed on the x surfaces (Fig. 3.6, 0123x; Figs. 3.7 and 3.8 0094x and 0095x respectively). These surfaces are perpendicular to the syn- and post-depositional deformation direction and parallel to the inferred flow direction. Thus the x surface cannot show any effects of static compaction, but would show the effect of elongation and orientation of particles during non-particulate flow if, for example, fiamme were lineated. A strong lineation however was not recorded from any of the cut sections (e.g. Fig. 3.6, 0123x).

SAMPLE 0123
TL1

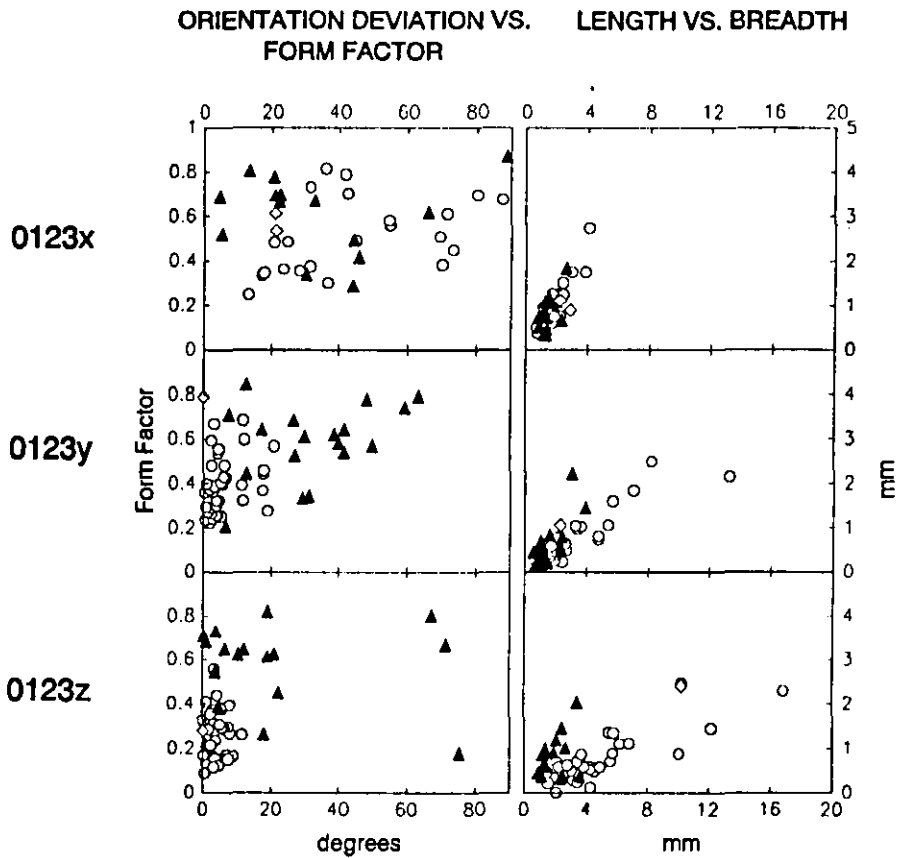
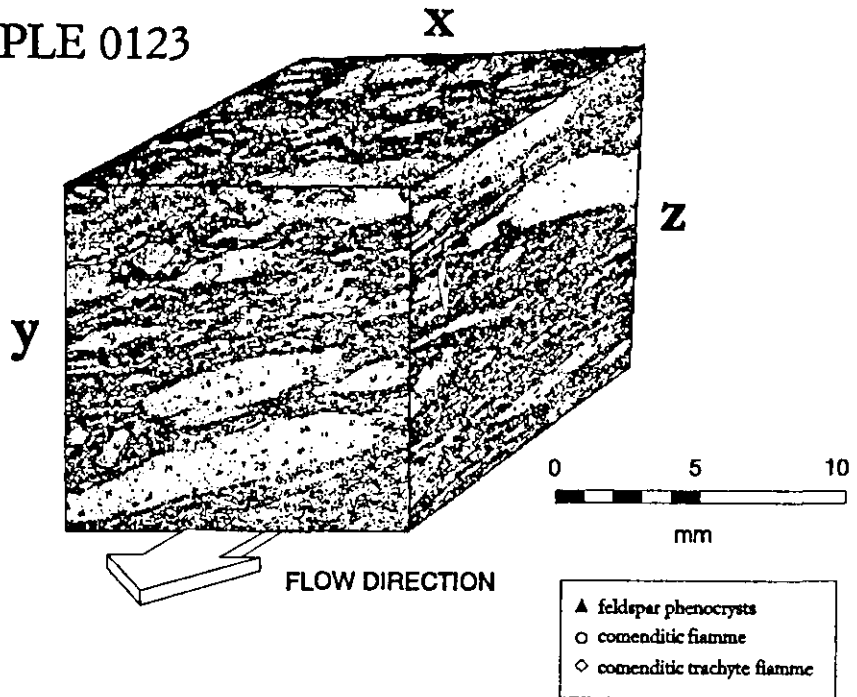


Figure 3.6. Microscopic image analyses of sample 0123, TL1, lithofacies C2D, Exp. 60, Montaña de las Carboneras. Orientation versus form factor and length versus breadth are plotted for individual particle populations on X, Y and Z surfaces. Details of cut sections are given in text.

In summary, the effect of syn- and post-depositional deformation can only be seen on y and z surfaces, and the effect of non-particulate flow can only be observed on x and z surfaces. Because the oriented samples were all taken parallel to the inferred flow direction the above relationships between the x, y and z surfaces are maintained for samples from both TL1 and TL2. Thus the variation in the measured parameters must be the result of the nature (e.g. viscosity, shape) of the individual particle populations measured.

VIDS analysis of TL1

The particle populations measured for TL1 (sample Q123) were; matrix feldspar phenocrysts, comenditic fiamme and comenditic trachyte fiamme. The best results were obtained for comenditic fiamme and feldspar phenocrysts since comenditic trachyte fiamme are rare and a statistically valid number could not be measured. The results are summarised on Figure 3.6:

On the x surface, both feldspar phenocrysts and comenditic fiamme show no detectable elongation or orientation. As this surface is cut such that it should show the effect of non-particulate flow, the lack of orientation and elongation of particles suggests that the extent of non-particulate flow was insufficient to cause detectable lineation, through shear, of the viscous comenditic fiamme in this plane.

On the y surface, comenditic fiamme show moderate orientation. This is noticeably better than that of feldspar phenocrysts, due to flattening of the viscous comenditic particles, which causes preferential alignment of the long axis. Comenditic fiamme also have a larger length:breadth ratio on the y surface compared to x. Since this surface would not show the effect of non-particulate flow, the orientation of comenditic fiamme on the y surface must be the result of syn- and post-depositional flattening of particles causing preferential alignment of the long axis.

On the z surface comenditic fiamme show excellent orientation ($0 \pm 17^\circ$) and have much larger length:breadth ratios than on than on the y surface. This difference indicates that as well as static compaction, there was also some elongation and shear of particles during non-particulate flow.

Feldspar phenocrysts also show moderate orientation, although three phenocrysts stand out with very poor orientations. In thin section, two of these phenocrysts are square cross sections which have a Form Factor approaching 0. Square-cut cross sections cannot show any orientation. The third is a tabular crystal surrounded by 'shear cavities' (cf. to those depicted in Fig. 2.11) which was rotated over during non-particulate flow and now lies at almost 90° to the inferred flow direction (see Figure 3.6, outlined crystal on the z surface).

Only the comenditic fiamme show an increase in the length:breadth ratio from x to y to z surfaces as the rigid feldspar phenocrysts could not be effected by flattening, or elongation during non-particulate flow.

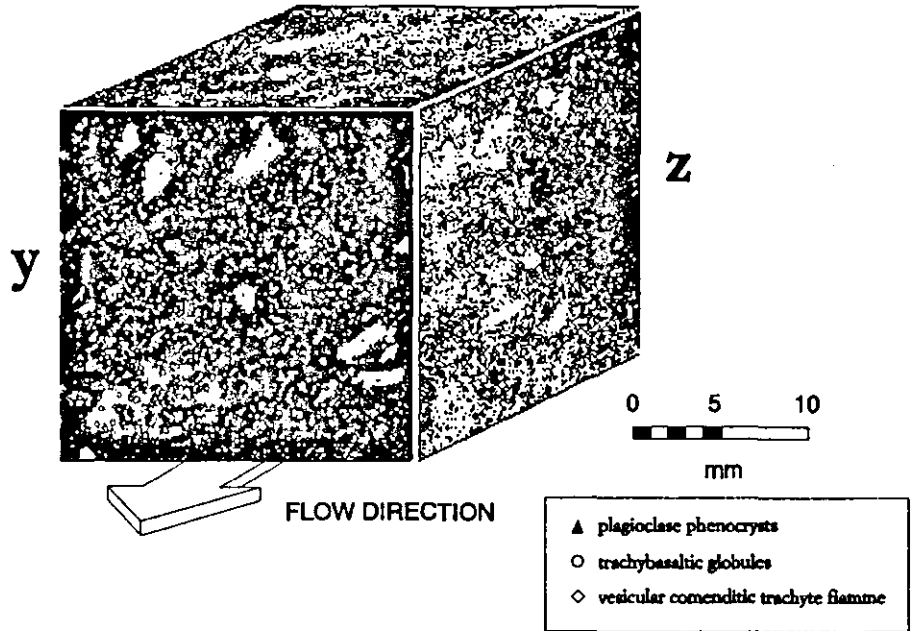
VIDS analysis of TL2

The particle populations measured for TL2 (samples 0094 and 0095) were; matrix feldspar phenocrysts, trachybasaltic globules and vesicular comenditic trachyte fiamme. The particle populations in TL2 generally show poorer orientation on all surfaces than in TL1. The length:breadth ratio and the Form Factor values (Fig. 3.7 and 3.8) indicate that most of the particles are approaching equidimensional and thus cannot show preferred orientation of the long axis. The trachybasalt globules and comenditic trachyte fiamme are approximately spherical and most of the feldspar phenocrysts are square or trapezoidal in cross section. Equidimensional bodies cannot show any preferred orientation, thus the lack of orientation of particles in TL2 cannot simply be attributed to the absence of non-particulate flow, this may have been considerable, but would not be recorded because of the shape of the particles.

SAMPLE 0094

X

TL2



ORIENTATION DEVIATION VS. LENGTH VS. BREADTH
FORM FACTOR

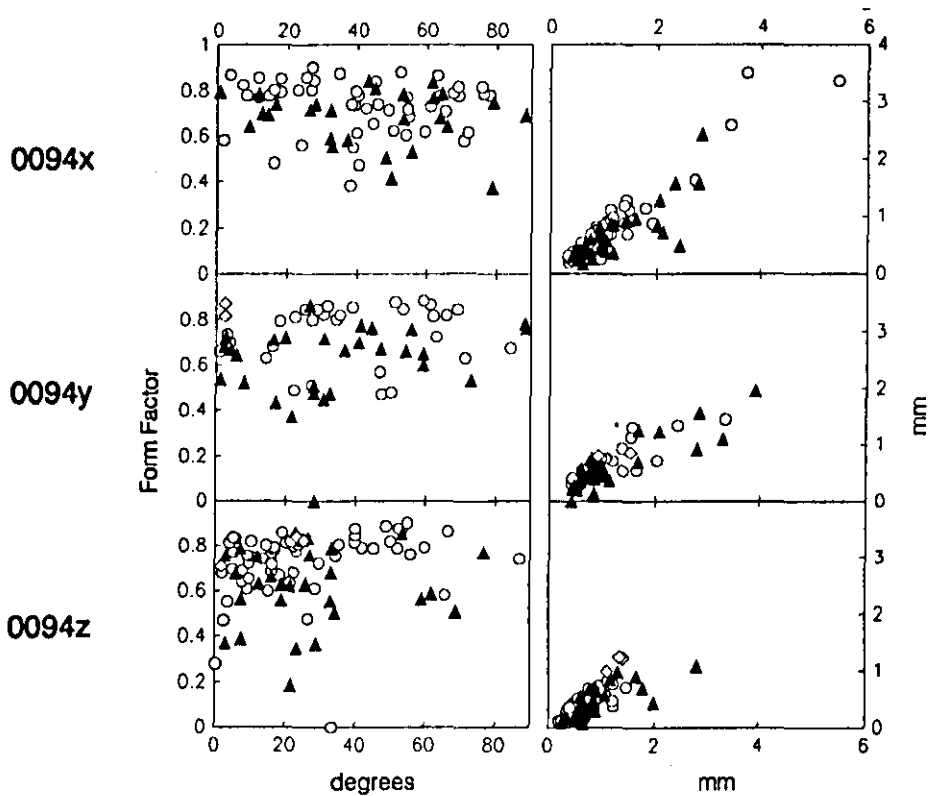


Figure 3.7. Microscopic image analyses of sample 0094, TL2, Big globule lithofacies (B.G.I.Z.), Exp. 58, Bco. de Lechugal. Orientation versus form factor and length versus breadth are plotted for individual particle populations on X, Y, and Z surfaces. Details of cut sections are given in text.

SAMPLE 0095
TL2

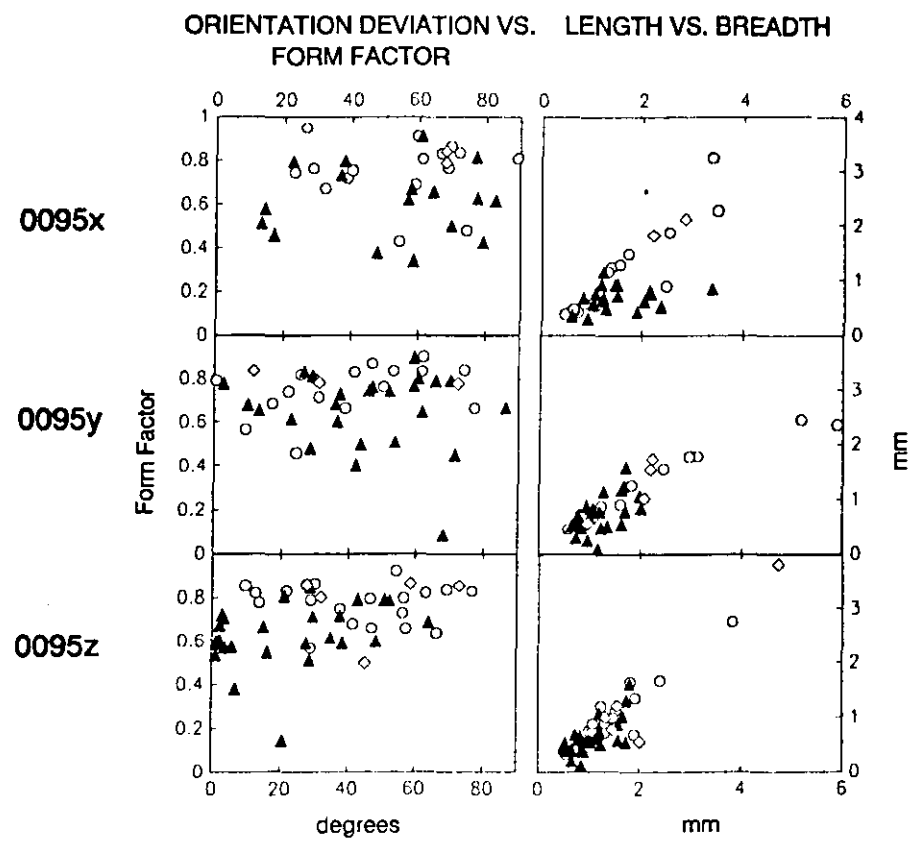
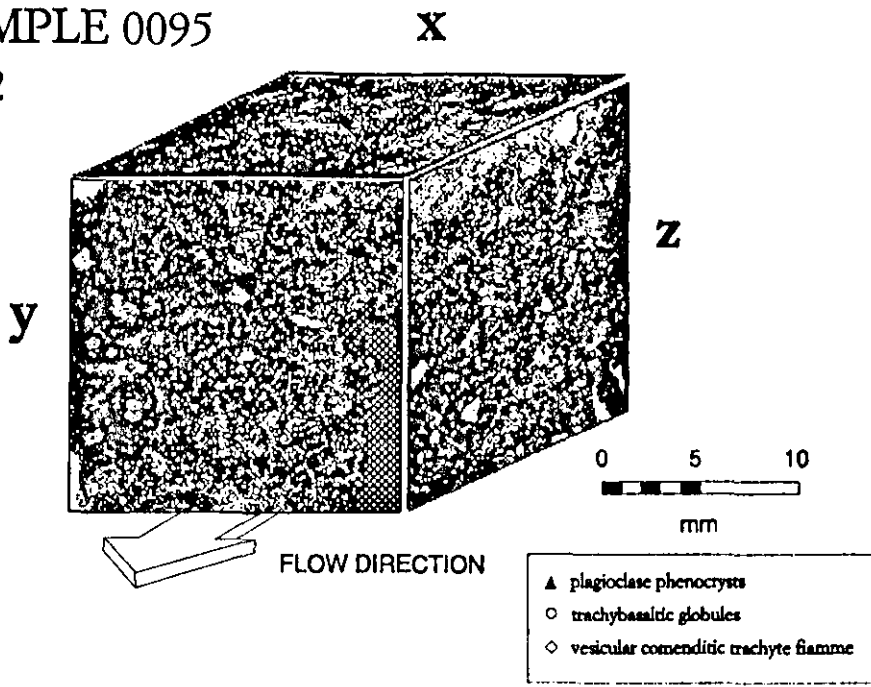


Figure 3.8. Microscopic image analyses of sample 0095, TL2, Big globule lithofacies (B.G.I.Z.), Exp. 58, Bco. de Lechugal. Orientation versus form factor and length versus breadth are plotted for individual particle populations on X, Y, and Z surfaces. Details of cut sections are given in text.

Syn- and post-depositional flattening of particles is also not recorded, but this is interpreted to be the result of the nature of the individual particle populations. Feldspar phenocrysts cannot be flattened, only rotated. The trachybasalt globules are glassy and must also have been rigid when incorporated in the depositional regime. Thus, similarly, they could not be flattened. The comenditic trachyte fiamme contain round vesicles which must have formed as the result of volatile exsolution, after post-depositional deformation. The fiamme must have had sufficiently low viscosity to allow the formation of these vesicles. However, the Form Factor of these particles suggests that during vesicle formation the comenditic trachyte fiamme, which may or may not have been previously flattened, re-inflated such that they are now almost perfectly spherical.

The only preferential orientation is shown by some feldspar phenocrysts (Fig. 3.8 0095z). In thin section these are tabular and are preferentially aligned forming weak trachytic texture.

Summary of results

Video image analysis has allowed textural comparisons to be made between TL1 and TL2 that could not be made in the field, due to the fine grained nature of TL2.

In TL1 comenditic fiamme have very low sphericity and are predominantly prolate in form, with a Form Factor approaching 0. As a result of attenuation and shear during non-particulate flow and static compaction, these particles have excellent orientation (Fig. 3.9a).

Comenditic trachyte fiamme similarly have low sphericity (Form Factor 0.3), but are not as prolate as the comenditic fiamme, this is interpreted to be due to their higher depositional viscosity, possibly the result of differential cooling. Comenditic trachyte fiamme have good orientation (Fig. 3.9a) which is interpreted to be the result of some flattening, and shear during non-particulate flow.

Feldspar phenocrysts have moderate sphericity (Fig. 3.9a), but form factor is higher than would normally be expected because the average value is affected by the measurement of square or trapezoidal cross sections. The predominance of these cross sections suggests that rather than columnar or tabular forms, the majority of the phenocrysts are equant. Due to their largely equant morphology the orientation of feldspar phenocrysts is only moderate, with the best orientation shown by columnar or lath shaped crystals.

In TL2 the feldspar phenocrysts show similar sphericity and orientation to those analysed in TL1, although in TL2 their orientation is slightly better due to the development of weak trachytic texture. The trachybasaltic globules and comenditic trachyte fiamme in TL2 both have very high sphericity (Fig. 3.9b) and as a result of their equidimensional form, these particles show very poor orientation. The lack of syn- and post depositional deformation of the glassy trachybasalt globules is interpreted to be the result of rigidity when they were incorporated into the depositional regime of the flow. The comenditic trachyte fiamme may have attained a spherical form during late stage vesiculation. Average values for Form Factor and the amount of orientation deviation for each particle population in TL1 and TL2 are given in Figure 3.9, and the conclusions are summarised in Table 3.2 (see also data Table in Appendix I).

Problems with the technique

The results of this pilot study indicate that video image analysis can be used to quantitatively describe microfabrics. However several problems were noted during the study and consolidation of the results, for example, in sample 0123 from TL1, the elongation and shear of particles on the z surface does not correspond with the absence of a lineation on the x surface. This discrepancy highlights one of the problems with this type of analysis. The elongation and shear of particles on the x surface may not have been detected because the sample area was too small. Further studies are

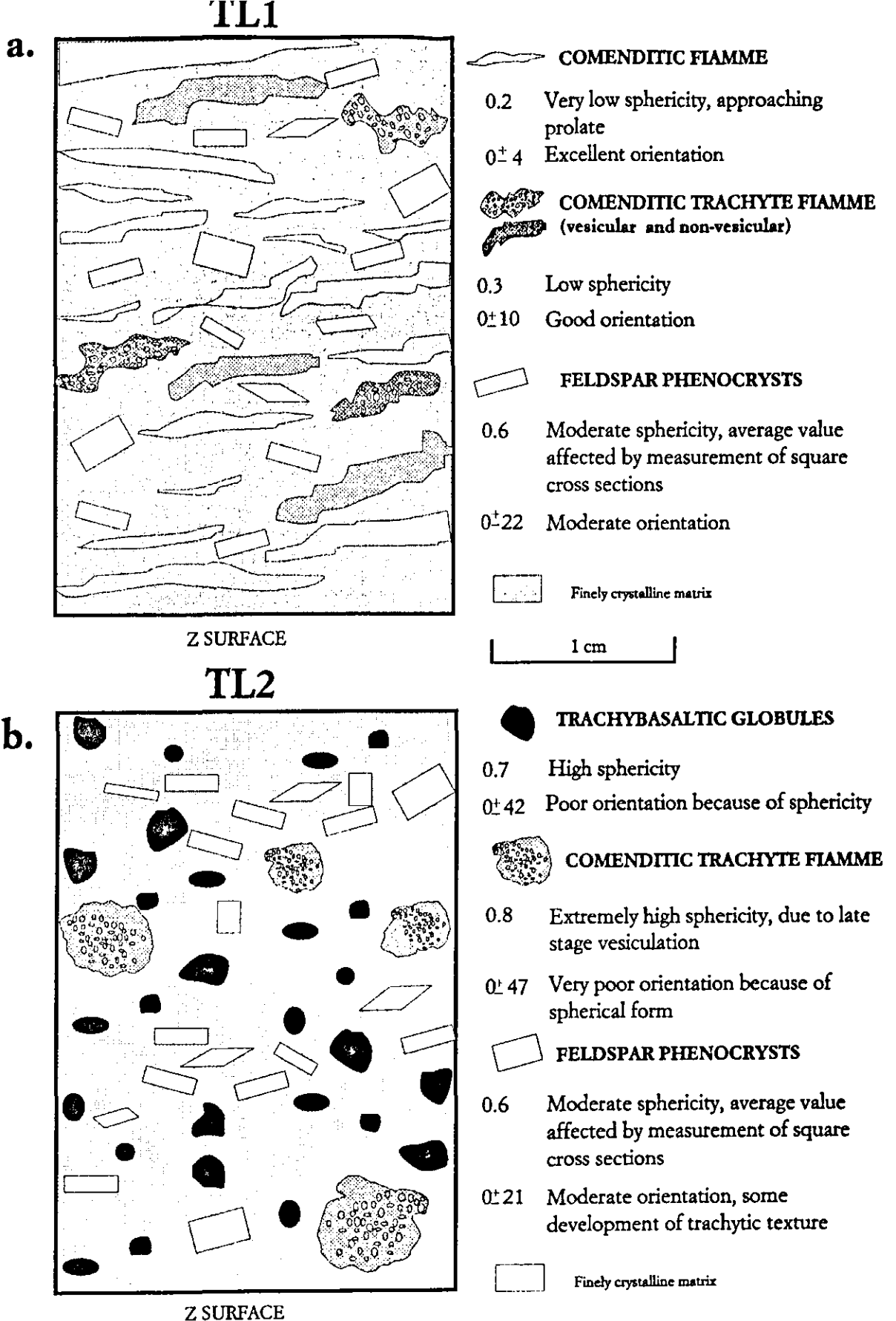


Figure 3.9. Summary diagram of orientation and sphericity of individual particle populations in (a) TL1 and (b) TL2.

necessary to test the statistical validity of the results. These would include analysis of larger samples, since in many cases, where the fiamme size is large the number of whole fiamme than can be measured is very limited. VIDS analyses of photographs of cut and polished surfaces of oriented blocks would provide larger sample areas and allow more fiamme and phenocrysts to be measured.

Table 3.2

PARAMETER	TL1	TL2
FELDSPAR PHENOCRYSTS		
Form Factor	moderate to high , some breakage and abrasion during transport. Average values also affected by measurement of square cross sections	moderate to high , no breakage or abrasion during transport, but some phenocrysts are rounded and embayed. Average values also affected by measurement of square cross sections
Orientation	moderate to low , sections with high form factor approaching equidimensional cannot be preferentially oriented	moderate to low , sections with high form factor approaching equidimensional cannot be preferentially oriented. Tabular sections show preferred alignment, forming weak trachytic texture.
length:breadth	moderate to low , rigid particles cannot be affected by syn- and post-depositional flattening.	moderate to low , rigid particles cannot be affected by syn- and post-depositional flattening.
COMENDITIC FIAMME		
Form Factor	Very low , approaching 1 (prolate) due to extreme syn- and post-depositional deformation of viscous particles.	absent
Orientation	Excellent , due to flattening which causes preferred orientation of the long axis of viscous particles and due to elongation, by shear, during non-particulate flow.	
length:breadth	Very high , due to syn- and post-depositional flattening and elongation during non-particulate flow.	
COMENDITIC TRACHYTE FIAMME		
Form Factor	Low , some syn- and post-depositional deformation of particles, but less than comenditic fiamme, possibly due to higher viscosity of particles on deposition.	Very high , (approaching 1) due to post-depositional deformation vesiculation, any affects of flattening or non-particulate flow are overprinted
Orientation	Good , as above, but less than observed in comenditic fiamme.	Very poor , due to the high sphericity of particles. Equidimensional particles cannot be preferentially oriented
length:breadth	Moderate , less than observed in comenditic fiamme, some syn- and post-depositional flattening and elongation during non-particulate flow.	Very low , because particles are almost spherical
TRACHYBASALT GLOBULES		
Form Factor	absent	Very high , due to original fluidal nature of particles and surface tension effects during ejection and transport, particles are also glassy suggesting that they may have been rigid when incorporated in the depositional regime
Orientation		Very poor , due to the high sphericity of particles. Equidimensional particles cannot be preferentially oriented
length:breadth		Very low , because particles are almost spherical, also rigid particles cannot be flattened

3.7 GEOGRAPHICAL DISTRIBUTION AND FLOW LINEATIONS

Regional variations in fabrics can be determined through measurement of the dip and strike of fiamme. The fabric in TL is defined by lineations, produced by syn- and post-depositional elongation and orientation of fiamme in the direction of flow (Fig. 3.10). In some cases the fiamme are pulled apart or have fractures, convex in the downflow direction, indicating that deformation continued to a point where fiamme were more brittle than the matrix (Schmincke and Swanson, 1967).



Figure 3.10. Lineated, fractured, comenditic fiamme in lithofacies C2V of TL2. The curving fractures (above black arrow indicating inferred flow direction) crossing the fiamme are perpendicular to the inferred flow direction, and convex in the downflow direction. The lense cap is 5.5 cm in diameter. (Exp. 108, Bco. de Tasarte).

The dip and strike of the fiamme in TL1 and in TL2 (where it is vitroclastic) were measured at localities around the caldera (Fig. 3.11). The computer programme ARIANE (Appendix I) has been used to project data onto lower hemisphere Schmidt nets. When the data for all barrancos is plotted together (Fig. 3.12A), the projection demonstrates that the lineation is at a low angle (<30 degrees) and shows a strong radial distribution. When these orientations are plotted onto a map of Gran Canaria they radiate outwards from the caldera margin (Fig. 3.11). As these structures are syn- and post-depositional it can be concluded that the pyroclastic flows depositing TL1 and TL2 flowed radially outward, from the caldera towards the coast, in a broad sheet covering the NNW to SE part of the island.

Measurement of lineations throughout the entire thickness of flow unit TL1 at Montaña de las Carboneras and Bco. de Mogán (Fig. 3.12B and C) shows that although flow was maintained in one general direction throughout the deposition of the entire unit, there were localised variations in flow direction. These variations are attributed to:

- (1) Migration or 'talweg' of the main flow axis during progressive aggradation of the deposit, as demonstrated by the progressive change in orientation of lineations with height through the unit. This was towards the west, in Bco. de Mogán (Fig. 3.12B) and towards the east at Montaña de las Carboneras (Fig. 3.12C).
- (2) Sinuosity of the flow axis as the flow waxed and waned, as shown by the widespread orientation of lineations in lithofacies C3f and M4F of TL1 at Montaña de las Carboneras and Bco. de Mogán.

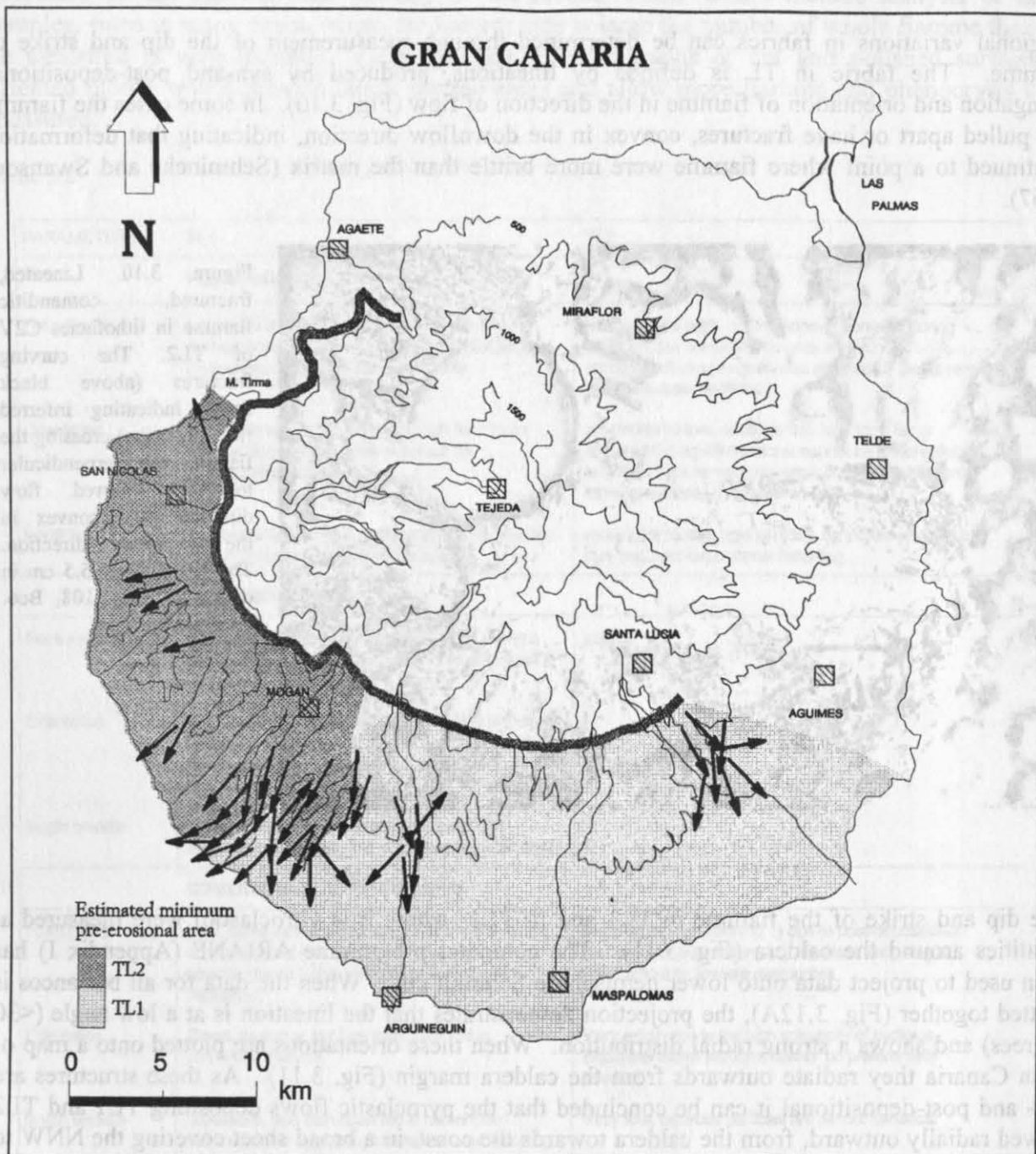


Figure 3.11. Inferred palaeoflow direction of TL1 (light grey) and TL2 (dark grey), deduced from azimuth orientation of fiamme lineations.

(3) Palaeotopography also caused localised variation in lineation directions e.g. Bco. de Taurito and Bco. de Arguineguin (Fig. 3.12D) where down slope drainage produced lineations in the opposite sense to the main transport direction.

Lineations occurring at a very high angle (Fig. 3.12D), have been recorded from TL2 in Bco. de Mogán and TL1 in Bco. de Arguineguin and Bco. de Taurito, these are related to ramp structures (Fig. 7.23) which are interpreted to be the result of the upward mass movement of material along shear planes (Section 7.11.2, Fig. 7.22) with a consequent increase in angle of imbrication and lineation of fiamme from ca. 30 degrees to ca. 80-90 degrees.

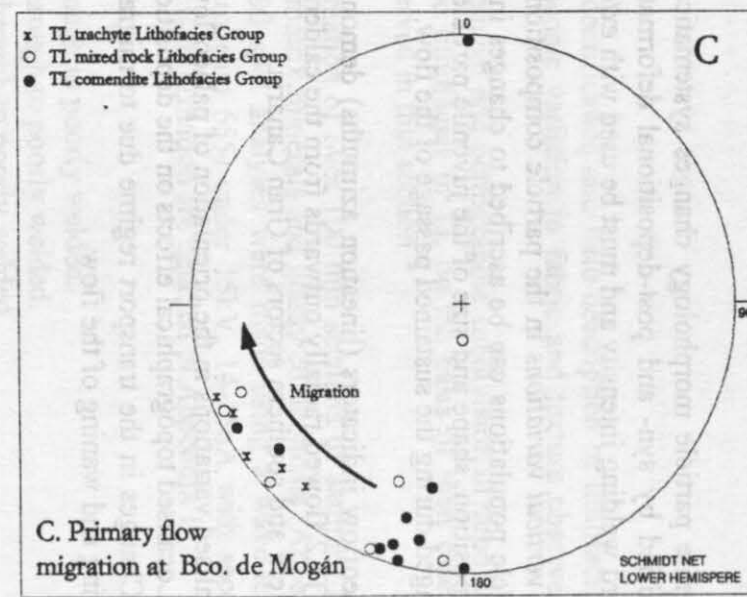
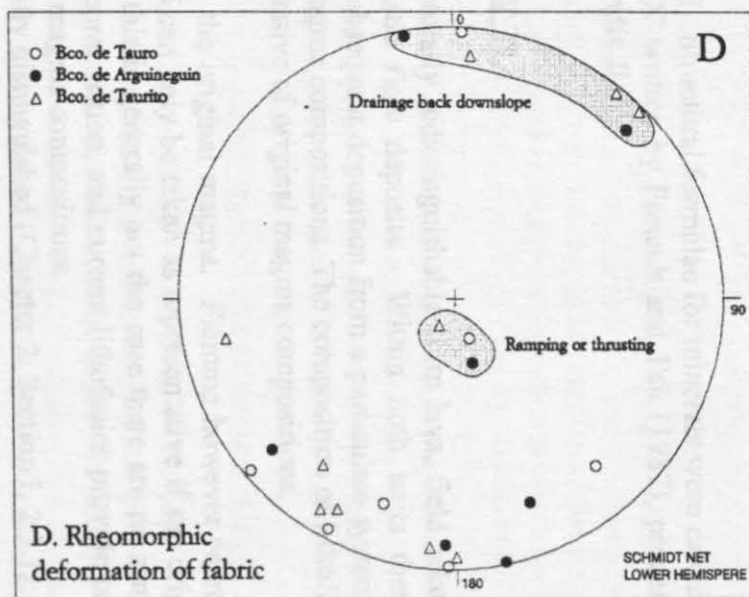
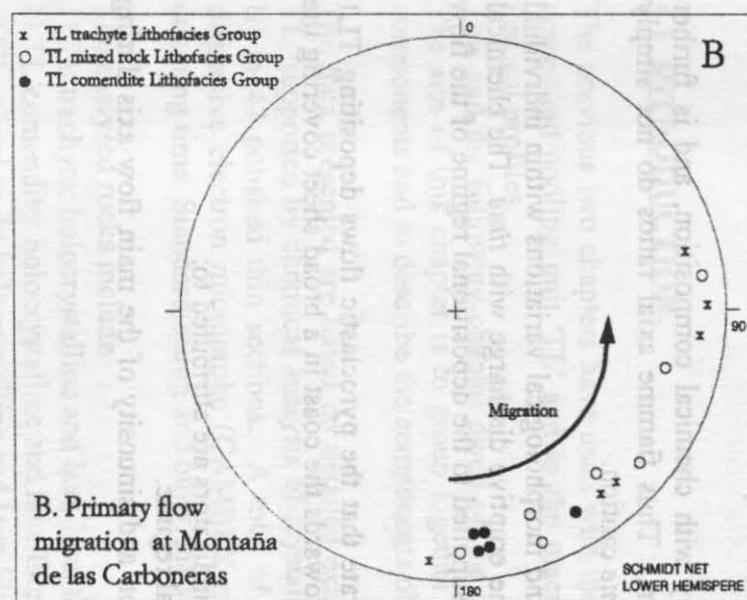
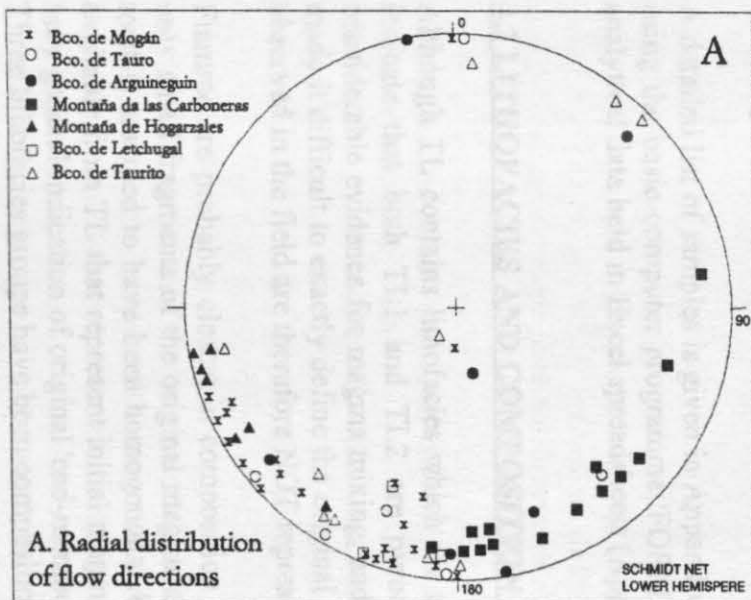


Figure 3.12. Lower hemisphere Schmidt net projections of the dip and strike of fiamme in TL1 and TL2. Details are given in section 3.7.

3.8. CONCLUSIONS

Three chemically discrete juvenile particle populations are represented by fiamme in TL. These are; comenditic fiamme, mixed fiamme and comenditic trachyte fiamme.

Juvenile particle morphology changes systematically with chemical composition, and is further modified by syn- and post-depositional deformation. Thus fiamme axial ratios do not simply record welding intensity and must be used with *extreme* caution.

The *vertical variations* in the particle composition and morphological variations within individual particle populations can be ascribed to changes in the eruptive discharge with *time*. The chemical composition, shape and size of the juvenile particles supplied to the depositional regime of the flow changed during the sustained passage of the flow.

Palaeoflow indicators (lineation azimuths) demonstrate that the pyroclastic flows depositing TL1 and TL2 flowed radially outwards from the caldera towards the coast in a broad sheet covering the western and southern sectors of Gran Canaria.

Localised variations in the orientation of palaeoflow indicators are attributed to:

- (1) Localised topographical effects on the depositional regime.
- (2) Changes in the transport regime due to migration and sinuosity of the main flow axis during waxing and waning of the flow.

CHAPTER 4

PETROGRAPHY OF TL LITHOFACIES

4.1 INTRODUCTION

The previous two chapters have dealt with the identification and field description of lithofacies in compound cooling unit 'TL' and in the macroscopic variation in fabric and texture observed in vertical profiles.

This and the following chapter dwell on the chemical and petrographic subdivision of lithofacies. The aim of this chapter is to group together the lithofacies in TL on the basis of their essential components and to describe the components observed in thin section.

The data presented are based on detailed examination of over 100 thin sections of samples from TL, supported by chemical analysis of crystals, matrix minerals and glassy components (Appendix II) in 47 polished thin sections. A total of 600 spot analyses were made using a wave-length dispersive electron microprobe (CAMBEX microbeam 655) under 15kV, 14-15nA with seconds counting time. Standardisation and other analytical information are detailed in Appendix II.

The analysed rocks include:

- 1) TL trachyte: holocrystalline and lava-like, through to poorly welded.
- 2) TL comendite: holocrystalline and lava-like through to poorly welded.
- 3) TL mixed rock: holocrystalline and lava-like through to poorly welded.
- 4) Fiamme of comenditic trachyte, comenditic and (mixed rock) intermediate composition.
- 5) Lava-like, mixed comendite and trachyte containing glassy to microcrystalline trachybasalt globules.
- 6) Glassy basal vitrophyres from 4 separate localities.

A detailed list of samples is given in Appendix II. Structural formulae for minerals were calculated using the basic computer programme 'FORMFIX' written by Freundt and Tait (1987), processing analytical data held in Excel spreadsheets (Appendix II).

4.2 LITHOFACIES AND COMPOSITION OF TL

Although TL contains lithofacies which are texturally indistinguishable from lava, field relations indicate that both TL1 and TL2 are pyroclastic flow deposits. Within both units there is considerable evidence for magma mixing, and subsequent deposition from a particulate system has made it difficult to exactly define the original magma compositions. The composition of lithofacies observed in the field are therefore NOT representative of original magma compositions.

Fiamme are probably closest in composition to the original magma. Fiamme however represent only small fragments of the original magma and can only be taken as representative if the original melt is assumed to have been homogenous. As this is generally not the case there are no samples available from TL that represent initial magma composition, and current lithofacies provide only a very general indication of original 'end-member' magma compositions.

Three lithofacies groups have been compositionally distinguished (Chapter 2, Section I, 2.3.1):

TL trachyte

TL comendite

TL mixed rock

Glass, mineral and fiamme compositions however, suggest that three original magma compositions are represented in TL: **comenditic trachyte, comendite and trachybasalt.**

TL trachyte consists of >60 volume percent comenditic trachyte components and <40 volume percent comendite components, with up to 2 volume percent trachybasalt.

TL comendite consists of >60 volume percent comendite components and <40 volume percent comenditic trachyte components.

TL mixed rock consists of 40-60 volume percent comenditic trachyte components and 40 -60 volume percent comendite components mingled in varying proportions (e.g. Table 2.3), with up to 2 volume percent trachybasalt.

The three lithofacies TL trachyte, TL comendite and TL mixed rock are composed of phenocrysts, glomerocrysts, fiamme (containing phenocrysts), glassy or formerly glassy shards, lenticules (vesicles), non-juvenile rock fragments and microcrystalline matrix.

TL trachyte and TL comendite are distinguished petrographically by their characteristic mineral assemblages. TL mixed rock contains mineral components from both TL comendite and TL trachyte. Trachybasalt which occurs as globules in TL trachyte is glassy and aphyric and has been identified by microprobe analysis only.

The first part of this chapter (Section I) concentrates on the mineralogy of TL. It contains petrographic descriptions of the mineral assemblages, followed by the analytical data and detailed discussion of the mineral compositions. The second part of the chapter (Section II) describes the other components in TL lithofacies and includes descriptions of the various matrix textures observed in TL.

SECTION I

4.3 MINERALOGY

The characteristic mineral assemblages for TL trachyte and TL comendite are given in Table 4.1, together with modal abundances and grain size. A total of 528 crystals and trachybasalt globules were modally analysed using the 'VIDS' video image analysis system (Appendix I). The perimeter, form factor (shape and roundness) and long axis were measured for each, processing data held in 'Excel' spreadsheets.

TL comendite is characterised by phenocrysts of anorthoclase feldspar, minor amphibole, accessory clinopyroxene and Fe-Ti oxide. TL trachyte has both plagioclase and alkali feldspar, with alkali feldspar being dominant. Minor phenocrysts are amphibole, with subordinate clinopyroxene and orthopyroxene, and Fe-Ti oxide as an accessory mineral.

4.3.1 Crystal assemblage in TL comendite

Lithofacies C1E, C2D and C3f of TL1, and lithofacies C2P, C3V, C2L and C3B of TL2 are composed of TL comendite (Fig. 2.4). The phenocryst population of TL comendite is dominated by large (<7mm) anorthoclase crystals. The minor phase is amphibole, with opaque oxides and rare pyroxene as accessories. The phenocryst content of TL comendite varies between 2-8 modal percent and anorthoclase accounts for 60-70% of the phenocryst fraction.

MODAL ABUNDANCE (mean %)									
ROCK TYPE	MAJOR PHENOCRYST PHASE	MINOR PHENOCRYST PHASE					ACCESSORY TRACE	VAPOUR PHASE	
		Anorthoclase	Plagioclase	Ca Amphibole	Alkali Amphibole	Cps		Opa	Fe-Ti Oxide
TL trachyte	5	2	t	1	< 1	< 1	A	vp	vp
TL comendite	7	x	< 1	2.	t	t	A	vp	vp
GRAIN SIZE (mm)									
Average	1.5	1	0.7	0.5	0.3	0.5	0.2		
Maximum	5	5	4	3	2	1.16	0.6	< 0.1	< 0.1

t = mineral present in only a few thin sections (< 1 % abundance)
 A = accessory mineral

vp = vapour phase mineral
 x = xenocrysts

Table 4.1. Modal abundance and grain size of phenocryst phases in TL trachyte and TL comendite.

Anorthoclase occurs predominantly as separate euhedral phenocrysts and more rarely as glomerocrysts. The phenocrysts are equant, tabular or prismatic and are randomly oriented throughout samples. They rarely show evidence of zoning or corrosion, but commonly exhibit albite pericline cross twinning and show signs of strain with in-situ breakage and inhomogeneous extinction. Small amphibole inclusions commonly occur towards the crystal margins (Fig. 4.1).

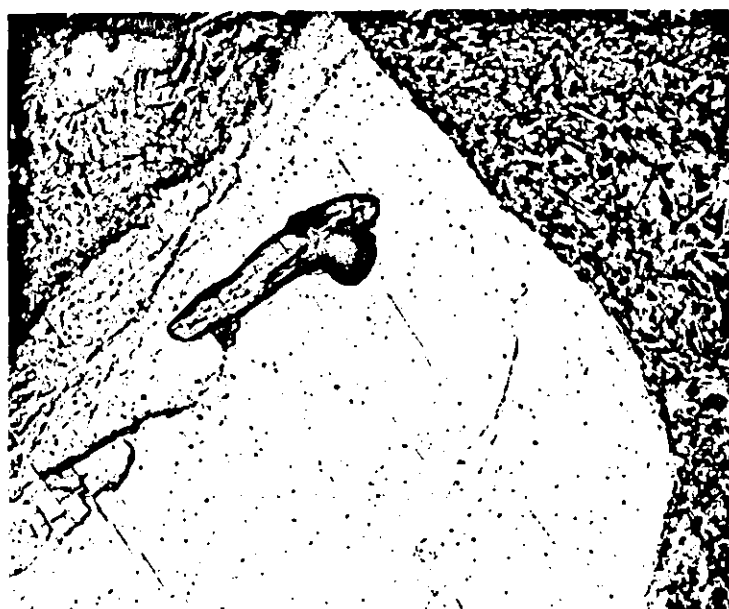


Figure 4.1. Opaque oxide partially enclosed in amphibole, enclosed in a large anorthoclase phenocryst (sample 0026, TL2, Exp. 26, Bco. de Tauro). Photomicrograph taken in plane polarised light.

0.25mm

Plagioclase phenocrysts are found in some samples (e.g. sample 0372, lithofacies C2P, Bco. de Tauro). They are embayed and rounded or highly irregular in outline. The embayment and rounding is interpreted to be the result of resorption and corrosion (Fig. 4.2). Their textures and scarcity, suggest that they may be xenocrystic.

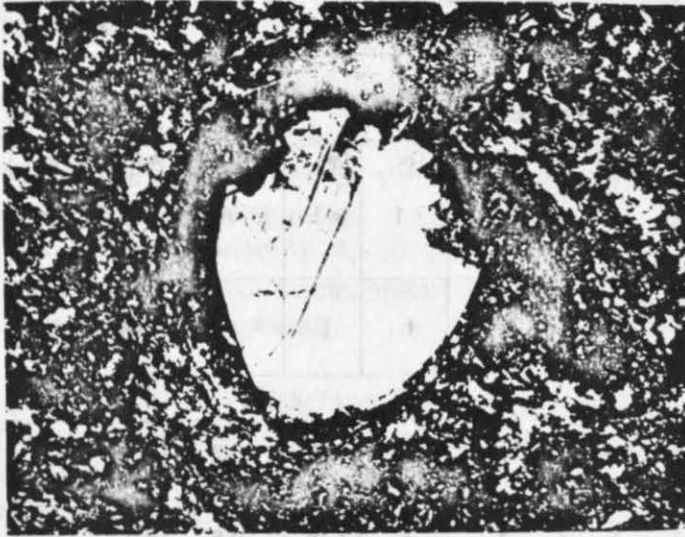
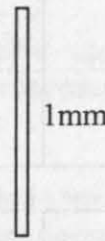


Figure 4.2. Rounded, embayed plagioclase phenocryst, interpreted as a xenocryst, in TL comendite (sample 0372, TL2, Exp. 101, Bco. de Tauro). Photomicrograph taken under crossed nicols.



TL comendite contains sodic-calcic and alkali amphiboles, distinguished by their pleochroism.

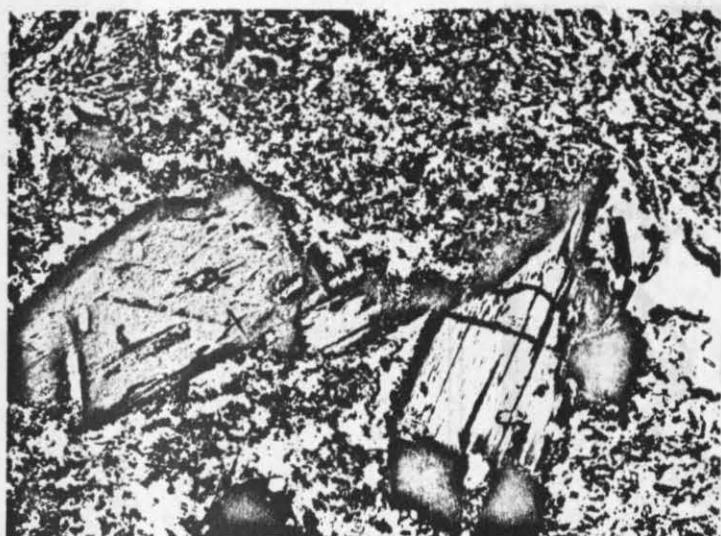
Sodic-calcic amphiboles are larger (<4mm), euhedral and more abundant than alkali amphibole (Table 4.1). The colour and pleochroism of the sodic-calcic amphiboles is variable. Pleochroism ranges from pale yellow to yellow-brown in amphiboles in TL comendite lithofacies at the base of TL1 and TL2 and in inclusions in anorthoclase, to orange-brown to dark red-brown in TL comendite lithofacies near the central portions of TL1 and TL2. This systematic variation suggests that the colour change may be the result of cooling rate and oxidation. Isolated phenocrysts often have an opaque oxide rim (Fig. 4.3a).

Alkali amphibole occurs as smaller phenocrysts (<3mm) which are more irregular in outline than the sodic-calcic amphiboles, and also as small acicular vapour phase crystals in vesicles and lenticules. They have distinctive pleochroism from pale violet-green to dark blue-green. Alkali amphibole phenocrysts commonly have an alteration rim of vermicular intergrown feldspar and pyroxene (aegirine) with spinel (Fig. 4.3b). This reaction rim is interpreted to be the result of dehydration of amphibole. A thicker vermicular alteration rim occurs around alkali amphiboles in TL mixed rock samples, compared to that observed in TL comendite samples. This suggests that the dehydration was probably due to reheating or superheating of the comendite during mingling with hotter comenditic trachytic, just prior to, or during eruption.

Clinopyroxene is present as rare augite phenocrysts. These are lath shaped or prismatic (<10 μ m) and are partly or completely enclosed in amphibole. Aegirine occurs predominantly a vapour phase mineral in vesicles and lenticules.

Opaque oxide occurs as small (<40 μ m), isolated, euhedral phenocrysts and as smaller anhedral crystals forming glomerocrysts together with amphibole.

The order of crystallisation, deduced from mutual inclusions (Fig. 4.1) is: opaque oxide, followed by amphibole, followed by anorthoclase.



a

0.5mm



b

0.5mm

Figure 4.3. Amphiboles in TL comendite:

(a) Sodic-calcic amphiboles (Katophorite, analysis C-Ap, An 4) show variable colour and pleochroism, crystals are slightly zoned towards the margins and an opaque oxide rim surrounds most crystals. (sample A, TL2, Exp. 6, Bco. de Mogán). (b) Alkali amphibole (Arfvedsonite, analysis Cf-0125p, An12) with a dehydration rim of vermicular intergrown feldspar and aegirine together with spinel (sample 0125, TL1, Exp. 60, Montaña de las Carboneras). Photomicrographs taken in plane polarised light.

4.3.2 Crystal assemblage in TL trachyte

Lithofacies T6w and T5W of TL1, and lithofacies T5V and T5L of TL2 are composed of TL trachyte (Fig. 2.4).

The phenocryst population of TL trachyte is dominated by alkali feldspar and plagioclase. Sodic-calcic amphibole, clinopyroxene (augite) and orthopyroxene (hypersthene) are the minor crystal phases. Opaque oxides are accessory minerals.

The crystal content of TL trachyte varies between 7-15 modal percent and feldspar accounts for 70-80% of the crystal fraction.

Alkali feldspar occurs most commonly as single, untwinned, large (<5mm), euhedral to subhedral phenocrysts. Phenocrysts are unzoned, but are occasionally angular and broken, with curving fractures. Phenocrysts are often sub-parallel aligned forming a trachytoid texture (Section 4.5, Fig. 4.26). Many of the larger phenocrysts (3-5mm) have inclusions of opaque oxide, or partly enclose small laths of amphibole and more rarely pyroxene. Rare phenocrysts are highly embayed and skeletal (Fig. 4.4), with glass filling the embayments and hollows. The texture of these crystals suggests they may be xenocrystic.

Plagioclase phenocrysts are less common than alkali feldspar. They are generally smaller (average 1mm), rounded phenocrysts showing simple twinning or albite cross twinning. Like the alkali

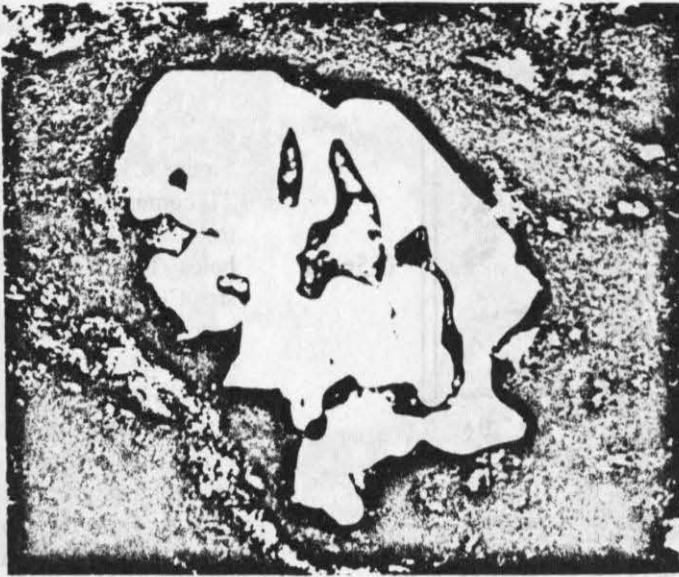


Figure 4.4. Embayed anorthoclase in TL trachyte, interpreted as xenocryst from TL comendite (sample 0277, TL2, Exp. 91, Bco. de Mogán). Photomicrograph taken in plane polarised light.

1mm

feldspars, they are often fractured and occasionally sub-parallel aligned. Plagioclase phenocrysts rarely have inclusions.

TL trachyte has both **sodic-calcic and alkali amphibole**, although sodic-calcic amphiboles predominate. These are generally less common in occurrence, and smaller (<3mm) than the amphibole phenocrysts in TL comendite, (Table 4.1). Phenocrysts are subhedral and subrounded in outline. Pleochroism is distinctive, yellow to dark yellow-brown, and margins of the phenocrysts are often slightly zoned. Like the sodic-calcic amphiboles in TL comendite, these also have an overgrowth rim of opaque oxide. Phenocrysts in samples taken from TL trachyte facies near the top of units TL1 and TL2 show alteration to limonite (Fig. 4.31)

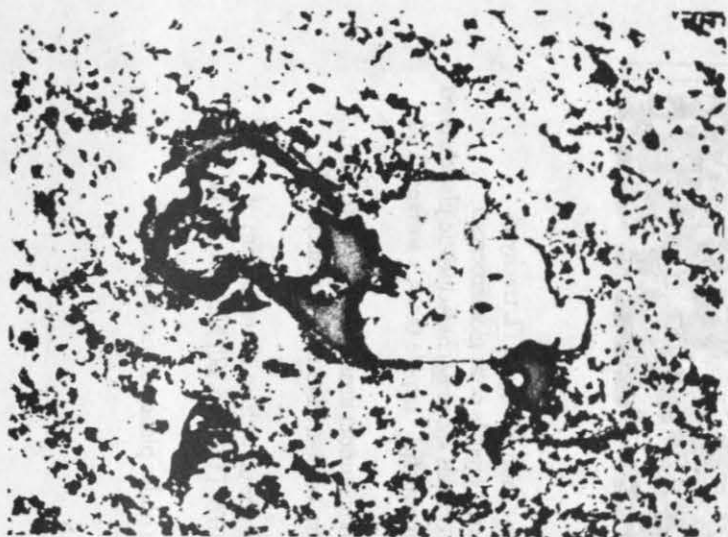
TL trachyte is characterised by two pyroxene crystal phases.

Clinopyroxene is present as phenocrysts, microlites and vapour phase crystals in vesicles. Small (<2mm), isolated, subhedral or euhedral augite phenocrysts are rare and are often partially enclosed in plagioclase feldspar and amphibole. Their pleochroism is variable. Augite phenocrysts which are enclosed in larger feldspar phenocrysts show pale green to dark green pleochroism. Isolated augite phenocrysts in the matrix show pale yellow-green to dark yellow-brown or green-brown pleochroism. This systematic variation suggests that the colour change is due to oxidation of the isolated phenocrysts, with the inclusion crystals remaining largely unaffected.

Microlites of aegirine occur throughout the matrix of TL trachyte. Larger, acicular, aegirine crystals occur in vesicles and lenticules in association with large (<0.5mm), fan shaped, very dark green/black, strongly pleochroic fassaite crystals (Fig. 4.29c). The two often occur as parallel or irregular intergrowths.

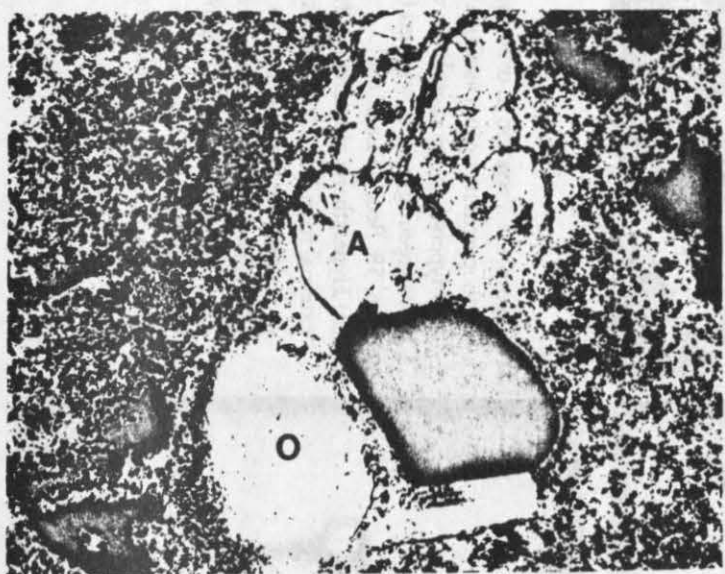
Orthopyroxene is less abundant than clinopyroxene. Orthopyroxenes range in size from microlites (25 microns) to phenocrysts (1.16mm). Phenocrysts are generally subhedral in outline (Fig. 4.5b and Fig. 4.6c), often occurring as glomerocrysts (Fig. 4.6a and b). The orthopyroxenes show the distinctive pink, yellow, yellow-green pleochroism of hypersthene.

The suggested sequence of crystallisation for TL trachyte, deduced from mutual mineral inclusions is: opaque oxides and orthopyroxene, followed by clinopyroxene and amphibole together with plagioclase, which continued crystallising, together with alkali feldspar, after clinopyroxene and amphibole.



a

0.5mm



b

0.5mm

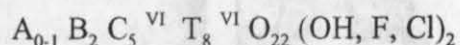
Figure 4.5. Pyroxene species in TL trachyte. (a) Rounded, corroded augite crystal (pale green, centre left), together with altered amphibole surrounded by black opaque oxide rim (centre right). (sample 0076, TL1, Exp. 60, Montaña de las Carboneras). (b) Augite (A) and orthopyroxene (O) together with opaque oxide, as a crystal cluster in TL trachyte. Note the subhedral, subrounded shape of augite and the fine grained granular alteration rim to the rounded orthopyroxene. The small, clear, high relief mineral (a) is apatite, which occurs rarely as an accessory mineral in some samples. (sample 0376, TL2, Exp. 101, Bco. de Tauro). Photomicrographs taken in plane polarised light.

TL trachyte has considerably more amphibole than pyroxene. However measured volatile contents for TL suggest that this is not anomalous. The predominance of amphibole over pyroxene is interpreted to be the result of high magmatic water content, which has resulted in the formation of more hydrous phases, such as amphibole, rather than anhydrous pyroxene (Section 4.3.3, stability considerations).

4.3.3 Mineral chemistry

AMPHIBOLE

The classification of amphiboles and the calculation of the structural formula follows the method of Leake (1978), in which the standard amphibole formula is taken to contain 8 tetrahedral sites and the general formula is:



Calculation of this formula is detailed in Leake (1978).

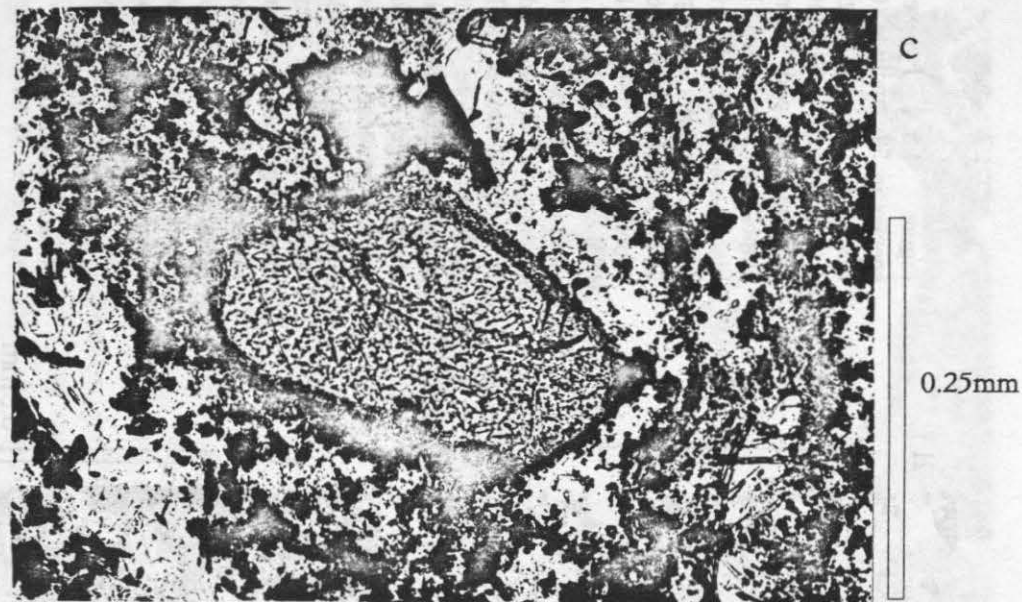
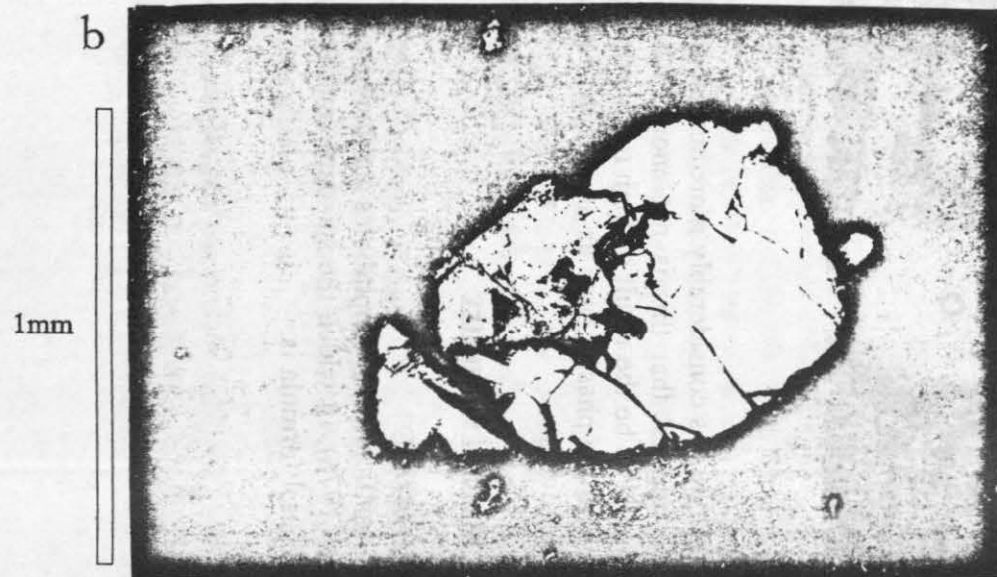
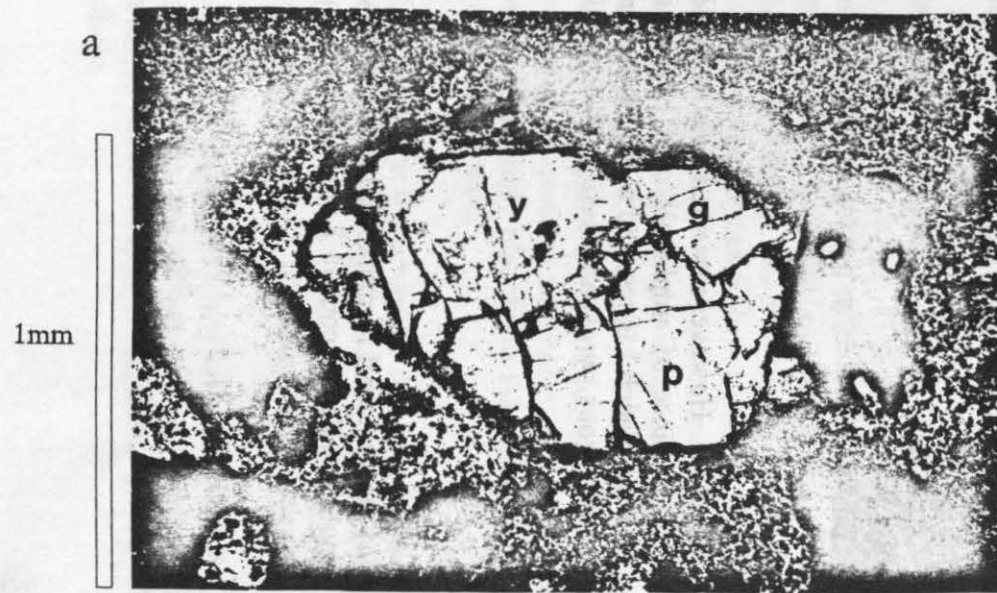


Figure 4.6. Variation in orthopyroxene morphology in TL trachyte. Orthopyroxene occurs as single isolated crystals or as glomerocrysts. (a) Hypersthene glomerocryst, with crystals showing characteristic pleochroism from green (g) to yellow-green (y) to pink (p). (sample 0095, z surface, TL2, Exp. 58, Bco. de Lechugal). (b) Hypersthene glomerocryst (as above) under crossed nicols. Note the external rounding to the glomerocryst, compared to the angularity of the crystals on the internal surfaces. (c) Isolated, rounded orthopyroxene crystal with an alteration rim of clinopyroxene and spinel (sample 0076, TL1, Exp. 60, Montaña de las Carboneras). Photomicrographs (a) and (c) taken under plane polarised light.

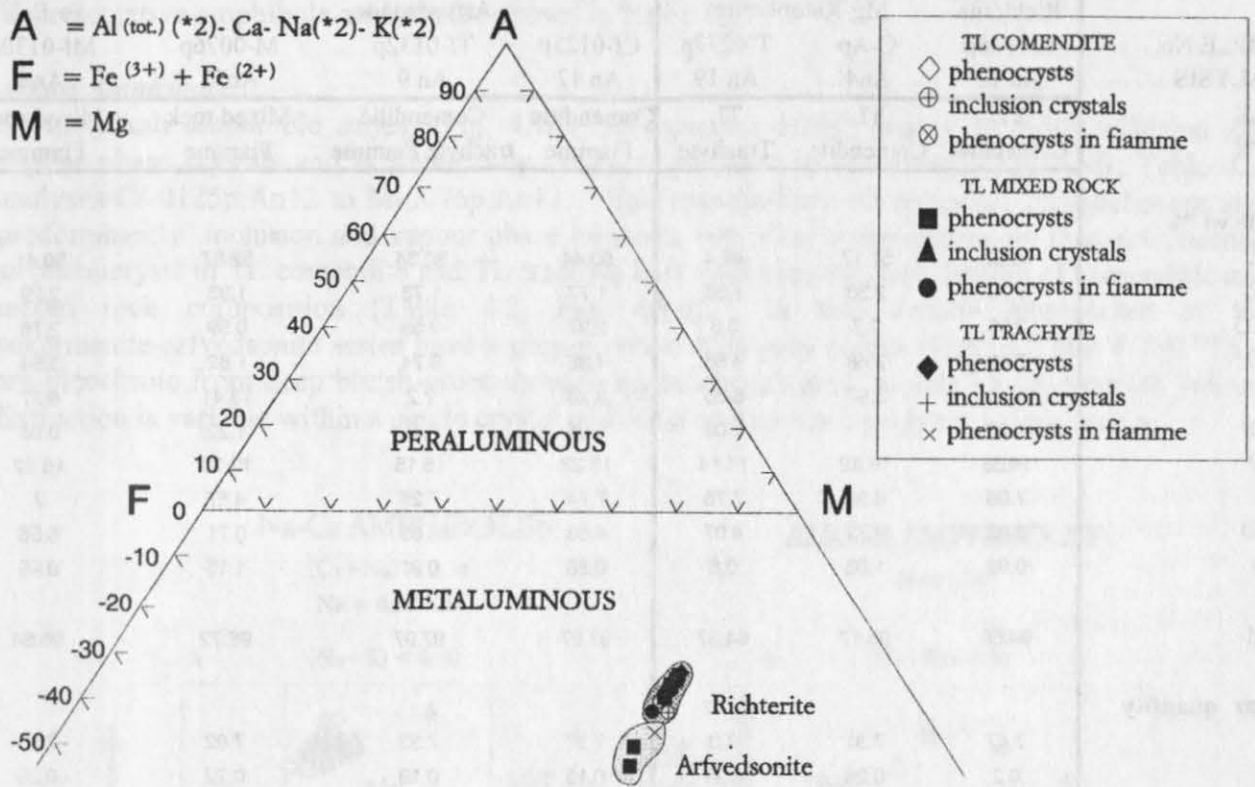


Figure 4.7. AFM diagram divided into metaluminous (below F-M line) and peraluminous (above F-M line) regions, with all amphibole analyses for TL plotting in the metaluminous region. Mineral compositions are plotted using molar quantities normalised to hundred, following the scheme of Abbott (1981).

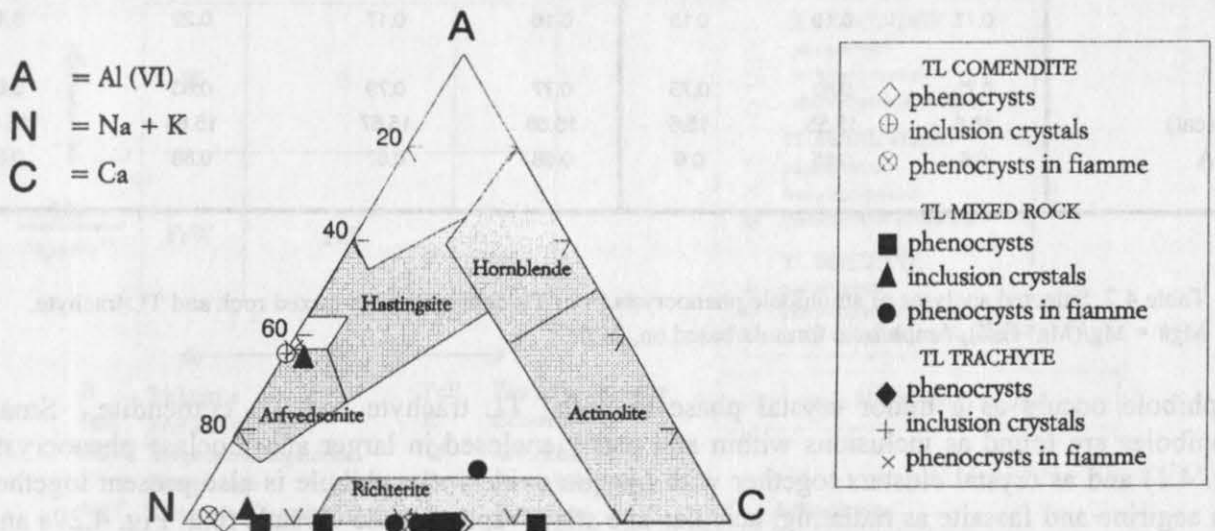


Figure 4.8. Chemical variation of sodic-calcic and alkali amphiboles in TL. Mineral compositions are plotted using molar quantities normalised to hundred, following the scheme of Tröger (1969).

SAMPLE No. ANALYSIS BULK ROCK	SODIC-CALCIC AMPHIBOLES			ALKALI AMPHIBOLES			
	Richterite	Mg-Katophorite		Arfvedsonite		Fe-Eck.	
	C-0046p An 16	C-Ap An4	T-0277p An 19	Cf-0125p An 12	Tf-0132p An 9	M-0076p An11	Mf-0130p An6
	TL Comendite	TL Comendite	TL Trachyte	Comenditic Fiamme	Comenditic trachyte Fiamme	Mixed rock Fiamme	Mixed rock Fiamme
Oxide wt %							
SiO ₂	49.67	51.17	48.4	50.44	50.34	52.57	50.41
TiO ₂	1.75	2.38	1.86	1.77	1.73	1.93	2.29
Al ₂ O ₃	2.55	2.7	3.3	2.97	2.55	0.59	2.76
Fe ₂ O	2.96	7.48	4.66	4.35	6.74	1.82	3.54
FeO	9.48	3.97	8.35	8.26	7.2	13.41	6.27
MnO	1.08	1	1.03	1.05	1.2	1.22	0.93
MgO	14.36	16.82	14.14	15.22	15.15	12.76	16.82
CaO	7.96	6.92	7.76	7.74	7.25	4.57	7
Na ₂ O	3.93	4.72	4.07	4.63	4.85	6.71	5.56
K ₂ O	0.89	1.03	0.8	0.86	0.91	1.15	0.95
Total	94.66	98.17	94.37	97.27	97.97	96.72	96.54
Molar quantity							
Si	7.47	7.31	7.3	7.37	7.32	7.82	7.35
Ti	0.2	0.26	0.21	0.19	0.19	0.22	0.25
Al(IV)	0.45	0.45	0.59	0.51	0.44	0.1	0.47
Al(VI)	0	0	0	0	0	0	0
Fe ³⁺	0.33	0.8	0.53	0.48	0.74	0.2	0.39
Fe ²⁺	1.19	0.47	1.05	1.01	0.88	1.67	0.76
Mn	0.14	0.12	0.13	0.13	0.15	0.15	0.12
Mg	3.22	3.58	3.18	3.31	3.28	2.83	3.66
Ca	1.28	1.06	1.25	1.12	1.13	0.73	1.09
Na	1.15	1.31	1.19	1.31	1.37	1.94	1.57
Na(A)	0.43	0.37	0.44	0.52	0.5	0.67	0.66
K	0.17	0.19	0.15	0.16	0.17	0.22	0.18
Mg#	0.73	0.88	0.75	0.77	0.79	0.63	0.83
Sum (cat)	15.6	15.55	15.6	15.68	15.67	15.88	15.84
Sum A	0.6	0.55	0.6	0.68	0.67	0.88	0.84

Table 4.2. Selected analyses of amphibole phenocrysts from TL comendite, TL mixed rock and TL trachyte. Mg# = Mg/(Mg+Fe²⁺), Amphibole formula based on, 23 O.

Amphibole occurs as a minor crystal phase in both TL trachyte and TL comendite. Small amphiboles are found as inclusions within and partly enclosed in larger anorthoclase phenocrysts (Fig. 4.1) and as crystal clusters together with opaque oxides. Amphibole is also present together with aegirine and fassaite as radiating, acicular late stage vapour phase crystals (e.g. Fig. 4.29a and b).

All of the amphiboles optically identified and analysed are metaluminous (Fig. 4.7) and belong to the sodic-calcic and alkali amphibole series, (Fig. 4.8). On a triangular ANC diagram (Fig. 4.8), most of the amphiboles plot in the richterite field, but further detailed classification, following Leake (1978) indicates that the amphiboles show varying compositions ranging over a continuous

series from ferro-winchite through Mg-katophorite to eckermanite and arfvedsonite. Representative amphibole analysis are shown in Table 4.2.

Alkali Amphibole

Of the alkali amphibole series, (Fig. 4.9B), arfvedsonite occurs mainly as small inclusion and vapour phase crystals and is found only rarely as phenocrysts in fiamme (Fig. 4.9B; Table 4.2, analyses Cf-0125p, An12 to M-0076p, An11). Eckermanite-ferro-eckermanite amphiboles are also predominantly inclusion and vapour phase minerals, but occur more commonly than arfvedsonite as phenocrysts in TL comendite and TL trachyte bulk rock samples, and fiamme of comenditic and mixed rock composition (Table 4.2, Fig. 4.9B). In thin section amphiboles of the eckermanite-arfvedsonite series have a grey-green or blue-grey colour (Figs. 4.1 and 4.3b). They are pleochroic from deep bluish-green through lavender-blue grey, to pale bluish-greenish yellow. Extinction is variable within a single crystal and often anomalous blue-green colours occur.

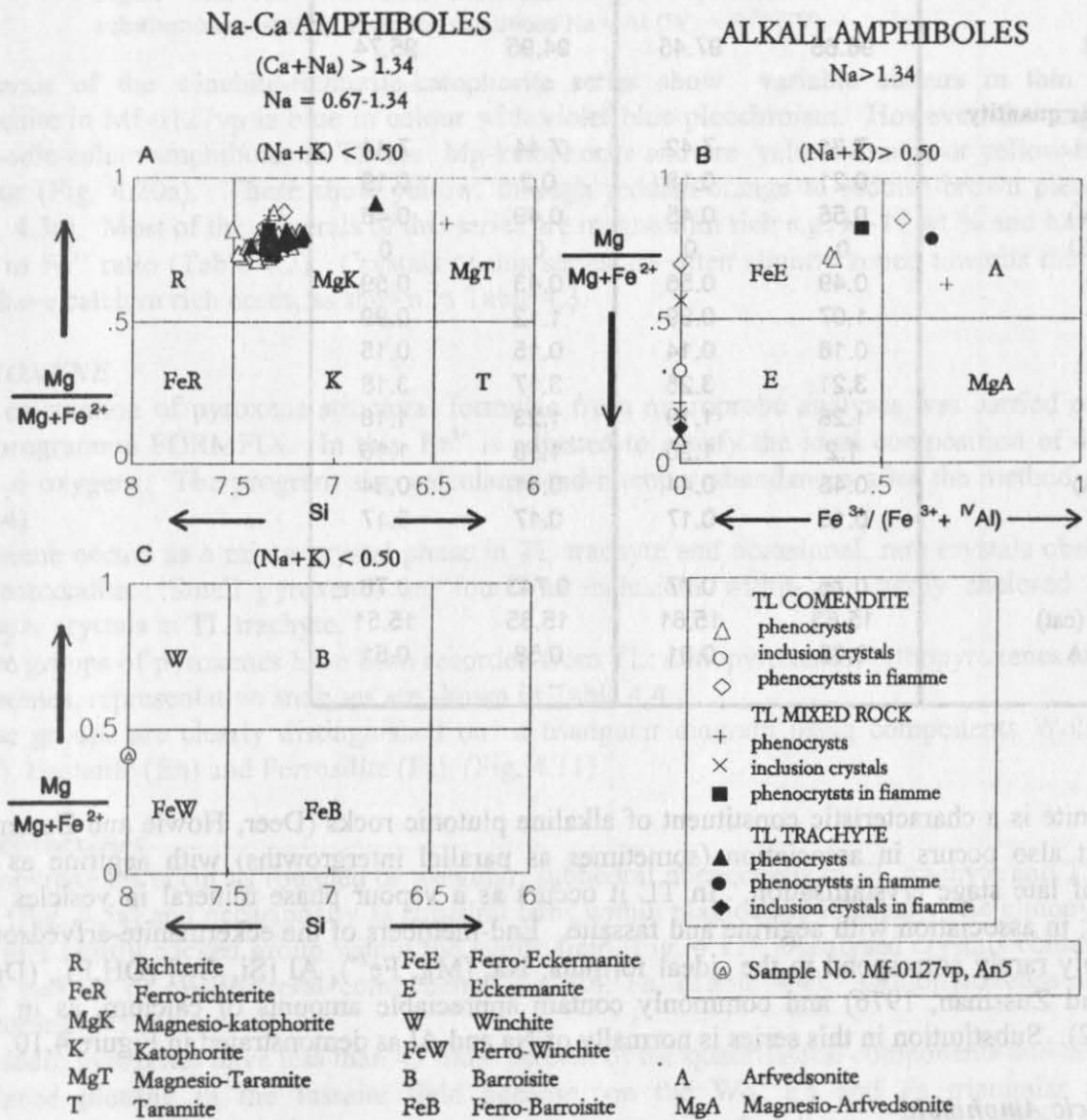


Figure 4.9. Classification of amphiboles after Leake (1978). Sodic-calcic and alkali amphiboles are distinguished using molar amount of (Na + K) and further subdivision is made according to variation in Mg/Mg+Fe²⁺ ratio.

SAMPLE No.	C-0118p		C-0109p	
ANALYSIS	An2-core	An3-rim	An18-core	An19-rim
BULK ROCK	TL Comendite		TL Comendite	
Oxide wt %				
SiO ₂	49.46	50.85	49.64	50.18
TiO ₂	1.88	1.66	1.75	1.68
Al ₂ O ₃	3.19	2.59	2.8	2.61
Fe ₂ O	4.41	5.15	3.86	5.29
FeO	8.65	8.14	8.91	7.98
MnO	1.27	1.15	1.17	1.18
MgO	14.59	14.98	14.22	14.4
CaO	8.11	7.59	7.64	7.46
Na ₂ O	4.2	4.42	4.08	4.02
K ₂ O	0.79	0.92	0.89	0.89
Total	96.65	97.45	94.95	95.74
Molar quantity				
Si	7.31	7.42	7.44	7.44
Ti	0.21	0.18	0.2	0.19
Al(IV)	0.55	0.45	0.49	0.46
Al(VI)	0	0	0	0
Fe ³⁺	0.49	0.56	0.43	0.59
Fe ²⁺	1.07	0.99	1.12	0.99
Mn	0.16	0.14	0.15	0.15
Mg	3.21	3.26	3.17	3.18
Ca	1.28	1.19	1.23	1.18
Na	1.2	1.25	1.18	1.16
Na(A)	0.48	0.44	0.41	0.34
K	0.15	0.17	0.17	0.17
Mg#	0.75	0.77	0.743	0.76
Sum (cat)	15.63	15.61	15.85	15.51
Sum A	0.63	0.61	0.58	0.51

Table 4.3. Selected analyses of amphibole phenocrysts showing the 'normal zoning' of Ca enriched cores and Ca poor rims, that develops during fractional crystallisation.

Arfvedsonite is a characteristic constituent of alkaline plutonic rocks (Deer, Howie and Zussman, 1976) but also occurs in association (sometimes as parallel intergrowths) with aegirine as the product of late stage crystallisation. In TL it occurs as a vapour phase mineral in vesicles and lenticules, in association with aegirine and fassaite. End-members of the eckermanite-arfvedsonite series only rarely correspond to the ideal formula: $\text{Na}_3(\text{Mg}, \text{Fe}^{2+})_4\text{Al}[\text{Si}_8\text{O}_{22}](\text{OH}, \text{F})_2$, (Deer, Howie and Zussman, 1976) and commonly contain appreciable amounts of calcium, as in TL, (Table 4.2). Substitution in this series is normally of Na and Al as demonstrated in Figure 4.10.

Sodic-calcic Amphibole

The bulk of the amphibole phenocrysts in TL are sodic-calcic amphiboles of the richterite-taramite series (Fig. 4.9A). These range in composition from richterite (Table 4.2, analysis C-0046p, An16) through to Mg-taramite, although the majority plot as Mg-katophorite close to the richterite-Mg-katophorite boundary (Fig. 4.9A, Table 4.2). One phenocryst analysis from a mixed-rock fiamme plotted as ferro-winchite (Fig. 4.9C).

Richterite: $\text{Na}_2\text{Ca}(\text{Mg}, \text{Fe}, \text{Mn})_5(\text{OH})_2\text{Si}_8\text{O}_{22}$

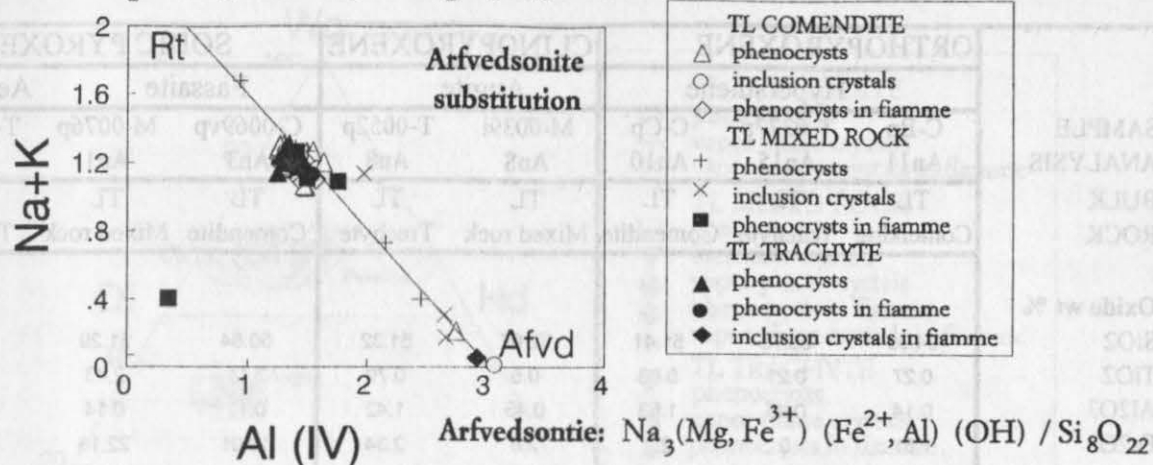


Figure 4.10. Na + K versus tetrahedral Al for amphiboles in TL. Arfvedsonite substitution is satisfied under the conditions $\text{Na} = \text{Al (IV)} + \text{Fe}^{3+} \text{ (IV)}$.

Minerals of the winchite-richterite-katophorite series show variable colours in thin section. Winchite in Mf-0127vp is blue in colour with violet blue pleochroism. However, the majority of the sodic-calcic amphiboles in TL are Mg-katophorite and are yellow-orange or yellow-brown in colour (Fig. 4.20a). These show yellow, through reddish-orange to reddish-brown pleochroism (Fig. 4.3a). Most of the minerals of this series are magnesium rich e.g. 14-17 wt % and have a high Fe^{2+} to Fe^{3+} ratio (Table 4.2). Crystals of this series are often slightly zoned towards the margins and have calcium rich cores, as shown in Table 4.3.

PYROXENE

The calculation of pyroxene structural formulae from microprobe analyses was carried out using the programme FORMFIX. In this, Fe^{3+} is adjusted to satisfy the ideal composition of 4 cations with 6 oxygens. The program also calculates end-member abundances after the method of Duda (1984).

Pyroxene occurs as a minor crystal phase in TL trachyte and occasional, rare crystals observed in TL comendite. Small pyroxenes are found as inclusions within and partly enclosed in large feldspar crystals in TL trachyte.

Three groups of pyroxenes have been recorded from TL: clinopyroxenes, orthopyroxenes and sodic pyroxenes, representative analyses are shown in Table 4.4.

These groups are clearly distinguished on a triangular diagram using components Wollastonite (Wo), Enstatite (En) and Ferrosilite (Fs), (Fig. 4.11).

Clinopyroxenes

Clinopyroxenes occur as rounded or irregular, subhedral phenocrysts in TL trachyte and TL mixed rock (Fig. 4.5a) and occasionally as euhedral laths within plagioclase feldspar. The clinopyroxenes plot in a tightly packed group within the augite field (Fig. 4.11). Analysed crystals contain 86-92 mole percent of quadrilateral components Wo, En, Fs, (Table 4.4). Orthopyroxenes are purer containing >95 mole percent.

The sodic pyroxenes have less than 43 mole percent of the quadrilateral components and aegirine is displaced plotting in the fassaite field because, on the Wo, En and Fs triangular plot the quadrilateral components do not account for the presence of sodium. Augites show some Fs enrichment with a slight decrease in the Wo component. However this is extremely restricted and the number of analysis is too small to describe any specific trend of iron enrichment.

SAMPLE ANALYSIS BULK ROCK	ORTHOPIYROXENE			CLINOPYROXENE		SODIC PYROXENE		
	Hypersthene			Augite		Fassaite	Aegirine	
	C-Bp An11	T-0277p An15	C-Cp An10	M-0039i An8	T-0052p An8	C-0069vp An3	M-0076p An1	T-0282vp An4
	TL Comendite	TL Trachyte	TL Comendite	TL Mixed rock	TL Trachyte	TL Comendite	TL Mixed rock	TL Trachyte
Oxide wt %								
SiO ₂	54.39	53.75	51.41	52.07	51.32	50.64	51.29	51.47
TiO ₂	0.27	0.21	0.88	0.5	0.79	3.11	2.43	0.66
Al ₂ O ₃	0.14	0.45	1.53	0.45	1.42	0.11	0.14	0.17
Fe ₂ O ₃	1.81	0	2.7	2.8	2.34	19.01	22.18	26.47
FeO	15.42	14.8	9.25	8.63	9.64	7.38	7.21	4.63
MnO	2.88	1.63	0.61	1.84	0.6	1.06	1.09	0.53
MgO	24.98	25.78	15	14.16	14.78	0.73	4.47	0.15
CaO	1.41	1.32	18.24	16.26	18.24	4.08	3.57	1.25
Na ₂ O	0.13	0.06	0.45	1.33	0.46	10.43	10.72	11.87
K ₂ O	0	0.01	0.06	0	0	0.01	0.02	0.01
Total	101.4	98.01	100.15	98.03	99.58	96.54	99.15	97.22
Molar quantity								
Si	1.97	1.99	1.92	0	1.93	2.02	2.01	2.04
Ti	0	0	0.02	0.01	0.02	0.09	0.07	0.02
Al(IV)	0	0.01	0.07	0.02	0.06	0	0	0
Al(VI)	0	0.01	0	0	0	0	0	0
Fe ³⁺	0.05	0	0.08	0.08	0.07	0.57	0.65	0.79
Fe ²⁺	0.47	0.46	0.29	0.27	0.3	0.25	0.24	0.15
Mn	0.09	0.05	0.02	0.06	0.02	0.04	0.04	0.02
Mg	1.35	1.42	0.84	0.8	0.83	0.04	0.03	0.01
Ca	0.05	0.05	0.73	0.66	0.74	1.15	1.16	1.29
Na	0.02	0.01	0.02	0.09	0.02	0.79	0.74	0.67
Mg#	0.72	0.76	0.7	0.69	0.69	0.05	0.03	0.01
En	0.67	0.71	0.42	0.4	0.41	0.02	0.01	0
Fs	0.28	0.25	0.15	0.17	0.16	0.14	0.14	0.09
Wo	0.02	0.02	0.33	0.33	0.34	0.63	0.6	0.61
Quad. (%)	96.26	98.7	91.6	90.29	92.52	53.7	51.69	49.01
AC	0.02	0	0.02	0.08	0.02	0.57	0.65	0.67

Table 4.4. Selected pyroxene analyses from the three pyroxene groups occurring in TL. In the sample number, p = phenocryst, i = inclusion crystal and vp = vapour phase crystal. Mg# = Mg/(Mg+Fe^{total}), En, Fs and Wo = Quadrilateral components as mole %, Quad. (%) = Molar abundance of quadrilateral components, AC = NaFe³⁺(SiO₃) Acmite. Structural formula based on 6 oxygens.

Orthopyroxenes

Orthopyroxene occurs predominantly in TL trachyte, as glomerocrysts (Fig. 4.6a and b). Only two crystals were observed in TL comendite samples (Fig. 4.11) and these are rounded with an alteration rim of clinopyroxene and spinel, and probably represent xenocrysts incorporated from TL trachyte. All analysed crystals plot within the hypersthene field with 50-70% Mg (Mg + Fe²⁺ + Fe³⁺ + Mn). For these samples the range in Wo is fairly constant at 0.01 to 0.03 mole percent.

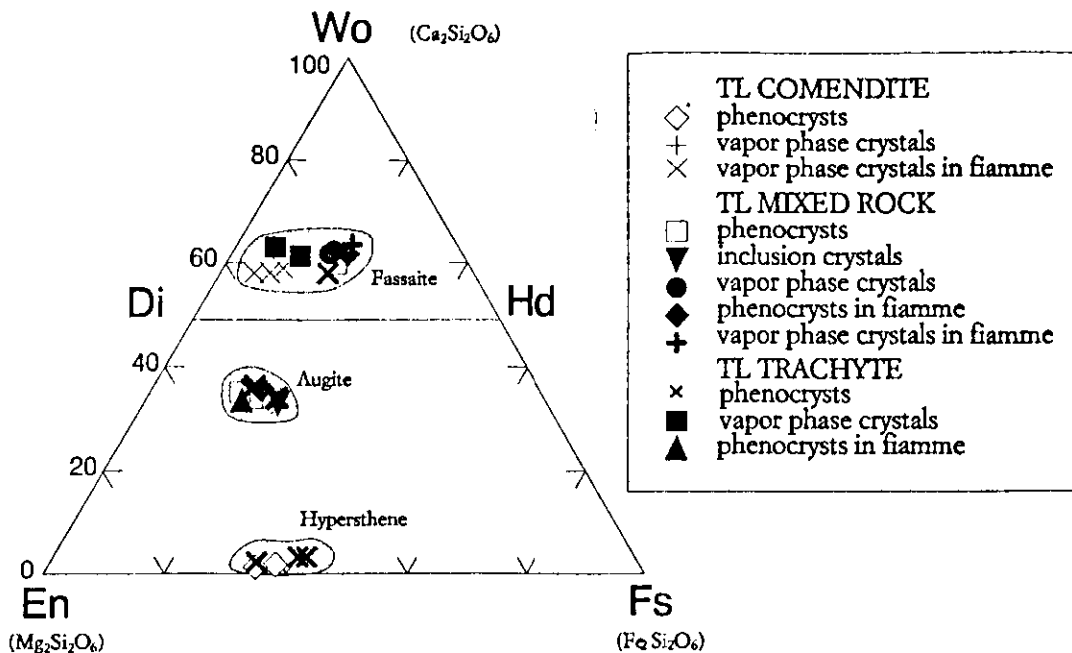
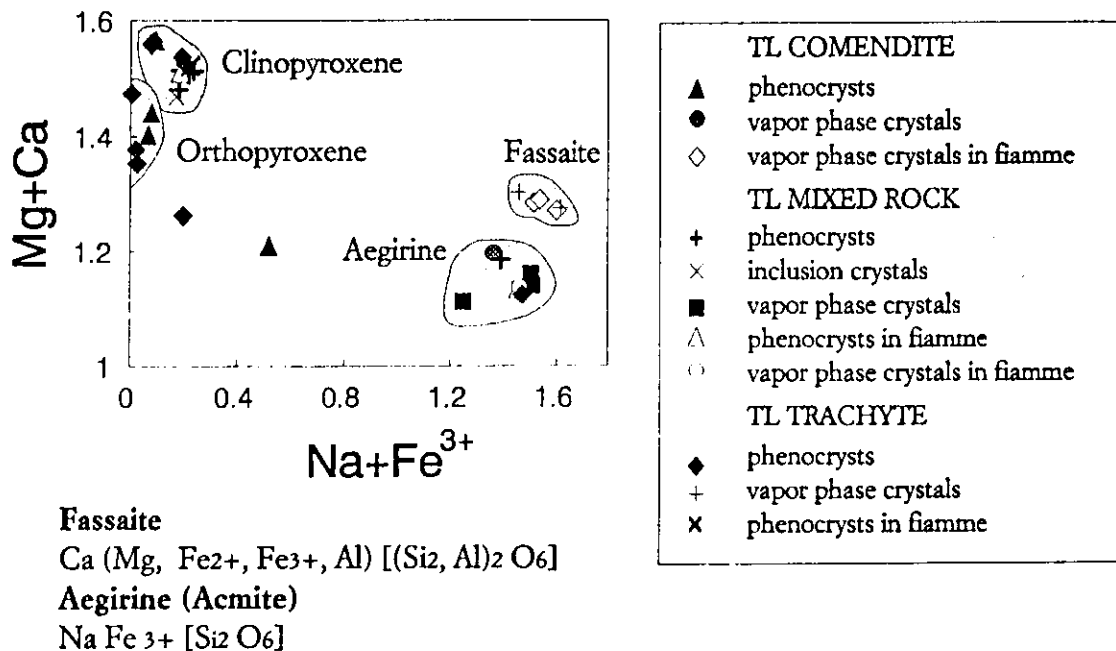


Figure 4.11. Pyroxene groups in TL, clinopyroxene (augite), orthopyroxene (hypersthene) and sodic-calcic rich vapour phase pyroxenes (above Di-Hd line) distinguished using triangular components Wo, En and Fs.

Figure 4.12. Plot of Mg+Ca versus Na+Fe³⁺ to distinguish Ca rich (Fassaite) and Na rich (Aegirine) pyroxenes in TL (After Tröger, 1969).



Sodic pyroxenes

The sodic pyroxenes together with amphibole, comprise most of the vapour phase minerals within TL, (Fig. 4.18). Most of the analyses plot within the fassaite field on the triangular Wo, En, Fs diagram, but this data is better represented on a plot of Ca + Mg versus Na + Fe³⁺, which distinguishes fassaite and aegirine end-members (Fig. 4.12).

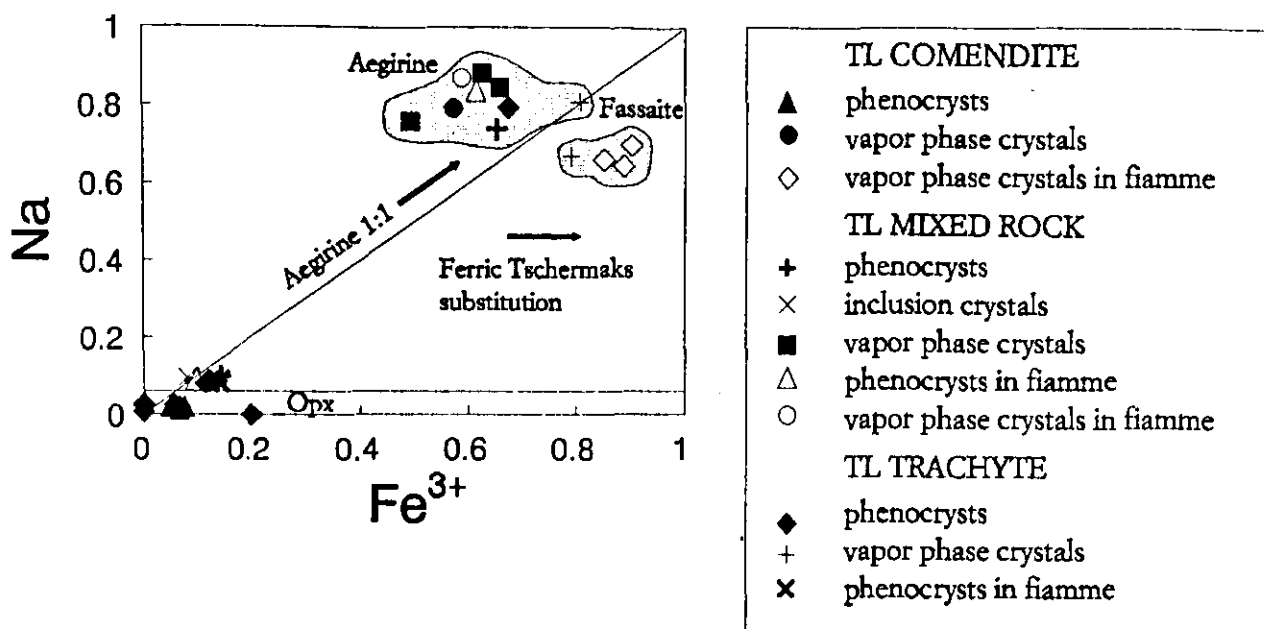


Figure 4.13. Plot of Na versus Fe^{3+} to show the main trend of aegirine substitution and minor ferric Tschermaks substitution in pyroxenes in TL.

The Fe^{3+} content of pyroxenes has been calculated assuming an ideal stoichiometric composition, which introduces a large error. However, a plot of Fe^{3+} versus Na (Fig. 4.13), shows that data plots either side of the Fe^{3+}/Na 1:1 ratio indicating that Fe^{3+} is substituted not only with Na in an acmite component ($Na Fe^{3+} Si_2O_6$) but also by substantial ferric Tschermaks (fassaite: $Ca Fe^{3+} Al SiO_6$) substitution. The number of crystals available for analysis was limited but Figure 4.13 indicates that pyroxenes in TL comendite, particularly vapour phase crystals have lower sodium contents and show a higher degree of ferric Tschermaks substitution compared to phenocrysts and vapour phase crystals in TL trachyte and TL mixed rock samples. However, most of the ferric iron trends start off on the $Fe^{3+}/Na = 1$ line (Fig. 4.13), suggesting that acmite substitution was the dominant process for Na incorporation, with ferric Tschermaks substitution affecting only the late stage vapour phase crystal compositions.

FELDSPAR

The structural formulae of feldspar has been calculated using the programme FORMFIX on the basis of 32 oxygens and Ca, Na and K are allotted to the respective end-members An, Ab and Or. TL contains two groups of feldspars: plagioclase feldspar and the alkali feldspars, anorthoclase and sanidine. These two groups are found in both TL comendite and TL trachyte, and in TL mixed rock samples (Fig. 4.14)

The feldspar population in TL comendite and TL trachyte is dominated by alkali feldspars. Plagioclase occurs as a subsidiary phase in TL trachyte.

Alkali feldspar

In TL comendite the alkali feldspar composition is predominantly anorthoclase (AB >63%) together with, less common, sanidine (Table 4.5 and Fig. 4.14A). TL mixed rock samples similarly have a predominance of anorthoclase over sanidine (Fig. 4.14B). In TL trachyte however, the bulk of the alkali feldspars are sanidine. This compositional difference and the occurrence of higher temperature forms in TL trachyte may be related to differing magmatic temperatures which are estimated (Fig. 4.17) to be in the range of minimum 810-910°C for TL trachyte and 650-811°C for

SAMPLE No. ANALYSIS	TL COMENDITE						TL MIXED ROCK		TL TRACHYTE			
	Andesine	Oligoclase	Albite	Sanidine	Anorthoclase		Oligoclase	Sanidine	Andesine	Oligoclase	Albite	Sanidine
	C-0023p An12	C-0277 An6	C-0010p An3	C-0023p An2	C-0065p An14	C-0227m An16	M-0001p An8	M-0002p An2	T-0282p An7	T-0282p An6	T-0282p An12	T-0132p An1
Oxide wt %												
SiO ₂	61.64	65.11	66	70.76	70.3	67.23	62.42	67.58	59.23	61.76	69.75	67.59
TiO ₂	0.12	0.13	0.12	0	0.07	0.44	0.08	0.04	0.13	0.09	0.06	0.02
Al ₂ O ₃	23.66	21	20.24	18.72	19.46	15.6	22.45	18.12	23.9	22.73	19.18	18.2
FeO	0.63	0.62	0.6	0.7	0.69	2.5	0.38	0.58	0.64	0.53	0.54	0.74
MnO	0	0	0.03	0.01	0.01	0.08	0	0	0.01	0.01	0	0
MgO	0.05	0.03	0.01	0.01	0	0.07	0.01	0	0.04	0.03	0	0
CaO	6.45	2.9	1.77	0.08	0.35	0.76	4.4	0.07	6.98	5.23	0.35	0.11
Na ₂ O	5.9	8.54	8.11	5.45	7.82	7.04	7.54	6.9	6.94	7.44	9.06	7.84
K ₂ O	0.88	0.47	2.17	6.05	3.06	4.38	1.16	9.23	0.88	1.25	2.21	5.13
Total	99.32	98.8	99.2	101.84	101.76	98.1	98.45	99.53	98.76	99.05	101.17	99.66
Molar quantity												
Si	11.02	11.59	11.74	12.27	12.12	12.27	11.24	12.12	10.75	11.11	12.1	12.08
Ti	0.02	0.02	0.02	0	0.01	0.06	0.01	0	0.02	0.01	0.01	0
Al	4.98	4.4	4.25	3.83	3.95	3.35	4.76	3.83	5.11	4.82	3.92	3.83
Fe ²⁺	0.09	0.09	0.09	0.1	0.01	0.38	0.06	0.09	0.1	0.08	0.08	0.11
Mn	0	0	0	0	0	0.01	0	0	0	0	0	0
Mg	0.01	0.01	0	0	0	0.02	0	0	0.01	0.01	0	0
Ca	1.23	0.55	0.34	0.01	0.06	0.15	0.85	0	1.36	1.01	0.06	0.02
Na	2.04	2.95	2.8	1.83	2.61	2.49	2.63	2.4	2.44	2.6	3.05	2.72
K	0.2	0.11	0.49	1.34	0.67	1.02	0.27	1.43	0.2	0.29	0.49	1.17
Sum Z	16	15.55	15.99	16.1	16.08	15.62	16	15.94	15.86	15.92	16.02	15.92
Sum X	3.48	3.61	3.63	3.18	3.35	3.66	3.75	3.84	4	3.89	3.6	3.91
OR	5.79	2.93	13.56	42.04	20.1	27.87	7.08	37.16	5.09	7.35	13.57	29.96
AB	58.75	81.75	77.12	57.52	77.99	68.07	70.27	62.5	61.02	66.75	84.64	69.53
AN	35.46	15.32	9.32	0.44	1.91	4.06	22.65	0.35	33.89	25.9	1.79	0.51

Table 4.5. Representative feldspar analyses for TL comendite, TL mixed rock and TL trachyte. Triangular components OR, AB and AN have been used to make the ternary diagram in Fig. 4.14.

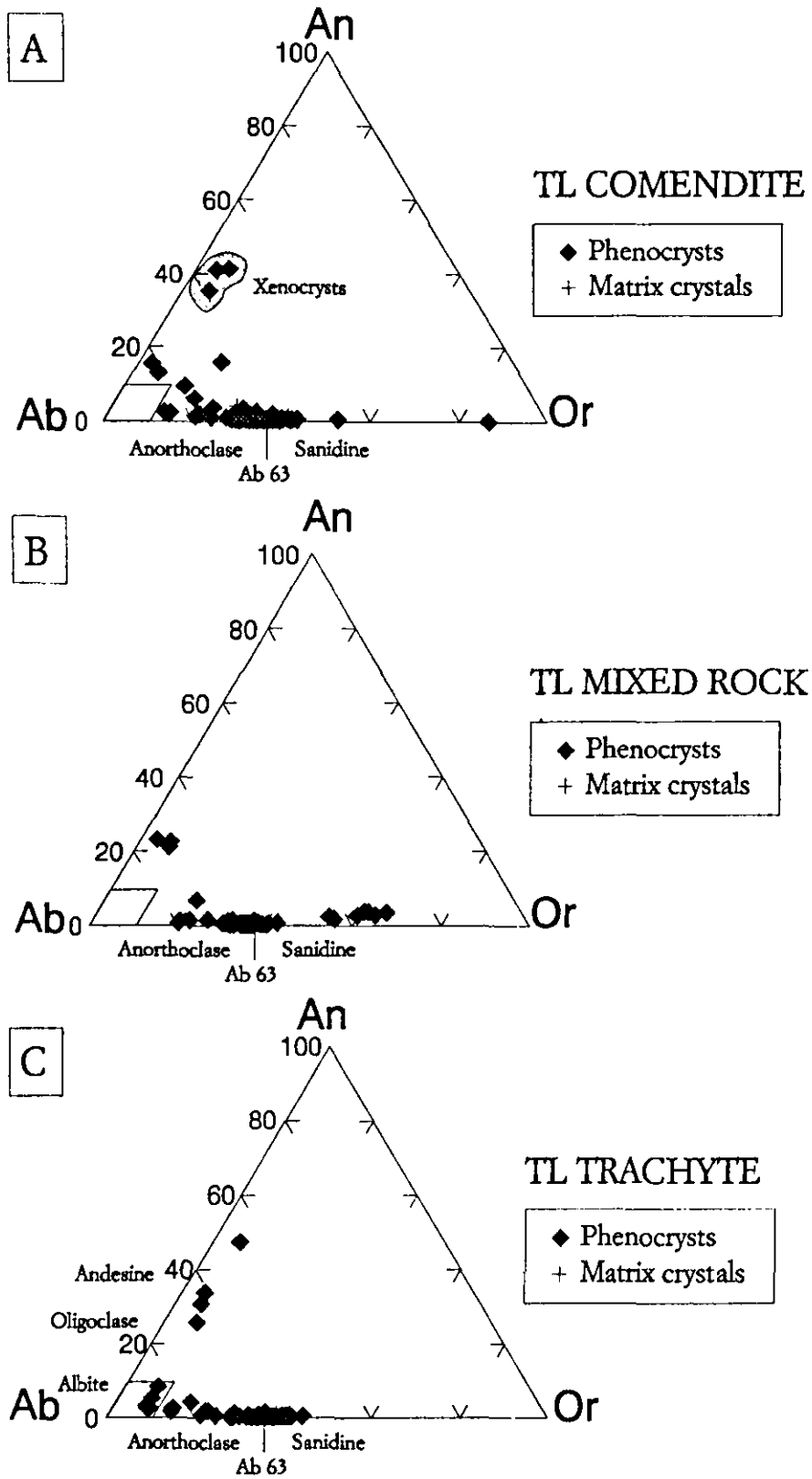


Figure 4.14. Variation in composition of feldspars in (A) TL comendite, (B) TL mixed rock and (C) TL trachyte. Phenocrysts within the shaded area in A, are interpreted as xenocrysts incorporated from TL trachyte. Significantly sodic plagioclase (Albite) occurs within TL trachyte (see text for discussion).

TL comendite. Occasionally anorthoclase crystals in TL trachyte are embayed and irregular in outline (Fig. 4.4), suggesting that they may be xenocrysts incorporated from comendite.

Plagioclase

TL trachyte shows the widest range in plagioclase composition from andesine to albite. Noticeably, albite is only found in TL trachyte (Fig. 4.14C) TL mixed rock samples and TL comendite lack this sodic end-member. The normal development of peralkalinity in volcanic suites shows progressive depletion of Na_2O in the melt by feldspar crystallisation. Absence of sodic feldspar in TL comendite may be due to the fractional crystallisation of feldspar which progressively reduced the Na_2O content of the melt (Fig. 5.6 and 5.7). The rounding and irregular embayment observed in plagioclase feldspars in TL comendite (Fig. 4.2) and TL mixed rock samples (e.g. phenocrysts with analyses plotting in the oligoclase and andesine fields in figure 4.19A and B), is typical of the texture produced by resorption of phenocrysts during the disequilibrium reaction with liquid of contrasting composition. This suggest that these may be xenocrysts incorporated from comenditic trachyte.

The feldspars in general, do not show any visible petrographic zoning, but analyses indicate some compositional inhomogeneity. Many phenocrysts have Ca rich cores and Ca poor rims (Appendix II), although this is a 'normal' zonation which typically develops during fractional crystallisation (Section 5.2.4).

OPAQUE OXIDE

Oxides of both the ilmenite-hematite solid-solution (rhombohedral) and the ulvöspinel-magnetite (spinel) solid-solution series are common accessory phases in TL. Structural formulae have been calculated from microprobe analysis using the appropriate $\text{Fe}^{2+}/\text{Fe}^{3+}$ distribution on the basis of 2

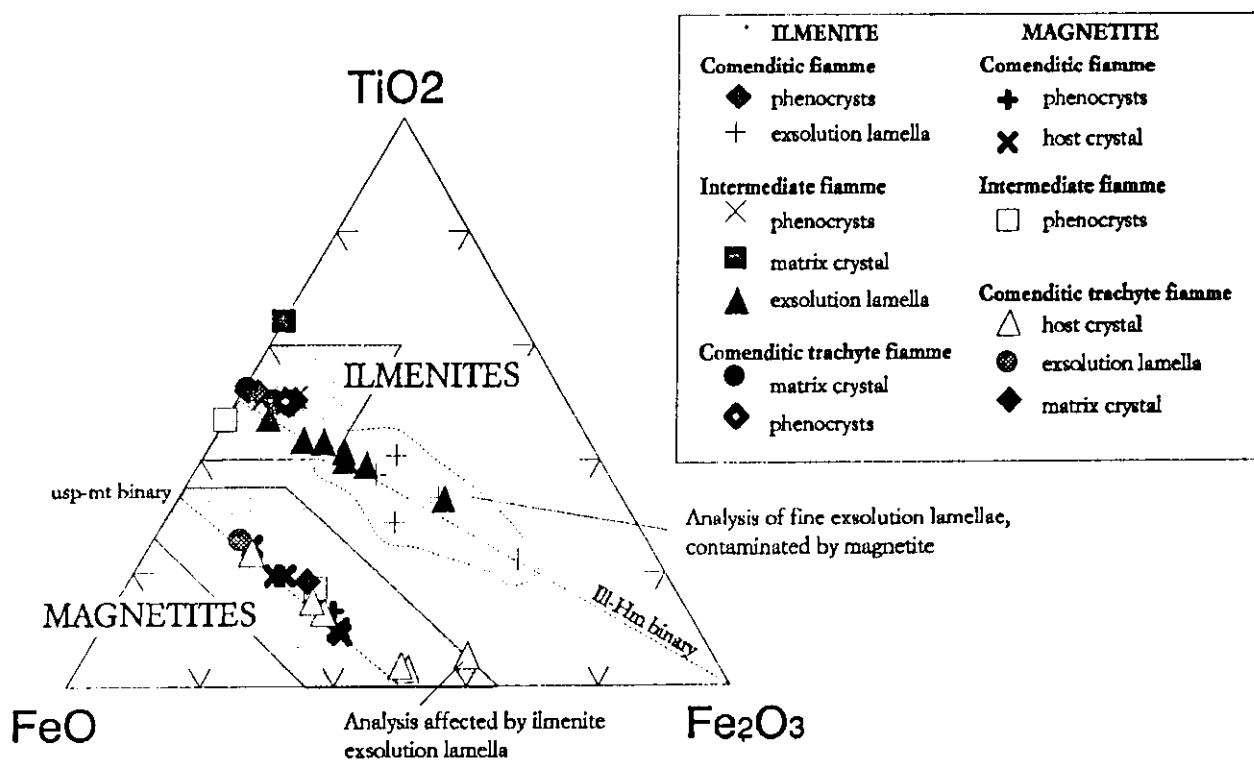


Figure 4.15. Composition of ulvöspinel-magnetite and ilmenite-hematite solid solutions in TL, shown on the Fe-Ti oxide ternary. Molar proportions normalised to a hundred are plotted.

SAMPLE ANALYSIS	ILMENITE					MAGNETITE			
	Cf-0120p	Cf-0120e	If-0115p	Tf-0068e	Tf-0125p	Cf-0120h	If-0115p	Tf-0068h	Tf-0125i
	An2	An4	An4	An11	An1	An6	An5	An8	An4
BULK ROCK	Comenditic Fiamme	Intermediate Fiamme	Comenditic Fiamme	trachyte Fiamme		Comenditic Fiamme	Intermediate Fiamme	Comenditic Fiamme	trachyte Fiamme
Oxide wt %									
SiO2	0.04	0.09	0.02	0.013	0.02	0.09	0.08	0.04	0.07
TiO2	49.78	29.01	45.57	42.21	45.46	6.86	13.14	1.99	14.06
Al2O3	0.02	0.022	0.07	0.27	0.05	0.18	0.48	0.61	0.42
Fe2O3	1.15	41.18	15.23	11.5	15.27	55.29	43.63	64.66	40.78
FeO	40.27	19.52	32.62	36.8	33.89	36.76	37.3	27.61	37.38
MnO	4.46	5.17	2.58	0.62	2.85	0.69	2.06	2.5	1.99
MgO	0	0.71	3.21	0.28	2.21	0.02	2.41	1.7	0.84
CaO	0	0.01	0.03	0	0.04	0	0.01	0.02	0
Na2O	0	0.04	0	0.04	0.03	0	0.01	0	0.54
K2O	0.01	0	0	0	0	0.02	0.01	0	0.02
CrO3	0.02	0.04	0	0	0	0	0	0.01	0
Total	96.1	95.98	99.3	91.84	99.81	99.9	99.14	99.13	96.08
Molar quantity									
Si	0	0	0	0	0	0	0	0	0
Ti	0.98	0.58	0.86	0.87	0.86	0.2	0.37	0.33	0.41
Al	0	0.01	0	0.01	0	0.01	0.02	0.04	0.02
Fe3+	0.03	0.83	0.29	0.24	0.29	1.59	1.23	1.13	1.19
Fe2+Mn	0.88	0.44	0.68	0.85	0.71	1.18	1.17	1.23	1.22
Mn	0.1	0.12	0.05	0.01	0.06	0.02	0.07	0.03	0.07
Mg	0	0.03	0.12	0.01	0.08	0	0.14	0.03	0.05
Xilm	0.98	0.55	0.84	0.88	0.84				
Xulv						0.2	0.34	0.33	0.39

p = phenocryst e = exsolution lamella
h = host crystal i = inclusion crystal

Structural formula for ilmenite based on 3 oxygens
Structural formula for ilmenite based on 4 oxygens

Table 4.6. Representative opaque oxide analyses, taken from comenditic fiamme (Cf), intermediate fiamme (If) and comenditic trachyte fiamme (Tf) in TL1 and TL2.

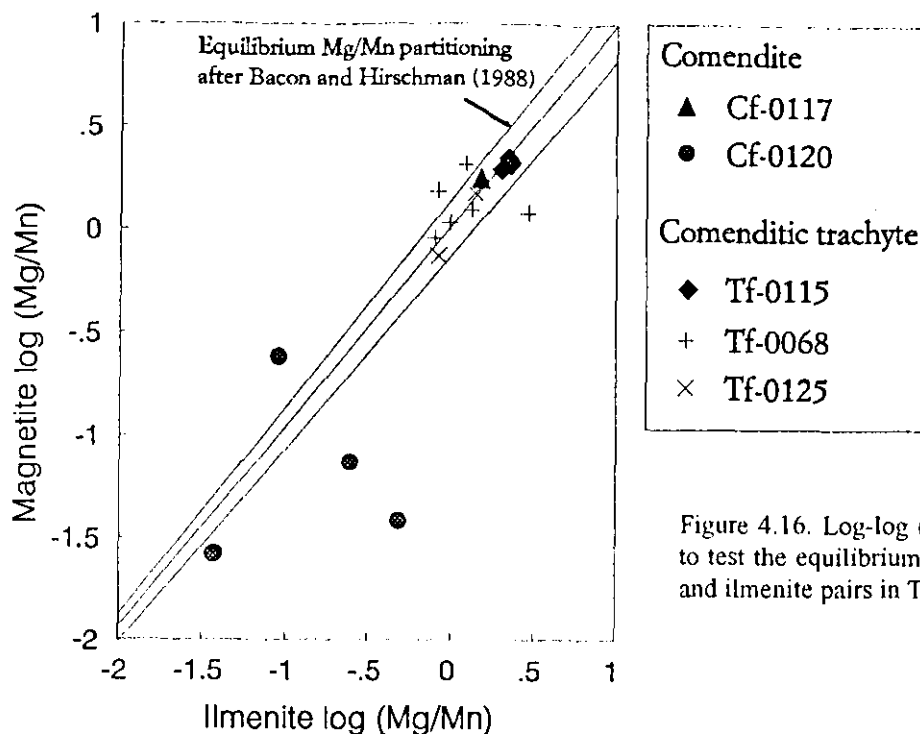


Figure 4.16. Log-log (Mg/Mn) plot to test the equilibrium of magnetite and ilmenite pairs in TL.

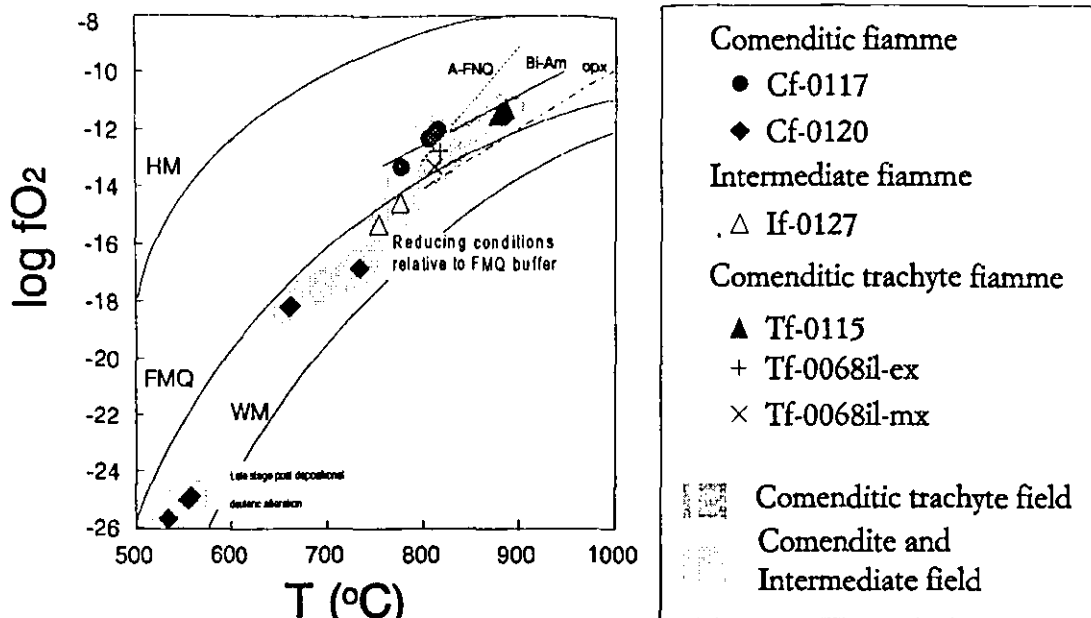
cations and 3 oxygens for ilmenite solid solution and 3 cations and 4 oxygens for magnetite solid solution.

The end-member concentrations of ulvöspinel, magnetite, ilmenite and hematite, and the end-member mole fractions $X_{usp} = \frac{usp}{usp+mt}$ and $X_{ilm} = \frac{ilm}{ilm+hem}$ have been calculated by the programme FORMFIX (Freundt and Tait, 1987) following the method of Stromer (1983). Oxides of these two series are clearly distinguished on the Fe-Ti oxide ternary (Fig. 4.15) and in both cases nearly all analysis plot on the ulvöspinel-magnetite binary (solid-solution line) and the ilmenite-hematite binary. This indicates that the amount of analytical error was minimal, other than for one analysis of a host crystal in comenditic trachyte fiamme (Fig. 4.15), ilmenite exsolution for example, has not affected magnetite measurements.

Crystals chosen for analysis include phenocryst, matrix and inclusion crystals in comenditic, intermediate (homogeneously mixed) and comenditic trachyte fiamme. Selected analysis are presented in Table 4.6. Phenocrysts in comenditic and comenditic trachyte fiamme show evidence of sub-solidus exsolution. Electron backscatter images reveal dark lamellae of ilmenite in magnetite grains. Lamellae are generally only a few microns wide, thus reliable microprobe measurements were difficult to obtain.

The Mg/Mn ratio has been used as a test for equilibrium for these phases (Bacon and Hirschman, 1988) and Figure 4.16 shows that most of the data scatter about the equilibrium conditions. Data from sample Cf-0120 plots over a wide range, as these points represent analyses of very fine exsolution lamella, and analyses have been contaminated by measurement of the host crystal. Samples plotting close to equilibrium were chosen to calculate temperature and oxygen fugacity (Fig. 4.17). The thermometric calculation was carried out using the programme CELCIUS (Freundt and Bednarz 1987, 1988, Appendix II) following the method of Spencer and Lindsley (1981).

Data are extremely limited, but give a rough guide to possible temperature ranges of comendite and comenditic trachyte in TL. The data are consistent with *conclusive field evidence* which demonstrates the considerable difference in temperature and related viscosity of TL comendite and TL trachyte for example, Figures 2.29, 2.35b, 2.40 and 2.41. Although these figures show



Buffer curves, calculated after Wones (1982)
 HM = Hematite/Magnetite
 FMQ = Fayalite/Magnetite + Quartz
 WM = Wustite + magnetite

A-FNQ = Acmite /Na disilicate + Magnetite + Quartz boundary estimated by Carmichael et al. (1974; p.287) for unit activities of these phases

opx = trend of orthopyroxene bearing rhyolites
 Bi-Am = trend of amphibole biotite bearing dacites (from Carmichael, 1967)

Figure 4.17. Fugacity of oxygen plotted against temperature. Data calculated from oxide pairs. (After Spencer and Lindsley, 1981).

structures which are interpreted as being post-depositional, and thus represent temperature and related viscosity during post-depositional deformation, they imply an *initial* difference in temperature, which was probably related to magmatic conditions.

All data for trachytic samples cluster above the FMQ buffer (Fig. 4.17) with a range in fO_2 of -14.5 to -11.7, and indicate a temperature range of 810-910°C. Data for intermediate and comenditic samples plot over a wider range from -18 to -12.2 fO_2 and indicate a range in temperature from 650-811°C. The three data points for Cf-0120 plotting below fO_2 -24 and 600°C are from exsolved crystals indicating strongly reduced conditions. As it is extremely unlikely that Fe-Ti oxides would crystallise at such low temperatures these probably represent modified crystals of the higher temperature group.

TL trachyte has an unusually high fO_2 compared to TL comendite and intermediate samples. The few data points indicate that the trend of comenditic trachyte oxides ranges from above the opx line across the Bi-Am line and over sodic pyroxene stability which is in agreement with the occurrence of sodic pyroxenes and amphiboles in TL trachyte samples.

Data from comenditic samples ranges from above the opx line to above the A-FNQ line (Fig. 4.17) and is similarly in agreement with petrographic observation of sodic pyroxenes and amphiboles in these samples.

STABILITY CONSIDERATIONS

It is generally believed that the presence of amphibole indicates 'wet' crystallisation conditions and that a minimum H_2O content is required to stabilise amphibole. The calculations of Naney (1983) indicate that hornblende, for example requires 3-4 wt.% H_2O in order to be stable. However

amphibole stability is not only controlled by $P(\text{H}_2\text{O})$, but also temperature (T), total pressure (P), oxygen fugacity ($f\text{O}_2$) and magma composition (Helz, 1982). Magma composition controls not only the stability but also the composition of the amphibole (e.g. Giret et al. 1980).

The predominance of amphibole over pyroxene in TL, particularly TL trachyte, argues for high volatile contents, and suggests a minimum H_2O content of ca. 3 wt.%. However as suggested above, other parameters such as $f\text{O}_2$ have a considerable influence on determining the mineral assemblage which crystallises from the melt. Thus the presence of amphibole in both TL comendite and TL trachyte only provides a rough guide to the probable magmatic water content.

SECTION II

4.4 OTHER COMPONENTS IN TL

As well as their characteristic mineral assemblages, TL comendite and TL trachyte contain a wide variety of other components. These include: (1) non-crystalline juvenile components, which range from: pyroclasts, including fiamme and shards of varying composition, to glassy and cryptocrystalline trachybasalt globules which are interpreted to have formed in the magma chamber; (2) non-juvenile lithic fragments; (3) coarsely crystalline, partially infilled vesicles (lenticules) and (4) finely crystalline matrix, showing a range of textures.

4.4.1 TL Trachybasalt globules

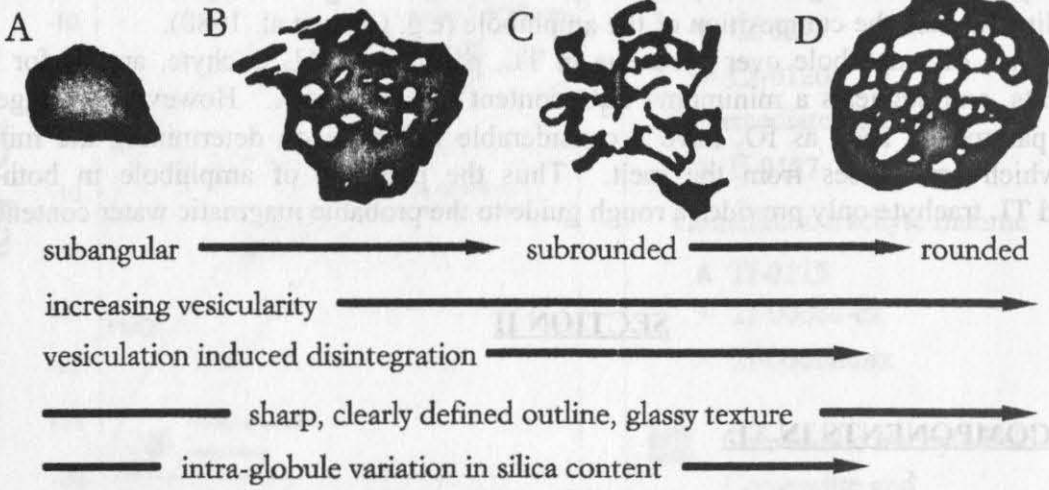
Trachybasalt is ONLY found within TL2, where it occurs as small (<7mm) globules or subangular fragments, which are finely dispersed through TL mixed rock lithofacies M4m and TL trachyte (lava-like) lithofacies T5L. Crushed rock separates could not be prepared for XRF analysis because of the intimate and very small scale relationship between the trachybasalt and the surrounding TL trachyte and TL mixed rock.

Trachybasalt globules have been subdivided into three categories on the basis of chemical composition (Fig. 5.1b), textural and morphological features, which are summarised in Table 4.7. The three types are quite distinctive in thin section, although they can show a range of morphologies, as illustrated in Figures 4.18 and 4.19.

Globule type 1: Trachybasalt end-member

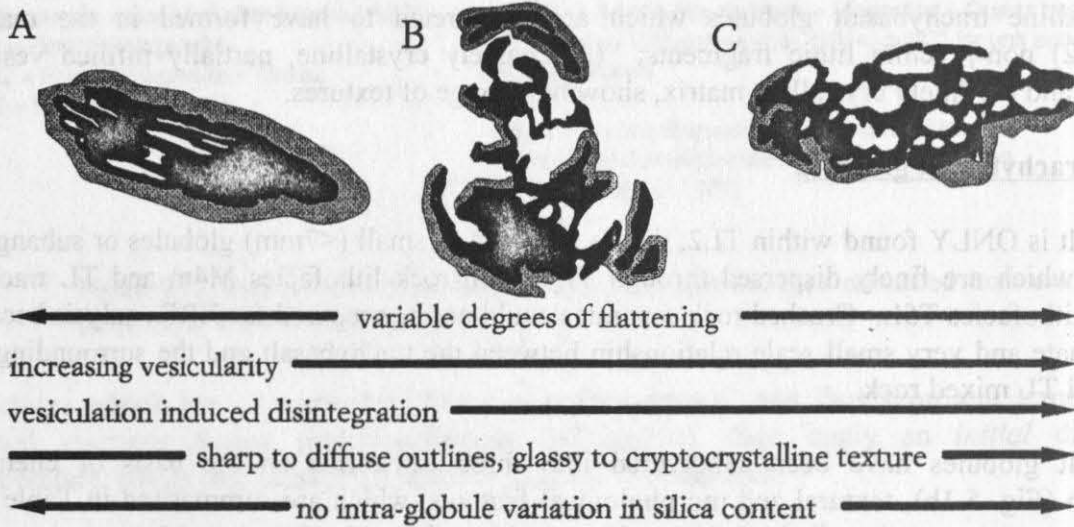
These globules have the lowest silica content and are composed of black, trachybasalt glass or *tachylite* (after MacDonald, 1972). They vary in outline from angular to subrounded or rounded (Fig. 4.19, 1a). Vesicularity is variable. Some fragments are non-vesicular others are highly expanded, skeletal in outline and partially fragmented (Fig. 4.19, 1b). These highly expanded fragments (Fig. 4.18, Globule type 1c) do not show signs of flattening and shear. Therefore the fragmentation is inferred to be the result of extreme vesiculation of particles during magma-mixing (Section 6.2.2) followed by cooling, rather than by vesiculation following deposition and breakage during rheomorphism, where particles should show evidence of flattening and shear. The degree of vesiculation is not size dependant. Some particles are vesicular throughout, others (for example, Fig. 4.18, 1d) are subspherical in outline and have a glassy non-vesicular rind with a concentration of vesicles in the centre of the globule. Often vesicle size increases towards the centre of these globules. Analysed globules of the type 1 category show an 'intra-globule' variation in composition. Margins of the globules have silica and alkali enriched margins e.g. 38 wt.% SiO_2 in the core compared to 57 wt.% SiO_2 at the margin, this was probably the result of contamination by the surrounding magma (Section 6.2.2).

GLOBULE TYPE 1: TRACHYBASALT END-MEMBER



GLOBULE TYPE 2: MANTLED

■ Comenditic trachyte mantle



GLOBULE TYPE 3: DIFFUSE



Granular, cryptocrystalline texture
 Diffuse, but rounded, amoeboid outline
 Non-vesicular or slightly vesicular
 No intra-globule variation in silica content

0.5 mm

Figure 4.18. Classification and morphology of trachybasalt globules in TL2. Diagrams are drawn from sections taken parallel to the inferred flow direction.

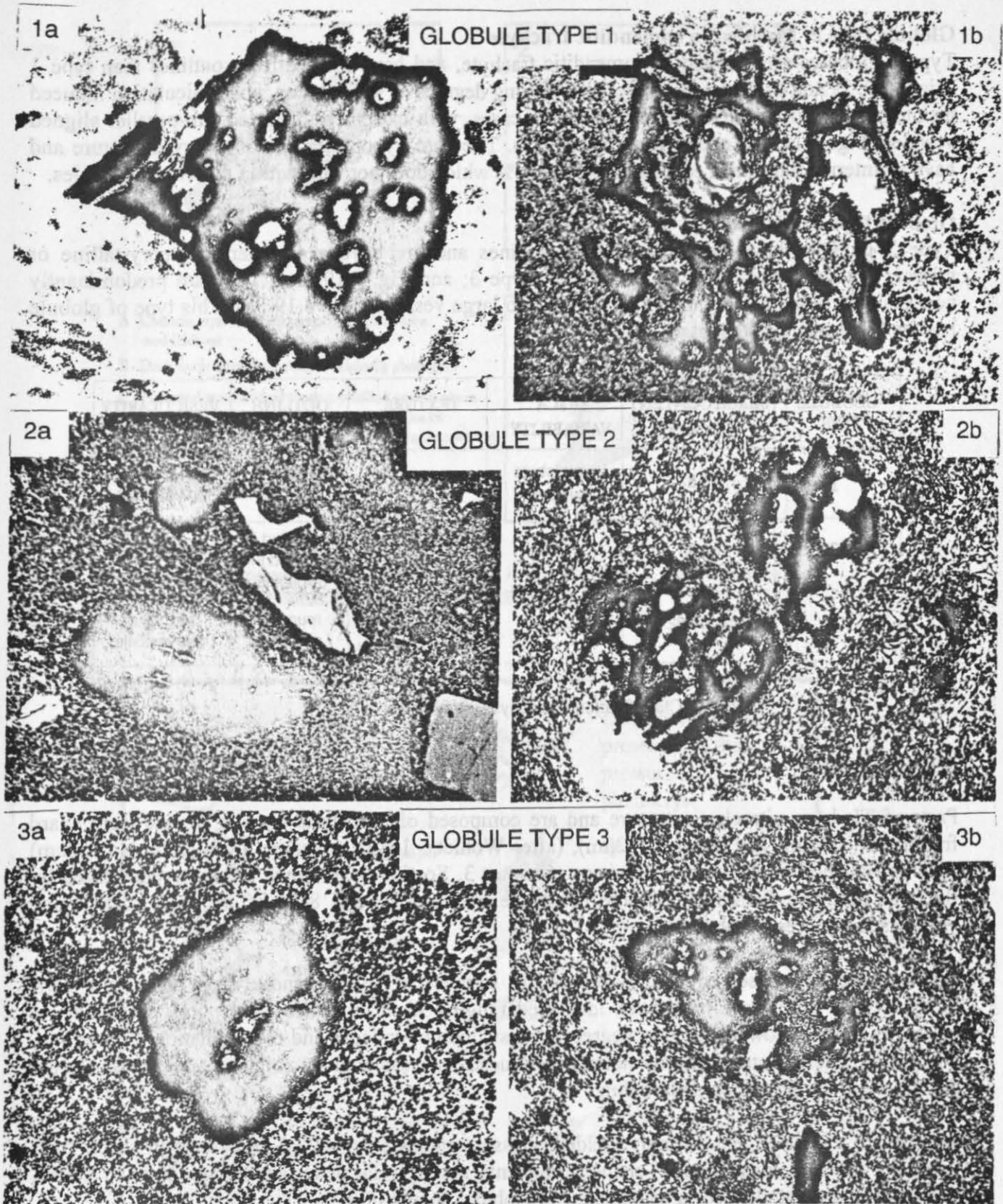


Figure 4.19. Photomicrographs (taken under plane polarised light) of the trachysalt globules classified in Figure 4.18.

Globule type 2: Mantled in comenditic trachyte

Type 2 globules are mantled in comenditic trachyte, and have more diffuse outlines than type 1 (Fig. 4.19, 2a and b). Similarly they show varying degrees of vesiculation, and vesiculation induced disintegration, but are also flattened in some cases, with extremely distorted sub-parallel aligned vesicles (Fig. 4.19, 2a) and ellipsoidal outlines. They are hypocrySTALLINE or glassy in texture and have an intermediate silica content of ca. 59 wt.% which does not vary within individual globules.

Globule type 3: Diffuse

Type 3 globules have diffuse amoeboid outlines and are have a granular cryptocrystalline or microcrystalline texture (Fig. 4.18, Globule type 3; and Fig. 4.19, 3a). They are predominantly non-vesicular although some contain one or two large vesicles (Fig. 4.19 3b). This type of globule has the highest silica content ca. 61-62 wt.%.

GLOBULE TYPE	SILICA CONTENT (wt %)	SILICA VARIABILITY	TEXTURE	OUTLINE	VESICULARITY
1	38-57	intra-globule variation	glassy	rounded to angular	non-vesicular to vesicular
2	ca.59	none	hypocrySTALLINE / glassy	mantled, rounded to ellipsoidal	vesicular
3	ca. 61-62	none	cryptocrystalline / microcrystalline	rounded / amoeboid	slightly to non-vesicular

Table 4.7. Classification of trachybasalt globules in TL2.

4.4.2 Pyroclasts

Parts of TL have vitroclastic texture and are composed of pyroclasts ranging in size from shard fragments (<62 μ m) and shards (>62 μ m), (after Wohletz, 1983), to larger juvenile clasts (<50cm) such as flattened pumice and scoria rags (Chapter 3, Section 3.3), which are now represented by flattened elongate fiamme. Fiamme constitute between 20 and 80% of the bulk rock where vitroclastic textures are observed.

Fiamme are best observed in thin section, in samples of TL comendite from flow unit TL1. Several types of fiamme have been identified ranging from devitrified and poorly vesicular, to glassy fragments showing varying degrees of vesiculation, collapse and revesiculation. Figure 4.20 details the internal structures of fiamme produced by vesiculation, collapse and revesiculation during eruption, deposition and cooling.

Shards are visible in less strongly welded, glassy samples (Fig. 4.27a) and range in shape from flattened tricusps, lunate and 'Y' shaped fragments, through flat plates and fibrous pumice shards, to less vesicular angular scoria fragments and globular shards (Fig. 4.21).

The shape of shards varies with composition and related vesicularity (Fig. 4.22). Comenditic shards are commonly cusped, platy or fibrous (Fig. 4.21); comenditic trachyte shards are angular, poorly vesicular fragments or globules (Fig. 4.23). Remnant shard outlines can be identified in some devitrified samples. In very highly welded samples, glass shards are extremely attenuated and are moulded tightly around larger particles (Fig. 4.27c) such that the shard structure is obscured. Individual shard outlines are only preserved in the pressure shadows behind large crystals or lithic fragments.

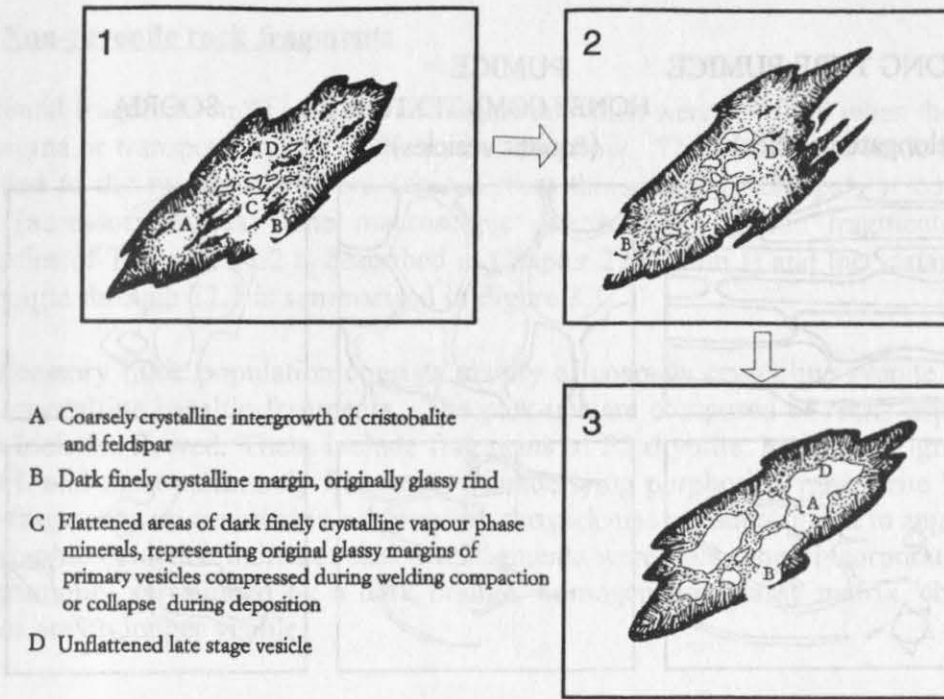


Figure 4.20. Progressive revesiculation of fiamme in TL1. Diagrams 1, 2 and 3 indicate how progressive revesiculation destroys evidence of earlier vesicles.

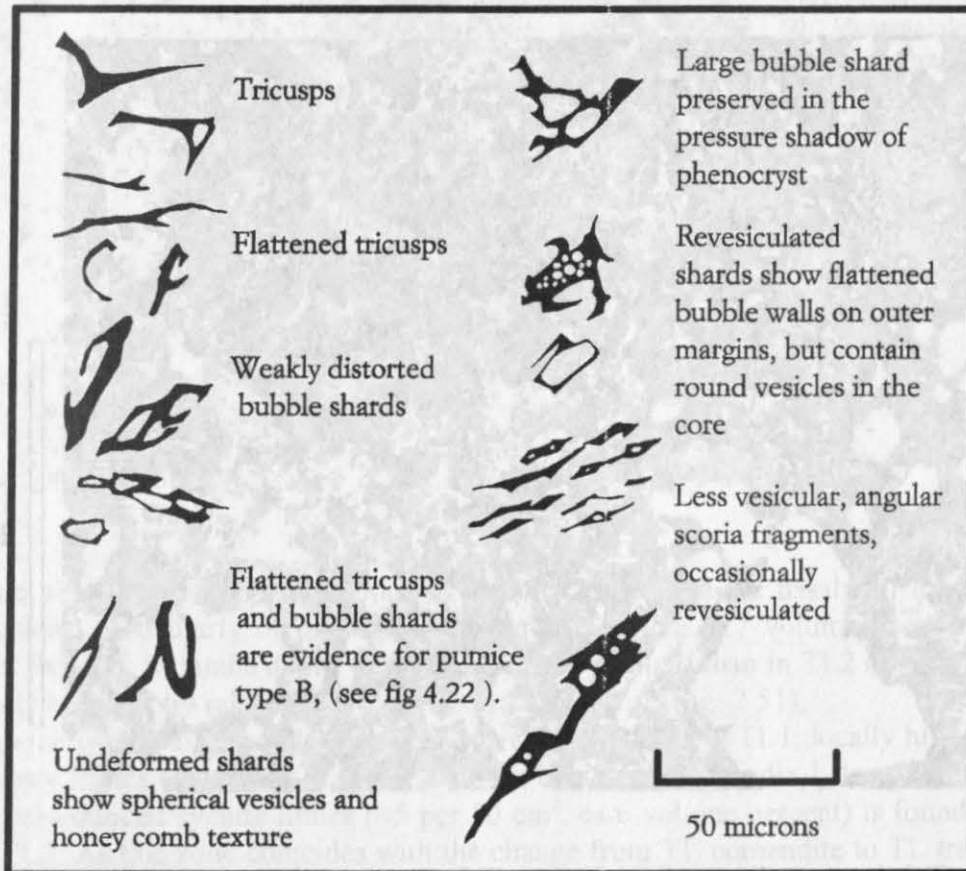


Figure 4.21. Details of shard shapes observed in TL. Shard morphology varies with chemical composition and related vesicularity of juvenile material. Comenditic shards are predominantly tricusps and flattened bubble shards. Comenditic trachyte shards are less vesicular scoria fragments or globular shards as shown in Fig. 4.23

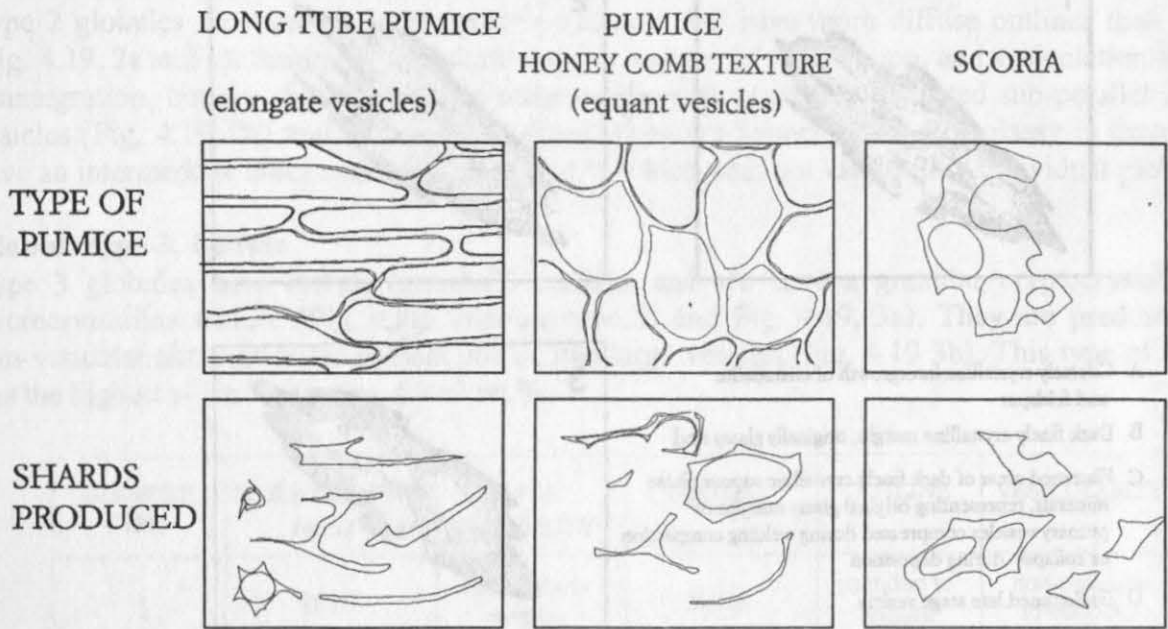


Figure 4.22. Variation in shard morphology with pumice type. Long tube pumice produces long, and platy or small, circular shards. Pumice with honey comb texture fragments to produce large bubble shards, short tricusps and 'Y' shaped shards. Scoria fragments to form poorly vesicular angular or blocky shards.

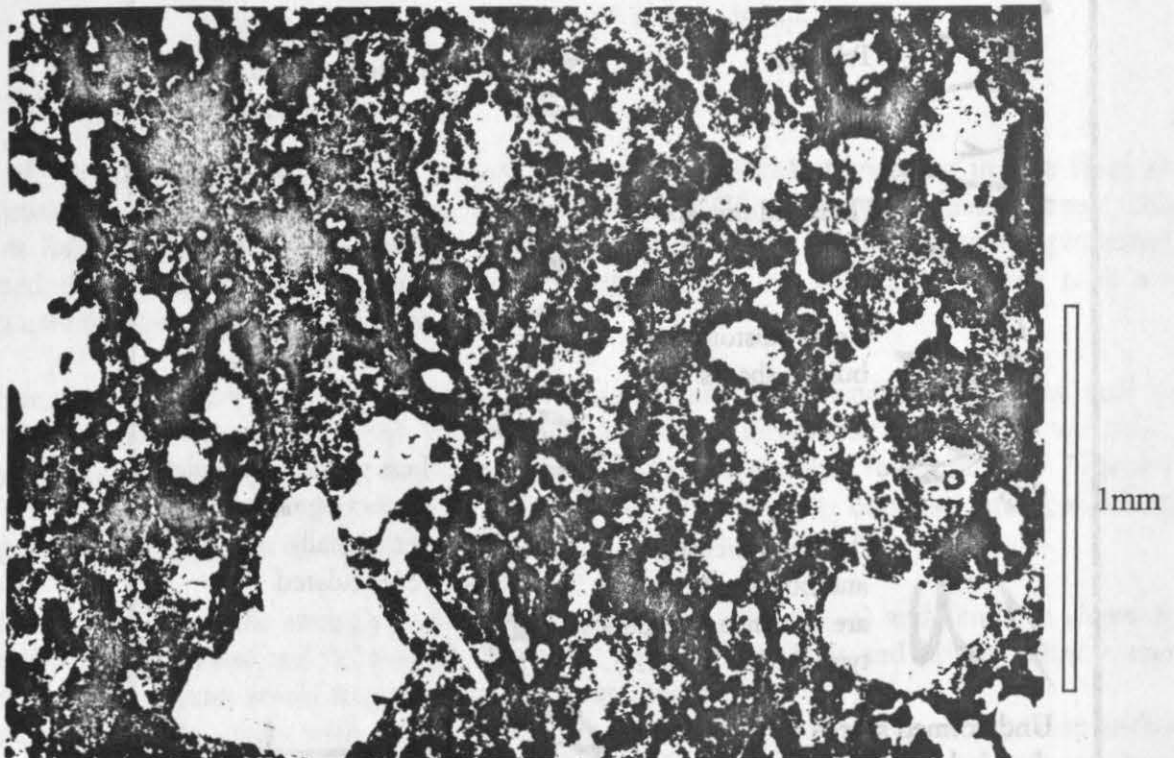


Figure 4.23. Globular comenditic trachyte shards in TL2. These probably represent chilled fluidal droplets, as opposed to the 'Y' shaped and cusped shards characteristic of more inflated pumice. (Sample 0378, Exp. 6, Bco. de Mogán, taken under plane polarised light).

4.4.3 Non-juvenile rock fragments

Accidental fragments in TL include all fragments which were not fluid when they were entrained in the magma or transport regime of the pyroclastic flow. These comprise lithic fragments which are unrelated to the magma and were derived from the surface (pick-ups), or conduit and vent wall rocks (accessory lithics). The macroscopic distribution of lithic fragments within individual lithofacies of TL1 and TL2 is described in Chapter 2 (Section 1) and the variation in lithic content with height through TL1 is summarised in Figure 3.1.

The accessory lithic population consists mainly of coarsely crystalline syenite and heavily altered, finely crystalline basaltic fragments. The pick-ups are composed of rocks exposed on the surface over which TL flowed. These include fragments of P1 rhyolite, high grade ignimbrite VI, rhyolite lava VL and most commonly fragments of underlying porphoritic ignimbrite P2. The syenite and basalt fragments are rounded to subrounded, the pick-ups are subrounded to angular.

Petrographic evidence indicates that the fragments were cold when incorporated (Fig. 4.24) They are commonly surrounded by a dark orange, homogeneous glassy matrix 'chill', in which shard outlines are no longer visible.

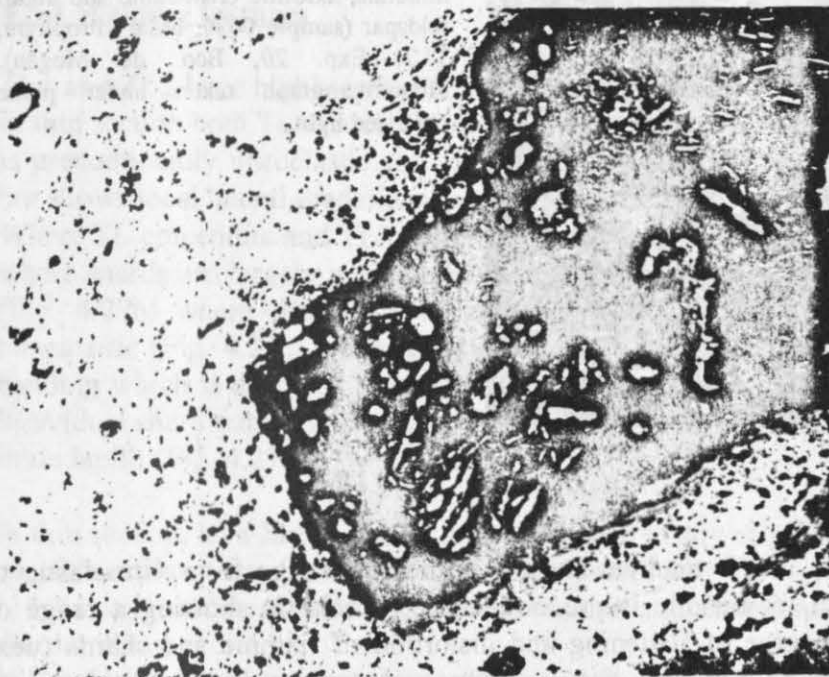


Figure 4.24. Accidental fragment within TL comendite. Note the loss of shard textures in the dark orange glassy matrix chill surrounding the subangular lithic clast (sample 0109, basal vitrophyre TL1, Exp. 60, Montaña de las Carboneras). Photomicrograph taken under plane polarised light.

1mm

The lithic abundances in TL are about 1-3 volume percent in the basal and lower portions. The lithic content, particularly of pick-ups is higher in TL1 (ca. 3.7 volume percent), and rarely for example, Exp. 60, Montaña de las Carboneras ca. 12 volume) than in TL2 (ca. <1 volume percent), and locally topography related higher concentrations occur (Fig. 2.51).

Although the overall lithic content is much lower in TL2 than in TL1, locally higher concentrations of accessory lithics occur, e.g.. Exp 58, Bco. de Lechugal (Appendix 1, Log 58). At this locality a zone of sub-rounded syenite lithics (<5 per 50 cm², ca 6 volume percent) is found ca. m from the base of TL2. As this zone coincides with the change from TL comendite to TL trachyte facies, the increase in number of accessory lithics may be the result of an increase in conduit erosion, related to the eruption of hotter, more basic, comenditic trachyte magma.

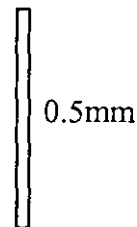
4.4.4 Lenticules

Both TL1 and TL2 are densely welded to within a few cm's of the upper surface (Section 4.5). TL2 contains lithofacies in which the particle outlines are no longer visible.

An increase in welding is commonly associated with progressive loss of pore space, accompanied by an increase in deformation of shards and larger juvenile clasts. The presence of lava like facies within TL2 suggests a degree of particle agglutination that would have obliterated any primary pore space. However, flattened elongate vesicles are found throughout TL2, even in the most highly welded lava like portions of the tuff. These elongate vesicles (lenticules, after Mackin, 1960) are interpreted as gas cavities, which were lengthened and flattened during and following emplacement of the tuff (Reedman et al., 1987a). Lenticules are up to 8mm long and 1.7mm wide show varying degrees of flattening and are distorted around lithic lapilli and large crystals. They generally have smooth margins and streaked out 'brush-like' terminations. Lenticules are commonly lined or filled with a fine-grained axiolitic intergrowth of cristabolite and alkali feldspar (Fig. 4.25) overgrown by inwardly radiating axiolitic aegirine and alkali amphibole.



Figure 4.25. Lenticule (flattened, ellipsoidal gas cavity), almost completely filled by vapour phase minerals, axiolitic cristabolite and alkali feldspar (sample 0020, basal vitrophyre, TL2, Exp. 20, Bco. de Mogán). Photomicrograph taken under plane polarised light.



4.5 MATRIX TEXTURES IN TL

In thin section the matrix textures in TL trachyte and TL comendite range from vitroclastic to holocrystalline. The matrix of TL comendite is predominantly vitroclastic showing a range of welding textures defined by the degree of flattening and distortion of fiamme and shards (next section). The matrix of TL trachyte similarly shows a range in texture from vitroclastic to holocrystalline, but lava-like holocrystalline textures predominate. Where holocrystalline texture is observed it is inferred to be the result of high temperature devitrification of welded glass particles and vapour phase crystallisation. In TL comendite this has produced a microcrystalline aggregate composed of alkali feldspar, amphibole, disseminated opaque oxides and aegirine in decreasing order of abundance. In TL trachyte the microcrystalline matrix is composed of anorthoclase, sodic feldspar, clinopyroxene, disseminated opaque oxides and aegirine, in decreasing order of abundance. Where the matrix is more coarsely crystalline (Fig. 4.26), lath shaped groundmass feldspars are sub-parallel aligned forming trachytic texture. This is particularly noticeable where crystals follow the outline of larger particles. Rather than being a single universal alignment, the trachytic texture appears to occur as domains, each having its own preferred feldspar alignment. These domains, rich in feldspar laths, account for the coloured flow banding observed in many hand specimens.

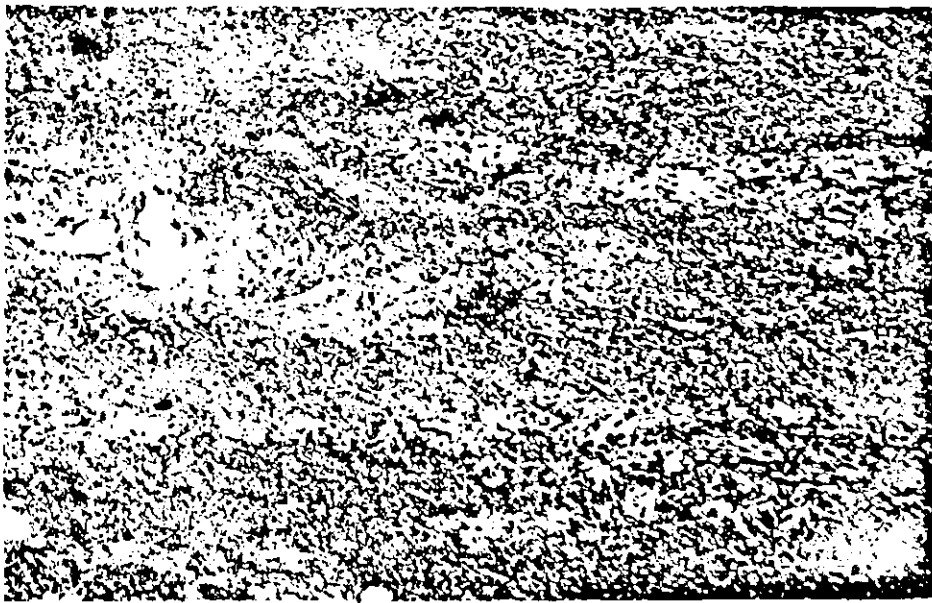
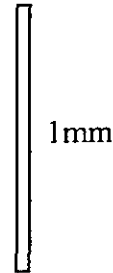


Figure 4.26. Trachytic texture (sub parallel alignment of feldspar laths) in lava-like TL trachyte subfacies T5Lp (sample 0277, TL2, Exp. 91, Bco. de Mogán). Photomicrograph taken under plane polarised light.



4.5.1 Welding textures

TL1 and TL2 have highly irregular welding profiles (Fig. 7.6, and Logs of TL2 in Appendix I) and in thin section both TL comendite and TL trachyte show a range of welding textures. TL comendite is predominantly vitroclastic and only locally lava-like, TL trachyte is largely lava-like in texture, but shows local lateral gradations to vitroclastic lithofacies (Fig. 2.25).

Where TL comendite and TL trachyte are vitroclastic, welding textures range from 'weakly welded' where shards are largely unflattened but point contacts are *sintered* (Fig. 4.27a), through *eutaxitic* (Fig. 4.27b) where shards are highly compressed and point contacts are no longer visible, to *parataxitic* (Fig. 4.27c) where glassy shards are highly attenuated and form a discontinuous flow banding which is distorted around lithic lapilli and large crystals. Where the texture is parataxitic, individual shard outlines are only discernible in the pressure shadows around large phenocrysts and lithic lapilli (Fig. 4.27c).

In thin section, lava-like facies retain no evidence of any original particulate texture. There are two possible explanations for the apparent holocrystallinity:

- 1) Intense *post depositional* welding compaction and rheomorphism may have obliterated original shard outlines.
- 2) Particle outlines may have been obliterated during the formation of a non-particulate layer (Fig. 7.9), where lower viscosity particles agglutinated or coalesced *during deposition*.

The spherical nature of preserved trachytic shards in TL (Fig. 4.23) demonstrates that particles were sufficiently fluidal to form spherical droplets similar to those observed in very fluidal basaltic fountain-fed eruptions (e.g., Pele's tears).

Similarity in morphology suggests that the spherical comenditic trachyte shards were probably originally "hot viscous droplets" with viscosities more typical of basalt than trachyte. Such hot fluidal droplets would be more likely to coalesce during deposition and would not require the presence of an over-lying load to weld. This suggests that agglutination and coalescence occurred *during* deposition, producing a non-particulate layer which then continued to flow in a lava-like manner and crystallised on cooling to form a fine grained holocrystalline matrix (Fig. 4.26). Non-particulate flow of coalesced material may also account for the sub-parallel alignment of matrix crystals (trachytic texture) and phenocrysts (trachytoid texture) observed in some TL

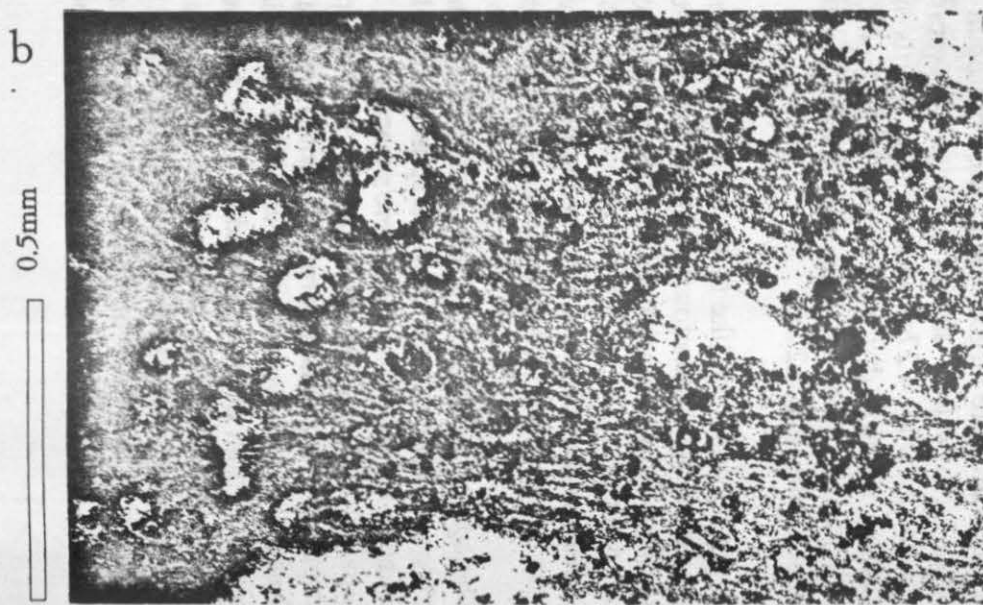
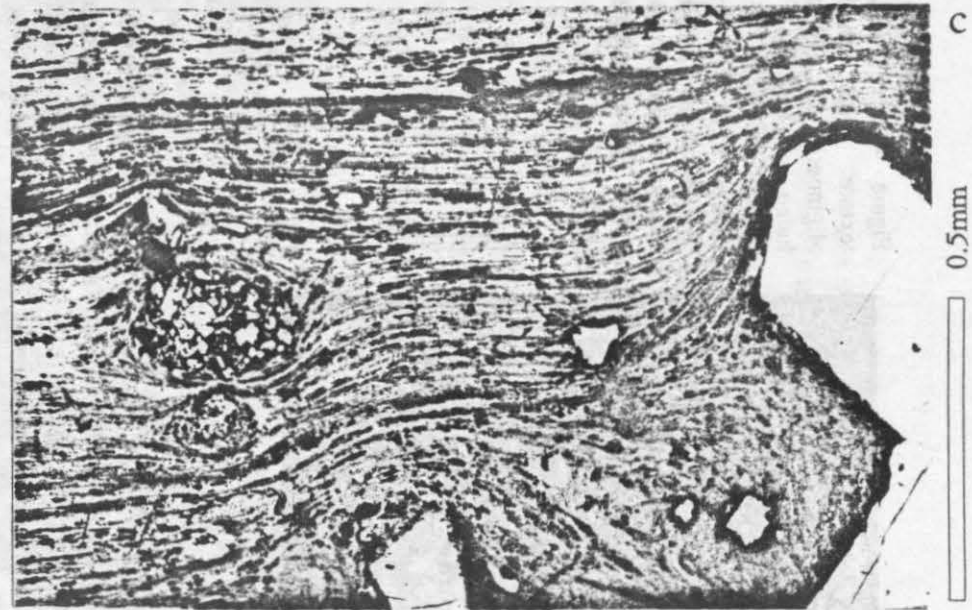
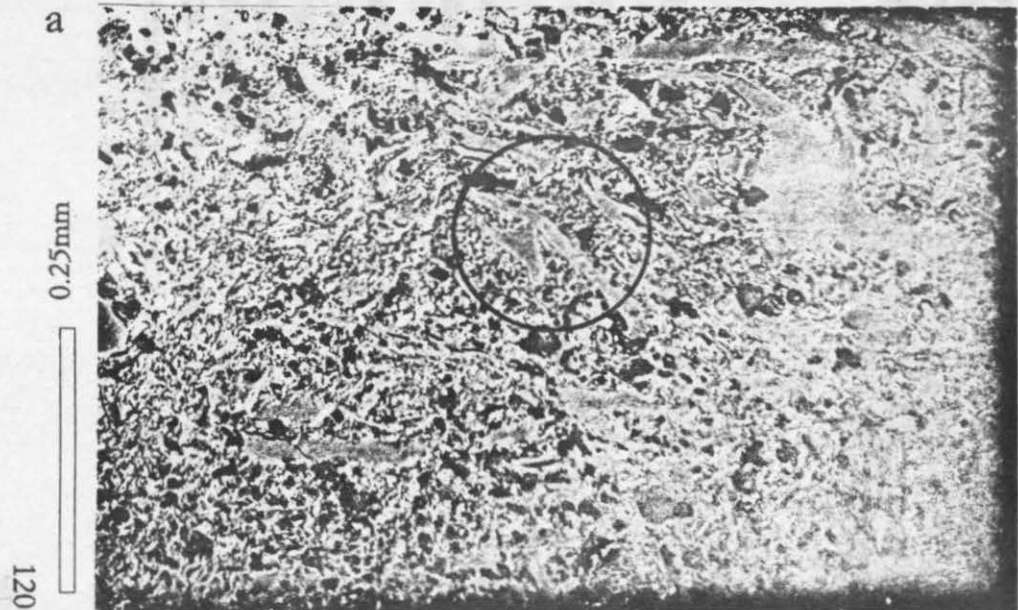


Figure 4.27. Welding textures in TL ranging from: (a) 'Weakly welded,' where the shards are largely unflattened, but the point contacts are sintered (see inset), (sample 0109, TL1, Exp. 60, Montaña de las Carboneras), through (b) Eutaxitic, where shards are compressed and point contacts are no longer visible (sample 0065, TL1, Exp. 55, Montaña de las Carboneras), to (c) Parataxitic, where shards are highly attenuated and form a discontinuous flow banding which is distorted around lithic lapilli and phenocrysts. Individual shard outlines are only discernible in the pressure shadows around rigid bodies (sample 0383, TL2, Exp. 101, Bco. de Tauro). Photomicrographs taken in plane polarised light.

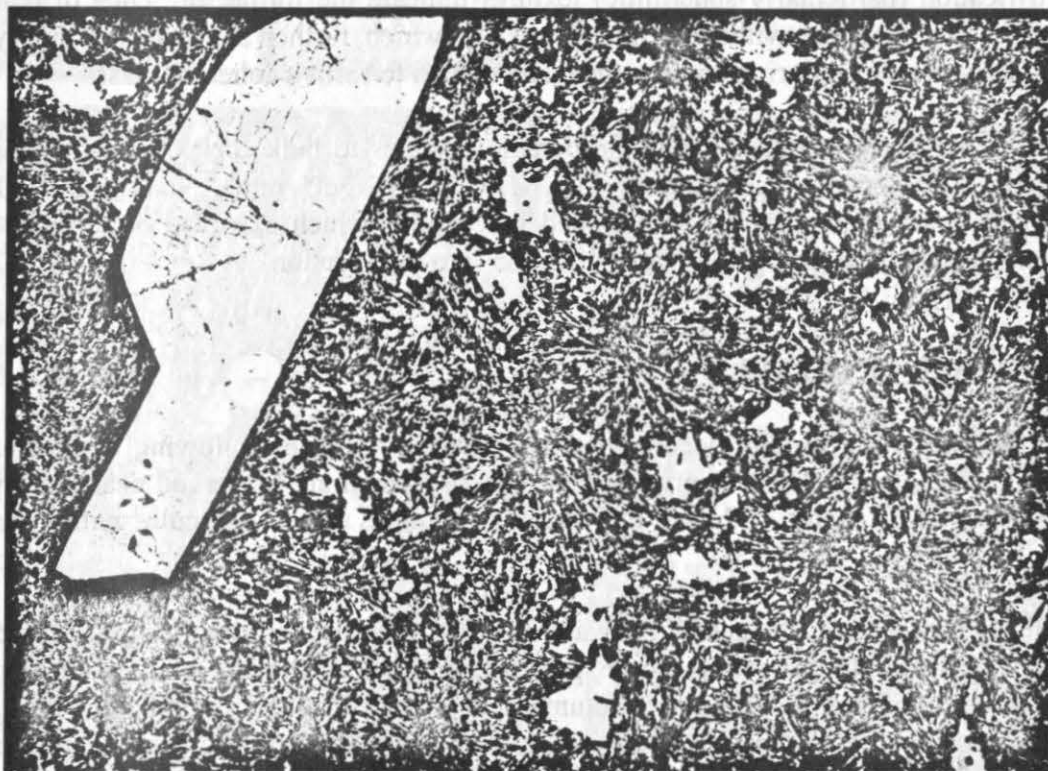
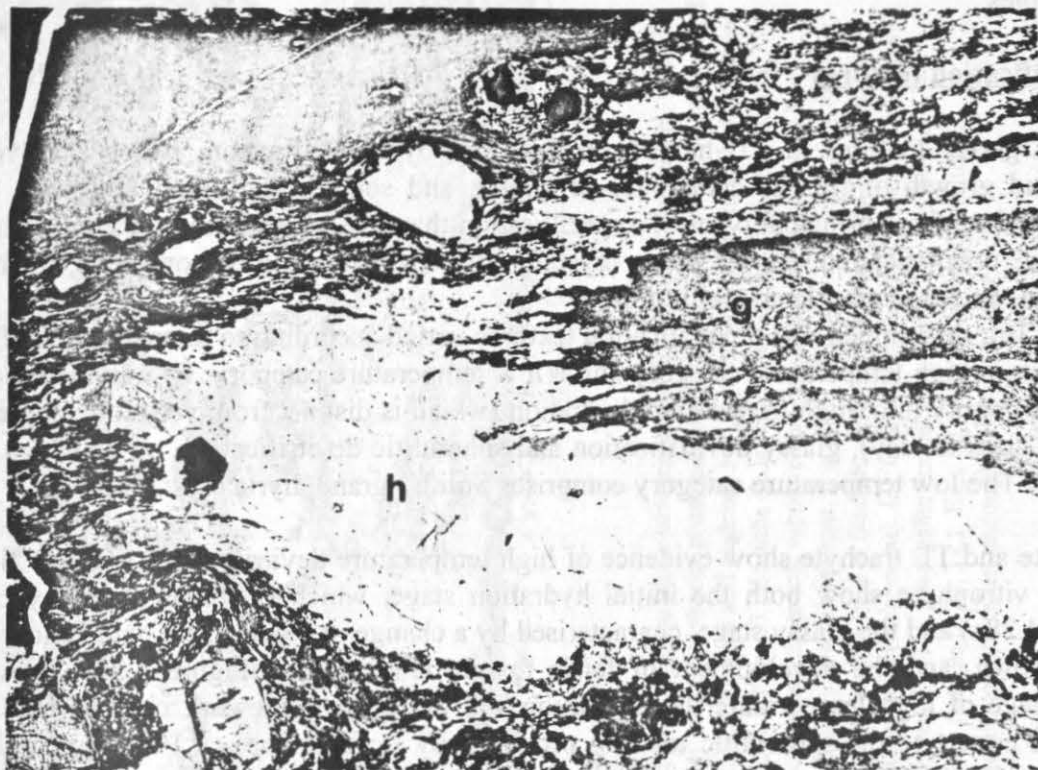


Figure 4.28. High temperature devitrification stages in TL; (a) Devitrification stages in glass from the basal vitrophyre of TL2, h = high temperature hydration stage, g = glassy stage (categories after Lofgren, 1971 b, see text for discussion) (sample 0020, Exp. 20, Bco. de Mogán). (b) Spherulitic stage of high temperature devitrification. Open framework, circular clusters of spaced fibres are comparable to those generated experimentally by Lofgren at temperatures at 700 °C. (sample 0125, TL1, Exp. 60, Montaña de las Carboneras) Photomicrographs are taken under plane polarised light.

trachyte samples.

4.5.2 Devitrification textures

The original glassy textures in TL have been modified by devitrification, which involves the nucleation and growth of fibrous crystallites of quartz, and sodium and alkali feldspar. Smith (1960b) recognised three principal types of crystallisation that take place during the cooling history of ignimbrites, devitrification, vapour phase crystallisation (which is contemporaneous, or follows devitrification) and granophyric crystallisation.

Lofgren (1971b), determined that devitrification textures varied according to temperature and could be divided into a high temperature category and a low temperature category. He divided the high temperature category into: high temperature hydration (which is distinct from very low temperature hydration of glass to clay), glassy devitrification and spherulitic devitrification, all of which occur above 400°C. The low temperature category comprises Smith's granophyric crystallisation.

TL comendite and TL trachyte show evidence of high temperature devitrification. Glassy fiamme in the basal vitrophyre show both the initial hydration stage, which is characterised by perlitic cracks (Fig. 4.28a) and the glassy stage, characterised by a change in colour from pale yellow-green to reddish-brown, and the development of felsic texture (Fig. 4.28a). Figure 4.28b, shows the spherulitic stage of high temperature devitrification and the open framework circular clusters of spaced fibres equate to the spherulitic textures produced by Lofgren (op. cit.) at temperatures of 700°C. Devitrification (particularly spherulitic) textures indicate the former presence of coherent glass. Spherulites are observed within the matrix of TL, which further supports the theory that particles had totally coalesced during emplacement and cooled to form a coherent glass.

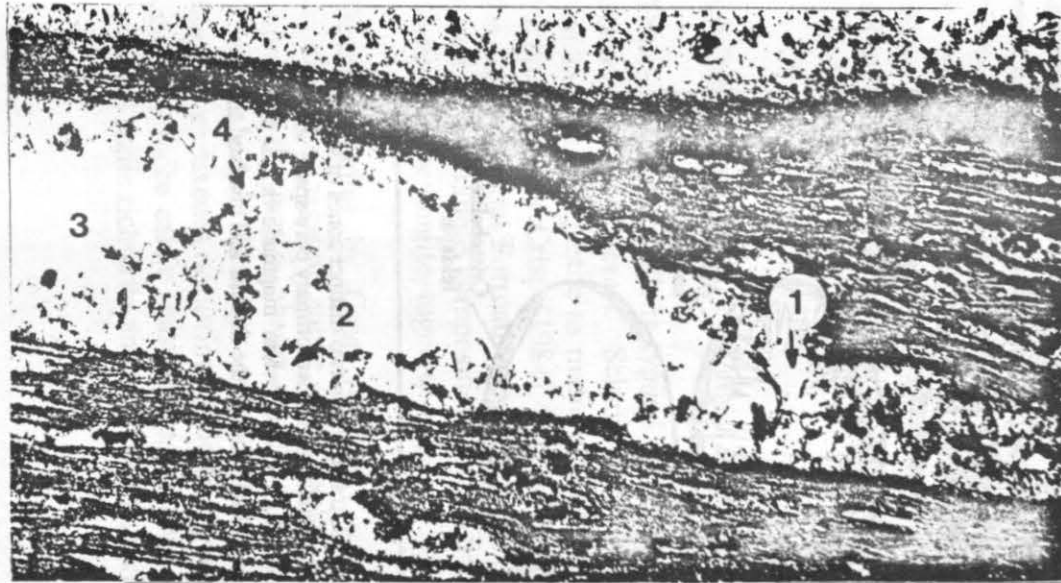
Devitrification is usually accompanied by considerable changes to bulk rock chemistry (Lipman 1965, Noble 1967), especially variations in SiO₂, H₂O, Fe₂O₃/FeO ratio, Na₂O and K₂O and secondary vapour phase minerals may be enriched in volatiles which exsolved or diffused from glassy fragments during high temperature devitrification (see next section).

4.6 VAPOUR PHASE CRYSTALLISATION

Vapour phase crystallisation usually occurs contemporaneously with or following devitrification. Vapour phase minerals in TL occur in primary pore spaces, which are preserved near the top less highly welded parts of TL1 and TL2, and in vesicles in fiamme and in lenticules within densely welded parts of the tuff.

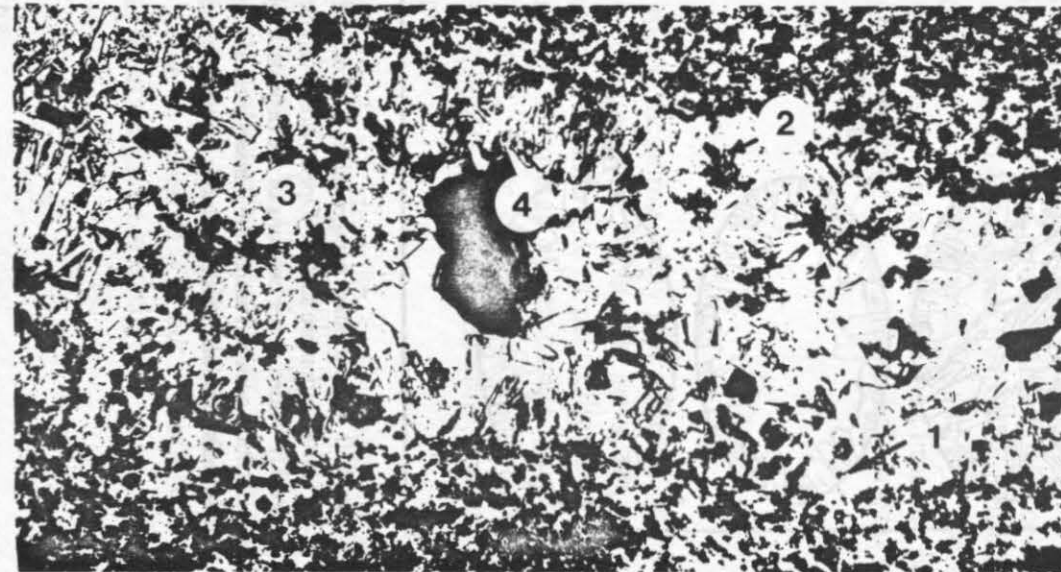
The vapour phase paragenesis, deduced from vapour phase crystal overgrowth, in TL comendite samples is usually inwardly grown tridymite prisms, axiolitic cristobalite and alkali feldspar, overgrown by inwardly radiating, acicular or columnar, aegirine and alkali amphibole (Fig. 4.29a). In TL trachyte, cristobalite and alkali feldspar are overgrown by axiolitic alkali feldspar and aegirine together with alkali amphibole, overgrown by large isolated crystals of fassaite (Fig. 4.29b).

Near the top of TL1 and TL2 where facies are weakly to incipiently welded, large open pores are partially filled with calcite plates and botryoidal to amorphous dark red brown limonite (Fig. 4.29c), and occasionally halite, although the latter is more likely to be the result of recent weathering. The vapour phase paragenesis of TL comendite and TL trachyte is shown in Figure 4.30.



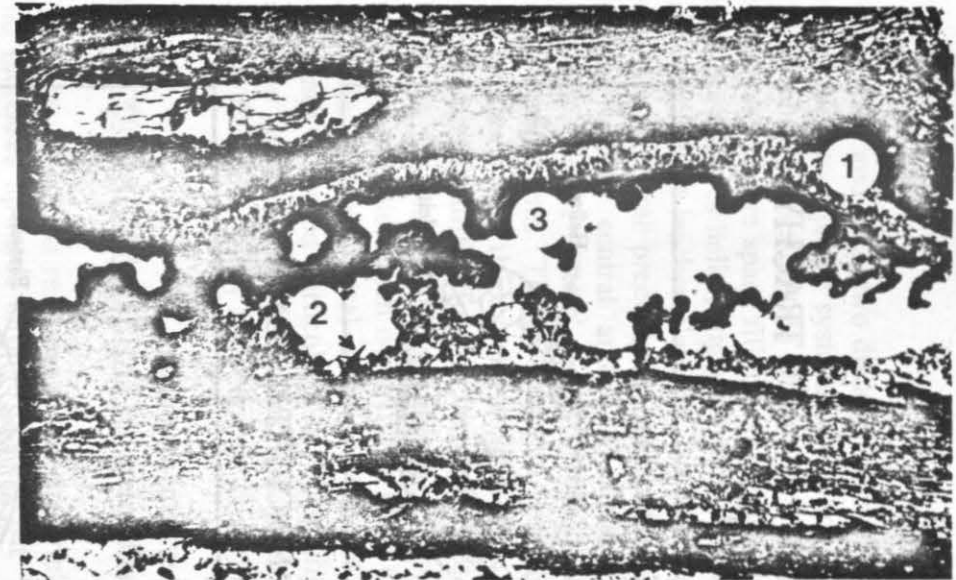
a

0.5mm



b

.025mm



c

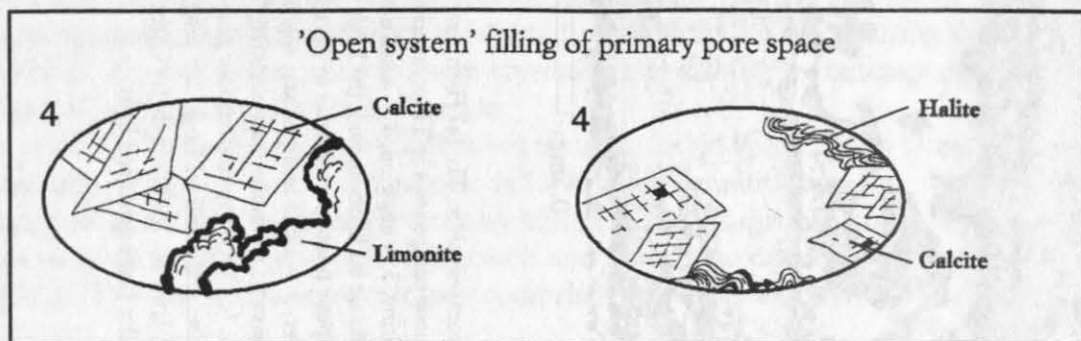
0.5mm

Figure 4.29. Vapour phase paragenesis in TL. (a) High temperature, 'closed system' magmatic vapour phase paragenesis in TL comendite; 1 = tridymite, 2 = axiolitic feldspar and aegirine, 3 = aegirine, 4 = alkali amphibole (sample 0118, TL1, Exp. 60, Montaña de las Carboneras). (b) High temperature, 'closed system' magmatic vapour phase paragenesis in TL trachyte; 1 = cristobalite and alkali feldspar, 2 = alkali feldspar and aegirine, 3 = aegirine and alkali amphibole, 4 = fassaitic pyroxene (sample 0076, TL1, Exp. 60, Montaña de las Carboneras). (c) 'Open system' vapour phase paragenesis in TL comendite; 1 = cristobalite and alkali feldspar, 2 = amphibole, 3 = limonite (sample 0123, TL1, Exp. 60, Montaña de las Carboneras). Photomicrographs taken under plane polarised light.

TL COMENDITE

TL TRACHYTE

WEAKLY WELDED TOP



DENSELY WELDED BASAL AND CENTRAL ZONES

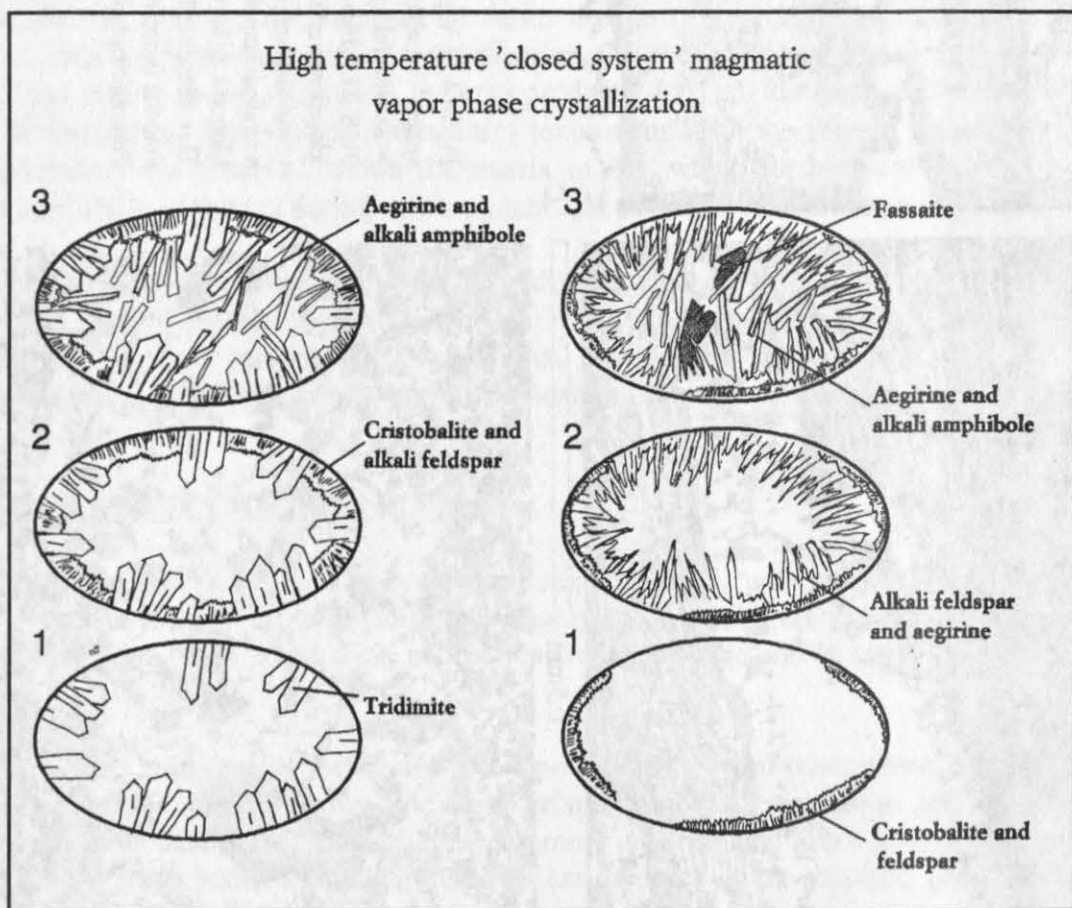


Figure 4.30. Vapour phase paragenesis in TL comendite and TL trachyte, the two distinct zones of vapour phase crystallisation are shown. 'Open system' vapour phase crystallisation filled primary pore space within the weakly welded upper portions of the deposit. High temperature 'closed system' magmatic vapour phase crystallization occurred within the densely welded, central and basal zones of the deposit and involved the simple redistribution of mobile phases within a closed system.

Within TL1 and TL2, two distinct zones of vapour phase crystallisation can be distinguished, and argues for two separate systems which account for the infilling of vesicles and pore spaces. The vapour phase crystallisation within the weakly welded top portions of TL1 and TL2 represent 'open system, pore space filling' typical of low grade ignimbrites. The presence of calcite, and some pore spaces halite, suggests the presence of non-magmatic fluids e.g. downward percolation of rainwater which leaches elements out of the porous glassy top of the ignimbrite and may lead to secondary mineral precipitation in open pore spaces. The vapour phase crystallisation of the densely welded central and basal zones however, probably represents a 'high temperature magmatic, closed system' vapour phase crystallisation involving a simple redistribution of the most stable components. The similarity in composition of vapour phase minerals to those of the bulk rock supports this theory and suggests that the vapour phase crystals formed during the high temperature devitrification of glassy particles. The vapour phase minerals are enriched in Na and Fe^{3+} . Na for example is particularly susceptible to leaching when in contact with hot fluids and may have migrated from devitrifying glass to be deposited from hydrothermal phases in near-surface lenticules. More unusual is the presence of Ca rich vapour phase minerals such as the fassaitic pyroxenes observed particularly in TL trachyte. Calcium is not especially mobile, however the presence of a hydrothermal CO_2 rich phase which combined preferentially with calcium may account for the mobility and redistribution of calcium into vapour phase minerals.

4.7 SECONDARY ALTERATION

Secondary alteration resulting from vapour phase activity is particularly well observed within TL and increases upwards through the deposit. The first evidence of minor alteration is exsolution lamella and magnetite rims in Fe-Ti oxides. Amphibole is also only fresh in densely welded basal parts of the deposit, and shows increasing oxidation and alteration upward. Amphiboles commonly have an opaque oxide rim, (Fig. 4.31a) due to the formation of magnetite by oxidation of iron, and are increasingly altered to limonite by dendritic overgrowth (for example, Fig. 4.31b). The color changes from pale green brown to dark orange. In the top portion of the deposit limonite crystals are only identified as being after amphibole, by retention of the original amphibole crystal outlines (fig. 4.31c).

4.8 DISCUSSION

The mineralogy of TL is typical of peralkaline rocks, including many characteristic sodium and potassium rich minerals. Schmincke (1974b) recorded aegirine, richterite, arfvedsonite, spinel, hematite and magnetite as mafic groundmass minerals characteristic of peralkaline ash-flow tuffs. Further work by Crisp (1984) detailed the mineralogy of a range of peralkaline ignimbrites from the Upper Mogán Formation on Gran Canaria. Like TL, these Upper Mogán ignimbrites show a wide range in amphibole compositions from edenite to richterite and Mg-katophorite, and contain clinopyroxene: augite, together with orthopyroxene.

Detailed studies by Crisp (op. cit.) on ignimbrite E-ET describe groundmass minerals including anorthoclase, aegirine, augite, amphibole and Fe-Ti oxides for this ignimbrite, which correspond closely to the matrix phases observed in TL. Recent work by Freundt (1989) on ignimbrite E (Gran Canaria), describes crystal phases of augite, orthopyroxene together with aegirine and fassaitic pyroxenes occurring in the trachytic end-member of P1. Amphibole phenocrysts in P1 are generally more calcic (hastingsite, edenite) than those observed in TL, but Freundt (op. cit.) also recorded sodic richterite and winchite occurring as matrix crystals in trachyte.

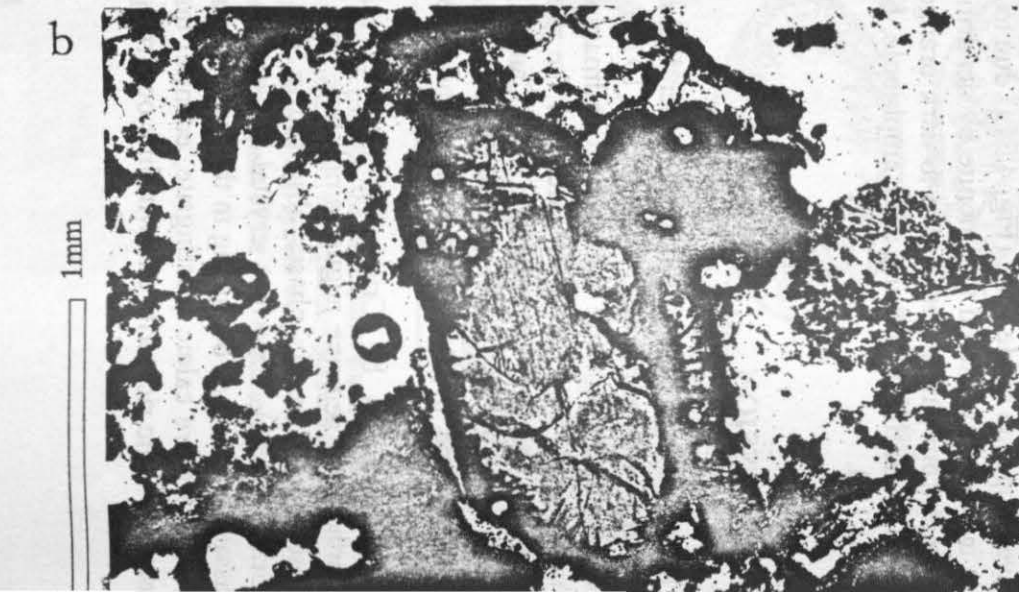
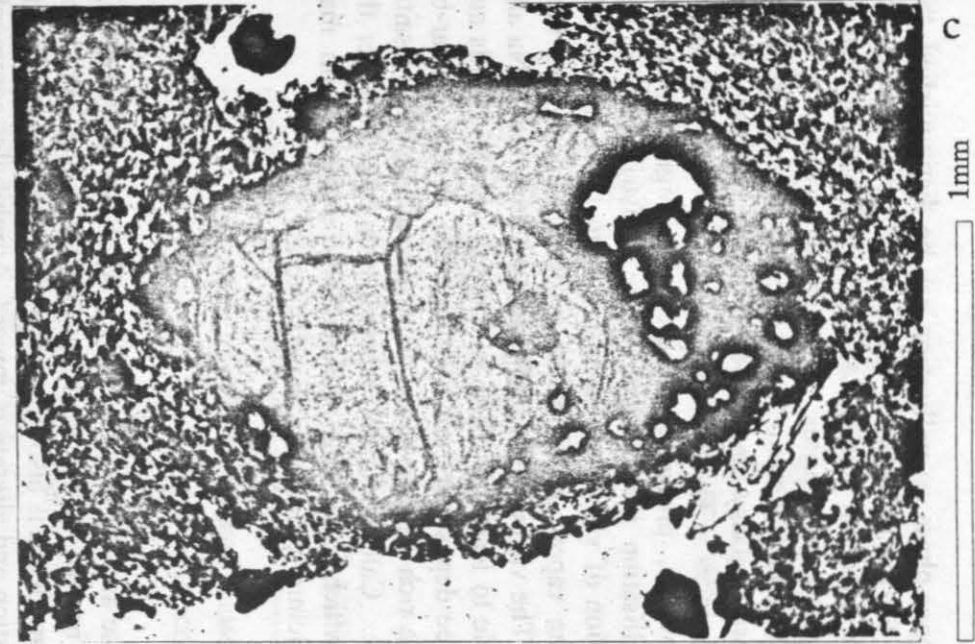
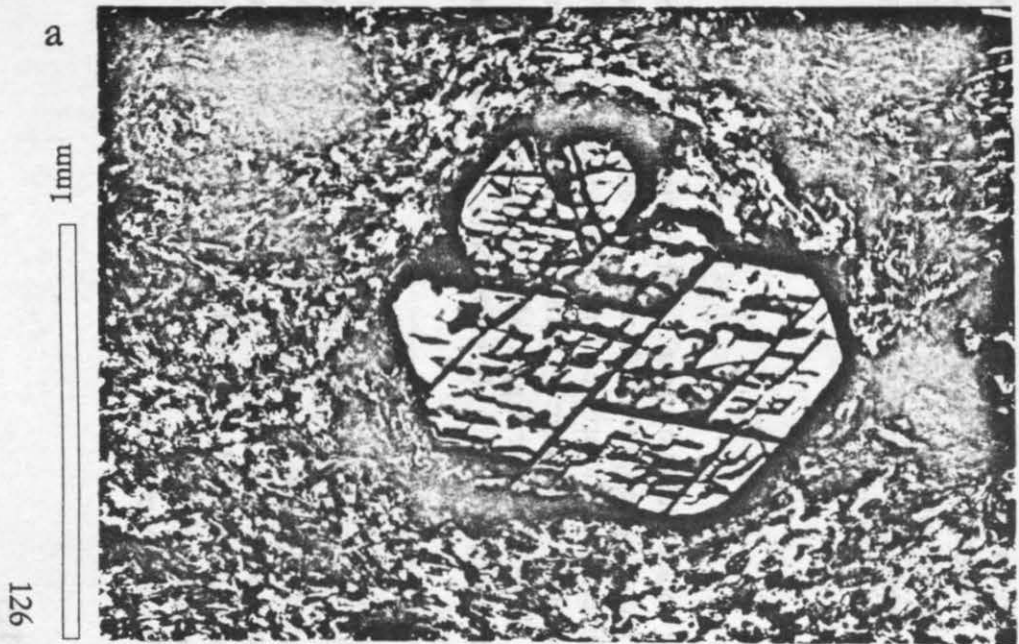


Figure 4.31. Stages of alteration of amphibole to limonite; (a) amphibole (Katophorite) with an opaque rim due to the formation of magnetite by the oxidation of iron (sample 0039, TL1, Exp. 39, Montaña de las Carboneras). (b) Progressive replacement of amphibole by limonite, around the margins and along the cleavage of the crystal (sample 0018, TL2, Exp. 6, Bco. de Mogán). (c) Limonite crystal after amphibole (sample 1284, TL2, Montaña Hogarzales). Photomicrographs taken under plane polarised light.

Mahood (1984) noted the importance of a predominance of alkali feldspar as the phenocryst phase over the comparative scarcity of quartz in a range of peralkaline rocks from e.g., Pantelleria and Mount Suswa, as being consistent with pantellerite liquidus relations at pressures of <100 MPa. This is also the case in TL, where there is an overwhelming predominance of alkali feldspar and total absence of quartz in both bulk rock samples and fiamme.

Although the mineralogy of TL is typical of peralkaline rocks the textural variations are extremely unusual. The textural evidence in TL indicates that both flow unit TL1 and particularly TL2 remained at high temperatures for prolonged periods compared to medium or low grade ignimbrites.

Evidence for high emplacement temperature and high post-emplacement temperature:

1) Both TL1 and TL2 are densely welded to within a few cm's of the upper surface, which indicates high emplacement and depositional temperatures, compared to weakly or incipiently welded low grade ignimbrites. Dense welding leads to the development of a 'closed system' in which heat is retained for prolonged periods. In TL this is supported by the occurrence of uncontaminated, high temperature magmatic, vapour phase minerals whose chemistry indicate a simple redistribution of mobile elements within a closed system.

2) High temperature devitrification textures, particularly spherulitic devitrification indicate the former presence of homogeneous glass. Development of spherulitic textures is favoured by relatively slow cooling and maintenance of high temperatures, together with the presence of aqueous solutions (especially alkali rich solutions). Spherulitic textures in the matrix of TL indicate the former presence of homogeneous glass which could only be produced by the total coalescence of particles. The rare occurrence of spherical trachytic shards preserved in TL indicates that particle viscosity and yield strength were low enough to be overcome by surface tension effects during transport. Such hot fluidal particles would be more likely to coalesce during deposition to form homogeneous glass. Causes of low viscosity are high eruption temperatures and strongly peralkaline chemistry, together with high halogen content and eruptive volatile content much higher than those preserved in the tuff.

3) Open gas cavities (lenticules) within very densely welded portions of TL could only have formed after emplacement and welding. This suggests that following emplacement of agglutinate or coalesced particles, temperatures were sufficiently high to allow the formation of vesicles by continued exsolution of volatiles.

Textural structures also provide evidence for the retention of volatiles in TL compared to other medium or low grade ignimbrites.

Evidence of volatile exsolution after deposition and welding:

1) Revesiculation of shards (Fig. 4.21), fiamme (Fig. 4.20) and matrix (lenticules) indicate the continued exsolution of volatiles following emplacement and welding. Many vesicles are unflattened indicating that volatile exsolution continued after post-depositional deformation.

2) The occurrence of high temperature magmatic vapour phase crystals within vesicles in TL indicates liberation, transport and redeposition of mobile phases such as Na, Fe³⁺ together with H₂O and possibly CO₂ together with Ca.

3) The bulk composition of glass is significantly altered during devitrification (Lipman 1965, Lofgren 1970). Hydration of glassy particles in TL and the occurrence of spherulitic structures in the matrix indicates that volatile phases were released during the high temperature devitrification of TL.

4.9 CONCLUSIONS

TL lithofacies consist of TL trachyte, TL comendite and TL mixed rock. The crystalline phases (phenocrysts and vapour phase crystals) in TL lithofacies are typical of peralkaline rocks. TL trachyte is characterised by the crystal phases: alkali feldspar, plagioclase feldspar, amphibole, clinopyroxene, orthopyroxene and accessory oxide listed in decreasing order of abundance. TL comendite is characterised by the crystal phases: alkali feldspar, alkali amphibole and accessory oxide together with rare pyroxene. TL mixed rock contains crystal phases characteristic of both TL trachyte and TL comendite.

The composition of vapour phase minerals in lenticules, in the densely welded portions of TL, indicate a high temperature 'closed system' redistribution of volatile phases, as opposed to the 'open system' pore space filling characteristic of low grade ignimbrites.

Matrix textures in TL suggest that compared to low grade ignimbrites;

- 1) TL remained at a high temperature post emplacement,
- 2) Volatile exsolution continued after deposition and welding.

CHAPTER 5

WHOLE ROCK CHEMISTRY

5.1 INTRODUCTION

The aim of this chapter is to show the major and trace element variation in TL comendite and TL trachyte, to present a plausible fractionation model and to discuss the implications of peralkaline chemistry. The chemical composition of TL lithofacies has been determined by bulk rock and glass analyses. A total of 53 chemical analyses are presented from bulk rock samples of TL comendite, TL mixed rock and TL trachyte lithofacies (described in Section 4.1), together with 21 analyses of separated comenditic, comenditic trachyte and mixed rock fiamme (Appendix II).

Analyses were obtained by Automatic X-ray fluorescence (XRF) of glass pellets by a Phillips PW 1400 and a Phillips PW 1480, using standard 'OXIQUANT' software. 230 International Reference Samples and 41 synthetic standards were used for calibration.

Major and trace elements have also been determined for the feldspar fraction in sample 0123 (TL1, comenditic facies, layer 2; Section 2.3.1) using 'UNIQUANT' software.

H₂O was determined by titration, sulphur and carbon by Infra-red Photometry, using standards CWA.5003 for CO₂ and H₂O, and CSA.5003 for carbon and sulphur. The analyses comprise up to 30 major and trace elements (Appendix II); chemical data are presented re-calculated as H₂O free.

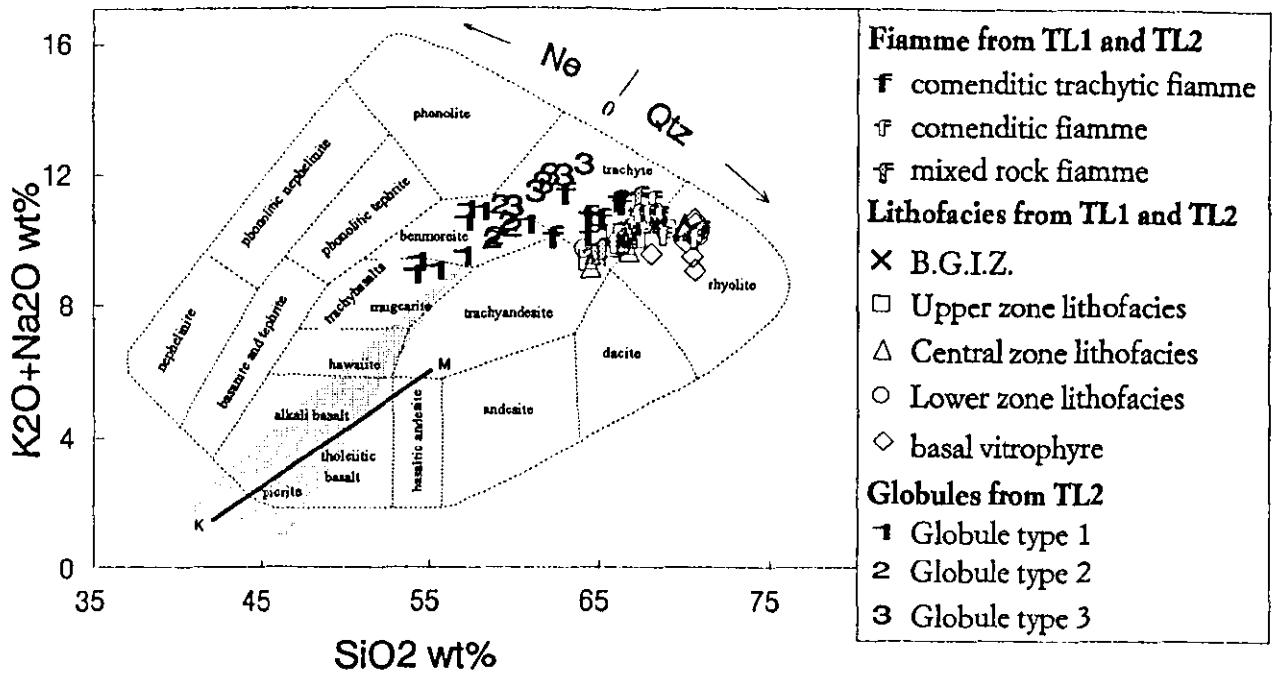
The amount of data available for the trachybasalt in TL2 is limited as it is present only as small (<7mm) globules within TL mixed rock and TL trachyte lithofacies. These minute globules are finely dispersed throughout these facies and crushed rock separates were not obtainable. The trachybasalt has been identified by microprobe analyses of glassy globules. Only major element variation has been established by this method, thus the composition of the trachybasalt is plotted for general comparative purposes. The majority of the data presented in this chapter concerns the genesis of TL comendite and TL trachyte.

5.2 GEOCHEMISTRY OF THE LITHOFACIES

5.2.1 Identification of Lithofacies Groups

TL is composed of three Lithofacies Groups; TL comendite, TL trachyte and TL mixed rock (Section 4.2). However, glass analyses and whole rock geochemistry suggest that three original magma compositions are represented in these lithofacies; comendite, comenditic trachyte and trachybasalt. These end-member magmatic compositions are not represented in TL lithofacies due to pre-eruption magma mixing and mixing of pyroclasts of different composition during subsequent transport and deposition. XRF analysis of separated comenditic and comenditic trachyte fiamme and microprobe analysis of glassy trachybasalt globules represent compositions closest to the original magmatic end-members.

The extreme compositional variation within TL is illustrated on a total alkalis versus silica classification (Cox et al, 1979) diagram (Fig. 5.1). Samples of bulk rock and fiamme range from trachyte (57-65 wt.% SiO₂) to rhyolite (>65 wt.% SiO₂). Microprobe analyses of glassy globules (globule Types 1 and 2), added for comparison, plot as trachybasalt (53-60 wt.% SiO₂). Type 3 globules are microcrystalline and show evidence of contamination through diffusion of alkalis and silica (Fig. 5.1) and plot in the trachyte field (60-65 wt.% SiO₂).



Silica saturated (*Hy only* in the norm) after Cox et al. (1979). Line M-K separates Hawaiian tholeiites from Hawaiian alkali basalts (Macdonald and Katsura, 1964).

Figure 5.1 a. Total alkalis versus silica diagram (compositional grid from Cox et al., 1979) for all analysed samples of TL with microprobe analyses of globules added for comparison.

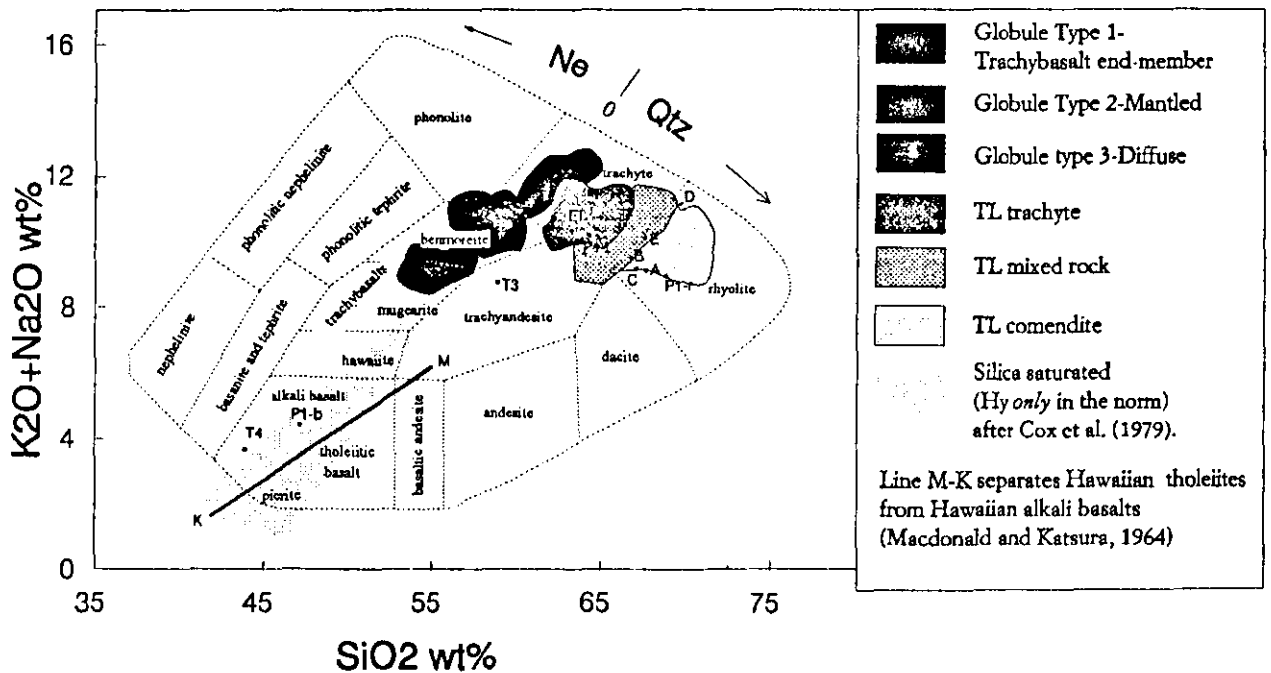


Figure 5.1 b. Total alkalis versus silica diagram comparing the composition of TL with other ignimbrites in the Mogán Formation, Gran Canaria. (Samples A, B, C, D, E, ET and T3, T4 are from Schmincke (1993); samples P1-r, P1-t and P1-b are from Freundt (1989).

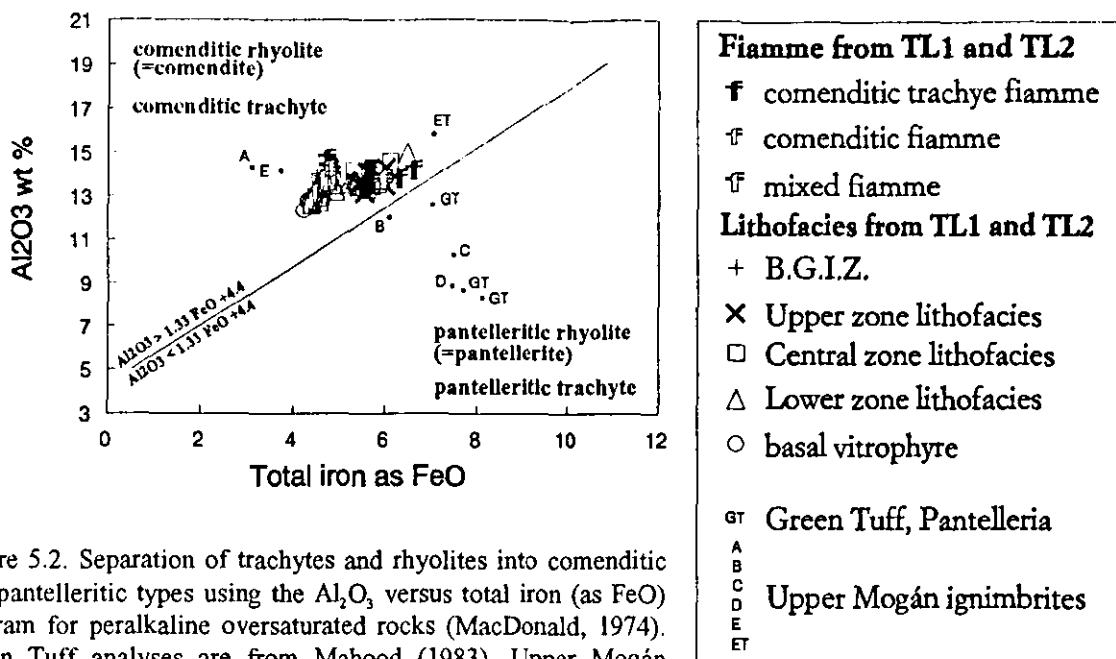


Figure 5.2. Separation of trachytes and rhyolites into comenditic and pantelleritic types using the Al_2O_3 versus total iron (as FeO) diagram for peralkaline oversaturated rocks (MacDonald, 1974). Green Tuff analyses are from Mahood (1983), Upper Mogán Formation ignimbrite analyses are from Schmincke (1993). Although the Upper Mogán Formation samples show a wide range in composition, all samples from TL plot as comenditic types.

Like most of the other ignimbrites on Gran Canaria (Schmincke, 1974 b), TL is **peralkaline**. Peralkalinity has been determined using the Peralkalinity Index ($\text{P.I.} = \text{Molecular Na}_2\text{O} + \text{K}_2\text{O} / \text{Al}_2\text{O}_3$). For peralkaline rocks the P.I. is >1 (Le Maitre et al., 1989). Virtually all the samples from TL have a P.I. of >1 , only eight samples have a P.I. of <1 , with values ranging from 0.86-0.98 (Appendix II). Samples plotting in the trachyte and rhyolite fields on the total alkalis versus silica diagram are therefore peralkaline rhyolite and peralkaline trachyte.

On an Al_2O_3 weight percent versus total iron as FeO diagram (MacDonald, 1974), samples from TL lie within the comendite sector (Fig. 5.2). Using this diagram, TL lithofacies can be further subdivided into comenditic trachyte (= TL trachyte) and comenditic rhyolite (comendite, after MacDonald 1974; = TL comendite). TL comendite and TL trachyte samples are all silica saturated (quartz and haüyne in the norm; Cox et al. 1979) and TL trachybasalt (represented by Globule type 1, Section 4.4.1) is silica undersaturated (nepheline only in the norm; Cox et al. 1979). Analyses from other rocks within the Mogán Formation (Schmincke, 1993) including: P1_T , P1_R (Lower Mogán Formation) and E, ET, D, B, C, and A (Middle Mogán Formation), have been plotted to demonstrate the compositional similarity between TL comendite and TL trachyte and other ignimbrites in the Mogán Formation. Selected analyses are shown on Table 5.1. Two analyses from lavas within the Mogán Formation T3 and T4 have also been plotted for comparison with TL trachybasalt (Fig. 5.1). TL trachybasalt is closest in composition to T3, but shows (ca. 2 wt.%) alkali enrichment compared to T3, and TL trachyte samples.

The bulk rock chemistry of TL is comparable to that recorded from rocks in other well known peralkaline volcanic provinces, e.g. the Green Tuff, Pantelleria (Schmincke, 1974b; Villari, 1974; Wright, 1980; Wolff and Wright 1981, 1982; Mahood and Hildreth, 1986) and Mount Suswa, Kenya (Johnson, 1968; Nash et al., 1969). Selected analysis from TL and the above areas are compared in Table 5.2 and plotted on Figure 5.2.

SAMPLE	TL1	TL2	TL1	TL2	P1-t	P1-r	E	ET	D	TL2*	TL2*	T4	T3
Sample No.	c. trachyte fiamme t-0038A	TL trachyte Upper zone t-70:30-0375	comendite fiamme c-0121	TL comendite Lower zone Lv-0077	trachyte TR-746	rhyolite R2-732	comendite fiamme S11,6	trachyte fiamme S6,1	trachyte fiamme GKa3	Globule type 1 0010-4	Globule type 1 0010-5	Hawaiite lava GC1721	Benmoreite lava 279869b
SiO ₂	63.6	64.86	69.04	68.81	64.58	67.87	67.7	58.4	64.6	57.14	56.98	44	57.6
TiO ₂	1.36	1.13	0.55	0.57	1.16	0.87	0.65	1.2	1.2	4.47	2.94	4.65	2.16
Al ₂ O ₃	13.82	13.72	12.87	12.8	15	15.65	14.26	15.93	14.5	14.95	14.61	14.78	13.83
Fe ₂ O ₃	6.31	5.48	4.36	4.41	nd	nd	3.68	7.31	5.33	nd	nd	6.28	8.05
FeO*	nd	nd	nd	nd	4.3	3.32	nd	nd	nd	6.63	7.82	6.55	1.73
MnO	0.21	0.17	0.21	0.19	0.27	0.22	0.22	0.23	0.23	0.37	0.28	0.19	0.19
MgO	1.43	0.88	0.27	0.3	1.12	0.9	0.39	1.25	0.96	0.09	1.49	5.58	1.7
CaO	2.08	1.27	0.25	0.27	1.97	1.07	0.29	1.45	1.03	2.77	3.56	11.49	4.74
Na ₂ O	6.52	6.05	5.08	5	7.43	5.14	6.15	6.36	7.38	6.48	6.68	2.68	4.54
K ₂ O	5.05	3.97	4.88	4.83	2.61	4.58	4.77	3.17	3.86	4.46	3.86	1.2	2.75
P ₂ O ₅	0.5	0.29	0.04	0.05	0.63	0.16	0.08	0.52	0.31	nd	nd	0.73	0.76
Total	101.3	98.3	98.32	98.12	98.5	98.17	98.5	97.85	99.6	98.2	98	99.28	99.19
V	49	39	14	17	19	26	nd	nd	nd	nd	nd	nd	nd
Cr	6	3<	6<	2<	8	22	4	<4	2	nd	nd	17	40
Co	3	8	15	0	4	1	2	<1	0	nd	nd	45	7
Ni	2	35	58	0	13	15	6	8	0	nd	nd	73	47
Cu	0	0	0	44	11	13	<3	6	12	nd	nd	137	24
Zn	217	175	183	169	195	179	182	306	138	nd	nd	140	180
Rb	58	75	126	120	54	94	105	26	58	nd	nd	25	72
Sr	218	116	15	15	265	210	8	562	62	nd	nd	895	515
Y	77	68	87	119	93	81	101	65	58	nd	nd	38	59
Zr	853	837	1283	1646	1247	1079	1471	564	552	nd	nd	394	726
Nb	120	120	197	213	128	158	216	115	94	nd	nd	64	112
Ba	1410	973	134	130	1158	534	159	1565	1360	nd	nd	552	491
P.I.	1.17	1.04		1.05	1	0.86	1.07	0.87	1.13	1.04	1.04	0.76	0.39

P.I = Peralkalinity index (Molecular Na₂O+K₂O/Al₂O₃)

nd= not determined

c.trachyte = comenditic trachyte

FeO* recalculated to FeO and Fe₂O₃, assuming Fe₂O₃/(Fe₂O₃+FeO)

TL2* = microprobe data included for comparison

(XRF analysis not possible due to the microscopic size of globules)

Table 5.1. Selected analyses from TL, together with analyses from Lower (P1) and Upper (D, ET) Mogán Formation ignimbrites for comparison

Two analyses from trachybasalt lavas in the Mogán Group (T3 & T4) are included for comparison with the trachybasalt globules in TL2.

SAMPLE	Green Tuff, Pantelleria			Mt. Suswa	La Primavera	TL1	TL2	TL1	TL1	TL1	TL1	TL2
Sample No.	Base	Middle	Top	Phonolitic trachyte W100	High-silica rhyolite 37	c.trachyte fiamme t-0068	TL trachyte Upper Zone Lt-0376	intermediate fiamme m-0130	TL mixed rock Central Zone MC50:50-0087	comendite fiamme c-0067	TL comendite Lower Zone c2-0123	Basal vitrophyre BV-0171
SiO ₂	69.5	65.6	63.3	60.3	76	62.42	64.4	65.59	65.61	69.29	69.25	67.21
TiO ₂	0.05	0.71	0.83	0.66	0.17	1.29	1.21	0.92	1.09	0.59	0.59	0.57
Al ₂ O ₃	8.7	12.9	15.6	15.4	15.4	14.3	13.5	13.89	14.19	12.57	12.65	12.38
Fe ₂ O ₃	n	n	n	n	n	5.6	6	4.79	5.3	4.28	4.39	4.23
FeO*	7.8	7	5.8	6.9	2.1	nd	nd	nd	nd	nd	nd	nd
MnO	0.32	0.32	0.24	0.38	0.07	0.17	0.16	0.2	0.26	0.19	0.18	0.2
MgO	0.13	0.39	0.52	0.5	0.04	0.99	0.8	0.62	0.55	0.36	0.28	0.3
CaO	0.39	0.92	1.47	1.69	0.28	1.74	1.28	0.37	0.66	0.37	0.29	0.29
Na ₂ O	5.9	5.9	6.7	7.3	4.6	6.85	5.71	6	6.12	5.29	5.2	4.7
K ₂ O	4.5	4.8	4.5	5.2	4.7	2.66	3.96	5.06	4.21	4.78	4.85	5.45
P ₂ O ₅	<0.05	0.11	0.21	0.07	0.01	0.59	0.36	0.11	0.22	0.06	0.03	0.03
Total	97.3	98.65	99.17	98.4	103.37	97.63	98.8	98.05	99.02	98.18	98.25	98.31
V	n	n	n	n	n	47	52	19	39	12	17	7<
Cr	n	n	n	n	n	6<	9<	8<	6<	8<	10<	3<
Co	n	n	n	n	n	0	8	0	10	1<	0	0
Ni	n	n	n	n	n	2	4	14	5	13	0	10
Cu	n	n	n	n	n	0	0	0	10	0	58	0
Zn	n	n	n	n	n	327	194	183	175	168	170	229
Rb	n	n	n	n	n	43	89	95	75	129	125	133
Sr	n	n	n	n	n	88	170	8	90	18	12	9
Y	n	n	n	n	n	151	81	83	65	68	62	93
Zr	n	n	n	n	n	563	1037	978	816	1551	1511	1559
Nb	n	n	n	n	n	108	141	134	121	193	183	206
Ba	n	n	n	n	n	2409	734	509	1149	105	111	112
P.I.	1.69	1.15	1.02	1.15	1.09	1.01	1.01	1.1	1.03	1.1	1.09	1.1

P.I. = Peralkalinity index (Molecular Na₂O+K₂O/Al₂O₃)

FeO* = Total Iron

c.trachyte = comenditic trachyte

nd = not determined

n = data not available

Table 5.2. Selected analyses of peralkaline rocks from Pantelleria, Mt. Suswa, Kenya and La Primavera, Mexico (from Mahood, 1984, trace element data not available) with analyses of TL for comparison.

5.2.2 Vertical Variation in the Composition of TL

The composition of individual lithofacies within compound cooling unit TL is highly variable (Sections 2.3.1 and 2.3.2). The lithofacies associations, particularly within flow unit TL2, are extremely complex (for example, Fig. 2.27). On a regional scale however, a relatively simple compositional stratification for both the lower unit TL1 and the upper unit TL2 can be defined (Fig. 2.2). TL comendite lithofacies form the basal and lower zones of both TL1 and TL2, and TL mixed rock lithofacies form the central zone. The upper zones of TL1 and TL2 are composed of TL trachyte lithofacies. This variation is illustrated in three vertical profiles (Figs 5.3, and 5.4a and b). Selected major elements from bulk rock analyses are plotted with increasing height from the base for each profile, to show absolute vertical variation in composition. Bulk rock analyses for profiles from both TL1 (Fig. 5.3) and TL2 (Fig. 5.4a and b) show a general decrease in SiO_2 , K_2O and Na_2O from the basal zone of TL comendite, through the central TL mixed rock zone to the upper TL trachyte zone. There is a corresponding increase in mafic major oxides and CaO . This chemical profile is characteristic of all localities, however the relative thickness of lithofacies and their associations varies at each locality. Thickness variation and the presence or absence of certain lithofacies causes a wide scatter in the chemical data when samples from all localities of both TL1 and TL2 are plotted together using normalised height within a flow unit (Fig. 5.5).

The composition of fiamme also varies with height through the deposit (Fig. 3.4, and Fig. 5.5B) and in all bulk rock samples the inclusion of fiamme has affected the bulk rock composition. The change in the composition of the particle population with height is shown in Figure 5.5 (A), and chemical composition of fiamme and bulk rock samples using selected major and trace elements are shown in Figure 5.5 (B) for comparison. The greater abundance of high silica comenditic fiamme in the lower or basal zone correlates to higher SiO_2 contents in bulk rock samples in this zone. The lower SiO_2 contents for bulk rock samples in the upper zone correlate to the predominance of low

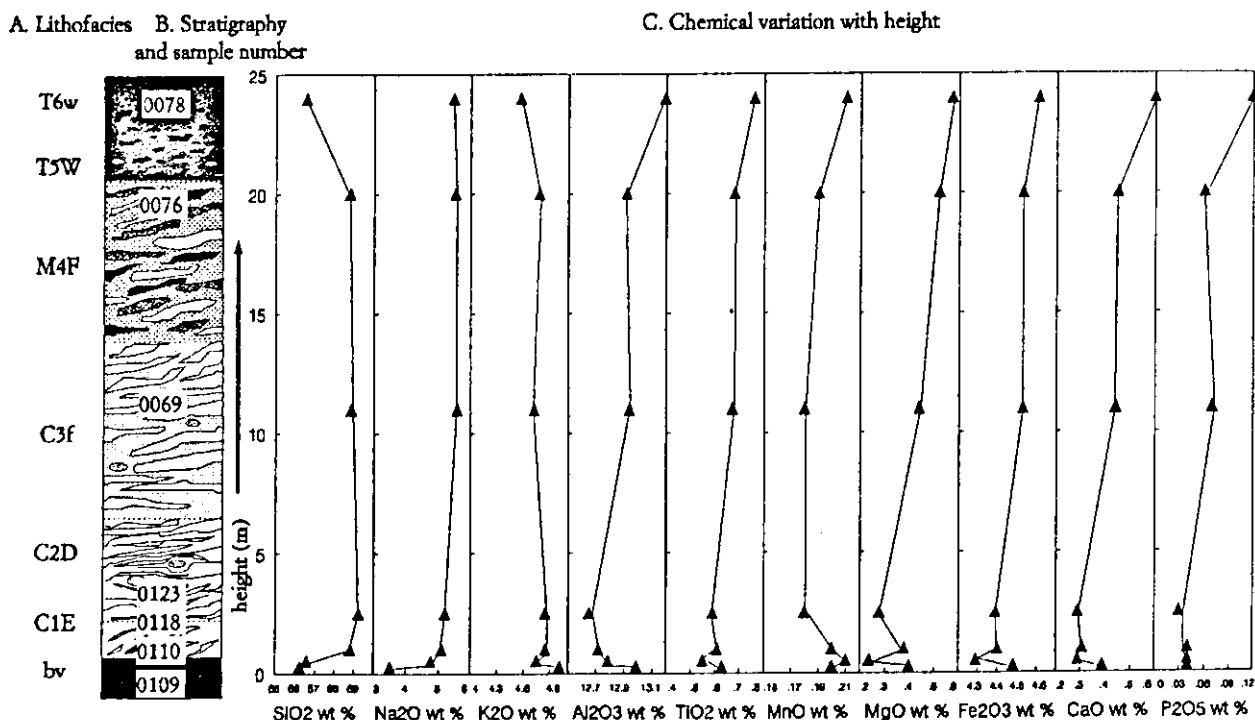


Figure 5.3. Variation in selected major oxides with height in TL1, Exp. 60, Montaña de las Carboneras. (lithofacies descriptions are summarised in Figure 2.5, details of log 60 are in Figure 2.7).

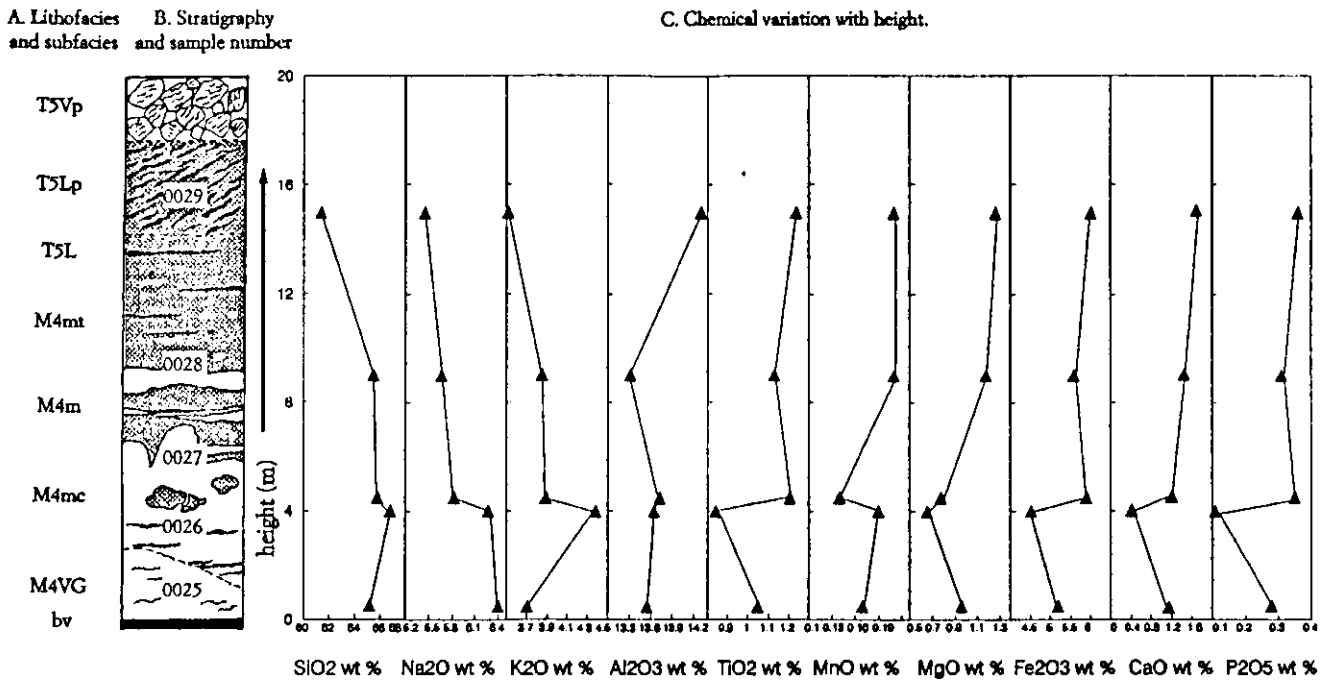


Figure 5.4a. Variation in selected major oxides with height in TL2, Exp. 26, Bco. de Tauro. (Lithofacies descriptions are summarised in Figure 2.5, details of log 26 are in Appendix I).

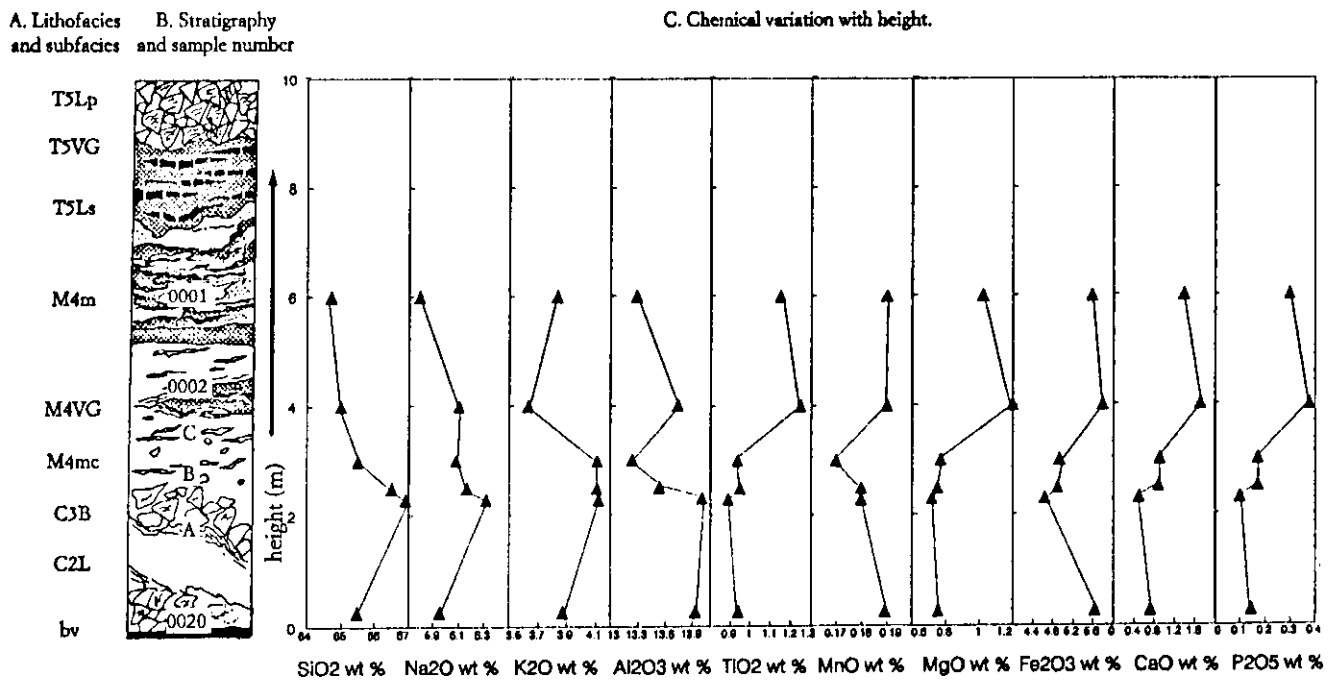


Figure 5.4b. Variation in selected major oxides with height in TL2, Exp. 90-II/6, Bco. de Mogán. (Lithofacies descriptions are summarised in Figure 2.5, details of log 90-II/6 are in appendix I).

A. FIAMME COMPOSITION

B. BULK ROCK ANALYSES OF LITHOFACIES AND FIAMME IN TL1 AND TL2

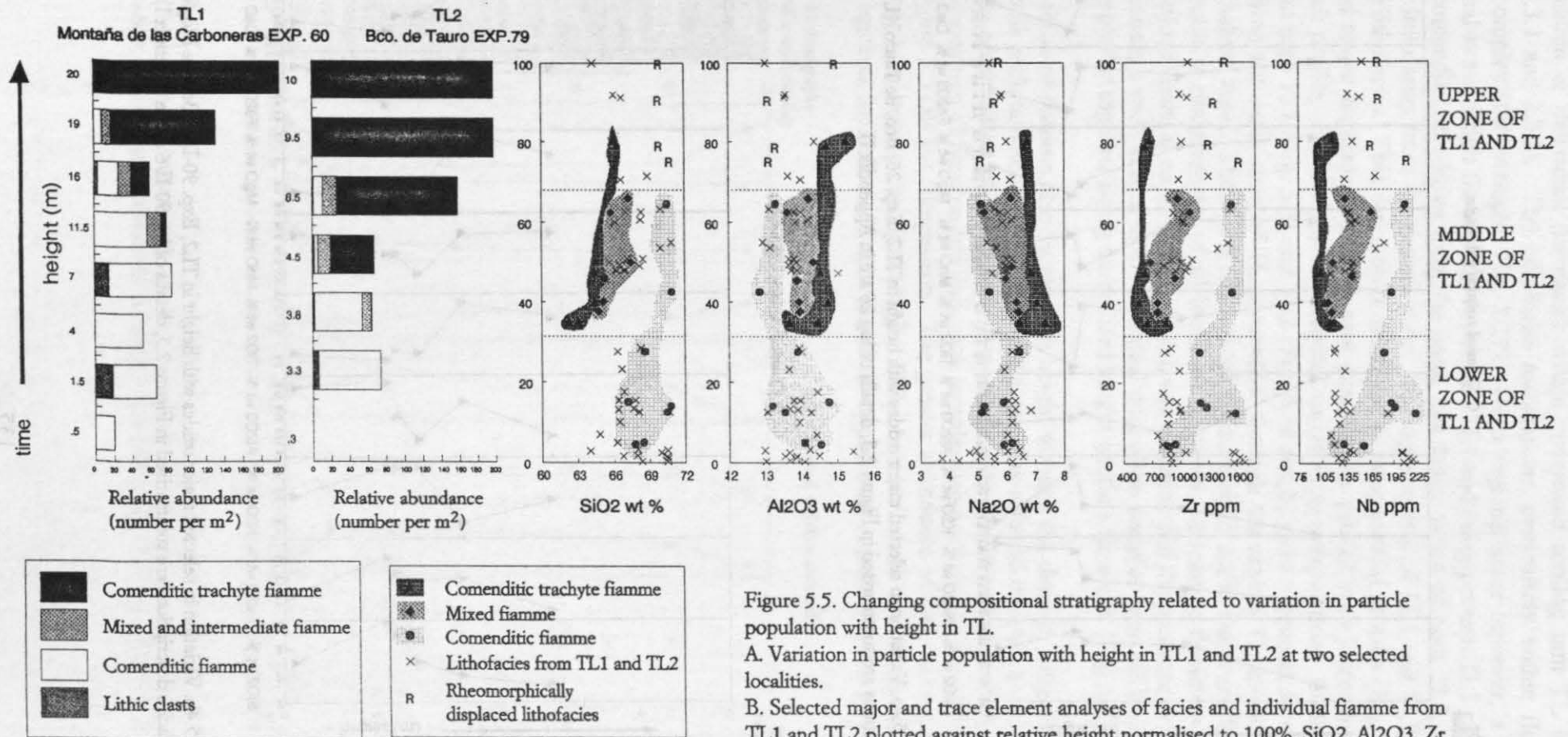


Figure 5.5. Changing compositional stratigraphy related to variation in particle population with height in TL.

A. Variation in particle population with height in TL1 and TL2 at two selected localities.

B. Selected major and trace element analyses of facies and individual fiamme from TL1 and TL2 plotted against relative height normalised to 100%. SiO₂, Al₂O₃, Zr and Nb decrease with height as the number of comenditic fiamme decreases and the number of comenditic trachyte fiamme increases.

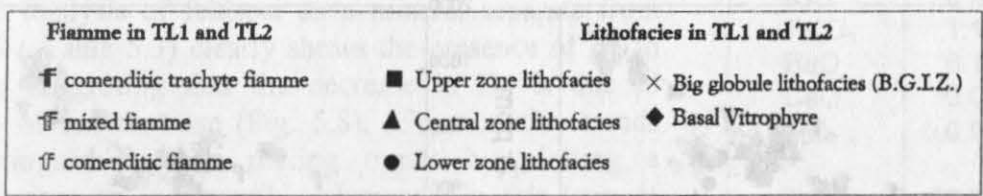
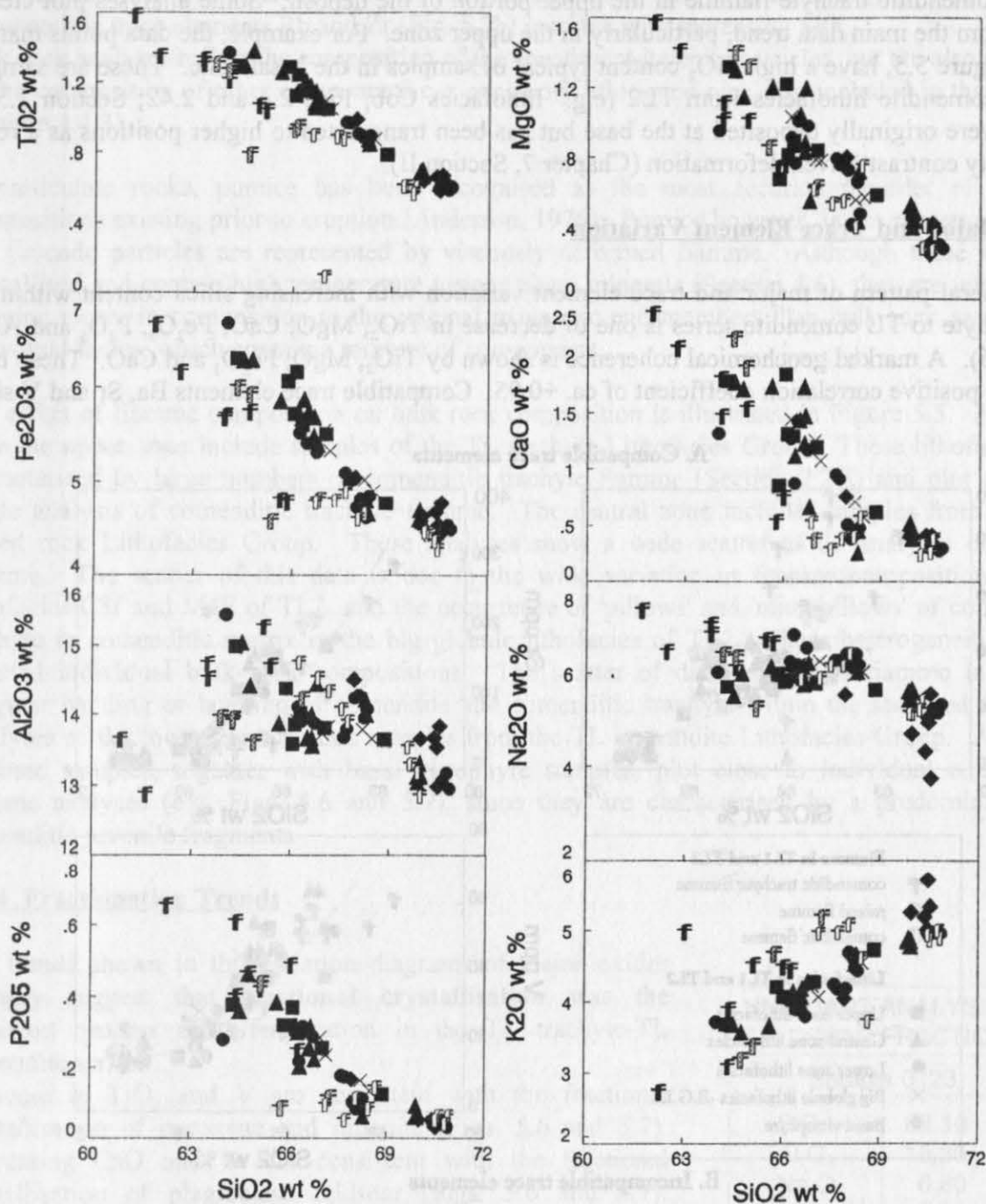


Figure 5.6. Major element versus silica variation diagram. Samples from the lower zone are predominantly TL comendite lithofacies and plot close to the single analyses of comenditic fiamme. Samples from the central and upper zones are predominantly TL mixed rock and TL trachyte lithofacies respectively. These show a wider compositional variation due to mechanical mixing of lithofacies during non-particulate flow (see section 6.5 for details of the mingling process). Comenditic trachyte fiamme stand out as the most basic end-member.

silica, comenditic trachyte fiamme in the upper portion of the deposit. Some analyses plot clearly away from the main data trend, particularly in the upper zone. For example, the data points marked 'R' in Figure 5.5, have a high SiO_2 content typical of samples in the basal zone. These are samples of TL comendite lithofacies from TL2 (e.g. lithofacies Cob, Figs 2.4 and 2.42; Section 2.5.2), which were originally deposited at the base but has been transported to higher positions as a result of density contrast driven deformation (Chapter 7, Section II).

5.2.3 Major and Trace Element Variation

The general pattern of major and trace element variation with increasing silica content within the TL trachyte to TL comendite series is one of decrease in TiO_2 , MgO , CaO , Fe_2O_3 , P_2O_5 and Al_2O_3 (Fig. 5.6). A marked geochemical coherence is shown by TiO_2 , MgO , Fe_2O_3 and CaO . These have a strong positive correlation coefficient of ca. +0.95. Compatible trace elements Ba, Sr and V show

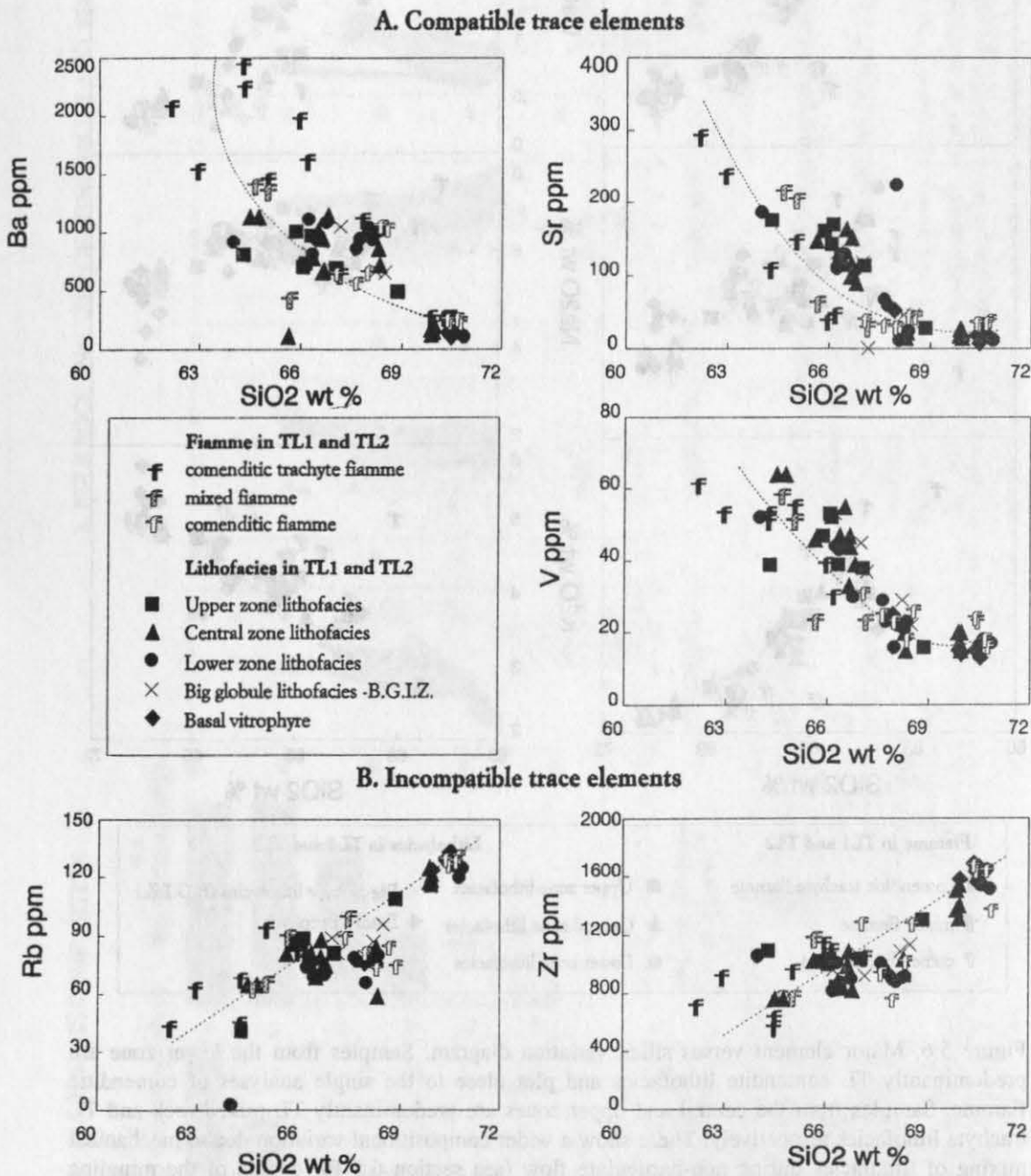


Figure 5.7. Selected trace elements Ba, Sr and V plotted against silica, show the fractional crystallisation trends of major crystal phases; potassium feldspar, plagioclase feldspar and, pyroxene and ilmenite respectively. Rb and Zr are incompatible and remain in the melt, and show a straight line trend when plotted against silica.

a similar decrease with increasing silica content (Fig. 5.7a). In contrast K_2O (Fig. 5.6) and the incompatible trace elements Rb and Zr (Fig. 5.7b) increase with increasing SiO_2 .

Bulk rock analyses reflect the composition of the constituent juvenile particles, but are also affected by the composition of other components e.g. accessory lithics and pick-ups, included in the deposit (Section 4.4.3).

In particulate rocks, pumice has been recognised as the most accurate recorder of magma compositions existing prior to eruption (Anderson, 1976). Pumice however, is not preserved in TL and juvenile particles are represented by viscously deformed fiamme. Although these are now crystallised and contain high temperature vapour phase minerals (Section 4.6), they are interpreted as being closer in composition to the original magmatic end-members than bulk rock samples of individual facies, which contain a mixture of components.

The effect of fiamme composition on bulk rock composition is illustrated in Figure 5.5. Analyses from the upper zone include samples of the TL trachyte Lithofacies Group. These lithofacies are characterised by large numbers of comenditic trachyte fiamme (Section 2.2.3) and plot close to single analysis of comenditic trachyte fiamme. The central zone includes samples from the TL mixed rock Lithofacies Group. These analyses show a wide scatter as do analyses of mixed fiamme. The scatter of this data is due to the wide variation in fiamme composition within lithofacies C3f and M4F of TL2, and the occurrence of 'pillows' and 'micropillows' of comenditic trachyte in comenditic matrix in the big globule lithofacies of TL2. These heterogeneities have affected individual bulk rock compositions. The scatter of data for mixed fiamme is due to irregular banding or layering of comendite and comenditic trachyte within the analysed fiamme. Analyses of the lower zone include samples from the TL comendite Lithofacies Group. Analyses of these samples, together with basal vitrophyre samples, plot close to individual comenditic fiamme analyses (e.g. Figs. 5.6 and 5.7), since they are characterised by a predominance of comenditic juvenile fragments.

5.2.4 Fractionation Trends

The trends shown in the variation diagrams of major oxides strongly suggest that **fractional crystallisation** was the dominant process of differentiation in the TL trachyte-TL comendite series.

Decrease in TiO_2 and V are consistent with the fractional crystallisation of pyroxene and ilmenite (Figs. 5.6 and 5.7). Decreasing CaO and Sr are consistent with the fractional crystallisation of plagioclase feldspar (Figs. 5.6 and 5.7). UNIQUANT analysis of feldspar as a mineral separate from sample 0123 (Table 5.3) clearly shows the presence of Ba in anorthoclase, suggesting that the decrease in Ba is due to fractionation of anorthoclase (Fig. 5.8). Fractionation trends can be distinguished from mixing trends by plotting a compatible versus an incompatible element. In this type of diagram mixing trends are linear functions while fractionation trends are hyperbolic (Cox, Bell and Pankhurst, 1979). Figure 5.9 illustrates the presence of both a fractionation and a mixing trend in TL lithofacies. When Ba is plotted against Nb and Th, the comenditic trachyte, intermediate, and comenditic fiamme plot along a hyperbolic fractionation curve. Banded fiamme and samples from the big globule lithofacies (B.G.I.Z.), which

UNIQUANT ANALYSIS FELDSPAR FRACTION	
Sample 0123	
SiO_2	69.10
Al_2O_3	16.30
Na_2O	6.80
K_2O	6.40
Fe_2O_3	1.10
BaO	0.11
CaO	0.05
TiO_2	0.05
Total	99.92

Table 5.3. UNIQUANT analysis of the anorthoclase crystal fraction in sample 0123 (TL1, comenditic facies layer 2), indicating the presence of Ba in the crystal lattice of anorthoclase.

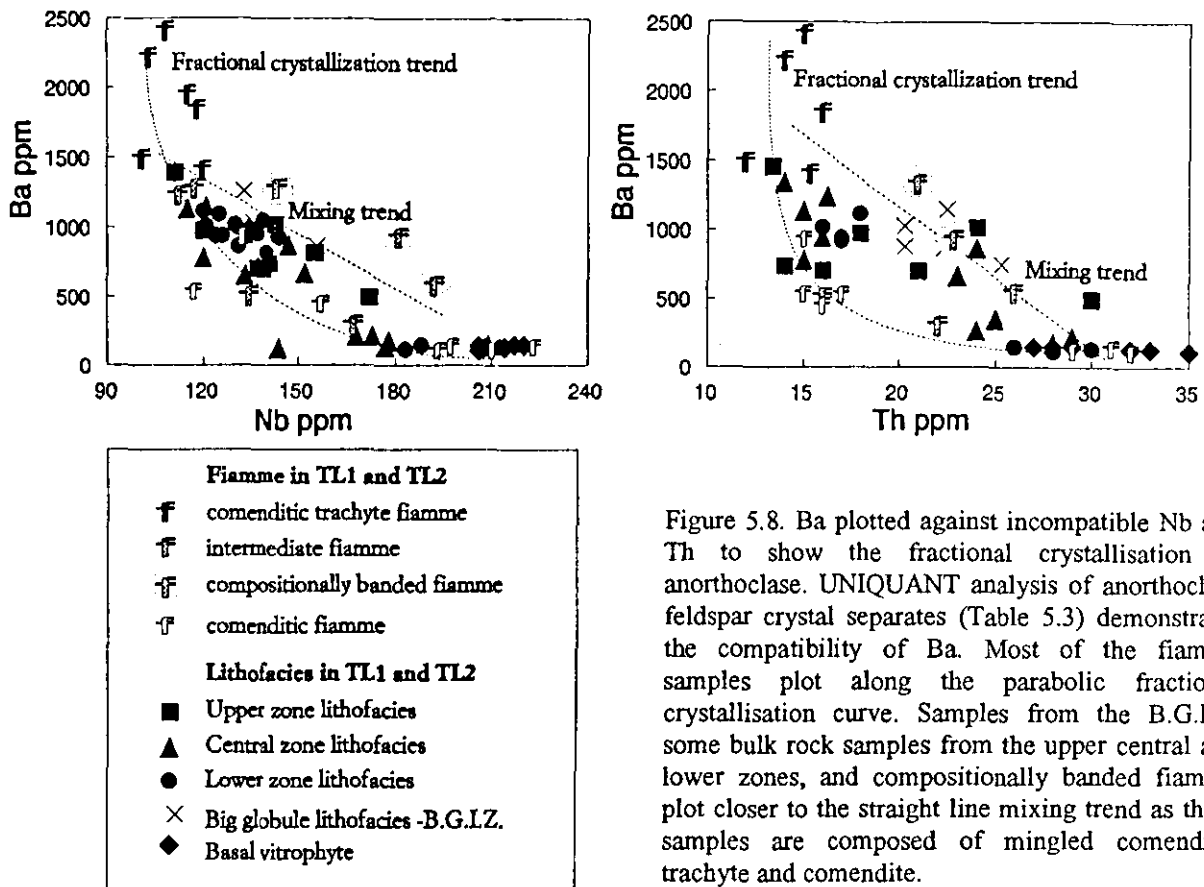


Figure 5.8. Ba plotted against incompatible Nb and Th to show the fractional crystallisation of anorthoclase. UNIQUANT analysis of anorthoclase feldspar crystal separates (Table 5.3) demonstrates the compatibility of Ba. Most of the fiamme samples plot along the parabolic fractional crystallisation curve. Samples from the B.G.I.Z., some bulk rock samples from the upper central and lower zones, and compositionally banded fiamme plot closer to the straight line mixing trend as these samples are composed of mingled comenditic trachyte and comendite.

are composed of mingled comenditic trachyte and comendite plot along a straight line mixing trend (Fig. 5.8).

Whole rock and fiamme analysis plotted together show a continuous variation with changing silica content (Figs. 5.6 and 5.7). Most of the bulk rock samples of individual lithofacies and subfacies from the upper, middle and lower zones of TL1 and TL2 show a wide range in composition, because they are composed of varying mixtures of particles. The inhomogeneity produced by this obscures the details of the fractional crystallisation trend. When only individual fiamme analyses are plotted (Fig. 5.9) they are seen to form a series of chemically discrete groups; A, B, C, D and E. These groups range from the lowest silica (<63 wt.% SiO₂) comenditic trachyte end-member (E), found in the 'upper zone' through intermediate fiamme (D and C), found in the central zone, and a low silica comenditic fiamme group (B) with <69-67 wt.% SiO₂, to the highest silica (>71 wt.% SiO₂) comenditic end-member (A), found in the basal zone. These chemically discrete groups of fiamme probably represent a series of discrete magma compositions generated by fractional crystallisation. The systematic change in fiamme composition with height (Fig. 5.9) indicates the progressive sampling of layers with discrete compositions, during eruption from a magma chamber zoned from the top down, with comendite overlying comenditic trachyte (see discussion).

The compositional variations shown by major and trace elements suggest that the comendite was probably derived from comenditic trachyte by a process of fractional crystallisation of pyroxene and Ti oxide together with plagioclase and anorthoclase.

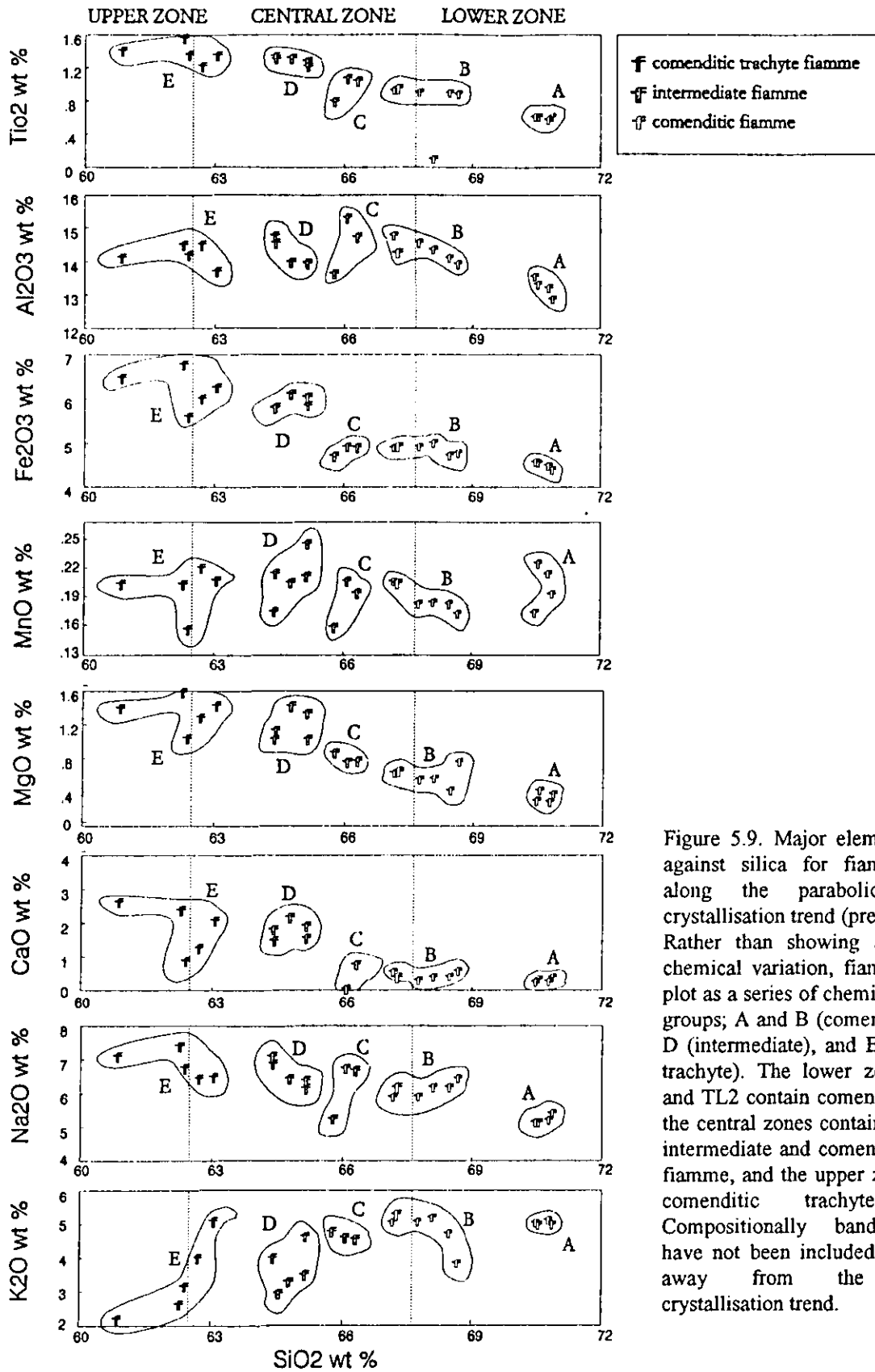


Figure 5.9. Major element variation against silica for fiamme plotting along the parabolic fractional crystallisation trend (previous figure). Rather than showing a continuous chemical variation, fiamme analyses plot as a series of chemically discrete groups; A and B (comenditic), C and D (intermediate), and E (comenditic trachyte). The lower zones of TL1 and TL2 contain comenditic fiamme, the central zones contain comenditic, intermediate and comenditic trachyte fiamme, and the upper zones contain comenditic trachyte fiamme. Compositionally banded fiamme have not been included as they plot away from the fractional crystallisation trend.

5.3 DISCUSSION

5.3.1 Differentiation of TL Magmas by Fractional Crystallisation and Mixing

As demonstrated in the previous four chapters, TL is the deposit of an extremely complex particulate system. TL lithofacies are not representative of the original magma compositions. However, sampling and analysis of individual fiamme (juvenile particles) has been possible and these have been used as the best available indicators of compositional variations existing in the magma chamber prior to eruption.

This study has concentrated on the chemical composition of TL lithofacies, thus the data presented is restricted to more evolved compositions, comendite and comenditic trachyte. Extrapolation of this data to consider possible parental magmas and the full fractionation series can only be made using data from more basic compositions.

TL is typical of many of the cooling units of the Mogán Formation (Fig. 1.3) in that it exhibits zoning and is composed of two magma types (Table 5.1): TL comendite and TL trachyte. Other examples, are ignimbrites, E-ET, A (comenditic trachyte and comendite), D (comenditic trachyte and pantellerite) and C (comendite and pantellerite). Ignimbrite P1 has proved particularly useful for geochemical study as it is zoned from basalt to rhyolite (Freundt, 1989; Freundt and Schmincke, 1992).

The importance of fractional crystallisation in the differentiation of Miocene magmatic rocks on Gran Canaria was first described by Schmincke (1969b, 1976). This work has since been supported by fractionation calculations for several of the Mogán Formation ignimbrites by Crisp (1984) and more recently by Freundt (1989), for Lower Mogán ignimbrite P1 (Fig. 5.10a).

Crisp (1984), using data compiled from least squares crystal fractionation analyses of ignimbrites from the Mogán Formation, produced a fractional crystallisation series (Fig. 5.10b), and demonstrated that TL comendite could be generated from comenditic trachyte (TL trachyte) by

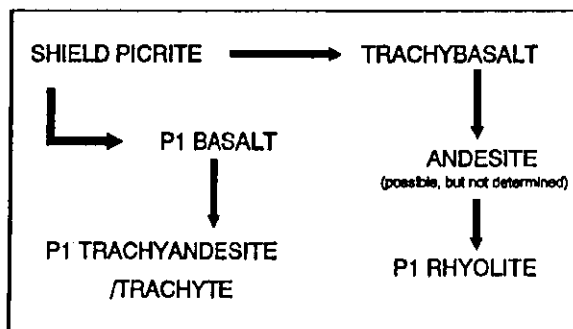


Figure 5.10 a. Differentiation of P1 (Lower Mogán Formation) magmas, with increasing differentiation from top to bottom. (After Freundt, 1989).

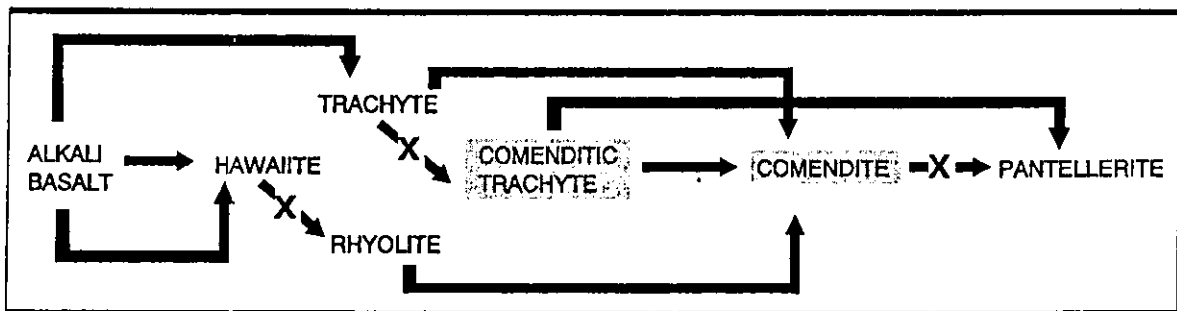


Figure 5.10 b. Chain of differentiation, with increasing differentiation from left to right. Solid arrows indicate genetic links, that can be generated using major element least squares crystal fractionation analysis, crossed lines cannot be generated. (After Crisp, 1984). TL compositions are outlined in grey.

least-squares fractionation analysis. This supports the geochemical data presented in Figures 5.6, 5.7, 5.8 and 5.9.

A process of simple fractional crystallisation cannot however, account for the presence of comenditic trachyte and trachybasalt in TL. Both mixing and mingling of magmas must have been involved to produce the compositions and textures observed in TL lithofacies.

Three successive processes are believed to account for the compositions and petrographic features in TL:

- 1) Mixing of basalt and comendite to produce comenditic trachyte (TL trachyte).
- 2) Fractional crystallisation to produce a magma chamber zoned from comenditic trachyte to comendite.
- 3) Mingling of magmas to produce the fine dispersion of trachybasalt throughout TL trachyte and TL mixed rock facies.

The geochemical implications are discussed in the following section, the mixing and mingling processes are described in Chapter 6.

Formation of comenditic trachyte by an early mixing event?

Least-squares crystal fractionation analysis is consistent with the formation of TL comendite from TL trachyte as part of a simple fractionation series (Fig. 5.10b). However, Crisp (op.cit) demonstrated that this series could not be generated progressively and produced a modified chain of differentiation showing feasible genetic links and highlighting those that could not be generated using least-squares analysis (Fig. 5.10b).

In Figure 5.10b TL compositions are outlined in grey. This diagram clearly demonstrates the problem of generation of *comenditic trachyte* (TL trachyte) because using least-squares analysis it cannot be generated simply from trachyte. In an attempt to resolve this problem Crisp also used least-squares analysis to determine if certain compositions could be generated by *mixing*. She concluded that the comenditic trachyte portion of TL (TL trachyte), could be derived by the addition of 13 wt.% T4 basalt (hawaiite, see Table 5.1) to TL comendite. An early mixing event between comendite and basalt (e.g. T4 basalt) may explain the presence of comenditic trachyte in TL. Subsequent fractional crystallisation of this lead to the development of a zoned magma chamber containing comenditic trachyte at the base overlain by a series of layers of intermediate composition, overlain by comendite (Fig. 6.1 and 6.2).

Development of a zoned magma chamber

Bulk rock analysis trends for TL lithofacies and individual analyses of fiamme, together with least squares crystal fractionation analysis, support the suggestion that comendite was generated from comenditic trachyte by a process of fractional crystallisation. Fiamme are preserved in TL1 which is less highly welded than TL2 (Section 3.1). The discrete chemical groupings of fiamme (Fig. 5.9) within TL1 suggest that the process of fractional crystallisation did not produce a magma chamber which was continuously gradationally zoned from comenditic trachyte to trachyte. Similarly, banded fiamme and a wide range in mixed rock compositions are not the result of homogenisation. This suggests that the development of the chemical zonation and subsequent mixing between comendite and comenditic trachyte was probably stepwise, through a series of individual 'mixing cells' each with a discrete chemical composition. A continuously, gradationally zoned magma chamber would produce a continuous range of juvenile clast compositions rather than chemically discrete groups.

Comenditic fiamme of groups A and B are found in the basal zones of TL1 suggesting that the more evolved material was the first sampled upon commencement of the eruption. Fiamme of group A are the most highly evolved and thus are probably closest to the true comendite end-member, representing the most evolved material residing under the chamber roof, drawn out

from the chamber in large lenses. Comenditic fiamme of group B are smaller and more highly vesicular than those of A, and probably represent more contaminated or less evolved comendite, since they plot closer to fiamme of intermediate compositions which characterise the central zone. The upper zone of TL1 contains fiamme of the least evolved composition, group E, which are probably most representative of the comenditic trachyte end-member. The composition and distribution of fiamme within TL has implications for the type of mixing, and the reconstruction of the magma chamber and eruptive sequence (Chapter 6).

Contamination of comenditic trachyte and comendite by trachybasalt

Geochemical and petrographic observations indicate that TL lithofacies contain compositions belonging to two magma series, (1) nepheline normative (e.g. trachybasalt) and (2) quartz normative (e.g. comenditic trachyte and comendite).

This can be explained either by:

- 1) Contamination of the quartz normative series by partial melts from wall rocks, or;
- 2) Direct contamination of the quartz normative series by trachybasalt, introduced at a later stage.

The presence of trachybasalt globules in some samples suggests that Ne normative trachybasalt incompletely mingled with comenditic trachyte and comendite prior to eruption, this is discussed in detail in Chapter 6.

5.3.2 Implications of Peralkaline Chemistry

Calculation of the peralkalinity index (Table 5.1 and 5.2) has demonstrated that TL lithofacies are peralkaline in composition.

A peralkaline magma composition has considerable effect on the physical character of the resultant pyroclastic deposit (Mahood, 1984). Petrographic and out-crop scale features of peralkaline pyroclastic deposits were first described by Schmincke (1974b). This section considers the properties of peralkaline magmas relating to temperature, chemistry, viscosity, volatile content, and related eruption column height.

Temperature

High magmatic temperature and peralkaline composition contribute to low magma viscosities (e.g. Schmincke, 1974b). Fe-Ti oxide temperatures are higher in rocks of peralkaline composition than those typical of calcalkaline rhyolites and rhyodacites (Carmichael, 1967). The pantellerites and trachytes at Pantelleria give 950-1025°C (Carmichael, 1967; Wolff and Storey, 1984; Mahood, unpublished data, 1983), and Wolff and Storey (1984) obtained 880-960°C for felsic tuffs at Agua de Pau, Sao Miguel. Temperature calculations for TL (Table 4.17, and Appendix II) are comparable to these values, ranging from 650-811°C for TL comendite and 810-910°C for TL trachyte.

Chemistry

The most detailed discussion of the effects of peralkaline chemistry is by Schmincke and Swanson (1967), who listed the following factors as being the most likely cause of inferred low viscosity:

- 1) High Fe/(Si+Al) ratios
- 2) High alkali contents
- 3) High Na/K ratios

High total iron and low Al₂O₃ were suggested as being especially significant, as high Fe/(Si + Al) ratios are known to decrease glass viscosities substantially (Barth, 1962, p.142). The presence of iron occurring principally in vapour phase aegirine in TL (Table 4.4, Figs. 4.29 and 4.30) indicates that most of the iron was contained in the glass particles, rather than phenocrysts. Also, as in the case of TL, when the sum of the molar concentration of Na and K exceeds Al (i.e. P.I. > 1), the alkalis behave as network modifiers and lower melt viscosity (Riebling, 1966; Scarfe, 1977).

SAMPLE	Green Tuff, Pantelleria*			Mt. Suswa*	La Primavera*	TL	TL
Sample No.	Base	Middle	Top	Phonolitic trachyte W100	High-silica rhyolite 37	comenditic trachyte t-0068	comenditic fiamme c-0120
VISCOSITY	Pantellerite	Pant-Trach	Trachyte	Phon-Trach	Rhyolite	Min. SiO ₂	Max. SiO ₂
0% H₂O							
810						<i>3.23E+07</i>	<i>4.68E+08</i>
850				6.90E+06	7.37E+09	1.58E+07	2.05E+08
980	2.00E+06	2.00E+06	1.50E+06	4.40E+05		2128436	2.00E+07
1010		1.10E+06	8.50E+05	2.50E+05		<i>1419698</i>	<i>1.25E+07</i>
1040			4.80E+05	1.50E+05		<i>964645.6</i>	<i>7998169</i>
1% H₂O							
810						<i>4503422</i>	<i>2.59E+07</i>
850				1.20E+06	3.38E+08	2398625	1.28E+07
980	2.80E+05	3.30E+05	2.80E+05	9.40E+04		408751.4	1769141
1010		1.90E+05	1.60E+05	5.70E+04		<i>285909.8</i>	<i>1186342</i>
1040			9.00E+04	3.50E+04		<i>203278.8</i>	<i>810192.8</i>
3% H₂O							
810						<i>310665.6</i>	<i>702259.6</i>
850				7.50E+04	4.20E+06	185394.8	404798.4
980	1.60E+04	2.00E+04	1.90E+04	8.00E+03		43483.05	86128.52
1010		1.30E+04	1.20E+04	5.00E+03		<i>32442.24</i>	<i>63007.29</i>
1040			8.00E+03	4.00E+03		<i>24530.97</i>	<i>46756.1</i>

Table 5.4. Calculated viscosities for a range of peralkaline rocks including two samples from TL for comparison. Samples from TL include the minimum SiO₂ wt.% (62.42) comenditic trachyte 'end-member' and the maximum SiO₂ wt.% (68.73) comenditic 'end-member'. * samples are from Mahood (1984), recalculated to poise. Numbers in italics for TL are values at temperatures not obtained by Fe-Ti oxide analysis, they are given for comparison.

Viscosity

As a result of the combined effects of temperature and composition, peralkaline magmas have calculated viscosities 1.5-3 orders of magnitude less than those of calc-alkaline rhyolites (Schmincke and Swanson, 1967; calculated using the atomic ratio $R=(Si+Al)/O$, after Shaw, 1965). Table 5.4 contains calculated viscosities (after the method of Shaw, 1972) for a range of peralkaline rocks (including data, recalculated to poise, from Mahood, 1984) with samples from TL included for comparison. These calculated values cannot be taken as accurate measures of viscosity, because they do not take into account volatiles other than water, or the effect of phenocrysts. Also, the original data were extrapolated by Shaw (1972) and Bottinga et al. (1982) from temperatures higher than magmatic. Similarly the data are not representative of viscosity of particles during transport and deposition as the temperatures used in the calculations are magmatic (chamber) temperatures. However, for comparative purposes the data serves to indicate that for peralkaline magmas, the calculated viscosities are more similar to those of silicic andesites despite SiO₂ contents as high as 70 wt.% (69.29 wt.% in TL comenditic fiamme, Appendix II).

Volatiles

Peralkaline magmas are thought to be relatively rich in CO₂, F and Cl and poor in H₂O (Bailey, 1980). However in TL, amphibole is present in much larger quantities than pyroxene, particularly

in TL trachyte. Amphibole, e.g. hornblende, requires a minimum water content of 3-4% (Naney, 1983) to become stable. This suggests that the water content in TL magmas was relatively high. Enrichment in CO₂ and H₂O in eruption columns favours column collapse (Sparks and Wilson, 1976). CO₂ and H₂O are the most important components of the gas phase in peralkaline eruption columns. However, the lower proportion of water *relative* to the denser F, Cl, C and S gases in peralkaline magmas should lead to an eruptive mix denser than one with pure water, and therefore lower eruption columns will result (Mahood, 1984).

Low eruption columns

Lower eruption columns allow for little cooling of the particles during fall out (Thomas and Sparks, 1992). The lack of any co-ignimbritic plinian fallout in association with TL supports the theory of a low column.

In summary, the peralkaline chemistry of TL, the associated high eruptive temperatures, the high volatile contents (H₂O), and the related low eruption columns, which prevented significant cooling during transport through the atmosphere and over the surface, produced hot low viscosity particles. This sequence of events together with selected evidence from TL is summarised in a flow chart, Figure 5.11.

The implications of such hot, low viscosity particles on the processes of transport, deposition and welding are discussed in Chapter 7, Section I.

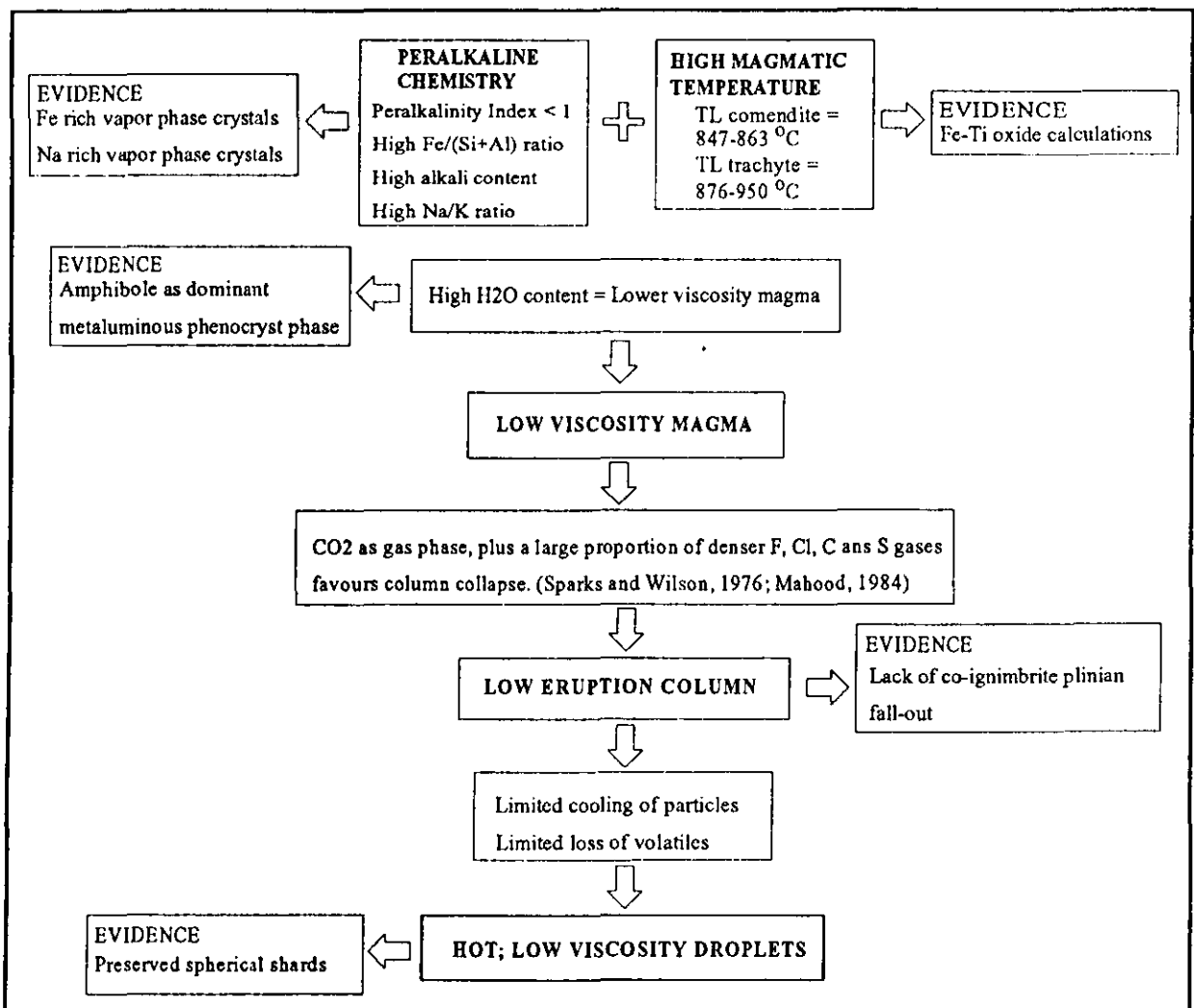


Figure 5.11. Flow chart summarising the implications of peralkaline chemistry on the physical properties of pyroclasts, with lines of evidence from ignimbrite TL.

5.4 CONCLUSIONS

TL consists of two overlapping cooling units, both of which are chemically zoned. Both TL1 and TL2 have a simple chemical stratification from TL comendite (Lower Zone), through TL mixed rock (Central Zone), to TL trachyte (Upper Zone).

TL lithofacies are particulate, thus the bulk rock compositions are effected by the relative proportions of particles of different composition. Silica rich comenditic fiamme are dominant in the lower zone of TL1 and TL2, the central zone of each flow unit has a diverse fiamme population ranging from comendite to comenditic trachyte, and comenditic trachyte fiamme dominate the upper zones of TL1 and TL2.

The wide scatter in chemical data with height is due to the physical mingling of up to three magma batches and to the complex facies associations produced by displacement of facies, by loading, thrusting and partial overturning of the deposit during post-depositional non-particulate flow.

The major and trace element trends indicate that fractional crystallisation of comenditic trachyte was the main process of differentiation in the TL trachyte - TL comendite series. Comendite is interpreted as being produced from comenditic trachyte by the fractional crystallisation of pyroxene and ilmenite together with plagioclase and anorthoclase feldspar, with anorthoclase feldspar being the most important phase.

The presence of comenditic trachyte (TL trachyte) cannot be explained by simple fractionation and is probably the result of an early magma mixing event between basalt and comendite.

A wide range in fiamme compositions plotting on a fractional crystallisation trend indicates that a zoned magma chamber, consisting of several discrete layers, was produced by the fractional crystallisation of comenditic trachyte.

Petrographic evidence indicates the presence of rocks belonging to two discrete fractionation series, one nepheline normative (e.g. trachybasalt globules in TL) and one quartz normative (e.g. TL trachyte and TL comendite). This is interpreted to be the result of contamination by incomplete mingling of magmas from these series, rather than contamination of magma by partial melting of wall rocks.

CHAPTER 6

MAGMA MIXING AND MINGLING IN TL

6.1 INTRODUCTION

Ignimbrite TL consists of two texturally and chemically complex flow units; TL1 and TL2, both of which show evidence of mixing and mingling of two or more end-member magmas. TL1 is composed of mixed and mingled comendite and comenditic trachyte and TL2 is composed of mixed and mingled comendite, comenditic trachyte and trachybasalt. Varying proportions of these end-members are present in the lithofacies TL comendite, TL trachyte and TL mixed rock:

TL trachyte consists of >60 volume percent comenditic trachyte and <40 volume percent comendite, with up to 2 volume percent trachybasalt.

TL comendite consists of >60 volume percent comendite and <40 volume percent comenditic trachyte.

TL mixed rock consists of 40-60 volume percent comenditic trachyte and 40-60 volume percent comendite, with up to 2 volume percent trachybasalt.

Several generations of mixing and mingling of magma have been identified in TL. Because of the extremely complex mixing history, this study distinguishes mixing and mingling processes.

Mixing: the process by which two or more compositionally distinct magmas are mixed together such that the melts of each are blended into a compositionally uniform *single* magma (Anderson, 1976). The most reliable criteria for defining magma mixing are: (1) if the present melt is reasonably uniform in composition, (2) if the identified composition of at least one liquid lies outside the compositional range defined by the composition of the whole rock and outside the composition of the remaining melt (glass), and (3) if mixing occurred for two or more magmas each containing some melt. The latter criterion is important because, although in porphyritic magmas the phenocrysts can still reflect the end-member magmas, disequilibrium assemblages of crystals can also result from the incorporation of solid rock.

Mingling: incomplete mixing of two or more compositionally distinct magmas, such that the magmas reach the surface without entirely losing their identity and are still texturally and compositionally distinguishable (Yoder, 1973). Evidence for magma mingling includes; compositionally banded pumice clasts (or compositionally banded fiamme in welded pyroclastic flow deposits), inhomogeneous glass compositions, and mafic clots, pillows or micro-pillows, showing distinctive quench textures, incorporated in more silicic pumice or lava.

Two other terms are used to describe mixing and mingling events which occurred in response to surface processes acting during the transport, deposition and non-particulate deformation of TL:

Particulate mixing: the process by which pre-existing juvenile particle populations are physically mixed, by semi-turbulent flow in the transport regime of a pyroclastic flow.

Mechanical mingling: the process by which lithofacies are physically mingled during post-depositional non-particulate flow of high grade ignimbrite.

TL is one of many compositionally zoned ignimbrites, other examples include: the deposit of the 1912 eruption of the Valley of Ten Thousand Smokes, Katmai (Hildreth, 1983); the Upper Mogán ignimbrites on Gran Canaria (Schmincke, 1969a); and the Bandelier Tuff (Smith and Bailey, 1966). The formation of these compositionally zoned ignimbrites has been related to compositionally zoned magma columns (e.g. Smith, 1979; Hildreth, 1981).

The chemical stratigraphy within TL1 and TL2 ranges from TL comendite, through TL mixed rock, to TL trachyte (Figs. 2.2 and 2.4). This suggests that the magma mixing and mingling processes in each case were similar, and that the two flows are genetically related (Section 6.6.2). Four sites and phases of mixing and mingling have been distinguished for TL:

- 1) Mixing and mingling in the magma chamber.
- 2) Mingling in the conduit during withdrawal.
- 3) Particulate mixing in the transport regime.
- 4) Mechanical mingling of lithofacies during non-particulate flow.

The field and petrographic evidence for these processes are presented and discussed here in interpreted genetic order.

6.2 MIXING AND MINGLING IN THE MAGMA CHAMBER

TL lithofacies and large individual juvenile clasts (fiamme), display both textural and compositional evidence for magma mixing and mingling. In a pyroclastic deposit reliable evidence for mingling within the magma chamber is only obtained from examination of juvenile particles (fiamme, shards and phenocrysts). Due to fractional crystallisation and syn- and post-eruptive mingling, evidence of magma mixing is best obtained from geochemical analysis.

6.2.1 Mixing

As discussed in Chapter 5 (Section 5.3.1), comenditic trachyte cannot be generated by simple fractional crystallisation of alkali basalt or trachyte (Fig. 5.10b). Least squares analysis by Crisp (1984) demonstrated that mixing of comendite and hawaiite was necessary to produce the comenditic trachyte in TL (Chapter 5, Section 5.3.1). This mixing event must have pre-dated fractional crystallisation and mingling since the petrographic evidence for mixing has been

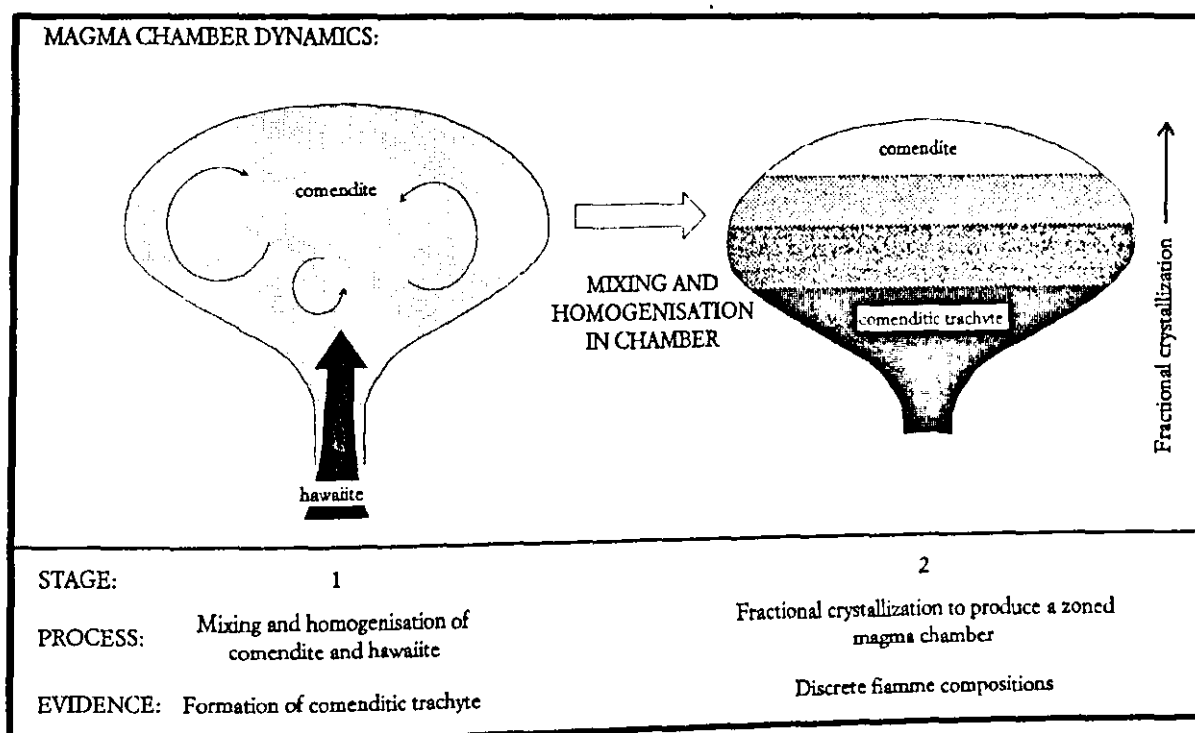


Figure 6.1. Early mixing event between comendite and hawaiite (Crisp, 1984) to account for the genesis of comenditic trachyte. Fractional crystallisation leads to the development of a zoned magma chamber containing comenditic trachyte, overlain by intermediate compositions, overlain by comendite.

overprinted. Subsequent fractional crystallisation of comenditic trachyte lead to the development of a layered magma chamber, zoned from comenditic trachyte at the base to comendite at the top (Fig. 6.1). The fiamme compositions in TL fall into a series of chemically discrete groups (Fig. 5.9) suggesting that these layers had discrete chemical compositions and that large-scale disruption of the zonation, with subsequent mingling (see below) of the discrete magma 'packages' must have taken place just prior to, or during, withdrawal and eruption.

6.2.2 Mingling

As well as mixing to produce comenditic trachyte, petrographic and geochemical evidence suggest that mingling between comenditic trachyte and trachybasalt occurred within the magma chamber.

Mingling through vesiculation induced disintegration of basic magma

Trachybasalt, identified by microprobe analysis, occurs as small (<7mm) globules in TL trachyte and TL mixed rock in flow unit TL2. The trachybasalt globules show a range of morphologies, textures and chemical composition. These features have been used to subdivide the globules into three groups (Section 4.4.1, Table 4.7, Figs. 4.18 and 4.19):

- 1) Type 1: trachybasalt end-member, consisting of black glass (tachylite, of MacDonald, 1972).
- 2) Type 2: tachylite mantled by comenditic trachyte.
- 3) Type 3: diffuse, crypto- or microcrystalline trachybasalt globules.

Three lines of evidence indicate that both the comenditic trachyte and trachybasalt were molten at the time of mingling and that mingling occurred in the magma chamber prior to eruption:

a) The most convincing evidence for mingling within the chamber, between comenditic trachyte and trachybasalt is provided by the occurrence of **mantled globules** (Globule Type 2). Many globules are completely coated in a layer of comenditic trachyte (e.g. Figs. 6.2,1a and 6.3a). This mantling could only have been produced by total immersion of trachybasalt blebs in fluidal comenditic trachyte and is therefore interpreted to have occurred in the magma chamber prior to eruption. The homogeneous composition of the mantle suggests that the mantling process did not occur in the conduit, during withdrawal. The bulk rock composition of TL trachyte and TL comendite (Section 6.1) indicate that the comendite and comenditic trachyte end-members were intimately mingled during withdrawal and eruption (Section 6.3). Thus, any globules mantled in the conduit would be expected to have a mantle composed of both comendite and comenditic trachyte, not just comenditic trachyte. Also, mechanical mingling by in conduit shear of two adjacent magma streams would produce banded rather than homogeneously mantled fragments (Section 6.3, Fig. 6.5,b5).

b) The **glassy condition** of the trachybasalt indicates that it was molten at the time of injection and mingling, and that it quenched on contact with comenditic trachyte. Tachylite (e.g. globule Type 1 and 2, Fig. 6.4a) forms during the very rapid chilling of magma to glass, and the black colour of the glass is due to the presence of quench crystallites of pyroxene (Kawachi et al., 1983). The temperatures calculated for TL trachyte are 810-910°C and temperature estimates for trachybasalt e.g. hawaiiite, from Mt. Etna (1970-75 eruption) are between 1050 and 1125°C (Archambault and Tanguy, 1976). A temperature difference of ca. 200°C would be sufficient to cause rapid chilling to glass (Dingwell and Webb, 1989).

The preservation of glassy globules indicates that mingling between trachybasalt and comenditic trachyte can only have occurred shortly before eruption. Textures are still dominantly glassy even in globules only a few mm's in diameter. Such inclusions could not survive in comenditic trachyte

CHAMBER

CONDUIT

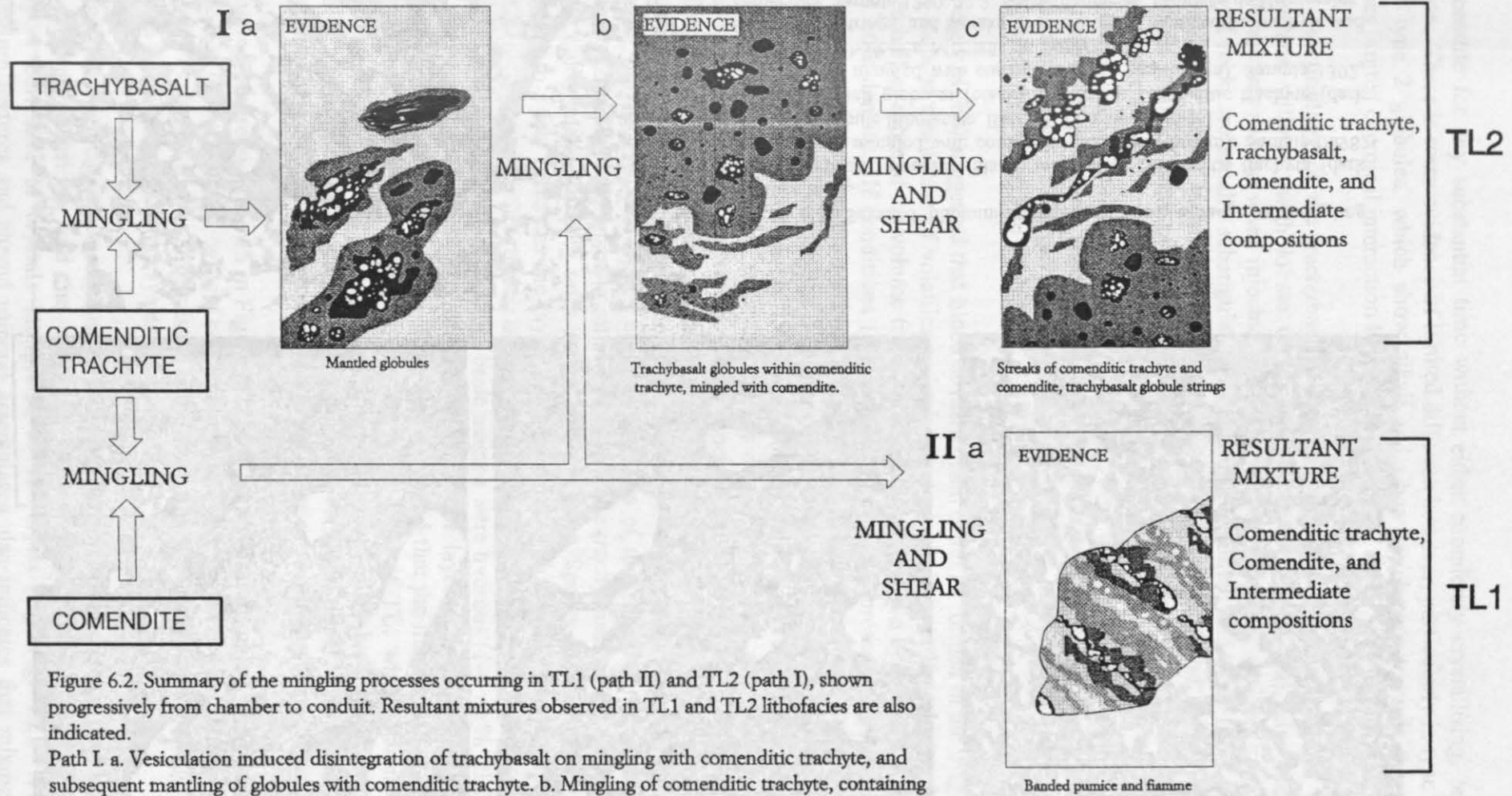


Figure 6.2. Summary of the mingling processes occurring in TL1 (path II) and TL2 (path I), shown progressively from chamber to conduit. Resultant mixtures observed in TL1 and TL2 lithofacies are also indicated.

Path I. a. Vesiculation induced disintegration of trachybasalt on mingling with comenditic trachyte, and subsequent mantling of globules with comenditic trachyte. b. Mingling of comenditic trachyte, containing trachybasalt, with comendite. c. Further mingling of comenditic trachyte containing trachybasalt with comendite and intermediate compositions during withdrawal by shear in the conduit, through the laminar flow of different compositions during simultaneous eruption.

Path II. a. Mingling in the conduit by shear of adjacent magma streams through the laminar flow of different compositions, during simultaneous eruption. Explosive fragmentation produces compositionally banded juvenile clasts.

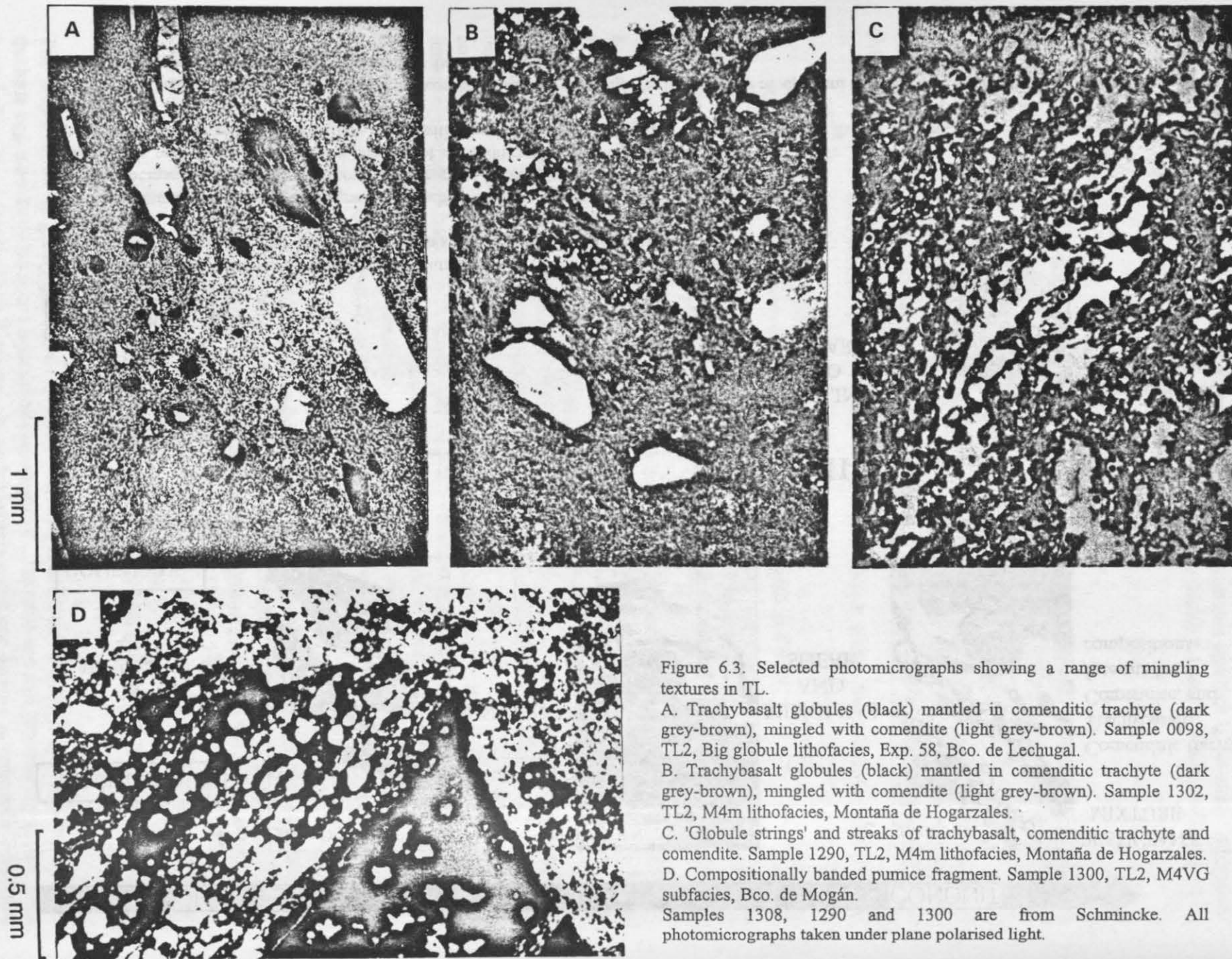


Figure 6.3. Selected photomicrographs showing a range of mingling textures in TL.

A. Trachybasalt globules (black) mantled in comenditic trachyte (dark grey-brown), mingled with comendite (light grey-brown). Sample 0098, TL2, Big globule lithofacies, Exp. 58, Bco. de Lechugal.

B. Trachybasalt globules (black) mantled in comenditic trachyte (dark grey-brown), mingled with comendite (light grey-brown). Sample 1302, TL2, M4m lithofacies, Montaña de Hogarzales.

C. 'Globule strings' and streaks of trachybasalt, comenditic trachyte and comendite. Sample 1290, TL2, M4m lithofacies, Montaña de Hogarzales.

D. Compositionally banded pumice fragment. Sample 1300, TL2, M4VG subfacies, Bco. de Mogán.

Samples 1308, 1290 and 1300 are from Schmincke. All photomicrographs taken under plane polarised light.

or comendite for any substantial time without either completely crystallising, or dissolving by diffusion. There is some evidence of limited diffusion however, particularly in type 3 globules, and also in type 2 globules, which show alkali and silica enrichment towards the margins. This indicates limited chemical interaction by ionic diffusion.

c) The **morphology** of the trachybasalt inclusions, which are mostly spherical or subspherical globules and 'pillows', with lobate or crenulate margins (Fig. 6.4 a), also indicates that the trachybasalt was molten when injected. Accessory lithic fragments, derived from solid or nearly solid wall rock, are usually subangular to subrounded in outline and those in TL commonly have holocrystalline igneous textures (e.g. Fig. 4.24). The morphology and texture suggests that the trachybasalt globules were produced when more mafic magma was injected into and quenched within, cooler more silicic magma (comenditic trachyte).

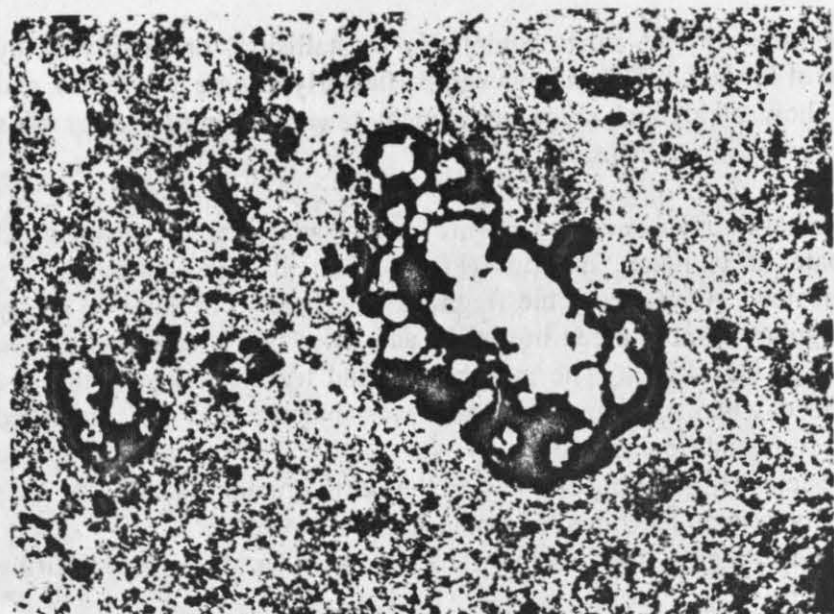
The globules contain abundant vesicles (Fig. 6.4b), even when the host contains no vesicles, thus the vesicularity of inclusions appears to be independent of the host.

The vesicular nature of the globules suggests that 'foaming' of the trachybasalt occurred during mingling with the comenditic trachyte.

Eichelberger (1980) suggested that blobs of mafic foam could be formed in the magma chamber by cooling induced exsolution of volatiles and subsequent vesiculation. He calculated that if vesicles occupied half or more of the volume fraction, then inclusions would be buoyant, forming a foam of reduced bulk density. If conditions (e.g. volatile content and pressure) permit the formation of mafic foam less dense than the reservoir magma, the interface between the two layers (in the case of TL, trachybasalt and comenditic trachyte) would become unstable in Raleigh-Taylor fashion (e.g. Ramberg, 1973; Berner et. al., 1972) and blobs of foam would rise into the reservoir magma. Large scale convection in the reservoir magma driven by heating and addition of low density material to its base would contribute to the dispersal and progressive breakdown of mafic foam (Eichelberger, 1975). The resultant pattern of chaotic mingling in the TL magma chamber would be predominantly affected by the localised flotation of trachybasalt foam or globules, and the intensity of mingling would depend upon the duration of this process. One drawback with this model however, is that the unstable interface between the trachybasalt and the comenditic trachyte would be quite small, probably only a few cm's (Huppert, Sparks and Turner, 1982) and would thicken only to a few meters as the layers exchanged heat. However, Huppert, Sparks and Turner (op. cit.), incorporating the model of Eichelberger (1980), went on to demonstrate that, for calcalkaline magmas, if the replenishing basic magma were hydrous (1-4 wt.% H₂O) the resultant density changes (due to exsolution of H₂O) in the *whole* layer of hydrous mafic magma would cause mingling through overturning. They also suggested that the magma in the upper layer need not be compositionally homogeneous, e.g. as in the case of TL, where fiamme compositions indicate that the reservoir contained comenditic trachyte overlain by intermediate compositions, overlain by comendite. The same processes would occur if the upper layer were compositionally zoned, although mingling would be confined to the lower parts of the system.

The mingling progression shown in Figure 6.2, from trachybasalt mingled with comenditic trachyte (Fig. 6.2,1a), to trachybasalt within comenditic trachyte mingled with comendite (Fig. 6.2,1b), supports the theory of Sparks, Sigurdsson and Turner, that in a zoned system mingling is initially confined to the lower parts of the system (Fig. 6.2,1c).

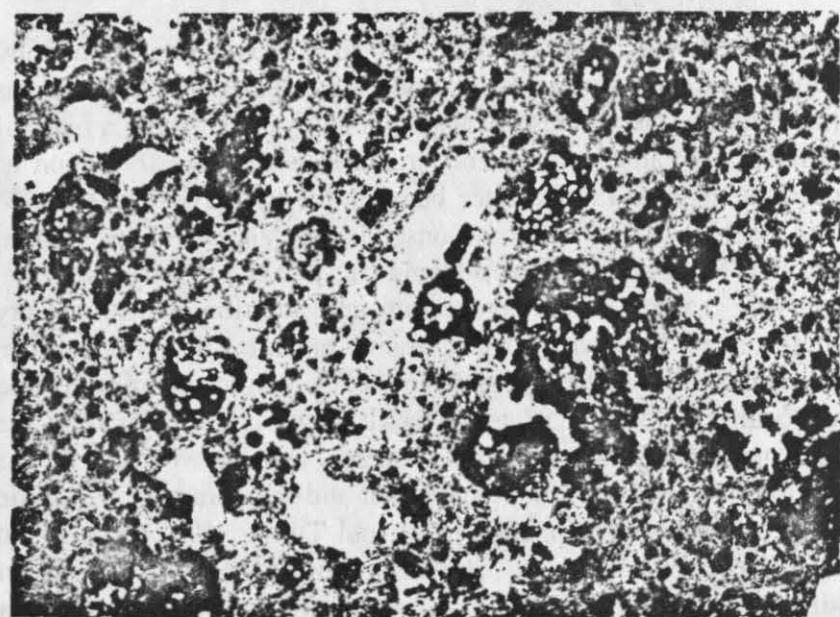
The suggestion that magmas were physically mingled rather than mixed is supported by the *lack* of mutual mineral inclusions, and the only rare occurrence of disequilibrium textures, such as rounding or corrosion of crystals interpreted as xenocrysts (e.g. Fig. 4.2). The absence of disequilibrium textures and shared mineral assemblages also indicates that mixing occurred just



a

0.5mm

Figure 6.4. Morphology of trachybasalt globules in TL2. a. The lobate margin of globule (Type 1) indicates that the trachybasalt was molten when injected. The glassy texture indicates that it was quenched on contact with comenditic trachyte. b. The vesicular texture of globules (Type 2 and 3), suggests that disintegration of the magma, through 'foaming', may have occurred (see text for details). Sample 1303 (from Schmincke), TL2, subfacies M4mt of TL2, Bco. de Mogán. Photomicrographs taken under plane polarised light.



b

2mm

prior to, or during eruption, with insufficient time for minerals to develop reverse zoning, through continued growth in a melt of contrasting composition.

6.3 MINGLING IN THE CONDUIT DURING WITHDRAWAL

In this study syn-eruptive mingling processes, occurring during simultaneous withdrawal, ascent through the conduit and fragmentation, are distinguished from transport out of the vent, and across the land surface, by which the *pre-existing* particle populations are mixed together during transport (Section 6.4).

The most convincing evidence for syn-eruptive mingling of magmas is the occurrence of banded pumice (e.g. Smith, 1979; Sparks, Sigurdsson and Wilson, 1977; Hildreth, 1981; Wolff and Storey, 1984) represented by compositionally banded fiamme (composed of comendite, comenditic trachyte and intermediate compositions) in TL (Fig. 6.3.D).

Several studies have modelled the withdrawal of magma from a zoned magma chamber, in which silicic magma overlies a more mafic magma, and the production of streaky and banded pumice during flow in a volcanic conduit (Blake, 1981b; Blake and Campbell, 1986; Blake and Ivey, 1986; Koyaguchi, 1985; Freundt and Tait, 1986). These studies modelled flow of two miscible fluids of differing viscosity, passing concentrically through a vertical pipe. The proportions in which the component magmas are withdrawn from the chamber depend on the outflow rate, the density and viscosity contrast between the magmas, the depth of the layers, and their geometrical configuration (Freundt and Schmincke, 1992).

Sectorial changes in the mixing patterns and the variation in thickness and distribution of TL lithofacies (Fig. 2.41) do not support a model of eruption through a single vent (Section 6.6.2), however this assumption does not effect consideration of the general withdrawal and mingling mechanisms.

Assuming that the TL magma chamber was evacuated from the top down (cf. Spera, 1984; Valentine, 1992; Hildreth 1981) the stratigraphic succession observed in both TL1 and TL2 (Fig. 2.2) indicates that in each case, the comenditic trachyte end-member was at the base of the magma chamber. This was overlain by a series of progressively more evolved intermediate compositions, generated by fractional crystallisation, with the most evolved (siliceous) magma; the comenditic end-member at the top of the chamber.

Using the experimental results obtained by Blake and Campbell (1986), and Koyaguchi (1985) the formation of compositionally banded fiamme in TL is interpreted as follows:

- 1) The eruption began with the withdrawal of the comenditic end-member (Fig. 6.5,b1) followed by the underlying more evolved intermediate compositions. When the volume of comendite and more evolved intermediate magma was reduced below a critical value (determined by outflow rate and viscosity- and density- contrast), the interface between the magma of more evolved intermediate composition and comenditic trachyte deformed into an inverted funnel (Fig. 6.5,b2). This led to the 'coning' of subjacent comenditic trachyte to the vent (cf. Mahood and Hildreth, 1986; Blake and Ivey, 1986).
- 2) With continued withdrawal, two or more magmas (comendite, intermediate compositions and comenditic trachyte) entered the vent simultaneously, and flowed concentrically, the outermost liquid being the more viscous comendite and magma of intermediate compositions (Fig. 6.5,b3).
- 3) During ascent through the conduit the boundary between the comendite and intermediate compositions, and comenditic trachyte became unstable (Fig. 6.5,b4) and mingling proceeded with an intensity controlled by discharge rate, viscosity contrast and length of conduit (Freundt and Tait, 1986)
- 4) Fragmentation of the variously mingled magmas led to the formation of compositionally banded juvenile fragments (Fig. 6.5,b5).

Due to their high viscosity, silicic magmas are calculated to flow in a laminar fashion even at high eruption rates (Wilson et al., 1980). Thus an initially concentric arrangement of mafic magma surrounded by more silicic magma would be stable in the conduit. However, experimental studies (e.g. Koyaguchi, 1985, 1986) have demonstrated that where the viscosity contrast between two fluids is high, instability results. In TL, the petrographic evidence (shard morphologies, Fig. 4.21), geochemical evidence (peralkalinity indices and calculated viscosities, tables 5.1, 5.2, and 5.4) and

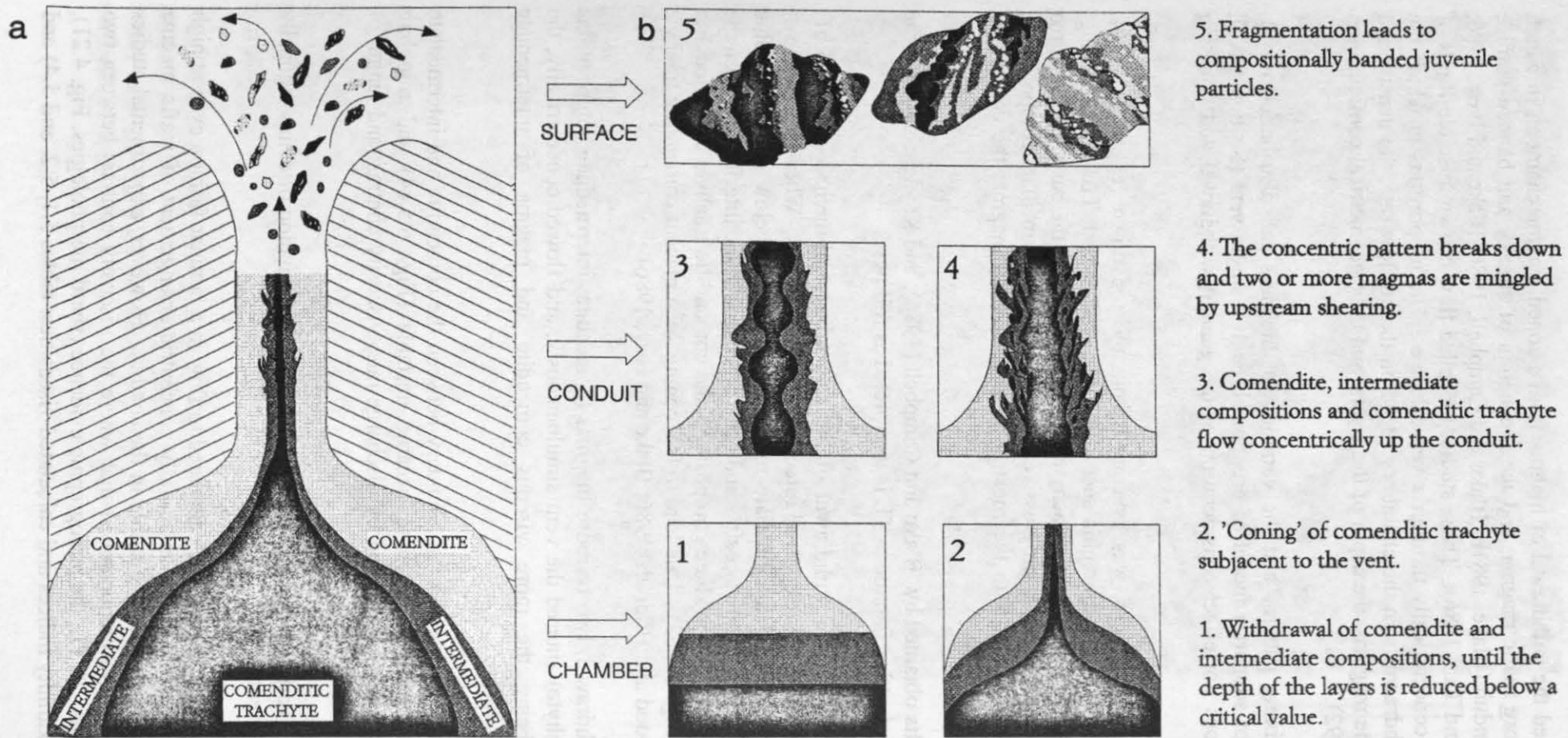


Figure 6.5. Summary diagram of the development of compositionally banded juvenile fragments in TL. a. Sketch showing the mingling of comendite (light grey), intermediate compositions (dark grey) and comenditic trachyte (black) during their simultaneous withdrawal (Modified from Blake and Campbell, 1986). The bottom part of the diagram shows comenditic trachyte being drawn up into the conduit together with intermediate compositions and comendite. At the base of the conduit, flow of the magma streams is laminar, with a concentric pattern of comenditic trachyte surrounded by intermediate compositions and comendite. At a higher level this pattern breaks down and the magmas are mingled. Banded and streaked pumice is erupted from the vent (upper part of diagram).

b. Schematic diagrams illustrating: 1. the disruption of the stable interface between comendite, intermediate compositions and comenditic trachyte during withdrawal, 2. 'coning' of comenditic trachyte adjacent to the vent, and 3. the subsequent breakdown of laminar concentric flow by the development of 'bead waves' (Koyaguchi, 1985). 4. Upstream shearing causes mingling of the magma streams. (Diagrams modified from Blake and Campbell, 1986; Koyaguchi, 1985). 5. Explosive fragmentation produces compositionally banded juvenile fragments.

mineralogy (calculated eruption temperatures, Fig. 4.17) suggest the comenditic trachyte had a much lower viscosity than the comendite.

Two magmas of contrasting viscosity become unstable during simultaneous withdrawal by forming asymmetric 'bead' waves (Koyaguchi, 1985) which are disrupted by upstream shear. This process strips shreds of mafic magma (comenditic trachyte) off the central magma column, which are then incorporated into the surrounding (comenditic, or magma of intermediate composition) silicic magma. This results in the formation of banded pumice on fragmentation. Thus the simultaneous eruption of silicic and mafic magmas can produce banded pumice even at high eruption rates (Bacon, 1983).

Wörner and Schmincke (1984) demonstrated that this process was especially effective in alkalic magmas were involved, because of their low viscosity. The very low viscosity of TL magmas related to their peralkaline chemistry and high eruption temperatures (Fig. 5.11) would further facilitate this process.

Blake and Campbell (1986) concluded that the high eruption rates associated with pyroclastic eruptions which permit the draw-up of a dense magma layer, should also allow the concentric flow pattern at the base of the volcanic conduit to become unstable. The occurrence of compositionally banded fiamme in ignimbrite TL supports this conclusion.

6.4 PARTICULATE MIXING DURING TRANSPORT

Analyses of bulk rock samples suggest that particulate mixing of the chemically discrete, juvenile particle populations (comendite, intermediate compositions, comenditic trachyte and compositionally banded juvenile fragments) occurred during transport out of the vent and over the land surface. The proportions of the component magmas supplied to the transport regime are determined by processes active in both the chamber and the conduit (Freundt and Schmincke, 1992). Fragmentation, transport, welding and non-particulate flow significantly modify mingling structures and bulk compositions of the lithofacies, but do not effect the composition of individual juvenile fragments.

Transport can act to both sort and mix particle populations. Sparks (1976) noted that many ignimbrites, for example the non-welded ignimbrites from Vulcini volcano, Italy, show coarse tail grading. The density-controlled segregation of large clasts produced deposits with pumice rich tops and lithic rich bases. Freundt and Schmincke (1985) for example, observed marginal pumice concentrations and pumice levees in the incipiently welded and non-welded ignimbrites of Laacher See (East Eifel, Germany). TL however, does not show this type of coarse tail grading. It is a high grade, densely welded, highly rheomorphic ignimbrite, containing no pristine pumice. Large juvenile fragments are highly flattened fiamme, the morphology of which (Section 3.2, Fig. 3.2) suggests that the majority were never highly expanded pumice clasts. In general the lithic content of TL is very low (<4 volume percent) which is typical of high grade lava-like ignimbrites (e.g. Branney, Kokelaar and McConnell, 1992). Observed local lithic concentrations can be directly related to topographic effects (Section 2.7.3, Fig. 2.51, Section 4.4.3). These features suggest that density-controlled sorting was not the dominant process occurring within the transport regime of TL.

The larger range of compositions in TL lithofacies compared to individual particle (represented by fiamme) groups (Table 6.1) indicates that mingling of the particle populations occurred. This increased the range of compositions in TL trachytic lithofacies compared to trachytic fiamme, and TL comenditic lithofacies compared to comenditic fiamme.

COMPOSITIONAL VARIATION		
	Range in SiO ₂ wt %	Difference in SiO ₂ wt %
TL comenditic trachyte fiamme	61.1 - 63.6	2.5
TL trachyte lithofacies	61.4 - 66.55	5.15
TL comendite fiamme	66.11 - 69.29	3.15
TL comendite lithofacies	62.15 - 69.25	7.1

Table 6.1. The wide variation in composition of TL trachyte and TL comendite lithofacies compared to comenditic and comenditic trachyte fiamme, using wt % SiO₂ as a general compositional indicator.

Poor sorting in ignimbrites has been attributed to high particle concentrations, not turbulence (Sparks, 1976), and coarse tail grading is consistent with theoretical settling rates of particles in a dispersion with a high particle concentration. Thus coarse tail grading as well as poor sorting can be attributed to flow (in a laminar fashion), of a high particle concentration dispersion.

Branney and Kokelaar (1992) however, suggest that the sorting character of ignimbrites only reflects the high particle concentrations within near depositing basal parts of a stratified, particulate gravity flow, undergoing laminar movement. They suggest that this does not preclude higher parts of the flow from undergoing expanded or turbulent flow. Semi-turbulent flow in the transport regime may have caused particulate mixing of the juvenile particles during the transport of TL.

6.5 MINGLING OF FACIES DURING POST-DEPOSITIONAL DEFORMATION

Complex variations in the chemical stratigraphy of TL suggest that large scale mechanical mingling of lithofacies occurred during post-depositional deformation. Flow unit TL2 is more highly welded than TL1 and thus provides the best evidence for the mechanical mingling of lithofacies during post-depositional deformation.

The depositional sequence of TL2, from first deposited TL comendite, overlain by TL mixed rock further overlain by TL trachyte, constitutes an inverse density stratification which is inherently unstable (Bottinga and Weill, 1970). This lead to deformation and mechanical mingling of lithofacies during non-particulate flow of the deposit. The coalesced and agglutinated particles continued to deform after deposition and the aggrading pile of agglutinate layers underwent loading, shear and auto intrusion prior to cooling and lithification. These processes and supportive evidence are discussed in detail in chapter 7, which is specifically concerned with deposition and post-depositional deformation of TL. However, a brief description is presented here as these processes represent the final stages in the mixing and mingling history of TL:

Loading caused by the inverse density stratification, acted to disrupt the original stratigraphic layering. TL trachyte loaded downwards in a series of lobate protrusions, displacing lower TL mixed rock lithofacies and underlying TL comendite lithofacies (Fig. 7.17). During displacement, lithofacies were mechanically mingled and sheared against one another. More competent lithofacies were autobrecciated, and fragments were sheared off and incorporated into the surrounding, more plastically deforming lava-like lithofacies.

Shear and auto-intrusion caused by viscosity differences related to differential cooling (Section 7.9) produced thrust or 'ramping' planes of plastically deforming TL comendite containing

fragments and streaks of autobrecciated and semi-plastically deformed TL trachyte and TL mixed rock (e.g. Fig. 2.32).

Where viscosity differences were minimal, due to thermal exchange and insulation (Section 7.9, Fig. 7.14), plastic deformation of TL comendite, TL mixed rock and TL trachyte lead to the intimate and complex juxtaposition of lithofacies, subfacies and microfacies, giving the rock a marbled appearance in the field (Fig. 2.30).

6.6 DISCUSSION

The field relations, geochemistry, petrographic and textural evidence indicate that TL underwent several stages of mixing and mingling. The mixing and mingling processes effected:

- 1) The component magmas prior to and during eruption.
- 2) The pyroclast populations created by explosive fragmentation, during transport and deposition.
- 3) The resultant extremely high grade ignimbrite, during post-depositional non-particulate flow.

There are several lines of evidence which demonstrate that all the component magmas of TL erupted from a common reservoir:

- 1) The comendite, comenditic trachyte and intermediate compositions are present in TL lithofacies as viscously deformed fiamme, indicating their molten state at the time of the eruption. Trachybasalt is present as glassy undeformed globules interpreted to have been present in the magma chamber because they are mantled in comenditic trachyte.
- 2) Comenditic trachyte cannot be generated by simple crystal fractionation of alkali basalt or trachyte. The mixing and homogenisation of comendite and hawaiite to produce comenditic trachyte could only have occurred in the magma chamber, from which the comenditic trachyte was later erupted.
- 3) Mingling structures such as compositional banding in fiamme, and mantling of trachybasalt in comenditic trachyte could only have occurred in the chamber or conduit.

6.6.1 Model for mixing, mingling and eruption of TL

Compositional zonation in magma chambers is commonly envisaged as a vertical change in composition corresponding to a stable vertical density stratification (e.g. Wörner and Schmincke, 1984; Fridrich and Mahood, 1987; Boden, 1989). The TL reservoir was probably composed of a simple vertical stack of magma layers, with comendite at the top, comenditic trachyte at the base and intermediate compositions in between.

There are many studies describing the mixing and mingling of magmas during evacuation of a zoned magma chamber (e.g. Blake, 1981 b; Blake and Ivëy, 1986; Wright, 1971; Wright and Fiske, 1971; Hildreth, 1981; Hildreth, 1983) and the initiation of eruption by injection of a more basic magma (Sparks, Sigurdsson and Wilson, 1977; O'Hara and Mathews, 1981; Huppert and Sparks, 1980).

Sparks, Sigurdsson and Wilson (op. cit.) presented the most comprehensive model for replenishment of a magma chamber by influx of more mafic magma, and although the geochemical and petrographic evidence suggest that more complex mixing and mingling processes were involved in TL, this model is applicable.

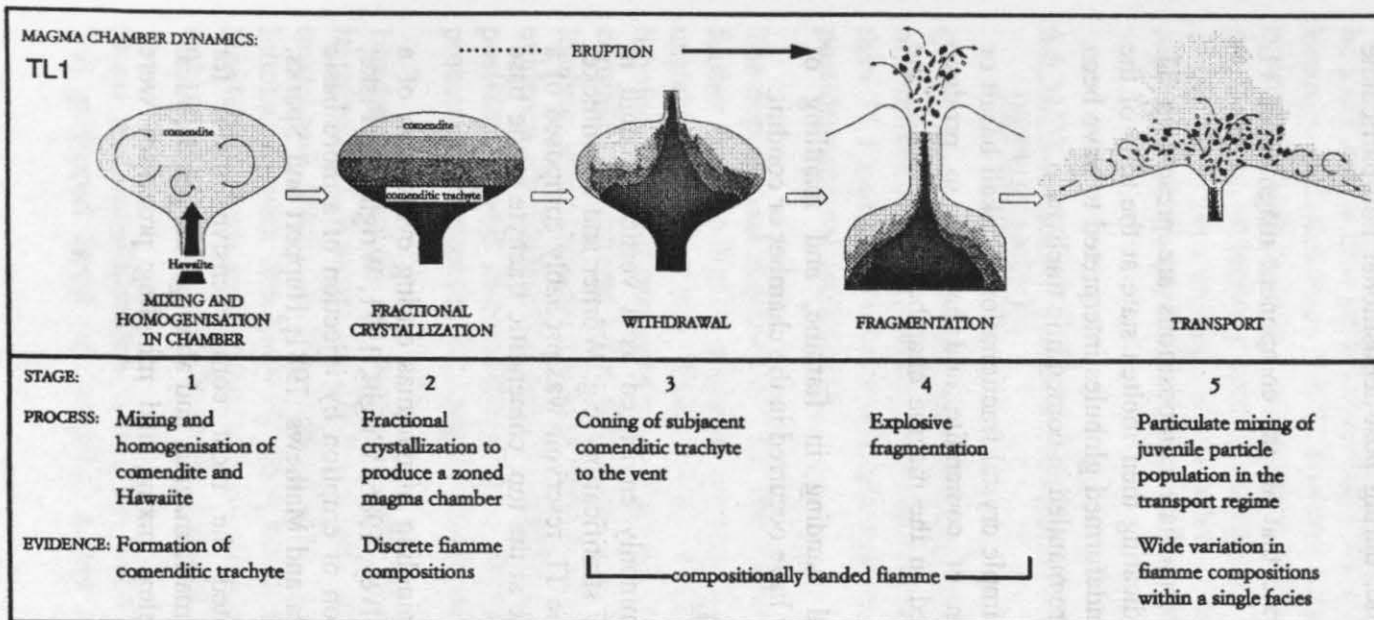


Figure 6.6. Summary of the changing magma chamber dynamics of TL1. Stages 1-5 describe the mixing and mingling processes in the chamber, through to explosive fragmentation and transport over the surface. (Details of processes are given in the text).

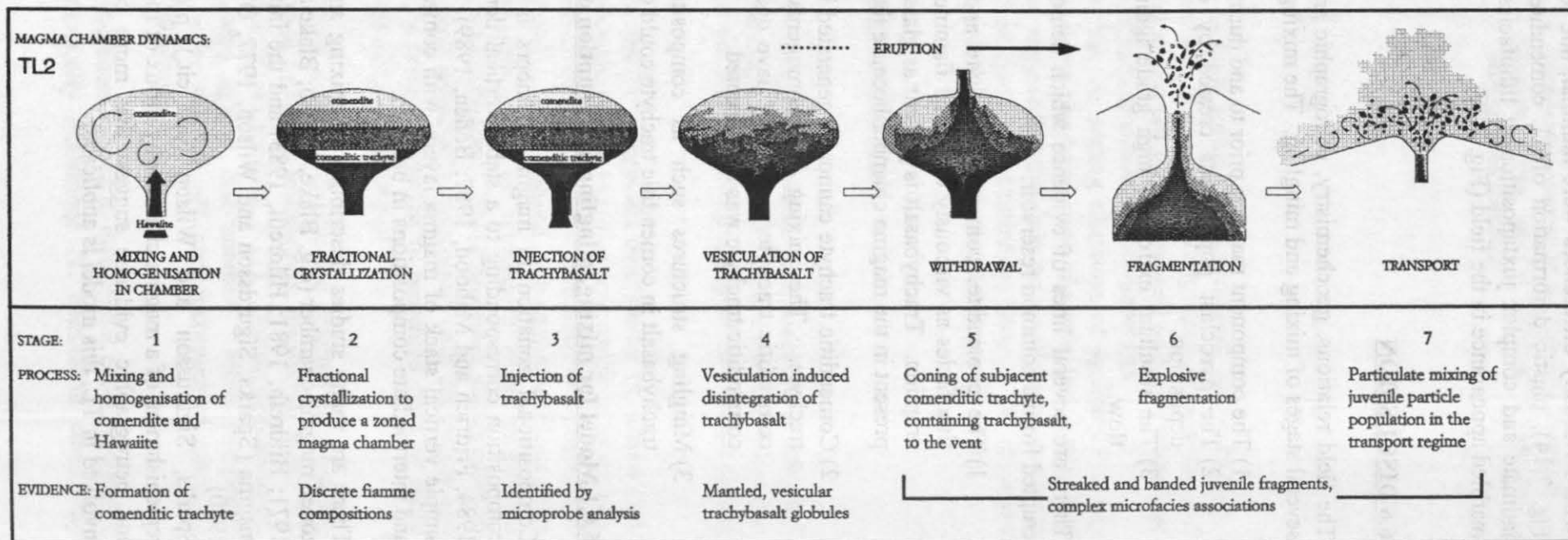


Figure 6.7. Summary of the changing magma chamber dynamics of TL2, including the injection and vesiculation of trachybasalt. (Details of processes are given in the text).

The sequence of events for mixing, mingling and eruption of TL is illustrated in Figures 6.6 and 6.7. The changing magma chamber dynamics of TL1 and TL2 have been summarised separately because TL1 contains no evidence of the trachybasalt characterising TL2. This suggests that TL1 and TL2 may be the result of two separate events. However, the identical vertical stratigraphy and composition of the comendite and comenditic trachyte in both TL1 and TL2 suggest that the two are genetically related and are probably the result of evacuation of a single magma chamber.

The following sequence of events would account for the compositional variation, mingling textures and compositional stratigraphy observed in TL1 and TL2.

1) Early mixing event

The pre-eruption TL magma chamber is envisaged as a stable, fractionating body of comenditic magma (Figs. 6.6 and 6.7, stage 1), the stable state of which was probably disrupted by the injection of trachybasalt (hawaiite).

Mixing and homogenisation of comendite and hawaiite lead to the formation of comenditic trachyte (Figs. 6.6 and 6.7, stage 2). Fractional crystallisation of the comenditic trachyte produced a zoned magma chamber containing comenditic trachyte overlain by comendite.

2) Intrusion of basic magma (only known for TL2)

The further intrusion of hotter basic magma, e.g. trachybasalt, lead to an unstable non-equilibrium system. Vesiculation induced disintegration of the basic magma (Fig. 6.7, stage 3), caused disruption of the stable comenditic trachyte-comendite zonation.

3) Initiation of the eruption

The presence of amphibole in both TL comendite and TL trachyte indicates water contents of ca. 3 wt.% (Section 4.3.3, stability considerations), suggesting that the magmas were comparatively volatile rich. The presence of lenticules (Fig. 4.25) in densely welded parts of TL1 and TL2 (Section 4.4.4) demonstrates, that even following transport and deposition, the volatile content was sufficient to produce vesicles during post emplacement cooling and degassing. If the TL magma towards the base of the chamber was saturated with volatiles it would become highly supersaturated as it rose. The increase in temperature, resulting from the injection of hotter trachybasalt, would also reduce the solubility of H_2O , thus providing a second independent mechanism for supersaturating the magma.

Exsolution of volatiles would lead to an increase in gas pressure, which together with the volume increase due to the intrusion of trachybasalt (increasing fluid pressure on the chamber walls) was probably sufficient to initiate the eruption of TL.

4) Eruptive sequence

Comendite was first erupted (TL comendite Lithofacies Group), and as the thickness of this layer was progressively reduced, intermediate compositions and comenditic trachyte were drawn up towards the conduit in the form of an inverted funnel (Figs. 6.6, stage 3 and 6.7, stage 4). Simultaneous eruption of comendite, intermediate compositions and comenditic trachyte lead to in-conduit mingling e.g. banded pumice and TL mixed rock Lithofacies Group (Figs. 6.6, stage 4 and 6.7, stage 5).

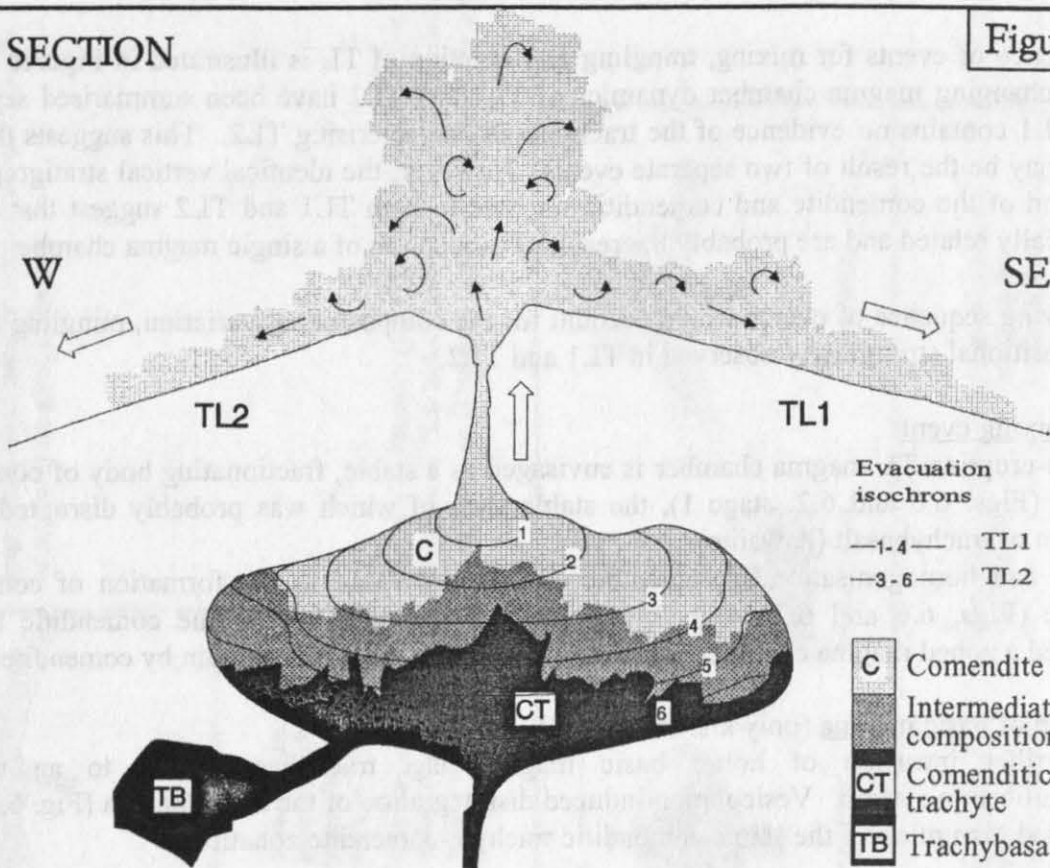
On continued eruption the amount of comenditic trachyte ejected gradually increased and finally dominated the eruption, leading to the deposition of the TL trachyte Lithofacies Group.

6.6.2 Generation of TL1 and TL2

One serious problem with the application of this model to ignimbrite TL is that there is no evidence of trachybasalt in TL1.

Figure 6.8

A SECTION



B PLAN

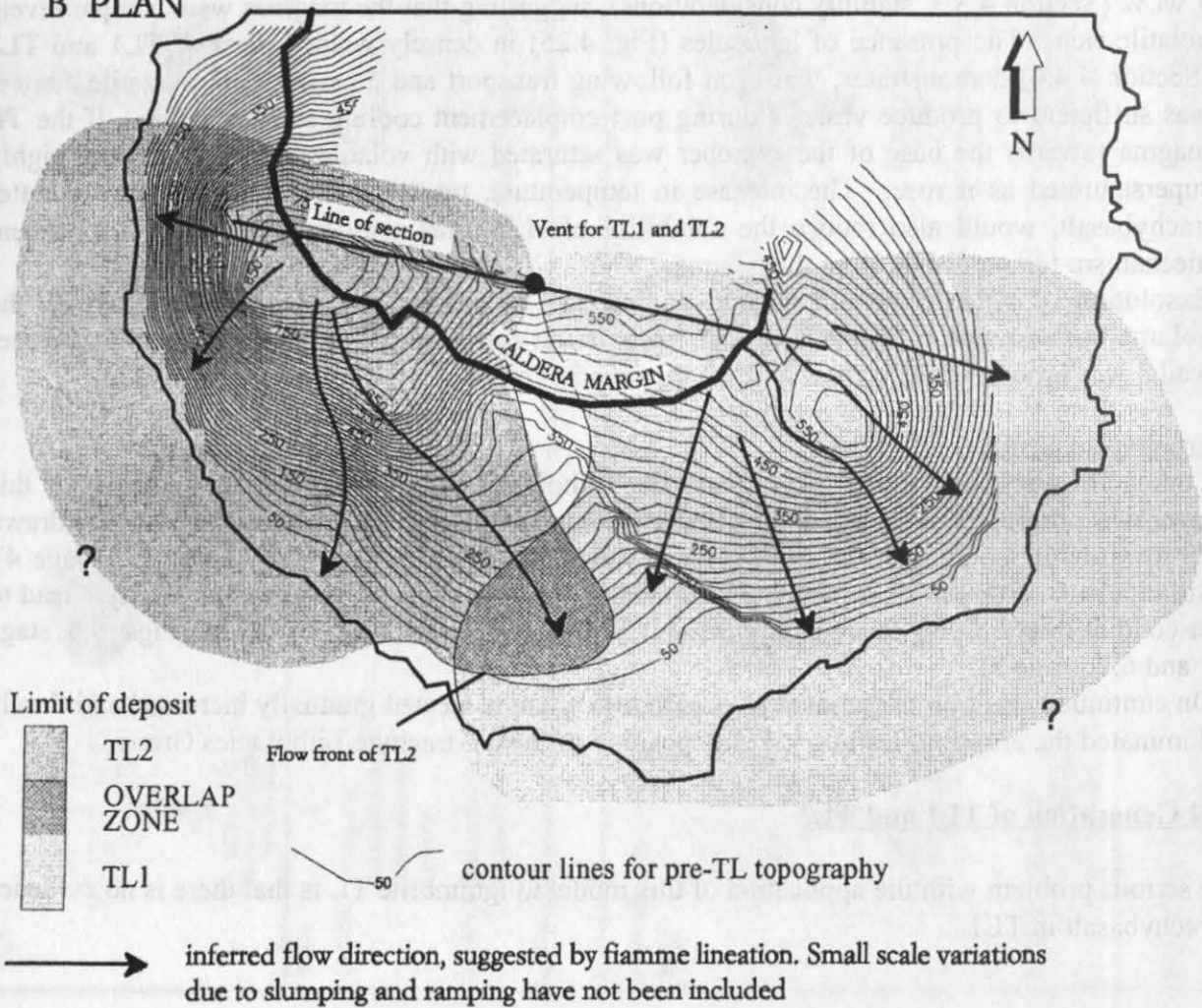


Figure 6.9

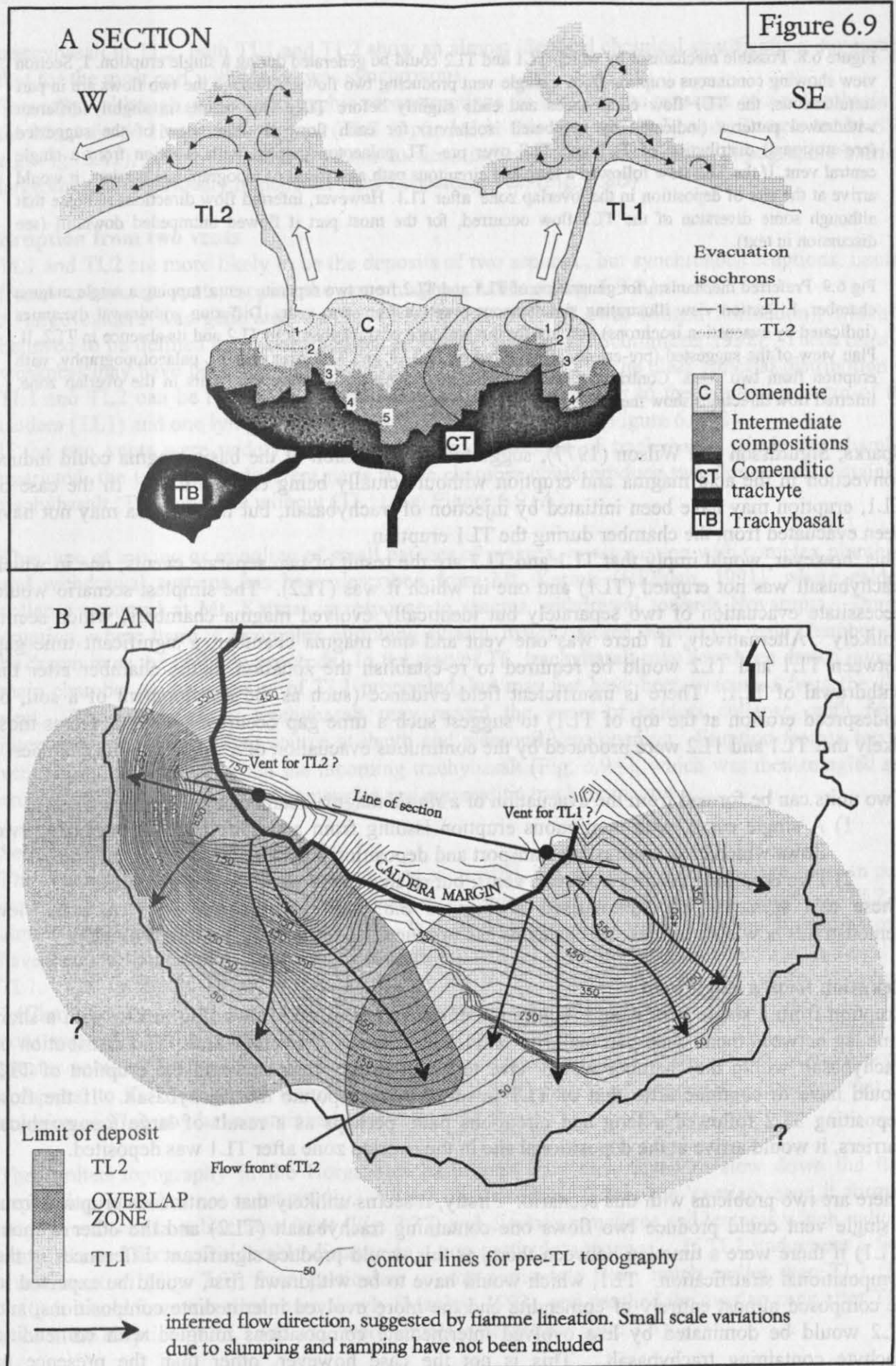


Figure captions on following page.

Figure 6.8. Possible mechanism by which TL1 and TL2 could be generated during a single eruption. I. Section view showing continuous eruption from a single vent producing two flows. Although the two flows are in part simultaneous, the TL1 flow commences and ends slightly before TL2. This results in slightly different withdrawal patterns (indicated by numbered isochrons) for each flow. II. Plan view of the suggested (pre-erosional) distribution of TL1 and TL2 over pre- TL palaeotopography, with eruption from a single central vent. If the TL2 flow followed a long and circuitous path as a result of topographical barriers, it would arrive at the site of deposition in the 'overlap zone' after TL1. However, inferred flow directions indicate that although some diversion of the TL2 flow occurred, for the most part it flowed unimpeded downhill (see discussion in text).

Fig 6.9. Preferred mechanism for generation of TL1 and TL2 from two separate vents, tapping a single magma chamber. I. Section view illustrating simultaneous eruption from two vents. Differing withdrawal dynamics (indicated by evacuation isochrons) account for the presence of trachybasalt in TL2 and its absence in TL1. II. Plan view of the suggested (pre-erosional) distribution of TL1 and TL2 over pre- TL palaeotopography, with eruption from two vents. Contrasting transport and flow dynamics produce two units in the overlap zone. Inferred flow directions show the influence of topography.

Sparks, Sigurdsson and Wilson (1977), suggested that intrusion of the basic magma could induce convection in the acid magma and eruption without actually being erupted itself. In the case of TL1, eruption may have been initiated by injection of trachybasalt, but this magma may not have been evacuated from the chamber during the TL1 eruption.

This, however, would imply that TL1 and TL2 are the result of two separate events; one in which trachybasalt was not erupted (TL1) and one in which it was (TL2). The simplest scenario would necessitate evacuation of two separately but identically evolved magma chambers, which seems unlikely. Alternatively, if there was one vent and one magma chamber, a significant time gap between TL1 and TL2 would be required to re-establish the zonation in the chamber after the withdrawal of TL1. There is insufficient field evidence (such as the development of a soil, or widespread erosion at the top of TL1) to suggest such a time gap occurred. Thus it seems most likely that TL1 and TL2 were produced by the continuous evacuation of a single magma chamber.

Two units can be formed from the evacuation of a *single* magma chamber by:

- 1) A single event, with continuous eruption issuing from a single vent, but producing two flows which have contrasting transport and depositional dynamics.
- 2) Two eruptions, issuing from two vents, but related to the same magma chamber.

These two scenarios are summarised in Figures 6.8. and 6.9. respectively. A plan view demonstrates how both of these mechanisms can produce two units in the region of overlap.

Eruption from a single vent

Eruption from a single vent would require the development of two flows (Fig. 6.8A) with a short time lag between them, such that majority of TL1 was withdrawn before TL2. The distribution of trachybasalt within the chamber would have to be extremely restricted and the eruption of TL2 would have to continue after that of TL1 in order to incorporate the trachybasalt. If the flow depositing TL2 followed a long and circuitous path, perhaps as a result of large topographical barriers, it would arrive at the depositional site in the overlap zone after TL1 was deposited.

There are two problems with this scenario. Firstly, it seems unlikely that continuous eruption from a single vent could produce two flows one containing trachybasalt (TL2) and the other without (TL1) if there were a time lag between them, as this would produce significant differences in the compositional stratification. TL1, which would have to be withdrawn first, would be expected to be composed almost entirely of comendite and the more evolved intermediate compositions, and TL2 would be dominated by less evolved intermediate compositions mingled with comenditic trachyte containing trachybasalt. This is not the case however, other than the presence of

trachybasalt in TL2, both TL1 and TL2 show an almost identical chemical stratification, suggesting that for the most part withdrawal was synchronous.

Secondly, although palaeotopographic reconstructions do indicate the presence of a palaeobasin in the Montaña de Horgazales region (TL2 is ponded in this area and in Bco. de Tasarte to the SW, e.g. Fig. 2.41), palaeotopographic reconstructions indicate that there were no topographic barriers large enough to seriously impede the flow depositing TL2 (Fig. 6.8B)

Eruption from two vents

TL1 and TL2 are more likely to be the deposits of two separate, but synchronous eruptions, issuing from two separate vents, tapping the same magma chamber (Fig. 6.9 A).

A large caldera was generated during the eruption of P1 (Lower Mogán Formation), which is believed to be defined by actual fractures at depth (Freundt and Schmincke, 1992). These lines of weakness may have been reactivated during the eruption of TL. The clear sectorial distribution of TL1 and TL2 can be related to eruption from two vents, one near to the southern margin of the caldera (TL1) and one lying towards the west (TL2), as shown on Figure 6.9 (B).

If the two vents were widely separated and the distribution of trachybasalt within the chamber restricted, the tapping of different parts of the chamber could produce two flows; one containing trachybasalt (TL2) and one without (TL1) e.g. Figure 6.9 (A).

This type of mixing or mingling of small batches of magma, in association with complex plumbing and withdrawal systems has been described from Mt. Katmai (Hildreth, 1991), where caldera collapse occurred at Mt. Katmai in response to magma withdrawal towards Novarupta. During eruption, where there is a complex plumbing system, magma stored outside the main chamber can be drawn in as the eruption proceeds. In the case of TL, trachybasalt may have been drawn into the main chamber as the eruption of TL1 proceeded, but may not have been evacuated from the TL1 vent. The incoming of trachybasalt may record the onset of caldera collapse, with faults intersecting the trachybasalt source at depth and a second vent opening. Eruption from a second vent (TL2), may have tapped the incoming trachybasalt (Fig. 6.9A), which was then mingled and erupted with the main body of comendite and comenditic trachyte magma.

Sequential or synchronous eruption

The eruption of TL1 and TL2 may have been sequential, but was more likely to have been, in part, synchronous as the magma chamber zonation, recorded in the chemical stratification of TL2, is almost identical to that in TL1 (Fig. 2.4). It is unlikely that the magma chamber zonation would have been so completely preserved if the eruption of TL2 followed the complete withdrawal of TL1. The relatively larger volume of comendite in TL1 however (minimum estimated volume 1.67km^3 , 32% of TL1), compared to TL2 (minimum estimated volume 1.07km^3 , 28.6% of TL2) does suggest that the eruption of TL1 may have commenced slightly before TL2. Similarly the greater volume of TL trachyte in TL2 (minimum estimated volume 1.45km^3 , 38.7% of the deposit) compared to TL1 (minimum estimated volume 1.82km^3 , 34.9% of the deposit) indicates that the eruption of TL2 may have continued after that of TL1.

The limited topography in the Horgazales basin area may have acted to slow down the flow depositing TL2, but not substantially. Where TL2 overlies TL1 in the 'overlap' zone it forms a steep brecciated lava-like flow front (Fig. 2.37) and displays structures and textures which indicate that it flowed for a considerable distance in a non-particulate manner. If TL2 underwent a flow transformation (Fig. 7.9), from particulate to non-particulate flow, much earlier than TL1 (Fig 7.10) it would have travelled more slowly (Manley, 1993), and reached the overlap zone after TL1, even if the eruption of TL1 and TL2 were almost synchronous (Fig. 7.3).

6.7 CONCLUSIONS

- 1) The field relations, geochemistry, petrographic and textural evidence indicate that TL underwent several stages of mixing and mingling which successively affected:
 - (a) The component magmas in the magma chamber, prior to and during eruption.
 - (b) The pyroclast populations created by explosive fragmentation, in the conduit, and in the transport regime during particulate flow.
 - (c) The resultant extremely high grade ignimbrite, during post-depositional non-particulate flow.
- 2) Several processes are believed to account for the varying compositions and mingling textures observed in TL1 and TL2:
 - (a) Mixing and homogenisation of hawaiite and comendite to produce comenditic trachyte.
 - (b) Mingling of comenditic trachyte and trachybasalt, by vesiculation induced disintegration of trachybasalt.
 - (d) Mingling of comendite, intermediate compositions and comenditic trachyte, by in-conduit shear of adjacent magma streams during withdrawal.
 - (e) Particulate mixing of juvenile particles by semi-turbulent flow in the transport regime.

A further stage of mingling has been defined for extremely high grade ignimbrite TL2:

- (f) Mechanical mingling of lithofacies by loading, shear and auto-intrusion during post-depositional non-particulate flow.
- 3) The compositional stratigraphy observed in TL1 and TL2 indicates that the composition of the erupting magma changed systematically with time, during the deposition of these two units. In both cases, comendite magma was discharged during the early phase of the eruption (TL comendite Lithofacies Group), comenditic trachyte gradually joined the comendite (TL mixed rock Lithofacies Group) and ultimately dominated the bulk composition (TL trachyte Lithofacies Group).
 - 4) The sectorial differences in the distribution of TL1 and TL2, together with presence of trachybasalt in TL2 and its absence in TL1, argue strongly for *two* simultaneous eruptions issuing from *two* vents, but related to single compositionally heterogeneous magma chamber.
 - 5) The actual vent locations of TL1 and TL2 can only be generally inferred because:
 - (a) TL is exposed at the Tejada caldera rim at only one locality (Exp. 113, Bco. de Mogán).
 - (b) The presently exposed caldera rim has been modified by Miocene volcanic, tectonic and erosional activity, post dating the TL eruption.
 - (c) Intra-caldera TL is totally covered by younger rocks.

However, the distribution of TL1 and TL2 is most simply explained by the vents being located on the caldera ring fissure system, rather than centrally within the caldera.

CHAPTER 7

DEPOSITION AND DEFORMATION OF TL

7.1 INTRODUCTION

The following discussion draws on data presented in Chapters 2-6. This chapter deals with: (1) the transport and depositional mechanisms of TL, and (2) the post emplacement deformation of TL. In the first section various models of high grade ignimbrite emplacement and deposition are reviewed and evidence is presented for a model of deposition of TL. In the second section, evidence for post-emplacement deformation is drawn mainly from TL2 which is higher grade and shows a greater degree of rheomorphism than TL1. The latter part of this discussion concentrates mainly on the large and unusual outcrop scale features of TL2 to provide an insight into the non-particulate flow of lava-like ignimbrites.

7.2 CHARACTERISTICS OF HIGH GRADE PERALKALINE IGNIMBRITES

Welding characteristics

Throughout this work, the term *grade* (Section 1.5), first proposed by Walker (1983), is used to refer to the intensity of welding exhibited by ignimbrites. The term embraces a concept of a grade continuum for ignimbrites. This reflects the variability of particle viscosity and yield strength during ignimbrite emplacement, without implying which of the many factors are the cause e.g. eruption temperature, magma chemistry, volatile content, cooling (Branney and Kokelaar, 1992). The continuum can be divided into a series of arbitrary grade categories ranging from fountain-fed lava flows to non-welded ignimbrites. The grade continuum is shown on Figure 7.1 and the general positions of TL1 and TL2, based on the product characteristics detailed in Chapters 2 and 3, are outlined in grey.

Using this classification TL1 is a *high grade* ignimbrite, which is welded to within a few cm's of the upper surface (Fig. 2.18), and has intensely welded and rheomorphic zones. TL2 is an *extremely high grade* ignimbrite which is intensely welded to its upper surface (Fig. 2.27) and includes 'lava-like' (Section 1.5) lithofacies (e.g. Fig. 2.37). Note that the different lithofacies of each flow unit may be different grades, so the given grades for TL1 and TL2 are generalised.

Physical properties of erupted magma

TL is peralkaline and has characteristics that relate to the physical properties of the erupted magma i.e. low viscosity, high eruptive temperature and high dissolved volatiles (Fig. 5.11). The presence of amphibole (Section 4.10.5), in both TL trachyte and TL comendite indicates a high (minimum 3 wt.%) magmatic water content. These features, together with a likely low eruption column, which is typical of peralkaline ignimbrites (Fig. 5.11), combined to produce hot low viscosity particles which were not significantly cooled during eruption. The particular rheological properties of these particles have implications for both the transport and depositional mechanism (Section 1).

High emplacement and post-emplacement temperature

Mineralogical and petrographic observations (Sections 4.5 and 4.6) suggest that TL was emplaced at high temperature and, compared to low grade ignimbrites, remained at high temperature after emplacement:

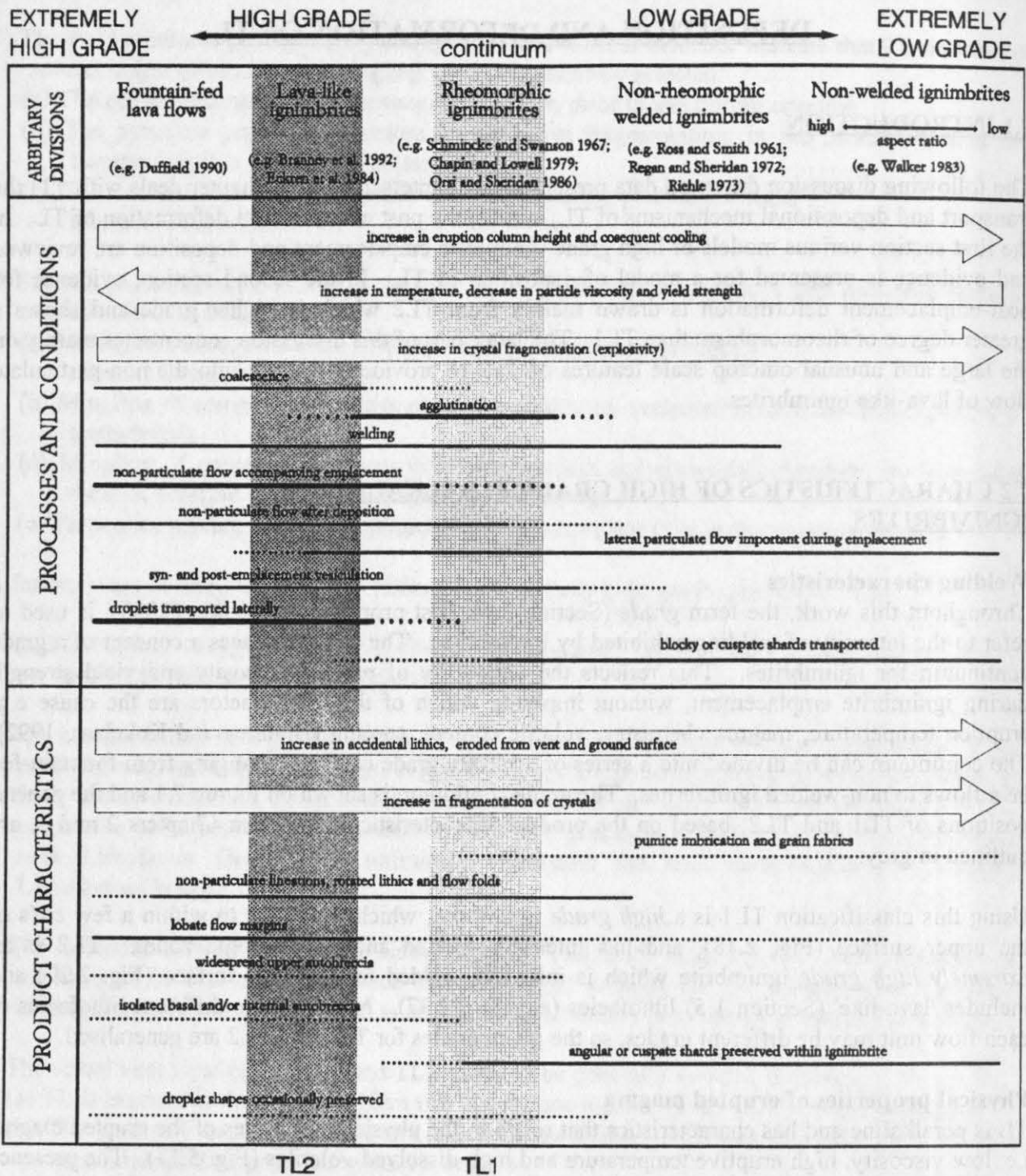


Figure 7.1. The grade continuum, with associated processes, conditions (Branney and Kokelaar, 1992). All gradations can occur within deposits of a single stratified flow since the processes vary both through time (i.e. vertically through a deposit), and with distance from source (laterally within a deposit). *Solid lines* indicate characteristic features, *dotted lines* indicate possible features. The position of TL1 and TL2, determined by product characteristics, are indicated by shaded columns. Details of the processes and conditions are given in the text.

- 1) Both TL1 and TL2 are welded to within a few cm's of the upper surface and their fiamme and matrix show high-temperature spherulitic devitrification (Section 4.5.2, Fig. 4.28)
 - 2) High-temperature vapour phase crystallisation has occurred within lenticules (Section 1.5) in the densely welded lithofacies of TL1 and TL2 (Section 4.6, Fig. 4.29). Mineral compositions (Figs. 4.12 and 4.13) indicate that this involved a simple redistribution of mobile phases within a closed system.
 - 3) The formation of lenticules (Fig. 4.25) and the deposition of vapour phase minerals within them indicates that volatile exsolution continued after deposition and after welding.
- That TL remained at high temperatures after emplacement has implications for the deformation processes (Section II).

7.3 FLOW DYNAMICS

The geographical distribution (Fig. 2.1) and the absence of internal flow unit boundaries (for example, Fig. 2.3) suggests that TL1 and TL2 were the deposits of two separate sustained flows. The deposits are restricted in extent (estimated minimum volumes: 18km³ for TL1 and 9km³ for TL2, ignoring any possible caldera fill). Flow direction indicators (fiamme lineations, Figs. 3.11 and 3.12) demonstrate that the flows depositing TL1 and TL2 spread radially outwards from the caldera, but were also channelled to some extent, such that they were deposited on top on one another in a zone of overlap at a palaeotopographic low (Fig. 7.2).

The sectorial distribution, the compositional stratigraphy, and the occurrence of the two units together only in a small zone of overlap suggests that rather than being the result of a single vent eruption, TL1 and TL2 were erupted from two separate vents, related to the same magma chamber (Section 6.6.2, Fig. 6.9). The larger volume of TL comendite in TL1, compared to TL2, suggests that the TL1 vent was active before that of TL2 (Fig. 7.3a). The larger volume of TL trachyte, including TL trachyte containing trachybasalt globules (Fig. 6.2), indicates that TL2 continued erupting after the eruption of TL1 had ended (Fig. 7.3c).

Although TL1 and TL2 appear as two separate units in the zone of overlap, at locality 113, near the caldera wall at the head of Bco. de Mogán, TL1 and TL2 have cooled together forming a single cooling unit with repeated stratigraphy (Appendix I, profile 113). This suggests that the eruptions were in part, synchronous (Fig. 7.3b).

Three dimensional palaeotopographical reconstructions (made with the program Surfer[®], Appendix II) were compiled using field data from TL1 and TL2. The height of the base of each flow unit, at over 40 localities, was used to create a palaeotopographical base map. There are two limitations with this model of palaeotopographic reconstruction:

1. The current coastline of Gran Canaria was used because the position of the coastline during emplacement of TL is not known. The Miocene coast was certainly very different and the large cliffs on the western coast of Gran Canaria were probably not present.
2. The lack of data points in areas where TL is not exposed at the surface necessitated a rough calculation of the palaeotopography, the sudden oversteepening of the topography, inland of the east coast, may be an artefact of the gridding method.

The path of each flow (deduced from palaeoflow indicators) was sketched onto the palaeotopographic base map for three consecutive time periods (Fig 7.3a, b and c). A wide channel between Bco. de Mogán and Bco. de Arguineguin effected the pyroclastic flows that deposited TL1 and TL2. The geographical distribution and lineation orientations indicate radial transport of the TL1 flow from a vent lying towards the southern margin of the caldera, and deposition of TL1 in the zone of overlap (Fig. 7.3a). Simple radial transport of the flow depositing TL2, from a vent

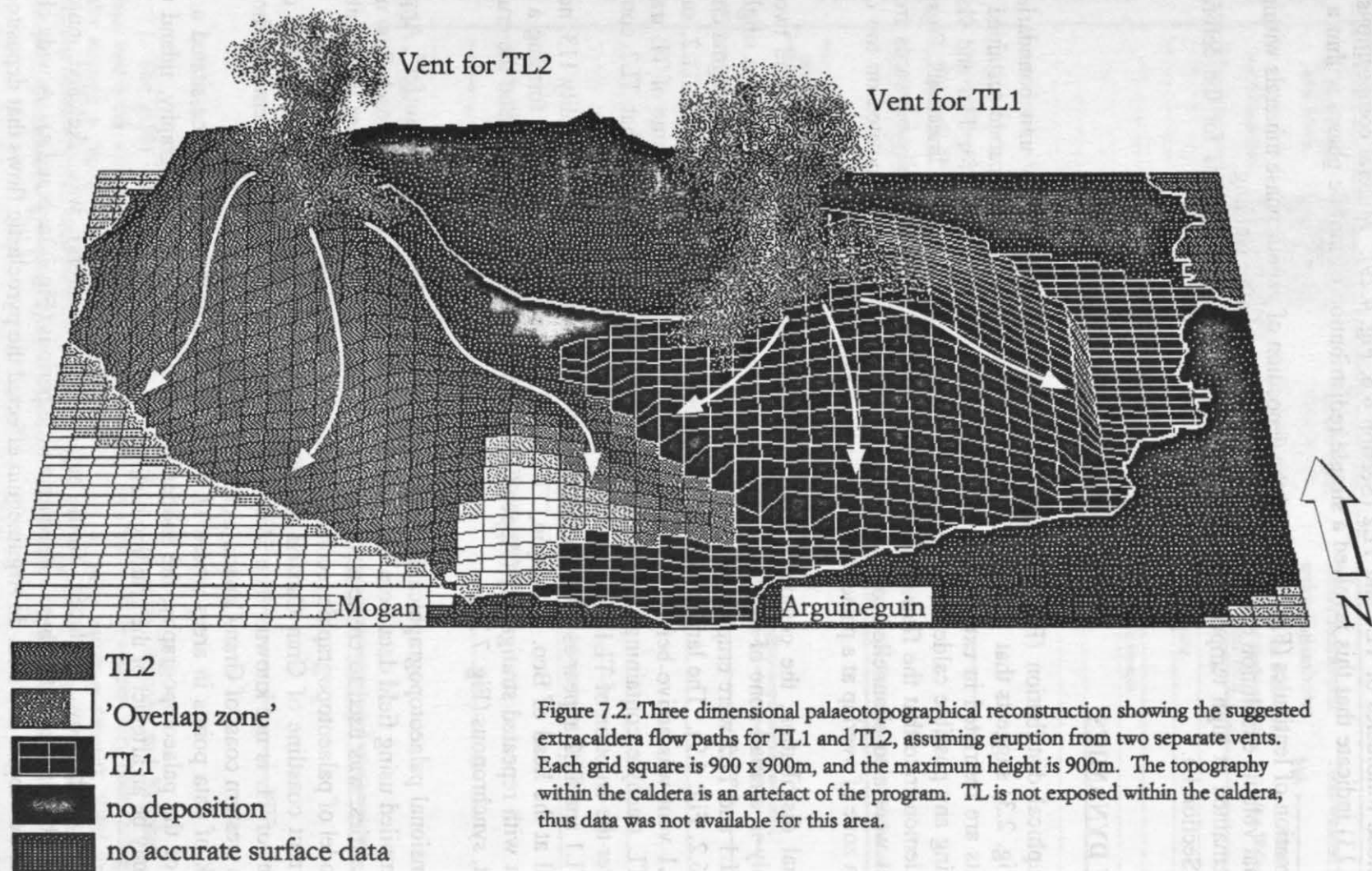


Figure 7.2. Three dimensional palaeotopographical reconstruction showing the suggested extracaldera flow paths for TL1 and TL2, assuming eruption from two separate vents. Each grid square is 900 x 900m, and the maximum height is 900m. The topography within the caldera is an artefact of the program. TL is not exposed within the caldera, thus data was not available for this area.

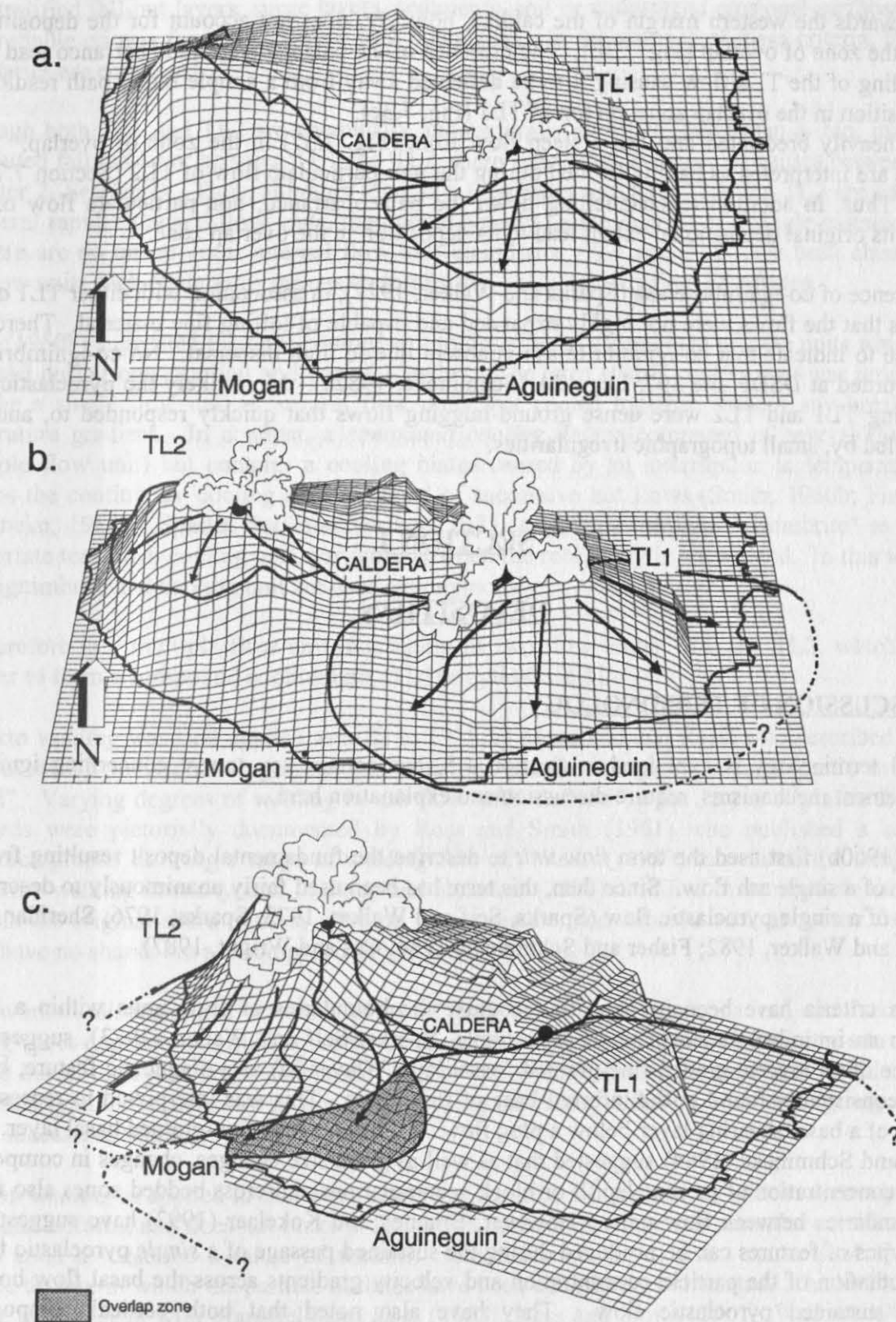


Figure 7.3. Flow distribution and changing flow dynamics, during the staggered eruption of TL1 and TL2. The flow paths are modeled over three consecutive time periods. (a) Eruption of TL1 slightly pre-dates TL2. The TL1 flow travels radially outwards from a vent near the southern margin of the caldera. (b) Period of simultaneous eruption of TL1 and TL2. TL1 is deposited in the overlap zone between Bco. de Mogán and Bco. de Arguineguin. (c) Eruption of TL1 wanes while TL2 continues erupting. A particulate to non-particulate flow transition occurs (Figs. 7.9 and 7.10) during the flow of TL2 and the non-particulate flow travels slowly down the wide palaeobarranco such that TL2 is deposited on top of TL1 in the overlap zone.

lying towards the western margin of the caldera, however, does not account for the deposition of TL2 in the zone of overlap (Fig. 7.3b). The presence of the palaeotopographic barranco lead to the channelling of the TL2 flow causing it to be deflected away from a simple radial path resulting in its deposition in the overlap zone, on top of TL1 (Fig. 7.3c).

TL2 is heavily brecciated and has a steep flow front (Fig. 2.37) in the zone of overlap. These features are interpreted as having formed during the non-particulate flow of TL2 (Section 7.7, Fig. 7.10). Thus, in addition to channelling down the palaeobarranco, non-particulate flow of TL2 *beyond* its original depositional extent lead to its deposition in the overlap zone.

The absence of co-ignimbrite ash (Sparks and Walker, 1977), in association with either TL1 or TL2 suggests that the flows were not highly expanded and capable of lofting fine material. There is no evidence to indicate that co-ignimbrite ash is absent due to high dispersal. No co-ignimbrite ash was recorded at DSDP site 397, Leg 47A (Schmincke, 1982a). More likely the pyroclastic flows depositing TL1 and TL2 were dense ground-hugging flows that quickly responded to, and were channelled by, small topographic irregularities.

SECTION I

DEPOSITION

7.4 DISCUSSION OF TERMINOLOGY

General terminology is explained in Section 1.5, but certain key terms, concerning ignimbrite emplacement mechanisms, require discussion and explanation here.

Smith (1960b) first used the term *flow unit* to describe the fundamental deposit resulting from the passage of a single ash flow. Since then, this term has been used fairly unanimously to describe the deposit of a single pyroclastic flow (Sparks, Self and Walker, 1973; Sparks, 1976; Sheridan, 1979; Wilson and Walker, 1982; Fisher and Schmincke, 1984; Cas and Wright, 1987).

Various criteria have been invoked to recognise the boundaries of flow units within a section through an ignimbrite succession. For example, Sparks, Self and Walker (1973), suggested the presence of an inverse-graded fine-grained "basal layer" (layer 2a) as a diagnostic feature, because it was consistently found at the inferred base of flow units. This was interpreted to represent the deposit of a basal shearing layer below a plug flow. TL has no such fine-grained basal layer.

Fisher and Schmincke (1984) suggested that as well as grain size changes, changes in composition, fabric, concentration of pumice lapilli or block accumulations and cross bedded zones also marked the boundaries between flow units. However, Branney and Kokelaar (1992) have suggested that these types of features can be produced during the sustained passage of a *single* pyroclastic flow by the fluctuation of the particle concentration and velocity gradients across the basal flow boundary of the sustained pyroclastic flow. They have also noted that both vertical compositional stratification and grain size changes have been recorded within massive units (L2 of Sparks, 1976), i.e. within individual flow units (e.g. Sheridan, 1979; Wright and Walker, 1981; Cas and Wright, 1987) and have drawn analogy with similar sorting, grain size variations and bedding structures produced during sustained deposition from aqueous flows, e.g. deposition from high density turbidity currents.

Interstratified fall-out layers, surge layers, sediments, soil or widespread erosional surfaces are the most reliable criteria for defining flow unit boundaries. In the absence of these criteria, flow unit boundaries are equivocal.

Although both TL1 and TL2 are chemically and texturally stratified, other than a thin, irregularly distributed fall out layer between TL1 and TL2, there is no other evidence of pauses between flows (Chapter 2, Section I). Thus, although there is a possibility that both TL1 and TL2 are composed of several rapidly stacked flow units, they could equally be the deposit of a single sustained flow. As there are no unequivocal internal flow unit boundaries, TL1 and TL2 have been classified as two flow units each containing various texturally and chemically distinct lithofacies.

Smith (1960b) suggested the term *cooling unit* to describe an assemblage of flow units which were produced during one eruption and cooled together. The term *simple cooling unit* was proposed to describe a single flow unit or several flow units that cooled together without any break in the temperature gradient. In contrast, a *compound cooling unit* is composed of several flow units (multiple flow unit) but contains a cooling hiatus caused by an interruption in temperature that disturbs the continuous 'cooling unit zonation' of successive hot flows (Smith, 1960b; Fisher and Schmincke, 1984). Sparks, Self and Walker (1973) suggested the term "ignimbrite" as a more appropriate term than cooling unit, particularly when the rock body is not welded. In this work the terms ignimbrite and cooling unit are used synonymously.

TL therefore is a multiple flow unit, consisting of two flow units; TL1 and TL2, which cooled together to form a compound cooling unit (TL) or ignimbrite TL.

The term *welding* was first applied to tuffs in 1935 by Mansfield and Ross, who described welded tuffs "in which individual fragments had remained plastic enough to become partly or wholly welded". Varying degrees of welding in ash flow tuffs, defined by the degree of plastic distortion of shards were pictorially documented by Ross and Smith (1961) who published a series of photomicrographs showing a range of welding fabrics. Walker (1983) introduced the term 'grade' to describe welding intensity, and Branney and Kokelaar (1992) modified this to include lithofacies in which the original shard outlines were no longer visible, and deposits such as spatter fed lavas, which have no shards but are composed of welded clasts (Fig. 7.1).

Many workers distinguished between "primary" (syn-depositional agglutination) and "secondary" welding (post-depositional welding compaction under the influence of a deposits in-situ cooling rate and burial load pressure). This is difficult to apply since there is no conclusive evidence that high grade ignimbrites form by an ash flow stopping en masse, deflating, then undergoing welding in neat successive stages.

The term *welding* is applied in this work simply to describe the process by which viscous particles adhere and deform, and does not make a distinction between primary and secondary welding. The term is used to describe a range of textures from the sintering of point contacts of shards to lava-like texture in which the particle outlines have been completely obliterated. This definition of welding is consistent with Mansfield and Ross (1953), Ross and Smith (1961), Walker (1983) and Branney and Kokelaar (1992). Where shard forms are preserved, specific degrees of welding have been described by analogy to the descriptions of Ross and Smith. Where particles weld rapidly on contact and the particle outlines are preserved the term agglutination is used (Branney and Kokelaar, 1992) and the process by which low viscosity droplets rapidly coalesce on contact and the original particle outlines are obliterated is termed coalescence (Branney and Kokelaar, 1992). These processes produce agglutinate beds and lava-like lithofacies respectively.

The term *rheomorphism* defined as "secondary mass flow" was used by Wolff and Wright (1981) to describe and ignimbrite or tuff that underwent deformation following emplacement and deposition. As with the use of primary and secondary welding, the concept of "secondary" flow is difficult to apply to high grade ignimbrites because non-particulate flow could occur during deposition and the flow would not necessarily halt abruptly before remobilising and undergoing "secondary" flow at some later time.

In this work, the term rheomorphism is used to describe any non-particulate deformation, including deformation during deposition as well as hot slumping or gravity sliding. This definition of rheomorphism includes the processes of syn-depositional deformation and post-depositional deformation. Structures are described as being the result of post-depositional deformation when the deformation structure effects the entire unit to the upper surface (Section II, this chapter), as these structures must have formed after deposition of the entire unit.

7.5 A REVIEW OF HIGH GRADE IGNIMBRITE EMPLACEMENT MECHANISMS

Three models have been presented to explain the emplacement mechanism of high grade ignimbrite:

- 1) En masse particulate deposition, followed by secondary mass flowage.
- 2) Laminar viscous flowage, with agglutination occurring during the final deceleration of a single pulse, dense pyroclastic flow.
- 3) Progressive aggradation and simultaneous changes from particulate to non-particulate flow.

These models are reviewed here with particular reference to three processes:

- 1) Type of particulate flow and flow dynamics.
- 2) Depositional mechanism.
- 3) Timing of welding.

Details of these models are given in the references listed in Figure 7.4, the most recent review is found in Branney and Kokelaar (1992) .

A. En Masse deposition, followed by secondary mass flowage

Flow dynamics

In the *en masse* deposition model, a pyroclastic flow was envisaged as a high concentration, poorly expanded, partially fluidised flow. This was turbulent proximally but became laminar and underwent plug flow distally (Fig. 7.4a). In this model, laminar and plug flow were invoked when Sparks (1976) attributed poor sorting in ignimbrites to high particle concentration in poorly expanded flows, rather than to turbulence.

Deposition

The flow is envisaged as undergoing deceleratory laminar or plug flow before stopping *en masse* to produce a deposit consisting of an inversely graded unit (Layer 2a) overlain by a massive unit (Layer 2b, terminology of Sparks et al., 1973). Together these represent a single flow unit, ergo the deposit of a single pyroclastic flow.

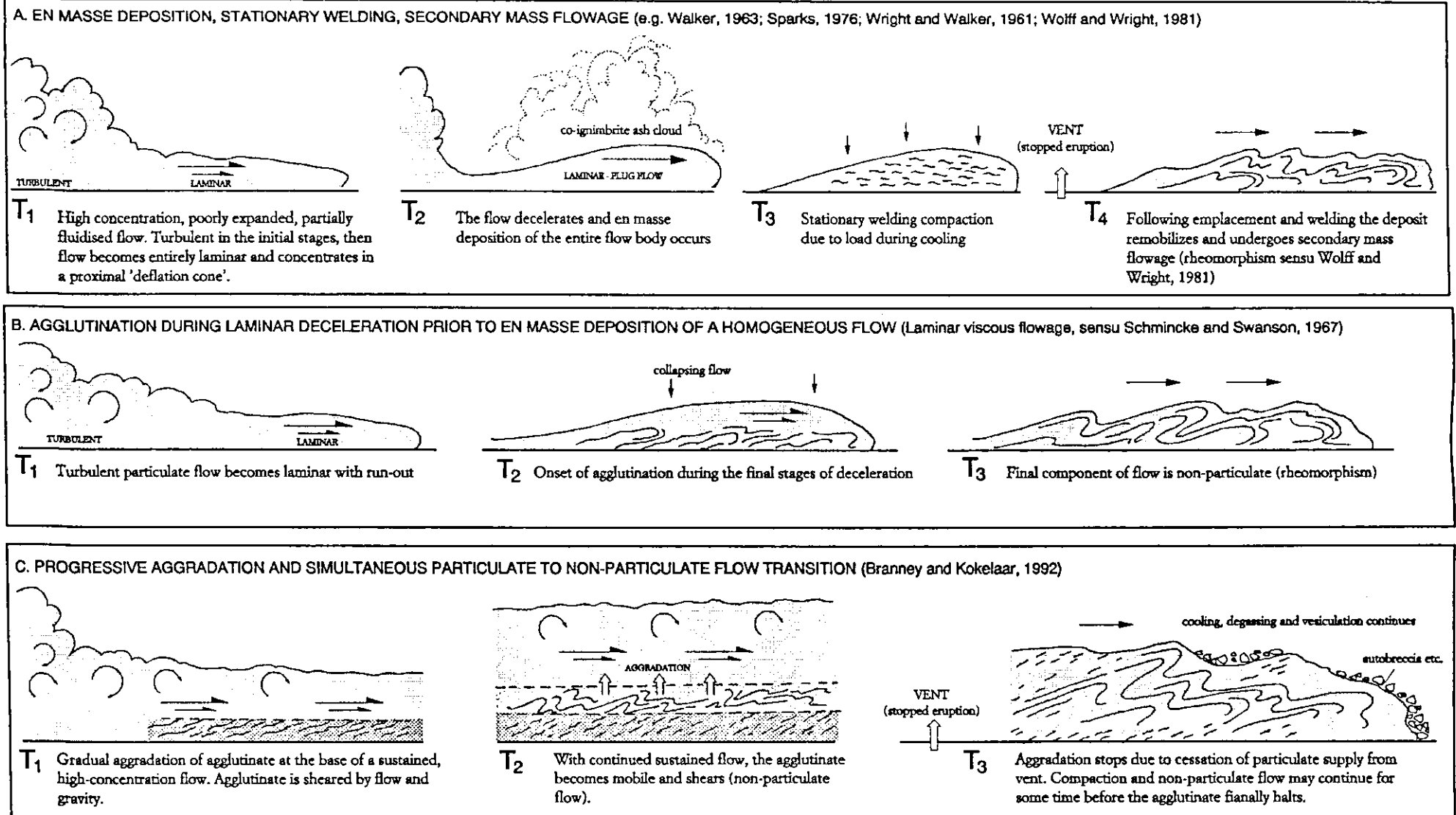


Figure 7.4. Summary of three models of high grade ignimbrite emplacement and deposition, with key references, and details of the major processes including: type of flow, depositional mechanism and timing of welding.

Welding

In this model all compaction and welding takes place after *en masse* deposition and is related to:

- 1) emplacement temperature,
- 2) thickness of the unit (rate of cooling),
- 3) the composition and physical properties of glass and residual volatiles.

Welding profiles, therefore reflect the cooling and loading profiles of *in situ* ignimbrite sheets. The degree of welding reflects the length of time at which loaded parts of the profile remained at high temperature (e.g. Ross and Smith 1961, Ragan and Sheridan, 1972).

Rheomorphism

Following welding the tuff can undergo *secondary mass flowage* (rheomorphism: *sensu* Wolf and Wright, 1981) as shown in Figure 7.4A.

Thus, in a model of *en masse* deposition followed by welding compaction, followed by secondary mass flowage, both welding and non-particulate deformation take place AFTER deposition has ceased.

Using this model, compositionally and texturally layered sequences must imply the stacking of flow units from successive pyroclastic flows.

B. Laminar viscous flowage with agglutination occurring during final deceleration of a single pulse, dense pyroclastic flow

This model (Fig. 7.4B) was presented by Schmincke and Swanson (1967), who described structures from peralkaline ignimbrites on Gran Canaria. Structures such as stretched pumice, broken and rotated pumice fragments, imbricated and lineated pumice fragments and hollows around lithics, were interpreted as being formed during *laminar viscous flowage* (non-particulate shear).

The particulate flow was again envisaged as initially turbulent and evolving to laminar on deceleration. In this model the structures (listed above) were interpreted as being formed by welding and lava-like flow during the final deceleration stages of *en masse* emplacement (Fig. 7.4B), just before the ash flows halted.

This was seen as a "simple end phase movement" (Schmincke and Swanson, 1967), prior to secondary mass flowage, but following the halt of the turbulent flow, with agglutination occurring throughout the body of a flow as it stops and deflates *en masse*.

In this case, welding and particle deformation occurred before and independently of post emplacement cooling and welding, thus for example, explaining ignimbrite sheets which are welded to the upper surface.

Using this model, compositionally and texturally layered sequences are again produced by the stacking of successive flow units.

C. Progressive aggradation and simultaneous particulate to non-particulate flow transition

Recent work by Branney and Kokelaar (1992) reviewed the theory of *en masse* emplacement and deposition, highlighted the problems with the application of this model (Branney and Kokelaar, 1992, page 507), and modified the model of Schmincke and Swanson (1967). Branney and Kokelaar suggest that massive ignimbrite and layered ignimbrite sequences can be formed by a process of *progressive aggradation* during the sustained passage of a single particulate flow, although they do not dispute that some ignimbrite sheets may record more than one pyroclastic flow.

Flow dynamics

In the progressive aggradation model, the flow is envisaged as a density stratified flow (Fig. 7.4C) in which the basal part undergoes laminar flow and higher parts show varying degrees of laminar flow or turbulence. Deposition occurs progressively at the base of the flow, where high particle concentration and flow boundary drag promote laminar flow. Thus laminar flow and high concentration are recorded in the deposit.

Deposition

In this model, deposition is suggested as being sustained and incremental. Thus bedding and sorting characteristics of an ignimbrite deposited by this method reflect mainly the depositional processes in the dense basal parts of the flow, rather than the transport processes of the entire flow, as is the case with sudden *en masse* deposition.

Welding

In the progressive aggradation model, welding occurs throughout the depositional history, and the degree of welding is related to the rheological properties of the particles supplied to the underlying depositional regime by the overriding transport regime. In this case, welding and non-particulate deformation occur during deposition and, like the model of laminar viscous flowage, independently of post emplacement cooling and loading. Agglutination and deposition of particles may continue as long as the transport regime supplies hot particulate material to the depositional regime.

Rather than stacking of successive flow units, the vertical facies successions developed in the deposit reflect temporal changes in flow steadiness, and in the material supplied to a sustained flow at source. This model thus accounts for vertical changes in, for example, grain size and welding intensity in the absence of unequivocal flow unit boundaries.

The key points of these three models, relating to flow dynamics, deposition and welding are compared and contrasted in Table 7.1.

MODEL	EN MASSE DEPOSITION AND SECONDARY MASS FLOW	LAMINAR VISCOUS FLOWAGE	PROGRESSIVE AGGRADATION AND PARTICULATE TO NON-PARTICULATE FLOW TRANSITION
FLOW PROCESSES	High concentration, poorly expanded partially fluidized flow Turbulent \longleftrightarrow Laminar or plug flow	High concentration, poorly expanded partially fluidized flow Turbulent \longleftrightarrow Laminar	Density stratified flow Basal depositional regime \leftrightarrow Laminar Overriding \longleftrightarrow Laminar to transport regime turbulent
METHOD OF DEPOSITION	Instantaneous, En masse	En masse with a laminar component as a 'simple end-phase movement'	Continuous and incremental throughout the passage of the flow
TIMING OF WELDING AND NON-PARTICULATE DEFORMATION	Post depositional welding compaction occurs AFTER deposition of the entire unit. Secondary mass flowage follows welding	Welding and non-particulate flow occurs during the FINAL stages of emplacement	Welding and non-particulate flow occurs THROUGHOUT the entire depositional history, and after deposition has ceased

Table 7.1. Comparison of the major aspects of the three models of ignimbrite emplacement, further details are given in the text.

7.6 EVIDENCE FOR PROGRESSIVE AGGRADATION OF TL

This section describes individual textural features in TL and then critically evaluates them in light of the three models of high grade ignimbrite emplacement to produce a model of deposition for TL:

- 1) en masse deposition followed by static welding, followed by secondary mass flowage,
- 2) laminar viscous flowage with agglutination occurring during final deceleration of a single-pulse, dense pyroclastic flow, and,
- 3) progressive aggradation with simultaneous particulate to non-particulate flow transition

Chemical and textural stratification

Compound cooling unit TL consists of two flow units, TL1 and TL2. Although TL1 and TL2 are chemically and texturally stratified (Fig. 2.2), internally they contain no definable flow unit boundaries. The boundaries between the chemically and texturally discrete layers, are gradational over 10's of cm's (Fig. 2.3). There are no features between the layers, such as fall-out deposits or surge deposits, sediments or soil and no erosional surfaces that would suggest a time interval before the deposition of a subsequent pyroclastic flow. Thus there is no evidence that shows that the chemical and textural layers within TL1 and TL2 are the deposits of small successive pyroclastic flows.

TL1 is locally bedded (Fig. 7.5) and shows both normal and inverse-graded layers. Figure 7.5 is a local section of TL1 that consists of three texturally discrete layers. The lower two layers are 2m and 68cm thick respectively, and show normal coarse-tail grading (Fig. 7.5). Fiamme size ranges from 3.5:0.8cm to 1:0.6cm for layer 1, and 2.5:1cm to 1:0.2cm for layer 2. Overlying these are two very thin (2.8 and 4cm respectively) inverse-graded layers. These are very fine grained and have an average fiamme size of 0.4:0.2cm. On top these is a layer (28cm thick) which has a fine grained base and top, grading into a more coarse central region. The profile is topped by coarse grained lithofacies T5W (Section 2.5.3).

The two coarsening upwards layers relate to the inversely graded layer 2a, of Sparks (1976). However, unlike layer 2a, which is widespread and characterises the base of flow units, this bedding is extremely localised (traceable in either direction for <8m) and passes laterally into massive ignimbrite (subfacies M4Fx).

TL2 has an even more complicated chemical and textural stratigraphy and consists of locally developed, interstratified lenses and layers of contrasting texture and composition, up to 5m thick and <20m in length (Fig. 7.6) which grade laterally into massive ignimbrite. The chemical stratigraphy commonly is gradational and not restricted to abrupt textural changes.

Evaluation

The features:

- 1) gradational chemical stratification,
- 2) rapid lateral and vertical facies changes, and
- 3) locally developed impersistent normal and inverse-graded bedding,

are not consistent with a model of *en masse* deposition (which would invoke the stacking of multiple flow units to account for the chemical and textural changes) for the following reasons:

1. The vertical and lateral chemical and textural changes do not correspond to unequivocal flow unit boundaries.

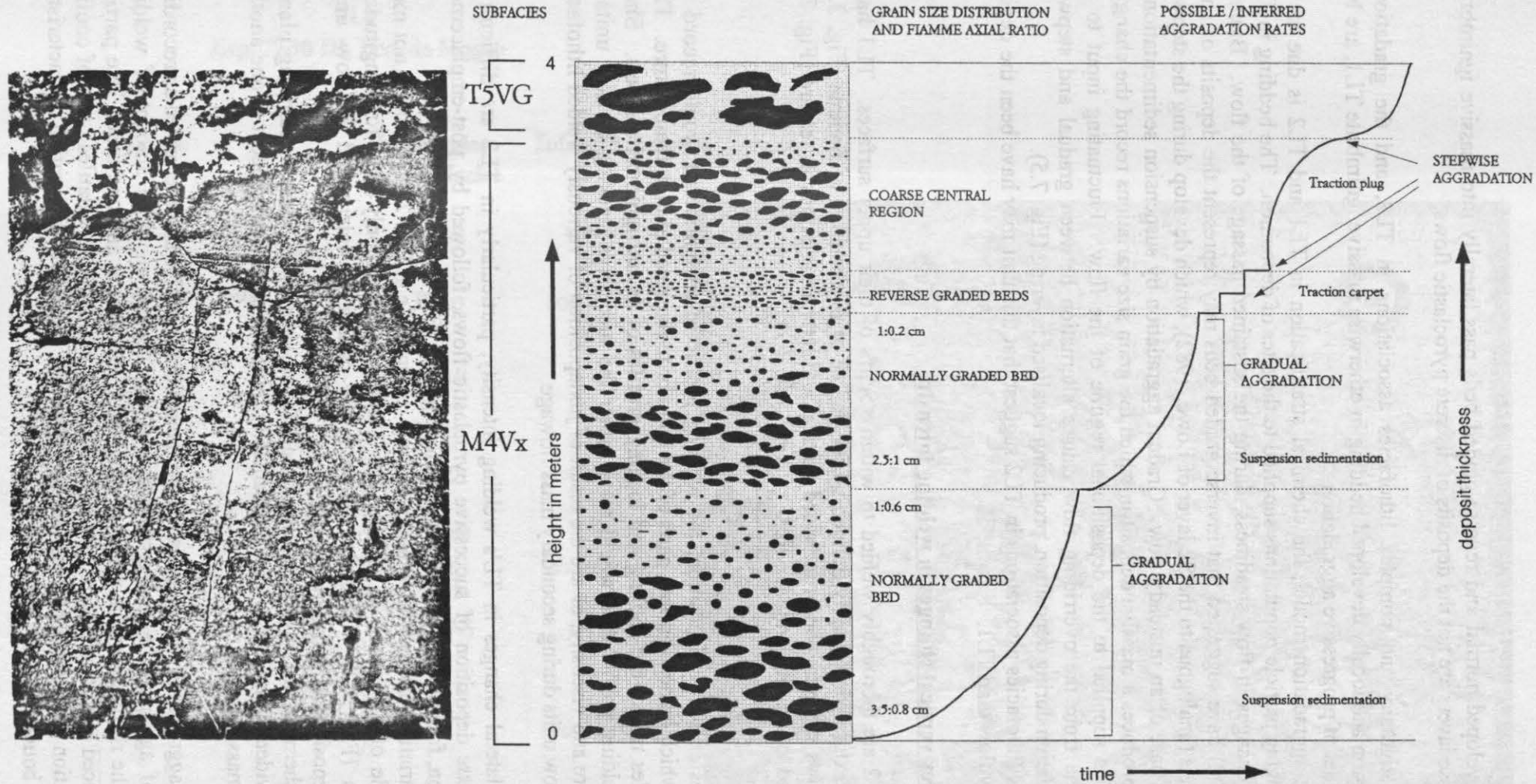


Figure 7.5. Localised sedimentary stratification (traceable laterally for 5-8 m) developed within a single lithofacies (M4Fx) in TL1. The changing grain size with height is interpreted as reflecting the changing size of the particle population supplied to the site of deposition over time. The two reverse graded layers are interpreted as being the deposits of short-lived traction carpets produced during stepwise aggradation during unsteady flow (see text for discussion). Possible aggradation rates, based on the textural and bedding features observed, are shown on the right. Exp. 89, Bco. de Mogán.

2. The locally developed normal and reverse graded beds pass laterally into massive ignimbrite, suggesting that these layers are not the deposits of discrete pyroclastic flows.

The chemical stratigraphy and complex lithofacies associations in TL2, and the gradational chemical stratification and locally developed bedding in otherwise massive ignimbrite TL1, are best explained by a model of progressive aggradation.

In the progressive aggradation model, the chemical stratification in TL1 and TL2 is due to the progressively changing particle populations supplied to the sites of deposition. The bedding in TL1 developed due to changes in flow steadiness, during the sustained passage of the flow. Branney and Kokelaar (1992) have suggested that inverse graded beds may represent the deposits of short lived traction carpets (analogous to the S2 layer of Lowe, 1982), which develop during the stepwise aggradation at the base of an unsteady flow. Gradual aggradation by suspension sedimentation of individual grains produces a massive deposit in which the grain size variations record the changing size of the particles supplied to the depositional regime of the flow. Fluctuating input to the depositional regime from the overriding flow causes alternation between gradual and stepwise progressive aggradation during deposition, producing localised layering (Fig. 7.5).

The more complex lithofacies associations in TL2 suggest that this unit may have been the deposit of a more unsteady flow than TL1.

Rapid and complex vertical changes in welding intensity

Both TL1 and TL2 are thoroughly welded to within <5cm's of their upper surfaces. TL1 has a relatively simple textural stratigraphy defined by the degree of deformation of fiamme (Fig. 3.4). TL2 however, shows complex and pronounced vertical and lateral variations in texture (Fig. 7.6) from poorly welded to eutaxitic and lava-like.

Evaluation

With instantaneous *en masse* deposition, the welding profile of an ignimbrite would record the length of time at which loaded (buried) parts of the ignimbrite remained at high temperature. Thus the welding profiles reflect the cooling and loading profiles of *in situ* ignimbrite sheets. Sharp changes in the welding profile thus would mean either the successive stacking of flow units of varying temperature and viscosity, or are the result of juxtaposition of variously welded lithofacies from successive flow units during secondary mass flowage.

The vertical and lateral changes in TL's welding intensity, particularly in TL2 are difficult to explain by *en masse* deposition of successive pyroclastic flows, followed by post-emplacment welding compaction, followed by secondary mass flowage (e.g. Fig. 7.4A) because:

1. The textural variations are not traceable over great distances (e.g. Fig. 2.27), usually not more than from one side of a barranco to another (ca. 1-2km) and commonly only for longitudinal sections of <3km (Fig. 7.7). Therefore these layers cannot be interpreted as flow units, representing the deposit of an entire pyroclastic flow.
2. Many of the chemical and textural changes are not associated with shear or ramping planes. Thus there is no evidence that layers were mechanically mixed or emplaced adjacent to one another during secondary mass flowage.

In the progressive aggradation model, variations in the welding profiles are interpreted as recording varying degrees of agglutination and coalescence *during* deposition. The amount of welding therefore reflects the rheology of the particles supplied to the flow at any one time. The particle rheology is influenced by strain rate, temperature, composition (including volatiles), rate of cooling and volatile exsolution during transport, as well as the particle size and concentration characteristics in the depositional boundary layer (Fig. 7.4C).

WELDING PROFILE
TL2
Exp. 77-90 III, Bco. de Mogán

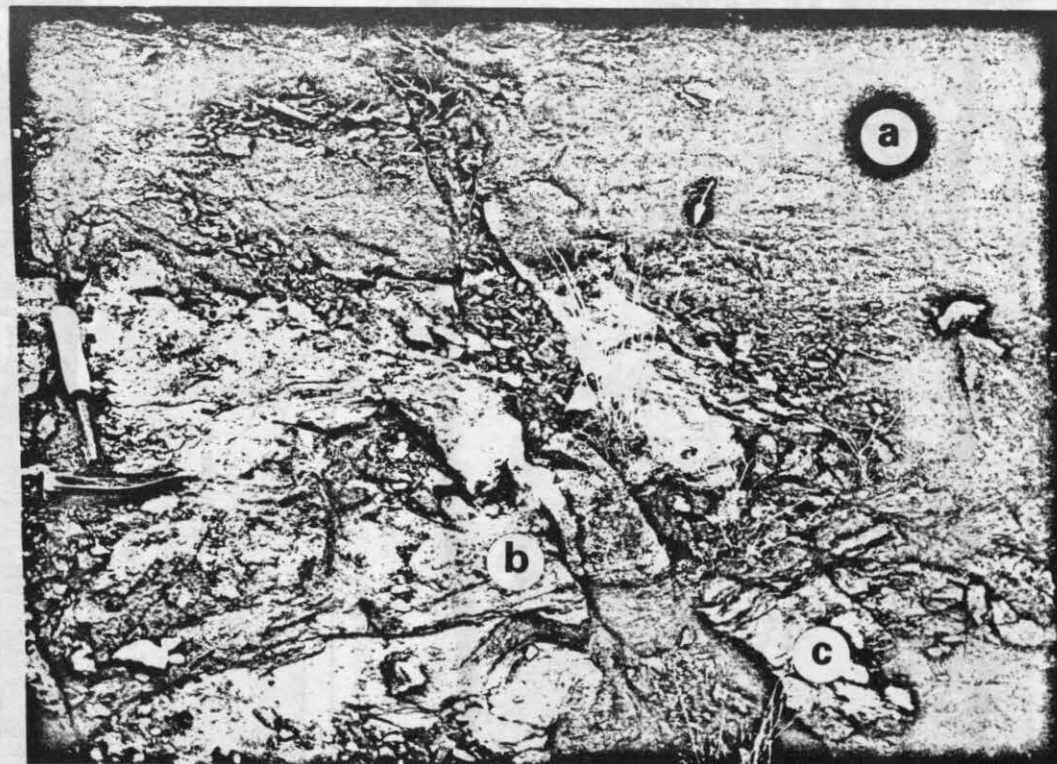
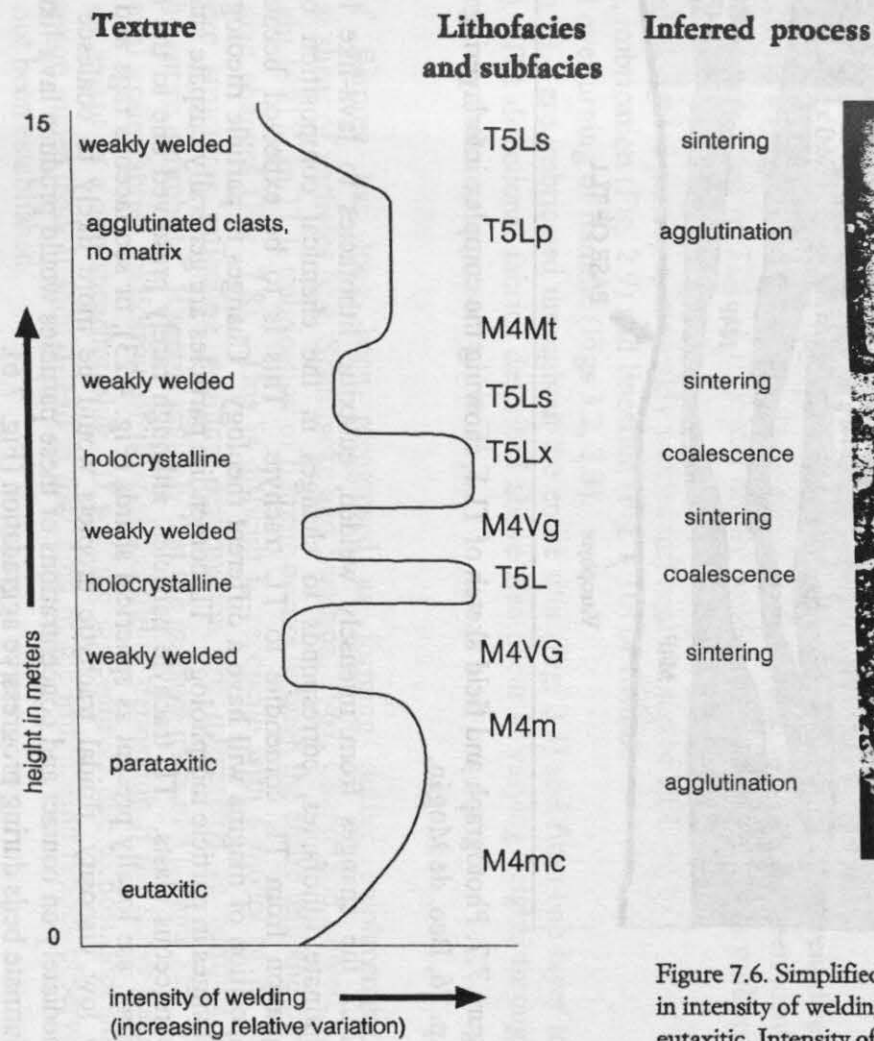


Figure 7.6. Simplified welding profile and photograph, showing the complex and irregular vertical and lateral changes in intensity of welding in TL2. Texture varies between; a. holocrystalline and lava-like, b. poorly welded, and c. eutaxitic. Intensity of welding has been estimated by the degree of plastic deformation of shards and by the percentage of particle outlines preserved.

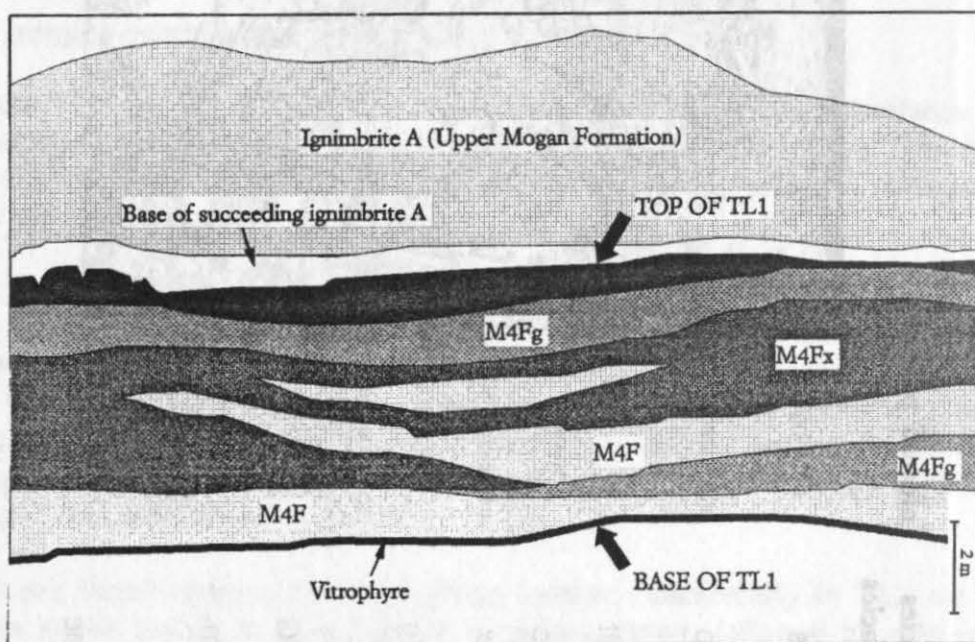
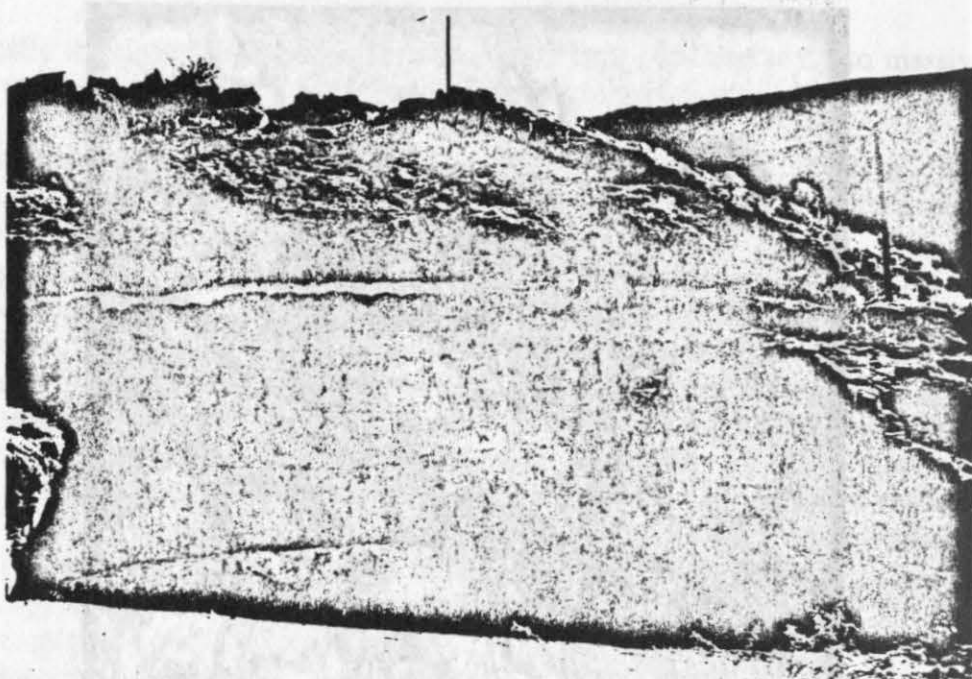
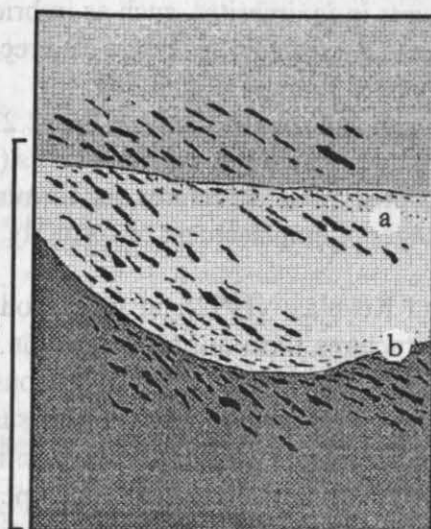
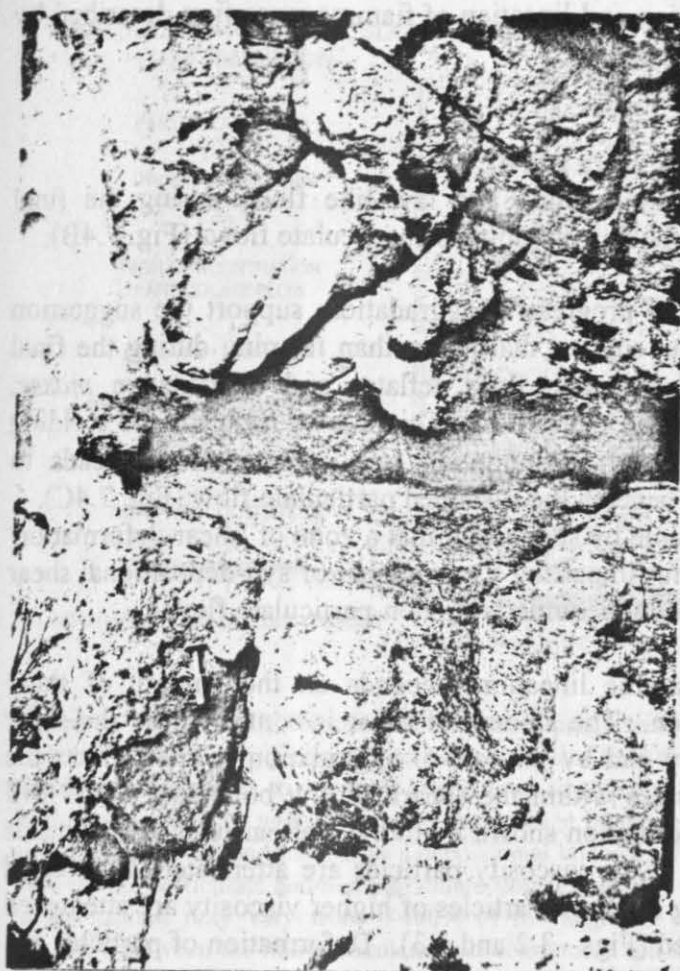


Figure 7.7. Photograph and field sketch of TL1, showing the complex interlayering of lithofacies. Exp. 76, Bco. de Mogán.

In TL2 the changes from intensely welded, eutaxitic lithofacies to lava-like lithofacies and agglutinate lithofacies, corresponds to changes in the chemical composition of the particle population from TL comendite to TL trachyte. This is to be expected because a different composition of magma will have a different rheology. Changes in particle rheology are reflected by changes in particle morphology. TL comendite particles are generally cusped shards (Fig. 4.21) or pumiceous clasts. TL trachyte particles, although rarely preserved due to the high degree of welding, are locally present as spherical shards (Fig. 4.23), or scoriaceous rags and ribbons. Hot, very low viscosity, fluidal trachytic droplets would be more likely to coalesce or agglutinate immediately on contact and concentrations of these particles would produce lava-like lithofacies or agglutinate beds during progressive aggradation (Fig. 7.6).



a. Continuous imbrication of fiamme persists across layers and through grain size changes

b. Locally developed planar contacts within massive ignimbrite

Figure 7.8. Imbrication of fiamme throughout sedimentary stratification developed within lithofacies M4F of TL1. This is best interpreted as recording imbrication during progressive aggradation, and is difficult to explain by instant *en masse* deposition of three separate flows. See text for discussion. Exp. 79, Bco. de Taurito.

Directional fabrics

Both TL1 and TL2 contain directional fabrics which have been used to infer palaeocurrent direction of the pyroclastic flow (Figs 3.11 and 3.12). Three types of directional fabrics have been identified and these are best preserved in TL1 as it is less highly welded as TL2 and particle outlines are easily identifiable:

- 1) Alignment of elongated particles, in weakly welded tuff near the top of TL1.
- 2) Attenuation, imbrication (Fig. 2.9) and lineation (Fig. 3.10) of fiamme.
- 3) Folding and overturning of fiamme (Figs 3.2, 3.3).

The fiamme in TL1 are imbricated throughout the entire unit (Fig. 2.3) and from one layer to the next (Fig. 7.8). The directional fabrics described above also occur at varying heights throughout TL1, and more rarely (where are preserved) in TL2.

Evaluation

Imbrication of fiamme has long been recognised as forming during emplacement by syn-depositional shear of particles (e.g. Schmincke and Swanson, 1967; Chapin and Lowell, 1979; Wolff and Wright 1981). In TL1, imbrication of fiamme occurs through the entire unit and persists through grain size changes (Fig. 7.8). This is difficult to reconcile with a model of *en masse* deposition where structures reflecting welding deformation are interpreted as forming *after* deposition of the entire ignimbrite. It seems unlikely that the massive parts of TL1 and TL2 would contain directional grain fabrics, indicative of flow at the site of deposition if the flows travelled and deposited *en masse* as a non shearing plug. If welding was entirely due to post-depositional welding compaction under load, it should lead to flattening of the imbrication fabrics observed in TL, which has not been established.

Flow structures in ignimbrites, such as imbrication and lineation of fiamme were first described by Schmincke and Swanson (1967) who also recognised:

- 1) Stretched fiamme (Fig. 3.10).
- 2) Broken and rotated fiamme (Fig. 2.23).
- 3) Hollows around rotated lithic clasts (Fig. 2.11a and b).

They interpreted these structures as forming by welding and lava-like flow, during the final (laminar) stages of emplacement of formerly turbulent, single-pulse particulate flows (Fig. 7.4B).

Branney and Kokelaar (1992), in their model of progressive aggradation, support the suggestion that these structures form during deposition, but suggest that rather than forming during the final stages of emplacement as a homogeneous particulate flow deflates and deposits *en masse*, agglutination occurs continuously during sustained deposition. This allows time for the welding deformation to occur. Sustained deposition and agglutination of viscous particles leads to formation of a non-particulate flow component beneath the sustained particulate flow (Fig. 7.4C).

The authors account for the imbrication of fiamme by suggesting that a zone of 'shear deformation' passes upwards with the aggrading surface. Thus imparting a component of syn-depositional shear to viscous particles as they become incorporated in the underlying non-particulate flow.

The intensity of a directional fabric, e.g. fiamme lineation, depends on the amount of shear imparted on the particles during their deposition. The amount of shear is controlled by the shear gradient within the depositional flow boundary and by the rate of aggradation, which effects the length of time any population of particles resides within the shearing flow boundary. This will change during unsteady flow. The type of deformation shown by individual particles also depends upon the particle viscosity during deposition. Low viscosity particles are attenuated, imbricated and lineated as they pass through the aggrading surface. Particles of higher viscosity are attenuated and fractured (Fig. 2.23) or folded and fractured (Figs. 3.2 and 3.3). Deformation of particles and agglutinate may continue after aggradation has ceased.

7.7 TEXTURAL EVIDENCE OF A PARTICULATE TO NON-PARTICULATE FLOW TRANSITION IN TL2

TL displays textures and features which have been considered diagnostic of lavas:

- 1) Basal autobreccia (Fig. 2.37).
- 2) Extensive upper autobreccia (Fig. 2.27).
- 3) Steep distal margin and marginal autobreccia (Fig. 2.37).
- 4) Locally holocrystalline trachytic texture (Fig. 4.26).

There are two possible methods of generating these lava-like lithofacies:

1. In a model of *en masse* deposition, hot, viscous particles weld following deposition of the entire sheet, under the influence of the deposits cooling rate and load pressure. The agglutinated deposit then remobilises and undergoes secondary mass flowage (rheomorphism; *sensu* Wolff and Wright, 1981). During welding and secondary mass flowage, the particle outlines become completely obliterated, producing lava-like layers. This theory however, does not account for the pronounced vertical and lateral changes between poorly welded and lava-like textures in TL2, because secondary mass flow would effect much larger packages of material. Also, many of the changes in intensity of welding would be associated with folds, shear or ramping planes and other structures formed during secondary mass flowage, this is not the case in TL2.

2. Branney and Kokelaar (1992), and Mahood (1984) suggested that if particles are sufficiently hot and fluidal they can agglutinate on contact.

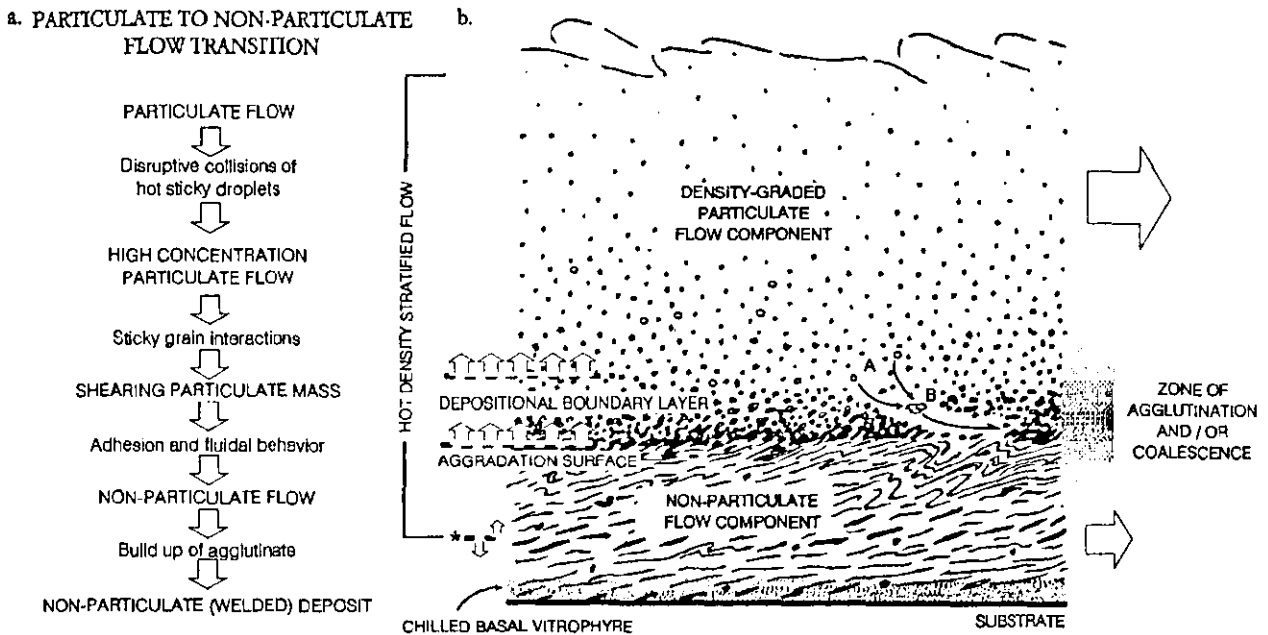


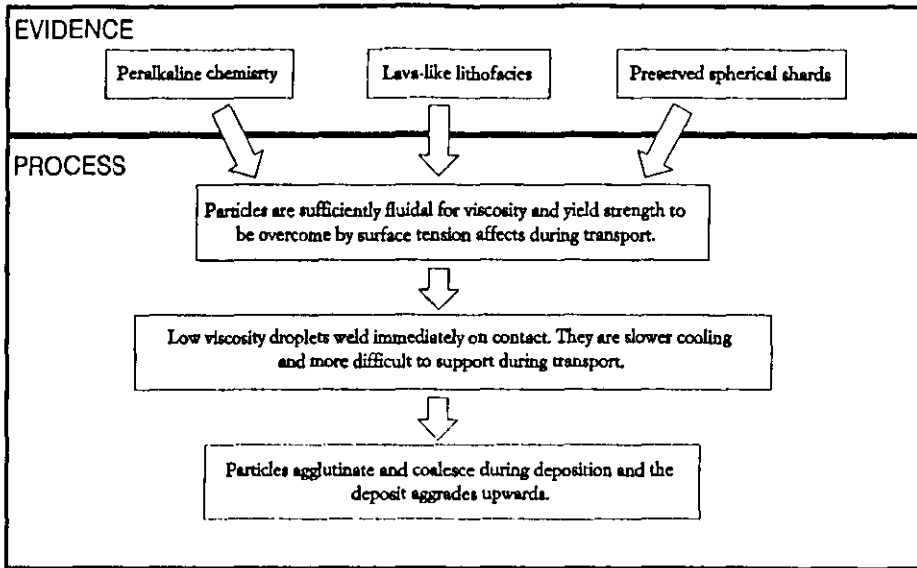
Figure 7.9. A schematic cross section showing progressive aggradation of high grade ignimbrite (Branney and Kokelaar, 1992). a. A particulate to non-particulate flow transition occurs as disruptive collisions of hot, sticky droplets give way, via sticky grain interactions, to adhesion and fluidal behavior, thus a non-particulate layer of agglutinate gradually aggrades during the passage of the flow. b. Hot, viscous particles (A) agglutinate and/or coalesce (B) within and just below a depositional boundary layer that migrates progressively upwards to a position between the particulate and non-particulate flow component. The thickness of the non-particulate flow component at any instant may vary from 0-100% of the aggraded non-particulate material. The asterisk indicates the boundary between the non-particulate flow component and the underlying stationary tuff at an instant in time, its vertical position varies with time

The model of Branney and Kokelaar involves a *particulate to non-particulate* transition which occurs in and just beneath a depositional boundary layer (Fig. 7.9). The particulate to non-particulate transition occurs where disruptive collisions of hot sticky droplets give way, via sticky grain interactions, to adhesion. Agglutination and coalescence of particles leads the development of a non-particulate flow component, which exhibits fluidal behaviour. During the initial incursion of the flow, agglutinate chills and freezes against the ground. However during sustained passage of the flow, as agglutination continues, the non-particulate layer thickens (aggrades) and becomes mobile, thus promoting lava-like flow.

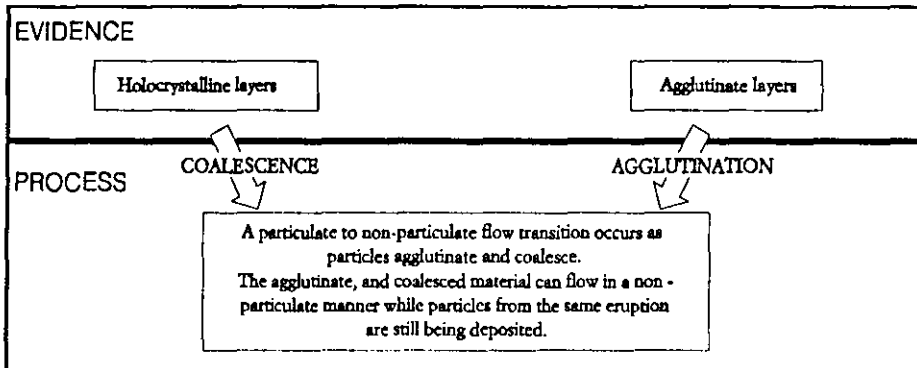
Four lines of evidence suggest that the particles in TL2 were hot, low viscosity droplets which were sufficiently fluidal to weld immediately on contact, rather than under the influence of post-emplacement cooling and loading:

- 1) The peralkaline chemistry of TL together with high eruptive temperatures, high volatile contents and an associated low eruption column combined to produce hot, low viscosity particles (Fig. 5.11).
- 2) The presence of preserved globular shards in TL2 (Fig. 4.23), indicates that the particles were sufficiently fluidal for viscosity and yield strength to be overcome by surface tension effects during transport. Less fluidal particles would retain angular shapes.
- 3) Occurrence of lava-like lithofacies in which remnant particle outlines are absent, indicates complete homogenisation to a coherent liquid.
- 4) Spherical post-welding vesicles indicate surface tension effects dominated over yield strength even after welding and rheomorphism.

1. AGGLUTINATION AND COALESCENCE OF FLUIDAL DROPLETS



2. PARTICULATE TO NON-PARTICULATE FLOW TRANSITION



3. NON-PARTICULATE FLOW

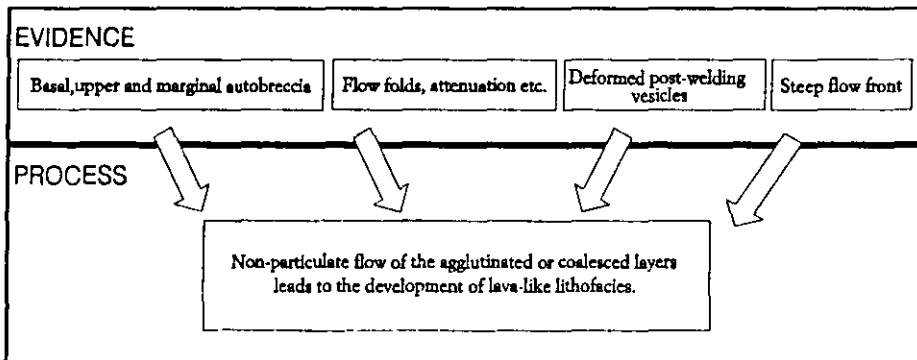


Figure 7.10. Evidence for agglutination and coalescence of particles and a particulate to non-particulate flow transition, leading to the development of lava-like lithofacies in TL2.

Similar globular particles occur in many high grade ignimbrites, e.g. Menegai, Kenya (Schmincke, 1972; Leat, 1985), Mt. Suswa, Kenya (Schmincke, 1974 b; Hay et al., 1979), Pantelleria and Gran Canaria (Schmincke, 1969 a, 1974 b), and in rhyolitic sheets interpreted as high temperature lava flows (Bonnichsen, 1982). Droplet-shaped particles have not been observed in low grade silicic tuffs or viscous obsidian lavas, however they do characterise Hawaiian magmatic fountaining (MacDonald, 1972), where they have been called 'achneliths' (Walker and Croasdale, 1972). Globular particles thus suggest rheologies more similar to typical basalt fountains, rather than those typical of lower grade silicic ignimbrites and lava flows.

The droplet shape of the particles in TL2 would enhance rapid agglutination or coalescence because the droplets are both slower to cool, as they have a minimum surface to volume ratio, and are more difficult to support during transport, due to larger settling velocity (Branney and Kokelaar, 1992). These hot, low viscosity particles would agglutinate and coalesce quickly and begin to flow in a non-particulate manner, while pyroclasts from the TL2 eruption were still being deposited.

There is evidence for both agglutination and coalescence in TL2. In layers of agglutinate (e.g. Exp. 114, Anden Verde; Exp. 113, Bco. de Mogán; Appendix I), the original particle outlines can still be identified. Holocrystalline layers (e.g. Exp. 96, Bco. de Mogán; Exp. 95 II, Bco. de Taurito) with trachytic texture, are interpreted to have formed by complete coalescence of fluidal droplets, such that particle outlines are completely obliterated, and crystal growth can occur in the resultant fluid.

The development of a steep distal margin, and marginal, upper and basal autobreccia, indicates that extensive non-particulate flow of agglutinate and coalesced material occurred. This sequence of events is summarised in Figure 7.10.

7.8 SUMMARY AND CONCLUSIONS

A model of virtually instantaneous *en masse* deposition of an entire ignimbrite sheet, followed by post depositional welding compaction (Section 1.5) cannot account for the chemical and textural changes observed in TL for the following reasons:

- 1) Chemical and textural stratigraphy is gradational, there is not a clear, unambiguous "flow unit boundary" (Section 1.5) where the chemistry changes. The sharp boundaries and reverses graded beds which do occur are *local* phenomenon which pass laterally into massive beds. Even if they were laterally continuous, this could equally reflect unsteadiness in the flow. Unsteadiness initiated at source (vent) would give a widespread change in texture or chemistry, whereas local unsteadiness, due to local topographical effects (e.g. turbulent eddies), would give a localised change in texture or chemistry.
- 2) Directional fabrics indicative of flow at the site of deposition occur *throughout* the thickness of TL1, suggesting that the whole unit cannot have been deposited *en masse* as a non-shearing plug with a basal shear zone.
- 3) Welding profiles, especially in TL2 are extremely irregular; suggesting that the temperature of clasts on deposition was variable. This resulted in varying degrees of sintering and agglutination of clasts *during* deposition. If deformation of clasts occurred by post depositional static welding of the entire deposit, the central portions of the flow which remained hottest longest, would display the highest degree of welding. This type of simple welding profile (cf. Ragan and Sheridan, 1972) is not observed in TL2.

DEPOSITION OF TL1- HIGH GRADE RHEOMORPHIC IGNIMBRITE

1. Rapid but sustained suspension sedimentation from a finite but, predominantly steady particulate flow produces massive ignimbrite.
2. Localized flow unsteadiness causes development of short-lived traction carpets, which produce thin inverse graded beds.
3. The particle population supplied to the depositional regime, by the overriding transport regime, changes gradually with time, producing a gradational chemical stratification from TL comendite to TL trachyte. More abrupt changes produce sharper boundaries.
4. Syn-depositional deformation of particles occurs: Low viscosity particles are agglutinated and attenuated, imbricated and folded. Higher viscosity particles are folded and fractured.
5. Limited non-particulate flow causes further attenuation and folding of sintered and agglutinated particles, but particle outlines are retained.

DEPOSITION OF TL2- EXTREMELY HIGH GRADE LAVA-LIKE IGNIMBRITE

1. Rapid suspension sedimentation takes place from an unsteady sustained flow.
2. Particle chemistry and viscosity changes rapidly with time at individual localities producing complex vertical and lateral facies associations and a highly irregular welding profile.
3. Hot, low viscosity particles agglutinate and coalesce immediately on contact, particle outlines are obliterated, producing lava-like lithofacies.
4. A particulate to non-particulate flow transition occurs continuously as the non-particulate flow component aggrades.
5. Extensive non-particulate flow leads to the development of lava-like lithofacies and autobreccias.

Figure 7.11. Summary of the suggested depositional mechanisms of TL1 and TL2.

4) Magmas of peralkaline chemistry are known to produce low viscosity particles (Mahood, 1984; Schmincke, 1974b), which would be more likely to weld rapidly (agglutinate or coalesce) *during* deposition, rather than by only post-depositional welding compaction under the influence of a deposits in-situ cooling rate and load pressure. Preserved globular shards in TL2 indicate the low viscosity of particles, although in this case their shape was preserved by cooling during transport.

The directional fabrics throughout TL1, the evidence for fluidal droplets in the form of preserved globular shards in TL2, and the occurrence of agglutinate and holocrystalline lava-like lithofacies in TL2, suggest that onset of deformation and welding of particles in TL was *syn-depositional*. Particles began agglutination and coalescence on impact and were deformed during deposition, as well as after deposition. The compositional and textural changes observed in both flow unit TL1 and TL2 can best be explained by *progressive aggradation*. The deposition and welding of the particles was sustained and incremental throughout the passage of two separate pyroclastic flows, one aggrading TL1 and one aggrading TL2. The pronounced textural variations in TL2 compared to TL1 suggest that flow that produced TL2 was more unsteady than the one that formed TL1.

The composition and degree of welding ultimately relates to *temporal* changes in the composition, viscosity and temperature of the particle population supplied at source. The higher grade of TL2 is interpreted as being the result of the supply of a larger volume of hotter, lower viscosity, comenditic trachyte particles to this flow, compared to the flow depositing TL1.

The proposed depositional sequences of TL1 and TL2 are summarised in figure 7.11.

SECTION II

POST-AGGLUTINATION DEFORMATION

7.9 AGGLUTINATE STABILITY AND VISCOSITY

This section focuses on the post-depositional deformation of TL. The best evidence of post-depositional deformation is in TL2.

TL2 is an 'extremely high grade' ignimbrite that displays several characteristics which have previously been considered as diagnostic of lavas (Section 7.6). These features are here interpreted as having formed during the continued non-particulate deformation of agglutinated and coalesced material (Fig. 7.10). The large-scale deformation features described in this section effect the whole of TL2 from the base to the upper surface and are therefore interpreted as having occurred after the deposition of the entire unit.

The rapid deposition of TL2 from a sustained flow produced a unit composed of a series of stacked layers of differing density, competency and temperature. This was particularly susceptible to loading, slumping and auto-intrusion. Under extension, features such as extensional fracturing and boudinage were produced. Conversely, under compression, ramp structures and thrusts were formed.

The chemical zonation in TL2 consisting of basal TL comendite, overlain by TL mixed rock, in turn overlain by last erupted TL trachyte produced an unstable reverse density layering. Calculated magmatic densities (Bottinga and Weill 1970), while not an accurate measurement of densities during and after emplacement (because they take no account of porosity and vesicles), indicate initial density differences. Furthermore TL trachyte is much less vesicular than underlying TL



Figure 7.12. Contrasting deformation behaviour of TL trachyte and TL comendite. Lava-like TL trachyte was more competent than TL comendite and has produced pinch and swell structures and boudinage blocks (30cm left of hammer). The hammer is 30cm long. TL2, Exp. 93 II, Bco. de Mogán.

comendite, thus compounding the instability.

There also was an initial temperature stratification within flow units TL1 and TL2. Fe-Ti oxide calculations indicate temperatures of 810-910°C for TL trachyte and 776-811°C for TL comendite. Although these magmatic temperatures may not necessarily directly represent emplacement temperatures (as some cooling likely accompanied particulate transport) they do indicate that there was an initial temperature difference. However, in spite of higher magmatic temperature, deformation structures indicate that TL trachyte was consistently more brittle than TL comendite. In TL1 this can be seen in the deformation of fiamme (e.g. Fig. 3.3) where TL trachyte fiamme are fractured and boudinaged.

This is observed on a large scale in TL2, in

the deformation of individual lithofacies. TL trachyte lithofacies and subfacies e.g. T5Ls and T5Lx are boudinaged and form autobreccia pockets which are surrounded by more plastically deformed TL comendite lithofacies (e.g. Fig. 7.12).

The contrasting competence of TL trachyte and TL comendite is attributed to:

- 1) Larger content of volatiles in TL comendite, which acted to give it lower viscosity even at lower temperatures (Williams and McBirney, 1979; Murase and McBirney, 1970).
- 2) Reheating and remobilisation of TL comendite by adjacent hotter TL trachyte, and slower prolonged cooling of TL comendite lithofacies which were thermally insulated by overlying TL trachyte lithofacies.
- 3) Rapid cooling, by convection, of TL trachyte in the top of the deposit.

Evidence for a higher volatile content in TL comendite during rheomorphism is indicated by a higher proportion of lenticules, in densely welded parts of the tuff, and by the occurrence of highly vesicular pumiceous lenses (e.g. Fig. 3.2f).

Evidence for reheating and remobilisation of TL comendite can be seen in zones of auto intrusion where fluidal TL comendite was injected into surrounding TL trachyte which deformed in a brittle manner (e.g. Fig. 2.35). Heat exchange between adjacent TL trachyte and TL comendite lead to the development of T5Lv subfacies in TL2 (Fig. 2.41). Where TL trachyte and TL comendite were brought into contact during post-depositional deformation (for example by loading, Section 7.10.3) lava-like TL comendite re-vesiculated, producing intensely vesicular zones adjacent to TL trachyte. Vesicles in these zones are slightly deformed and parallel to the margin of the TL trachyte

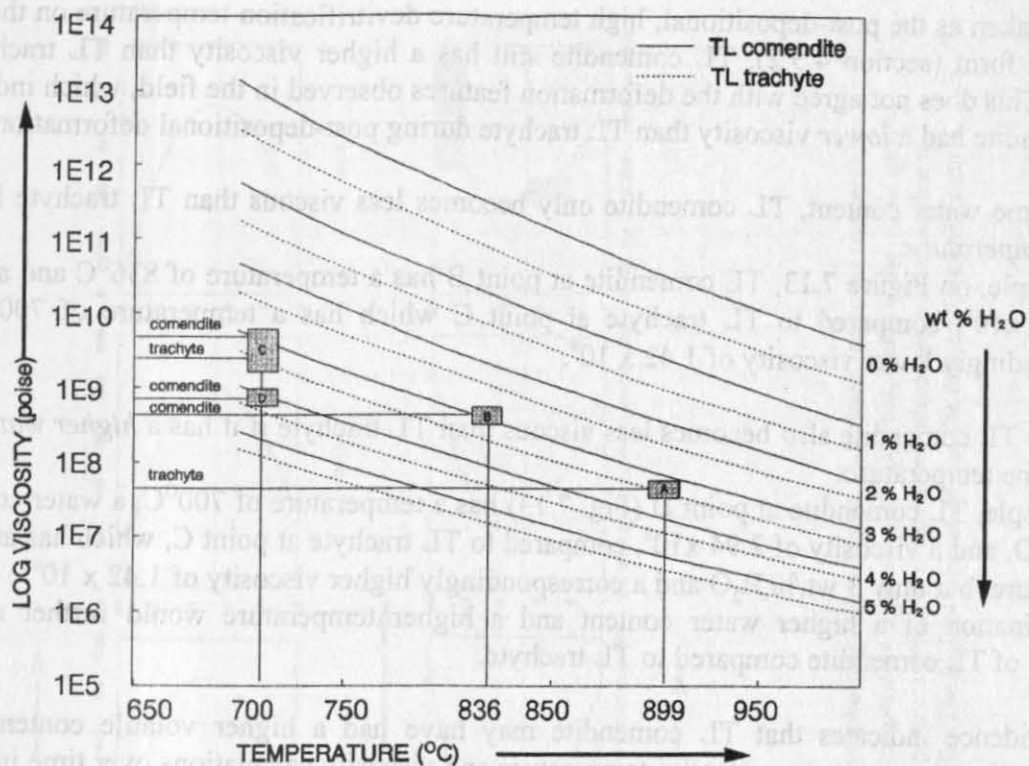


Figure 7.13. Plot of log magmatic viscosity versus temperature, with different water contents for TL comendite and TL trachyte.

A- viscosity of TL trachyte with 3 wt.% water at the calculated magmatic temperature 899 °C = 2.55×10^7 . B- viscosity of TL comendite with 3 wt.% water at the calculated magmatic temperature 836 °C = 3.03×10^8 . C- viscosity of TL comendite = 4.74×10^9 and TL trachyte = 1.42×10^9 with 3 wt.% water at 700 °C, which is taken as the high temperature devitrification temperature on the basis of spherulite form. D- viscosity of TL comendite at 700 °C with a water content of 4 wt.% = 2.94×10^8 . For discussion, see text.

lithofacies (Fig. 2.41) indicating that vesiculation occurred both during and after plastic deformation.

The autobreccia and large boudinage blocks (Fig. 7.17) of TL trachyte lithofacies in the upper zone of TL2 indicate that these lithofacies were cooled and subsequently deformed in a brittle manner.

Viscosity calculations

Fe-Ti oxide temperature calculations (Fig. 4.17) suggest that TL trachyte had a higher magmatic temperature and therefore probably lower viscosity on eruption than TL comendite. Thus, significant viscosity changes must have occurred during transport, deposition and degassing to account for the deformation features observed at outcrop. These viscosity changes are most likely to be related to the effects of cooling, degassing, insulation and thermal transfer.

Figure 7.13 shows a relative comparison of viscosities of TL trachyte and TL comendite, using water as the major volatile. A range of water contents is shown, since it is virtually impossible to calculate the volatile content of TL while it was being deformed, due to degassing before and after deformation. The presence of amphibole as the secondary phenocryst phase in both TL comendite and TL trachyte (Table 4.1) indicates relatively high magmatic water contents, since a minimum of 3 wt.% H₂O is required to stabilise amphibole phases (Naney, 1983).

Using the calculated magmatic temperatures and 3 wt.% H₂O, TL trachyte (Fig. 7.13A) is always less viscous than cooler TL comendite (Fig. 7.13B). If the same temperature is used i.e. 700 °C, which is taken as the post-depositional, high temperature devitrification temperature on the basis of

which is taken as the post-depositional, high temperature devitrification temperature on the basis of spherulite form (section 4.5.2), TL comendite still has a higher viscosity than TL trachyte (Fig. 7.13C). This does not agree with the deformation features observed in the field, which indicate that TL comendite had a *lower* viscosity than TL trachyte during post-depositional deformation.

At the same water content, TL comendite only becomes less viscous than TL trachyte if it has a *higher temperature*:

For example, on Figure 7.13, TL comendite at point B has a temperature of 836°C and a viscosity of 13.03×10^8 , compared to TL trachyte at point C which has a temperature of 700°C and a correspondingly lower viscosity of 1.42×10^9 .

Similarly TL comendite also becomes less viscous than TL trachyte if it has a *higher water content* at the same temperature:

For example, TL comendite at point D (Fig. 7.13) has a temperature of 700°C, a water content of 4 wt.% H₂O, and a viscosity of 2.94×10^8 , compared to TL trachyte at point C, which has an identical temperature, but only 3 wt.% H₂O and a correspondingly higher viscosity of 1.42×10^9 .

A combination of a higher water content and a higher temperature would further reduce the viscosity of TL comendite compared to TL trachyte.

Field evidence indicates that TL comendite may have had a higher volatile content than TL trachyte. However more importantly, temperature and viscosity calculations over time indicate that the temperature profile through the unit was not uniform during cooling.

Figure 7.14 shows a simple model of the changing temperature and viscosity profiles for TL over a period of 8 days, following deposition. The chemical stratification of the unit has been simplified to include TL comendite at the base and TL trachyte at the top. Initial magmatic temperatures with corresponding viscosities (Appendix II) have been used to produce the initial temperature and viscosity profiles. The effect of cooling has been extrapolated using the BASIC program NEWDIFF6 (Dehn, 1993; Appendix II).

This program calculates only the *maximum* cooling effect, since the thermal diffusivity was estimated using the specific heat conductivity constant of single crystal silicon ceramic as the maximum and the specific heat conductivity constant of vitreous silica as the minimum. The average value used is not the actual thermal diffusivity of TL comendite and TL trachyte. The program also does not include the effect of latent heat of crystallisation, however this does not effect the relative relationships between TL comendite and TL trachyte.

Figure 7.14 clearly shows the inverse relationship between viscosity and temperature. The curves for temperature and viscosity are progressively smoothed with time, due to the effects of cooling at (1) the basal parts of the deposit against the ground and (2) the upper surface of the deposit by convection to the surrounding air. In the central portion of the unit the temperature falls from 899°C (maximum temperature for TL trachyte) to only 750°C after 8 days of cooling, clearly demonstrating that in comparison to low grade ignimbrites TL remained at high temperatures post emplacement. This is an important consideration for both high temperature devitrification (Section 4.5.2) and the formation of high temperature magmatic closed-system vapour phase minerals (Section 4.6).

The significance of cooling for the deformation structures observed in TL is shown in the changing viscosity profiles related to temperature. The central portion of the unit remained hottest longest and correspondingly has the lowest viscosity for longest. This is especially important in TL because TL trachyte in the central portion of the unit (Fig. 7.14A) maintains the lowest viscosity

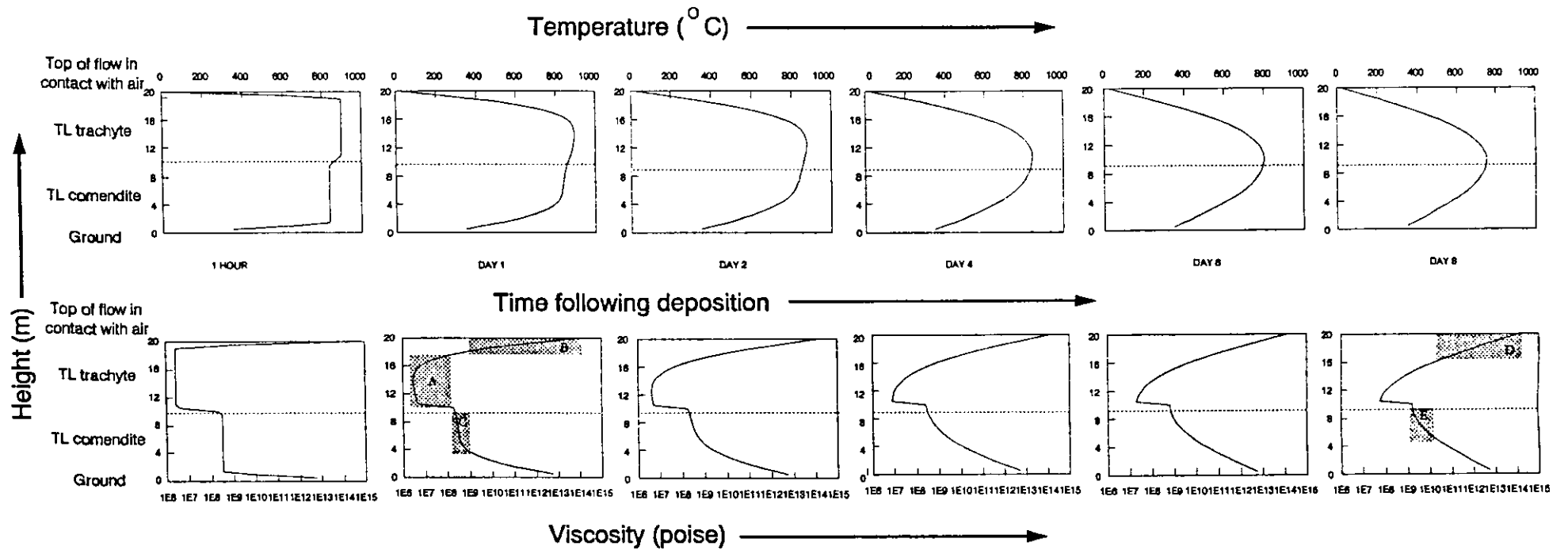


Figure 7.14. A model of changing temperature and viscosity profiles for TL during a period of 8 days following emplacement. Calculated magmatic temperatures for TL comendite and TL trachyte have been used to calculate the initial viscosity profile. Ground temperature is taken as 350 degrees, which is the stable ground temperature 5 hours after emplacement. Air temperature remains constant at 20 degrees. The temperature profile is progressively smoothed over time, due to cooling effects at the top and base of the unit. There is a corresponding change in the viscosity profile. The highest temperature and the related lowest viscosity is maintained in the central portion of the unit. Details of the shaded areas A-E are given in the text.

throughout cooling, however, TL trachyte in the upper portion of the deposit cools significantly. After only one day, the top 2 m of TL trachyte (Fig. 7.14B) has a *higher* viscosity than TL comendite in the central portion of the unit (Fig. 7.14C). After 8 days this increases to a thickness of 4 m of TL trachyte (Fig. 7.14D) which has a higher viscosity than TL comendite (Fig. 7.14E). The preferential cooling of TL trachyte on the upper surface, together with the comparative insulation of TL comendite in the central portion of the unit caused the TL trachyte lithofacies at the top of the deposit to deform in a brittle manner during loading and slumping. The less viscous TL comendite deformed less competently as it flowed around boudinage blocks and autobreccia.

Drawbacks with the model

Since this model considers only Newtonian viscosity it takes no account of the abundant vesicles, remnant shard margins and groundmass crystallites known to be abundant in many lithofacies. It does not include the effect of cooling during progressive aggradation and due to degassing, or viscosity increase due to volatile exsolution. Note that agglutinate competence is also dependent on yield strength, as the agglutinates were not Newtonian. The yield strength and the effect of porosity (both initial, matrix and vesicles) on diffusivity are not included.

Summary

There is change in deformation behaviour from agglutination and coalescence of TL trachyte particles during syn-depositional deformation, to brittle high viscosity behaviour of TL trachyte lithofacies during post-depositional deformation. This is consistent with a corresponding relative decrease in the viscosity of TL comendite during post-depositional deformation. These changes in the deformation behaviour are interpreted to be the result of:

- (1) preferential cooling and degassing of TL trachyte in the top portion of the flow and
- (2) insulation of TL comendite, coupled with reheating by heat transfer from TL trachyte and possibly also retention of dissolved volatiles in TL comendite due to overlying impermeable TL trachyte.

7.10 POST-DEPOSITIONAL DEFORMATION OF TL2

The deformation structures and resultant lithofacies associations in TL2 are complex (for example Fig. 2.27). In the simplest case, on near horizontal surfaces, the post-depositional deformation of TL2 is predominantly density and gravity driven and field relationships indicate that processes such as lateral spreading, slumping, brecciation and loading occurred.

7.10.1 Lateral spreading and slumping: the effect of competency contrasts

Lateral spreading (Varnes, 1978) or the slumping of unstable, inadequately supported agglutinate on horizontal surfaces, resulted in the disruption of the textural and chemical stratigraphy in TL2. In profiles that show marked variations in the intensity of welding, the competency of individual layers effects the type of deformation structures produced.

The competency of individual layers is the result of :

- 1) Initial composition and related viscosity, volatile content and temperature of particles.
- 2) The degree of welding, related to emplacement temperature and viscosity of particles during deposition.
- 3) The rate of cooling and volatile exsolution.

Figure 7.15 shows two vertical sections through TL2, (a) shows the pre- non-particulate deformation stratigraphy, which has been reconstructed from less strongly deformed sections (e.g.

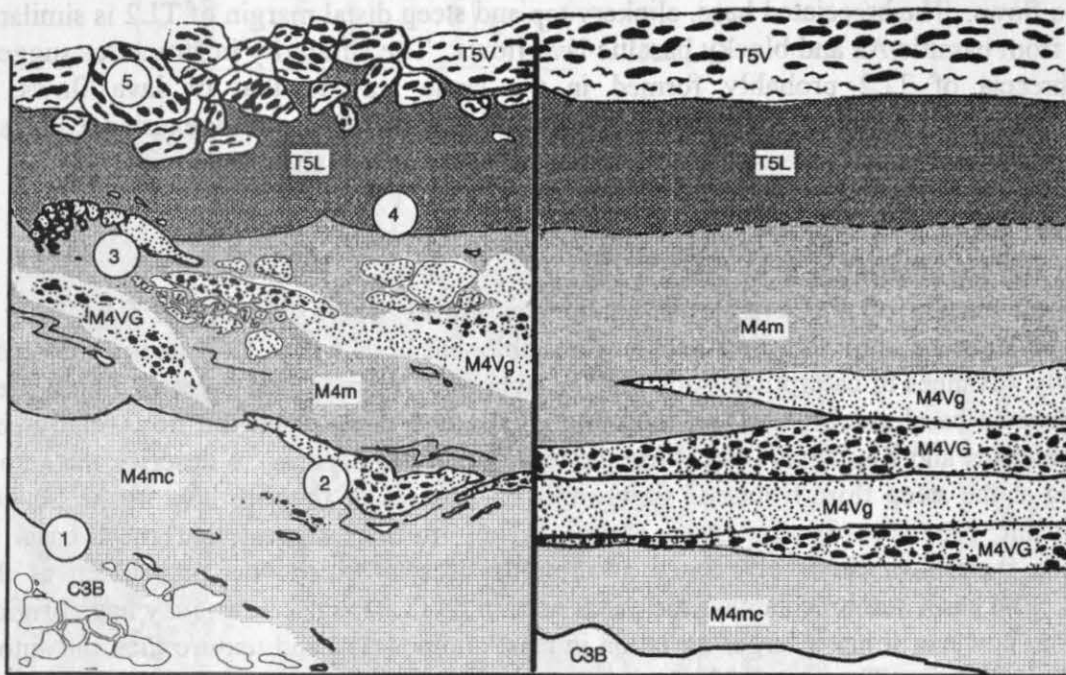


Figure 7.15. The effects of contrasting competency of lithofacies during non-particulate flow of TL2. (a) shows the original pre non-particulate deformation stratigraphy, (b) shows the post non-particulate deformation facies associations.

1. C3B lithofacies deforms plastically, producing ramps or shear plane, but brecciates on further deformation, forming basal autobreccia.
2. Weakly welded subfacies M4Vg and M4VG are ripped up and incorporated into surrounding plastically deforming lava-like facies, forming discrete lenses and pods.
3. With continued deformation, subfacies M4Vg and M4VG break up to form pockets of in situ autobreccia.
4. Lava-like lithofacies (M4m and T5L) deform plastically, shearing around M4Vg and M4VG lenses and breccia pockets.
5. At the top of the deposit, cooler, less strongly welded lithofacies T5V is 'rafted' along, breaking up to form upper autobreccia.

from post-depositional non-particulate flow (e.g. Exp. 90-III and 93-II, Fig. 2.27). The interstratified competent and incompetent layers are inferred to have thinned and distorted during lateral spreading. The layers which are more competent as a result of:

1. cooling, e.g. lithofacies T5V at the top of the unit, and
 2. a lower degree of welding, e.g. subfacies M4Vg and M4VG
- have deformed in a brittle manner (Fig. 7.15b). These lithofacies appear to have been 'ripped up' forming discrete lenses and pods surrounded by plastically deforming lava-like TL comendite and TL mixed rock lithofacies (e.g. lithofacies M4m and associated subfacies). With continued deformation the competent weakly welded lenses have been broken up to form pockets of internal autobreccia, resembling the internal autobreccia within lava flows. The cool upper surface also fractured to produce upper autobreccia (see next section). The lava-like TL trachyte and TL mixed rock lithofacies continued to deform plastically, and sheared around the M4Vg and M4VG lenses and breccia pockets (Fig. 7.15).

7.10.2 Brecciation: Brittle deformation

Extensive non-particulate flow of TL2 (Section 7.6, Fig. 7.10) has led to the development of autobreccia at the distal margin, top and base of the unit (Fig. 2.37)

The marginal, basal and upper autobreccias in TL2 resemble the autobreccias of viscous obsidian block lava flows. The brecciated base, clinkery top and steep distal margin of TL2 is similar to that recorded from basaltic Aa and blocky basaltic lava flows. The similarity in structures suggests that the autobreccia of TL2 probably formed in the same way to that of lava flows, during non-particulate deformation and degassing of the welded tuff. Where flow exerted a stress on the welded tuff that exceeded its tensile strength, fracturing occurred, and blocks were formed. These were rotated and fractured further as flow continued.

Marginal and basal autobreccia

At the distal margin of Aa lava-flows, autobreccia forms where the jagged flow front creeps forward and steepens until a section becomes unstable and breaks off. Collapse is repeated as the flow slowly advances in caterpillar track fashion over an autobrecciated layer of fragmented lava. This produces a basal autobreccia and thick marginal autobreccia when the flow finally comes to rest. Bonnicksen and Kauffman (1987) use the term '**crumble breccia**' to describe the autobreccia originating at the steep flow fronts of slowly moving masses of rhyolite lava in the Snake River Plain volcanic province (Southwestern Idaho). They further suggest that most basal breccia observed in these lava flows originated as crumble breccia which was overridden as the lava advanced. The basal autobreccia near the distal margin of TL2 (Fig. 2.37a), may have originated in this fashion, however it has a larger variation in clast composition and texture than the autobreccia at the distal margin. The marginal autobreccia is monolithologic, composed of large, slipped blocks of subfacies T5La (Fig. 2.37a), while the basal autobreccia is composed of vitrophyre blocks, agglutinate blocks and flow-banded blocks in a devitrified matrix (Fig. 2.37a). The heterolithologic nature of the basal autobreccia indicates that brecciation of the vitrophyre and basal flow banded lithofacies of TL2 occurred. The greater thickness of the marginal autobreccia was probably produced by collapse of the distal margin. Evidence of instability at the steep distal margin is indicated by the presence of sub-vertical fractures extending from the top, nearly to the base of the flow (Fig. 7.19). These are filled with blocks of breccia welded together, and may represent fractures which developed due to oversteepening of the flow front.

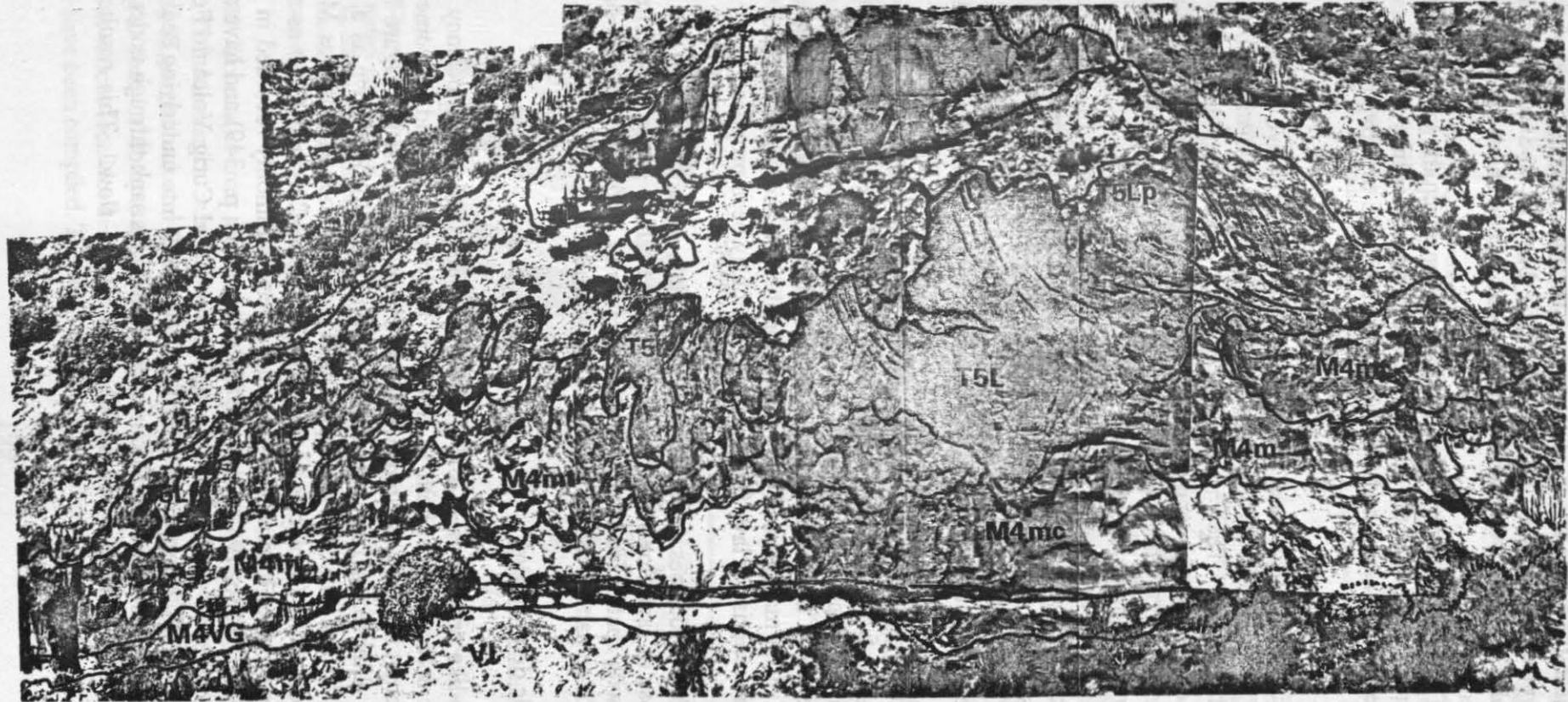
In-situ autobreccia

Approximately 10 m away from the distal margin, the distribution of basal autobreccia becomes extremely irregular. Pockets of basal autobreccia occur in association with ramping planes, suggesting that this autobreccia developed in place (Fig. 7.19). Bonnicksen and Kauffman (op. cit.) have also described lenses and irregular zones of basal autobreccia in extensive silicic lavas which they suggest also formed in-situ. These are similar to the pockets of basal autobreccia in TL2 (Fig. 7.19). The in-situ autobreccia is clast-supported and is generally monolithologic, composed of tightly packed (including jigsaw fit) angular fragments of comenditic C3B lithofacies (e.g. Figs. 2.27 and 7.15). The tight packing and monolithologic composition of this autobreccia distinguishes it from the loosely packed basal autobreccia near the distal margin. The angularity of the particles suggests that the fragments have undergone little transport.

In situ autobreccia also occurs within TL2, as irregular lenses and 'breccia pockets' (Fig. 7.15) which must have formed in place, since the brecciated zones pass laterally into non-brecciated material of the same composition (Fig. 7.15 and Fig. 2.31). This autobreccia is similar to 'internal autobreccia' within lava flows (Manley and Fink, 1987).

Upper autobreccia

Most of the upper surface of TL2 is covered with irregularly distributed autobreccia. This autobreccia is loosely packed, clast supported, and is composed of cobble to boulder sized blocks (<2m in diameter) of lithofacies T5V, subfacies T5VG and T5Lp (Fig. 7.15), and more rarely lithofacies C0b.



X	
T5Lp	TL2
T5L	
M4mt	
M4m	
M4mc	
M4VG	
P2	
VI	

2 m

Figure 7.16. Load structures in TL2 (Exp. 101, Bco. de Tauro). TL trachyte lithofacies have loaded down into underlying TL mixed rock and TL comendite. The lithofacies associations in TL2 have been outlined together with an indication of the angle of imbrication of fiamme and flow banding, to highlight the ramp structures near the top of the deposit. Overlying Middle Mogan Formation ignimbrite X is also marked, together with underlying units P2 and VI. The length of outcrop is 57m and the inferred direction of flow is from right to left.

Similar upper autobreccias composed of glassy to devitrified flow-banded breccia blocks have been recorded from other high grade ignimbrites, e.g. The Barrel Springs Tuff, Trans-Pecos Texas (Henry and Wolff, 1991) and The Bad Step tuff, English Lake District (Branney, Kokelaar and McConnell, 1992). Bonnicksen and Kauffman (1987) have described autobreccia composed of vitrophyre blocks found near the upper zones of the extensive rhyolite lava-flows of the Snake River Plain volcanic province. They describe this as '**jostle breccia**' and suggest that it was probably formed when cooled, glassy rhyolite was broken up and jostled about by movement in the underlying, hotter less viscous lava.

The upper autobreccia of TL2 probably formed in a similar manner, when the yield strength of less strongly agglutinated tuff at the surface of the deposit increased during cooling and degassing (Fig. 7.14). The tuff blocks were rafted along and ultimately fractured due to movement of the more fluidal tuff below.

Both Bonnicksen and Kauffman (1987) and Henry and Wolff (1992) have proposed that the features of the distal ends of extensive rhyolite lava-flows can be used to distinguish them from highly rheomorphic ignimbrites. They note that distally, extensive silicic lava flows characteristically have thick, blunt ends and marginal flow lobes with thick accumulations of crumble breccia. In comparison to the distal parts of high grade ignimbrites which commonly thin to 3 to 6 m and lack marginal and basal autobreccia.

Henry and Wolff (op. cit.) also suggest that the presence or absence of autobreccia, and autobreccia composition can also be used to distinguish between high grade ignimbrites and extensive silicic lava flows. They note that where high grade ignimbrites (e.g. The Barrel Springs Tuff) have autobreccia, it is commonly composed only of the immediately surrounding lithofacies and does not show the diverse clast composition of for example, rhyolite lava flow breccias.

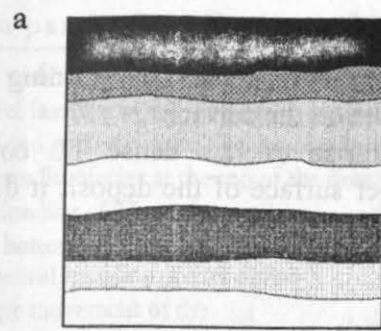
TL2 is clearly pyroclastic in origin, since the lava-like lithofacies pass gradationally, vertically and laterally into vitroclastic lithofacies and yet it has both a thick, steep distal margin with a considerable accumulation of marginal autobreccia, and basal and upper autobreccias. Also, the basal autobreccia near the distal margin show considerable diversity in clast composition (Fig. 2.37a). Thus the shape of distal margins and the presence or absence and composition of breccias, cannot be used as diagnostic criteria for lava flows, as has previously been proposed.

The post agglutination flow processes in extremely high grade ignimbrites may be virtually indistinguishable from those of lava-flows. For example, compare high grade ignimbrites fed by low pyroclastic fountains with spatter fed or fountain fed lava flows, both will undergo substantial non-particulate flow and so are liable to develop identical flow structures.

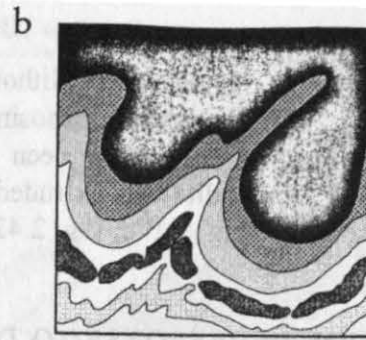
7.10.3 Hot loading: Plastic deformation

In highly welded and lava-like profiles of TL2 (Fig. 7.16) that lack marked competency contrasts between lithofacies, plastic deformation of both TL trachyte, TL mixed rock and TL comendite has produced a number of different field relationships which have been summarised in Figure 7.17.

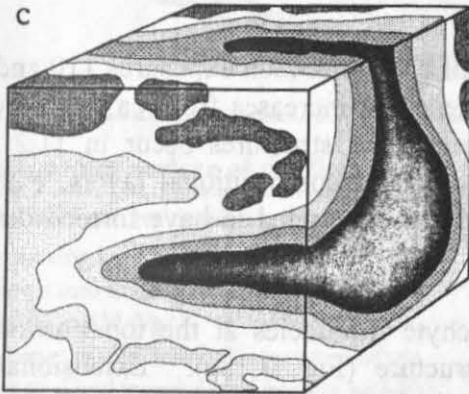
The lava-like TL trachyte (lithofacies T5L and subfacies M4mt) has loaded down as a series of lobate protrusions (Fig. 7.16 and Fig. 7.17b) displacing TL mixed rock (lithofacies M4m) and underlying lava-like TL comendite (subfacies M4mc and lithofacies C3B and C2L) as shown in Figure 7.17c and d. These types of loading structures have been commonly recorded in liquefied sediments (e.g. Kuenen 1953a, 1953b, 1957; Lowe, 1982; Allen, 1982; p. 349) and have also been observed in the distal lithofacies of welded ash flow tuff in the Capel Curig Volcanic Formation, North Wales (Howells et al., 1985), where 'pods' of ash flow tuff sank into underlying sediment. In TL2, the loading is restricted to *within* the unit; TL trachyte lithofacies sank through underlying TL mixed rock and TL comendite lithofacies towards the base of the flow. This resulted in the



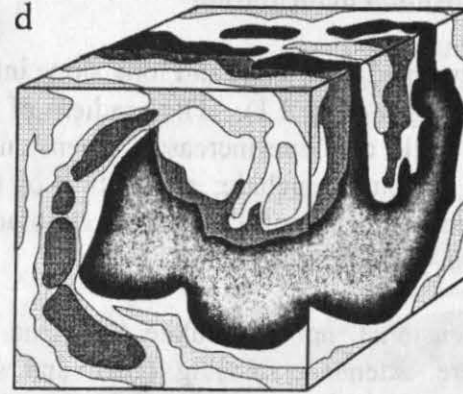
Pre-deformation stratigraphy consists of rapidly stacked hot layers of different density and competence. There is an inverse density stratification, with last deposited TL trachyte overlying earlier deposited TL comendite, this leads to instability.



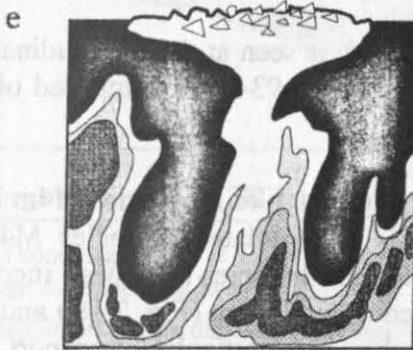
TL trachyte deforms downwards in a series of lobate protrusions, displacing lower layers. This is aided by bouyant rise of TL comendite, which results in spine-like protrusions into the base of more competent TL trachyte.



TL trachyte layers continue to sink towards the base of the flow, breaking up into large boudinage blocks and forming load balls. This promotes late-stage mechanical mixing between adjacent facies and forces less dense TL comenditic layers towards the top of the flow.



Large parts of the originally overlying TL trachyte lithofacies are disrupted and sink towards the base of the flow. TL comendite is displaced and rises diapirically to the top of the flow. This results in late-stage partial overturning of the flow.



Complete overturning of the flow results in the surface expression of TL comendite. TL comendite commonly brecciates on exposure to the surface as a result of extreme deformation and increase in competency due to prolonged cooling.

Lithofacies and subfacies	Lithofacies Group
T5L	TL trachyte
M4mt	
M4m	TL mixed rock
M4mt	
C3B	TL comendite

Figure 7.17. Schematic cross sections showing the progressive post-depositional deformation and mechanical mixing in TL2. Mechanical mixing is caused by the downloading of TL trachyte which displaces less dense, underlying TL mixed rock and TL comendite. All the components behave viscously, but viscosity varies according to chemical composition and degree of cooling. Cross sections have been compiled from field data recorded at various localities in Bco. de Mogán. Where data was available (e.g. diagrams c and d) block diagrams have been compiled. The sections are 10m by 10m.

mechanical displacement of the lower lithofacies, leading to a partial overturning of the lithostratigraphy (Fig. 7.17d) sometimes exposing TL comendite on the surface.

The process of overturning may have been assisted by uprise of less dense TL comendite lithofacies. Where TL comendite was extruded onto the upper surface of the deposit it deformed brittly forming autobreccia (Fig. 7.17e, Fig. 2.42).

7.11 DEFORMATION IN RESPONSE TO TOPOGRAPHY

The most extreme deformation in TL2 occurs near the distal margin and in areas of steep topography. Two broad categories of deformational structures have been identified: (1) extensional structures, (2) compressional structures.

7.11.1 Extensional deformation

TL2 was deposited over a hill and long slope into a small basin, between exposures 110 and 93 IV, in Bco de Mogán (Fig. 2.1). The gradient of the palaeoslope increases from ca. 20° to ca. 45°. Where the angle of slope increases, extensional deformational structures occur in TL2. These extensional structures include; attenuation of the textural and compositional layers, extensional fractures and boudinage of TL trachyte lithofacies, and are interpreted to have formed during the downhill non-particulate flow of TL2.

During extensional, non-particulate flow, the TL trachyte lithofacies at the top portion of the deposit were extended, forming pinch and swell structure (Fig. 7.18a). Extensional cracks developed on the cool, top surface of the deposit in the 'pinch zones' (Fig. 7.18b). At the maximum slope angle TL trachyte lithofacies were broken up, forming a series of large boudinage blocks (Fig. 7.18c) which sunk down through underlying lava-like lithofacies M4m and M4mc. These lithofacies were, in-turn, displaced upwards towards the top of the deposit. In the same way in which the loading structures developed on horizontal surfaces, this caused mechanical mingling and shear of adjacent lithofacies, and produced comenditic upper autobreccia (lithofacies C0b), where TL comendite was forced to the upper surface (Fig. 7.18c).

The effect of extension on lithofacies of contrasting competency is seen at the longitudinal section in Bco. de Mogán. The base of TL2 between Exp. 92 and Exp. 93-III is composed of weakly welded subfacies M4VG and M4Vg.

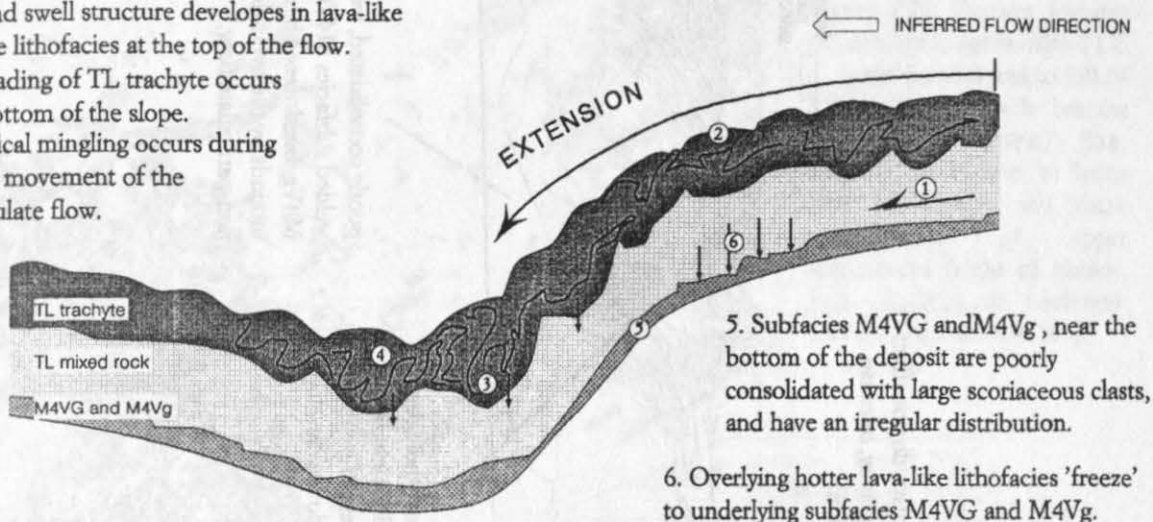
The hotter, more ductile and therefore faster moving overlying lava-like lithofacies M4m and T5L appear to have ploughed down into the underlying poorly consolidated subfacies M4VG and M4Vg, stripping them from the lower surface. Lenses of these lithofacies have been incorporated into the surrounding lava-like lithofacies which have sheared around them (Fig. 7.18b and c). The lenses of M4VG and M4Vg were broken up during further non-particulate transport to form pockets of internal autobreccia (Fig. 2.31a and b).

7.11.2 Compressional deformation

Beyond the long palaeoslope and basin described in the previous section, the pre- TL topography is a small, low mound, over which the most distal portion of TL2 was deposited. TL2 does not completely cover this mound and forms a steep distal margin near the crest of the hill. The compressional structures observed in this part of TL2 indicate that the front of the flow halted and formed a barrier. The rest of the flow which was still moving, with the added impetus of having come downhill, piled up behind the distal margin, forming a series of large compressional 'ramp'

a. Non-particulate flow travels fast downhill, undergoing extension.

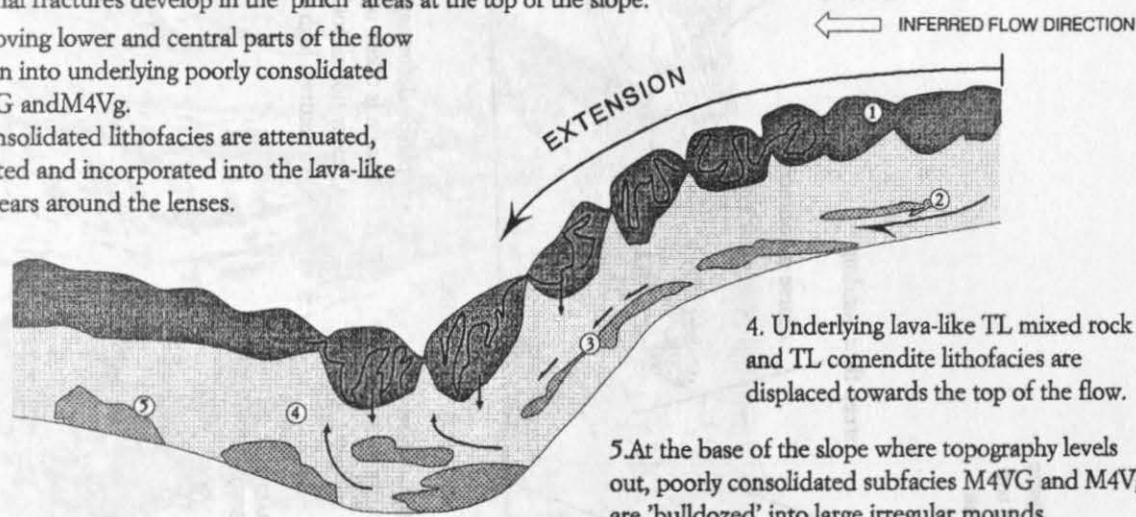
1. Shear within the flow, as the lower and central parts of the flow travel faster than the top, due to cooling effects.
2. Pinch and swell structure develops in lava-like TL trachyte lithofacies at the top of the flow.
3. Downloading of TL trachyte occurs near the bottom of the slope.
4. Mechanical mingling occurs during downslope movement of the non-particulate flow.



5. Subfacies M4VG and M4Vg, near the bottom of the deposit are poorly consolidated with large scoriaceous clasts, and have an irregular distribution.
6. Overlying hotter lava-like lithofacies 'freeze' to underlying subfacies M4VG and M4Vg.

b. Upper, cooler surface of the flow breaks up under extension.

1. Extensional fractures develop in the 'pinch' areas at the top of the slope.
2. Faster moving lower and central parts of the flow plough down into underlying poorly consolidated layers M4VG and M4Vg.
3. Poorly consolidated lithofacies are attenuated, autobrecciated and incorporated into the lava-like flow as it shears around the lenses.



4. Underlying lava-like TL mixed rock and TL comendite lithofacies are displaced towards the top of the flow.
5. At the base of the slope where topography levels out, poorly consolidated subfacies M4VG and M4Vg are 'bulldozed' into large irregular mounds.

c. Loading and sinking of TL trachyte boudinage blocks

1. Isolated boudinage blocks of TL trachyte lithofacies sink through the underlying lava-like lithofacies.
2. Underling lithofacies are displaced and forced towards the upper surface where they form upper autobreccia

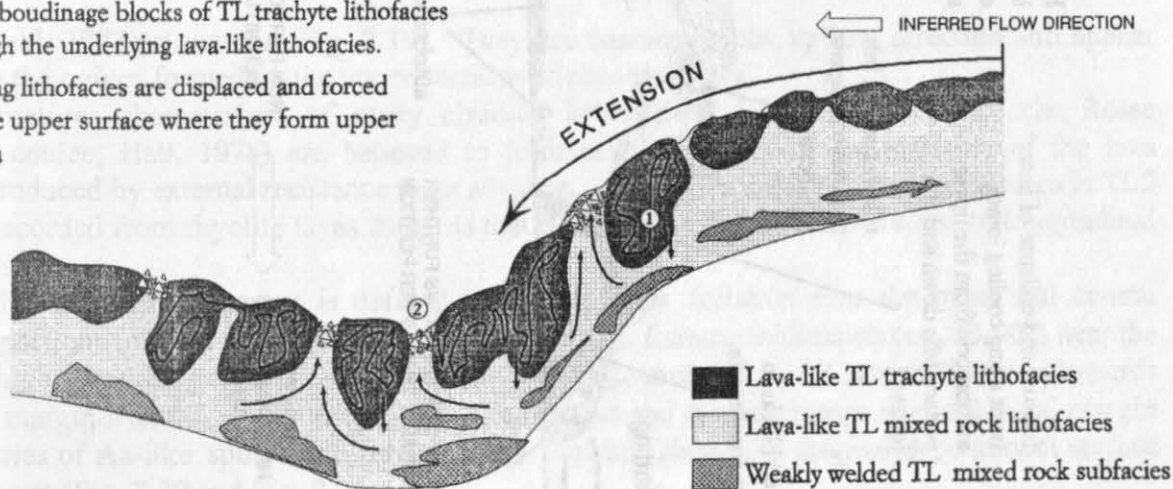


Figure 7.18. Development of extensional boudinage structures in TL2, Bco. de Mogan.

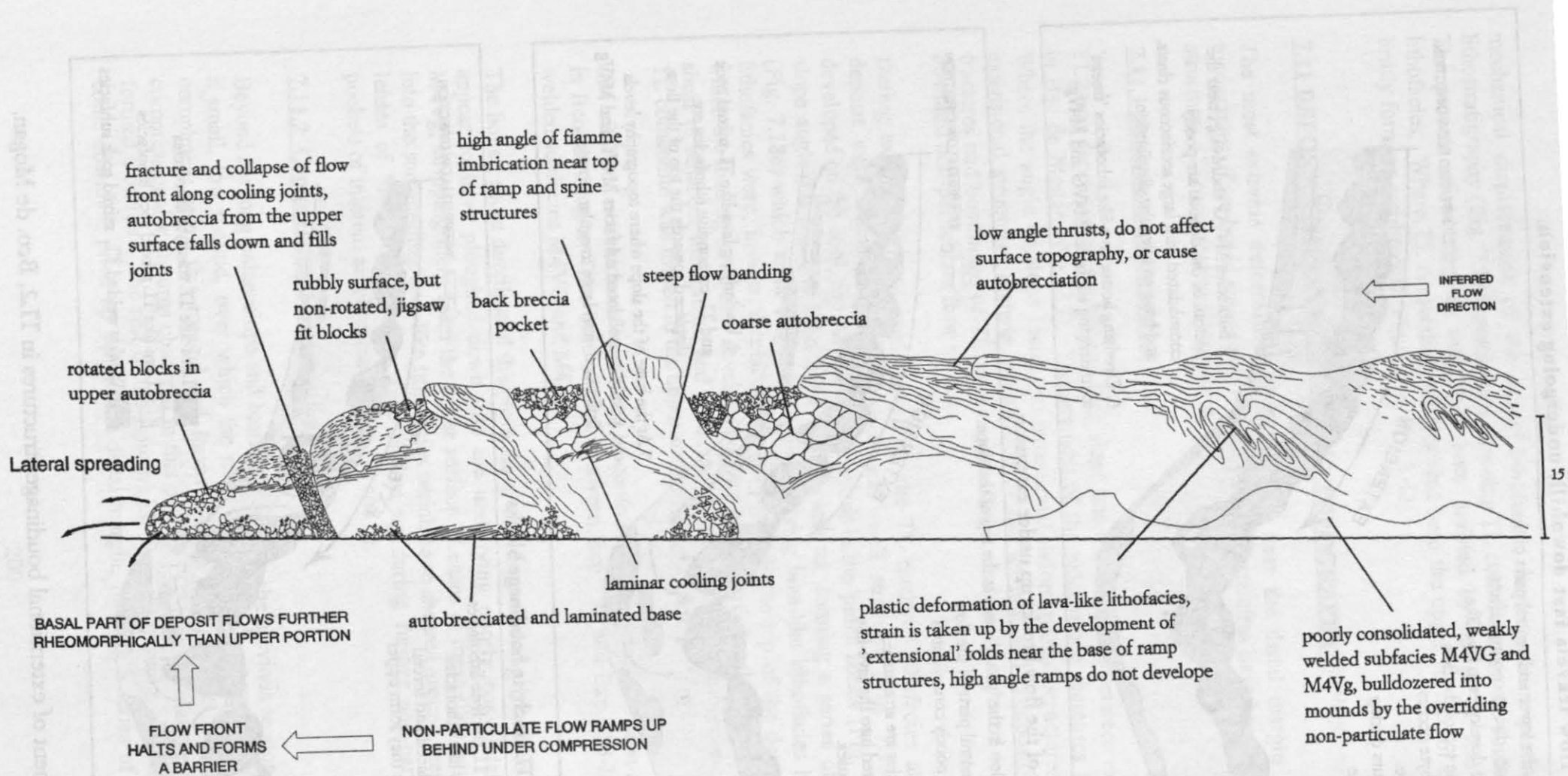
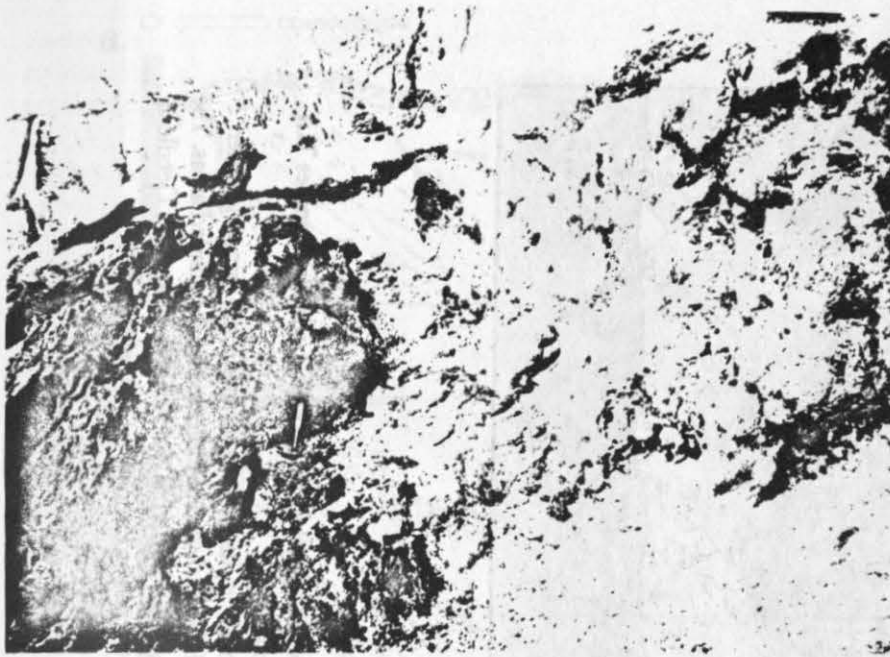
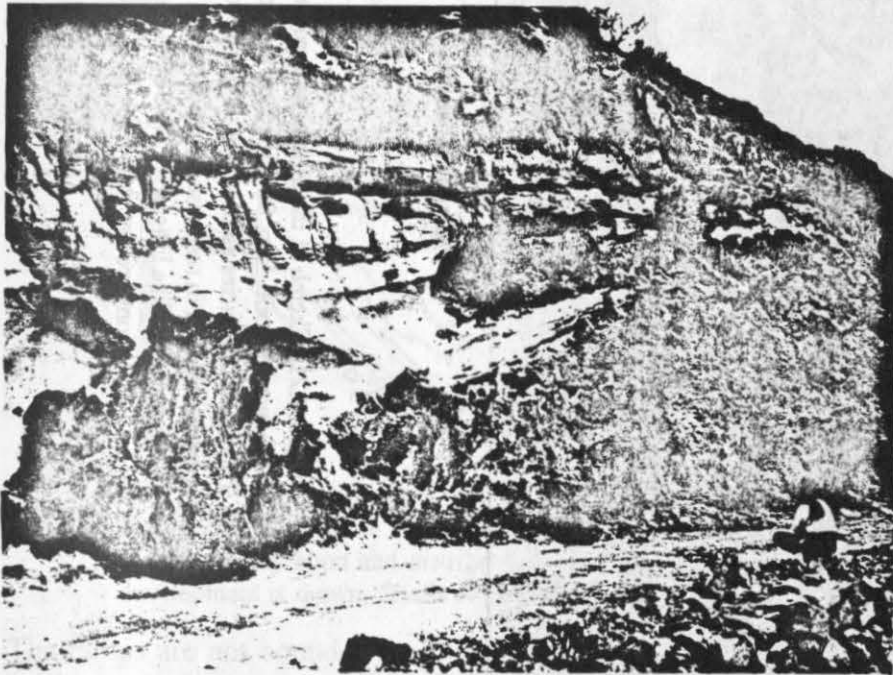


Figure 7.19. Compressional deformation structures at the distal margin of TL2, Bco. de Mogán.



a.



b.

Figure 7.20. Surface features of high grade ignimbrite TL2. a. Spine (behind and to left of hammer) and 'back breccia' (right of photograph), Exp. 98, Bco. de Taurito. b. Spine (left of photo) and thick accumulation of upper autocbreccia (right of photo), Exp. 58, Bco. de Lechugón. The hammer is 30cm long.

(MacDonald, 1972) structures (Fig. 7.19). They are concave in the upflow direction and appear similar to the ogives formed on the upper surfaces of rhyolite flows.

Ramp structures characteristic of many obsidian lava flows (for example the Rocche Rosse Obsidian coulee; Hall, 1978) are believed to form under longitudinal compression of the lava stream, produced by external resistance to its advance. The similarity of the ramp structures in TL2 to those recorded from rhyolite lavas suggests that they formed by the same process of longitudinal compression.

In TL2 the angle of the ramps is defined by a steep flow foliation near the basal and central lava-like portions of the unit, and by an exceptionally high fiamme inclination (ca. 80-90°) near top, less highly welded portions of the deposit. The angle and size of the ramps increases toward the distal margin from 40° to 80° (Fig. 7.19). The largest and steepest ramps near the distal margin form a series of Aa-like 'spines' and ridges, which protrude above the original depositional surface of the deposit (Fig. 7.20 and Fig. 7.21).

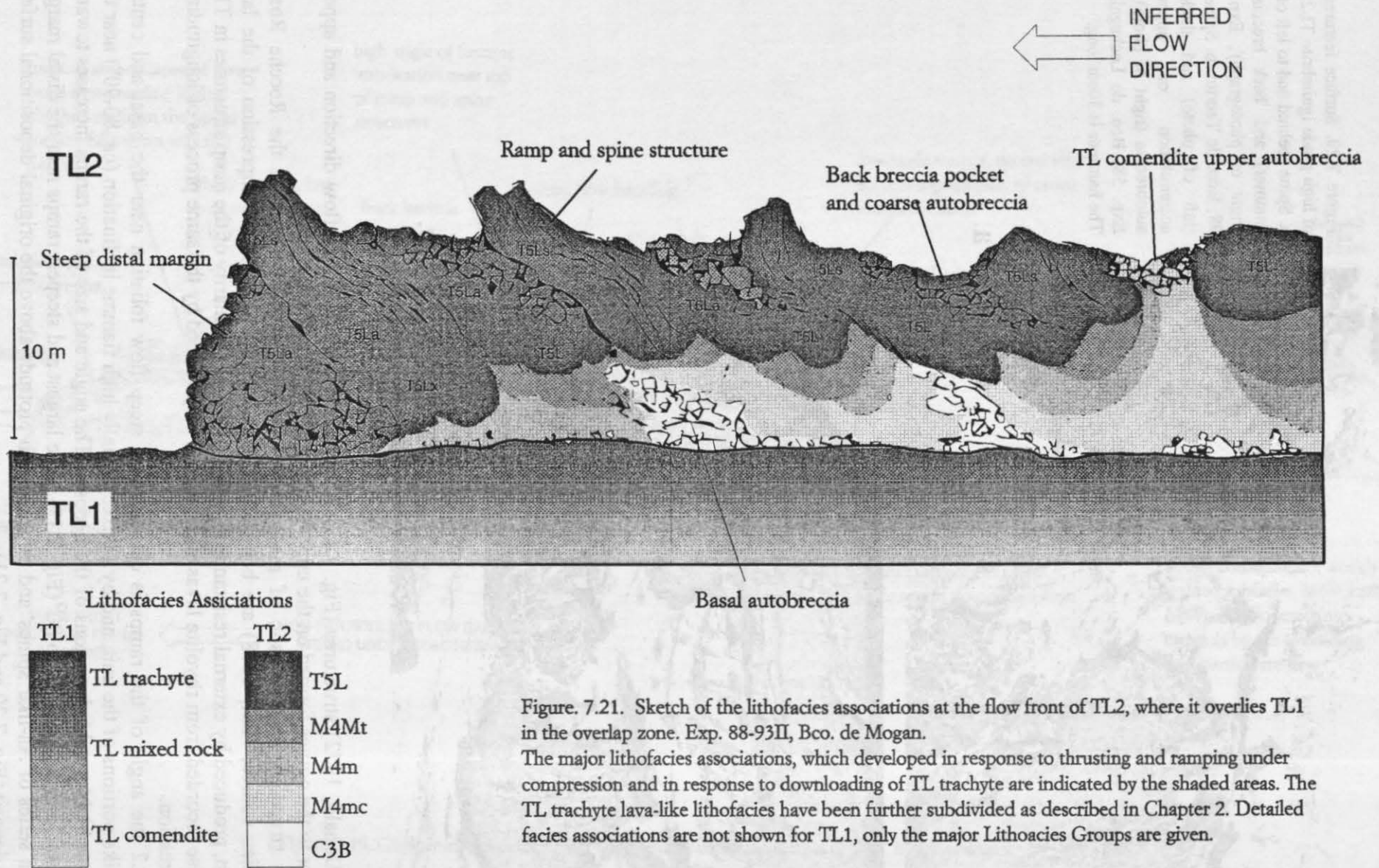
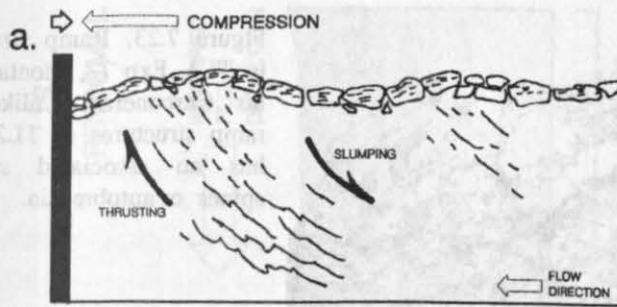


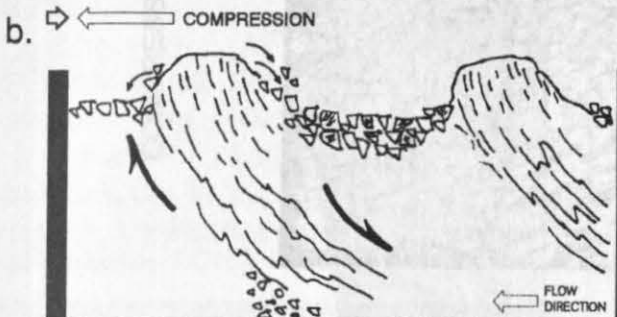
Figure 7.21. Sketch of the lithofacies associations at the flow front of TL2, where it overlies TL1 in the overlap zone. Exp. 88-93II, Bco. de Mogan.

The major lithofacies associations, which developed in response to thrusting and ramping under compression and in response to downloading of TL trachyte are indicated by the shaded areas. The TL trachyte lava-like lithofacies have been further subdivided as described in Chapter 2. Detailed facies associations are not shown for TL1, only the major Lithofacies Groups are given.



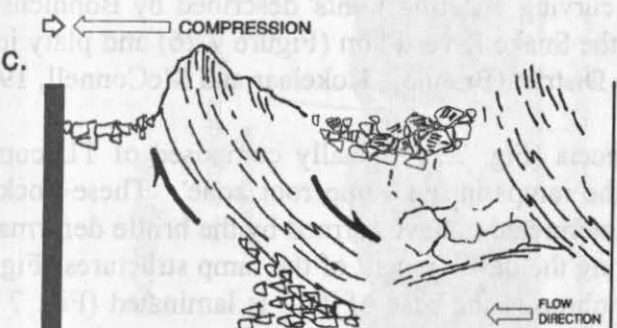
1. Autobrecciation of cooled, moderately welded upper surface (non-rotated blocks).
2. Development of ramps, as faster moving material rides up against the flow front barrier.
3. Ramps are not bounded by clearly defined shear planes, but are formed by the upward mass movement of material in a wide shear zone.

FLOW FRONT BARRIER



4. Surface expression of ramp structure as a spine or ridge.
5. The surface is disrupted as the spine protrudes. Breccia blocks roll off the surface of the spine and fill the depression left by the upward displacement of material along the ramp zone. Breccia blocks are rotated.

FLOW FRONT BARRIER



6. As ramping continues and more material is displaced, slumping occurs in the area between the ramp and spine structures. Lithofacies are broken up into large blocks forming coarse autobreccia.
7. Basal autobreccia develops near the foot of the ramp and is sheared out along the base of the ramp zone.

FLOW FRONT BARRIER

Figure 7.22. Successive stages (a, b, c) in the development of compressional ramp structures and the associated formation and distribution of autobreccia, near the distal margin of TL2. Only structural development is shown, details of lithofacies associations are given in Figure 7.21.

The ramps are not bounded by clearly defined shear planes, and they appear to have been formed by the upward mass movement of viscously deforming non-particulate (welded) material.

The distribution of autobreccia within the distal margin area appears to be related to the development of these large scale compressional structures. Pockets of 'back breccia' are on the upper surface behind the spines and ridges produced by ramping (Fig. 7.20), and coarse autobreccia occurs in the central, massive parts of the tuff between the spines and ridges (Fig. 7.19). These breccias are interpreted to have formed during the development of the ramps. The uppermost cool, weakly welded surface of the deposit deformed brittly to produce upper autobreccia (Fig. 7.22a). During protrusion of the spines, breccia blocks rolled down off the back of the spines filling the depressions produced by the upward mass movement of material within the ramp zone (Fig. 7.22b). Between the ramp structures the upper and central portions of the deposit have been broken into coarse autobreccia which may have formed in response to slumping, produced by the upward mass movement of material in the ramp zone (Fig. 7.22c).

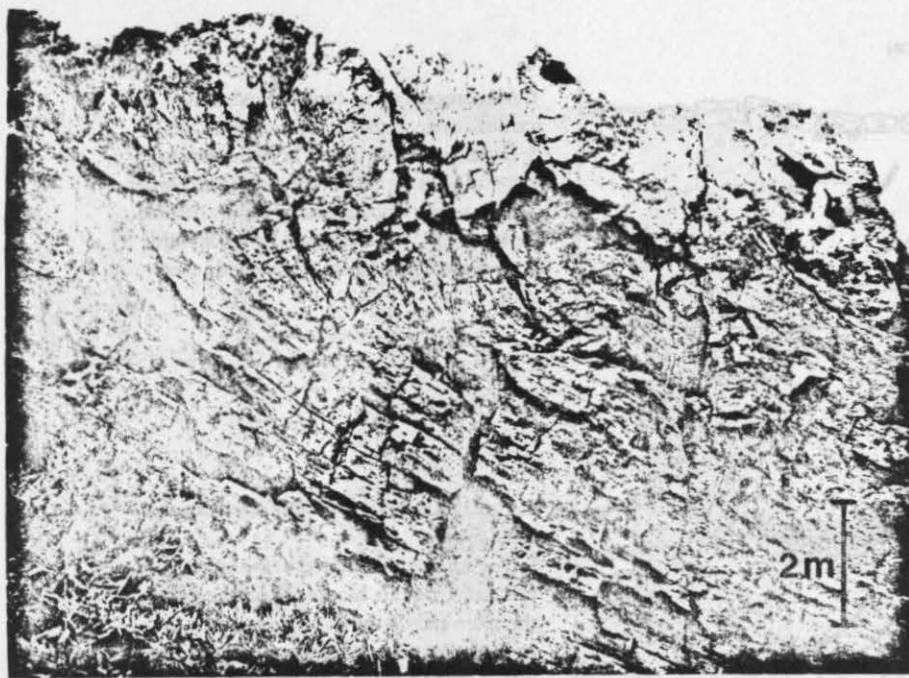


Figure 7.23. Ramp structure in TL1, Exp 72, Montaña de las Carboneras. Unlike the ramp structures in TL2, this has no associated surface spines or autobreccia.

Between the pockets of back breccia and coarse autobreccia, and the underlying plastically deformed lava-like lithofacies are sub-horizontal cooling joints (e.g. Fig. 7.19, and Fig. 7.22c). These features resemble the sub-horizontal, curving 'sheeting joints' described by Bonnicksen and Kauffman (1987) from the rhyolite lavas of the Snake River Plain (Figure 7.26) and platy joints in rheomorphic ignimbrites of the English Lake District (Branney, Kokelaar and McConnell, 1992).

Roughly triangular pockets of basal autobreccia (Fig. 7.21) usually composed of TL comendite lithofacies (C3B) are found at the base of the ramps in the 'ramp root zone'. These pockets are sheared out along the ramp zone. They are interpreted to have formed by the brittle deformation of cooler material near the base of the flow during the development of the ramp structures (Fig. 7.22b and c). In between the pockets of basal autobreccia the base of TL2 is laminated (Fig. 7.19 and Fig. 2.40).

The steep (ca. 70°) distal margin of TL2 consists of a large mound of autobreccia composed of various lithofacies (Fig. 2.37a and b); and large slipped blocks (Fig. 2.38), of agglutinate (T5La). Wide (<1.5m), sub-vertical fracture zones containing autobreccia occur between the agglutinate blocks (Fig. 7.19). They pass from the base to the upper surface of the deposit. These are interpreted to have formed during cooling, fracture and collapse of the distal margin by lateral spreading. The fractures were filled with breccia blocks which tumbled in from the irregular upper surface.

Thrusts (ramp structures) also occur in TL1 (Fig. 7.23) however they are not widely developed. TL1 most commonly has a planar upper surface and although it has areas of upper autobreccia, no basal autobreccia has been observed.

7.12 THE MORPHOLOGY OF A LAVA-LIKE IGNIMBRITE

The post-depositional deformation structures observed in TL2, in longitudinal section (ca. 20km) down Bco. de Mogán, indicate that the degree of rheomorphic deformation increased from proximal to distal localities, because the following deformation styles occur from proximal to distal localities:

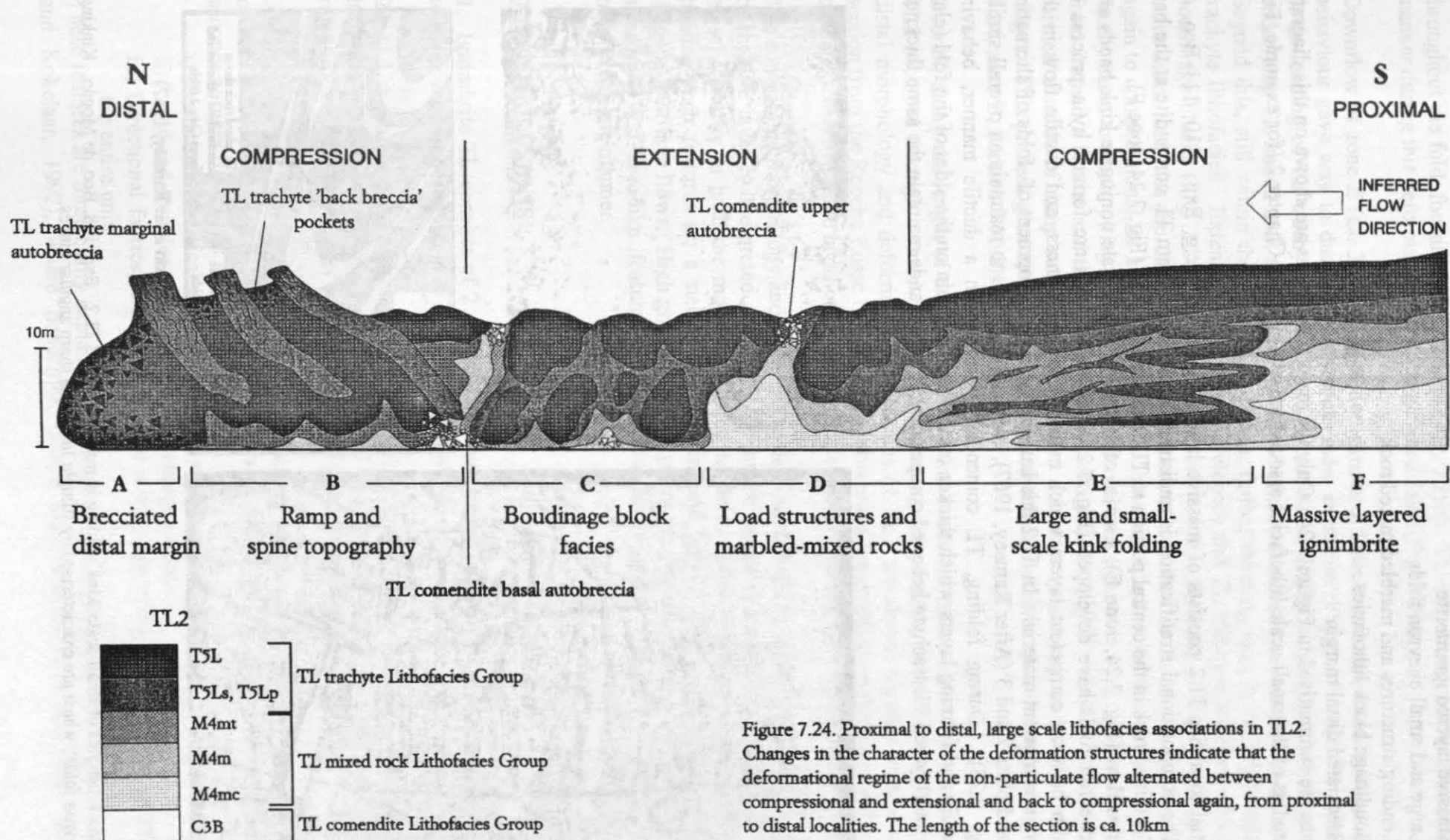


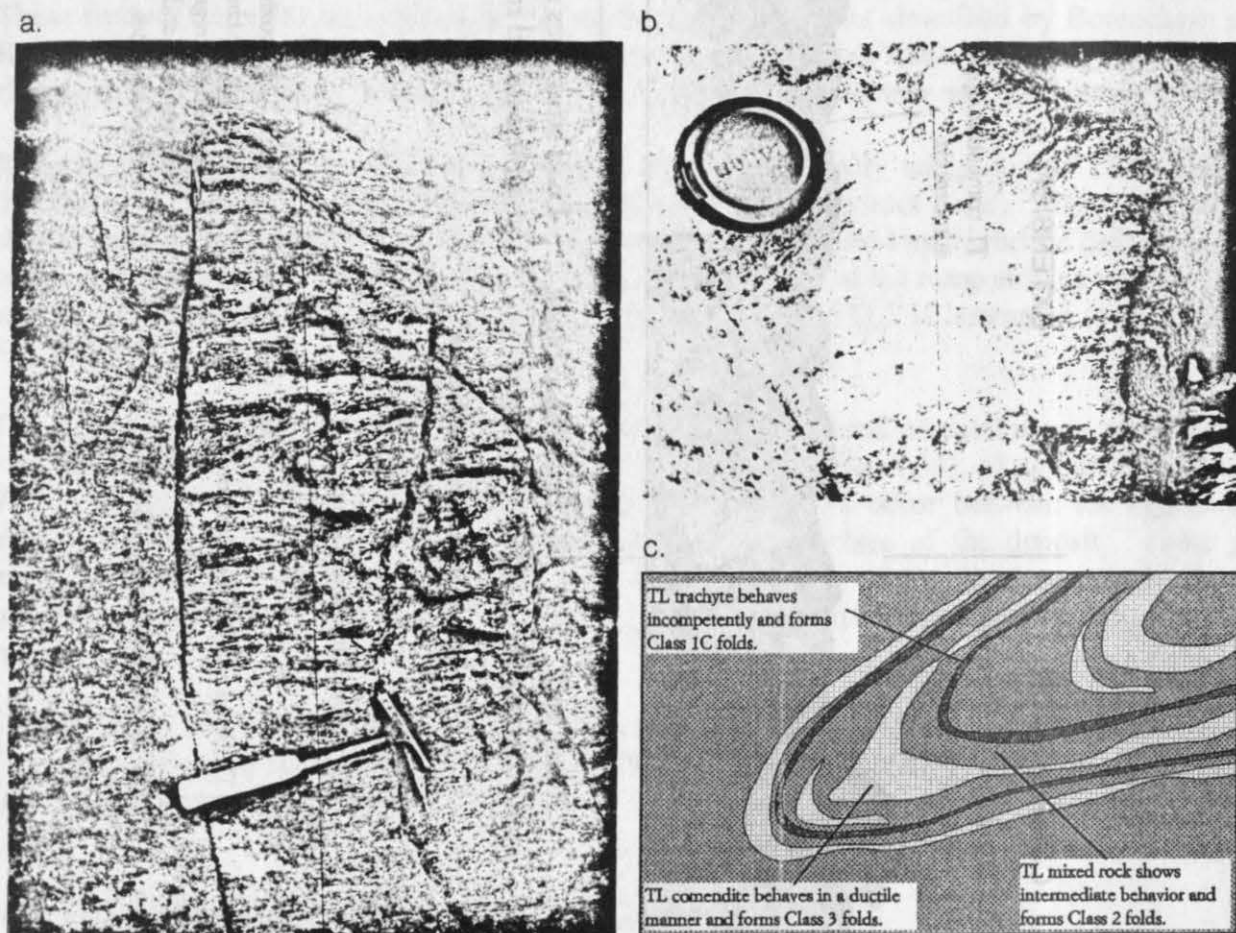
Figure 7.24. Proximal to distal, large scale lithofacies associations in TL2. Changes in the character of the deformation structures indicate that the deformational regime of the non-particulate flow alternated between compressional and extensional and back to compressional again, from proximal to distal localities. The length of the section is ca. 10km

- 1) Massive layered ignimbrite
- 2) Large and small chevron folds
- 3) Loading structures and marbled mixed rock
- 4) Boudinage block lithofacies
- 5) Brecciated distal margin

These zones are summarised in Figure 7.24. Only the major lithofacies are shown on this diagram, detailed studies of the small-scale lithofacies associations are given in Chapter 2 (for example, Fig. 2.27).

At proximal localities TL2 consists of massive layered ignimbrite (e.g. Exp. 110, 111 Bco. de Mogán) The compositional stratification is undisturbed and passes from TL comendite at the base through TL mixed rock in the central portion to TL trachyte at the top (Fig. 7.24, zone F).

Further downflow (Fig. 7.24, zone E), a series of large and small scale conjugate kink bands and multiple chevron folds have developed (Fig. 7.25). Chevron folds are formed by a process of flexural slip between competent layers which maintain their thickness, and ductile flow in the intervening incompetent material. In TL2 this has led to the development of folds of alternating class 1c, and class 2 and 3 (After Ramsey, 1967), enabling the folds to maintain an overall similar form (Fig. 7.25). During folding, TL comendite deformed in a ductile manner, behaving incompetently and forming layers which thicken on the crest and thin on the sides of the fold (class 3 folds). Interlayered TL trachyte behaved competently and the bands maintain the same thickness



(Classification after Ramsey, 1967)

Figure 7.25. Examples of small scale 'kink' folding in massive layered TL2. Exp. 108, Bco. de Mogán. Kinking forms 'chevron folds', which are characterised by straight limbs and sharp angular hinges.

throughout the fold, forming class 1c folds (Fig. 7.25c). TL mixed rock behaved in a semi-ductile manner during this deformation, producing class 2 folds (Fig. 7.25c).

Downflow of zone E (ca. 3km) deformation structures indicate that the more brittle, compressive behaviour gave way to ductile deformation under extension (Fig. 7.24, zone D). Thinning and down-loading of TL trachyte lithofacies with associated displacement and mechanical mixing of underlying TL mixed rock and TL comendite lithofacies occurred (as described in Section 7.10.3). Beyond this, still within the zone of extension, further thinning lead to the brittle failure of TL trachyte lithofacies. Extensional fractures developed, and TL trachyte lithofacies broke up into boudinage blocks (Fig. 2.24, zone C), which sunk towards the base of the flow (Fig 7.18). At more distal localities the deformational structures indicate that the deformational regime changed again to compressional, as a result of the gradual slowing down of the flow front. The flow front finally came to a halt, piling up a mound of autobreccia in front of it (Fig. 7.24, zone A). The flow front formed a barrier and the material upflow, which had a higher viscosity, piled up behind and formed a series of ramp structures, which have a surface expression in the form of spines and ridges. This process generated associated upper and basal autobreccia and coarse autobreccia (Fig. 7.24, zone B, Section 7.10.2).

Overall, along the length of the TL2, deformation structures indicate that non-particulate flow of TL2 occurred through a series of zones of alternating compression and extension. The proximal to distal morphology and deformational structures of TL2 are shown together with a longitudinal section from the Rocche Rosse Obsidian lava flow and a longitudinal profile compiled from studies of the extensive rhyolite lavas of the Snake River Plain volcanic province on Figure 7.26.

The comparable morphology and similarity in deformation structures between TL2 and the profiles of rhyolite lavas is interpreted as resulting from the extensive non-particulate flow of TL2. The close similarity in both the morphology and the deformation structures highlights the danger of treating such features as; a steep distal margin, and upper, basal and marginal autobreccia, as diagnostic of lava flows. High grade lava-like ignimbrites, such as TL2, can develop identical flow structures and lava-like features if they flow for a large proportion of their length in a non-particulate manner.

7.13 CONCLUSIONS

1. Ignimbrite TL consists of 2 separate but overlapping flow units, TL1 and TL2, which cooled together in a zone of overlap to form a compound cooling unit.
2. TL1 is a high grade ignimbrite which is welded to within a few cm's of the upper surface and has intensely welded and rheomorphic zones. TL2 is an extremely high grade ignimbrite which is intensely welded to the upper surface and includes lava-like lithofacies.
3. Both TL1 and TL2 display textures and structures which are difficult to reconcile with a model of instantaneous *en masse* deposition, followed by subsequent welding compaction, followed by secondary mass flowage in successive stages:
 - i) Gradational chemical and textural stratigraphy
 - ii) Rapid and complex changes through welding profiles
 - iii) Directional fabrics, indicative of flow at the sight of deposition which occur throughout the entire unit.

These features are more easily explained by invoking a model of progressive aggradation (Branney and Kokelaar, 1992), where deposition occurs incrementally from the base upwards with

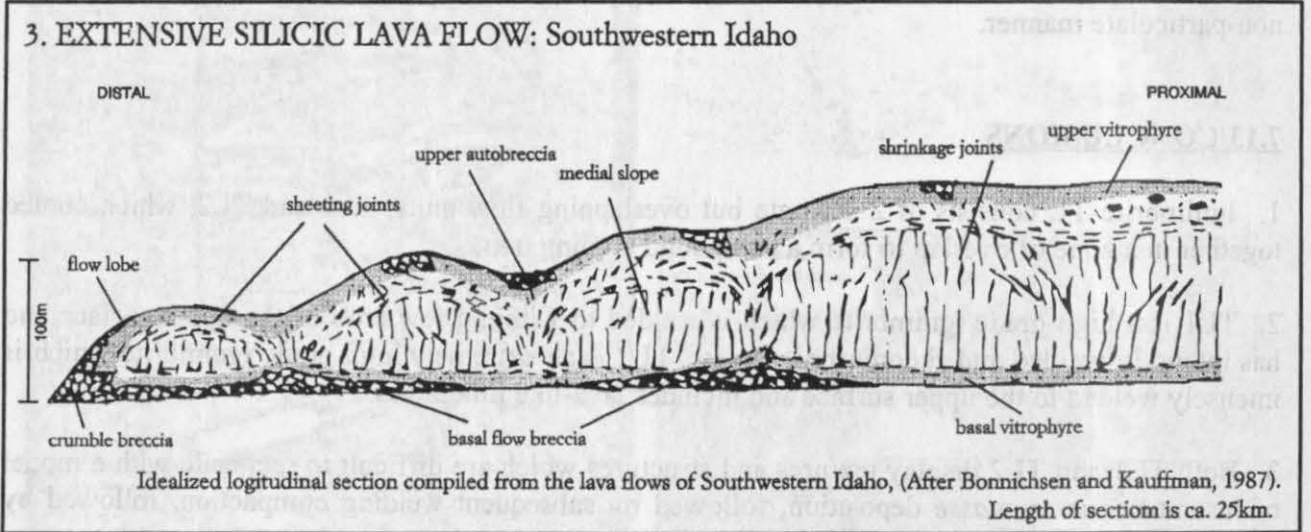
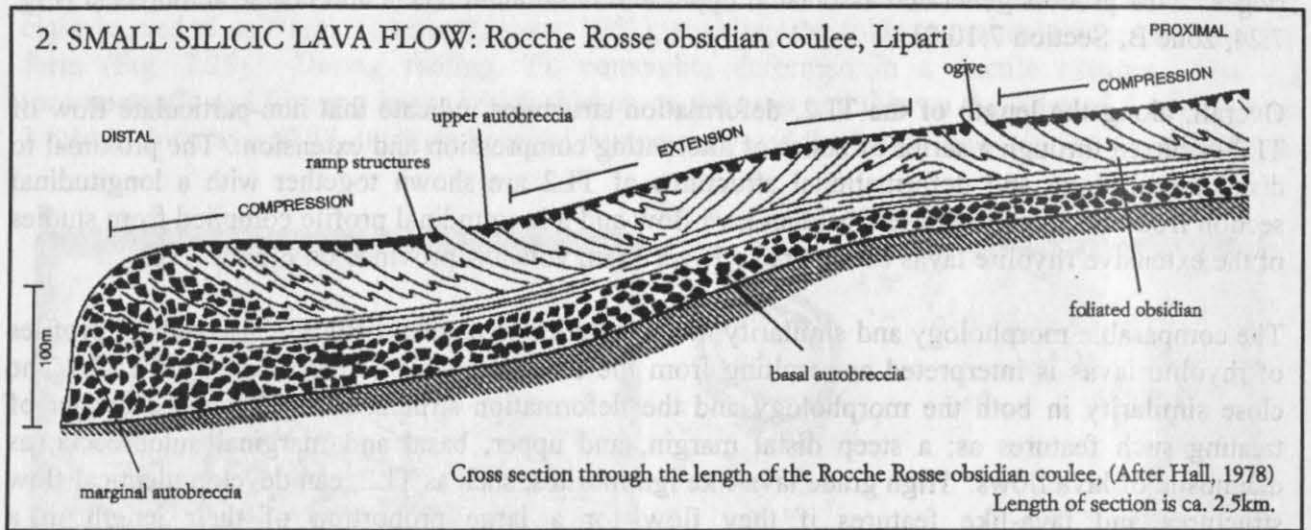
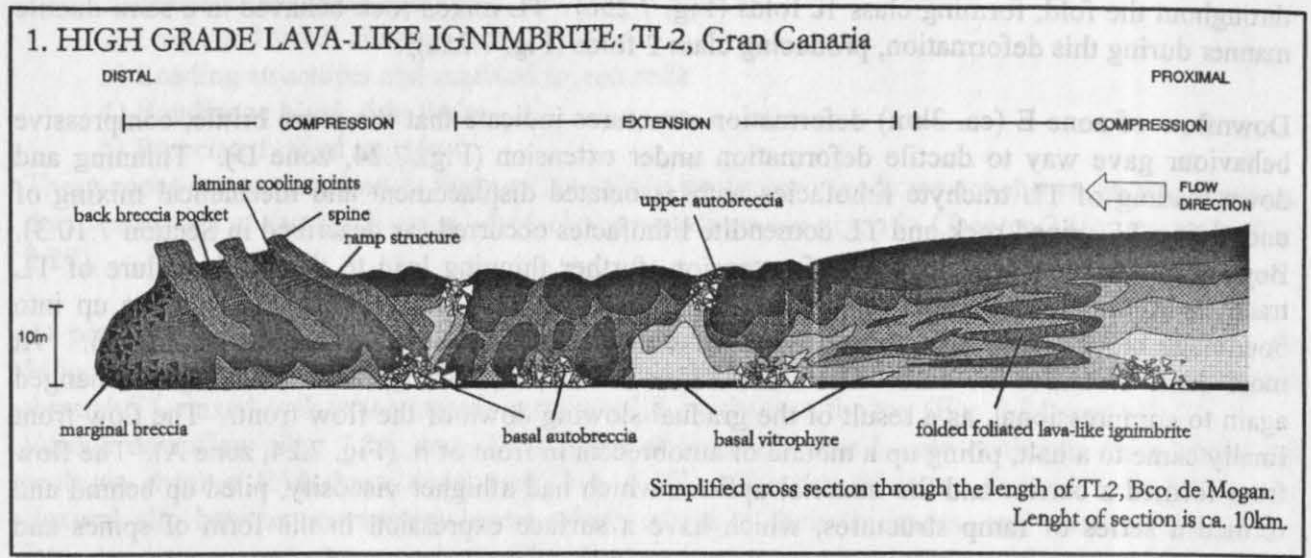


Figure 7.26. Comparison between; (a) High grade ignimbrite TL2, (b) the Rocche Rosse Obsidian rhyolite lava flow and (c) the extensive silicic lavas of Southwestern Idaho, highlighting the similarities and contrasts between basal, internal and surface deformation structures. Note the similarity in breccia distribution and the undulating surface topography between TL2 and the extensive silicic lava flows of Southwestern Idaho. The ramp and spine structures of TL2 closely resemble the ogive structures in the Rocche Rosse Obsidian lava flow, suggesting a similar origin. On a regional scale, from proximal to distal localities, the changes from a compressional to an extensional and back to a compressional regime, are directly comparable to those in the Rocche Rosse Obsidian coulee.

agglutination and rheomorphism occurring during as well as after deposition. The variations from slightly welded to eutaxitic and lava-like lithofacies in TL1 and TL2 reflect the viscosity variations of the successive particle populations supplied to the two flows over time. The more complex lithofacies variations in TL2 suggest that this was the deposit of a more unsteady flow than TL1.

4. TL2 is composed of rapidly stacked layers of differing density and viscosity, which were gravitationally unstable and so underwent lateral spreading, loading, hot slumping and brecciation during non-particulate flow.

5. Contrasting deformational features were produced in TL2 under varying stress regimes: extensional stress caused the development of pinch and swell structures and boudinage, at the top of slopes. Compressional stress, at the base of slopes, resulted in the formation of thrusts and ramp structures with associated autobreccia.

6. Extensive non-particulate flow caused the development of lava-like features in TL2, such as a steep distal margin and associated marginal autobreccia, and upper and basal autobreccia. Structures such as these have been used to distinguish extensive silicic lava-flows from highly rheomorphic ignimbrites, a practice which this study shows to be untenable.

CHAPTER 8

CONCLUSIONS

Peralkaline ignimbrite TL, of the Lower Mogán Formation on Gran Canaria, is a multiple flow unit consisting of two overlapping flow units, TL1 and TL2. TL1 forms a widespread sheet deposited over an area of 106km² on the southern flanks of the shield volcano. TL2 was deposited over a more restricted area of 51km², to the southwest. The two overlap between Bco. de Mogán and Bco. de Tauro, where TL2 overlies TL1. Close to the caldera margin, where the two overlap, they have cooled together to form a compound cooling unit.

Flow unit TL1 is a 'high grade' ignimbrite which is welded to the upper surface and contains rheomorphic zones. TL2 is an 'extremely high grade' ignimbrite, which is welded to the upper surface, and shows vertical and lateral gradations to lava-like lithofacies.

Both units have an extremely complicated textural stratigraphy, but there is a relatively simple compositional stratigraphy based on the varying proportions of comenditic trachyte and comendite. Both units consist of a base dominated by TL comendite lithofacies, a central zone of TL mixed rock lithofacies and an upper zone dominated by TL trachyte lithofacies.

TL comendite lithofacies are mostly vitroclastic and are only locally lava-like. TL mixed rock lithofacies show both vitroclastic and lava-like lithofacies and are marbled and flow banded.

TL trachyte lithofacies are generally lava-like, but locally even these grade vertically and laterally into vitroclastic lithofacies.

The thickness and composition of TL1 and TL2 and the lithofacies within them varies regionally around the caldera. These variations are interpreted to reflect the variation in magma withdrawal patterns, the discharge rate around the caldera rim, the duration of deposition (at any one locality) during sustained passage of the flow and the subsequent distribution over the palaeorelief. The thickness variations are a result of the flows' ability to surmount elevations which increases as the topography is buried. Post depositional welding compaction and late stage hot slumping downslope also influence the thickness of the flow unit and the lithofacies within it.

TL lithofacies consist of TL trachyte, TL mixed rock, and TL comendite. Glass, mineral and fiamme compositions however suggest that three original magma compositions are represented in TL: comenditic trachyte, comendite and trachybasalt, these are mingled in varying proportions.

TL trachyte consists of >60 volume percent comenditic trachyte components and <40 volume percent comendite components, with up to 2 volume percent trachybasalt.

TL comendite consists of >60 volume percent comendite components and <40 volume percent comenditic trachyte components.

TL mixed rock consists of 40-60 volume percent comenditic trachyte components and 40-60 volume percent comendite components mingled in varying proportions, with up to 2 volume percent trachybasalt.

Both TL1 and TL2 show considerable evidence for magma mixing, and are the deposits of particulate systems. Thus, TL lithofacies are not representative of the original magma compositions. Fiamme, although representing only small fragments of the original magma, are probably closest in composition to the original magma compositions.

Three chemically discrete juvenile particle populations are represented by fiamme in TL, these are; comenditic fiamme, mixed fiamme and comenditic trachyte fiamme. The juvenile particle

morphology changes systematically with chemical composition, and the composition of juvenile particles changes with height through TL1 and TL2. The vertical variations in the particle composition and the morphological variations within individual particle populations are ascribed to changes in the eruptive processes over *time*. This reflects the chemical composition, shape, and size of the juvenile particles supplied to the depositional regime of the flow during its sustained passage.

Like most of the other ignimbrites on Gran Canaria, TL is peralkaline. However, because the rock is particulate, the bulk rock compositions, determined by XRF analysis, are effected by the relative proportions of particles of different composition.

Silica rich comenditic fiamme are dominant in the lower zone of TL1 and TL2, and samples from this zone plot as comenditic rhyolite (= TL comendite). The central zone of each flow unit has a diverse fiamme population ranging from comendite to comenditic trachyte, thus TL mixed rock samples show extreme compositional variation. Comenditic trachyte fiamme dominate the upper zones of TL1 and TL2 and bulk rock analyses from these zones plot as comenditic trachyte (= TL trachyte).

The wide variation in chemical composition in TL is due to the physical mingling of up to three magma batches and to the complex lithofacies associations produced by displacement of lithofacies by loading, thrusting and partial overturning of the deposit during rheomorphism.

The major and trace element trends indicate that fractional crystallisation of comenditic trachyte was the main process of differentiation in the TL trachyte - TL comendite series.

Comendite is interpreted as being produced from comenditic trachyte by the fractional crystallisation of pyroxene and ilmenite together with plagioclase and anorthoclase feldspar, with anorthoclase feldspar being the most important phase. A wide range in fiamme composition plotting on a fractional crystallisation trend indicate that a zoned magma chamber, consisting of several discrete layers, was produced by the fractional crystallisation of comenditic trachyte.

The presence of comenditic trachyte (TL trachyte) cannot be explained by simple fractionation and is probably the result of an early magma mixing event between basalt and comendite.

Petrographic evidence indicates the presence of rocks belonging to two discrete fractionation series: one nepheline normative (e.g. trachybasalt globules in TL) and one quartz normative (e.g. TL trachyte and TL comendite). This is interpreted to be the result of contamination by incomplete mingling of magmas from these series, rather than contamination of magma by partial melting of wall rocks.

TL lithofacies are poorly sorted, and as well as fiamme, are composed of phenocrysts, glomerocrysts, glassy or formerly glassy shards, lenticules (vesicles), non-juvenile rock fragments, and microcrystalline matrix.

TL comendite and TL trachyte have been distinguished petrographically by their characteristic mineral assemblages. Trachybasalt, which occurs as globules in TL trachyte is glassy and aphyric and has been identified by microprobe analysis only.

The crystalline phases (phenocrysts and vapour phase crystals) in TL lithofacies are typical of peralkaline rocks. TL trachyte is characterised by the crystal phases: alkali feldspar, plagioclase, feldspar, amphibole, clinopyroxene, orthopyroxene and accessory oxide. TL comendite is characterised by the crystal phases: alkali feldspar, alkali amphibole and accessory oxide together with rare pyroxene. TL mixed rock contains crystal phases characteristic of both TL trachyte and TL comendite.

The non-crystalline phases in TL included shards, non-juvenile rock fragments and microcrystalline matrix.

Shards are visible in less strongly welded, glassy samples from TL1 and TL2. As with fiamme, the shape of shards varies with composition, and related vesicularity. Comenditic shards are commonly cusped, platy or fibrous; comenditic trachyte shards are angular, poorly vesicular fragments or globules.

Non-juvenile rock fragments in TL include all fragments which were not fluid when they were entrained in the magma or transport regime of the pyroclastic flow. These comprise accidental lithic fragments which are unrelated to the magma and were derived from the surface (pick-ups), or conduit and vent wall rocks (accessory lithics). The distribution of accidental lithics varies with height through TL1 and TL2 as well as locally in relation to topographic irregularities. The general decrease in the number of accidental lithics with height is consistent with a changing particle supply to the depositional regime of the flow. This may relate to the progressive burial of the landscape by aggrading tuff, and a decrease in wall erosion at the conduit and vent during the course of the eruption. Lithics are absent in the upper four or five metres of TL1 and TL2, this is interpreted to be the result of deposition during waning flow conditions, when lithic transport limits had migrated considerably upstream and dense lithics could no longer be transported for large distances. Localised Zones of lithic concentration generally correspond to a marked change in the composition of juvenile particles from comendite to comenditic trachyte. These are interpreted to be the result of increasing conduit erosion associated with eruption of comenditic trachyte.

The composition of vapour phase minerals in lenticules, in the densely welded portions of TL, indicate a high temperature 'closed system' redistribution of volatile phases, as opposed to the 'open system' pore space filling characteristic of low grade ignimbrites. Matrix textures in TL such as holocrystalline and trachytic texture, high temperature spherulite forms and partially infilled lenticules, suggest that compared to low grade ignimbrites, TL remained at a high temperature post emplacement, and that volatile exsolution continued after deposition and welding.

The field relations, geochemistry, petrographic and textural evidence indicate that TL underwent several stages of mixing and mingling which successively affected:

- 1) The component magmas in the magma chamber, prior to and during eruption.
- 2) The pyroclast populations created by explosive fragmentation, in the conduit, and in the transport regime during particulate flow.
- 3) The resultant extremely high grade ignimbrite, during post-depositional non-particulate flow.

Several processes are believed to account for the varying compositions and mingling textures observed in TL1 and TL2:

- 1) Mixing and homogenisation of hawaiite and comendite to produce comenditic trachyte.
 - 2) Mingling of comenditic trachyte and trachybasalt, by vesiculation induced disintegration of trachybasalt.
 - 3) Mingling of comendite, intermediate compositions and comenditic trachyte, by in-conduit shear of adjacent magma streams during withdrawal.
 - 4) Particulate mixing of juvenile particles by semi-turbulent flow in the transport regime.
- A further stage of mingling has been defined for extremely high grade ignimbrite TL2:
- 5) Mechanical mingling of lithofacies by loading, shear and auto-intrusion during non-particulate flow.

The compositional stratigraphy observed in TL1 and TL2 indicates that the composition of the erupting magma changed systematically with time, during the deposition of these two units. In both cases, comendite magma was discharged during the early phase of the eruption (TL comendite lithofacies). Comenditic trachyte gradually joined the comendite (TL mixed rock lithofacies) and ultimately dominated the bulk composition (TL trachyte lithofacies).

The sectorial differences in the distribution of TL1 and TL2, together with presence of trachybasal in TL2 and its absence in TL1, argue strongly for *two* simultaneous eruptions issuing from *two* vents, but related to single compositionally heterogeneous magma chamber.

The actual vent locations of TL1 and TL2 can only be generally inferred because TL is exposed at the Tejeda caldera rim at only one locality and intra-caldera TL is totally covered by younger rocks. Also the presently exposed caldera rim has been modified by Miocene volcanic, tectonic and erosional activity, post dating the TL eruption. However, the distribution of TL1 and TL2 is most simply explained by the vents being located on the caldera ring fissure system, rather than centrally within the caldera.

Both TL1 and TL2 display textures and structures which are difficult to reconcile with a model of *en masse* deposition, followed by post depositional welding compaction, followed by secondary mass flow. Although TL1 and TL2 are chemically and texturally stratified, internally they contain no definable flow unit boundaries. Within flow units TL1 and TL2 boundaries between compositional or textural lithofacies are gradational and where sharp contacts do occur they are traceable for only ten or twelve meters. There are no features between the lithofacies, such as fallout deposits, or surge deposits, sediments or soil, and no erosional surfaces that would suggest a time interval before the deposition of the next pyroclastic flow. Thus there is no evidence that suggests that the chemical and textural layers within TL1 and TL2 are the deposits of small, successive pyroclastic flows.

Both TL1 and TL2 are thoroughly welded to within a few centimetres of their upper surfaces. TL1 has a relatively simple textural stratigraphy defined by the degree of deformation of fiamme. TL2 however, shows complex and pronounced vertical and lateral variations in texture, from poorly welded to eutaxitic and lava-like. These changes are difficult to explain by a model of *en masse* deposition followed by welding compaction followed by secondary mass flowage because; the textural variations are not traceable over great distances and thus cannot be interpreted as flow units, representing the deposit of an entire pyroclastic flow. Also, many of the chemical and textural changes are not associated with deformational features indicating that layers were mechanically mixed or emplaced adjacent to each other during secondary mass flowage.

Both TL1 and TL2 contain directional fabrics which have been used to infer the palaeocurrent direction of the pyroclastic flow. In TL1 the fiamme are imbricated throughout the entire unit, and from one layer to the next, where imbrication persists through grain size changes. This is difficult to reconcile with a model of *en masse* deposition where structures reflecting welding deformation are interpreted as forming *after* deposition of the entire ignimbrite. It seems unlikely that the massive parts of TL1 and TL2 would contain directional grain fabrics, indicative of flow at the site of deposition if the flows travelled and deposited *en masse* as a non shearing plug. If welding was entirely due to post-depositional welding compaction under load, it should lead to flattening of the imbrication fabrics observed in TL, which has not been established.

The laterally impersistent and gradational changes in composition and texture, the complex change through welding profiles, and the persistence of fiamme imbrication through grain size changes are more easily explained by invoking a model of progressive aggradation (Branney and Kokelaar

1992). In this model deposition occurs throughout the passage of a sustained flow. Deposition is incremental from the base upwards, and agglutination and rheomorphism occur during as well as after deposition.

The variation in composition in TL1 and TL2 thus reflects the changing composition of the particles supplied to the depositional regimes of the two flows at any one time.

The textural variations from slightly welded to eutaxitic and lava-like lithofacies reflect the viscosity variations of the successive particle populations supplied to the two flows over time.

The persistence of fiamme imbrication through grain size changes and through out entire flow units is the result syn-depositional shear of viscous particles as they pass through the depositional boundary layer of the aggrading flow. Shear of particles continues as they become incorporated in the underlying non-particulate flow.

Flow unit TL2 can be clearly divided in to a proximal ponded region and a distal region. The distal portion of TL2 is dominated by holocrystalline lava-like textures and features, which have been considered diagnostic of lavas: basal autobreccia, extensive upper autobreccia, a steep distal margin and marginal autobreccia and locally holocrystalline trachytic texture. These features are interpreted to have formed during the non-particulate flow of TL2.

If hot low viscosity particles are sufficiently fluidal they will agglutinate or coalesce immediately on contact, rather than under the influence of post-emplacement cooling and loading. Agglutination or coalescence of particles leads to the development of a non-particulate flow component, which aggrades during the sustained passage of the flow. As the non-particulate layer thickens, it becomes mobile thus promoting lava-like flow.

The post agglutination flow processes in extremely high grade ignimbrites may be virtually indistinguishable from those of lava-flows. High grade ignimbrites fed by low pyroclastic fountains and spatter fed or fountain fed lava flows will both undergo substantial non-particulate flow and so are liable to develop identical flow structures.

Structures such as a steep distal margin and associated marginal autobreccia, and upper and basal autobreccia have been used to distinguish extensive silicic lava-flows from highly rheomorphic ignimbrites, a practice which this study concludes to be untenable.

REFERENCES

- Abbott RN jr. (1981) AFM liquidus projections for granitic magmas, with special reference to hornblende, biotite, and garnet. *Can Mineral* 19: 103-110
- Abich H (1982) Geologische Forschungen in den Kaukasischen Ländern. (Geologie des Armenischen Hochlands) *Wein, Alfred Holder* 2: 1-478
- Allen JRL (1982) Sedimentary structures; their character and physical basis: *Developments in Sedimentology* 30: 1-663. Elsevier, Oxford, United Kingdom
- Anderson AT (1976) Magma mixing: Petrological process and volcanological tool. *J Volcanol Geotherm Res* 1: 3-33
- Archambault C and Tanguy JC (1976) Comparative temperature measurements on Mount Etna lavas: problems and techniques. *J Volcanol Geotherm Res* 1: 113-25
- Bacon CR (1983) Eruptive history of Mount Mazama and Crater Lake caldera, Cascade Range, U.S.A. In *Arc Volcanism*, S. Aramaki and I. Kushiro (eds) *J Volcanol Geotherm Res* 18: 57-115
- Bacon CR and Hirschman MM (1988) Mg/Mn partitioning as a test for equilibrium between coexisting Fe-Ti oxides. *Am Mineral* 73: 57-61
- Barth TFW (1962) Theoretical petrology (2d ed.): *New York, John Wiley and Sons*, 416p.
- Berner H, Ramberg H, and Stephansson O (1972) Diapirism in Theory and Experiment. *Tectonophysics* 15: 197-218
- Blake DH, Elwell RWD, Gibson IL, Skelhorn RR, Walker GPL (1965) Some relationships resulting from the intimate association of acid and basic magmas. *Quart J Geol Soc London* 121: 31-49
- Blake S (1981 b) Eruptions from zoned magma chambers. *J Geol Soc London* 138: 281-287
- Blake S and Campbell IH (1986) The dynamics of magma-mixing during flow in volcanic conduits. *Contrib Mineral Petrol* 94: 72-81
- Blake S and Ivey GN (1986) Density and viscosity gradients in zoned magma chambers, and their influence on withdrawal dynamics. *J Volcanol Geotherm Res* 30: 201-230
- Boden DR (1989) Evidence for step-function zoning of magma and eruptive dynamics., Toquima Caldera Complex, Nevada. *J. Volcanol Geotherm Res* 27: 153-178
- Bogaard Pvd, Schmincke H-U, Freundt A, Hall CM, York D (1988) Eruption ages and magma supply rates during the Miocene evolution of Gran Canaria. *Naturwissenschaften* 75: 616-617
- Bonnichsen B and Kauffman DF (1987) Physical features of rhyolite lava flows in the Snake River Plain volcanic province, southwestern Idaho. In Fink JH (ed) The emplacement of silicic domes and lava flows. *Geol Soc Am Spec Pap* 212: 118-145

- Bottinga Y and Weill DF (1970) Densities of liquid silicate systems calculated from partial molar volumes of oxide components. *Am J Sci* 269: 1669-182
- Bottinga Y, Weill DF and Richet P (1982) Density calculations for silicate liquids. I. Revised method for aluminosilicate compositions. *Geochim Cosmochim Acta* 46: 909-919
- Branney MJ and Kokelaar BP (1992) A reappraisal of ignimbrite emplacement: progressive aggradation and changes from particulate to non-particulate flow during emplacement of high grade ignimbrite. *Bull Volcanol* 54: 504-520
- Branney MJ and Sparks RSJ (1990) Fiamme formed by diagenesis and burial-compaction in soils and subaqueous sediments. *J Geol Soc Lond* 147: 919-922
- Branney MJ, Kokelaar BP and McConnell (1992) The Bad Step Tuff: a lava-like rheomorphic ignimbrite in a calc-alkaline piecemeal caldera, English Lake District. *Bull Volcanol* 53: 187-199
- Buesch DC and Valentine GA (1989) Thickness and flow dynamics as factors controlling welding variations in ignimbrites (abstract) IAVCEI General Assembly on Continental Magmatism, Santa Fe. *New Mexico Bur Mines Mineral Resources Bull* 131: 364-65
- Carmichael ISE (1967) The Iron-Titanium oxides of silicic volcanic rocks and their associated ferromagnesian silicates. *Contrib Mineral Petrol* 14: 36-64
- Carmichael ISE, Turner FJ and Verhoogen J (1974) *Igneous Petrology*. New York: McGraw-Hill
- Cas RAF and Wright JV (1987) Volcanic successions: modern and ancient. Allen and Unwin, London: 1-528
- Chapin CE and Lowell GR (1979) Primary and secondary flow structures in ash-flow tuffs of the Gribbles Run Palaeovalley, central Colorado. In Chapin CE and Elson WE (eds) Ash Flow Tuffs. *Geol Soc Amer Spec Pap* 180: 137-154
- Cook EF (ed) Tufflavas and ignimbrites: a survey of soviet studies. Elsevier Publishing Co. NY: 1-121
- Cox KG, Bell JD and Pankhurst RJ (1979) The interpretation of igneous rocks. George Allen and Unwin, London: 1-450
- Crisp JA (1984) The Mogán and Fataga Formations of Gran Canaria (Canary Islands) Geochemistry, petrology, and compositional zonation of the pyroclastic and lava flows; intensive thermodynamic variables within the magma chamber; and the depositional history of pyroclastic flow E/ET. Unpubl PhD thesis, Princeton University, New Jersey: 1-304
- Deer WA, Howie RA and Zussman J (1976) An introduction to the rock-forming minerals. Longman Group Ltd. London: 1-528
- Dingwell DB and Webb SL (1989) Structural relaxation in silicate melts and non-newtonian melt rheology in geological processes. *Phys Chem Minerals* 16: 508-516

- Duda A (1984) Die petrographische Bedeutung der "Grunkern"-Pyroxene und andere Einsprenglingsphasen in den Foiditen und Basaniten der Westeifel. *Bochumer Geol Geogr Arb* 16: 1-170
- Eichelberger JC (1975) Origin of andesite and dacite: Evidence of mixing at Glass Mountain in California and at other Circum-Pacific volcanoes. *Geol Soc Am Bull* 86: 1381-1391
- Eichelberger JC (1980) Vesiculation of mafic magma during replenishment of silicic magma reservoirs. *Nature* 288: 446-450
- Ekren EB, McIntyre DH and Bennet EH (1984) High-temperature large-volume, lava-like ash-flow tuffs without calderas in southwestern Idaho. *US Geol Surv Pro Pap* 1272: 1-76
- Fisher RV and Schmincke (1984) Pyroclastic rocks. Springer Verlag, Berlin: 1-472
- Freundt A (1989) Composite flow P1 on Gran Canaria: Evolution of a rhyolite-trachyte-basalt magma system culminating in mixed-magma eruption and formation of silicic and basaltic welded ignimbrite. Unpubl PhD thesis Rhur-Universität Bochum (FRG): 1-444
- Freundt A and Schmincke H-U (1985) Lithic-enriched segregation bodies in pyroclastic flow deposits of Laacher See volcano (E-Eifel, Germany). *J Volcanol Geotherm Res* 25: 193-224
- Freundt A and Schmincke H-U (1992) Mixing of rhyolite, trachyte and basalt magma erupted from a vertically and laterally zoned reservoir, composite flow P1, Gran Canaria. *Contrib Mineral Petrol* 112: 1-19
- Freundt A and Tait SR (1986) The entrainment of high viscosity magma into low viscosity magma in eruption conduits. *Bull Volcanol* 48: 325-339
- Fridrich CJ and Mahood GA (1987) Compositional layers in the zoned magma chamber of the Grisly Peak Tuff. *Geology* 15: 299-303
- Furster JM, Hernandez-Pacheco A, Muñoz M, Badiola ER and Garcia Cacho L (1968) Geology and Volcanology of the Canary Islands, Gran Canaria Inst. (Lucas Mallada) *Consejo Superior de Investigacione Cientificas Madrid*, 243 pp.
- Gibson IL and Tazieff H (1967) Additional theory on the origin of fiamme in ignimbrites. *Nature* 215: 1473-4
- Giret A, Bonin B, Leger JM (1980) Amphibole compositional trends in oversaturated and undersaturated alkaline plutonic ring-complexes. *Can Mineral* 18: 481-495
- Hall SH (1978) The stratigraphy of northern Lipari and the structure of the Rocche Rosse rhyolite flow and its implications. Unpubl PhD thesis, University of Leeds, UK.
- Hay RL, Hildreth W and Lambe RN (1979) Globule ignimbrite of Mount Suswa, Kenya. In Chap and Elson (1979):167-75

- Helz RT (1982) Phase relations and compositions of amphiboles produced in studies of the melting behaviour of rocks. In Veblen DR and Ribbe PH (eds) *Amphiboles: Petrology and experimental phase relations. Reviews in Mineralogy 9b: 279-353*
- Henry CD and Wolff JA (1992) Distinguishing strongly rheomorphic tuffs from extensive silicic lavas. *Bull Volcanol 54: 171-186*
- Hildreth W (1981) Gradients in silicic magma chambers: Implications for lithospheric magmatism. *J Geophys Res 86:10153-10192*
- Hildreth W (1983) The compositionally zoned eruption of 1912 in the Valley of Ten Thousand Smokes, Katmai National Park, Alaska. *J Volcanol Geotherm Res 18: 1-56*
- Hildreth W (1991) The timing of caldera collapse at Mount Katmai in response to magma withdrawal toward Novarupta. *Geophys Res Letters 18: 1541-1544*
- Howells MF, Campbell SDG and Reedman AJ (1985) Isolated pods of subaqueous welded ash-flow tuff; a distal facies of the Capel Curig Formation (Ordovician) North Wales. *Geol Mag 122(2): 175-180*
- Huppert HE and Sparks RSJ (1980) The fluid dynamics of a basaltic magma chamber replenished by influx of hot dense ultrabasic magma. *Contrib Mineral Petrol 75: 279-289*
- Huppert HE, Sparks RSJ and Turner JS (1982) Effects of volatiles on mixing in calc-alkaline magma systems. *Nature 297: 554-557*
- Johnson RW (1968) Volcanic globule rock from Mount Suswa, Kenya. *Geol Soc Am Bull 79: 647-652*
- Kawachi Y, Pringle IJ and Coombs DS (1983) Pillow lavas of the Eocene Oamaru volcano, North Otago. Tour Bh 3. *Pacific Sci Congr, Dunedin, New Zealand*
- Koyaguchi T (1985) Magma mixing in a conduit. *J Volcanol Geotherm Res 25: 365-369*
- Koyaguchi T (1986) Textural and compositional evidence for magma mixing and its mechanism, Abu Volcanic Group, Southwestern Japan. *Contrib Mineral Petrol 93: 33-45*
- Kuenen PH (1953 a) Significant features of Graded Bedding. *Bull Am Assoc Pet Geol 37: 1044-1066*
- Kuenen PH (1953 b) Graded Bedding, with Observations on Lower Palaeozoic Rocks of Britain. *Verh K Ned Akad Wet (1)20(3):1-47*
- Leake BE (1978) Nomenclature of amphiboles. *Can Mineral 16:501-520*
- Leat PT (1985) Facies variations in peralkaline ash-flow tuffs from the Kenya Rift Valley. *Geol Mag 22: 139-150*

- Le Maitre RW, Bateman P, Dudek A, Keller J, Lameyre J, Le Bas MJ, Sabine PA, Schmid R, Sørensen H, Streckeisen A, Woolley AR, and Zanettin B (1989) A classification of igneous rocks and glossary of terms. Recommendation of the IUGS subcommission on the systematics of igneous rocks. *Blackwell Scientific Publ, Oxford, UK: 1-35*
- Lipman PW (1965) Chemical comparison of glassy and crystalline volcanic rocks. *US Geol Survey Bull 1201-D, D1-D24*
- Lipman PW (1971) Iron-Titanium oxide phenocrysts in compositionally zoned ash-flow sheets from southern Nevada. *J Geol 79:438-456*
- Lofgren G (1971 b) Experimentally produced devitrification textures in natural rhyolitic glass. *Geol Soc Am Bull 82: 111-24*
- Lowe DR (1979) Sediment gravity flows: their classification and some problems of application to natural flows and deposits. In Doyle LJ and Pilkey OH (eds) *Geology of continental slopes. SEPM Spec Pub 27: 75-82*
- Lowe DR (1982) Sediment gravity flows: II. Depositional models with special reference to high-density turbidity currents. *J Sed Petrol 52: 279-297*
- MacDonald GA (1972) *Volcanoes*. Englewood Cliffs, New Jersey: Prentice-Hall.
- Macdonald R (1974) Nomenclature and Petrochemistry of the Peralkaline Oversaturated Extrusive Rocks. *Bull Volcanol 88: 411-437*
- MacDonald GA and Katsura T (1964) Chemical composition of Hawaiian Lavas. *J Petrol 5:82-133*
- Mackin JH (1960) Structural significance of Tertiary volcanic rocks in southwestern Utah.. *Amer J Sci 258: 81-131*
- Mahood GA (1984) Pyroclastic rocks and calderas associated with strongly peralkaline volcanic rocks. *J Geophys Res 89: 8540-8552*
- Mahood GA and Hildreth W (1986) Geology of the peralkaline volcano at Pantelleria, Straights of Sicily. *Bull Volcanol 48: 143-172*
- Manley CR and Fink JH (1987) Internal textures of rhyolite flows as revealed by research drilling. *Geology 15: 549-552*
- Mansfield GR and Ross CS (1935) Welded rhyolitic tuffs in southeastern Idaho. *Am Geophys Union Trans, 16 th Ann. Mtg. pt. 1: 308-321. Natl Research Council, Aug. 1935.*
- McBirney AR (1979) Mixing and unmixing of magmas. *J Volcanol Geotherm Res 7: 357-371*
- McDougall I and Schmincke H-U (1977) Geochronology of Gran Canaria, Canary Islands: Age of shield building volcanism and other magmatic phases. *Bull Volcanol 40: 1-21*
- Millward D and Lawrence DJD (1986) The Stockdale (Yarlside) rhyolite - a rheomorphic ignimbrite? *Proc Yorks Geol Soc 45 (14): 299-306*

- Murase T and McBirney AR (1973) Properties of some common igneous rocks and their melts at high temperatures. *Geol Soc Am Bull* 84: 3563-3592
- Naney MT (1983) Phase equilibria of rock-forming ferromagnesian silicates in granitic system. *Am J Sci* 283:999-1033
- Nash WP, Carmichael ISE and Johnson RW (1969) The mineralogy and petrology of Mount Suswa, Kenya. *J Petro* 10: 409-439
- Noble DC (1967) Sodium, potassium and ferrous iron contents of some secondarily hydrated natural silicic glasses. *Am Mineral* 52: 280-285
- O'Hara MJ and Mathews RE (1981) Geochemical evolution in an advancing, periodically replenished, periodically tapped, continuously fractionated magma chamber. *J Geol Soc Lond* 138: 237-77
- Ragan IB and Sheridan MF (1972) Compaction of the Bishop Tuff, California. *Geol Soc Am Bull* 83:95-106
- Ramberg IB (1973) Gravity studies of the Fen Complex, Norway, and Their Petrological significance. *Contrib Mineral Petrol* 38: 115-134
- Ramsay JC (1967) Folding and fracturing of rocks. New York, McGraw-Hill
- Reedman AJ, Park KH, Merriman RJ and Kim SE (1987 a) Welded tuff infilling a volcanic vent at Weolseong, Republic of Korea. *Bull Volcanol* 49: 541-546
- Riebling EF (1966) Structure of sodium aluminosilicate melts containing at least 50 mole % SiO_2 at 1500 °C. *J Chem Phys* 44: 2857-2865
- Ross CS and Smith RL (1961) Ash-flow tuffs, their origin, geological relations and identification. *US Geol Surv Prof Pap* 366: 1-77
- Scarfe CM (1977) Viscosity of pantellerite melt at one atmosphere. *Can Mineral* 15:185-189
- Schmincke H-U (1969 a) Ignimbrite sequence on Gran Canaria. *Bull Volcanol* 33:1199-1219
- Schmincke H-U (1969 b) Petrologie der phonolithischen bis rhyolithischen Vulkanite auf Gran Canaria, Kanarische Inseln, Habilitationsschrift, Universität Heidelberg, 1-151
- Schmincke H-U (1972) Froth flows and globules flows in Kenya. *Naturwissenschaften* 11: 1-2
- Schmincke H-U (1974 b) Volcanological aspects of peralkaline silicic welded ash-flow tuffs. *Bull Volcanol* 38: 594-636
- Schmincke H-U (1982 a) Volcanic and chemical evolution of the Canary Islands. In von Rad U, Hinz K, Sarnthein M and Seibold E (eds) *Geology of the Northwest African Continental Margin*. Springer Verlag, Berlin, Heidelberg, New York. 273-308
- Schmincke H-U (1976) Geology of the Canary Islands. In Kunkel G (ed). *Biogeography and Ecology in the Canary Islands*. W Junk, The Hague. 67-184

- Schmincke (1993) Geological Field Guide Gran Canaria. (6th edition) 1-227, Pluto Press, Witt
FRG
- Schmincke H-U and Swanson DA (1967) Laminar viscous flowage structures in ash-flow tuffs
from Gran Canaria, Canary Islands. *J Geol* 75: 641-664
- Shaw HR (1965) Comments on viscosity, crystal settling, and convection in granitic magmas. *Am
Sci* 263: 120-152
- Shaw HR (1972) Viscosities of magmatic silicate liquids: An empirical method of prediction. *Am
Sci* 272: 870-893
- Sheridan MF (1979) Emplacement of pyroclastic flows: A review. *Geol Soc Am Spec Pap* 180:
125-136
- Smith RL (1960 b) Zones and zonal variations in welded ashflows. *US Geol Survey Prof Pap*
354-F, 149-159
- Smith RL (1979) Ash-flow magmatism. In Chapin CE and Elston WE (eds) Ash-flow tuffs. *Geol
Soc Am Spec Pap* 180: 5-27
- Smith RL and Bailey RA (1966) The Bandelier Tuff: a study of ash flow eruption cycles from
zoned magma chambers. *Bull Volcanol* 29: 83-104
- Sparks RSJ (1976) Grain size variations in ignimbrites and implications for the transport of
pyroclastic flows. *Sedimentology* 23: 147-188
- Sparks RSJ and Walker GPL (1977) The significance of vitric-enriched air-fall ashes associated
with crystal-enriched ignimbrites. *J Volcanol Geotherm Res* 2: 329-341
- Sparks RSJ and Wilson L (1976) A model for the formation of ignimbrite by gravitational column
collapse. *J Geol Soc Lond* 132: 441-451
- Sparks RSJ, Self S and Walker GPL (1973) Products of ignimbrite eruption. *Geology* 1: 115-118
- Sparks RSJ, Sigurdsson H and Wilson L (1977) Magma mixing: A mechanism for triggering ac-
tively explosive eruptions. *Nature* 267: 315-318
- Spencer KJ and Lindsley DH (1981) A solution model for coexisting iron-titanium oxides. *Amer
Mineral* 66: 1189-1201
- Spera FJ (1984) Ascent of basaltic magma. *Contrib Mineral Petrol*
- Stromer JC (1983) The effects of recalculation on the estimates of temperature and oxygen fugacity
from analyses of multicomponent iron-titanium oxides. *Am Mineral* 68: 586-594
- Thomas RME and Sparks RSJ (1992) Cooling of tephra during fallout from eruption columns. *Bull
Volcanol* 338: 1-12
- Tröger WE (1969) Optische Bestimmung der gesteinsbildenden Minerale. *E. Schweizerbart Sc
Verlagsbuchhandlung; Stuttgart (1982)*

- Valentine GA (1992) Magma chamber dynamics. *Encyclopaedia of Earth System Science* 3
- Villari L (1974) The island of Pantelleria. *Bull Volcanol* 38: 680-724
- Walker GPL (1983) Ignimbrite types and ignimbrite problems. *J Volcanol Geotherm Res* 1:
- Walker GPL and Croasdale R (1972) Characteristics of some basaltic pyroclasts. *Bull Volca*
303-317
- Wilson CJN and Walker GPL (1982) Ignimbrite depositional facies: The anatomy of a py
flow. *J Geol Soc Lond* 139: 581-592
- Wilson CJN, Sparks RSJ and Walker GPL (1980) Explosive volcanic eruptions IV: The co
magma properties and conduit geometry on eruption column behaviour. *Geophys J*
Soc 63: 117-148
- Wohletz KH (1983) Mechanisms of hydrovolcanic pyroclast formation: grain-size, s
electron microscopy, and experimental studies. *J Volcanol Geotherm Res* 17: 31-63
- Wolff JA and Storey M (1984) Zoning in highly alkaline magma bodies. *Geol Mag*
563-575
- Wolff JA and Wright JV (1981) Rheomorphism of welded tuffs. *J Volcanol Geotherm* 1
13-34
- Wolff JA and Wright JV (1982) Formation of the Green Tuff, Pantelleria. *Bull Volcanol*
681-90
- Wones DR (1982) Biotites and amphiboles in igneous rocks: Dehydration redox reactio
Veblen DR and Ribbe PH (eds) Amphiboles: Petrology and experimental phase rel
Rev Mineral 9B: 357-371
- Wörner G and Schmincke H-U (1984) The Laacher See Volcano I: Mineralogy and geoch
evolution of the Laacher See magma chamber. *J Petrol* 25:
- Wright JV (1980) Stratigraphy and geology of the welded air-fall tuffs of Pantelleria, Italy
Rundsch 69: 263-91
- Wright TL (1971) Chemistry of Kilauea and Mauna Loa lava in space and time. *US Geol*
Prof Pap 735: 1-40
- Wright TL and Fiske RS (1971) Origin of differentiated hybrid lavas of Kilauea volcano, Ha
Petrol 12: 1-65
- Wright JV and Walker GPL (1981) Eruption, transport and deposition of ignimbrite: a cas
from Mexico. *J Volcanol Geotherm Res* 9: 11-31
- Wright JV, Smith AL and Self S (1980) A working terminology of pyroclastic deposits. *J Vol*
Geotherm Res 8: 315-36
- Yoder HS jr (1973) Contemporaneous basaltic and rhyolitic magmas. *Am Mineral* 58: 153-1



GEOMAR REPORTS

- 1 GEOMAR FORSCHUNGSZENTRUM FÜR MARINE GEOWISSENSCHAFTEN
DER CHRISTIAN-ALBRECHTS-UNIVERSITÄT ZU KIEL
BERICHT FÜR DIE JAHRE 1987 UND 1988. 1989. 71 + 6 pp.
In German
- 2 GEOMAR FORSCHUNGSZENTRUM FÜR MARINE GEOWISSENSCHAFTEN DER CHRISTIAN-
ALBRECHTS-UNIVERSITÄT ZU KIEL
JAHRESBERICHT / ANNUAL REPORT 1989. 1990. 96 pp.
In German and English
- 3 GEOMAR FORSCHUNGSZENTRUM FÜR MARINE GEOWISSENSCHAFTEN
DER CHRISTIAN-ALBRECHTS-UNIVERSITÄT ZU KIEL
JAHRESBERICHT / ANNUAL REPORT 1990. 1991. 212 pp.
In German and English
- 4 ROBERT F. SPIELHAGEN
DIE EISDRIFT IN DER FRAMSTRASSE WÄHREND DER LETZTEN 200.000 JAHRE. 1991. 133 pp.
In German with English summary
- 5 THOMAS C. W. WOLF
PALÄO-OZEANOGRAPHISCH-KLIMATISCHE ENTWICKLUNG DES NÖRDLICHEN NORDATLANTIKS
SEIT DEM SPÄTEN NEOGEN (ODP LEGS 105 UND 104, DSDP LEG 81). 1991. 92 pp.
In German with English summary
- 6 SEISMIC STUDIES OF LATERALLY HETEROGENOUS STRUCTURES - INTERPRETATION AND
MODELLING OF SEISMIC DATA.
Edited by ERNST R. FLUEH
Commission on Controlled Source Seismology (CCSS), Proceedings of the 8th Workshop Meeting, held at
Kiel - Feilhorst (Germany), August 27-31, 1990. 1991. 359 pp.
In English
- 7 JENS MATTHIESSEN
DINOFLAGELLATEN-ZYSTEN IM SPÄTQUARTÄR DES EUROPÄISCHEN NORDMEERES:
PALÖKOLOGIE UND PALÄO-OZEANOGRAPHIE. 1991. 104 pp.
In German with English summary
- 8 DIRK NÜRNBERG
HAUPT- UND SPURENELEMENTE IN FORAMINIFERENGHÄUSEN - HINWEISE AUF KLIMATISCHE
UND OZEANOGRAPHISCHE ÄNDERUNGEN IM NÖRDLICHEN NORDATLANTIK WÄHREND DES
SPÄTQUARTÄRS. 1991. 117 pp.
In German with English summary
- 9 KLAS S. LACKSCHEWITZ
SEDIMENTATIONSPROZESSE AM AKTIVEN MITTELOZEANISCHEN KOLBEINSEY RÜCKEN (NÖRDLICH
VON ISLAND). 1991. 133 pp.
In German with English summary
- 10 UWE PAGELS
SEDIMENTOLOGISCHE UNTERSUCHUNGEN UND BESTIMMUNG DER KARBONATLÖSUNG IN
SPÄTQUARTÄREN SEDIMENTEN DES ÖSTLICHEN ARKTISCHEN OZEANS. 1991. 106 pp.
In German with English summary
- 11 FS POSEIDON - EXPEDITION 175 (9.10.-1.11.1990)
175/1: OSTGRÖNLÄNDISCHER KONTINENTALRAND (65° N)
175/2: SEDIMENTATION AM KOLBEINSEYRÜCKEN (NÖRDLICH VON ISLAND)
Hrsg. von J. MIENERT und H.-J. WALLRABE-ADAMS. 1992. 56 pp. + app.
In German with some English chapters
- 12 GEOMAR FORSCHUNGSZENTRUM FÜR MARINE GEOWISSENSCHAFTEN
DER CHRISTIAN-ALBRECHTS-UNIVERSITÄT ZU KIEL
JAHRESBERICHT / ANNUAL REPORT 1991. 1992. 152 pp.
In German and English
- 13 SABINE E. I. KÖHLER
SPÄTQUARTÄRE PALÄO-OZEANOGRAPHISCHE ENTWICKLUNG DES NORDPOLARMEERES UND
EUROPÄISCHEN NORDMEERES ANHAND VON SAUERSTOFF- UND KOHLENSTOFF-
ISOTOPFENVERHÄLTNISSEN DER PLANKTISCHEN FORAMINIFERE *Neogloboquadra pachyderma*
(sin.). 1992. 104 pp.
In German with English summary
- 14 FS SONNE - FAHRTBERICHT SO 78 PERUVENT
BALBOA, PANAMA - BALBOA, PANAMA, 28.2.1992-16.4.1992
Hrsg. von ERWIN SUESS. 1992. 120 pp.
In German with some English chapters
- 15 FOURTH INTERNATIONAL CONFERENCE ON PALEOCEANOGRAPHY (ICP IV)
SHORT- AND LONG-TERM GLOBAL CHANGE: RECORDS AND MODELLING
21-25 SEPTEMBER 1992, KIEL/GERMANY
PROGRAM & ABSTRACTS. 1992. 351 pp.
In English
- 16 MICHAELA KUBISCH
DIE EISDRIFT IM ARKTISCHEN OZEAN WÄHREND DER LETZTEN 250.000 JAHRE. 1992. 100 pp.
In German with English summary

- 17 PERSISCHER GOLF: UMWELTGEFÄHRDUNG, SCHADENSERKENNUNG, SCHADENSBEWERTUNG AM BEISPIEL DES MEERESBODENS; ERKENNEN EINER ÖKOSYSTEMVERÄNDERUNG NACH ÖLEINTRÄGEN. Schlußbericht zu den beiden BMFT-Forschungsvorhaben 03F0055 A+B. 1993. 108 pp. In German with English summary
- 18 TEKTONISCHE ENTWÄSSERUNG AN KONVERGENTEN PLATTENRÄNDERN / DEWATERING AT CONTINENTAL MARGINS. Hrg. von / ed. by ERWIN SUESS. 1993. 106+32+68+16+22+38+4+18 pp. Some chapters in English, some in German
- 19 THOMAS DICKMANN
DAS KONZEPT DER POLARISATIONSMETHODE UND SEINE ANWENDUNGEN AUF DAS SEISMISCHE VEKTORWELLENFELD IM WEITWINKELBEREICH. 1993. 121 pp. In German with English summary
- 20 GEOMAR FORSCHUNGSZENTRUM FÜR MARINE GEOWISSENSCHAFTEN
DER CHRISTIAN-ALBRECHTS-UNIVERSITÄT ZU KIEL
JAHRESBERICHT / ANNUAL REPORT 1992. 1993. 139 pp. In German and English
- 21 KAI UWE SCHMIDT
PALYNO MORPHE IM NEOGENEN NORDATLANTIK - HINWEISE ZUR PALÄO-OZEANOGRAPHIE UND PALÄOKLIMATOLOGIE. 1993. 104+7+41 pp. In German with English summary
- 22 UWE JÜRGEN GRÜTZMACHER
DIE VERÄNDERUNGEN DER PALÄO GEOGRAPHISCHEN VERBREITUNG VON *BOLBOFORMA* - EIN BEITRAG ZUR REKONSTRUKTION UND DEFINITION VON WASSERMASSEN IM TERTIÄR. 1993. 104 pp. In German with English summary
- 23 RV PROFESSOR LOGACHEV - Research Cruise 09 (August 30 - September 17, 1993)
SEDIMENT DISTRIBUTION ON THE REYKJANES RIDGE NEAR 59°N
Edited by H.-J. WALLRABE-ADAMS & K.S. LACKSCHEWITZ. 1993. 66+30 pp. In English
- 24 ANDREAS DETTMER
DIATOMEEN-TAPHOZÖNOSEN ALS ANZEIGER PALÄO-OZEANOGRAPHISCHER ENTWICKLUNGEN IM PLIOZÄNEN UND QUARTÄREN NORDATLANTIK. 1993. 113+10+25 pp. In German with English summary
- 25 GEOMAR FORSCHUNGSZENTRUM FÜR MARINE GEOWISSENSCHAFTEN
DER CHRISTIAN-ALBRECHTS-UNIVERSITÄT ZU KIEL
JAHRESBERICHT / ANNUAL REPORT 1993. 1994. In German and English
- 26 JÖRG BIALAS
SEISMISCHE MESSUNGEN UND WEITERE GEOPHYSIKALISCHE UNTERSUCHUNGEN AM SÜD-SHETLAND TRENCH UND IN DER BRANSFIELD STRASSE - ANTARKTISCHE HALBINSEL. 1994. 113 pp. In German with English summary
- 27 JANET MARGARET SUMNER
THE TRANSPORT AND DEPOSITIONAL MECHANISM OF HIGH GRADE MIXED-MAGMA IGIMBRITE TL, GRAN CANARIA: THE MORPHOLOGY OF A LAVA-LIKE FLOW. 1994. 224 pp. In English with German summary